

X-582-76-77

PREPRINT

NASA TM X- 71106

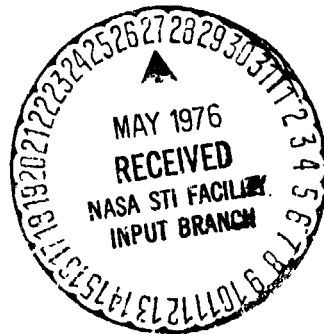
# MATHEMATICAL THEORY OF THE GODDARD TRAJECTORY DETERMINATION SYSTEM

(NASA-TM-X-71106) MATHEMATICAL THEORY OF  
THE GODDARD TRAJECTORY DETERMINATION SYSTEM  
(NASA) 529 p HC \$13.00 CSCL 22A

N76-24291  
THRU  
N76-24302  
Unclas  
40073

G3/13

APRIL 1976



**GSFC**

**GODDARD SPACE FLIGHT CENTER**

**GREENBELT, MARYLAND**

MATHEMATICAL THEORY OF THE GODDARD  
TRAJECTORY DETERMINATION SYSTEM

Edited by

J. O. Cappellari  
Computer Sciences Corporation

and

C. E. Velez and A. J. Fuchs  
Goddard Space Flight Center

April 1976

GODDARD SPACE FLIGHT CENTER  
Greenbelt, Maryland

## ACKNOWLEDGMENT

The editors wish to acknowledge the many individuals at Goddard Space Flight Center and at Computer Sciences Corporation who contributed to this document. These individuals are:

C. L. Ayres	CSC	D. H. Novak	CSC
J. A. Behuncik	GSFC	R. S. Pajerski	GSFC
J. O. Cappellari, Jr.	CSC	J. S. Reece	CSC
A. J. Fuchs	GSFC	G. P. Spears	CSC
T. J. Grenchik	GSFC	H. E. Stull	CSC
A. C. Long	CSC	C. E. Velez	GSFC
F. E. McGarry	GSFC	W. E. Wagner	CSC
G. D. Mistretta	GSFC	W. H. Wooden	CSC

A special acknowledgment is given to E. J. Smith of CSC, who made an invaluable contribution in the preparation of the figures and text for the final document.

In addition, the authors wish to acknowledge the efforts of the individuals who contributed to the previous description of the mathematics contained in GTDS.<sup>1</sup>

---

<sup>1</sup>Wagner, W. E. and Velez, C. E. (editors): 1972, Goddard Trajectory Determination System Mathematical Specifications, Goddard Space Flight Center Report X-552-72-244, March 1972.

## PREFACE

GTDS is documented in several parts in order to satisfy the specific requirements of different audiences. The Mathematical Theory of the Goddard Trajectory Determination System presents the derivations of all algorithms (including observation modeling equations) used in the system. This document is specifically directed to the analyst.

The GTDS Design Manual<sup>1</sup> presents a comprehensive overview of GTDS capabilities for the programmer who is totally unfamiliar with GTDS. This manual emphasizes the structure of the software system and the relationships among the individual components of the system. For this reason, the design manual is most suited as an introduction to GTDS for programmers who must maintain and enhance the system. It is also helpful, however, to the analyst who must be familiar with the system at the algorithm level.

The GTDS User's Guide<sup>2</sup> is directed to a general audience which includes analysts, programmers, and data technicians. Although a brief description of the system is provided in this document, the principal contents are a description of the specific requirements for data card input to the system.

---

<sup>1</sup> Zavaleta, E. L.: 1975, Goddard Trajectory Determination System Design Manual, Computer Sciences Corporation Report CSC/SD-75/6092, March 1975.

<sup>2</sup> Zavaleta, E. L. and Smith, E. J.: 1975, Goddard Trajectory Determination System User's Guide, Computer Sciences Corporation Report CSC/SD-75/6005, April 1975.



## ABSTRACT

This document presents a description of the mathematical theory underlying the Goddard Trajectory Determination System (GTDS), and includes an overview of the system capabilities. The basic mathematical formulations presented include mathematical descriptions of coordinate and time systems, perturbation models, orbit propagation techniques, numerical integration techniques, observation models, statistical estimation methods, and early orbit determination techniques.

PRECEDING PAGE BLANK NOT FILMED

# TABLE OF CONTENTS

	<u>Page</u>
<u>Chapter 1 - Introduction</u> . . . . .	1-1
<u>Chapter 2 - GTDS Overview</u> . . . . .	2-1 <del>D-1</del>
2.1 GTDS Programs . . . . .	2-1
2.1.1 Differential Correction Program . . . . .	2-2
2.1.2 Ephemeris Generation Program . . . . .	2-2
2.1.3 Ephemeris Comparison Program . . . . .	2-2
2.1.4 Filter Program . . . . .	2-2
2.1.5 Early Orbit Determination Program . . . . .	2-3
2.1.6 Data Simulation Program . . . . .	2-3
2.1.7 Error Analysis Program . . . . .	2-3
2.1.8 Data Management Program . . . . .	2-4
2.2 System Capabilities . . . . .	2-4
2.2.1 Trajectory Generation . . . . .	2-6
2.2.2 Observation Modeling . . . . .	2-9
2.2.3 Estimation Techniques . . . . .	2-13
2.2.4 Early Orbit Determination . . . . .	2-14
2.2.5 Optional Modes of Operation . . . . .	2-16
2.3 Spacecraft Dynamics . . . . .	2-17
2.4 Near Real-Time Operation and Postflight Processing . . . . .	2-19
<u>Chapter 3 - Coordinate and Time Systems</u> . . . . .	3-1
3.1 General Comments and Definitions . . . . .	3-1
3.2 Coordinate System Descriptions . . . . .	3-3
3.2.1 Body-Centered Equatorial Inertial (Geocentric, Selenocentric, or Planetocentric) . . . . .	3-3
3.2.2 Body-Centered Rotating . . . . .	3-4
3.2.3 Local Plane System . . . . .	3-5
3.2.4 Topocentric Local Tangent (East/North/Up). . . . .	3-6
3.2.5 Orbit Plane . . . . .	3-7
3.2.6 Orbital Elements . . . . .	3-8
3.2.7 Vehicle-Fixed . . . . .	3-10

	<u>Page</u>
3.3 Specific Transformations . . . . .	3-10
3.3.1 1950.0 Inertial to True of Date . . . . .	3-11
3.3.2 True of Date to Body-Fixed . . . . .	3-18
3.3.3 Selenocentric True of Date to Selenographic . . . . .	3-26
3.3.4 Spherical-Cartesian Transformations . . . . .	3-34
3.3.5 Body-Centered True of Date to Orbit Plane . . . . .	3-39
3.3.6 Body-Fixed to Geographic Transformations . . . . .	3-40
3.3.7 Earth-Fixed to Topocentric Local Tangent (East, North, Up) . . . . .	3-47
3.3.8 Keplerian-Cartesian Transformations . . . . .	3-49
3.3.9 Equinoctial-Cartesian Transformations . . . . .	3-58
3.3.10 Herrick-Cartesian Transformations . . . . .	3-62
3.3.11 Keplerian to Equinoctial and Herrick Transformations . . . . .	3-64
3.3.12 Vehicle-Fixed to Body-Centered True of Date Transformations . . . . .	3-65
3.4 Time Systems . . . . .	3-66
3.4.1 Ephemeris Time, ET. . . . .	3-67
3.4.2 Atomic Time, A.1 . . . . .	3-67
3.4.3 Universal Time, UT . . . . .	3-67
3.4.4 Uncorrected Universal Time, UT0 . . . . .	3-69
3.4.5 Universal Time, UT1 . . . . .	3-69
3.4.6 Universal Time, UT2 . . . . .	3-70
3.4.7 Universal Time Coordinated, UTC. . . . .	3-70
3.4.8 Station Time, ST. . . . .	3-71
3.5 Transformations Between Time Systems . . . . .	3-71
3.5.1 Transformations by Standard Formula . . . . .	3-71
3.5.2 Transformations by Time Polynomials . . . . .	3-72
3.6 Polynomial Representation of Ephemeris Data . . . . .	3-73
3.7 References . . . . .	3-80
<u>Chapter 4 - Perturbation Models and Variational Equations</u> . . . . .	4-1
4.1 Total Perturbation Model and Variational Equations . . . . .	4-2
4.2 Point Mass Effects . . . . .	4-4
4.2.1 N-Point Masses Perturbation Model . . . . .	4-5
4.2.2 Associated Partial Derivatives . . . . .	4-8

	<u>Page</u>
4.3 Nonspherical Gravitational Effects . . . . .	4-9
4.3.1 Nonspherical Gravitational Perturbation Model . . . . .	4-9
4.3.2 Associated Partial Derivatives . . . . .	4-14
4.4 Indirect Oblation Perturbation Model . . . . .	4-18
4.5 Aerodynamic Forces and Atmospheric Models . . . . .	4-22
4.5.1 Introduction . . . . .	4-22
4.5.2 Aerodynamic Force Modeling . . . . .	4-24
4.5.3 Associated Partial Derivatives . . . . .	4-29
4.5.4 Jacchia-Roberts Atmospheric Model . . . . .	4-33
4.5.5 Associated Partial Derivatives . . . . .	4-50
4.5.6 Modified Harris-Priester Atmospheric Model . . . . .	4-53
4.5.7 Associated Partial Derivatives . . . . .	4-57
4.5.8 Comparison of Atmospheric Models . . . . .	4-60
4.6 Solar Radiation Pressure . . . . .	4-60
4.6.1 Solar Radiation Pressure Perturbation Model . . . . .	4-60
4.6.2 Associated Partial Derivatives . . . . .	4-63
4.7 Attitude Control Effects . . . . .	4-64
4.7.1 Attitude Control Perturbation Model . . . . .	4-64
4.7.2 Associated Partial Derivatives . . . . .	4-66
4.8 Thrust Effects . . . . .	4-66
4.8.1 Thrust Acceleration Model . . . . .	4-67
4.8.2 Associated Partial Derivatives . . . . .	4-69
4.9 Replacement Acceleration . . . . .	4-73
4.9.1 Replacement Acceleration Model . . . . .	4-73
4.9.2 Associated Partial Derivatives . . . . .	4-74
4.10 Analytic Partial Derivatives . . . . .	4-75
4.10.1 Definition of the Perturbation Variables . . . . .	4-75
4.10.2 State Transition Matrix Elements . . . . .	4-79
4.10.3 Conversion of Differential Corrections . . . . .	4-83
4.11 References . . . . .	4-87
<u>Chapter 5 - Formulation of the Orbital Equations of Motion . . . . .</u>	<u>5-1</u>
5.1 Introduction . . . . .	5-1

	<u>Page</u>
5.2 Cowell Method . . . . .	5-8
5.3 Time Regularized Cowell . . . . .	5-9
5.4 Kustaanheimo-Stiefel (KS) Formulation . . . . .	5-10
5.4.1 The KS Variation of Parameters (VOP) Equations of Motion . . . . .	5-11
5.4.2 Transformation from Cartesian Position and Velocity to KS Parametric Values . . . . .	5-13
5.4.3 Transformation from KS Parametric Variables to Cartesian Position and Velocity . . . . .	5-15
5.5 Delaunay-Similar (DS) Elements . . . . .	5-16
5.5.1 The DS Variation of Parameters (VOP) Equations of Motion . . . . .	5-17
5.5.2 Transformation from Cartesian Position and Velocity to DS Elements . . . . .	5-20
5.5.3 Transformation from DS Elements to Cartesian Position and Velocity . . . . .	5-24
5.6 Picard Iteration Using Chebyshev Series . . . . .	5-26
5.7 Gaussian Variation of Parameters Formulations . . . . .	5-30
5.7.1 Keplerian Elements . . . . .	5-31
5.7.2 Equinoctial Elements . . . . .	5-33
5.7.3 Rectangular Formulation . . . . .	5-34
5.8 Numerical Averaging Formulations . . . . .	5-37
5.8.1 The Averaged Equations of Motion . . . . .	5-38
5.8.2 Numerical Evaluation of the Averaged Equations of Motion . . . . .	5-39
5.8.3 Averaged Equinoctial Variation of Parameters Formulation . . . . .	5-40
5.8.4 Averaged Keplerian Variation of Parameters Formulation . . . . .	5-40
5.8.5 Transformation from Osculating Orbital Elements to Averaged Elements . . . . .	5-40
5.9 Brouwer Theory . . . . .	5-42
5.9.1 Transformation from Osculating Orbital Elements to Brouwer Mean Elements . . . . .	5-45

	<u>Page</u>
5.9.2 Transformation from Brouwer Mean Elements to Osculating Keplerian Elements . . . . .	5-46
5.10 Brouwer-Lyddane Theory . . . . .	5-51
5.10.1 Transformation from Osculating Orbital Elements to Brouwer Mean Elements . . . . .	5-52
5.10.2 Transformation from Brouwer Mean Elements to Osculating Keplerian Elements . . . . .	5-52
5.11 Intermediate Orbit . . . . .	5-58
5.12 Vinti Theory . . . . .	5-59
5.13 References . . . . .	5-61
<u>Chapter 6 - Numerical Integration of the Equations of Motion and Variational Equations . . . . .</u>	<u>6-1</u>
6.1 Adams-Cowell Ordinate Second Sum Formulas . . . . .	6-2
6.2 Predict-Pseudo Correct Algorithm for Equations of Motion . . .	6-7
6.3 Corrector-Only Cowell Integration for Linear Systems . . . . .	6-9
6.4 Corrector-Only Algorithm for Variational Equations . . . . .	6-11
6.5 Mapping of Position Partial Derivatives . . . . .	6-15
6.6 The Runge-Kutta Integration Method . . . . .	6-16
6.7 The Starting Procedure . . . . .	6-19
6.7.1 Iterative Starter . . . . .	6-19
6.7.2 Runge-Kutta Starter . . . . .	6-20
6.8 Interpolation . . . . .	6-21
6.9 Local Error Control . . . . .	6-21
6.10 Time Regularization . . . . .	6-22
6.11 References . . . . .	6-26

	<u>Page</u>
<u>Chapter 7 - Observation Models</u> . . . . .	7-1
7.1 General Description . . . . .	7-1
7.2 Ground Based Tracker Models . . . . .	7-4
7.2.1 Tracking Process . . . . .	7-4
7.2.2 Local Tangent Plane Coordinates . . . . .	7-5
7.2.3 Measurement Equations and Partial Derivatives . . . . .	7-7
7.3 Satellite-to-Satellite Tracking (SST) Model . . . . .	7-18
7.3.1 Introduction . . . . .	7-18
7.3.2 Light Time Modeling . . . . .	7-21
7.3.3 The Range Observation . . . . .	7-21
7.3.4 The Doppler Observation . . . . .	7-27
7.4 Radar Altimeter Model . . . . .	7-34
7.4.1 Surface Model . . . . .	7-34
7.4.2 Measurement Equation . . . . .	7-38
7.4.3 Partial Derivatives . . . . .	7-40
7.5 Very Long Baseline Interferometer (VLBI) Model . . . . .	7-41
7.6 Atmospheric Effects . . . . .	7-43
7.6.1 Troposphere Model . . . . .	7-43
7.6.2 Ionosphere Models . . . . .	7-44
7.6.3 Chapman Profile Refraction Corrections . . . . .	7-52
7.6.4 Segmented Profile Refraction Corrections . . . . .	7-64
7.7 Additional Corrections . . . . .	7-76
7.7.1 Light-Time Correction . . . . .	7-76
7.7.2 Antenna Mount Corrections . . . . .	7-76
7.7.3 Transponder Delay Correction . . . . .	7-77
7.8 Estimation Model . . . . .	7-77
7.9 References . . . . .	7-80
<u>Chapter 8 - Estimation</u> . . . . .	8-1
8.1 Description of the Problem . . . . .	8-1

	<u>Page</u>
8.2 The Batch Estimator Algorithm . . . . .	8-5
8.2.1 Mean and Covariance of Estimate . . . . .	8-8
8.2.2 Observation Partial Derivatives . . . . .	8-12
8.2.3 Covariance Matrix Transformations . . . . .	8-15
8.2.4 Computational Procedure for the Differential Correction Program . . . . .	8-19
8.3 Error Analysis Application . . . . .	8-22
8.4 Sequential Estimation . . . . .	8-27
8.4.1 Derivation and Applications of the Extended Kalman Filter . . . . .	8-28
8.4.2 Dynamic Model Compensation Filtering . . . . .	8-37
8.4.3 Statistical Adaptive Filtering . . . . .	8-42
8.4.4 Computational Procedure for the Filter Program . . . . .	8-47
8.5 Covariance Matrix Interpretation . . . . .	8-50
8.5.1 Augmented Vector and Covariance . . . . .	8-50
8.5.2 Hyperellipse Probabilities . . . . .	8-51
8.5.3 Hyperrectangle Probabilities . . . . .	8-54
8.5.4 Correlation Coefficient . . . . .	8-56
8.6 Estimation Related Techniques . . . . .	8-57
8.6.1 Matrix Inversion . . . . .	8-57
8.6.2 Editing of Observation Residuals . . . . .	8-60
8.6.3 Iteration Control for the Differential Correction Program . . . . .	8-60
8.6.4 Weighted Least Squares and Filter Statistics . . . . .	8-61
8.7 References . . . . .	8-64
<u>Chapter 9 - Early Orbit Methods</u> . . . . .	9-1
9.1 Angles Only Methods . . . . .	9-1
9.1.1 Transformation of Topocentric Gimbal Angles to Inertial Coordinates . . . . .	9-2
9.1.2 Gauss Method . . . . .	9-6
9.1.3 Double r-Iteration Method . . . . .	9-14
9.2 Range and Angles Method . . . . .	9-24
9.3 References . . . . .	9-31



	<u>Page</u>
<u>Appendix A - Trajectory Sensor System Functional Descriptions and Preprocessing</u> . . . . .	A-1
A.1 Goddard Range and Range-Rate (GRARR) System and Applications Technology Satellite Range and Range-Rate (ATSR) System. . . . .	A-1
A.1.1 Functional Description . . . . .	A-1
A.1.2 Preprocessing Description . . . . .	A-4
A.2 C-Band Radar System . . . . .	A-9
A.2.1 Functional Description . . . . .	A-9
A.2.2 Preprocessing Description . . . . .	A-10
A.3 Unified S-Band (USE) System . . . . .	A-10
A.3.1 Functional Description . . . . .	A-10
A.3.2 Preprocessing Description . . . . .	A-13
A.4 Minitrack System . . . . .	A-14
A.4.1 Functional Description . . . . .	A-14
A.4.2 Preprocessing Description . . . . .	A-17
A.5 Very Long Baseline Interferometer (VLBI). . . . .	A-27
A.6 Radar Altimeter . . . . .	A-29
A.7 Satellite-to-Satellite Tracking . . . . .	A-30
A.8 References . . . . .	A-34
<u>Appendix B - Time Elements</u> . . . . .	B-1
B.1 Unperturbed Motion . . . . .	B-2
B.1.1 Time Element Corresponding to the Eccentric Anomaly ( $\alpha = 1$ ) . . . . .	B-2
B.1.2 Time Element Corresponding to the True Anomaly ( $\alpha = 2$ ). . . . .	B-3
B.2 Perturbed Motion . . . . .	B-3
B.2.1 Time Element Equation Corresponding to the KS Formulation ( $\alpha = 1$ ) . . . . .	B-3
B.2.2 Time Element Equation Corresponding to the DS Formulation ( $\alpha = 2$ ) . . . . .	B-5

	<u>Page</u>
<u>Appendix C - Development of Range-Rate Formulas</u> . . . . .	C-1
<u>Appendix D - Observation Weighting</u> . . . . .	D-1
<u>Appendix E - Matrix Identities Associated With</u> <u>Sequential Estimation</u> . . . . .	E-1
E.1 Derivation of the Recursive Form of the Covariance Matrix of Error, $P_{\Delta x_m+1}$ . . . . .	E-1
E.2 Derivation of an Alternative Form of the Optimal Linear Gain . . . . .	E-3
<u>Glossary</u> . . . . .	G-1
<u>Index</u> . . . . .	I-1

# LIST OF ILLUSTRATIONS

<u>Figure</u>		<u>Page</u>
2-1	Schematic Diagram of the Differential Correction Process . . . . .	2-5
2-2	Schematic Diagram of the Ephemeris Generation Process . . . . .	2-7
2-3	Schematic Diagram of the Data Simulation Process . . . . .	2-11
2-4	Schematic Diagram of the Error Analysis Process . . . . .	2-15
3-1	Body-Centered Inertial Coordinate System . . . . .	3-4
3-2	Body-Centered Rotating Coordinate System . . . . .	3-5
3-3	Local Plane System . . . . .	3-6
3-4	Topocentric Coordinates . . . . .	3-7
3-5	Orbit Plane Coordinates . . . . .	3-8
3-6	Orbital Parameters . . . . .	3-9
3-7	Vehicle-Fixed Coordinates . . . . .	3-10
3-8	Precession Angles . . . . .	3-13
3-9	Nutation Angles . . . . .	3-15
3-10	Greenwich Sidereal Time . . . . .	3-18
3-11	Polar Motion Schematic . . . . .	3-21
3-12	Polar Motion Errors . . . . .	3-23
3-13	Selenocentric/Selenographic Geometry . . . . .	3-27
3-14	Selenographic Transformation Angles . . . . .	3-29
3-15	Ellipsoid Geometry . . . . .	3-42
3-16	Greenwich Hour Angle . . . . .	3-68
4-1	Schematic of Point Mass Gravitational Bodies . . . . .	4-6
4-2	Body-Fixed System . . . . .	4-11
4-3	Sample Deviations of Jacchia-Roberts Densities from Jacchia 1971 Values . . . . .	4-48
4-4	Best-fit Value of $\rho$ as a Function of the Exospheric Temperature $T_{\infty}$ . . . . .	4-49
4-5	Cylindrical Shadow Model . . . . .	4-62
4-6	Orbital Geometry . . . . .	4-76
7-1	SST Tracking Geometry . . . . .	7-20
7-2	Geoid Undulation . . . . .	7-35
7-3	Geoid Geometry . . . . .	7-39
7-4	Empirical Worldwide Electron Density Profile . . . . .	7-45
7-5	Refraction Correction Comparison of Ray Trace vs. GIDS Algorithms (CSC Model) . . . . .	7-57
7-6	Uplink Path Geometry at Spacecraft Signal Reception . . . . .	7-62
8-1	Computational Sequence for the Differential Correction Program . . . . .	8-20

# LIST OF ILLUSTRATIONS (Cont'd.)

<u>Figure</u>		<u>Page</u>
8-2	Computational Sequence for the Filter Program . . . . .	8-49
8-3	Error Ellipse and Rectangle . . . . .	8-54
9-1	Position Vector Geometry . . . . .	9-6
9-2	Gauss Method Computational Sequence . . . . .	9-12
9-3	Double r-Iteration Computation Sequence . . . . .	9-21
9-4	Range and Angles Method Computational Sequence . . . . .	9-30
A-1	Schematic of GRARR Gimbal Angles . . . . .	A-3
A-2	GRARR and ATSR Data Preprocessor Computations and Interfaces . . . . .	A-5
A-3	Minitrack Baseline and Signal Reception Geometry . . . . .	A-15
A-4	Minitrack Preprocessor and Interface Schematic . . . . .	A-18
A-5	Simplified Schematic of VLBI . . . . .	A-28
A-6	Interferometer Fringes . . . . .	A-28
A-7	Radar Altimeter Cone . . . . .	A-30
A-8	Range Sum Geometry and Transmission Legs . . . . .	A-31
C-1	Signal Propagation Geometry . . . . .	C-4

# LIST OF TABLES

<u>Table</u>		<u>Page</u>
3-1	Polar Motion Coefficients . . . . .	3-25
3-2	Time Difference Coefficients . . . . .	3-74
3-3	Bounds for Truncation Error When Using Fifth-Order Everett Interpolation Formula . . . . .	3-76
4-1	Aerodynamic Force Coefficients for Elementary Surfaces . . .	4-26
4-2	Atmospheric Constituents and Related Constants . . . . .	4-42
4-3	Polynomial Coefficients for Constituent Densities at 125 km . . . . .	4-46
4-4	Density Altitude Tables . . . . .	4-55
4-5	DODS Variable Dependency . . . . .	4-78
5-1	Characteristics of High Precision Orbit Generators . . . . .	5-6
5-2	Characteristics of Approximate Orbit Generators . . . . .	5-7
5-3	Partial Derivatives of the Auxiliary Parameters $\tau_1, \tau_2, \tau_3, x_4$ . . . . .	5-21
5-4	Partial Derivatives of the Auxiliary Parameters q, p, e, r . . . . .	5-22
7-1	Sea Surface-Geoid Deviation Sources . . . . .	7-35
8-1	Hyperellipse Probabilities . . . . .	8-53
8-2	Hyperrectangle Probabilities . . . . .	8-55
A-1	GRARR and ATSR Stations . . . . .	A-2
A-2	C-Band Radar Sites . . . . .	A-9
A-3	Unified S-Band (USB) Stations . . . . .	A-10
A-4	Minitrack Stations . . . . .	A-14
A-5	Minitrack Counter Sequence . . . . .	A-17
D-1	Dynamic Weighting Factors . . . . .	D-1
D-2	Typical A Priori Data Standard Deviation . . . . .	D-2

## CHAPTER 1

### INTRODUCTION

This publication presents a description of the mathematical theory for the earth/lunar/interplanetary Goddard Trajectory Determination System (GTDS). GTDS is a multipurpose computer system designed

"to provide operational support for individual earth, lunar, and planetary space missions and for the research and development requirements of the various projects of the NASA/Goddard Space Flight Center scientific community" (Reference 1)

This orbit determination program includes many of the capabilities of previous orbit determination programs developed by GSFC (References 2 and 3).

GTDS is, by its very nature, an evolutionary system. The first document describing the GTDS mathematical theory (Reference 4) corresponded to a developmental version of GTDS. Since then, GTDS has evolved through several operational versions, and a Research and Development (R & D) version has been developed to permit evaluation of promising methods for operational, nonroutine, and highly precise orbit determination. This document corresponds approximately to GTDS Version 3.0, which will be implemented at GSFC in the spring of 1976. As additional capabilities are added to the system, this document will be updated or appended.

This document is not intended to represent a set of mathematical specifications for developing the GTDS software, but rather is a development of the basic mathematical formulations used in GTDS. The format varies somewhat from section to section, ranging from a straightforward presentation of the basic equations used in the program to a tutorial approach which delves into some of the underlying theory, depending on the topic under discussion.

In addition to describing the basic mathematical formulations of this particular system, this document is also intended to provide the reader with a comprehensive overview of the key physical and mathematical models required by orbit determination systems which have been developed in recent years, and the results of various evaluations and improvements developed at GSFC as a result of years of operational orbit determination experience.

An overview of GTDS is presented in Chapter 2. This overview includes a discussion of the programs available in GTDS, system capabilities, and schematic diagrams of the differential correction, ephemeris generation, data simulation, and error analysis processes, along with an indication of which chapters in this document contain the algorithms associated with each function.

Chapter 3 presents the coordinate and time systems necessary to accurately model the spacecraft's dynamic motion and tracking observations. Chapter 4 details the acceleration models which constitute the Cowell equations of motion and the variational equations. Chapter 5 details the formulation of the orbital equations of motion, including general perturbation and special perturbation methods. Chapter 6 describes the numerical integration of the equations of motion and variational equations, while Chapter 7 describes the observation models and systematic error corrections applied to the observations. Chapter 8 contains a description of the estimators and statistical models, and Chapter 9 presents early orbit techniques which can be used to obtain deterministically an estimate of the vehicle state from observations.

Several appendices are also included in this document. Appendix A gives functional descriptions of various tracking systems and preprocessing techniques. A detailed description of time elements as used in the regularized equations of motion can be found in Appendix B, and Appendix C contains a rigorous discussion of the conversion of Doppler measurements to range rate. Appendix D presents information on typical a priori standard deviations and dynamic weighting factors for several observation types, and Appendix E presents a derivation of matrix identities associated with the sequential estimation process.

Finally, a glossary and an index are provided for the convenience of the reader.

## REFERENCES

1. Goddard Space Flight Center: 1970, Functional Requirements for the Lunar/Planetary Orbit Determination Subsystem of the Goddard Trajectory Determination System.
2. Velez, C. E. and Brodsky, G. P.: 1969, GEOSTAR-I, A Geopotential and Station Position Recovery System, Goddard Space Flight Center Report X-553-69-544, December 1969.

3. Goddard Space Flight Center: 1971, Definitive Orbit Determination Operating System Description, Edition II, Goddard Space Flight Center Report X-544-71-296, July 1971.
4. Wagner, W. E. and Velez, C. E. (editors): 1972, Goddard Trajectory Determination System Mathematical Specifications, Goddard Space Flight Center Report X-552-72-244, March 1972.



## CHAPTER 2

## GTDS OVERVIEW

Orbit determination in GTDS involves a complex mathematical process which combines the disciplines of orbital dynamics, observation modeling, and estimation theory. This process is implemented through the use of several separate programs which are briefly described in Section 2.1.

The capabilities of the system are discussed in Section 2.2. These capabilities include trajectory generation, observation modeling, and estimation techniques. Also included is a discussion of the early orbit determination process, which allows a crude initial estimate of the orbit to be obtained from early tracking data. In addition, the orbit determination system combines capabilities which are frequently useful in mission analysis studies when executed independently; GTDS has been provided with several modes of operation in order to permit utilization of these separate capabilities.

The acceleration sources which are accounted for in the GTDS dynamic model are described in Section 2.3, while Section 2.4 discusses near real-time operation and postflight processing.

## 2.1 GTDS PROGRAMS

To meet the varying demands imposed upon the system by operational support of the research and development requirements of various projects, GTDS includes the following programs:

- Differential Correction Program
- Ephemeris Generation Program
- Ephemeris Comparison Program
- Filter Program
- Early Orbit Determination Program
- Data Simulation Program
- Error Analysis Program
- Data Management Program
- Permanent File Report Generation Program

This document presents the mathematical models and procedures for all of these programs except the Permanent File Report Generation Program. A brief description of each of the programs is given in the remainder of this section.

### 2.1.1 Differential Correction Program

The primary purpose of the Differential Correction Program is to estimate the satellite orbit and associated parameters. The estimation algorithm used in the Differential Correction Program is called the weighted least squares with a priori algorithm or the Bayesian weighted least squares algorithm. It minimizes the sum of the squares of the weighted residuals between actual and computed observations, while simultaneously constraining the model parameters to satisfy the a priori conditions to within a specified uncertainty. Both first- and second-order statistics (i.e., the mean and covariance matrices) are determined for the estimated variables.

### 2.1.2 Ephemeris Generation Program

The function of the Ephemeris Generation Program is to compute, from prescribed initial conditions, the value at a specific time of the vehicle state and, optionally, the state partial derivatives. In order to meet varying precision and efficiency requirements, several orbital theories have been provided, ranging from a first-order analytic theory to a high-precision Cowell-type numerical integration. The state partial derivatives can be computed by precision numerical integration of variational equations. The state partial derivatives with respect to the initial state, i.e., the state transition matrix, can optionally be generated by a two-body analytic approximation.

### 2.1.3 Ephemeris Comparison Program

The Ephemeris Comparison Program compares two input ephemerides. The comparison can be specified over a particular arc or over the arc of overlap between the ephemerides. The radial, along-track, and cross-track differences are computed and output.

### 2.1.4 Filter Program

The Filter Program provides an alternative to the Differential Correction Program for estimating the satellite orbit and associated parameters. The Filter Program contains four sequential estimation algorithms called the

Extended Kalman Filter (EKF), the Modified Extended Kalman Filter (MEKF), the Jazwinski Filter (JF), and the Modified Jazwinski Filter (MJF). These sequential filters differentially correct (update) the satellite state recursively at each observation point processed. As a result, these methods are referred to as sequential processing methods, in contrast to the batch processing method used in the Differential Correction Program. Other elements of the Filter Program, such as model parameters and observation handling, are the same as in the Differential Correction Program.

#### 2.1.5 Early Orbit Determination Program

The Early Orbit Determination Program is designed to determine approximately an initial estimate of an earth orbit when there is no a priori estimate available to start a differential correction process. The program provides three methods for doing this: (1) the Gauss Method, (2) the Double r-iteration Method, and (3) the Range and Angles Method.

#### 2.1.6 Data Simulation Program

The Data Simulation Program computes simulated observations of a spacecraft from specified ground tracking sites. The simulated data are generated for specified observation intervals and sampling frequencies. The program also has the capability to simulate attitude sensor measurements. Optionally, random and bias errors can be added to the observations. Observations can also be modified to account for the effects of atmospheric refraction, antenna mount errors, transponder delays, and signal propagation time delays.

#### 2.1.7 Error Analysis Program

The GTDS Error Analysis Program provides the capability of analyzing the effect of tracking error uncertainties, solve-for vector uncertainties, and consider parameter uncertainties associated with a specified orbit and station-dependent tracking schedule. Since the Error Analysis Program functions are similar to those performed in the Differential Correction and Data Simulation programs, these programs share common mathematical processing subroutines, input processors, and data management options. The Error Analysis Program features which are common to the Differential Correction and Data Simulation programs include the use of a tracking schedule, selection of tracking stations, selection of observation measurement types, specification of observation standard deviations and weights, and specification of the a priori state covariance matrix.

Construction of the normal matrix and the use of the consider mode to account for the effect of consider parameter statistics on the covariance matrix of the solve-for vector are performed in the same manner as in the Differential Correction Program.

#### 2.1.8 Data Management Program

The primary function of the Data Management Program is to create working files of data to be used by other programs in GTDS.

### 2.2 SYSTEM CAPABILITIES

The key elements of the differential correction process are shown schematically in Figure 2-1. The chapters of this document which contain algorithms associated with each function are indicated in this and succeeding figures. Both the batch and sequential modes for estimating the orbital state are shown. The use of common modules to perform key functions is basic to the GTDS structure. For this reason, algorithms derived in this document are applicable to many areas of GTDS. As shown in Figure 2-1, an estimate of the orbital state at an initial epoch must first be specified a priori from an independent source. Observation measurements to be processed are retrieved from an observation file, and an orbit generator determines the satellite trajectory (position and velocity) at times corresponding to the measurement sampling times. In addition, at each sampling time estimates of the observation measurements are computed as a function of the satellite trajectory.

In a batch mode, this process is performed sequentially from data time to data time, and constitutes the inner loop of the process (see Figure 2-1). In addition to the computed measurements, partial derivatives of the measurements with respect to the epoch state must be computed in the inner loop for use in the statistical regression process. Upon completion of the inner loop processing at the measurement times, the epoch state is differentially corrected by means of a Bayesian weighted least squares method. The updated epoch state is then used to perform another inner loop iteration. Repeated iteration of the inner loop, culminating each time with a differential correction to the epoch state, constitutes the outer loop. As the iterations proceed, the epoch state converges to the Bayesian weighted least squares solution to the nonlinear orbit determination problem.

In the sequential filter mode, a single loop is used to perform these measurement calculations and partial derivative calculations, and the state and covariance matrices are updated after each measurement to obtain the final state. It should

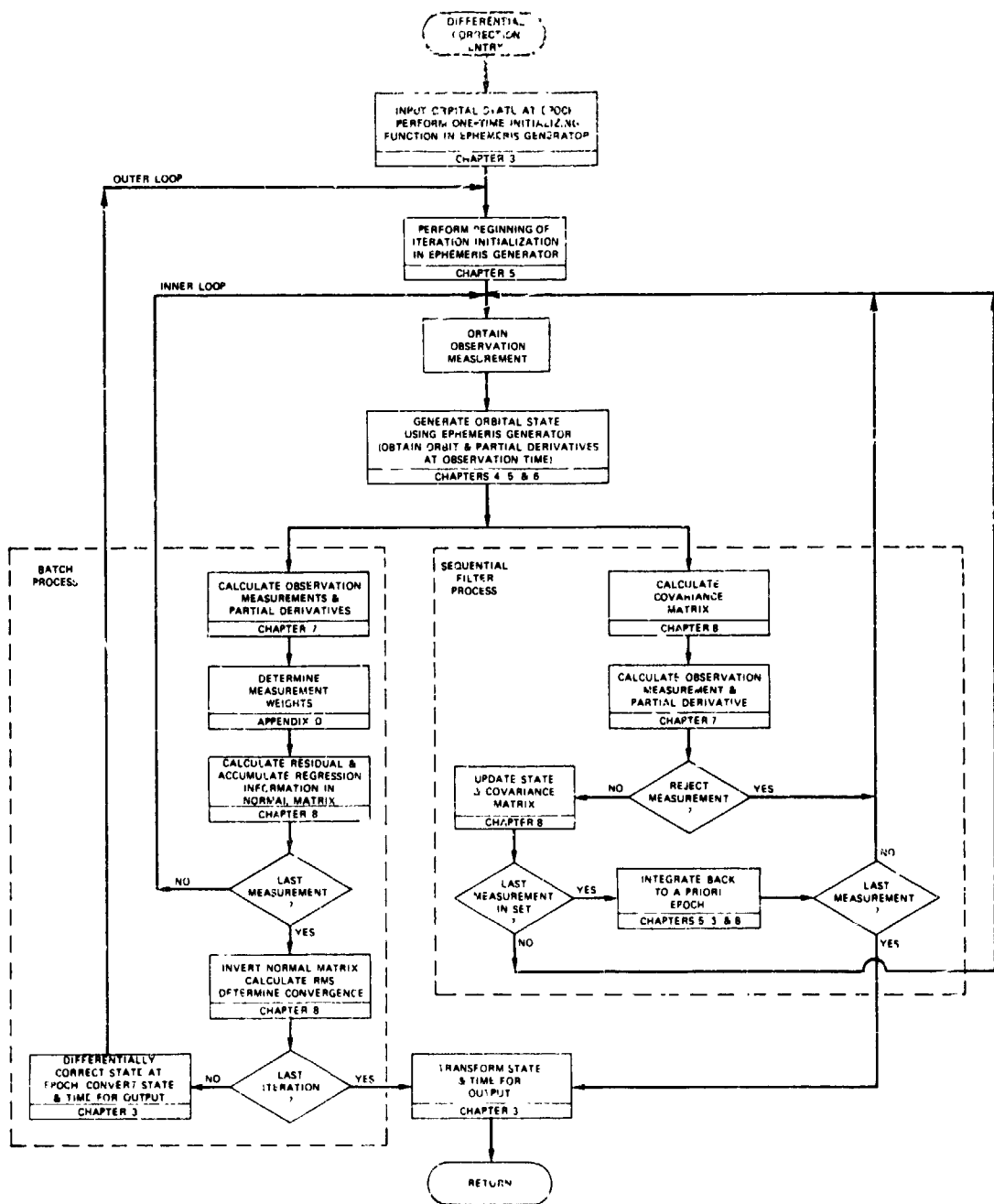


Figure 2-1. Schematic Diagram of the Differential Correction Process

be noted that Figure 2-1 depicts functional relationships and not the actual GTDS structure. Within the GTDS structure, the filter mode logic is separate from the batch mode logic.

### 2.2.1 Trajectory Generation

Trajectory generation is performed through integration of the orbital equations of motion in the Ephemeris Generation Program. Ephemeris generation can be performed as a standalone function as shown in Figure 2-2. In addition, trajectory generation is a key element of the differential correction process shown in Figure 2-1. The analytic and numerical theories available in GTDS are discussed in this section.

The orbital equations of motion can be expressed most simply in terms of the rectangular components of the acceleration vector acting on the satellite. Considerable research has focused on the problem of transforming the orbital equations of motion into a more desirable form. The general approach is to reformulate the equations in terms of a new set of orbital elements, to solve the transformed set of equations for the value of the orbital elements at the desired time, and then to transform these elements to the desired element set (e.g., Cartesian or Keplerian).

In the general perturbations approach, this reformulation of the equations of motion yields a set of equations which can be integrated analytically. The chief advantage of such trajectory generation methods is their high efficiency. However, reformulation of the orbital equations such that an analytic solution is possible usually requires some approximations. For example, in Brouwer theory, which is a general perturbations method in GTDS, the perturbation model includes only the effects of a point mass earth and the low-order zonal harmonics in the gravitational potential. For the generation of satellite trajectories for which these are the dominant perturbations, Brouwer theory is sufficiently accurate.

Solution of the equations of motion via numerical integration is classified as a special perturbations method. The numerical integration techniques available in GTDS are discussed in detail in Chapter 6. In the high-precision special perturbations approach, the perturbing acceleration which acts on the satellite is modeled as accurately as possible. The various perturbation models and numerical integration techniques which are available in GTDS are discussed in Chapters 4 and 6, respectively. The chief advantage of the special perturbations approach is high accuracy; however, these methods are considerably more expensive, in terms of computer time, than the general perturbation methods.

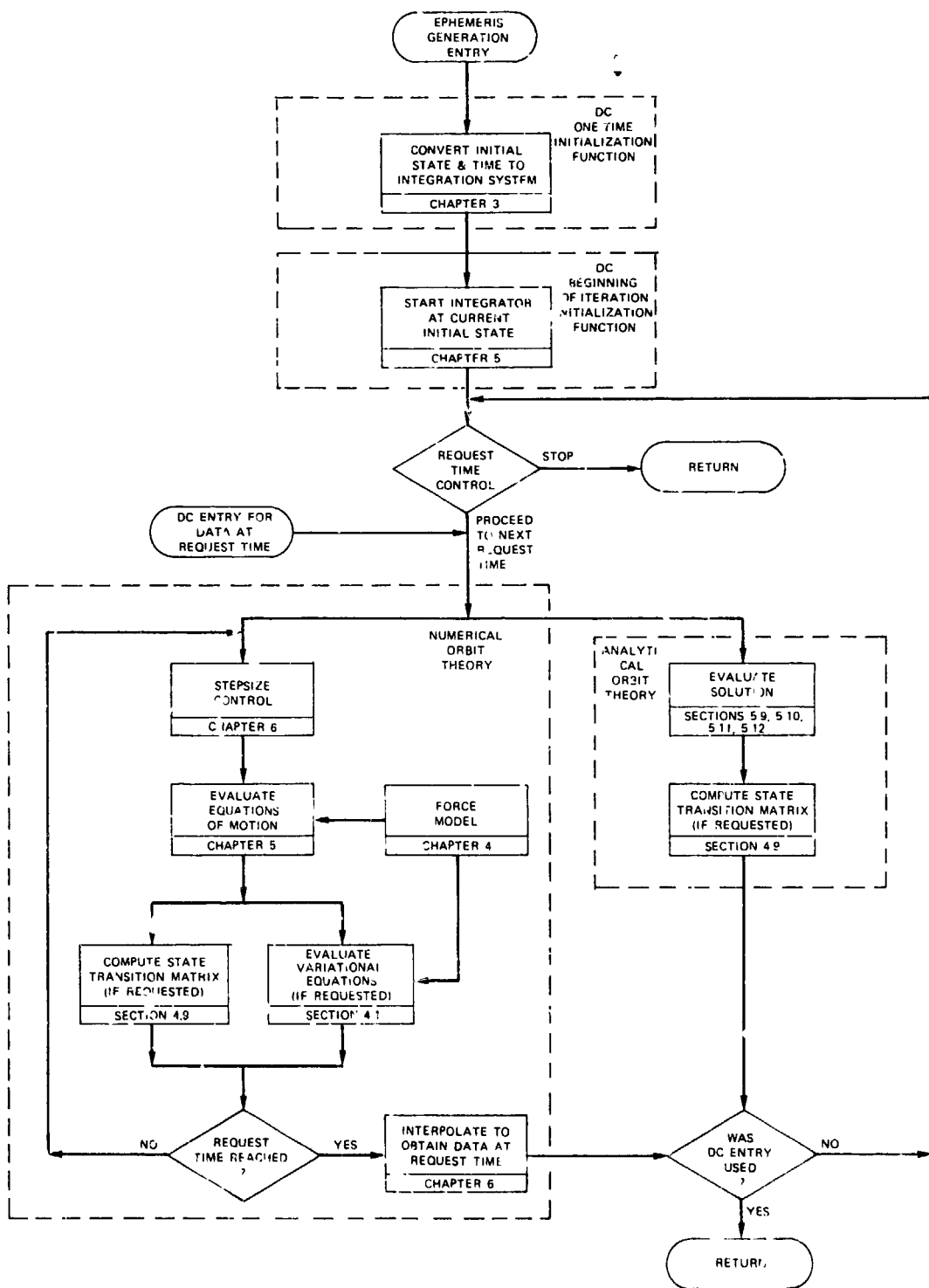


Figure 2-2. Schematic Diagram of the Ephemeris Generation Process

Numerical integration of the orbital equations expressed in terms of the Cartesian components of the acceleration vector acting on the satellite is called the Cowell Method. In both the Variation of Parameters (VOP) and Intermediate Orbit approaches, the Cowell equations of motion are reformulated to obtain equations that are better conditioned for numerical integration. In the VOP approach, a transformation is made to a set of orbital elements which provide an exact solution to the two-body problem. The orbital equations expressed in terms of these elements include variations in orbital elements arising only from the perturbing acceleration vector, i.e., the point mass effects of the earth are integrated exactly. In cases where inaccurate numerical integration of the point mass gravitational effect of the earth is a significant error source (e.g., geosynchronous orbits), VOP methods are superior to the Cowell Method.

In the Intermediate Orbit approach, an approximate solution obtained by an analytic theory is used as a reference solution, and the time rate-of-change of the difference between the true solution and this reference solution is numerically integrated to obtain an improved solution. Intermediate Orbit methods can be developed for any analytic theory; however, only two Intermediate Orbit methods have been considered for implementation in GTDS. The first is the Brouwer Intermediate Orbit with only first-order short-period terms due to  $J_2$  or with the first-order short- and long-period terms and second-order secular terms due to  $J_2$ . The second method is a similar orbit developed using Poincare variables so that orbits of low eccentricity and low inclination can be considered. The Intermediate Orbit approach should be optimal for an orbit for which numerical inaccuracies in the integration of the element rates arising from two-body or  $J_2$  effects are a major error source. The major drawback of both the VOP and Intermediate Orbit approaches is the computational cost associated with the required transformation of the orbital elements to and from the Cartesian state vector.

Fixed-step numerical integration is inefficient for the computation of highly eccentric orbits (i.e., eccentricity greater than 0.1) if time is used as the independent variable. For such applications, an automatic mechanism is required to force a small stepsize in the region of larger perturbations and a large stepsize in the region of small perturbations. A variable-stepsize option is available in GTDS; however, stepsize changes are costly and frequently introduce errors. Therefore, an alternative analytic stepsize control mechanism is also available. In this procedure, the equations of motion are reformulated in terms of a new independent variable  $s$  instead of time  $t$ , such that

$$ds \propto \frac{1}{r^n} dt \quad (2-1)$$



where  $r$  is the magnitude of the satellite's position vector. The effect of this transformation is to "regularize" the independent variable so that fixed steps in  $s$  correspond to variable steps in  $t$  that are smaller when  $r$  is small (i.e., where the perturbations are usually larger) and larger when  $r$  is large.

Several regularized trajectory generation methods are currently implemented in GTDS. The Time-Regularized Cowell Method was developed by reformulating the Cowell orbital equations in terms of the independent variable  $s$  (with  $n = 3/2$  as the default value) in Equation (2-1). The Kustaanheimo-Stiefel (KS) Method is a regularized VOP formulation which uses the eccentric anomaly as the independent variable ( $n = 1$  in Equation (2-1)). The Delaunay-Similar (DS) Method is a regularized VOP formulation in which the true anomaly is used as the independent variable ( $n = 2$  in Equation (2-1)). This form of analytic stepsize control works well when the forces vary inversely with distance from the central body. The DS approach has the strongest regularization, followed by the Time-Regularized Cowell, and then the KS Method. The chief disadvantage of the regularized methods is that they require numerical integration of an additional equation, the time equation. For orbits with low eccentricity (i.e., less than 0.1), analytic stepsize control is not needed and the error introduced by numerical integration of the time equation may even degrade the solution.

Special perturbation methods are also included in GTDS for generation of a mean trajectory, representing only the long-term evolution of the orbit. Numerical averaging is one such long-term orbit prediction method in GTDS. The numerical averaging method is a VOP approach in which the short-periodic perturbing effects are numerically averaged out of the equations of motion, leaving only the long-term motion to be integrated. The cost of each integration step is high, but is usually far outweighed by the large stepsizes that are possible in the integration of the averaged dynamics. The averaged prediction model is most efficient for applications where knowledge of the short-period perturbations is not required (e.g., mission analysis or prediction of tracking station acquisition times) or where the cost of numerically integrating the precision equations of motion is prohibitively high (e.g., determination of gravitational models from large amounts of tracking data).

### 2.2.2 Observation Modeling

Observation measurements provide the means by which the estimate of the orbit of a spacecraft is compared with its true flight. The orbit estimate is expressed in terms of the conceptual abstractions of position, velocity, and time, whereas the observations may involve measurements of some physical property of electromagnetic wave propagations between the tracking station and the

spacecraft. The propagation measurements are selected such that they can be easily related (via theoretical postulates) to the spacecraft state. This process of analytically relating the measurement quantities to the spacecraft state is referred to as "observation modeling" and is vitally important to the accuracy of the orbit estimate.

The observation models in GTDS are employed in the differential correction and data simulation processes, and, as shown in Figure 2-1, the algorithms are presented in Chapter 7. The relationship of these models to the GTDS Data Simulation Program is shown in Figure 2-3.

#### 2.2.2.1 Observation Types

GTDS provides for the processing of the following types of observations:

- Goddard Range and Range-Rate (GRARR) radar data (including the antenna X and Y gimbal angles)
- C-Band radar range, azimuth, and elevation data
- Minitrack interferometer direction cosine data
- Unified S-Band (USB) radar propagation time delay, Doppler shift, and X and Y gimbal angle data
- Satellite-to-Satellite Tracking (SST) propagation time delay and Doppler shift data

#### 2.2.2.2 Data Preprocessing

Before introduction into GTDS, data from the GRARR, C-Band, and Minitrack systems undergo considerable preprocessing to convert from measured quantities to estimates of the spacecraft state components relative to the tracking station. The preprocessing of observation data is normally done by means of a computer program completely independent of GTDS. Raw data are converted from the form received from the tracking stations to forms suitable for storage in the data base and for use in GTDS. Wild points are edited out, calibration corrections are applied to eliminate known instrumentation errors, ambiguities in the data measurement and/or recording are resolved, conversions are made from the measurement units to units which are more physically meaningful or convenient, and the data are optionally smoothed and possibly compacted if large amounts of raw data are measured.

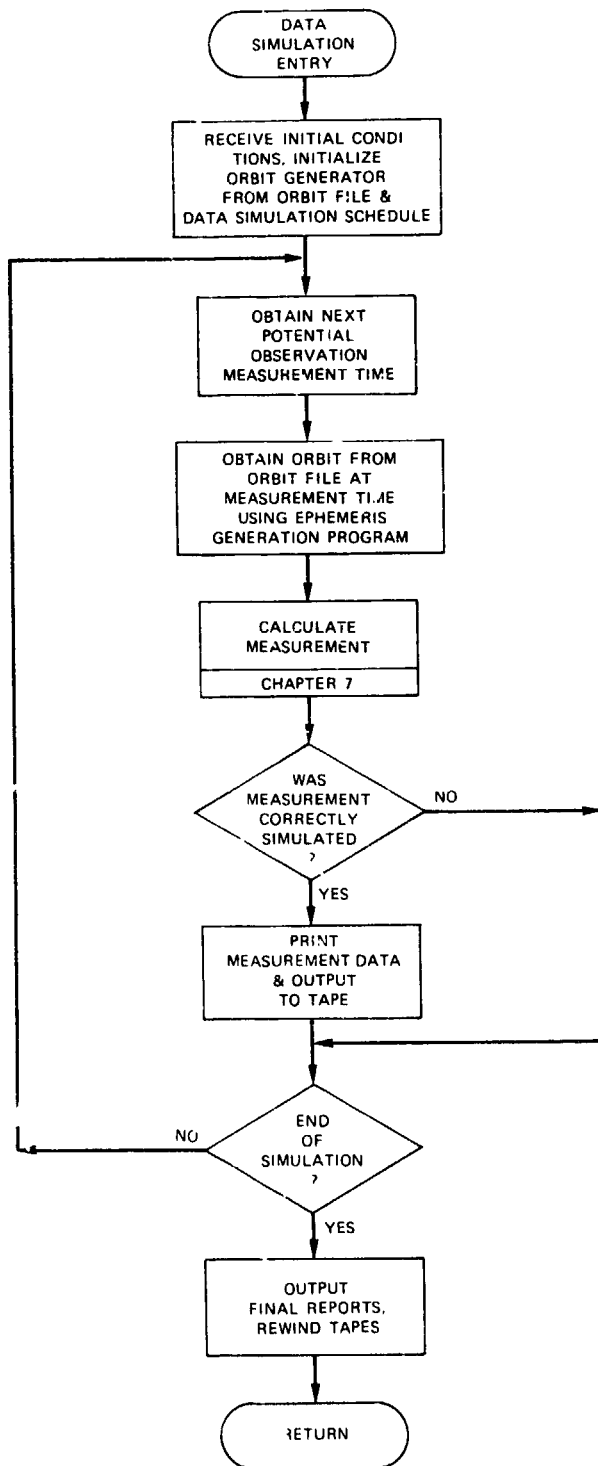


Figure 2-3. Schematic Diagram of the Data Simulation Process

More specifically, this preprocessing includes:

- Two-way propagation time delay conversion to approximate one-way (instantaneous) relative ranges
- Doppler-plus-bias cycle count conversion to approximate one-way (instantaneous) relative range rate
- C-Band radar gimbal angle conversion to line-of-sight azimuth and elevation angles
- Minitrack interferometer fractional phase count augmentation with whole cycle counts to resolve ambiguities, and conversion into line-of-sight direction cosines relative to the station east-west and north-south baselines

The modeling within GTDS is thus greatly simplified. It is only necessary to compute the appropriate quantity from the relative position vector between the tracking station and the spacecraft in local tangent coordinates.

The minimal preprocessing of USB and SST data consists of simple reformatting and conversion of reference frequency cycle counts to time intervals.

#### 2.2.2.3 Observation Models

The GTDS observation modeling requires rigorous iterative solutions for the two-way USB propagation paths and for the round-trip propagation path from the ground radar to the synchronous relay satellite to the target satellite and back for SST. These finite speed propagation paths are computed as straight lines in inertial coordinates. A round-trip circuit represents the modeling of the "range" time delay measurement, and two round-trip circuits are necessary to model the Doppler measurements in terms of the round-trip light time difference. The USB Doppler measurement is implemented as a nondestruct count, whereas the SST measurement is implemented in the form of either a destruct or a nondestruct count.

All of these observation models assume vacuum propagation of the electromagnetic wave. Corrections to the actual observations are computed for the refraction effects due to the presence of the atmosphere (the nondispersive troposphere and the dispersive ionosphere). In addition, other corrections to the observations are estimated for tracking antenna location errors and spacecraft transponder delay characteristics.

The modeling of the observations also includes the calculation of the partial derivatives with respect to the solve-for and consider variables. Variations of all the variables except two, the tracking station locations and the tracking data biases, result in changes in the estimate of the spacecraft orbit. For the remaining variables, the partial derivatives of the observations are computed in terms of variations of the spacecraft state at the time of the tracking signal turnaround. This variation with respect to the local state is then related back to the epoch time via the appropriate elements of the state transition matrix. This matrix maps changes in the initial state vector components into changes in spacecraft state components at any subsequent time of interest. Elements of this state transition matrix are calculated by numerical integration of the variational equations associated with the trajectory.

### 2.2.3 Estimation Techniques

As stated in Section 2.1.1, the primary estimation algorithm available in GTDS is called the weighted least squares with a priori or Bayesian weighted least squares algorithm (see Chapter 8). This algorithm minimizes the sum of the squares of the weighted residuals between actual and computed observations, while simultaneously constraining the state to satisfy an a priori state to within a specified uncertainty. The iterative estimation process differentially corrects the estimated variables and ultimately determines the weighted least squares solution. Both first- and second-order statistics (i.e., the mean and covariance matrices) are determined for the estimated variables.

A second method available in GTDS is the Extended Kalman Filter (EKF) sequential estimator (see Chapter 8). Several features have been incorporated to prevent divergence due to model errors in the dynamics or measurements. These vary from artificially constraining the covariance gain to using adaptive techniques.

Two classes of variables can be accommodated in the statistical computations. The first class, called solve-for variables, includes model parameters whose values are known with limited certainty and are being estimated. The second class, called consider variables, includes model parameters which are not being estimated, but whose uncertainty will affect the statistics of the solve-for variables. Model parameters which can be included in either the solve-for or consider classes include the following:

- Position and velocity components of the spacecraft in Cartesian, Keplerian, or spherical coordinates
- Atmospheric drag parameters

- Solar radiation pressure parameter
- Gravitational potential coefficients
- Thrust parameters
- Tracking station locations
- Observation biases

Specified subsets of the spacecraft position and velocity components can optionally be estimated in mean of 1950.0 or true of date inertial Cartesian coordinates, classical orbital elements, spherical coordinates, or Definitive Orbit Determination System (DODS) type elements (Reference 1).

GTDS can also operate in an error analysis mode, wherein only the covariance matrix of the solve-for variables is differentially corrected and propagated through the process. The error analysis process, shown in Figure 2-4, relies heavily on functions in the differential correction process, such as the computation of observations and the update of the normal matrix. The solve-for variables are unchanged from their a priori specified values. In this mode, only the uncertainties of the tracking data, not the data, are required. This mode permits simulation and analysis of the uncertainties resulting from the estimation process prior to mission operations.

#### 2.2.4 Early Orbit Determination

Occasionally, a priori state value estimates of sufficient accuracy to yield convergence of the iterative process are unavailable, as when mission anomalies occur and preflight estimates of the state are no longer valid. For such cases, GTDS has the capability of rapidly determining approximations of the spacecraft's position and velocity from a limited amount of early tracking data. These approximations provide starter values for the differential correction process.

Three early orbit approximation methods, described in Chapter 9, are available in GTDS. These methods are: (1) the Gauss Method, (2) the Double r-Iteration Method, and (3) the Range and Angles Method. The Gauss and Double r-Iteration Methods use three sets of radar gimbal angle observations to determine the state vector. The Range and Angles Method uses multiple sets of radar range and gimbal angle data to obtain the state vector.

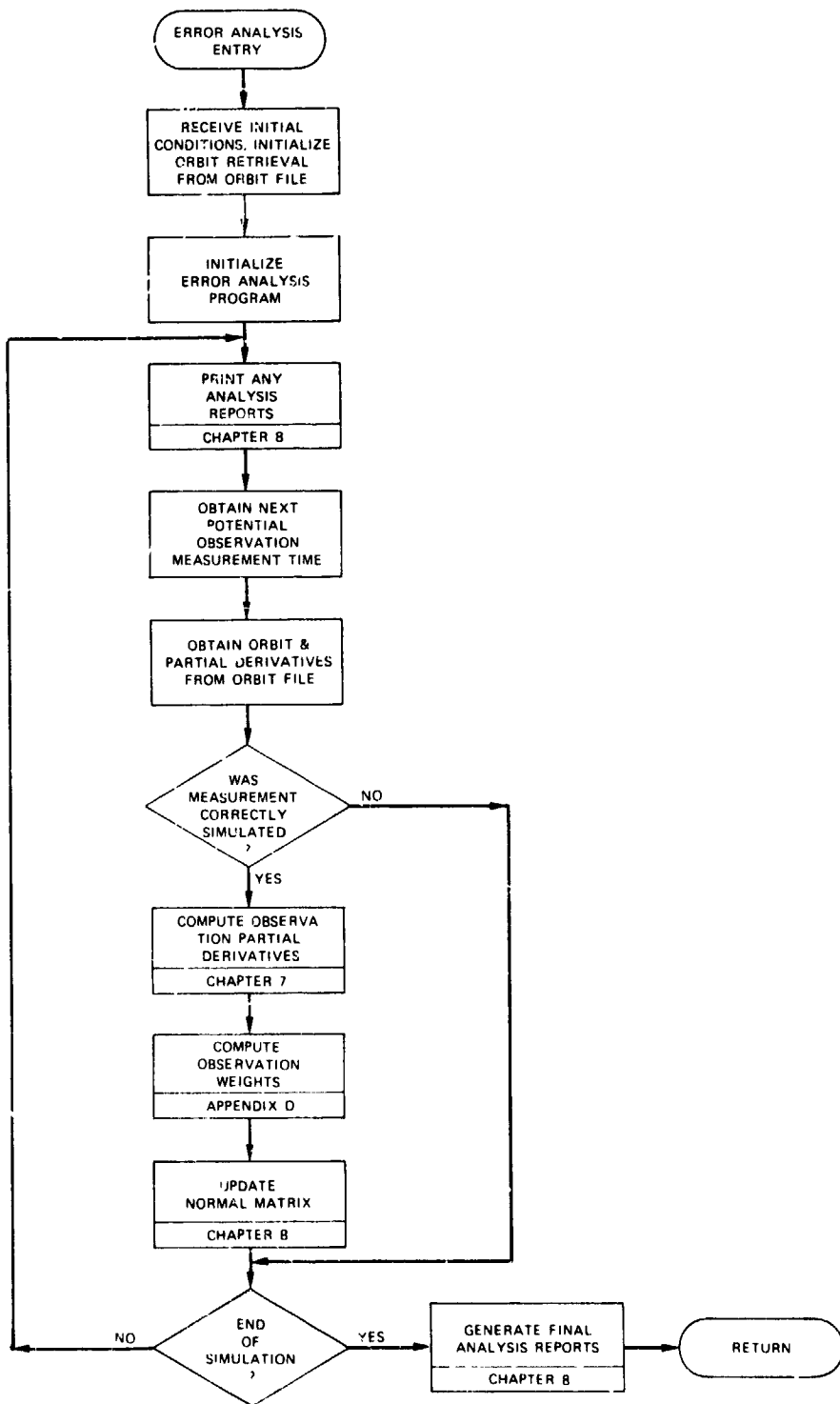


Figure 2-4. Schematic Diagram of the Error Analysis Process

### **2.2.5 Optional Modes of Operation**

Each of the programs which make up GTDS can be utilized in a number of different modes, depending on the needs of the user.

The Ephemeris Generation Program can be used to propagate a vehicle state from a given epoch to some specified time. This program is useful for several purposes:

- To generate a spacecraft ephemeris report on the online printer
- To generate a spacecraft ephemeris tape in either the ORBIT, EPHEM, or ORB1 (for Cowell integration only) format
- To perform vehicle lifetime studies
- To generate state partial derivatives over a given time span

The Differential Correction Program employs a Bayesian weighted least squares algorithm to estimate vehicle state, various force model parameters, and non-dynamic parameters such as station locations and observation biases. The Differential Correction Program uses the Ephemeris Generation Program with any of the available orbit theories to satisfy integration requirements. The Differential Correction Program can also be used to:

- Determine a definitive orbit during near real-time operational mission support or during postflight support
- Determine better estimates of the harmonic coefficients, the coefficient of drag, the solar radiation constant, etc.
- Save the results of a differential correction in the form of updated elements on an elements file or an orbit history on an ORB1, EPHEM, or ORBIT File

The Data Simulation Program is designed to compute simulated observations at a specified frequency for given sets of tracking stations and observation intervals. The program can create observational data in either the DODS or GTDS format. Simulated data are useful for controlled tests which require that the data conform to certain criteria (e.g., particular force model, biases, or corrections for particular portions of the orbit). The Data Simulation Program allows the observation tracking schedule to be specified in one of the four following forms:

- Periodic detailed schedule
- Spacecraft pass
- Function of special events
- Function of times on actual observation tape



The Data Simulation Program also provides for random and bias errors in the computed observations as well as the effects of atmospheric refraction, antenna mount errors, transponder delays, and light time. It uses the same modeling algorithms employed by the Differential Correction Program and data from the GTDS ORBIT File to compute observations.

The Error Analysis Program provides the capability to perform analysis of tracking errors for an arbitrary orbit, given the station-dependent tracking schedule and other scheduling information. The program provides a variety of statistical output reports, including the following:

- The epoch covariance matrix and correlation coefficients associated with an entire tracking span, and standard deviations associated with elements and solve-for parameters in various coordinate systems. Sensitivity information about the considered parameters and the noise effect on the epoch state is also available.
- The user may optionally request that the epoch covariance matrix and sensitivity matrix be mapped to requested times. Trajectory standard deviations and the root sum square of position and velocity sigmas are provided at each mapping time. At the last mapping time, the covariance matrix and associated correlation coefficients are also printed.

The Error Analysis Program uses the Data Simulation Program tracking schedule, the differential correction matrix accumulation, and data from the GTDS ORBIT File to construct the required statistical matrices.

## 2.3 SPACECRAFT DYNAMICS

In order to accommodate the varying requirements at GSFC in near-earth, lunar, and interplanetary mission analysis, the GTDS dynamic model includes the following acceleration sources:

- N-Body Point Mass Gravitational Accelerations – These include all planets in the solar system, the sun, and the earth's moon.
- Nonspherical Gravitational Accelerations – The nonspherical gravitational acceleration model allows the inclusion of up to a  $21 \times 21$  potential field for the earth and moon. The acceleration due to the mutual nonspherical gravitational attraction of the earth and moon can also be included.
- Aerodynamic Force Accelerations – The aerodynamic force acceleration model for the earth includes a dynamic atmosphere model which

accounts for variations in the solar flux on the earth's upper atmosphere. A modified Harris-Priester model and Robert's analytical formulation of the Jacchia (1971) model are available.

- Solar Radiation Accelerations – The solar radiation model includes shadowing and variations with distance from the sun.
- Attitude Control System Accelerations – A generalized model is included to account for the small accelerations resulting from the use of attitude control systems.
- Thrusting Maneuver Accelerations – A generalized model is included to account for the accelerations resulting from propulsive maneuvers.
- Replacement Accelerations – Provision is made for replacing all non-potential accelerations with the total acceleration measured by onboard accelerometers.

The reference coordinate system for the equations of motion is optionally either the mean equator and equinox of 1950.0 or a true of date system at a specified epoch. Coordinate transformations account for precession, nutation, and polar motion of the earth's spin axis. Planetary positions are determined from a peripheral ephemeris file containing Chebyshev polynomial coefficients derived from JPL ephemeris data.

The program is provided with a "flight sectioning" capability, wherein the complete trajectory arc can be partitioned into multiple subarcs. The dynamic model options, numerical integration characteristics, and output quantities and frequency can be suitably tailored for each subarc. The criteria for crossover from one subarc to the next are based on either time or spatial conditions which can be specified for each subarc.

The state transition matrix, required by the estimator algorithm, is obtained by numerically integrating the variational equations. A Cowell predictor-corrector numerical integration algorithm is used to integrate the second order equations of motion and associated variational equations. Automatic or semi-automatic error control is provided by adjusting the integration stepsize by using a time-regularization process.

Various options are provided in the dynamic models and numerical integration algorithms to give the versatility to accommodate both high-speed near real-time applications and precision postflight applications.

## 2.4 NEAR REAL-TIME OPERATION AND POST FLIGHT PROCESSING

To provide operational support, GTDS includes a near real-time capability with interactive graphics report and control facilities. The interactive capabilities allow the user to edit individual data points based on graphical displays of their residuals; to modify iterative convergence criteria; to modify editing criteria such as data time spans, processing, rates, data types, etc.; or even to change modes during a run.

Near real-time operation usually necessitates a compromise in computational precision compared with that generally achieved during postflight processing. Several options are included for this purpose. These options permit more rapid computation without seriously jeopardizing precision, and effect orbit generator type selection, model approximation, and control over the number of variables being estimated or considered.

## CHAPTER 3

## COORDINATE AND TIME SYSTEMS

The orbit determination process involves measurements that are taken and forces that are modeled in several different space and time coordinate systems. This chapter defines these systems and gives the necessary transformations between them.

## 3.1 GENERAL COMMENTS AND DEFINITIONS

The GTDS coordinate systems consist of the fundamental astronomical reference systems and other systems that were originally borrowed from aeronautics or originated from special requirements of space exploration. Requirements for different coordinate systems occur from the following three sources:

- input data
- internal computations
- output requirements.

For example, the input ephemerides of the planets are heliocentric and refer to the mean equator and equinox of 1950.0.\* The input observational data are in a topocentric coordinate system. The integration is done in either geocentric, selenocentric, planetocentric, or heliocentric rectangular coordinates referred to the mean equator and equinox of 1950.0 or of a specified epoch. The force model includes terms referred to a coordinate system that is fixed in the rotating earth and terms that are referred to the moon and planets. The output requirements may be osculating elements with respect to the earth, moon, or planets. These specific coordinate systems are defined and discussed later in this chapter.

Since several different coordinate systems are used in GTDS, these systems must be defined and provision must be made for transforming from one coordinate system to another. A coordinate system is defined by specifying the origin of the coordinates, a reference plane, and a principal direction in the reference plane. This specification of the reference plane includes an identification of the positive, or north, or outward sense along the normal to the plane. The reference plane is an equivalence class of mutually parallel planes. For example, the equator is defined to be the plane normal to the earth's axis of rotation. Usually, this plane contains the earth's center of mass; however, in selenocentric equatorial coordinates

---

The beginning of the Besselian solar year is denoted by the notation .0 after the year. The notation 1950.0 corresponds to January 0<sup>d</sup>923, 1950 ephemeris time. For a detailed explanation, see Reference 1, pages 22, 30, and 69.

the parallel plane contains the moon's center of mass. To avoid any such difficulty, the celestial sphere of infinite radius is introduced, and the celestial equator is the intersection of the equatorial plane with the celestial sphere. This is another way of identifying the equivalence classes of parallel planes and parallel lines. The reference plane often refers to that member of the equivalence class that contains the origin of coordinates. The corresponding statement holds for the equivalence of parallel lines in defining a principal direction.

The designations of coordinate systems, according to the location of the origin, are given in the following table:

<u>Origin of Coordinates</u>	<u>Designation of System</u>
The observer	Topocentric
The center of the earth	Geocentric
The center of the moon	Selenocentric
The center of the sun	Heliocentric
The center of mass	Barycentric

The following reference planes are used:

- The Horizon. Without further designation, the horizon is the plane tangent to the oblate ellipsoid earth model at a specified point on the surface. The outward normal is directed away from the earth model. For topocentric coordinates, the reference plane is the geographic horizon corresponding to the point on the earth model whose normal passes through the observer.
- The Equator. The equator is the earth's equator, unless otherwise specified. This is the plane normal to the earth's axis of rotation, and north is in the direction of the angular velocity vector of the rotation, also called the celestial pole. The moon's equator is defined in a corresponding way.
- The Plane of an Orbit. The plane of an orbit is defined by two-body motion and north is the direction of the angular momentum. In the problem of more than two bodies, the osculating plane corresponds to the state at a given epoch or the mean plane that has the periodic perturbations removed.
- The Ecliptic. The ecliptic is the earth-sun orbital plane and is a special case of the plane of an orbit. North is the direction of the system's angular momentum, also called the ecliptic pole.

The principal direction is usually specified by giving the sense along the intersection of the reference plane with some other plane. The other plane may be a meridian plane, an equatorial plane, or another orbital plane. A meridian plane is defined as any plane that contains the axis of rotation of one of the principal gravitating bodies. Commonly used meridians of the earth and moon which are used to determine principal directions are:

- The Greenwich or Prime Meridian. The Greenwich meridian is the earth's meridian plane that passes through the former Royal Observatory at Greenwich, England.
- The Lunar Prime Meridian. The lunar prime meridian is the moon's meridian plane that passes through the mean center of the apparent lunar disk (that point on the lunar surface that would be intersected by the earth-moon line, were the moon to be at the mean ascending node when this node coincided with either the mean perigee or the mean apogee).
- The Local Meridian. The local meridian is the earth's or moon's meridian plane that passes through the observer's position. This concept is not meaningful when the observer is situated on the axis of rotation.

Other principal directions frequently used in astronomy are:

- The Vernal Equinox or Equinox. The equinox is the fundamental principal direction used in astronomy. It is defined as the intersection of the ecliptic and the earth's equator with the positive sense being from the earth to the sun as the sun crosses the equator from south to north.
- The Ascending Node. The ascending node is the intersection of an orbital plane and the reference plane with the positive sense being from the origin toward the orbiting body as it crosses the reference plane from the south to the north. Thus, the vernal equinox is an ascending node.

### 3.2 COORDINATE SYSTEM DESCRIPTIONS

#### 3.2.1 Body-Centered Equatorial Inertial (Geocentric, Selenocentric, or Planetocentric)

Origin:	Center of the reference body
Reference Plane:	Equatorial plane of earth at epoch
Principal Direction:	Vernal equinox of epoch

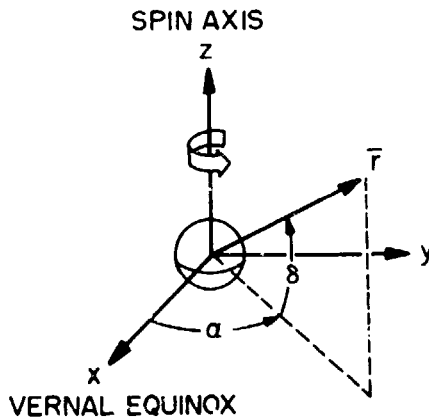


Figure 3-1. Body-Centered Inertial  
Coordinate System

Rectangular Cartesian Coordinates (See Figure 3-1):

- x-axis ~ the principal direction
- y-axis ~ the normal to the x and z axes to form a right-handed system
- z-axis ~ the normal to the equatorial plane of epoch in the direction of the angular momentum vector.

Within the following formulation,  $\bar{R}$ ,  $X$ ,  $Y$ , and  $Z$  designate the position vector and Cartesian coordinates referred to the mean equator and equinox of 1950.0. Similarly,  $\bar{r}_E$ ,  $x_E$ ,  $y_E$ , and  $z_E$  designate the position vector and Cartesian coordinates referred to the mean equator and equinox of epoch and  $\bar{r}$ ,  $x$ ,  $y$ , and  $z$  designate the position vector and Cartesian coordinates referred to the true equator and equinox of epoch.

Spherical Polar Coordinates:

- $r$  ~ radial distance from the origin to the point being measured
- $\alpha$  ~ right ascension measured east from the vernal equinox,  $\tan^{-1} (y/x)$
- $\delta$  ~ declination measured north from the equator,  $\sin^{-1} (z/r)$

### 3.2.2 Body-Centered Rotating

- |                      |   |
|----------------------|---|
| Origin:              | Center of the reference body                        |
| Reference Plane:     | Equatorial plane of reference body at epoch         |
| Principal Direction: | Intersection of the prime meridian with the equator |

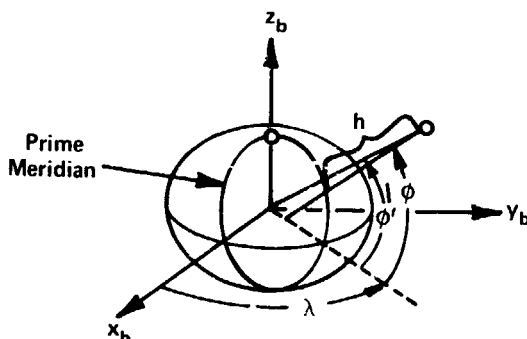


Figure 3-2. Body-Centered Rotating  
Coordinate System

Rectangular Cartesian Coordinates (see Figure 3-2):

$x_b$ -axis  $\sim$  the principal direction

$y_b$ -axis  $\sim$  the normal to the  $x_b$  and  $z_b$  axes to form a right-handed system

$z_b$ -axis  $\sim$  the normal to the equatorial plane of epoch in the direction of the north celestial pole

Spherical Polar Coordinates:

$r$   $\sim$  radial distance from the origin to the point being located

$\lambda$   $\sim$  longitude angle measured east from the prime meridian,  
 $\tan^{-1} (y_b/x_b)$

$\phi'$   $\sim$  geocentric latitude angle measured north from the equator,  
 $\sin^{-1} (z_b/r_b)$

Geodetic Coordinates

$h$   $\sim$  height measured normal to local body surface to the point being located

$\lambda$   $\sim$  longitude angle described above

$\phi$   $\sim$  geodetic latitude angle measured north from the equatorial plane to the vector normal to the ellipsoidal body surface passing through the point being located (see Figure 3-2)

### 3.2.3 Local Plane System

Origin: Center of reference body (see Figure 3-3)

Reference Plane: Plane containing  $\bar{r}$ , the geocentric position vector to point P, and the z-axis

Principal Direction: Geocentric position vector to point P



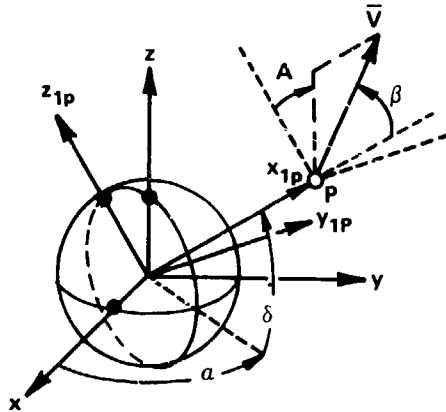


Figure 3-3. Local Plane System

### Rectangular Cartesian Coordinates (see Figure 3-3)

- $x_{1p}$ -axis ~ directed along geocentric position vector to point P
- $y_{1p}$ -axis ~ the axis displaced from the inertial y-axis by the origin's right ascension and lying in the equatorial plane
- $z_{1p}$ -axis ~ the north pointed axis lying in the reference plane normal to the principal direction.

### Spherical Velocity Coordinates:

- $V$  ~ the velocity vector's magnitude ( $|\dot{\mathbf{r}}|$ )
- $A$  ~ the azimuth angle measured clockwise from the  $z_{1p}$ -axis to the projection of the velocity vector onto the  $y_{1p}$ - $z_{1p}$  plane.
- $\beta$  ~ the flight path angle measured from the  $x_{1p}$ -axis to the velocity vector.

### 3.2.4 Topocentric Local Tangent (East/North/Up)

- Origin: Observer (topocentric)
- Reference Plane: Plane tangent to the ellipsoidal earth model at the observer
- Principal Direction: Vector in reference plane pointed north

### Rectangular Cartesian Coordinates (See Figure 3-4):

- $x_{1t}$ -axis ~ the axis lying in the reference plane that points east
- $y_{1t}$ -axis ~ the principal direction
- $z_{1t}$ -axis ~ the upward direction along the geodetic vertical

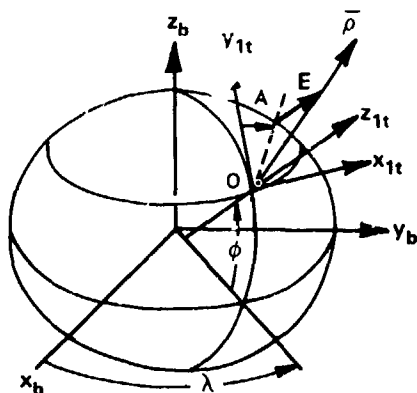


Figure 3-4. Topocentric Coordinates

### Spherical Position Coordinates:

(The origin coincides with the tracking station and  $\bar{\rho}$  is directed at satellite)

$\rho$  ~ the station to spacecraft range

A ~ the azimuth angle measured clockwise from the principal direction to the projection of the position vector in the reference plane

E ~ the elevation angle measured from the reference plane to the station-to-spacecraft position vector

### 3.2.5 Orbit Plane

Origin: Center of the reference body

Reference Plane: The plane of the orbit

Principal Direction: The radius vector from the origin to the satellite

$x_{op}$ -axis ~ the principal direction

$y_{op}$ -axis ~ in the orbital plane 90 degrees ahead of the satellite in the sense of the motion

$z_{op}$ -axis ~ the direction along the vector  $\bar{r} \times \dot{\bar{r}}$

The following two alternative orbit plane systems are defined. Both have the same origin and reference plane as the basic system described above.

- The Keplerian system, denoted by  $x_p$ ,  $y_p$  and  $z_p$ , has its  $x_p$ -axis (principal direction) directed towards the perifocus of the satellite orbit (see Figures 3-5 and 3-6).

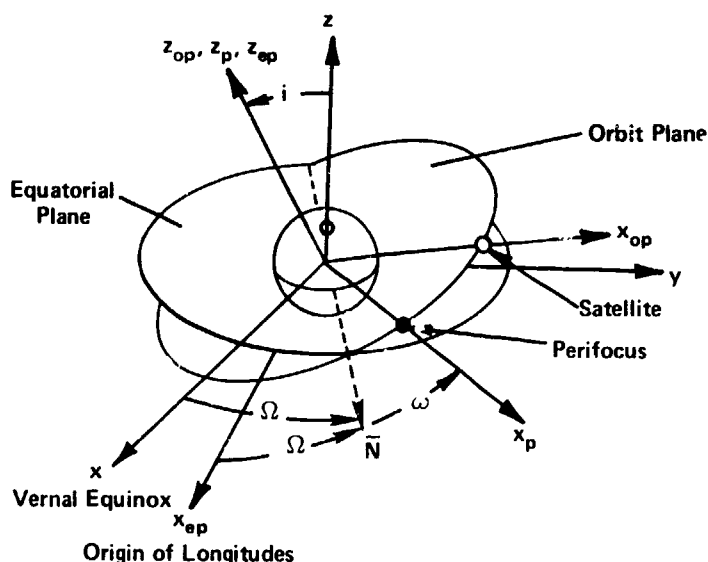


Figure 3-5. Orbit Plane Coordinates

- The equinoctial system, denoted by  $x_{ep}$ ,  $y_{ep}$ , and  $z_{ep}$ , has its  $x_{ep}$ -axis (principal direction) directed towards the "origin of longitudes." The "origin of longitudes" lies in the plane of the orbit and is displaced by the angle  $\Omega$  from the ascending node  $\bar{N}$ , where  $\Omega$  is the right ascension of the ascending node. Unit vectors along the coordinate directions  $x_{ep}$ ,  $y_{ep}$  and  $z_{ep}$  are denoted by  $\hat{f}$ ,  $\hat{g}$  and  $\hat{w}$  respectively.

### 3.2.6 Orbital Elements

Three types of orbital coordinates are presented below which can be used to describe closed orbits. Two sets of equinoctial and Herrick elements are defined such that the elements and the corresponding equations of motion are non-singular for inclinations of both 0 degrees (direct set) and 180 degrees (retro-grade set).

Keplerian Elements (see Figures 3-5 and 3-6):

- $a$  ~ the semimajor axis
- $e$  ~ the eccentricity specifying the elongation of the orbital conic section
- $i$  ~ the inclination specifying the orientation of the satellite's orbital plane with respect to the equator of the central body
- $\Omega$  ~ the right ascension of the ascending node, i.e., the angle measured eastward along the equator between the vernal equinox and the point where the satellite crosses the equator traveling in a northerly direction

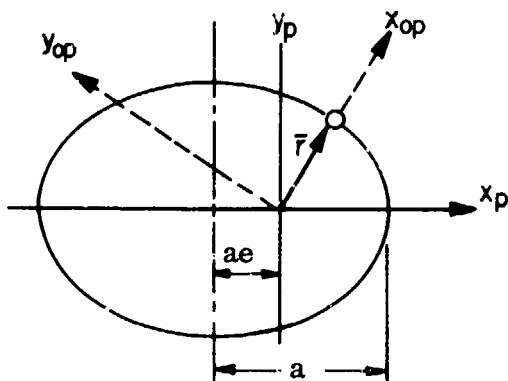


Figure 3-6. Orbital Parameters

$\omega$  ~ the argument of perigee, i.e., angle between the ascending node and the perifocal point measured positive with increasing mean anomaly

$M$  ~ the mean anomaly, i.e., the sum of the mean anomaly at epoch and the product of the mean motion and the elapsed time from epoch.

Equinoctial Elements (see Figure 3-5):

$a$  ~ the semimajor axis

$h$  ~ the projection of the vector  $\vec{e}$  on the  $y_{ep}$ -axis

$k$  ~ the projection of the vector  $\vec{e}$  on the  $x_{ep}$ -axis

$p$  ~ the projection of the vector  $\vec{N}$  on the  $y_{ep}$ -axis

$q$  ~ the projection of the vector  $\vec{N}$  on the  $x_{ep}$ -axis

$\lambda$  ~ the mean longitude

where

$\vec{e}$  ~ eccentricity vector pointing in the direction of the  $x_p$ -axis (perifocus) and having a magnitude equal to the eccentricity,  $e$

$\vec{N}$  ~ nodal vector pointing in the direction of the ascending node and having a magnitude equal to

$$\left[ \tan \left( \frac{i}{2} \right) \right]^j,$$

where  $i$  denotes the orbital inclination and  $j = +1$  for direct orbits, and  $j = -1$  for retrograde orbits

Herrick Elements:

$\vec{e}$  ~ the eccentricity vector (defined above) expressed in inertial Cartesian coordinates

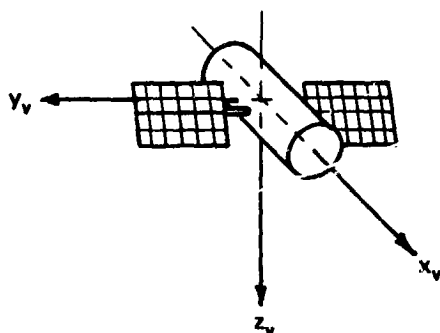


Figure 3-7. Vehicle-Fixed Coordinates

$\bar{\ell}$  ~ the angular momentum vector divided by  $\sqrt{\mu}$ , where  $\mu$  is the gravitational constant, i.e.,

$$\bar{\ell} = \frac{\bar{r} \times \dot{\bar{r}}}{\sqrt{\mu}}$$

The vector  $\bar{\ell}$  is expressed in inertial Cartesian coordinates.

$n$  ~ the Kepler mean motion

$\lambda$  ~ the mean longitude

(Note: Only six of the eight scalar components above are independent. Single components of the vectors  $\bar{e}$  and  $\bar{\ell}$  are dependent upon the remaining six elements.)

### 3.2.7 Vehicle- Fixed

Origin:	Center-of-gravity of the spacecraft
Reference Plane:	Plane containing the longitudinal and vertical axes defined by the spacecraft designer
Principal Direction:	Longitudinal axis directed toward front of spacecraft

Rectangular Cartesian Coordinates (see Figure 3-7)

$x_v$ -axis ~ the longitudinal (roll) axis along principal direction

$y_v$ -axis ~ the lateral (pitch) axis

$z_v$ -axis ~ the vertical (yaw) axis

## 3.3 SPECIFIC TRANSFORMATIONS

The spacecraft's state vector at a given time is obtained by integrating the equations of motion. The equations of motion equate the acceleration of the vehicle to the sum of the various accelerations acting on the vehicle, and are valid only

in an inertial reference frame. However, the principal acceleration sources which act on the vehicle, i.e., gravity and aerodynamic drag, are most easily expressed in terms of a body-fixed system. The inertial position and velocity must therefore be transformed to body-fixed coordinates for use in computing the gravity and drag accelerations. These accelerations, expressed in terms of body-fixed axes, must then be transformed to the inertial coordinate system for use in the numerical integration process. The tracking measurement computations, used in the estimation process, also require body-fixed position and velocity coordinates of the spacecraft. Thus, one of the most basic transformations in GTDS is that between the inertial coordinate system and the body-fixed system. The following coordinate systems are also used in GTDS to express spacecraft position, velocity and/or acceleration for various purposes.

- **Body-Centered Equatorial Inertial:** This system, when "frozen" at a specified date, provides the basic coordinates for expressing the equations of motion derived from Newton's laws. In GTDS the 1950.0 reference date is used to locate the planets, moon, and spacecraft.
- **Body-Centered Rotating:** This system is used to characterize the gravitational field and the atmospheric properties of the body.
- **Local Plane:** This system is used to orient the spacecraft velocity vector.
- **Topocentric Local Tangent:** This system is used to characterize ground based radar tracking observations of the spacecraft.
- **Orbit Plane:** This system is used to characterize the spacecraft orbital position and motion.
- **Vehicle-Fixed:** This system is used to characterize propulsive and aerodynamic forces acting on the spacecraft.

In the following subsections, the transformation between the mean equator and equinox of 1950.0 inertial coordinate system and the body-fixed system is presented. This is followed by descriptions of transformations relating the inertial coordinates to the various other coordinate systems used in GTDS.

### 3.3.1 1950.0 Inertial to True of Date

The equinox is defined as the intersection of the planes of the earth's equator and the ecliptic. The equator is defined as being normal to the earth's polar axis. The motion of the equinox is due to the combined motions of the two planes, the equator and the ecliptic, that define it. The motion of the celestial pole or of

the equator is due to the gravitational attraction of the sun and moon on the earth's equatorial bulge. It consists of two components: lunisolar precession and nutation (References 1, 2, 3). Lunisolar precession is the smooth long-period westward motion of the equator's mean pole around the ecliptic pole and has an amplitude of approximately 23.5 degrees and a period of approximately 26,000 years. Nutation is a relatively short-period motion that carries the actual (or true) pole around the mean pole in a somewhat irregular curve with an amplitude of approximately 9 seconds of arc and a period of approximately 18.6 years. The motion of the ecliptic (i.e., the mean plane of the earth's orbit) is due to the plane's gravitational attraction on the earth and consists of a slow rotation of the ecliptic. This motion is known as planetary precession and consists of an eastward movement of the equinox of approximately 12 seconds of arc a century and a decrease of the obliquity of the ecliptic, the angle between the ecliptic and the earth's equator, of approximately 47 seconds of arc a century. In astronomical work the precessional motion of the equator and ecliptic, called general precession, is considered separately from the nutational motion. Thus the "mean" equator and equinox are determined by neglecting nutation. The "true" equator and equinox can then be obtained by correcting the mean equator and equinox for nutation.

### 3.3.1.1 1950.0 Inertial to Mean of Date

The 1950.0 inertial coordinates are transformed into the mean equator and equinox of date by correcting only for precession. This is done by the following three rotations (see Figure 3-8).

$R_z(\pi/2 - \zeta_0) \sim$  the rotation about the Z-axis that rotates the X-axis to the ascending node of the mean equator of date

$R_x(\theta_p) \sim$  the rotation of the 1950.0 equatorial plane into the mean equatorial plane of date about an axis that coincides with the ascending node of the mean equator of date on the 1950.0 equatorial plane

$R_z(\pi/2 + \xi_p) \sim$  the rotation about the  $z_E$ -axis that rotates the  $x_E$ -axis to the descending node of the mean equator of 1950.0

The orthogonal transformations are defined as follows:

$$R_x(\alpha) = \begin{bmatrix} \cos \alpha & \sin \alpha & 0 \\ -\sin \alpha & \cos \alpha & 0 \\ 0 & 0 & 1 \end{bmatrix} \quad R_z(\alpha) = \begin{bmatrix} 1 & 0 & 0 \\ 0 & \cos \alpha & \sin \alpha \\ 0 & -\sin \alpha & \cos \alpha \end{bmatrix} \quad (3-1)$$

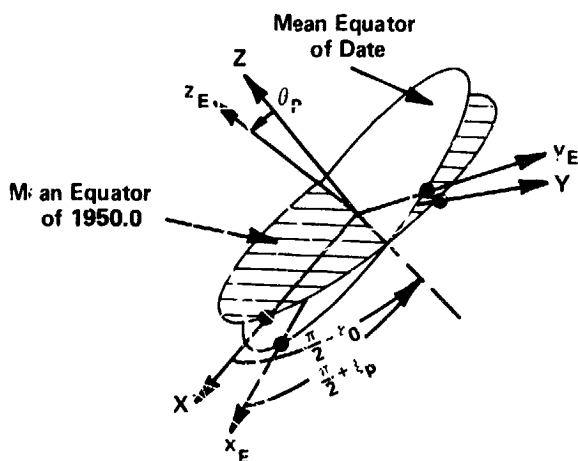


Figure 3-8. Precession Angles

The angles  $\zeta_0$ ,  $\theta_p$ , and  $\xi_p$  are given by (Reference 4)

$$\zeta_0 = 2304''.9969 T_U + 0''.302000 T_U^2 + 0''.01808 T_U^3 \quad (3-2a)$$

$$\theta_p = 2004''.2980 T_U - 0''.425936 T_U^2 - 0''.04160 T_U^3 \quad (3-2b)$$

$$\xi_p = 2304''.9969 T_U + 1''.092999 T_U^2 + 0''.019200 T_U^3 \quad (3-2c)$$

where

$T_U$  is measured in Julian centuries (of 36525 days) from 1950.0.

The total rotation matrix may be expressed as

$$A = R_z(-90^\circ - \xi_p) R_x(\theta_p) R_z(90^\circ - \zeta_0) = \{a_{ij}\}. \quad (3-3)$$

Denoting the 1950.0 coordinates by  $\bar{R}$  and the mean equator and equinox of date by  $\bar{r}_E$ , we have

$$\bar{r}_E = A \bar{R} \quad (3-4)$$



where the elements of A are

$$\begin{aligned}
 a_{11} &= -\sin \zeta_o \sin \xi_p + \cos \zeta_o \cos \xi_p \cos \theta_p \\
 a_{12} &= -\cos \zeta_o \sin \xi_p - \sin \zeta_o \cos \xi_p \cos \theta_p \\
 a_{13} &= -\cos \xi_p \sin \theta_p \\
 a_{21} &= \sin \zeta_o \cos \xi_p + \cos \zeta_o \sin \xi_p \cos \theta_p \\
 a_{22} &= \cos \zeta_o \cos \xi_p - \sin \zeta_o \sin \xi_p \cos \theta_p \\
 a_{23} &= -\sin \xi_p \sin \theta_p \\
 a_{31} &= \cos \zeta_o \sin \theta_p \\
 a_{32} &= -\sin \zeta_o \sin \theta_p \\
 a_{33} &= \cos \theta_p.
 \end{aligned} \tag{3-5}$$

The time derivative of A is assumed to be negligible; therefore, the velocity coordinates are transformed as follows

$$\dot{\vec{r}}_E = A \dot{\vec{R}}. \tag{3-6}$$

### 3.3.1.2 Mean of Date to True of Date

The transformation from the mean equator and equinox of date to the true of date system involves correcting for the nutation effect. Nutation is measured as cyclic changes in the obliquity, the angle between the equatorial plane and the ecliptic, and the longitude of the equinox. These changes in obliquity,  $\delta \epsilon$ , and longitude,  $\delta \psi$ , are assumed known. They are input to GTDS by fitting polynomials through the JPL ephemeris data (Reference 5) as described in Section 3.6.

To compute the transformation, the mean obliquity is first determined (Reference 1)

$$\bar{\epsilon} = 23.452294 - 9.130125 \times 10^{-1} T_E - 9.164 \times 10^{-5} T_E^2 + 9.503 \times 10^{-6} T_E^3 \tag{3-7}$$

where

$T_E$  ~ the time in Julian centuries (36525 Julian days) elapsed from 1900 Jan 0<sup>d</sup> 12<sup>h</sup> ET (JD 2415020.0) to specified date.

Then, defining

$\delta\epsilon$  ~ the difference between the true and the mean obliquity

$\tilde{\epsilon} = \bar{\epsilon} + \delta\epsilon$  ~ the true obliquity measured from the true equator to the ecliptic

$\delta\psi$  ~ the nutation in longitude, which is the true longitude of date of the mean equinox of date

the rotation from the mean equator and equinox of date to the true equator and equinox is given by the following three rotations: (see Figure 3-9).

$R_x(\bar{\epsilon})$  ~ the rotation about the  $x_E$ -axis through the mean obliquity to the ecliptic of date

$R_z(-\delta\psi)$  ~ the rotation about the ecliptic pole, through the nutation in longitude

$R_x(-\tilde{\epsilon})$  ~ the rotation about the x-axis through the true obliquity to the true equator of date

where  $R_x$  and  $R_z$  are given by Equation (3-1).

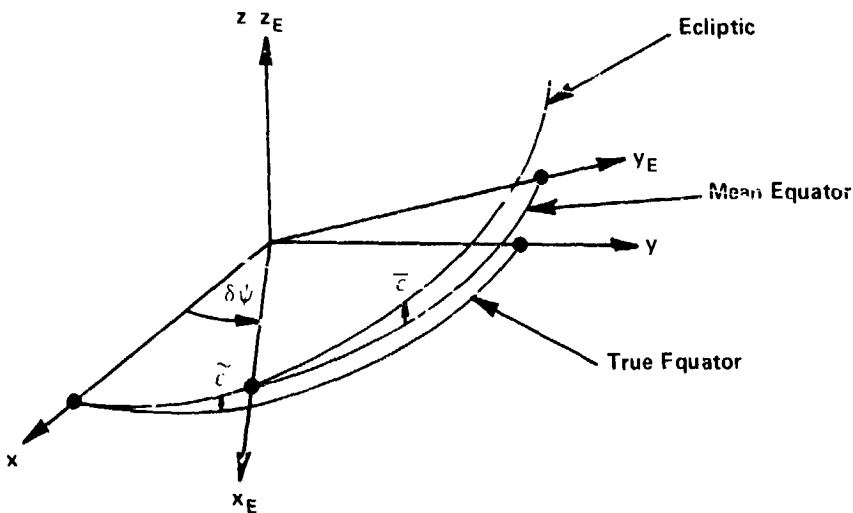


Figure 3-9. Nutation Angles

The total rotation matrix may be expressed as

$$N = R_x(-\tilde{\epsilon}) R_z(-\delta\psi) R_x(\tilde{\epsilon}) = \{n_{ij}\}. \quad (3-8)$$

Denoting the true of date coordinates by  $\bar{\mathbf{r}}$ , we have

$$\bar{\mathbf{r}} = N \bar{\mathbf{r}}_E \quad (3-9)$$

where the elements of N are

$$\begin{aligned} n_{11} &= \cos \delta\psi \\ n_{12} &= -\sin \delta\psi \cos \bar{\epsilon} \\ n_{13} &= -\sin \delta\psi \sin \bar{\epsilon} \\ n_{21} &= \sin \delta\psi \cos \tilde{\epsilon} \\ n_{22} &= \cos \delta\psi \cos \tilde{\epsilon} \cos \bar{\epsilon} + \sin \tilde{\epsilon} \sin \bar{\epsilon} \\ n_{23} &= \cos \delta\psi \cos \tilde{\epsilon} \sin \bar{\epsilon} - \sin \tilde{\epsilon} \cos \bar{\epsilon} \\ n_{31} &= \sin \delta\psi \sin \tilde{\epsilon} \\ n_{32} &= \cos \delta\psi \sin \tilde{\epsilon} \cos \bar{\epsilon} - \cos \tilde{\epsilon} \sin \bar{\epsilon} \\ n_{33} &= \cos \delta\psi \sin \tilde{\epsilon} \sin \bar{\epsilon} + \cos \tilde{\epsilon} \cos \bar{\epsilon}. \end{aligned} \quad (3-10)$$

The time derivative of N is assumed to be negligible. Therefore the velocity coordinates are transformed as follows

$$\dot{\bar{\mathbf{r}}} = N \dot{\bar{\mathbf{r}}}_E. \quad (3-11)$$

### 3.3.1.3 Summary

The transformation matrix from inertial mean of 1950.0 to true of date coordinates is given by

$$\bar{r} = C\bar{R} \quad (3-12)$$

where

$$C = N(\delta\psi, \delta\epsilon) A(\zeta_0, \theta_p, \xi_p). \quad (3-13)$$

The elements of the precession matrix, A, are given in Equation (3-5), and the elements of the nutation matrix, N, are given in Equation (3-10). In GTDS the C-matrix is synthesized during preprocessing computations using precession angles obtained by means of Equations (3-2), and nutation angles obtained from an ephemeris tape provided by the Jet Propulsion Laboratory. The elements of C are stored on the SLP (Solar/Lunar/Planetary) file, as described in Section 3.6, for retrieval and use during program execution.

GTDS has also been provided with the optional capability to solve the equations of motion in a true of "reference date" coordinate system where the reference date is specified. The orthogonal transformation in Equation (3-12) involves two times, the date of the true coordinates denoted by t, and the epoch of the mean inertial system, denoted by 1950.0. Therefore, Equation (3-12) can be written

$$\bar{r}(t) = C(t, 1950.0) \bar{R} \quad \text{or} \quad \bar{R} = C^T(t, 1950.0) \bar{r}(t) \quad (3-14)$$

where the superscript T denotes transpose.

Specifying the reference date by t\* then

$$\bar{r}(t^*) = C(t^*, 1950.0) \bar{R} \quad \text{or} \quad \bar{R} = C^T(t^*, 1950.0) \bar{r}(t^*) \quad (3-15)$$

The transformation from the true of reference date to true of date coordinates is obtained from Equations (3-14) and (3-15) to be

$$\bar{r}(t) = C(t, 1950.0) C^T(t^*, 1950.0) \bar{r}(t^*) \quad (3-16)$$

This equation permits problems to be solved using a true of reference date coordinate system as the inertial frame, but requires only the precession/nutation matrix,  $C(t, 1950.0)$ , which is available on the SLP files.

Note that the transformation matrix in Equation (3-16) is the identity matrix when  $t = t^*$ . GTDS utilizes this property and neglects precession and nutation when a true of reference date option is specified. This requires that the problem time, spanned by  $t$ , must be relatively short and in the proximity of the reference date,  $t^*$ .

### 3.3.2 True of Date to Body-Fixed

The transformation that relates the true of date coordinates to the body-fixed coordinates accounts for two separate effects. The first relates the true vernal equinox to the prime meridian of the rotating earth by means of the angle  $\alpha_g$ , the true of date right ascension of Greenwich (see Figure 3-10). The second effect, called polar motion, accounts for the fact that the pole of the body-fixed axis,  $z_b$ , does not coincide with the body's spin axis,  $z$ , the pole of the true of date geocentric axes. The first of these effects transforms the true of date coordinates to pseudo body-fixed coordinates,  $x'_b, y'_b, z'_b$ . These pseudo coordinates would be precisely the body-fixed coordinates  $x_b, y_b, z_b$ , if  $z'_b = z_b$ , that is, if polar motion were omitted.

#### 3.3.2.1 True of Date to Pseudo Body-Fixed

The transformation from the true of date to the pseudo body-fixed coordinates consists of a rotation about the true of date  $z$ -axis through the true right ascension of Greenwich  $\alpha_g$  (see Figure 3-10), yielding

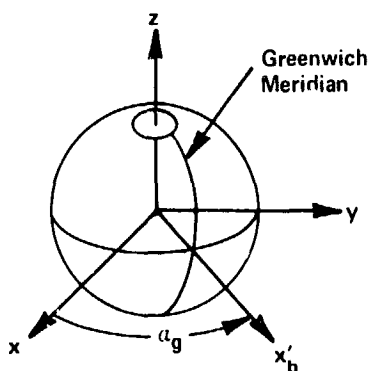


Figure 3-10. Greenwich Sidereal Time

$$B_1 = R_z^T(\alpha_g) = \begin{bmatrix} \cos \alpha_g & \sin \alpha_g & 0 \\ -\sin \alpha_g & \cos \alpha_g & 0 \\ 0 & 0 & 1 \end{bmatrix} \quad (3-17)$$

The true of date right ascension of Greenwich,  $\alpha_g$ , is measured easterly from the true vernal equinox to Greenwich. A related quantity is the Greenwich hour angle, also called the true Greenwich sidereal time, which is measured westerly in the plane of the equator from Greenwich to the true vernal equinox. Thus, although their definitions differ, the right ascension of Greenwich,  $\alpha_g$ , and the Greenwich sidereal time and hour angle are equal in magnitude. The true Greenwich sidereal time is obtained from the mean Greenwich sidereal time (Reference 2)

$$\alpha_{GM} = UT1 + 6^h 38^m 45^s 836 + 8640184^s 542 T_u + 0^s 0929 T_u^2 \quad (3-18)$$

by applying the correction

$$\alpha_g = \alpha_{GM} + \Delta H \quad (3-19)$$

where

$$\Delta H = \delta\psi \cos(\bar{\epsilon} + \delta\epsilon). \quad (3-20)$$

The nutation in longitude,  $\delta\psi$ , and obliquity,  $\delta\epsilon$ , is discussed in Section 3.3.1.2. The times UT1 and  $T_u$  in Equation (2-18) are

UT1 = Greenwich universal time measured from midnight (epoch) to time  $t$ .  
UT1 is positive for  $t$  after midnight and negative for  $t$  before midnight.

$T_u \sim$  the number of Julian centuries elapsed from 12 hours UT1 January 0, 1900 (JD = 2415020.0) to the UT1 time of epoch\*

The true of date coordinates transform into the pseudo body-fixed coordinates as follows

$$\bar{r}_b = B_1 \bar{r}. \quad (3-21)$$

---

\*UT1 and hence  $T_u$  are known only by observation of the polar motion and rotation of the Earth. GTDS uses empirical polynomials to compute the difference A.1-UT1. Since A.1 is known, UT1 can then be determined.

Differentiation yields the velocity transformation

$$\dot{\bar{r}}_b = B_1 \dot{\bar{r}} + \dot{B}_1 \bar{r} \quad (3-22)$$

where

$$\dot{B}_1 = \begin{bmatrix} -\sin \alpha_g & \cos \alpha_g & 0 \\ -\cos \alpha_g & -\sin \alpha_g & 0 \\ 0 & 0 & 0 \end{bmatrix} \dot{\alpha}_g \quad (3-23)$$

and where  $\dot{\alpha}_g$  is considered constant.

### 3.3.2.2 Pseudo Body-Fixed to Body-Fixed (Reference 3)

The earth's axis of figure (i.e., principal moment of inertia) is not coincident with the spin axis and it moves with respect to the latter causing the polar motion effect. The path of the spin axis on the earth's surface is "semi-regular" but unpredictable due to random shifts in the earth's crust, etc. Therefore, motion of the spin axis pole is given with respect to the pole at some established epoch. The pole at the established epoch is referred to as the adopted pole ( $P_A$ ) and corresponds to the pole of the body fixed axes,  $x_b, y_b, z_b$ , while the present position of the spin axis pole is referred to as the true pole ( $P_T$ ).

The adopted pole used in GTDS corresponds to the mean pole of 1903.0 which is consistent with that used by the International Polar Motion Service. Due to the small size of the polar motion correction (it takes place in squares of < 30 meters), the polar region of the earth may be considered a plane. A geocentric rectangular coordinate system is established with the  $z_b$ -axis passing through  $P_A$ , the  $x_p$ -axis parallel to the  $x_b$ -axis and directed along the Greenwich meridian, and the  $y_p$ -axis parallel to the negative  $y_b$ -axis and directed along the meridian of 90° west (see Figure 3-11). The coordinates of the instantaneous pole,  $P_T$ , are measured in terms of  $x_p$  and  $y_p$  components using units of seconds of arc. (The coordinates  $x_p$  and  $y_p$  are periodically measured by the International Polar Motion Service and supplied to interested users by the U. S. Naval Observatory.)

In order to derive the expressions for the effects of  $x_p$  and  $y_p$  on a point's latitude and longitude, these two quantities are shown in relation to a regular right-handed orthogonal-rectangular coordinate system whose  $z_b$  axis passes through  $P_A$  and whose  $x_b - z_b$  plane passes through Greenwich. In this system, the adopted longitude of a point  $\lambda_A$  is measured positive in an eastward direction from  $x_b$ . The following notation is used:

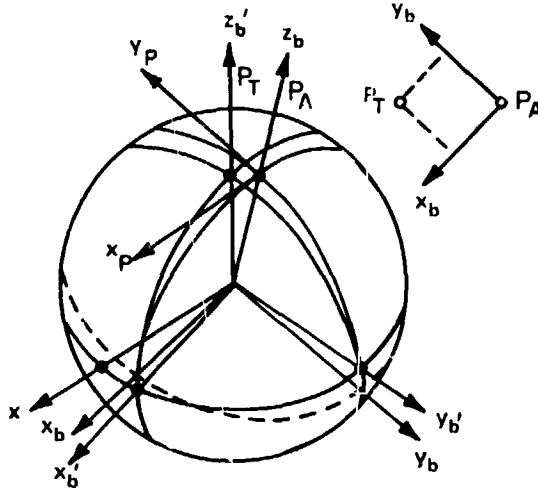


Figure 3-11. Polar Motion Schematic

$\lambda_A \sim$  the adopted longitude

$\phi_A \sim$  the adopted latitude

$\lambda_T \sim$  the instantaneous longitude with respect to  $(x'_b, y'_b, z'_b)$

$\phi_T \sim$  the instantaneous latitude with respect to  $(x'_b, y'_b, z'_b)$

$\Delta\phi \sim \phi_T - \phi_A$ , the difference between adopted and true latitude

$\Delta\lambda \sim \lambda_T - \lambda_A$ , the difference between adopted and true longitude

Let  $\phi_T$  and  $\lambda_T$  be measured in the pseudo body-fixed coordinate system  $(x'_b, y'_b, z'_b)$  whose  $z'_b$  axis passes through  $P_T$  and whose  $x'_b$  axis lies in the  $z_b - x_b$  meridian, displaced from  $x_b$  by the angle  $x_p$ . The vector in the  $(x_b, y_b, z_b)$  and  $(x'_b, y'_b, z'_b)$  systems may be written

$$\begin{bmatrix} x_b \\ y_b \\ z_b \end{bmatrix} = r_b \begin{bmatrix} \cos \phi_A \cos \lambda_A \\ \cos \phi_A \sin \lambda_A \\ \sin \phi_A \end{bmatrix} \quad (3-24)$$

and

$$\begin{bmatrix} x'_b \\ y'_b \\ z'_b \end{bmatrix} = r_b \begin{bmatrix} \cos \phi_T \cos \lambda_T \\ \cos \phi_T \sin \lambda_T \\ \sin \phi_T \end{bmatrix} \quad (3-25)$$



The two systems are related by

$$\begin{bmatrix} x_b \\ y_b \\ z_b \end{bmatrix} = R_y^T(x_p) \cdot R_x^T(y_p) \begin{bmatrix} x'_b \\ y'_b \\ z'_b \end{bmatrix} \quad (3-26)$$

where  $R_x$  is given in Equation (3-1) and  $R_y$  is

$$R_y(a) = \begin{bmatrix} \cos a & 0 & -\sin a \\ 0 & 1 & 0 \\ \sin a & 0 & \cos a \end{bmatrix} \quad (3-27)$$

The resulting transformation is

$$\bar{r}_b = \begin{bmatrix} \cos x_p & \sin x_p \sin y_p & \sin x_p \cos y_p \\ 0 & \cos y_p & -\sin y_p \\ -\sin x_p & \cos x_p \sin y_p & \cos x_p \cos y_p \end{bmatrix} \bar{r}'_b \quad (3-28)$$

The error made by neglecting the polar motion transformation defined by Equation (3-28) increases linearly with  $|\bar{r}_b|$ . A worst-case, order-of-magnitude indication of this error is given in Figure 3-12.

The figure also shows the band of uncertainty in  $|\bar{r}_b - \bar{r}'_b|$  as a result of a  $\pm 2$ -meter uncertainty in the measurement of the polar motion coordinates,  $x_p$  and  $y_p$ .

Since  $x_p$  and  $y_p$  are small, all cosine terms are equated to unity, all sine terms equated to their angles, and all products neglected. Thus the transformation defined by Equation (3-28) simplifies to

$$\bar{r}_b \approx \begin{bmatrix} 1 & 0 & x_p \\ 0 & 1 & -y_p \\ -x_p & y_p & 1 \end{bmatrix} \bar{r}'_b = B_2 \bar{r}'_b \quad (3-29)$$

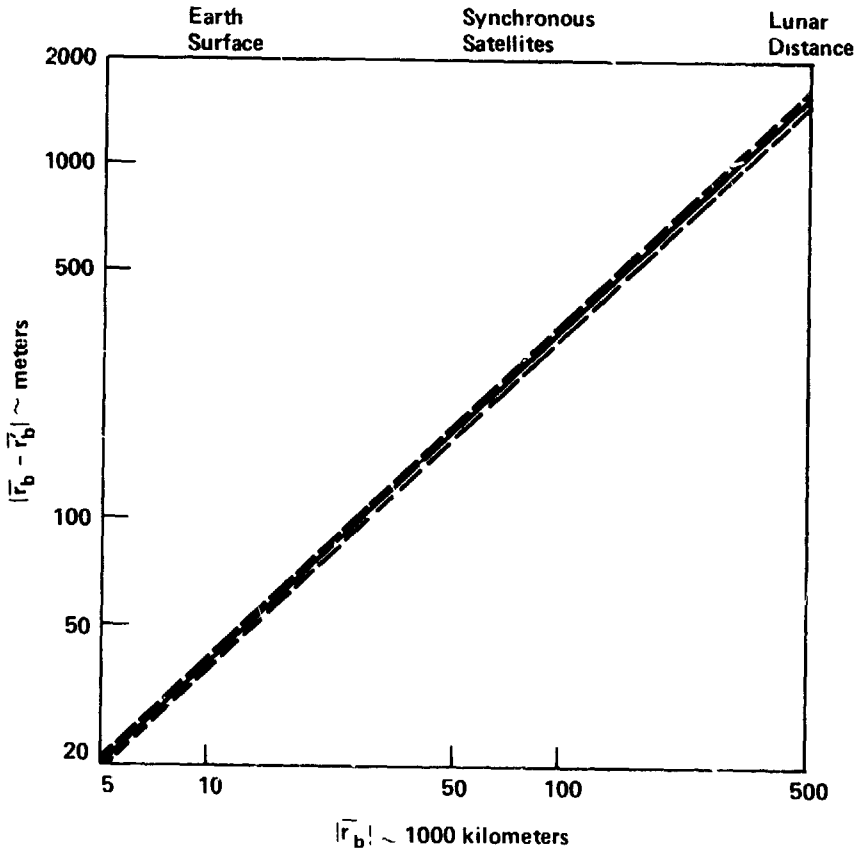


Figure 3-12. Polar Motion Errors

The worst-case error made by using the simplified transformation matrix is insignificant. For example, at lunar distances the error amounts to less than a centimeter.

In order to obtain the relationships between  $\lambda_T$ ,  $\lambda_A$ ,  $\phi_A$ , and  $\phi_T$ , the following formulas may be used

$$\phi_T - \phi_A = \Delta\phi = x_p \cos \lambda_A - y_p \sin \lambda_A \quad (3-30)$$

$$\lambda_T - \lambda_A = \Delta\lambda = \tan \phi_A (x_p \sin \lambda_A + y_p \cos \lambda_A). \quad (3-31)$$

The Goddard Trajectory Determination Program uses the simplified transformation matrix defined in Equation (3-29). The instantaneous coordinates of the pole,  $x_p$  and  $y_p$ , are obtained by evaluating predefined cubic polynomials at the given date.

$$x_p = a_{i1} + a_{i2}T + a_{i3}T^2 + a_{i4}T^3 \quad (3-32)$$

$$y_p = a_{i5} + a_{i6}T + a_{i7}T^2 + a_{i8}T^3$$

where

$x_p$  ~ x-polar coordinate, seconds of arc  
 $y_p$  ~ y-polar coordinate, seconds of arc  
 $T$  ~ number of days from the beginning of the time span covered by the polynomial, e.g.,  $T = 1, 2, \dots$ . For a given modified Julian date, MJD

$$T = \text{MJD} - \text{MJD}_i + 1 \quad (3-33)$$

where  $\text{MJD}_i$  is the tabular modified Julian date which bounds the interval from below, i.e.,

$$\text{MJD}_i \leq \text{MJD} < \text{MJD}_{i+1} \quad (3-34)$$

The coefficients  $a_{ij}$  are given in Table 3-1 next to modified Julian dates (mod 2,430,000) defining the time spans for which the coefficients are applicable. These coefficients and associated time spans were determined by least-squares fitting of cubic polynomials to published daily polar motion data. The time spans were determined by constraining the maximum deviation (between the data and polynomial) to be less than 0.01 seconds of arc.

The table begins on January 1, 1958, and is updated periodically as current data from the U. S. Naval Observatory becomes available. The last row of coefficients in the table can be used to obtain extrapolated values of the polar motion coordinates for a short time in the future.

### 3.3.2.3 Summary

The complete transformation between the true of date coordinate system and the body-fixed system is given by

$$\bar{r}_b = B_2(x_p, y_p) B_1(a_g) \bar{r} = B\bar{r} \quad (3-35)$$

where  $B = B_2 B_1$  with  $B_1$  given in Equation (3-17) and  $B_2$  in Equation (3-29).

**Table 3-1**  
**Polar Motion Coefficients**

Gregorian Date	Modified Julian Date	X-Polar Coordinate				Y-Polar Coordinate			
		a <sub>1,1</sub>	a <sub>1,2</sub>	a <sub>1,3</sub>	a <sub>1,4</sub>	a <sub>1,5</sub>	a <sub>1,6</sub>	a <sub>1,7</sub>	a <sub>1,8</sub>
01-01-58	6204	-0.19767D-00	-0.17397D-02	0.15792D-04	0.56537D-07	-0.54697D-01	0.19489D-02	0.57555D-04	-0.43444D-06
04-08-58	6291	-0.13488D-00	0.33695D-02	0.47862D-05	-0.47248D-07	0.37801D-00	0.29935D-02	-0.21848D-04	-0.36396D-07
08-28-58	6443	0.32567D-00	0.46392D-02	-0.81859D-04	0.17757D-06	0.27723D-00	-0.31136D-02	-0.33444D-04	0.28654D-06
11-27-58	6534	0.22133D-00	-0.63734D-02	0.18865D-04	0.61318D-07	-0.77337D-01	-0.70363D-03	0.17730D-04	0.46371D-08
03-24-59	6651	-0.17608D-00	0.25367D-03	0.97388D-05	0.27892D-07	0.84864D-01	0.41445D-02	-0.47648D-05	-0.75084D-07
09-09-59	6820	0.27773D-00	0.26658D-02	-0.42458D-04	0.10380D-06	0.28460D-00	-0.14203D-02	-0.10745D-04	0.60890D-07
04-24-60	7048	-0.85171D-01	-0.14450D-02	0.27010D-04	-0.70824D-07	0.12111D-00	0.11216D-02	0.63648D-05	-0.39237D-07
12-21-60	7289	0.14300D-00	0.15746D-03	-0.36863D-05	-0.83591D-09	0.22349D-00	-0.60969D-03	-0.10727D-04	0.61740D-07
07-05-61	7485	0.29412D-01	-0.72621D-03	0.82974D-06	0.97399D-08	0.14527D-00	0.20816D-02	-0.19450D-04	0.60625D-07
12-31-61	7664	-0.30430D-01	-0.12198D-02	0.21743D-04	0.12057D-08	0.23238D-00	0.10180D-02	0.39270D-05	-0.74242D-07
01-07-62	7761	0.50266D-01	0.63817D-03	0.10950D-05	-0.35036D-07	0.28686D-00	0.27306D-03	-0.20762D-04	0.75204D-07
10-23-62	7960	-0.36791D-01	-0.32778D-02	0.15180D-04	0.28784D-07	0.10175D-00	0.15825D-02	0.15937D-04	-0.85935D-07
04-01-63	8120	-0.63786D-01	0.28084D-02	0.14871D-04	-0.15351D-06	0.41375D-00	0.17397D-02	-0.44163D-04	0.12549D-06
09-03-63	8275	0.17377D-00	-0.24358D-02	-0.20183D-04	0.11286D-06	0.10492D-00	-0.35173D-02	0.39067D-04	-0.73909D-07
04-05-64	8490	-0.16637D-00	0.29283D-02	-0.64009D-07	0.36926D-07	0.41861D-00	0.29369D-02	-0.38429D-04	0.95676D-07
07-21-64	8597	0.17983D-00	0.26943D-02	-0.32600D-04	0.38477D-07	0.39884D-00	-0.25630D-02	-0.17647D-04	0.12983D-06
12-13-64	8742	0.23795D-01	-0.38284D-02	0.42512D-05	0.86298D-07	0.62704D-01	-0.13271D-02	0.39303D-04	-0.10542D-05
04-25-65	8875	-0.20109D-00	0.22095D-03	0.45378D-04	-0.19490D-06	0.32931D-00	0.38914D-02	-0.29382D-04	0.12412D-07
09-17-65	9020	0.17408D-00	0.20348D-02	-0.37014D-04	0.94791D-07	0.32932D-00	-0.28118D-02	-0.19542D-05	0.56443D-07
03-21-66	9205	-0.10598D-00	-0.29328D-02	0.37716D-04	-0.91061D-07	0.91055D-01	0.23065D-02	0.42261D-05	-0.49763D-07
09-29-66	9397	0.49071D-01	0.31195D-02	-0.76784D-04	0.97913D-07	0.35151D-00	-0.54344D-03	-0.23239D-04	0.12751D-06
02-09-67	9630	0.52058D-01	-0.18656D-02	0.13707D-04	-0.28621D-07	0.16365D-00	-0.12220D-03	0.67445D-05	-0.24437D-07
05-28-67	9761	-0.73559D-02	-0.40375D-03	0.50173D-05	-0.12649D-07	0.19478D-00	0.82581D-03	0.85707D-06	-0.19473D-07
01-10-68	9956	0.13935D-01	0.48635D-04	0.14791D-04	-0.89143D-07	0.26201D-00	-0.21272D-03	-0.12867D-04	0.64764D-07
09-17-68	10116	0.30342D-01	0.11158D-02	-0.63582D-04	0.33552D-06	0.15523D-00	-0.67421D-03	-0.71484D-05	0.22442D-06
12-25-68	10215	-0.15879D-00	0.77670D-03	0.16188D-04	-0.94824D-07	0.23023D-00	0.21761D-02	-0.11560D-04	0.28478D-07
04-30-69	10341	0.19964D-01	0.77886D-05	0.59554D-04	-0.24501D-06	0.37012D-00	0.11803D-03	-0.18108D-04	0.66953D-08
08-28-69	10461	0.11558D-00	-0.22065D-02	0.21487D-04	-0.15407D-06	0.13604D-00	-0.10302D-02	0.66636D-05	0.15805D-07
01-02-70	10588	-0.11561D-00	-0.41135D-02	0.86956D-04	-0.44075D-06	0.13167D-00	0.38634D-02	0.92753D-06	-0.11853D-06
04-21-70	10697	-0.98390D-01	0.16807D-02	0.32544D-04	-0.21161D-06	0.40615D-00	0.27255D-02	-0.51460D-04	0.13757D-06
09-02-70	10831	0.20618D-00	-0.10215D-03	-0.37373D-05	-0.30877D-06	0.20956D-00	-0.28568D-02	-0.49458D-05	0.19036D-06
11-15-70	10905	0.60462D-01	-0.22317D-02	-0.12960D-04	0.10771D-06	0.51276D-01	-0.27159D-02	0.52385D-04	-0.13978D-06
05-02-71	11073	-0.17706D-00	0.10542D-02	0.17511D-04	0.30257D-06	0.40436D-00	0.27322D-02	0.14680D-04	-0.44955D-06
07-10-71	11142	0.69938D-01	0.40489D-02	-0.12296D-04	-0.10366D-06	0.51538D-00	-0.17856D-02	-0.23130D-04	0.98062D-07
11-15-71	11270	0.17483D-00	-0.11171D-02	-0.28500D-04	0.14516D-06	0.11980D-00	-0.13099D-02	-0.11916D-04	0.17953D-06
03-30-72	11406	-0.18151D-00	-0.13452D-02	0.37202D-04	-0.91763D-07	0.16428D-00	0.37311D-02	-0.95525D-05	-0.24061D-07
08-21-72	11550	0.12046D-00	0.10719D-02	-0.19086D-05	-0.34012D-07	0.14018D-00	-0.23298D-02	0.19733D-05	-0.37883D-08
12-24-72	11675	0.16047D-00	-0.18834D-02	-0.45416D-06	-0.12531D-07	0.16675D-00	-0.35614D-02	0.17651D-04	-0.15218D-06
04-26-73	11798	-0.10713D-00	-0.81736D-03	0.19310D-04	-0.49338D-07	0.16691D-00	0.21438D-02	-0.44737D-05	-0.93690D-08
01-04-74	12051	0.12471D-00	-0.37360D-03	-0.14384D-04	0.68151D-07	0.24257D-00	-0.21067D-02	0.21696D-04	-0.59668D-07
07-25-74	12253	0.14009D-01	0.23838D-03	0.51712D-05	-0.15292D-06	0.21680D-00	0.53697D-03	-0.25801D-04	0.32254D-06
09-10-74	12300	-0.22000D-01	0.36157D-16	-0.28847D-17	0.62670D-19	0.25641D-00	-0.99723D-03	0.46992D-04	-0.11840D-05
10-09-74	12329	0.21593D-01	-0.15765D-02	0.12341D-04	-0.19666D-07	0.23639D-00	0.84515D-06	-0.35713D-05	0.28599D-07
03-30-75	12501	0.99919D-02	0.19124D-02	-0.24541D-01	0.16709D-06	0.31184D-00	0.75109D-03	-0.40138D-04	0.23771D-06

REPRODUCIBILITY OF THE  
(ORIGINAL PAGE IS POOR)

The time derivative of  $B_2$  is negligible; therefore, the velocity is transformed as follows

$$\dot{\vec{r}}_b = B_2 B_1 \dot{\vec{r}} + B_2 \dot{B}_1 \vec{r} \quad (3-36)$$

where  $\dot{B}_1$  is given by Equation (3-23).

### 3.3.3 Selenocentric True of Date to Selenographic (References 1, 3, 4 and 6)

The lunar landmarks and gravitational potential are referenced to a lunar-centered body-fixed (selenographic) coordinate system. Similar to the earth's geographic system, the selenographic system reference plane is the lunar equator which contains the  $x_b$ - and  $y_b$ -axes. The  $z_b$ -axis is directed towards the lunar axis of rotation.

The moon's mean rotation is described by the following three empirical laws of Cassini.

- (1) The mean axis of rotation is fixed in the moon, perpendicular to the mean lunar equator; the mean period of rotation is equal to the mean sidereal period of revolution of the moon around the earth.
- (2) The mean lunar equator intersects the ecliptic of date at a constant inclination,  $I_M$ , for which the currently accepted value is  $1^\circ 32'.1$ .
- (3) The mean lunar equator, the ecliptic, and the lunar orbit plane meet in the line of nodes of the lunar orbit, with the descending node of the equator at the ascending node of the orbit. The angle  $i$ , between the lunar orbit plane and the ecliptic, is a constant (the currently accepted value is  $5^\circ 8'$ ) as is the angle  $i + I_M$  between the mean lunar equator and the lunar orbit plane. The ecliptic is seen to always lie between the mean lunar equator and the lunar orbit plane.

The oscillation of the actual rotational motion about the mean rotation is called the physical libration. The physical libration consists of small pendulous oscillations, never exceeding approximately  $0^\circ.04$  (in selenographic latitude and longitude), and are caused by deformations in the moon's figure.

As a result of the first law of Cassini, the principal direction of the selenographic system ( $x_b$ -axis direction) defines the lunar prime meridian and has been chosen so that it is, on the average, directed towards the center of the earth disc. The  $x_b$ -axis passes through the Sinus Medii (Central Bay) on the lunar surface. Specifically, the  $x_b$ -axis is defined to be coincident with the vector pointing from the center of the moon to the center of the earth, if the moon were at the mean ascending node when the node coincided with either mean perigee or mean apogee.

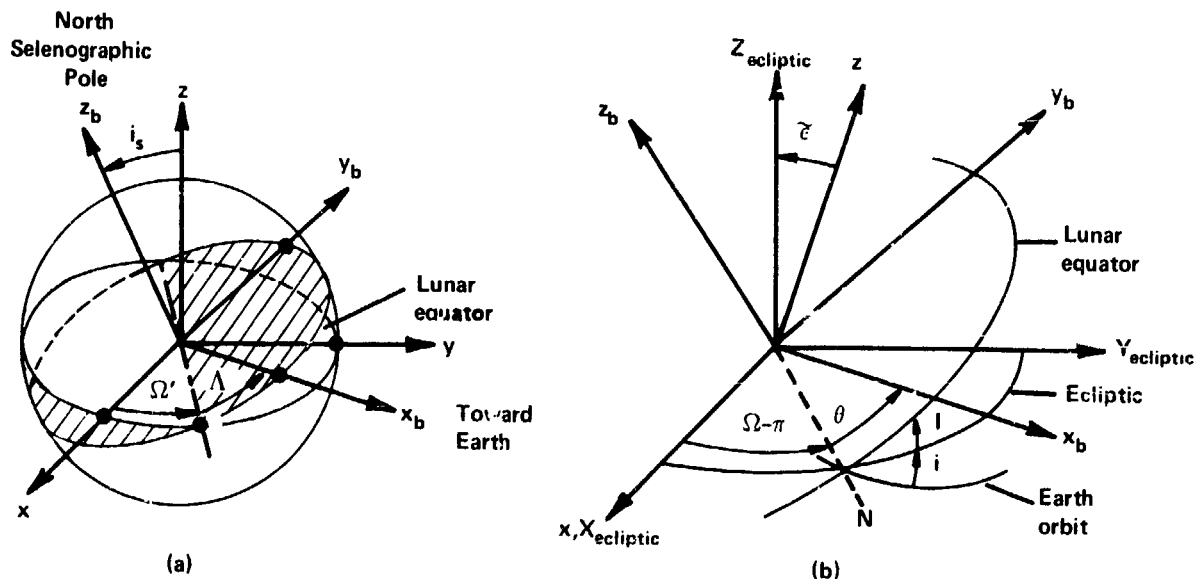


Figure 3-13. Selenocentric/Selenographic Geometry

To transform from the inertial system to the selenographic system, a lunar-centered (selenocentric) coordinate system is defined which is parallel to the earth-centered Cartesian true of date system. The selenographic system  $(x_b, y_b, z_b)$  is oriented relative to the selenocentric system  $(x, y, z)$  by the Euler angles  $\Omega'$ ,  $i_s$ , and  $\Lambda$  shown in Figures 3-13a and 3-14. The transformation between the selenocentric and selenographic systems is

$$\bar{r}_b = M \bar{r} \quad (3-37)$$

where

$$M = R_z(\Lambda) R_x(i_s) R_z(\Omega') \quad (3-38)$$

with  $R_x$  and  $R_z$  given by Equation (3-1). The elements of  $M$  are

$$\begin{aligned} m_{11} &= \cos \Lambda \cos \Omega' - \sin \Lambda \sin \Omega' \cos i_s \\ m_{12} &= \cos \Lambda \sin \Omega' + \sin \Lambda \cos \Omega' \cos i_s \\ m_{13} &= \sin \Lambda \sin i_s \\ m_{21} &= -\sin \Lambda \cos \Omega' - \cos \Lambda \sin \Omega' \cos i_s \\ m_{22} &= -\sin \Lambda \sin \Omega' + \cos \Lambda \cos \Omega' \cos i_s \\ m_{23} &= \cos \Lambda \sin i_s \end{aligned} \quad (3-39)$$

$$m_{31} = \sin \Omega' \sin i_s$$

$$m_{32} = -\cos \Omega' \sin i_s$$

$$m_{33} = \cos i_s$$

Because of the relationship between the moon's mean position and the orientation of the lunar selenographic coordinates, the determination of the Euler angles  $\Omega'$ ,  $i_s$ , and  $\Lambda$  necessarily involves the moon's mean orbit.

Figure 3-13b can be used to relate orbital motion to the lunar centered axes system. It shows the "ecliptic" plane ( $X_{\text{ecliptic}} - Y_{\text{ecliptic}}$ ) which passes through the center of the moon and is parallel to the ecliptic. The lunar equator and orbit planes are shown intersecting in a line on the "ecliptic" plane. The  $x_b$ -axis is shown in the lunar equator. In this moon relative coordinate frame, the earth can be considered as orbiting the moon (the origin) in exactly the same orbit as the moon orbits the earth except that longitude angles measured in the orbit plane must be reduced by 180 degrees. For example, when the earth is at the descending node and the  $x_b$ -axis points towards N in Figure 3-13b, the moon is, in reality, at its ascending node, 180 degrees advanced from N. Therefore, the longitude of the ascending node  $\Omega$  and the mean longitude  $\lambda$  must be reduced by 180 degrees when used in the moon relative frame. The selenographic axes can be oriented to the selenocentric axes by means of the following four angles:  $\xi$ , the true obliquity;  $\Omega - 180^\circ$ , the longitude of the descending node;  $I$ , the inclination of the lunar equator to the ecliptic; and  $\theta$ , the angle measured in the lunar equator between the descending node and the moon's prime meridian. These angles are shown in Figure 3-13b and the transformation is

$$\bar{r}_b = M' \bar{r} \quad (3-40)$$

where

$$M' = R_z(\theta) R_x(I) R_z(\Omega - \pi) R_x(\xi) \quad (3-41)$$

The elements of  $M'$  are

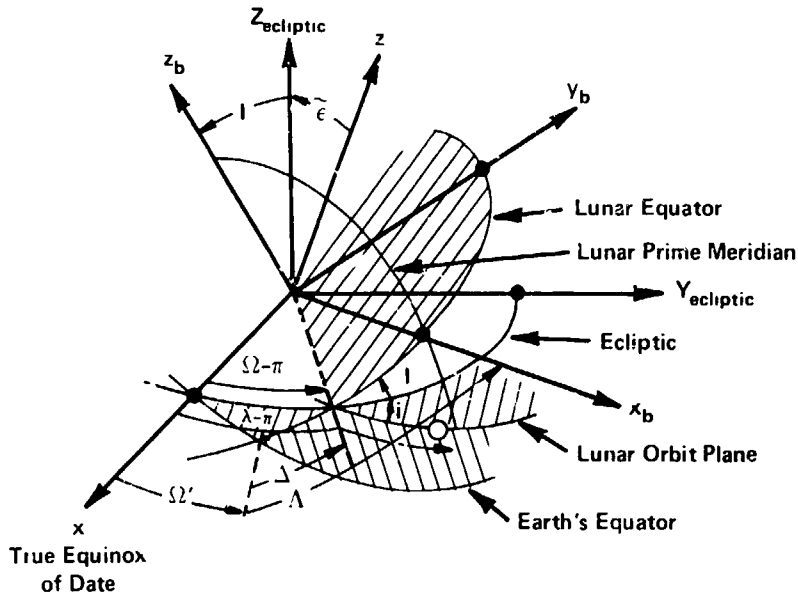


Figure 3-14. Selenographic Transformation Angles

$$m'_{11} = -\cos \theta \cos \Omega + \sin \theta \cos I \sin \Omega$$

$$m'_{12} = -\cos \theta \sin \Omega \cos \tilde{\epsilon} - \sin \theta (\cos I \cos \Omega \cos \tilde{\epsilon} + \sin I \sin \tilde{\epsilon})$$

$$m'_{13} = -\cos \theta \sin \Omega \sin \tilde{\epsilon} - \sin \theta (\cos I \cos \Omega \sin \tilde{\epsilon} - \sin I \cos \tilde{\epsilon})$$

$$m'_{21} = \sin \theta \cos \Omega + \cos \theta \cos I \sin \Omega$$

$$m'_{22} = \sin \theta \sin \Omega \cos \tilde{\epsilon} - \cos \theta (\cos I \cos \Omega \cos \tilde{\epsilon} + \sin I \sin \tilde{\epsilon}) \quad (3-42)$$

$$m'_{23} = \sin \theta \sin \Omega \sin \tilde{\epsilon} - \cos \theta (\cos I \cos \Omega \sin \tilde{\epsilon} - \sin I \cos \tilde{\epsilon})$$

$$m'_{31} = -\sin I \sin \Omega$$

$$m'_{32} = \sin I \cos \Omega \cos \tilde{\epsilon} - \cos I \sin \tilde{\epsilon}$$

$$m'_{33} = \sin I \cos \Omega \sin \tilde{\epsilon} + \cos I \cos \tilde{\epsilon}$$

The Euler angles  $\Omega'$ ,  $i_s$ , and  $\Lambda$  are determined as functions of the orbital parameters  $\tilde{\epsilon}$ ,  $\Omega$ ,  $I$ , and  $\theta$  by equating elements of the  $M$  and  $M'$  matrices. Equating  $m_{33}$  and  $m'_{33}$  yields



$$\cos i_s = \sin I \cos \Omega \sin \tilde{\epsilon} + \cos I \cos \tilde{\epsilon} \quad (3-43)$$

$$\sin i_s = \sqrt{1 - \cos^2 i_s}$$

Equating  $m_{31}$  and  $m_{32}$  to  $m'_{31}$  and  $m'_{32}$ , respectively, yields

$$\sin \Omega' = -\sin I \sin \Omega / \sin i_s \quad (3-44)$$

$$\cos \Omega' = (\cos I \sin \tilde{\epsilon} - \sin I \cos \Omega \cos \tilde{\epsilon}) / \sin i_s$$

Equating  $m_{13}$  and  $m_{23}$  to  $m'_{13}$  and  $m'_{23}$ , respectively, yields

$$\Lambda = \Delta + \theta \quad (3-45)$$

where the parameter  $\Delta$ , shown in Figure 3-14, is obtained from

$$\sin \Delta = -\sin \Omega \sin \tilde{\epsilon} / \sin i_s \quad (3-46)$$

$$\cos \Delta = (\sin I \cos \tilde{\epsilon} - \cos I \cos \Omega \sin \tilde{\epsilon}) / \sin I_s.$$

The angle  $\theta$ , measured along the lunar equator from the descending node to the lunar prime meridian, must be determined from the orbital motion of the moon. As a result of Cassini's first law the mean rate of rotation is equated to the mean orbital rate, resulting in

$$\theta_M = \lambda_M - \Omega_M \quad (3-47)$$

where  $\lambda$  is the mean longitude of the moon,  $\Omega$  the longitude of the ascending node, and the subscript M denotes mean values. Correcting Equation (3-47) for lunar physical librations gives the true value of  $\theta$

$$\theta = (\lambda_M + \tau_M) - (\Omega_M + \sigma_M). \quad (3-48)$$

Correcting  $\Omega$  and  $I$  in Equations (3-43) through (3-46) for nutation and libration yields their true values

$$\Omega = \Omega_M + \sigma_M + \delta\psi \quad (3-49)$$

$$I = I_M + \rho_M \quad (3-50)$$

The longitude of the mean ascending node of the lunar orbit is (Reference 4)

$$\begin{aligned} \Omega_M = & 12^\circ 1127902 - .0529539222 d_e + .20795(10^{-2}) T_e \\ & + .2081(10^{-2}) T_e^2 + .2(10^{-5}) T_e^3, \end{aligned} \quad (3-51)$$

the inclination of the mean lunar equator to the ecliptic is

$$I_M = 1^\circ 32' 1, \quad (3-52)$$

and the geocentric mean longitude of the moon is

$$\begin{aligned} \lambda_M = & 64^\circ 37545167 + 13^\circ 1763955268 d_e - .1131575(10^{-2}) T_e \\ & - .113015(10^{-2}) T_e^2 + .19(10^{-5}) T_e^3. \end{aligned} \quad (3-53)$$

The  $T_e$ -variable and  $d_e$ -variable in the above equations correspond to the number of Julian centuries of 36525 Julian ephemeris days past 0<sup>h</sup> January 1, 1950 ET, and the number of ephemeris days past the same date, respectively.

The nutation in longitude,  $\delta\psi$ , and the true obliquity,  $\varepsilon$ , are given in Section 3.3.1.2. The physical librations, determined by Hayn, in longitude of the ascending node,  $\sigma_M$ , inclination,  $\rho_M$ , and mean longitude,  $\tau_M$ , are as follows:

$$\sigma_M = [-0.0302777 \sin(g) + 0.0102777 \sin(g + 2\omega_M) - 0.305555(10^{-2}) \sin(2g + 2\omega_M)] / \sin I_M. \quad (3-54)$$

$$\rho_M = -0.0297222 \cos(g) + 0.0102777 \cos(g + 2\omega_M) - 0.305555(10^{-2}) \cos(2g + 2\omega_M). \quad (3-55)$$

$$\tau_M = -0.3333(10^{-2}) \sin(g) + 0.0163888 \sin(g') + 0.5(10^{-2}) \sin(2\omega_M). \quad (3-56)$$

where the parameter  $g$  is the moon's mean anomaly

$$g = 215.954013 + 13.064992 d_e \quad (3-57)$$

the parameter  $g'$  is the sun's mean anomaly

$$g' = 358.909067 + 0.9856005 d_e \quad (3-58)$$

and  $\omega_M$  is the moon's argument of perigee

$$\omega_M = 196.745632 + 0.1643586 d_e \quad (3-59)$$

The variables above are substituted into Equations (3-43) through (3-45) to yield the Euler angles  $\Omega'$ ,  $i_s$ , and  $\Lambda$  required in the selenocentric to selenographic transformation given by Equations (3-37) through (3-39).

The velocity transformation from selenocentric to selenographic coordinates is obtained by differentiating Equation (3-37), yielding

$$\dot{\vec{r}}_b = \dot{M} \vec{r} + \dot{M} \vec{r} \quad (3-60)$$

The time derivative of  $M$  is obtained by differentiating its elements in Equation (3-39) with  $\dot{\Omega}$  and  $i_s$  assumed zero, i.e.,

$$\dot{M} = \dot{\Lambda} \begin{bmatrix} m_{21} & m_{22} & m_{23} \\ -m_{11} & -m_{12} & -m_{13} \\ 0 & 0 & 0 \end{bmatrix} \quad (3-61)$$

The time derivative of  $\Lambda$  is obtained by differentiating Equation (3-45) after substituting Equation (3-48) for  $\theta$ . The resulting time derivative is

$$\dot{\Lambda} = \dot{\Delta} + \dot{\lambda}_M + \dot{\tau}_M - \dot{\Omega}_M - \dot{\sigma}_M \quad (3-62)$$

where

$$\dot{\Delta} = [-\cos(\Omega_M + \sigma_M + \Delta\psi) \sin \tilde{\epsilon}(\dot{\Omega}_M + \dot{\sigma}_M)] / (\sin i_s \cos \Delta) \quad (3-63a)$$

$$\dot{\lambda}_M = .266170762(10^{-5}) - .12499171(10^{-13}) T_e \quad (3-63b)$$

$$\dot{\Omega}_M = -.1069698435(10^{-7}) + .23015329(10^{-13}) T_e \quad (3-63c)$$

and

$$\dot{\tau}_M = -.1535272946(10^{-9}) \cos g + .569494067(10^{-10}) \cos g' \quad (3-64a)$$

$$+ .579473484(10^{-11}) \cos 2\omega_M$$

$$\begin{aligned} \dot{\sigma}_M = & -.520642191(10^{-7}) \cos g \\ & + .1811774451(10^{-7}) \cos(g + 2\omega_M) \end{aligned} \quad (3-64b)$$

$$- .1064057858(10^{-7}) \cos(2\omega_M + 2g)$$

### 3.3.4 Spherical-Cartesian Transformations (Reference 7)

#### 3.3.4.1 Spherical Position and Velocity to Cartesian Coordinates

Using the spherical position coordinates,  $r$ ,  $\alpha$ , and  $\delta$ , that are defined in Section 3.2.1, the transformation to Cartesian coordinates is seen from Figure 3-1 to be

$$\begin{bmatrix} x \\ y \\ z \end{bmatrix} = r \begin{bmatrix} \cos \delta \cos \alpha \\ \cos \delta \sin \alpha \\ \sin \delta \end{bmatrix} \quad (3-65)$$

To transform the spherical velocity coordinates,  $V$ ,  $\beta$ , and  $A$ , described in Section 3.2.3, it is convenient to transform to the local plane coordinate system (see Figure 3-3) and then to the body-centered inertial Cartesian coordinate system. If the local plane coordinates,  $x_{lp}$ ,  $y_{lp}$ , and  $z_{lp}$ , are fixed inertially (nonrotating),  $\dot{\bar{r}}_{lp}$  may be expressed as

$$\dot{\bar{r}}_{lp} = \begin{bmatrix} \dot{x}_{lp} \\ \dot{y}_{lp} \\ \dot{z}_{lp} \end{bmatrix} = V \begin{bmatrix} \cos \beta \\ \sin A \sin \beta \\ \cos A \sin \beta \end{bmatrix} \quad (3-66)$$

The transformation between the local plane and the body-centered inertial Cartesian coordinate systems is

$$\bar{r}_{lp} = D\bar{r} \quad (3-67)$$

where

$$D = \begin{bmatrix} \cos \delta \cos \alpha & \cos \delta \sin \alpha & \sin \delta \\ -\sin \alpha & \cos \alpha & 0 \\ -\sin \delta \cos \alpha & -\sin \delta \sin \alpha & \cos \delta \end{bmatrix} \quad (3-68)$$

Since the local plane system is fixed inertially, the velocity vector in Equation (3-66) may be transformed to the body-centered inertial Cartesian axes by means of the transformation D as follows

$$\dot{\bar{\mathbf{r}}} = \mathbf{D}^T \dot{\mathbf{r}}_{1p}. \quad (3-69)$$

The partial derivatives of  $x$ ,  $y$ ,  $z$ ,  $\dot{x}$ ,  $\dot{y}$ , and  $\dot{z}$  with respect to  $r$ ,  $\alpha$ ,  $\delta$ ,  $V$ ,  $A$ , and  $\beta$  are

$$\frac{\partial \bar{\mathbf{r}}}{\partial r} = \frac{\bar{\mathbf{r}}}{r} \quad (3-70)$$

$$\frac{\partial \bar{\mathbf{r}}}{\partial \alpha} = \begin{bmatrix} -y \\ x \\ 0 \end{bmatrix} \quad (3-71)$$

$$\frac{\partial \bar{\mathbf{r}}}{\partial \delta} = \begin{bmatrix} -z \cos \alpha \\ -z \sin \alpha \\ \sqrt{x^2 + y^2} \end{bmatrix} \quad (3-72)$$

$$\frac{\partial \bar{\mathbf{r}}}{\partial V} = \frac{\partial \bar{\mathbf{r}}}{\partial A} = \frac{\partial \bar{\mathbf{r}}}{\partial \beta} = \frac{\partial \dot{\bar{\mathbf{r}}}}{\partial r} = 0 \quad (3-73)$$

$$\frac{\partial \dot{\bar{\mathbf{r}}}}{\partial \alpha} = \begin{bmatrix} -\dot{y} \\ \dot{x} \\ 0 \end{bmatrix} \quad (3-74)$$

$$\frac{\partial \dot{\bar{\mathbf{r}}}}{\partial \delta} = \begin{bmatrix} -\dot{z} \cos \alpha \\ -\dot{z} \sin \alpha \\ V(\cos \beta \cos \delta - \cos A \sin \beta \sin \delta) \end{bmatrix} \quad (3-75)$$

$$\frac{\partial \dot{\bar{\mathbf{r}}}}{\partial V} = \frac{\dot{\bar{\mathbf{r}}}}{V} \quad (3-76)$$

$$\frac{\partial \dot{\bar{\mathbf{r}}}}{\partial A} = V \begin{bmatrix} \sin \beta (\sin A \sin \delta \cos \alpha - \cos A \sin \alpha) \\ \sin \beta (\sin A \sin \delta \sin \alpha + \cos A \cos \alpha) \\ -\sin A \cos \delta \sin \beta \end{bmatrix} \quad (3-77)$$

and

$$\frac{\partial \dot{\bar{\mathbf{r}}}}{\partial \beta} = -V \begin{bmatrix} \cos \alpha (\cos \delta \sin \beta + \sin \delta \cos \beta \cos A) + \sin \alpha \cos \beta \sin A \\ \sin \alpha (\cos \delta \sin \beta + \sin \delta \cos \beta \cos A) - \cos \alpha \cos \beta \sin A \\ \sin \beta \sin \delta - \cos \beta \cos \delta \cos A \end{bmatrix} \quad (3-78)$$

### 3.3.4.2 Cartesian Position and Velocity to Spherical Coordinates

The inverse of the preceding transformations is described in the following text. The spherical radius,  $r$ , is given by

$$r = \sqrt{x^2 + y^2 + z^2}. \quad (3-79)$$

From Figure 3-1 the right ascension,  $\alpha$ , and declination,  $\delta$ , of  $\bar{\mathbf{r}}$  are

$$\sin \alpha = \frac{y}{\sqrt{x^2 + y^2}} \quad \cos \alpha = \frac{x}{\sqrt{x^2 + y^2}} \quad 0 \leq \alpha \leq 2\pi, \quad (3-80)$$

and

$$\sin \delta = \frac{z}{r} \quad \cos \delta = \frac{\sqrt{x^2 + y^2}}{r} \quad -\frac{\pi}{2} \leq \delta \leq \frac{\pi}{2} \quad (3-81)$$

The right ascension is measured positive east from the inertial x-axis. The declination is measured positive north from the x-y plane.

The velocity vector's magnitude is

$$V = \sqrt{\dot{x}^2 + \dot{y}^2 + \dot{z}^2} \quad (3-82)$$

and the azimuth,  $A$ , and flight path angle,  $\beta$ , are obtained from the local plane components of velocity

$$\sin A = \frac{\dot{y}_{1p}}{\sqrt{\dot{y}_{1p}^2 + \dot{z}_{1p}^2}} \quad \cos A = \frac{\dot{z}_{1p}}{\sqrt{\dot{y}_{1p}^2 + \dot{z}_{1p}^2}} \quad 0 \leq A \leq 2\pi. \quad (3-83)$$

and

$$\sin \beta = \frac{\sqrt{\dot{y}_{1p}^2 + \dot{z}_{1p}^2}}{V} \quad \cos \beta = \frac{\dot{x}_{1p}}{V} \quad -\frac{\pi}{2} \leq \beta \leq \frac{\pi}{2} \quad (3-84)$$

The azimuth and flight path angles may be obtained alternatively from the vector products of  $\bar{r}$  and  $\dot{\bar{r}}$  as follows

$$\sin A = \bar{U}_{z_{1p}} \cdot \bar{U}_N \quad \cos A = \frac{\bar{U}_{z_{1p}} \cdot (\bar{U}_N \times \bar{r})}{r} \quad (3-85)$$

and

$$\sin \beta = \frac{|\bar{r} \times \dot{\bar{r}}|}{rV} \quad \cos \beta = \frac{\bar{r} \cdot \dot{\bar{r}}}{rV} \quad (3-86)$$

where  $\bar{U}_{z_{1p}}$  is the unit vector in the  $\bar{z}_{1p}$ -axis direction and has components expressed in the body-centered Cartesian system

$$\bar{U}_{z_{1p}} = \begin{bmatrix} -\sin \delta \cos \alpha \\ -\sin \delta \sin \alpha \\ \cos \delta \end{bmatrix} \quad (3-87)$$

and  $\bar{U}_N$  is the unit vector normal to  $\bar{r}$  and  $\dot{\bar{r}}$



$$\bar{U}_N = \frac{\bar{r} \times \bar{V}}{|\bar{r} \times \bar{V}|} \quad (3-88)$$

Substituting Equations (3-87) and (3-88) into Equation (3-85) yields

$$\sin A = \frac{(x\dot{y} - y\dot{x})}{rV \sin \beta \cos \delta}, \quad \cos A = \frac{y(y\dot{z} - z\dot{y}) + x(x\dot{z} - \dot{x}z)}{r^2V \sin \beta \cos \delta} \quad (3-89)$$

The partial derivatives of  $r$ ,  $\alpha$ ,  $\delta$ ,  $V$ ,  $A$ , and  $\beta$  with respect to  $x$ ,  $y$ ,  $z$ ,  $\dot{x}$ ,  $\dot{y}$ , and  $\dot{z}$  are

$$\frac{\partial r}{\partial \bar{r}} = \frac{\bar{r}^T}{r} \quad (3-90)$$

$$\frac{\partial \alpha}{\partial \bar{r}} = \frac{1}{(x^2 + y^2)} \begin{bmatrix} -y \\ x \\ 0 \end{bmatrix}^T \quad (3-91)$$

$$\frac{\partial \delta}{\partial \bar{r}} = \frac{1}{r^2 \sqrt{x^2 + y^2}} \begin{bmatrix} -zx \\ -zy \\ (x^2 + y^2) \end{bmatrix}^T \quad (3-92)$$

$$\frac{\partial V}{\partial \bar{r}} = [0]^T \quad (3-93)$$

$$\frac{\partial A}{\partial \bar{r}} = \frac{1}{(V^2 - \dot{r}^2)(x^2 + y^2)} \begin{bmatrix} \dot{y}(r\dot{z} - z\dot{r}) - (x\dot{y} - y\dot{x}) \left( x\dot{z} - z\dot{x} + \frac{xz\dot{r}}{r} \right) / r \\ \dot{x}(r\dot{z} - z\dot{r}) + (x\dot{y} - y\dot{x}) \left( y\dot{z} - z\dot{y} + \frac{yz\dot{r}}{r} \right) / r \\ (x\dot{y} - y\dot{x})(x^2 + y^2) \dot{r} / r^2 \end{bmatrix}^T \quad (3-94)$$

$$\frac{\partial \beta}{\partial \bar{r}} = \frac{1}{r^2 \sqrt{V^2 - \dot{r}^2}} \left( \frac{\bar{r}^T \dot{\bar{r}}}{r} - \frac{\dot{\bar{r}}^T \bar{r}}{\dot{r}} \right) \quad (3-95)$$

$$\frac{\partial \bar{r}}{\partial \dot{\bar{r}}} = \frac{\partial \alpha}{\partial \dot{\bar{r}}} = \frac{\partial \delta}{\partial \dot{\bar{r}}} = 0 \quad (3-96)$$

$$\frac{\partial V}{\partial \dot{\bar{r}}} = \frac{\dot{\bar{r}}^T}{V} \quad (3-97)$$

$$\frac{\partial \mathbf{A}}{\partial \dot{\bar{r}}} = \frac{1}{r(V^2 - \dot{r}^2)} \begin{bmatrix} (z\dot{y} - y\dot{z}) \\ (x\dot{z} - z\dot{x}) \\ (y\dot{x} - x\dot{y}) \end{bmatrix}^T \quad (3-98)$$

and

$$\frac{\partial \beta}{\partial \dot{\bar{r}}} = \frac{1}{r^2 \sqrt{V^2 - \dot{r}^2}} \left( \dot{\bar{r}}^T \frac{\dot{\bar{r}}^T \bar{r}}{V^2} - \bar{r} \right)^T \quad (3-99)$$

### 3.3.5 Body-Centered True of Date to Orbit Plane

The unit vectors in the  $x_{op}$ ,  $y_{op}$ , and  $z_{op}$  directions (see Figure 3-5), measured in the body-centered true of date coordinate system, are

$$\begin{aligned} \bar{U} &= \frac{\bar{r}_0}{|\bar{r}_0|} \\ \bar{V} &= \bar{W} \times \bar{U} \\ \bar{W} &= \frac{\bar{r}_0 \times \dot{\bar{r}}_0}{|\bar{r}_0 \times \dot{\bar{r}}_0|} \end{aligned} \quad (3-100)$$

where  $\bar{r}_0$  and  $\dot{\bar{r}}_0$  are the earth-centered position and velocity vectors used to determine the orbit plane coordinate system. If Equations (3-100) are expanded, they yield the following transformation relations between the orbit plane coordinates and the body-centered inertial Cartesian coordinates

$$\bar{\mathbf{r}}_{op} = \mathbf{E} \bar{\mathbf{r}} \quad (3-101)$$

where

$$\mathbf{E} = \begin{bmatrix} U_x & U_y & U_z \\ V_x & V_y & V_z \\ W_x & W_y & W_z \end{bmatrix} \quad (3-102)$$

Regarding the orbit plane system as fixed inertially, the velocity transforms as follows

$$\dot{\bar{\mathbf{r}}}_{op} = \mathbf{E} \dot{\bar{\mathbf{r}}} \quad (3-103)$$

and the position and velocity partial derivatives are

$$\frac{\partial \bar{\mathbf{r}}_{op}}{\partial \bar{\mathbf{r}}} = \frac{\partial \dot{\bar{\mathbf{r}}}_{op}}{\partial \dot{\bar{\mathbf{r}}}} = \mathbf{E}. \quad (3-104)$$

### 3.3.6 Body-Fixed to Geographic Transformations

The transformations between the body-centered rotating coordinate system and the geographic coordinates are described in Section 3.2.2. The transformation involves modeling the body's mean figure. The following subsections present the equations for an ellipsoidal earth model as well as the transformations and partial derivatives relating the geodetic coordinates ( $h, \lambda, \phi$ ) to the body-centered rotating coordinates ( $x_b, y_b, z_b$ ).

#### 3.3.6.1 Earth Figure (Reference 7)

The shape of the earth's surface is very nearly an ellipsoid of revolution. A satisfactory means for modeling the earth is to characterize it as such and, where necessary, correct local deflections of the vertical (e.g., correct local astronomic zenith to ellipsoidal vertical). The polar axis of symmetry of the ellipsoid,  $z_b$ , is nearly colinear with the earth's spin axis. The ellipsoid's radius is greatest in the  $x_b - y_b$  equatorial plane. Letting  $R_e$  denote the equatorial radius,  $R_p$  the polar radius, and  $x_s, y_s$ , and  $z_s$  the coordinates of

a point  $s$  on the ellipsoidal surface expressed in the body-centered rotating axis, then the coordinates of  $s$  must satisfy the following equation

$$\frac{x_s^2}{R_e^2} + \frac{y_s^2}{R_e^2} + \frac{z_s^2}{R_p^2} = 1 \quad (3-105)$$

Two convenient parameters which describe the elliptical cross-section are the flattening coefficient,  $f$ , defined by

$$f = \frac{R_e - R_p}{R_e} > 0 \quad (3-106)$$

and the eccentricity,  $e$

$$e^2 = 1 - \left(\frac{R_p}{R_e}\right)^2 = f(2 - f). \quad (3-107)$$

Since the ellipsoid is symmetrical about the  $z_b$ -axis, there is no loss of generality in restricting the analysis to the  $x_b - z_b$  plane. The two-dimensional analysis utilizes the symbol  $x_{s'}$  to denote that the  $y$  component is omitted.

The equation of the cross-section of the ellipsoid is

$$x_{s'}^2 + \frac{z_s^2}{(1 - e^2)} = R_e^2. \quad (3-108)$$

The equation for the normal to the ellipsoid is

$$\tan \phi = - \frac{dx_{s'}}{dz_s} \quad (3-109)$$

where  $\phi$  is the geodetic latitude shown in Figure 3-15. Differentiating Equation (3-108) and substituting the results into Equation (3-109) yields

$$\frac{z_s}{x_{s'}} = (1 - e^2) \tan \phi. \quad (3-110)$$

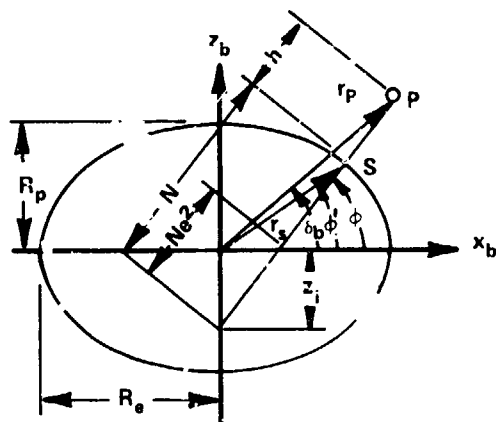


Figure 3-15. Ellipsoid Geometry

Solving Equations (3-108) and (3-110) simultaneously for  $x_s$ , yields

$$x_s = \frac{R_e \cos \phi}{\sqrt{1 - e^2 \sin^2 \phi}} \quad (3-111)$$

From Figure 3-15, it is evident that

$$x_s = N \cos \phi \quad (3-112a)$$

$$z_s = r_s \sin \phi' = N(1 - e^2) \sin \phi \quad (3-112b)$$

where  $N$  is the distance from the point  $s$  to the  $z_b$  axis measured along the normal vector to the ellipsoid at point  $s$ . Substituting Equation (3-111) into Equation (3-112a) yields

$$N = \frac{R_e}{\sqrt{1 - e^2 \sin^2 \phi}} = \frac{R_t}{\sqrt{1 - (2f - f^2) \sin^2 \phi}} \quad (3-113)$$

The ellipsoidal radius is

$$r_s = \sqrt{x_s^2 + z_s^2} \quad (3-114)$$

Substituting Equations (3-108) and (3-114) into Equation (3-114) yields

$$r_s = \frac{a_e(1-f)}{\sqrt{1-e^2 \cos^2 \phi'}} \quad (3-115)$$

where  $\phi'$  is the geocentric latitude.

### 3.3.6.2 Geodetic to Earth-Fixed Transformation

Assume that point P in Figure 3-15 has the coordinates  $x_b$ ,  $y_b$ , and  $z_b$  in the body-axis system and is located a distance  $h$  from the reference ellipsoid. From Equation (3-110) and Figure 3-15, the  $x_b$  and  $z_b$  coordinates are

$$x_b = x_s + h \cos \phi = (N + h) \cos \phi \quad (3-116)$$

and

$$z_b = z_s + h \sin \phi = [N(1 - e^2) + h] \sin \phi \quad (3-117)$$

Transforming Equations (3-116) and (3-117) to three dimensions yields

$$\begin{bmatrix} x_b \\ y_b \\ z_b \end{bmatrix} = \begin{bmatrix} (N + h) \cos \phi \cos \lambda \\ (N + h) \cos \phi \sin \lambda \\ [N(1 - e^2) + h] \sin \phi \end{bmatrix} \quad (3-118)$$

The partial derivatives of  $x_b$ ,  $y_b$ , and  $z_b$  with respect to  $h$ ,  $\lambda$ , and  $\phi$  are

$$\begin{bmatrix} \partial x_b / \partial h \\ \partial y_b / \partial h \\ \partial z_b / \partial h \end{bmatrix} = \begin{bmatrix} \cos \phi \cos \lambda \\ \cos \phi \sin \lambda \\ \sin \phi \end{bmatrix} \quad (3-119)$$

$$\begin{bmatrix} \partial x_b / \partial \lambda \\ \partial y_b / \partial \lambda \\ \partial z_b / \partial \lambda \end{bmatrix} = \begin{bmatrix} -(N+h) \cos \phi \sin \lambda \\ (N+h) \cos \phi \cos \lambda \\ 0 \end{bmatrix} \quad (3-120)$$

$$\begin{bmatrix} \partial x_b / \partial \phi \\ \partial y_b / \partial \phi \end{bmatrix} = \left( N+h - \frac{Ne^2 \cos^2 \phi}{1 - e^2 \sin^2 \phi} \right) \begin{bmatrix} -\sin \phi \cos \lambda \\ -\sin \phi \sin \lambda \end{bmatrix} \quad (3-121a)$$

and

$$[\partial z_b / \partial \phi] = \left( h + N(1 - e^2) \left( 1 + \frac{e^2 \sin^2 \phi}{1 - e^2 \sin^2 \phi} \right) \right) [\cos \phi]. \quad (3-121b)$$

### 3.3.6.3 Earth-Fixed to Geodetic

In transforming geodetic coordinates  $(h, \phi, \lambda)$  to earth-fixed coordinates  $(x_b, y_b, z_b)$ , the point of intersection of the height normal vector and the ellipsoid (i.e., point  $s$ ) is given. In transforming from earth-fixed to geodetic coordinates, this point is not known a priori, complicating the transformation.

Two solutions are presented. The first solution is iterative and can yield any required degree of accuracy. The second solution is a truncated binomial expansion that may be used when accuracy requirements are not so stringent.

The iterative technique is used primarily to determine geodetic tracking station positions where high accuracy is required. For this use (and for near earth satellites), the approximation  $h \ll N$  is satisfied, and since the earth's figure is nearly spherical,  $e^2 \ll 1$ . Therefore, from Equation (3-118), the following approximation can be made:

$$N \sin \phi \approx z_b. \quad (3-122)$$

Introducing  $z_i$ , the  $z_b$  intercept of the normal vector, it is apparent from Figure 3-15 that

$$z_i = -Ne^2 \sin \phi. \quad (3-123)$$

Combining Equations (3-122) and (3-123), the following approximation for  $z_i$  is obtained

$$z_i = -e^2 z_b. \quad (3-124)$$

Using Equation (3-124) as an initial estimate for  $z_i$ , the following sequence of equations may be solved iteratively to yield a solution for  $h$  and  $\phi$

$$z_{ib} = z_b - z_i \quad (3-125)$$

$$N + h = \sqrt{x_b^2 + y_b^2 + z_{ib}^2} \quad (3-126)$$

$$\sin \phi = \frac{z_{ib}}{N + h} \quad (3-127)$$

$$N = \frac{R_e}{\sqrt{1 - e^2 \sin^2 \phi}} \quad (3-128)$$

$$z_i = -Ne^2 \sin \phi. \quad (3-129)$$

Upon convergence of  $z_i$ , the altitude,  $h$ , and latitude,  $\phi$ , are obtained from Equations (3-126) and (3-127). The longitude  $\lambda$ , is

$$\lambda = \tan^{-1} \left( \frac{y_b}{x_b} \right), \quad 0 \leq \lambda \leq 2\pi \quad (3-130)$$



A second, computationally simpler, procedure for computing the values of  $\phi$  and  $h$  to a specified point, P, is useful when accuracy requirements are less stringent. The latitude,  $\phi$ , is solved for from Equation (3-110) as follows

$$\tan \phi = \frac{z_s}{(1 - e^2) x_s} = \frac{z_s}{(1 - e^2) \sqrt{x_s^2 + y_s^2}} \quad (3-131)$$

where  $x_b$ ,  $y_b$ , and  $z_b$  of point P are used to approximate the subvehicle point on the ellipsoid,  $(x_s, y_s, z_s)$ , required in Equation (3-131).

This approximation yields the geodetic latitude to the normal vector of an expanded ellipse through point P. For  $h \ll N$  and  $e^2 \ll 1$ , it is a good approximation for the geodetic latitude.

Applying the Binomial Theorem to Equation (3-115) yields

$$r_s = R_e \left[ 1 - \left( f + \frac{3}{2} f^2 \right) \sin^2 \phi' + \frac{3}{2} f^2 \sin^4 \phi' \right] \quad (3-132)$$

where terms of  $f$  higher than second order are neglected. The geodetic height is nearly

$$h = r_b - r_s. \quad (3-133)$$

Substituting Equation (3-132) into Equation (3-133) yields

$$h = \sqrt{x_b^2 + y_b^2 + z_b^2} - R_e + \left( R_e f + \frac{3}{2} R_e f^2 \right) \sin^2 \phi' - \frac{3}{2} R_e f^2 \sin^4 \phi'. \quad (3-134)$$

The geocentric latitude required in Equation (3-134) is approximated by

$$\phi' = \sin^{-1} \left( \frac{z_b}{r_b} \right). \quad (3-135)$$

The partial derivatives of  $h$ ,  $\lambda$ , and  $\phi$  with respect to  $x_b$ ,  $y_b$ , and  $z_b$  are obtained by differentiating Equations (3-126), (3-130), and (3-127) to yield

$$\begin{bmatrix} \partial h / \partial x_b \\ \partial h / \partial y_b \\ \partial h / \partial z_b \end{bmatrix} = - \left( \frac{e^2 a (1 - e^2) \sin \phi \cos \phi}{(1 - e^2 \sin^2 \phi)^{3/2}} + \frac{z_b \cos \phi}{\sin^2 \phi} \right) \begin{bmatrix} \partial \phi / \partial x_b \\ \partial \phi / \partial y_b \\ \partial \phi / \partial z_b \end{bmatrix} \quad (3-136)$$

$$\begin{bmatrix} \partial \lambda / \partial x_b \\ \partial \lambda / \partial y_b \\ \partial \lambda / \partial z_b \end{bmatrix} = \frac{1}{(x_b^2 + y_b^2)} \begin{bmatrix} -y_b \\ x_b \\ 0 \end{bmatrix} \quad (3-137)$$

and

$$\begin{bmatrix} \partial \phi / \partial x_b \\ \partial \phi / \partial y_b \\ \partial \phi / \partial z_b \end{bmatrix} = \frac{(1 - e^2)}{\sqrt{x_b^2 + y_b^2} [(1 - e^2 \sin^2 \phi) (x_b^2 + y_b^2) + z_b^2]} \begin{bmatrix} -x_b z_b \\ -y_b z_b \\ (x_b^2 + y_b^2) \end{bmatrix}. \quad (3-138)$$

### 3.3.7 Earth-Fixed to Topocentric Local Tangent (East, North, Up)

The topocentric local tangent system, described in Section 3.2.4, is used in processing ground based observation data. The transformation from geocentric earth-fixed coordinates  $(x_b, y_b, z_b)$  to local tangent coordinates  $(x_{lt}, y_{lt}, z_{lt})$  requires a translation along the geocentric radius vector to the station and a rotation of the axis through the station's longitude and latitude angles. The station parameters are defined as follows

- $\bar{r}_s \sim$  the body-fixed coordinates of the station
- $\phi_s \sim$  the geodetic latitude of the station (positive north)
- $\phi'_s \sim$  the geocentric latitude of the station
- $\lambda_s \sim$  the longitude of the station (positive east)
- $h_s \sim$  the height of the station above the reference ellipsoid.

The magnitude of the normal vector to the reference spheroid's surface at the station is given by Equation (3-113) to be

$$N_s = \frac{R_e}{\sqrt{1 - (2f - f^2) \sin^2 \phi_s}} \quad (3-139)$$

The components of the geocentric radius vector to the station along the  $x_b$ ,  $y_b$ , and  $z_b$  axes are given by Equation (3-118) to be

$$\begin{bmatrix} x_s \\ y_s \\ z_s \end{bmatrix} = \begin{bmatrix} (N_s + h_s) \cos \phi_s \cos \lambda_s \\ (N_s + h_s) \cos \phi_s \sin \lambda_s \\ [N_s(1 - e^2) + h_s] \sin \phi_s \end{bmatrix} \quad (3-140)$$

To bring the  $x_b$ ,  $y_b$ , and  $z_b$  axes parallel to the  $x_{lt}$ ,  $y_{lt}$ , and  $z_{lt}$  axes, a rotation is made about the  $z_b$  axis by the angle  $(\pi/2 + \lambda_s)$  and about the new  $x_b$  axis by the angle  $(\pi/2 - \phi_s)$ . The resulting transformation matrix  $M_{lt}$  may be written as

$$M_{lt} = \begin{bmatrix} -\sin \lambda_s & \cos \lambda_s & 0 \\ -\sin \phi_s \cos \lambda_s & -\sin \phi_s \sin \lambda_s & \cos \phi_s \\ \cos \phi_s \cos \lambda_s & \cos \phi_s \sin \lambda_s & \sin \phi_s \end{bmatrix} \quad (3-141)$$

The local tangent coordinates of a point in space,  $x_b$ ,  $y_b$ , and  $z_b$ , may be written as

$$\bar{r}_{lt} = M_{lt} (\bar{r}_b - \bar{r}_s). \quad (3-142)$$

This translates the system from the earth's center to the station and rotates it to the local tangent system.

The earth-fixed velocity in the local tangent system is given by

$$\dot{\bar{r}}_{lt} = M_{lt} \dot{\bar{r}}_b \quad (3-143)$$

since  $\dot{M}_{lt} = 0$  and  $\dot{\bar{r}}_s = 0$ .

The partial derivatives of the local tangent components with respect to the earth-fixed components are the respective elements of the  $M_{1t}$  matrix given by

$$\frac{\partial \bar{r}_{1t}}{\partial \bar{r}_b} = \frac{\partial \dot{\bar{r}}_{1t}}{\partial \dot{\bar{r}}_b} = M_{1t}. \quad (3-144)$$

### 3.3.8 Keplerian-Cartesian Transformations (References 7 and 8)

#### 3.3.8.1 Keplerian Elements to Body-Centered True of Date Coordinates

Consider the orbit geometry illustrated in Figure 3-5. The origin is the center of the reference body, the x-axis points to the vernal equinox, and the z-axis lies along the reference body's rotation axis. The satellite orbital plane intersects the equator at the nodes. The angle  $\Omega$  is the right ascension of the ascending node. The axis  $z_{op}$  is normal to the orbital plane defining the orbit's inclination. The angle  $\omega$  is the argument of perifocus. In Figure 3-6, the eccentricity,  $e$ , and semimajor axis,  $a$ , specify the orbit's shape and size. The final element necessary to predict a body's position and velocity is the mean anomaly  $M$ . However, the eccentric anomaly,  $E$ , or true anomaly,  $f$ , can be used instead of  $M$  to define the satellite's position in its orbit.

First, consider the transformation from the orbital elements ( $a, e, i, \Omega, \omega, m$ ) to the orbital rectangular coordinates ( $x_p, y_p, z_p, \dot{x}_p, \dot{y}_p, \dot{z}_p$ ). The  $x_p$  axis is directed toward perifocus, the  $y_p$  axis is in the plane of motion advanced  $\pi/2$  from the  $x_p$ -axis in the direction of motion, and the  $z_p$  axis is normal to the orbit plane and completes a right-handed system. The transformations for elliptic, hyperbolic and parabolic orbits are given below.

- Ellipse:  $0 \leq e < 1$

$$\begin{bmatrix} x_p \\ y_p \\ z_p \end{bmatrix} = a \begin{bmatrix} \cos E - e \\ \sin E \sqrt{1 - e^2} \\ 0 \end{bmatrix} \quad (3-145)$$

and

$$\begin{bmatrix} \dot{x}_p \\ \dot{y}_p \\ \dot{z}_p \end{bmatrix} = \frac{\sqrt{\mu/a}}{(1 - e \cos E)} \begin{bmatrix} -\sin E \\ \cos E \sqrt{1 - e^2} \\ 0 \end{bmatrix} \quad (3-146)$$

where

$E \sim$  the eccentric anomaly

$\mu \sim$  the gravitational parameter of the reference body.

The eccentric anomaly,  $E$ , is computed by Kepler's equation

$$M = E - e \sin E \quad (3-147)$$

where  $M$  is the mean anomaly defined in Section 3.2.6. This equation is solved by the following iteration scheme

$$\mathfrak{F}(E_n) = E_n - e \sin E_n - M \quad (3-148)$$

$$D_n = 1 - e \cos [E_n - .5 \mathfrak{F}(E_n)] \quad (3-149)$$

$$E_{n+1} = E_n - \frac{\mathfrak{F}(E_n)}{D_n} \quad n = 0, 1, 2, 3, \dots \quad (3-150)$$

where

$$E_0 = M + e \sin M \quad (3-151)$$

- Hyperbola:  $e > 1$

$$\begin{bmatrix} x_p \\ y_p \\ z_p \end{bmatrix} = a \begin{bmatrix} \cosh F - e \\ -\sqrt{e^2 - 1} \sinh F \\ 0 \end{bmatrix} \quad (3-152)$$

$$\begin{bmatrix} \dot{x}_p \\ \dot{y}_p \\ \dot{z}_p \end{bmatrix} = \frac{\sqrt{-\mu/a}}{(e \cosh F - 1)} \begin{bmatrix} \sinh F \\ -\sqrt{e^2 - 1} \cosh F \\ 0 \end{bmatrix} \quad (3-153)$$

where

$F \sim$  the hyperbolic anomaly computed using Kepler's equation for a hyperbola,  $M = e \sinh F - F$ .

The hyperbolic Kepler equation may be solved by a Newton-Raphson iteration of the following form

$$F_{n+1} = F_n - \frac{(e \sinh F_n - F_n - M)}{e \cosh F_n - 1} \quad (3-154)$$

$$n = 0, 1, 2, 3, \dots$$

where  $F_0 = M/2$ . (Note: The preceding equation is singular for orbits with  $e \approx 1$ .)

- Parabola:  $e = 1$

$$\begin{bmatrix} x_p \\ y_p \\ z_p \end{bmatrix} = \begin{bmatrix} q - D^2/2 \\ \sqrt{2qD} \\ 0 \end{bmatrix} \quad (3-155)$$

$$\begin{bmatrix} \dot{x}_p \\ \dot{y}_p \\ \dot{z}_p \end{bmatrix} = \frac{1}{(q + D^2/2)} \begin{bmatrix} -D \\ \sqrt{2q} \\ 0 \end{bmatrix} \quad (3-156)$$

where

$$q \sim \text{pericentric distance} \quad (3-157)$$

and  $D$  is computed from Barker's equation, that is

$$D^3 + 6qD = 6M. \quad (3-158)$$

The orbital rectangular coordinates are transformed to inertial Cartesian position and velocity coordinates as follows

$$\begin{bmatrix} x \\ y \\ z \end{bmatrix} = P \begin{bmatrix} x_p \\ y_p \\ z_p \end{bmatrix} \quad (3-159)$$

and

$$\begin{bmatrix} \dot{x} \\ \dot{y} \\ \dot{z} \end{bmatrix} = P \begin{bmatrix} \dot{x}_p \\ \dot{y}_p \\ \dot{z}_p \end{bmatrix} \quad (3-160)$$

The elements,  $p_{ij}$ , of the rotation matrix,  $P$ , are

$$\begin{aligned} p_{11} &= \cos \Omega \cos \omega - \sin \Omega \cos i \sin \omega \\ p_{12} &= -\cos \Omega \sin \omega - \sin \Omega \cos i \cos \omega \\ p_{13} &= \sin \Omega \sin i \\ p_{21} &= \sin \Omega \cos \omega + \cos \Omega \cos i \sin \omega \\ p_{22} &= -\sin \Omega \sin \omega + \cos \Omega \cos i \cos \omega \\ p_{23} &= \cos \Omega \sin i \\ p_{31} &= \sin i \sin \omega \\ p_{32} &= \sin i \cos \omega \\ p_{33} &= \cos i \end{aligned} \quad (3-161)$$

### 3.3.8.2 Keplerian to Cartesian Partial Derivatives

The functional relationships expressed in Equations (3-159) and (3-160) are

$$\begin{aligned}\bar{\mathbf{r}} &= \mathbf{P}(\Omega, \omega, i) \bar{\mathbf{r}}_p(a, e, M) \\ \text{and} \\ \dot{\bar{\mathbf{r}}} &= \mathbf{P}(\Omega, \omega, i) \dot{\bar{\mathbf{r}}}_p(a, e, M).\end{aligned}\tag{3-162}$$

The partial derivatives of  $\bar{\mathbf{r}}$  with respect to the orbital elements may be written

$$\frac{\partial \bar{\mathbf{r}}}{\partial \zeta} = \mathbf{P} \frac{\partial \bar{\mathbf{r}}_p}{\partial \zeta}$$

and

$$\frac{\partial \dot{\bar{\mathbf{r}}}}{\partial \zeta} = \mathbf{P} \frac{\partial \dot{\bar{\mathbf{r}}}_p}{\partial \zeta}\tag{3-163}$$

for  $\zeta = a, e,$  and  $M$ , and

$$\frac{\partial \bar{\mathbf{r}}}{\partial \zeta} = \frac{\partial \mathbf{P}}{\partial \zeta} \bar{\mathbf{r}}_p$$

and

$$\frac{\partial \dot{\bar{\mathbf{r}}}}{\partial \zeta} = \frac{\partial \mathbf{P}}{\partial \zeta} \dot{\bar{\mathbf{r}}}_p\tag{3-164}$$

for  $\zeta = \Omega, \omega,$  and  $i$ .

The partial derivatives of  $\bar{\mathbf{r}}_p$  and  $\dot{\bar{\mathbf{r}}}_p$  for elliptical orbits are

$$\frac{\partial \bar{\mathbf{r}}_p}{\partial(a, e, M)} = \begin{bmatrix} \frac{x_p}{a} & \left(-a - \frac{y_p^2}{r(1-e^2)}\right) & \left(-\frac{a y_p}{r \sqrt{1-e^2}}\right) \\ \frac{y_p}{a} & \left(\frac{x_p y_p}{r(1-e^2)}\right) & \left(\frac{a \sqrt{1-e^2}(x_p + a e)}{r}\right) \\ 0 & 0 & 0 \end{bmatrix}\tag{3-165}$$

and



$$\frac{\partial \dot{\vec{r}}_p}{\partial (a, e, M)} = \begin{bmatrix} -\frac{\dot{x}_p}{2a} & \dot{x}_p \left(\frac{a}{r}\right)^2 \left(2\left(\frac{x_p}{a}\right) + \frac{e}{1-e^2} \left(\frac{y_p}{a}\right)^2\right) & -n \left(\frac{a}{r}\right)^3 x_p \\ -\frac{\dot{y}_p}{2a} & \frac{n}{\sqrt{1-e^2}} \left(\frac{a}{r}\right)^2 \left(\frac{x_p^2}{r} - \frac{y_p^2}{a(1-e^2)}\right) & -n \left(\frac{a}{r}\right)^3 y_p \\ 0 & 0 & 0 \end{bmatrix} \quad (3-166)$$

where the mean motion,  $n$ , is

$$n = \frac{1}{a} \sqrt{\frac{\mu}{a}}. \quad (3-167)$$

The partial derivatives of  $P$  with respect to  $\Omega$ ,  $\omega$ , and  $i$  are

$$\frac{\partial P}{\partial \Omega} = \begin{bmatrix} -P_{21} & -P_{22} & 0 \\ P_{11} & P_{12} & 0 \\ 0 & 0 & 0 \end{bmatrix} \quad (3-168)$$

$$\frac{\partial P}{\partial \omega} = \begin{bmatrix} P_{12} & -P_{11} & 0 \\ P_{22} & -P_{21} & 0 \\ P_{32} & -P_{31} & 0 \end{bmatrix} \quad (3-169)$$

$$\frac{\partial P}{\partial i} = \begin{bmatrix} \sin \Omega \sin i \sin \omega & \sin \Omega \sin i \cos \omega & 0 \\ -\cos \Omega \sin i \sin \omega & -\cos \Omega \sin i \cos \omega & 0 \\ \cos i \sin \omega & \cos i \cos \omega & 0 \end{bmatrix} \quad (3-170)$$

### 3.3.3.3 Body-Centered True of Date Coordinates to Keplerian Elements

Given the position,  $\bar{r}$ , and velocity,  $\dot{\bar{r}}$ , at time  $t$ , the standard Keplerian elements ( $a$ ,  $e$ ,  $i$ ,  $\Omega$ ,  $\omega$ ,  $M$ ) are calculated as follows. Let the magnitude of the position, velocity, and angular momentum vectors be denoted by

$$r = |\bar{r}| \quad (3-171)$$

$$V = |\dot{\bar{r}}| \quad (3-172)$$

$$h = |\bar{h}| \quad (3-173)$$

where

$$\bar{h} = \bar{r} \times \dot{\bar{r}}.$$

The equations for the orbital elements and related parameters are then

Semimajor Axis

$$a = \frac{\mu r}{(2\mu - rV^2)} \quad (3-174)$$

Semilatus Rectum

$$p = \frac{1}{\mu}[(rV)^2 - (\bar{r} \cdot \dot{\bar{r}})^2] \quad (3-175)$$

Eccentricity

$$e = \sqrt{1 - \frac{p}{a}} \quad (3-176)$$

## Inclination

$$\sin i = \frac{|(\bar{\mathbf{r}} \times \dot{\bar{\mathbf{r}}}) \times \bar{\mathbf{u}}_z|}{|\bar{\mathbf{r}} \times \dot{\bar{\mathbf{r}}}|} = \frac{\sqrt{h_x^2 + h_y^2}}{h} \quad (3-177)$$

$$\cos i = \frac{(\bar{\mathbf{r}} \times \dot{\bar{\mathbf{r}}}) \cdot \bar{\mathbf{u}}_z}{|\bar{\mathbf{r}} \times \dot{\bar{\mathbf{r}}}|} = \frac{h_z}{h}$$

where  $\bar{\mathbf{u}}_x$ ,  $\bar{\mathbf{u}}_y$ , and  $\bar{\mathbf{u}}_z$  are unit vectors in the body-centered true of date Cartesian coordinate system and  $h_x$ ,  $h_y$ , and  $h_z$  are components of the angular momentum vector,  $h$ .

### Elliptic Motion

$$a > 0$$

#### Eccentric Anomaly

$$\sin E = \frac{1}{e} \left( \frac{\bar{\mathbf{r}} \cdot \dot{\bar{\mathbf{r}}}}{\sqrt{\mu a}} \right)$$

$$\cos E = \frac{1}{e} \left( 1 - \frac{r}{a} \right)$$

#### Mean Anomaly

$$M = E - \frac{\bar{\mathbf{r}} \cdot \dot{\bar{\mathbf{r}}}}{\sqrt{\mu a}}$$

#### Period

$$P = 2\pi \sqrt{\frac{a^3}{\mu}}$$

### Hyperbolic Motion

$$a \leq 0$$

#### Hyperbolic Anomaly

$$\sinh F = \frac{1}{e} \left( \frac{\bar{\mathbf{r}} \cdot \dot{\bar{\mathbf{r}}}}{\sqrt{-\mu a}} \right) \quad (3-178)$$

$$\cosh F = \frac{1}{e} \left( 1 - \frac{r}{a} \right)$$

$$M = \frac{\bar{\mathbf{r}} \cdot \dot{\bar{\mathbf{r}}}}{\sqrt{-\mu a}} - F \quad (3-179)$$

$$(3-180)$$

### Elliptic Motion

$$a > 0$$

### Hyperbolic Motion

$$a \leq 0$$

Energy (per unit mass)

$$\text{Energy} = -\frac{\mu}{2a}$$

$$\text{Energy} = \frac{\mu}{2a} \quad (3-181)$$

Longitude of Ascending Node

$$\sin \Omega = \frac{h_x}{h \sin i} \quad (3-182)$$

$$\cos \Omega = \frac{-h_y}{h \sin i}$$

True Anomaly

$$\sin f = \sqrt{\frac{p}{\mu}} \frac{(\bar{r} \cdot \dot{\bar{r}})}{re} \quad (3-183)$$

$$\cos f = \frac{(p - r)}{re}$$

Argument of Perifocus

$$\sin(\omega + f) = \frac{z}{r \sin i} \quad (3-184)$$

$$\cos(\omega + f) = \frac{yh_x - xh_y}{hr \sin i}$$

Perifocal and Apofocal Radius

$$r_p = a(1 - e) \quad (3-185)$$

$$r_a = a(1 + e) \quad (3-186)$$

## Perifocal and Apofocal Height

$$h_p = r_p - r_s \quad (3-187)$$

$$h_a = r_a - r_s \quad (3-188)$$

The partial derivatives of the Keplerian coordinates with respect to the Cartesian coordinates are given by the inverse of the Keplerian to Cartesian partial derivatives in Equations (3-163) and (3-164), i.e.,

$$\begin{bmatrix} \partial a / \partial x & \partial a / \partial y & \dots & \partial a / \partial z \\ \partial e / \partial x & \partial e / \partial y & \dots & \\ \partial i / \partial x & \partial i / \partial y & \dots & \\ \vdots & \vdots & & \\ \partial M / \partial x & \partial M / \partial y & \dots & \partial M / \partial z \end{bmatrix} = \begin{bmatrix} \partial x / \partial a & \partial x / \partial e & \partial x / \partial i & \dots & \partial x / \partial M \\ \partial y / \partial a & \partial y / \partial e & \partial y / \partial i & \dots & \\ \vdots & \vdots & \vdots & & \\ \partial z / \partial a & \partial z / \partial e & \partial z / \partial i & \dots & \partial z / \partial M \end{bmatrix}^{-1} \quad (3-189)$$

### 3.3.9 Equinoctial-Cartesian Transformations (References 9 and 10)

The following sections present the transformations between the equinoctial elements, described in Section 3.2.6, and the inertial Cartesian system. The equinoctial elements are used only to describe closed orbits.

#### 3.3.9.1 Equinoctial Elements to Cartesian Coordinates

Conversion from equinoctial elements,  $a, h, k, p, q, \lambda$ , to inertial Cartesian coordinates,  $\bar{r}$  and  $\dot{\bar{r}}$ , is performed in the following manner. First, the generalized Kepler equation for equinoctial elements,

$$\lambda = F + h \cos F - k \sin F \quad (3-190)$$

is iteratively solved for the eccentric longitude  $F$ , which is the sum of the eccentric anomaly, argument of perigee, and right ascension of the ascending node.

Next, the position and velocity coordinates in the equinoctial coordinate system  $(x_{ep}, y_{ep}, z_{ep})$  are obtained as follows for both the direct and retrograde cases

$$X_1 = a[(1 - h^2\beta) \cos F + hk\beta \sin F - k] \quad (3-191)$$

$$Y_1 = a[(1 - k^2\beta) \sin F + hk\beta \cos F - h]$$

$$\dot{X}_1 = \frac{na^2}{r} [hk\beta \cos F - (1 - h^2\beta) \sin F] \quad (3-192)$$

$$\dot{Y}_1 = \frac{na^2}{r} [(1 - k^2\beta) \cos F - hk\beta \sin F]$$

where

$$\beta = \frac{1}{1 + \sqrt{1 - h^2 - k^2}} \quad (3-193)$$

The transformation from the equinoctial system to the inertial Cartesian system is given by

$$\bar{r} = X_1 \hat{f} + Y_1 \hat{g} \quad (3-194)$$

$$\dot{\bar{r}} = \dot{X}_1 \hat{f} + \dot{Y}_1 \hat{g} \quad (3-195)$$

where  $\hat{f}$  and  $\hat{g}$  are unit vectors directed along the  $x_{ep}$  and  $y_{ep}$  axes, respectively (see Figure 3-5). These vectors are computed in the inertial Cartesian coordinates as follows

$$[\hat{f}, \hat{g}, \hat{w}] = \frac{1}{1 + p^2 + q^2} \begin{bmatrix} 1 - p^2 + q^2 & 2pqj & 2p \\ 2pq & (1 + p^2 - q^2)j & -2q \\ -2pj & 2q & (1 - p^2 - q^2)j \end{bmatrix} \quad (3-196)$$

where

$j = 1$  for direct orbits ( $0 \leq i < 180^\circ$ )

$j = -1$  for retrograde orbits ( $0 < i \leq 180^\circ$ )

In GTDS the operational choice of direct elements was made for  $0 \leq i \leq 90^\circ$  and of retrograde elements for ( $90^\circ < i \leq 180^\circ$ ).

### 3.3.9.2 Cartesian Coordinates to Equinoctial Elements

The equinoctial orbit elements,  $a, h, k, p, q, \lambda$ , are calculated from the Cartesian position,  $\bar{r}$ , and velocity,  $\dot{\bar{r}}$ . The semi-major axis is computed as follows:

$$a = \left( \frac{2}{r} - \frac{|\dot{\bar{r}}|^2}{\mu} \right)^{-1} \quad (3-197)$$

The eccentricity vector is given by

$$\bar{e} = -\frac{\bar{r}}{r} - \frac{(\bar{r} \times \dot{\bar{r}}) \times \dot{\bar{r}}}{\mu} \quad (3-198)$$

The unit vector  $\hat{w}$  is defined as follows (see Section 3.2.5)

$$\hat{w} = \frac{\bar{r} \times \dot{\bar{r}}}{|\bar{r} \times \dot{\bar{r}}|} \quad (3-199)$$

The unit vectors  $\hat{f}$  and  $\hat{g}$  can then be computed as follows

$$f_x = 1 - \frac{w_x^2}{1 + w_z^j} \quad f_y = -\frac{w_x w_y}{1 + w_z^j} \quad f_z = -w_x^j \quad (3-200)$$

where  $j$  is defined following Equation (3-196).

$$\hat{\mathbf{g}} = \hat{\mathbf{w}} \times \hat{\mathbf{f}} \quad (3-201)$$

The equinoctial elements  $h$ ,  $k$ ,  $p$ , and  $q$  are given by

$$h = \bar{\mathbf{e}} \cdot \hat{\mathbf{g}} \quad (3-202)$$

$$k = \bar{\mathbf{e}} \cdot \hat{\mathbf{f}} \quad (3-203)$$

$$p = \frac{w_x}{1 + w_z^j} \quad (3-204)$$

$$q = - \frac{w_y}{1 + w_z^j} \quad (3-205)$$

The mean longitude is computed using the generalized Kepler equation

$$\lambda = F + h \cos F - k \sin F \quad (3-206)$$

where

$$F = \tan^{-1} \left( \frac{\sin F}{\cos F} \right) \quad (3-207)$$

with

$$\cos F = k + \frac{(1 - k^2 \beta) X_1 - hk \beta Y_1}{a \sqrt{1 - h^2 - k^2}} \quad (3-208)$$

$$\sin F = h + \frac{(1 - h^2 \beta) Y_1 - hk \beta X_1}{a \sqrt{1 - h^2 - k^2}}$$

The parameter  $\beta$  in Equation (3-208) is given by Equation (3-193).



Finally, the position coordinates  $x_{ep}$  and  $y_{ep}$  relative to the equinoctial coordinate system are given by

$$\begin{aligned} X_1 &= \bar{r} \cdot \hat{f} \\ Y_1 &= \bar{r} \cdot \hat{g} \end{aligned} \tag{3-209}$$

### 3.3.10 Herrick-Cartesian Transformations (References 11 and 12)

#### 3.3.10.1 Herrick Elements to Cartesian Coordinates

The following method is used for conversion from Herrick elements,  $\bar{e}, \bar{\ell}, n$ , and  $\lambda$ , to inertial Cartesian coordinates. The unit vectors  $\hat{f}, \hat{g}$  and  $\hat{w}$  along the equinoctial orbit plane coordinate directions (see Section 3.2.5) must first be determined. The unit vector  $\hat{w}$  is given by

$$\hat{w} = \frac{\bar{\ell}}{|\ell|} \tag{3-210}$$

The unit vectors  $\hat{f}$  and  $\hat{g}$  are determined from Equations (3-200) and (3-201) as functions of  $\hat{w}$ .

The Kepler equation for Herrick elements is solved by iteration for the eccentric longitude  $F$ ,

$$\lambda = F + n \cos F - k \sin F \tag{3-211}$$

where  $h$  and  $k$  are calculated from Equations (3-202) and (3-203) as functions of the known vectors  $\bar{e}, \hat{f}$  and  $\hat{g}$ .

The coordinates of position and velocity in the direct equinoctial system,  $X_1, Y_1, \dot{X}_1, \dot{Y}_1$ , are given by Equations (3-191) and (3-192), with

$$a = \left( \frac{\mu}{n^2} \right)^{1/3} \tag{3-212}$$

Finally, the position and velocity in the inertial Cartesian system are computed via the following transformations

$$\bar{\mathbf{r}} = X_1 \hat{\mathbf{f}} + Y_1 \hat{\mathbf{g}} \quad (3-213)$$

$$\dot{\bar{\mathbf{r}}} = \dot{X}_1 \hat{\mathbf{f}} + \dot{Y}_1 \hat{\mathbf{g}} \quad (3-214)$$

### 3.3.10.2 Cartesian Coordinates to Herrick Elements

Given the Cartesian position and velocity vectors,  $\bar{\mathbf{r}}$  and  $\dot{\bar{\mathbf{r}}}$ , the Herrick variables  $\bar{\mathbf{e}}$ ,  $\bar{\ell}$ ,  $n$  and  $\lambda$  are computed as follows:

$$\bar{\mathbf{e}} = -\frac{\bar{\mathbf{r}}}{r} - \frac{(\bar{\mathbf{r}} \times \dot{\bar{\mathbf{r}}}) \times \dot{\bar{\mathbf{r}}}}{\mu} \quad (3-215)$$

the angular momentum vector is

$$\bar{\ell} = \frac{\bar{\mathbf{r}} \times \dot{\bar{\mathbf{r}}}}{\sqrt{\mu}} \quad (3-216)$$

and the Kepler mean motion is

$$n = \sqrt{\frac{\mu}{a^3}} \quad (3-217)$$

where the semimajor axis,  $a$ , is given by

$$a = \left[ \frac{2}{r} - \frac{|\dot{\bar{\mathbf{r}}}|^2}{\mu} \right]^{-1} \quad (3-218)$$

The mean longitude,  $\lambda$ , is computed from the generalized Kepler equation given in Equation (3-206) to be

$$\lambda = F + h \cos F - k \sin F$$

where the variables  $h$  and  $k$  are determined from Equations (3-202) and (3-203), with vectors  $\hat{w}$ ,  $\hat{f}$  and  $\hat{g}$  calculated from Equations (3-210), (3-200), and (3-201). The eccentric longitude  $F$  is determined from Equations (3-207) and (3-208) with  $\beta$  from Equation (3-193) and  $X_1$  and  $Y_1$  from Equation (3-209).

### 3.3.11 Keplerian to Equinoctial and Herrick Transformations

#### 3.3.11.1 Keplerian to Equinoctial Elements

The conversion from Keplerian elements ( $a, e, i, \Omega, \omega, M$ ) to equinoctial elements is performed via the following equations.

##### Direct Set ( $0^\circ \leq i < 180^\circ$ )

$$a = a$$

$$h = e \sin(\omega + \Omega)$$

$$k = e \cos(\omega + \Omega)$$

$$p = \tan(i/2) \sin \Omega$$

$$q = \tan(i/2) \cos \Omega$$

$$\lambda = M + \omega + \Omega$$

##### Retrograde Set ( $0^\circ < i \leq 180^\circ$ )

$$a = a$$

$$h_r = e \sin(\omega - \Omega)$$

$$k_r = e \cos(\omega - \Omega)$$

$$p_r = \cot(i/2) \sin \Omega$$

$$q_r = \cot(i/2) \cos \Omega$$

$$\lambda_r = M + \omega - \Omega$$

(3-219)

#### 3.3.11.2 Keplerian to Herrick Elements

Conversion from Keplerian to Herrick elements is performed using the equations

$$e_x = e \cos \Omega \cos \omega - e \sin \Omega \sin \omega \sin i$$

$$e_y = e \sin \Omega \cos \omega + e \cos \Omega \sin \omega \cos i \quad (3-220)$$

$$e_z = e \sin \omega \sin i$$

$$|\ell| = \sqrt{a(1 - e^2)} \quad (3-221)$$

$$\begin{aligned} \ell_x &= |\ell| \sin \Omega \sin i \\ \ell_y &= -|\ell| \cos \Omega \sin i \\ \ell_z &= |\ell| \cos i \end{aligned} \quad (3-222)$$

$$n = \sqrt{\mu/a^3} \quad (3-223)$$

$$\lambda = M + \omega_r \Omega. \quad (3-224)$$

where  $j$  is defined following Equation (3-196).

### 3.3.12 Vehicle-Fixed to Body-Centered True of Date Transformations

The propulsive and aerodynamic accelerations are modeled in the vehicle-fixed coordinate system described in Section 3.2.7. These vehicle oriented accelerations must be transformed to the inertial Cartesian system to be consistent with other terms in the dynamical equations of motion.

The following three angular transformations are required to orient the vehicle-fixed coordinates with respect to the inertial Cartesian axes:

$R_z (\alpha_v)$  the rotation about the inertial  $z$ -axis, through the right ascension,  $\alpha_v$ , of the vehicle's (longitudinal)  $x_v$ -axis.

$R_y (-\delta_v)$  the negative rotation about the new  $y$ -axis, through the declination,  $\delta_v$ , of the vehicle's (longitudinal)  $x_v$ -axis.

$R_x (\phi_v)$  the rotation about the new  $x$ -axis (which is aligned with the  $x_v$ -axis), through the roll angle,  $\phi_v$ , to the vehicle-fixed axes.

where  $R_x$  and  $R_z$  are given by Equation (3-1), and  $R_y$  is

$$R_y(\alpha) = \begin{bmatrix} \cos \alpha & 0 & -\sin \alpha \\ 0 & 1 & 0 \\ \sin \alpha & 0 & \cos \alpha \end{bmatrix} \quad (3-225)$$

Denote an arbitrary vector by  $\bar{\zeta}_v$  when expressed in the vehicle-fixed coordinates, and  $\bar{\zeta}$  when expressed in inertial Cartesian coordinates. Then the transformation between coordinates can be written

$$\begin{aligned}\bar{\zeta} &= R_x(\phi_v) R_y(-\delta_v) R_z(\alpha_v)^T \bar{\zeta}_v \\ &= Q \bar{\zeta}_v\end{aligned}\tag{3-226}$$

where the elements of  $Q$  are

$$\begin{aligned}q_{11} &= \cos \delta_v \cos \alpha_v \\ q_{12} &= -\sin \phi_v \sin \delta_v \cos \alpha_v - \cos \phi_v \sin \alpha_v \\ q_{13} &= -\cos \phi_v \sin \delta_v \cos \alpha_v + \sin \phi_v \sin \alpha_v \\ q_{21} &= \cos \delta_v \sin \alpha_v \\ q_{22} &= -\sin \phi_v \sin \delta_v \sin \alpha_v + \cos \phi_v \cos \alpha_v \\ q_{23} &= -\cos \phi_v \sin \delta_v \sin \alpha_v - \sin \phi_v \cos \alpha_v \\ q_{31} &= \sin \delta_v \\ q_{32} &= \sin \phi_v \cos \delta_v \\ q_{33} &= \cos \phi_v \cos \delta_v\end{aligned}\tag{3-227}$$

### 3.4 TIME SYSTEMS

The GTDS orbit determination program uses the atomic time system, A.1, in the integration of the equations of motion. However, the program must interface with external input-output data sets which are referenced to other time systems, such as ephemeris time (ET) for the solar/lunar/planetary ephemerides, universal time (UT1) for computing Greenwich sidereal time, and universal time coordinated (UTC) for input-output epochs and tracking data. A brief description of the relevant time systems and their interrelationships follows (References 1, 13, and 14).

### 3.4.1 Ephemeris Time, ET

This is the uniform measure of time, which is the independent variable of the equations of motion, and the argument for the ephemerides of the planets, the moon, and the satellite. The unit of ET is the ephemeris second, which is defined as the fraction  $1/31,556,925.9747$  of the tropical year for  $12^h$  ET of Jan 0<sup>d</sup>, 1900. Ephemeris time is determined from the instant near the beginning of the calendar year 1900 when the geometric mean longitude of the sun referred to the mean equinox of date was  $279^h 41'48''.04$ , at which instant the measure of ephemeris time was 1900 Jan 0<sup>d</sup>  $12^h$ .

### 3.4.2 Atomic Time, A.1

A.1 time is one of several types of atomic time. It is obtained from oscillations of the US Cesium Frequency Standard located at Boulder, Colorado. In 1958, the US Naval Observatory established the A.1 system based on an assumed frequency of 9,192,631,770 oscillations of the isotope 133 of cesium atom per A.1 second. The reference epoch of A.1 was established so that on Jan 1, 1958,  $0^h 0^m 0^s$  UT2 the value of A.1 was  $0^h 0^m 0^s$ , Jan 1, 1958.

### 3.4.3 Universal Time, UT

This is the measure of time that is the theoretical basis for all civil time keeping. UT is related to the rotation of the earth on its axis. Compared to ephemeris time, which is uniform time, UT does not take into account the irregularities of the earth's rate of rotation.

The quantity UT is defined as 12 hours plus the Greenwich hour angle (GHA) of a point (representing the fictitious mean sun) on the mean equator of date whose right ascension measured from the mean equinox of date is

$$R_u = 18^h 38^m 45^s.836 + 8,640,184^s.542 T_u + .0929 T_u^2 \quad (3-228)$$

where  $T_u$  is defined following Equation (3-20).

The Greenwich hour angle of this point, denoted by  $S_u$  in Figure 3-16, is

$$\text{GHA of } S_u = \alpha_{GM} - R_u \quad (3-229)$$

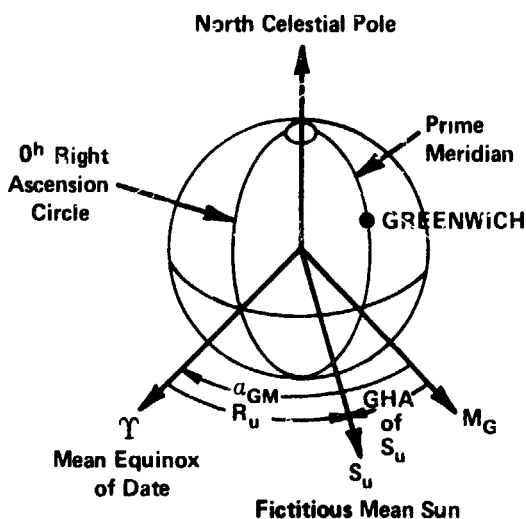


Figure 3-16. Greenwich Hour Angle

where  $\alpha_{GM}$  is the Greenwich mean sidereal time; hence,

$$UT = 12^h + \alpha_{GM} - R_u. \quad (3-230)$$

Adding 12 hours to both sides of the above equation yields

$$UT + 12^h = \alpha_{GM} - R_u \quad (3-231)$$

and solving for  $\alpha_{GM}$

$$\alpha_{GM} = 12^h + UT + R_u. \quad (3-232)$$

In practice, the point whose right ascension is  $R_u$  cannot be observed. Consequently, the practical determinations of UT are obtained, through the intermediary of sidereal time, from observations of the diurnal motion of the stars. Sidereal time is a measure of the rotation of the earth relative to the stars, and is defined as the hour angle of the vernal equinox. Therefore, the meridian transit of a star occurs at a sidereal time equal to its right ascension.

Universal time varies from uniform time due to variations of the meridian, arising principally from polar motion, and variations in the rotational rate of the earth consisting of secular, irregular, periodic seasonal, and periodic tidal terms.

The tidal variations are very small, the secular variation is significant only over large time intervals, and the irregular variations, while they may be relatively large, are highly erratic. The periodic seasonal variation appears stable enough to be predictable.

There are three measures of UT in common usage: (1) UT0, which is determined from observations of local mean sidereal time, (2) UT1, obtained by correcting UT0 for polar motion, and (3) UT2, which results from the removal of the seasonal inequality from UT1.

#### 3.4.4 Uncorrected Universal Time, UT0

This measure of time is obtained by assuming an adopted conventional value  $\lambda_A$  of the longitude of each observing station (see Section 3.3.2.2). The local mean sidereal time at transit is generally determined through observation of meridian transits of stars, omitting from the apparent right ascension the nutation terms that are independent of the coordinates of the star (the equation of the equinoxes). Subtracting the east longitude of the observing station gives  $\gamma_{GM}$ , the Greenwich mean sidereal time or Greenwich hour angle of the mean equinox of date. UT0 is then obtained from Equation (3-230) by adding  $12^h$  and subtracting  $R_u$  from this value. Since the motion of the pole causes variations in the meridian, UT0 is dependent on the location of the observing station.

#### 3.4.5 Universal Time, UT1

This measure of time is obtained from UT0 by applying an appropriate correction in longitude due to the motion of the pole and is the form of universal time used in GTDS. UT1 reflects the actual orientation of the earth with respect to the vernal equinox at that instant. UT1 will be the same for all observatories. In contrast, UT0 time, as determined by different observatories using their adopted longitude in calculations, results in a different value of UT0 for each observatory.

Then

$$UT1 = UT0 - \Delta\lambda \quad (3-234)$$

where  $\Delta\lambda$  is given in Equation (3-31).

UT1 time is used by GTDS to compute the  $\alpha_{GM}$  as given in Equation (3-19).



### 3.4.6 Universal Time, UT2

If the extrapolated value of UT1 time is corrected for periodic seasonal variations, SV, in the earth's speed of rotation, the resulting time is UT2. UT2 does not represent the actual orientation of the earth with respect to the vernal equinox. UT1 should always be used when the actual orientation of the earth is required. UT2 is often referred to as GMT, Greenwich Mean Time, and ZULU time. The equations for UT2 are

$$UT2 = UT1 + SV \quad (3-235)$$

where

$$SV = .022 \sin 2\pi t - .017 \cos 2\pi t - .007 \sin 4\pi t + .006 \cos 4\pi t \quad (3-236)$$

or

$$SV = .022 \sin 2\pi t - .012 \cos 2\pi t - .006 \sin 4\pi t + .007 \cos 4\pi t. \quad (3-237)$$

Equation (3-236) was used prior to 1962 and Equation (3-237) has been in use since 1962. The quantity  $t$  equals the fraction of the tropical year elapsed from the beginning of the Besselian year for which the calculation is made. (One tropical year = 365.2422 days.) Since seasonal variations can be known precisely only after their occurrence, UT2 itself is rarely used. The Bureau International de l'Heure also issues corrections for  $\Delta\lambda$  and SV.

### 3.4.7 Universal Time Coordinated, UTC

This is the standard time scale to which tracking stations are synchronized. UTC time is derived from atomic time, A.1, in a manner which makes it almost synchronous with UT2.

Up to January 1, 1972, the UTC time scale operated at a frequency offset from the atomic time scale. The value of the offset was periodically changed by international agreement so that the UTC scale would correspond more closely to UT2.

On January 1, 1972, a new improved UTC system, adopted by the International Radio Consultative Committee (CCIR), was internationally implemented by the time-keeping laboratories and time-broadcast stations.

The new UTC system eliminates the frequency offset from atomic time, thus making the UTC second constant and equal in duration to the A.1 second (References 15 and 16). The new UTC time scale is now kept in synchronism with the rotation of the earth to within  $\pm 0.7$  seconds by step-time adjustments of exactly one second, when needed.

#### 3.4.8 Station Time, ST

This measure of time is obtained at each station by counting cycles of a rubidium atomic frequency standard. The difference between ST and UTC is tabulated by each station. The observables are recorded in ST and then transformed to UTC.

### 3.5 TRANSFORMATIONS BETWEEN TIME SYSTEMS

Desired transformations between the time systems, ET, A.1, UTC, and UT1 are carried out in the GTDS orbit determination program by evaluating either a standard formula or an appropriate time polynomial.

#### 3.5.1 Transformations by Standard Formula

For most purposes, the difference between A.1 and ET may be considered a constant. The suspected discrepancy is roughly two parts in  $10^9$ . The actual transformation between A.1 and ET time is given by

$$\begin{aligned}
 (ET - A.1) = & \Delta T_{1958} - \frac{(JD - 2,436,204.5) (86,400)}{9,192,631,770} \times \Delta f_{\text{cesium}} \\
 & + \frac{2e(\mu a) 1/2 \sin E}{c^2}
 \end{aligned}
 \tag{3-238}$$

where

- $\Delta T_{1958} \sim$  the ET - UT2 on 1 January 1958,  $0^h 0^m 0^s$  UT2 minus the periodic term in Equation (3-238) evaluated at this same epoch
- JD  $\sim$  the Julian date
- 2,436,204.5  $\sim$  the Julian date on 1 January 1958,  $0^h 0^m 0^s$
- $\Delta f_{\text{cesium}} \sim$  the correction to  $f_{\text{cesium}} = 9,192,631,770$  cycles of cesium per ephemeris second
- $\mu \sim$  the gravitational constant of the sun,  
 $1.327,154,45 \times 10^{11} \text{ km}^3/\text{sec}^2$

- a ~ the semimajor axis of the heliocentric orbit of the earth-moon barycenter, 149,599,000 km
- e ~ the eccentricity of the heliocentric orbit of the earth-moon barycenter .01672
- c ~ the speed of light at an infinite distance from the sun, 299,792.5 km/sec
- E ~ the eccentric anomaly of the heliocentric orbit of the earth-moon barycenter.

The first term of Equation (3-238) arises because A.1 was set equal to UT2 at the beginning of 1958. The second term accounts for the difference between the lengths of ET and A.1 seconds (if  $\Delta f_{\text{cesium}}$  is nonzero). The periodic term arises from general relativity. It accounts for the fact that A.1, UTC, and ST times are measures of proper time observed on earth, and that ET is a measure of coordinate time in the heliocentric (strictly barycentric) space-time frame of reference. The contribution of the last two terms in Equation (3-238) is negligible for the range of applications currently contemplated for GTDS. Hence, the transformation between ET and A.1 is accomplished using the approximate formula,

$$ET - A.1 = 32^s.15 \quad (3-239)$$

### 3.5.2 Transformations by Time Polynomials

The remaining transformations between the time systems A.1, UTC, and UT1 are accomplished using the time difference data A.1-UTC, and A.1-UT1, supplied by the U. S. Naval Observatory. These data have been conveniently reduced by quadratic polynomial fits in order to improve the efficiency of the transformation procedure. The time difference polynomials derived for use by the GTDS program have the form

$$(A.1 - UTC)_i = a_{i1} + a_{i2}T + a_{i3}T^2 \quad (3-240)$$

$$(A.1 - UT1)_i = a_{i4} + a_{i5}T + a_{i6}T^2 \quad (3-241)$$

where

A.1-UTC ~ the difference between A.1 and UTC time, in seconds.

A.1-UT1 ~ the difference between A.1 and UT1 time, in seconds.

i ~ the number of days from the beginning of the time span covered by the polynomial,  $T = 1, 2, \dots$ . For the given date, MJD,

$$T - \text{MJD} - \text{MJD}_i + 1 \quad (3-242)$$

where  $\text{MJD}_i$  is the tabular modified Julian date which bounds the interval from below, i.e.,

$$\text{MJD}_i \leq \text{MJD} < \text{MJD}_{i+1} \quad (3-243)$$

The coefficients  $a_{ij}$  are given in Table 3-2 next to modified Julian dates (mod 2, 430, 000) defining the time interval for which the coefficients are applicable. These coefficients and associated time spans were determined by least-squares fitting second order polynomials to published time difference data. The time spans were determined by constraining the maximum deviation (between the data and polynomial) to be less than .0005 seconds for (A.1-UTC), and less than .005 seconds for (A.1-UT1). The table covers the time span from January 1, 1958, and is updated periodically. Provision is made for inserting future A.1-UTC offsets (leap seconds) as predicted by the U. S. Naval Observatory. Extrapolation of A.1-UT1 is achieved by performing a linear least squares fit on the data for the last six months to obtain  $a_{i5}$ , the A.1-UT1 rate. The second order coefficient,  $a_{i6}$ , is set equal to zero. This extrapolation is used for one year from the date of the last available observation; after this, both  $a_{i5}$  and  $a_{i6}$  are set equal to zero.

### 3.6 POLYNOMIAL REPRESENTATION OF EPHEMERIS DATA

In GTDS, planetary and lunar positions and velocities, as well as the earth's nutation, are determined by evaluating multiple-day-arc Chebyshev polynomials whose coefficients are derived from ephemeris data contained on tapes supplied by the Jet Propulsion Laboratory (JPL) (References 5, 17, and 18). These Chebyshev polynomial representations maintain the accuracy of the original data while increasing efficiency by eliminating the need to interpolate on the JPL ephemeris data. The data contained on the JPL tapes are the positions and velocities of the planets Mercury, Venus, Earth-Moon barycenter, Mars, Jupiter, Saturn, Uranus, Neptune, and Pluto, the Earth's Moon, plus the nutation rates in longitude and obliquity. These data are generated by weighted least-squares estimation of the appropriate orbital models using source positions obtained on the basis of current planetary theories. Positions and velocities on the tapes are referred to the rectangular equatorial system of the mean equator and equinox of 1950.0, with planetary data being heliocentric and lunar data geocentric.

The data needed to determine the lunar ephemeris and nutations were obtained by evaluating the Improved Brown Lunar Theory with corrections suggested by Dr. W. J. Eckert using values of astronomical constants adopted by the IAU in

**Table 3-2 (1 of 2)**  
**Time Difference Coefficients**

Gregorian Date	Modified Julian Date	A.1-UTC			A.1-UT1		
		a <sub>i1</sub>	a <sub>i2</sub>	a <sub>i3</sub>	a <sub>i4</sub>	a <sub>i5</sub>	a <sub>i6</sub>
01-01-58	6204	-0.1618000D-01	0.9745798D-03	-0.3991597D-05	0.1858875D-01	0.2017377D-02	-0.1409314D-04
01-16-58	6219	0.1758511D-01	0.9402134D-03	-0.2288330D-05	0.4548636D-01	0.1618852D-02	0.1799831D-05
02-06-58	6240	0.5616044D-01	0.8366484D-03	-0.1373626D-05	0.8011670D-01	0.1662466D-02	-0.2698772D-05
02-20-58	6254	0.8754361D-01	0.8397126D-03	0.4555439D-06	0.1028026D 00	0.1625878D-02	0.2606312D-05
04-10-58	6303	0.1496110D 00	0.9429822D-03	-0.2131837D-05	0.1874593D 00	0.1994024D-02	-0.6054242D-05
05-31-58	6354	0.1926477D 00	0.8642007D-03	0.2022977D-05	0.2728259D 00	0.1228771D-02	-0.6293706D-05
06-12-58	6366	0.2223144D 00	0.9408642D-03	-0.1432435D-05	0.2866422D 00	0.1092088D-02	-0.1028374D-04
07-03-58	6387	0.2626176D 00	0.8881868D-03	0.1373626D-05	0.3050101D 00	0.6156755D-03	0.3038138D-05
07-17-58	6401	0.2952014D 00	0.9007887D-03	-0.1810101D-06	0.3165780D 00	0.2966259D-03	0.6605071D-05
10-23-58	6499	0.4016215D 00	0.8420982D-03	-0.2598091D-06	0.4096507D 00	0.1671038D-02	-0.1379641D-06
11-27-58	6534	0.4508753D 00	0.7688908D-03	0.2232538D-05	0.4681985D 00	0.1664009D-02	-0.8183690D-06
12-25-58	6562	0.4940484D 00	0.8903961D-03	0.4597416D-06	0.5142490D 00	0.1485226D-02	0.3096075D-05
01-29-59	6597	0.5458328D 00	0.9169140D-03	0.4557703D-06	0.5700569D 00	0.1393824D-02	-0.1394801D-05
02-26-59	6625	0.5918885D 00	0.9479880D-03	-0.2074632D-06	0.6028216D 00	0.1705016D-02	-0.3217583D-05
08-02-59	6782	0.7350500D 00	0.1110000D-02	-0.5000000D-04	0.7885600D 00	0.8714286D-03	0.2857143D-04
08-06-59	6786	0.7587371D 00	0.8704235D-03	-0.2258611D-06	0.7918877D 00	0.5915514D-03	0.7643986D-05
08-27-59	6807	0.7969748D 00	0.8567179D-03	0.4459769D-06	0.8076672D 00	0.9517989D-03	0.6897709D-05
10-01-59	6842	0.8472612D 00	0.8507324D-03	0.1213704D-05	0.8492754D 00	0.1595855D-02	0.2668635D-05
11-05-59	6877	0.8893352D 00	0.9424176D-03	-0.3296703D-05	0.9081024D 00	0.1771395D-02	0.2658371D-05
11-19-59	6891	0.9309792D 00	0.8688708D-03	0.4694539D-06	0.9234968D 00	0.1775083D-02	-0.4568603D-05
12-17-59	6919	0.9762195D 00	0.6729432D-03	0.1359837D-04	0.9790332D 00	0.1469490D-02	-0.3076611D-05
01-14-60	6947	0.1005776D 01	0.1276327D-02	-0.2546813D-07	0.1015154D 01	0.1431175D-02	0.6904889D-06
06-30-60	7084	0.1179992D 01	0.1276583D-02	-0.7058271D-07	0.1223733D 01	0.6918611D-03	-0.1706175D-05
09-07-60	7184	0.1306970D 01	0.1251737D-02	0.2006400D-06	0.1277845D 01	0.1272192D-02	0.1663052D-05
01-01-61	7300	0.1459942D 01	0.1290565D-02	-0.1259551D-07	0.1442413D 01	0.7002162D-03	0.5207392D-05
04-20-61	7409	0.1600435D 01	0.1288668D-02	-0.4508204D-07	0.1572890D 01	0.1431424D-02	-0.4865981D-05
08-01-61	7512	0.1682730D 01	0.1297609D-02	-0.1611287D-07	0.1666425D 01	0.6024381D-03	0.4223422D-05
12-17-61	7650	0.1861600D 01	0.1300000D-02	-0.1262726D-15	0.1826452D 01	0.5920023D-03	0.6454468D-04
01-01-62	7665	0.1881260D 01	0.1121344D-02	0.9459211D-08	0.1843717D 01	0.1287215D-02	0.1332452D-05
06-02-62	7817	0.2051849D 01	0.1116318D-02	0.2776893D-07	0.2070910D 01	0.4724146D-03	0.1963054D-05
09-12-62	7919	0.2165931D 01	0.1120481D-02	0.5828122D-09	0.2141475D 01	0.1490751D-02	0.1756295D-05
01-05-63	8034	0.2294768D 01	0.1115182D-02	0.6620223D-07	0.2336628D 01	0.5611055D-03	0.7101327D-05
04-13-63	8132	0.2404600D 01	0.1111988D-02	-0.4262574D-08	0.2460437D 01	0.2022677D-02	-0.6346917D-05
08-14-63	8255	0.2542758D 01	0.1118567D-02	0.1036236D-07	0.2618246D 01	0.1139977D-02	0.6860039D-05
11-01-63	8334	0.2731246D 01	0.1111958D-02	0.1542096D-06	0.2750605D 01	0.2253339D-02	-0.1975578D-05
01-06-64	8400	0.2805812D 01	0.1298018D-02	-0.1044524D-07	0.2891822D 01	0.1992589D-02	0.7474964D-06
04-01-64	8486	0.3017345D 01	0.1293842D-02	0.1384168D-08	0.3063530D 01	0.26884157D-02	-0.6935132D-05
07-07-64	8583	0.3142858D 01	0.1294845D-02	-0.4926524D-07	0.3254806D 01	0.9664385D-03	0.4236349D-05
09-01-64	8639	0.3315311D 01	0.1287598D-02	0.3103647D-06	0.3321821D 01	0.1515276D-02	0.1055086D-04
10-01-64	8669	0.3355178D 01	0.1295054D-02	-0.1298027D-08	0.3379279D 01	0.2285529D-02	-0.4295243D-06
01-01-65	8761	0.3574267D 01	0.1294804D-02	0.4588893D-08	0.3587570D 01	0.2039134D-02	0.5294157D-06
03-01-65	8820	0.3750694D 01	0.1297441D-02	-0.1153898D-07	0.3705315D 01	0.2902436D-02	-0.4622248D-05
07-01-65	8942	0.4008834D 01	0.1296214D-02	-0.8656292D-08	0.3991956D 01	0.1542490D-02	0.1237396D-05
09-01-65	9004	0.4189151D 01	0.1296106D-02	-0.1562328D-08	0.4089639D 01	0.2405161D-02	0.2545870D-05
12-09-65	9103	0.4317425D 01	0.1298000D-02	-0.1337040D-16	0.4347453D 01	0.2446044D-02	-0.1489223D-04
01-02-66	9127	0.4348522D 01	0.2591633D-02	0.1658375D-08	0.4396586D 01	0.2342899D-02	0.1221517D-05
06-14-66	9290	0.4770985D 01	0.2594067D-02	-0.1855570D-07	0.4811298D 01	0.1594668D-02	0.3251986D-05
09-25-66	9393	0.5038040D 01	0.2590933D-02	0.1948657D-07	0.5012240D 01	0.2862011D-02	0.5936044D-06
12-01-66	9460	0.5210963D 01	0.2592218D-02	-0.4296877D-08	0.5211300D 01	0.2090521D-02	0.2751869D-05
04-23-67	9603	0.5581668D 01	0.2593321D-02	-0.8806318D-08	0.5570056D 01	0.2681584D-02	-0.6356829D-05
08-11-67	9713	0.5866922D 01	0.2585386D-02	0.3473871D-07	0.5793786D 01	0.1666173D-02	0.7210946D-05
11-30-67	9824	0.6154340D 01	0.2590120D-02	0.3398956D-07	0.6063976D 01	0.2472966D-02	0.9022760D-06
02-01-68	9887	0.6217630D 01	0.2592005D-02	-0.3637691D-10	0.6227322D 01	0.2259530D-02	0.2955707D-05
06-01-68	10008	0.6531262D 01	0.2591999D-02	0.6570560D-11	0.6559410D 01	0.1846400D-02	0.2752718D-05
12-26-68	10216	0.7070398D 01	0.2592008D-02	-0.6112177D-10	0.7039445D 01	0.2375908D-02	0.3412215D-05
05-18-69	10359	0.7441054D 01	0.2591984D-02	0.1292516D-09	0.7448662D 01	0.2318877D-02	-0.17309471D-05

**Table 3-2 (2 of 2)**  
**Time Difference Coefficients**

Gregorian Date	Modified Julian Date	A.1-UTC			A.1-UT1		
		a <sub>i1</sub>	a <sub>i2</sub>	a <sub>i3</sub>	a <sub>i4</sub>	a <sub>i5</sub>	a <sub>i6</sub>
09-07-69	10471	0.7731358D 01	0.2592001D-02	-0.5477020D-11	0.7693900D 01	0.2938450D-02	-0.7218456D-07
04-14-70	10690	0.8299006D 01	0.2592000D-02	0.2959026D-11	0.8339493D 01	0.3331022D-02	-0.7547016D-05
08-17-70	10315	0.8623006D 01	0.2592000D-02	-0.6895982D-16	0.8639866D 01	0.2150943D-02	0.5655341D-05
12-08-70	10328	0.8915902D 01	0.2592000D-02	-0.2521662D-11	0.8955715D 01	0.2377667D-02	0.2334677D-05
04-17-71	11058	0.9252862D 01	0.2592000D-02	0.2260392D-16	0.9318675D 01	0.3177070D-02	-0.4467255D-05
08-27-71	11190	0.9595006D 01	0.2591993D-02	0.8745209D-10	0.9663368D 01	0.2525044D-02	0.8834257D-05
11-26-71	11281	0.9830878D 01	0.2592018D-02	-0.5629834D-16	0.9961526D 01	0.3439684D-02	-0.1127429D-04
01-01-72	11317	0.1003438D 02	0.0	0.0	0.1006682D 02	0.3204370D-02	0.1683766D-05
05-25-72	11462	0.1003438D 02	0.0	0.0	0.1056214D 02	0.3100347D-02	-0.7556443D-05
07-01-72	11499	0.1103438D 02	0.0	0.0	0.1066897D 02	0.2153567D-02	0.5068341D-05
12-01-72	11652	0.1103438D 02	0.0	0.0	0.1111230D 02	0.3029462D-02	0.8200901D-05
01-01-73	11683	0.1203438D 02	0.0	0.0	0.1121122D 02	0.3275744D-02	0.1268116D-05
05-22-73	11824	0.1203438D 02	0.0	0.0	0.1169615D 02	0.2739495D-02	-0.1989802D-05
09-12-73	11937	0.1203438D 02	0.0	0.0	0.1198002D 02	0.3151757D-02	0.7251402D-06
12-23-73	12039	0.1203438D 02	0.0	0.0	0.1230448D 02	0.3394470D-02	-0.7916667D-04
01-01-74	12048	0.1303438D 02	0.0	0.0	0.1232661D 02	0.2490510D-02	0.4120220D-05
05-10-74	12177	0.1303438D 02	0.0	0.0	0.1270751D 02	0.3751944D-02	-0.2040723D-04
07-12-74	12240	0.1303438D 02	0.0	0.0	0.1286793D 02	0.1846049D-02	-0.1615431D-05
08-12-74	12271	0.1303438D 02	0.0	0.0	0.1296430D 02	-0.4005000D-01	0.1035000D-01
08-15-74	12274	0.1303438D 02	0.0	0.0	0.1292856D 02	0.5957143D-02	-0.3214286D-03
08-22-74	12281	0.1303438D 02	0.0	0.0	0.1294253D 02	0.1314643D-02	0.5946429D-03
08-28-74	12287	0.1303438D 02	0.0	0.0	0.1296817D 02	-0.3707143D-02	0.6738095D-03
09-05-74	12295	0.1303438D 02	0.0	0.0	0.1297733D 02	-0.1032143D-03	0.6053571D-03
09-11-74	12301	0.1303438D 02	0.0	0.0	0.1299306D 02	0.2219481D-02	0.5864136D-04
09-23-74	12313	0.1303438D 02	0.0	0.0	0.1307627D 02	-0.4386500D-01	0.8875000D-02
09-27-74	12317	0.1303438D 02	0.0	0.0	0.1307670D 02	-0.4800000D-01	0.1290000D-01
09-30-74	12320	0.1303438D 02	0.0	0.0	0.1306024D 02	-0.1315714D-01	0.2742857D-02
10-05-74	12325	0.1303438D 02	0.0	0.0	0.1305110D 02	0.4583001D-13	-0.8881784D-14
10-09-74	12329	0.1303438D 02	0.0	0.0	0.1307236D 02	0.3154490D-02	-0.1800921D-05
01-01-75	12413	0.1403438D 02	0.0	0.0	0.1331909D 02	0.3057353D-02	-0.6523143D-06
04-08-75	12510	0.1403438D 02	0.0	0.0	0.1361908D 02	0.2120486D-02	0.3011148D-04
05-03-75	12535	0.1403438D 02	0.0	0.0	0.1366022D 02	0.2498500D-01	-0.4375000D-02
05-07-75	12539	0.1403438D 02	0.0	0.0	0.1368984D 02	0.4292143D-02	-0.3535714D-03
05-13-75	12545	0.1403438D 02	0.0	0.0	0.1371077D 02	0.2625874D-03	0.2807692D-03
05-24-75	12556	0.1403438D 02	0.0	0.0	0.1374876D 02	-0.2339286D-02	0.4821429D-03
05-31-75	12563	0.1403438D 02	0.0	0.0	0.1375854D 02	-0.4590000D-02	0.1850000D-02
06-05-75	12568	0.1403438D 02	0.0	0.0	0.1376146D 02	0.8219048D-02	-0.8952381D-03
06-12-75	12575	0.1403438D 02	0.0	0.0	0.1377704D 02	0.1030643D-01	-0.1253571D-02
06-18-75	12581	0.1403438D 02	0.0	0.0	0.1379992D 02	0.3318864D-02	-0.1541667D-03
06-28-75	12591	0.1403438D 02	0.0	0.0	0.1384005D 02	0.2864403D-02	0.0
07-01-75	12594	0.1403438D 02	0.2000000D-07	0.0	0.1384864D 02	0.2864403D-02	0.0
07-03-75	12596	0.1403439D 02	0.2000000D-07	0.0	0.1488556D 02	0.0	0.0

1964. However, spacecraft trajectory data obtained more recently indicate that some of the constants still require significant corrections. The uncertainty in the geocentric position of the moon's center of mass at the data points of the ephemeris is estimated at 150 meters and the uncertainty in the distance is about 60 meters.

The evaluation of the orbital models of the planets needed in the least-squares fitting process was carried out by numerical integration of their differential equations of motion using a 1/2-day step-size for Mercury, a 2-day step-size for Venus and the Earth-Moon barycenter, and a 4-day step-size for Mars and the outer planets. A second-sum predictor-corrector integrator was used with fourteenth differences of the accelerations retained. The tabular ephemeris data obtained in this manner can be used directly by interpolating for intermediate values or they can be reduced by curve-fitting techniques at the sacrifice of additional accuracy.

The JPL software used to retrieve data from a JPL ephemeris tape provides interpolated values of position and velocity vectors of any requested set of bodies relative to any requested central body. Bounds for the truncation error associated with the fifth-order Everett interpolation formula are given in Table 3-3.

Table 3-3  
Bounds for Truncation Error When Using Fifth-Order  
Everett Interpolation Formula

Body	Position	Velocity
Mercury	$8890.00 \times 10^{-12}$ AU	$4420.00 \times 10^{-12}$ AU/day
Venus	$4.73 \times 10^{-12}$ AU	$0.62 \times 10^{-12}$ AU/day
Earth-Moon barycenter	$5.19 \times 10^{-12}$ AU	$2.50 \times 10^{-12}$ AU/day
Mars	$6.47 \times 10^{-12}$ AU	$5.77 \times 10^{-12}$ AU/day
Jupiter	$6.64 \times 10^{-12}$ AU	$5.72 \times 10^{-12}$ AU/day
Saturn	$6.64 \times 10^{-12}$ AU	$5.72 \times 10^{-12}$ AU/day
Uranus	$6.64 \times 10^{-12}$ AU	$5.72 \times 10^{-12}$ AU/day
Neptune	$6.64 \times 10^{-12}$ AU	$5.72 \times 10^{-12}$ AU/day
Pluto	$6.64 \times 10^{-12}$ AU	$5.72 \times 10^{-12}$ AU/day
Moon	$1.0100 \times 10^{-5}$ earth radii	$1.4500 \times 10^{-5}$ earth radii/day
Nutation in Longitude	$0.46 \times 10^{-12}$ radians	$1.16 \times 10^{-12}$ radians/day
Nutation in Obliquity	$0.23 \times 10^{-12}$ radians	$0.58 \times 10^{-12}$ radians/day

The Chebyshev polynomial coefficients are obtained from the JPL ephemeris data in the following manner. Let the function values provided by the JPL software at requested times  $t_i, i = 1, 2, \dots, m + 1$ , for a single component of position, velocity, or nutation, be designated  $y_i$ . An  $m^{\text{th}}$  order interpolating function in the interval  $[t_i, t_{m+1}]$  can be obtained as a linear combination of basic functions  $F_j(t)$

$$Y_m(t) = \sum_{j=1}^{m+1} c_j F_j(t) \tag{3-244}$$

by requiring that the differences between the data and the function vanish, i.e.,

$$Q = \sum_{i=1}^{m+1} \left[ y_i - \sum_{j=1}^{m+1} c_j F_j(t_i) \right]^2 = 0 \tag{3-245}$$

The choice of the functions,  $F_j(t), j = 1, 2, \dots, m + 1$ , in Equation (3-244) has important ramifications both on the obtainable accuracy of  $Y_m(t)$  for  $t \neq t_i$  and the ease of determining the  $c_j$ .

The interval  $[t_1, t_{m+1}]$  is transformed to  $[1, -1]$  by the linear transformation of variables

$$x = \frac{2t - (t_{m+1} + t_1)}{t_{m+1} - t_1} \tag{3-246}$$

The functions  $F$  are then chosen as the orthogonal Chebyshev polynomials of degree  $j - 1$ , i.e.,

$$T_j(x) = \cos [(j - 1) \cos^{-1} x] \tag{3-247}$$

where

$$T_1(x) = 1$$

$$T_2(x) = x$$

$$T_3(x) = 2x^2 - 1 \tag{3-248}$$

$$\vdots$$

$$T_{j+1}(x) = 2xT_j(x) - T_{j-1}(x)$$



Under these conditions Equations (3-244) and (3-245) can be reformulated as

$$Y_m(x) = \sum_{j=1}^{m+1} c_j T_j(x) \quad (3-249)$$

and

$$Q = \sum_{i=1}^{m+1} \left[ y_i - \sum_{j=1}^{m+1} c_j T_j(x_i) \right]^2 = 0 \quad (3-250)$$

Data reduction can be achieved by selecting the largest possible interval  $[t_1, t_{m+1}]$  for which

$$\max_x \left\{ \left| y - \sum_{j=1}^{m+1} c_j T_j(x) \right| \right\} < \epsilon \quad (3-251)$$

for  $x$  in  $[1, -1]$ . This is satisfied if the coefficient of the truncated term  $c_{m+2} < \epsilon$ , because of the min max property of Chebyshev polynomials. For a given interval  $[t_1, t_{m+1}]$ , the discrepancy between  $y$  and  $Y_m(x)$  is minimized and the amount of work required to determine the  $c_j$  substantially reduced by selecting the base points  $x_i$  as the roots of the Chebyshev polynomial of degree  $m+1$ .

$$x_i = \cos \frac{(2i-1)}{2(m+1)} \quad i = 1, 2, \dots, m+1 \quad (3-252)$$

At these points the polynomials have the following orthogonality property with respect to summation as well as integration,

$$\sum_{a=1}^{m+1} T_j(x_a) T_k(x_a) = 0 \quad j \neq k \quad (3-253)$$

$$\sum_{a=1}^{m+1} T_j(x_a) T_k(x_a) = \frac{m+1}{2} \quad j = k, \quad j, k < m+1$$

This property is derived from the corresponding orthogonality property of the cosine functions and makes it possible to determine the  $c_j$  from

$$c_1 = \frac{1}{m+1} \sum_{i=1}^{m+1} y_i T_1(x_i) \quad (3-254a)$$

$$c_j = \frac{2}{m+1} \sum_{i=1}^{m+1} y_i T_j(x_i), \quad j = 2, 3, \dots, m+1 \quad (3-254b)$$

Once the coefficients,  $c_j$ , of the linear combination of  $T_j$  have been determined,  $Y_m(x)$  may be conveniently transformed into the equivalent Chebyshev interpolating polynomial in  $[1, -1]$

$$Y_m(x) = \sum_{i=1}^{m+1} b_i x^{i-1} \quad (3-255)$$

as follows.

Let

$$a_{1j} = (-1)^{j+1} c_{2j-1} \quad j = 1, 2, \dots, (2j-1) \leq m \quad (3-256a)$$

$$a_{i1} = 2^{i-2} c_i \quad i = 2, 3, \dots, m+1 \quad (3-256b)$$

and

$$a_{ij} = c_{[i+2(j-1)]} [2a_{i-1,j} - a_{i,j-1}] \quad i = 2, 3, \dots, [i+2(j-1)] \leq m+1 \quad (3-256c)$$

$$j = 2, 3, \dots, [i+2(j-1)] \leq m+1$$

Then, the coefficients,  $b_i$ , of the interpolating polynomial can be determined from

$$b_i = \sum_j a_{ij} \quad i = 1, 2, \dots, m+1$$

$$j = 1, 2, \dots, [i+2(j-1)] \leq m+1 \quad (3-257)$$

Finally, the polynomial so determined can be used to interpolate in the interval  $[t_1, t_{m+1}]$  by means of the transformation of variables defined by Equation (3-246).

The present version of GTDS can handle any of 10 bodies, one of which is the central body. A solar/lunar/planetary file by Chebyshev approximating polynomials is generated covering the entire time interval of interest. The file contains polynomials for each component of position and velocity and for each element of the matrices which transform from the selenocentric true of date to the selenographic coordinate system and from the mean equator and equinox of date to the true of date coordinate system, as required by the application. The file also contains coefficients for the equation of the equinoxes,  $\Delta H$ , used to correct the mean Greenwich sidereal time as given in Equation (3-19).

### 3.7 REFERENCES

1. Her Majesty's Stationery Office: 1961, Explanatory Supplement, Nautical Almanac Office, London.
2. U. S. Government Printing Office: 1967, The American Ephemeris and Nautical Almanac, Nautical Almanac Office, Washington, D. C.
3. Melbourne, W. G., Mulholland, J. D., Sjogren, W. L., and Sturms, F. M.: 1968, Constants and Related Information for Astrodynamic Calculations, 1938, Jet Propulsion Laboratory Technical Report 32-1306, July 1968.
4. Kalensher, B. E.: 1961, Selenographic Coordinates, Jet Propulsion Laboratory Technical Report 32-41, February 1961.
5. Peabody, P. R., Scott, J. F., and Orozco, E. G.: 1964, User's Description of JPL Ephemeris Tapes, Jet Propulsion Laboratory Technical Report 32-580, March 1964.
6. TRW Systems Group Report TRW 70-FMT-792A: 1970, Houston Operations Predictor/Estimator (HOPE) Engineering Manual, June 1970.
7. Escobal, P. R.: 1965, Methods of Orbit Determination, New York, John Wiley and Sons, inc.
8. Battin, R. H.: 1964, Astronautical Guidance, New York, McGraw Hill.
9. Cefola, P. J., Long, A. C., and Nimitz, K. S.: 1972, The Next Generation of Orbit Prediction Formulations for Artificial Satellites, Computer Sciences Corporation Report 9101-053000-01TF, September 1972.

10. Cefola, P. J.: 1972, Equinoctial Orbit Elements — Application to Artificial Satellite Orbits, AIAA Paper 72-937, presented at the AIAA/AAS Astrodynamics Conference, Palo Alto, California, September 11-12, 1972.
11. Baker, R. M. L., Jr.: 1961, Astrodynamics, Applications, and Advanced Topics. New York, Academic Press.
12. Dallas, S. S., and Rinderle, E. A.: 1972, A Comparison of Cowell's Method and a Variation-of-Parameters Method for the Computation of Precision Satellite Orbits, Jet Propulsion Laboratory Technical Memorandum 392-101, Final Report, September 1972.
13. Brodie, R. A., Newell, F. F., Ekelund, J. E., and Warner, M. R.: 1969, Double Precision Orbit Determination Program, Vol. III, Jet Propulsion Laboratory Technical Report JPL-900-56; also, NASA Report NASA-CR-105589, June 1969.
14. Goddard Space Flight Center: 1968, Satellite Geodesy Theory and Applications, Wolf Research and Development Corp.
15. Curtright, J.: 1972, DSN Frequency and Time Scale Change from UTC to IAT or New UTC, Jet Propulsion Laboratory Technical Report 32-i526, Vol. VIII.
16. Chi, A. R. and Fosque, H. S.: 1971, Changes in Standard Frequency and Time-Signal Broadcast — January 1, 1972, Goddard Space Flight Center Report X-810-71-489, November 1971.
17. Devine, C. J.: 1967, JPL Development Ephemeris Number 19, Jet Propulsion Laboratory Technical Report 32-1181, November 1967.
18. Armstrong, Michael G. and Tomaszewski, Isabel B.: 1973, Generation and Use of the GTDS SLP Ephemeris Files, Goddard Space Flight Center Report X-552-73-20, January 1973.

## CHAPTER 4

## PERTURBATION MODELS AND VARIATIONAL EQUATIONS

For orbital prediction using the method of special perturbations, the equations of motion of the satellite are integrated numerically. The perturbing acceleration vector is required to construct these equations, which are presented in Chapter 5. The sources of these perturbations are identified and the appropriate perturbation models presented in this chapter. The perturbations discussed include:

- the gravitational acceleration due to n-point masses,  $\ddot{\mathbf{R}}_{PM}$
- the gravitational acceleration due to nonsphericity of the gravitational potential,  $\ddot{\mathbf{R}}_{NE}$
- the acceleration due to the mutual nonspherical gravitational attraction of the earth and moon,  $\ddot{\mathbf{R}}_{IO}$
- the acceleration due to aerodynamic forces,  $\ddot{\mathbf{R}}_D$
- the acceleration due to solar radiation pressure,  $\ddot{\mathbf{R}}_{SR}$
- the acceleration due to thrusting of the spacecraft engines,  $\ddot{\mathbf{R}}_T$
- the acceleration due to attitude control system corrections,  $\ddot{\mathbf{R}}_{TAC}$
- model replacement accelerations,  $\ddot{\mathbf{R}}_A$

All or any subset of these effects can be included in the perturbing acceleration vector which is used in the construction of the equations of motion using either the Cowell or Variation of Parameters formulations.

The partial derivatives of the current state vector with respect to the initial state vector are required in the differential correction process. These partial derivatives, which constitute the state transition matrix, can be obtained by numerically integrating a system of variational equations in conjunction with the Cowell orbit generator. The construction of these variational equations is discussed in detail for each of the perturbing accelerations. Accelerations which are included in the equations of motion, but for which the estimation process is insensitive, can be omitted in the construction of the variational equations.

A method of computing the partial derivatives analytically is discussed in Section 4.10. This analytical approach is always used in the differential correction process in GTDS when the Variation of Parameters or Brouwer orbit generators are used, and is optional in the Cowell differential correction process.

#### 4.1 TOTAL PERTURBATION MODEL AND VARIATIONAL EQUATIONS

The total acceleration vector is the sum of the accelerations induced by each of the sources listed above (expressed in an inertial Cartesian coordinate system, i.e., mean equator and equinox of 1950.0 or true of reference date.)

$$\ddot{\mathbf{R}} = \ddot{\mathbf{R}}_{PM} + \ddot{\mathbf{R}}_{NS} + \ddot{\mathbf{R}}_{IC} + \ddot{\mathbf{R}}_D + \ddot{\mathbf{R}}_{SR} + \ddot{\mathbf{R}}_{TAC} + \ddot{\mathbf{R}}_T. \quad (4-1)$$

The total perturbing acceleration vector is usually defined as the total acceleration excluding the point mass gravitational acceleration caused by the central body.

The Cowell equations of motion of the satellite may be written in the form

$$\ddot{\mathbf{R}} = \mathbf{f}(\bar{\mathbf{R}}, \dot{\mathbf{R}}, t, \bar{\mathbf{p}}) \quad (4-2)$$

where

$\bar{\mathbf{R}} \sim$  column vector of vehicle position coordinates  
 $\bar{\mathbf{p}} \sim$  vector of dynamic parameters of dimension  $n$

and

$$\bar{\mathbf{p}} = (\bar{\mathbf{R}}(t_0), \dot{\bar{\mathbf{R}}}(t_0), \bar{\mathbf{p}}^*)^T \quad (4-3)$$

where

$\bar{\mathbf{p}}^* \sim$  constant model parameters pertaining to drag, gravitational harmonic coefficients, etc.

The model parameters  $\bar{\mathbf{p}}$ , which may be included in the variational equations, are as follows:

- Position and velocity of the spacecraft in mean of 1950.0 coordinates, true of date coordinates, classical orbital elements at epoch, spherical coordinates, or DODS variables
- Gravitational parameter of the central body
- Harmonics of the central body
- Gravitational parameters of perturbing bodies
- Aerodynamic drag parameter
- Solar radiation pressure parameter
- Powered flight parameters
- Attitude control parameters.

These parameters are determined in such a way as to reduce the differences between a computed and an observed orbit. This orbit determination process requires the computation of variations in the state variables,  $\bar{\mathbf{R}}(t)$  and  $\dot{\bar{\mathbf{R}}}(t)$ , as functions of variations in this parameter set.

If Equation (4-2) is differentiated with respect to  $\bar{\mathbf{p}}$ , the matrix equation

$$\frac{\partial \ddot{\bar{\mathbf{R}}}}{\partial \bar{\mathbf{p}}} = \frac{\partial \ddot{\bar{\mathbf{R}}}}{\partial \bar{\mathbf{R}}} \frac{\partial \bar{\mathbf{R}}}{\partial \bar{\mathbf{p}}} + \frac{\partial \ddot{\bar{\mathbf{R}}}}{\partial \dot{\bar{\mathbf{R}}}} \frac{\partial \dot{\bar{\mathbf{R}}}}{\partial \bar{\mathbf{p}}} + \left( \frac{\partial \ddot{\bar{\mathbf{R}}}}{\partial \bar{\mathbf{p}}} \right)_{\text{explicit}} \quad (4-4)$$

is obtained. If time  $t$  and the parameter set  $\bar{\mathbf{p}}$  are independent, the differentiation with respect to  $t$  and  $\bar{\mathbf{p}}$  may be interchanged to give

$$\frac{d^2}{dt^2} \left( \frac{\partial \bar{\mathbf{R}}}{\partial \bar{\mathbf{p}}} \right) = \frac{\partial \ddot{\bar{\mathbf{R}}}}{\partial \bar{\mathbf{R}}} \frac{\partial \bar{\mathbf{R}}}{\partial \bar{\mathbf{p}}} + \frac{\partial \ddot{\bar{\mathbf{R}}}}{\partial \dot{\bar{\mathbf{R}}}} \frac{d}{dt} \left( \frac{\partial \bar{\mathbf{R}}}{\partial \bar{\mathbf{p}}} \right) + \left( \frac{\partial \ddot{\bar{\mathbf{R}}}}{\partial \bar{\mathbf{p}}} \right)_{\text{explicit}} \quad (4-5)$$

Defining the matrices

$$\begin{aligned} \mathbf{A}(t) &= \left[ \frac{\partial \ddot{\bar{\mathbf{R}}}(t)}{\partial \bar{\mathbf{R}}} \right]_{3 \times 3} & \mathbf{C}(t) &= \left[ \left( \frac{\partial \ddot{\bar{\mathbf{R}}}(t)}{\partial \bar{\mathbf{p}}} \right)_{\text{explicit}} \right]_{3 \times l} \\ \mathbf{B}(t) &= \left[ \frac{\partial \ddot{\bar{\mathbf{R}}}(t)}{\partial \dot{\bar{\mathbf{R}}}} \right]_{3 \times 3} & \mathbf{Y}(t) &= \left[ \frac{\partial \ddot{\bar{\mathbf{R}}}(t)}{\partial \bar{\mathbf{p}}} \right]_{3 \times l} \end{aligned} \quad (4-6)$$

Equation (4-5) takes the form of a system of linear differential equations

$$\ddot{\mathbf{Y}} = \mathbf{A}(t) \mathbf{Y} + \mathbf{B}(t) \dot{\mathbf{Y}} + \mathbf{C}(t) \quad (4-7)$$

called the variational equations.

Just as the basic Equation (4-1) is numerically integrated to obtain the position  $\bar{\mathbf{R}}(t)$  and velocity  $\dot{\bar{\mathbf{R}}}(t)$  of the satellite, the variational equations are integrated to obtain the matrices  $\mathbf{Y}(t)$  and  $\dot{\mathbf{Y}}(t)$ , which yield the required partial derivatives. These partial derivatives are used to form the observation partial derivatives required for differential correction of the orbit. This application is discussed in Chapter 7.

The matrices  $\mathbf{A}$ ,  $\mathbf{B}$ , and  $\mathbf{C}$  are formulated for the case where  $\ddot{\bar{\mathbf{R}}}$  is of the form given in Equation (4-1)

$$\mathbf{A} = \frac{\partial \ddot{\bar{\mathbf{R}}}_{\text{PM}}}{\partial \bar{\mathbf{R}}} + \frac{\partial \ddot{\bar{\mathbf{R}}}_{\text{NS}}}{\partial \bar{\mathbf{R}}} + \frac{\partial \ddot{\bar{\mathbf{R}}}_{\text{D}}}{\partial \bar{\mathbf{R}}} + \frac{\partial \ddot{\bar{\mathbf{R}}}_{\text{SR}}}{\partial \bar{\mathbf{R}}} + \frac{\partial \ddot{\bar{\mathbf{R}}}_{\text{TAC}}}{\partial \bar{\mathbf{R}}} + \frac{\partial \ddot{\bar{\mathbf{R}}}_{\text{T}}}{\partial \bar{\mathbf{R}}} \quad (\text{a})$$

$$\mathbf{B} = \frac{\partial \ddot{\bar{\mathbf{R}}}_{\text{D}}}{\partial \dot{\bar{\mathbf{R}}}} \quad (\text{b}) \quad (4-8)$$

$$\mathbf{C} = \left( \frac{\partial \ddot{\bar{\mathbf{R}}}}{\partial \bar{\mathbf{p}}} \right)_{\text{explicit}} = \left[ \frac{\partial \ddot{\bar{\mathbf{R}}}}{\partial \bar{\mathbf{r}}_0}, \frac{\partial \ddot{\bar{\mathbf{R}}}}{\partial \dot{\bar{\mathbf{r}}}_0}, \frac{\partial \ddot{\bar{\mathbf{R}}}}{\partial \bar{\mathbf{p}}^*} \right]_{\text{explicit}} = \left[ \mathbf{0}_3, \mathbf{0}_3, \frac{\partial \ddot{\bar{\mathbf{R}}}}{\partial \bar{\mathbf{p}}^*} \right] \quad (\text{c})$$

where

$$\mathbf{0}_3 \sim 3 \times 3 \text{ null matrix}$$

$\frac{\partial \ddot{\bar{\mathbf{R}}}}{\partial \bar{\mathbf{p}}^*} \sim$  columns of explicit partial derivatives of acceleration with respect to model parameters:

$$\frac{\partial \ddot{\bar{\mathbf{R}}}_{\text{PM}}}{\partial \mu}, \quad \frac{\partial \ddot{\bar{\mathbf{R}}}_{\text{PM}}}{\partial \mu_k}, \quad \frac{\partial \ddot{\bar{\mathbf{R}}}_{\text{NS}}}{\partial C_n^m}, \quad \dots \text{etc.}$$

## 4.2 POINT MASS EFFECTS

To first order, the gravitational attraction of a perturbing body of mass  $m$  can be approximated as that arising from a dimensionless particle of mass  $m$  located at the center of mass of the body. An expression for the perturbing acceleration arising from  $n$ -point masses is developed in this section.



#### 4.2.1 N-Point Masses Perturbation Model

In the development of the perturbation model for the gravitational effect of n-massive bodies, the starting point is Newton's second law of motion and law of gravitation (References 1, 2, 3).

The second law of motion for a body of mass  $m$ , acted upon by a force  $\bar{F}$ , is given by

$$\bar{F} = \frac{d}{dt} \left( m \frac{d\tilde{R}}{dt} \right) \quad (4-9)$$

which reduces to

$$\bar{F} = m \frac{d^2\tilde{R}}{dt^2} \quad (4-10)$$

when  $m$  is constant. Here  $\tilde{R}$  is a vector from the center of an inertial coordinate system to the satellite.

The gravitational force acting on a satellite of mass  $m$  due to the attraction of a body of mass  $m_k$ , which is assumed to act as a point mass, is given by

$$\bar{F}_k = - \frac{Gmm_k}{R_{kp}^3} \bar{R}_{kp} \quad (4-11)$$

where  $G$  is the universal gravitational constant and  $\bar{R}_{kp}$  the vector from the body  $k$  to the satellite (see Figure 4-1).

In order to obtain the total contribution from all perturbing bodies, a summation over  $k$  is performed

$$\bar{F} = - \sum_{k=1}^n \frac{Gmm_k}{R_{kp}^3} \bar{R}_{kp} \quad (4-12)$$

When this expression is substituted into Equation (4-10), the acceleration experienced by a satellite attracted by n-point masses is obtained in an inertial coordinate system

$$\frac{d^2\tilde{R}}{dt^2} = - \sum_{k=1}^n \frac{Gm_k}{R_{kp}^3} \bar{R}_{kp} \quad (4-13)$$

For convenience and ease in the interpretation of results, it is advantageous to refer the motion of the satellite to one of the perturbing bodies. The force on body  $j$ , the reference or central body, is given by

$$\bar{F}_j = \sum_{\substack{k=1 \\ k \neq j}}^n \frac{Gm_j m_k}{R_k^3} \bar{R}_k \quad (4-14)$$

where  $\bar{R}_k$  is a vector from the reference  $j^{\text{th}}$  body to the  $k^{\text{th}}$  body. The acceleration of the reference body with respect to the inertial coordinate system is given by

$$\frac{d^2 \tilde{R}_j}{dt^2} = \sum_{\substack{k=1 \\ k \neq j}}^n \frac{Gm_k}{R_k^3} \bar{R}_k \quad (4-15)$$

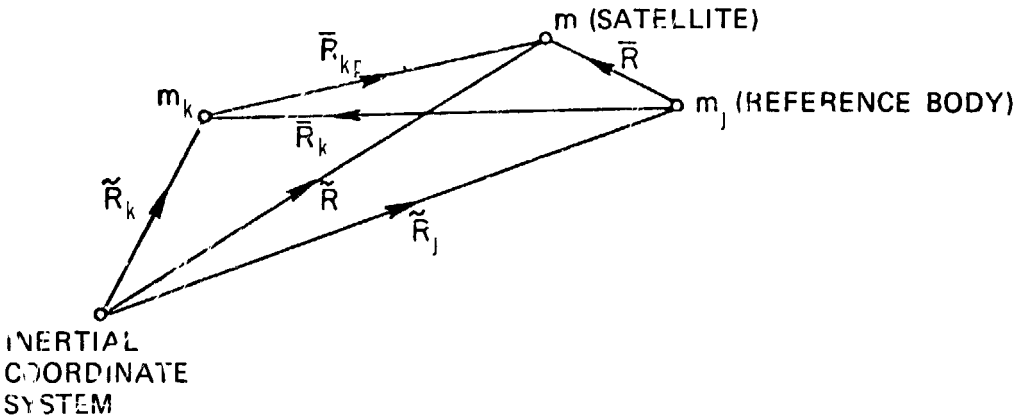


Figure 4-1. Schematic of Point Mass Gravitational Bodies

A subtraction of Equation (4-15) from Equation (4-13) yields

$$\frac{d^2 \tilde{R}}{dt^2} - \frac{d^2 \tilde{R}_j}{dt^2} = - \sum_{k=1}^n \frac{Gm_k}{R_{kp}^3} \bar{R}_{kp} - \sum_{\substack{k=1 \\ k \neq j}}^n \frac{Gm_k}{R_k^3} \bar{R}_k \quad (4-16)$$

Substituting  $\tilde{\mathbf{R}} - \tilde{\mathbf{R}}_j = \bar{\mathbf{R}} - \bar{\mathbf{R}}_j$  and  $\tilde{\mathbf{R}}_{kp} = \bar{\mathbf{R}} - \bar{\mathbf{R}}_k$  into Equation (4-16) yields the acceleration due to n-point masses

$$\ddot{\bar{\mathbf{R}}}_{PM} = \frac{d^2 \bar{\mathbf{R}}}{dt^2} = -\frac{\mu}{\bar{R}^3} \bar{\mathbf{R}} + \sum_{\substack{k=1 \\ k \neq j}}^n \mu_k \left( \frac{(\bar{\mathbf{R}}_k - \bar{\mathbf{R}})}{|\bar{\mathbf{R}}_k - \bar{\mathbf{R}}|^3} - \frac{\bar{\mathbf{R}}_k}{|\bar{\mathbf{R}}_k|^3} \right) \quad (4-17)$$

where  $\bar{\mathbf{R}}_{PM}$ ,  $\bar{\mathbf{R}}$ , and  $\bar{\mathbf{R}}_k$  are expressed in mean of 1950.0 coordinates or true of reference date coordinate whichever is the basic coordinate frame. The gravitational parameter  $\mu$  is the product of the mass of a given body and the universal gravitational constant. In particular,  $\mu_k = Gm_k$  for the  $k^{\text{th}}$  body, and  $\mu = Gm_j$  for the central body.

When only the effects of the central body are included in Equation (4-17), an analytic solution can be obtained. This solution is the basis for construction of the Variation of Parameters methods which are discussed in Chapter 5. Special perturbation methods are required for orbit propagation only when additional perturbation effects are considered. Consequently, the perturbing acceleration vector does not include the first term on the right hand side of Equation (4-17).

When the satellite is in a close orbit around the reference body, significant round-off errors may occur in the computation of Equation (4-17) due to the differencing of nearly equal numbers. When the earth is the central body, this error has not been found to be significant. However, it may be important in the computation of third body effects due to the earth when the moon is the central body. This difficulty can be removed by rewriting the equations of motion in a different, but equivalent, form.

Designate  $|\bar{\mathbf{R}}_{kp}|$  by  $r_{kp}$ ,  $|\bar{\mathbf{R}}_k|$  by  $r_k$ ,  $|\bar{\mathbf{R}}|$  by  $r$ , and the included angle between  $\mathbf{R}$  and  $\mathbf{R}_k$  by  $\psi$ ; then

$$r_{kp}^2 = r^2 + r_k^2 - 2r r_k \cos \psi \quad (4-18)$$

The ratio  $1/r_{kp}$  can be expanded in terms of Legendre functions as

$$\frac{1}{r_{kp}} = \frac{1}{r_k} \{P_0(\cos \psi) + P_1(\cos \psi) \frac{r}{r_k} + P_2(\cos \psi) \left(\frac{r}{r_k}\right)^2 + \dots\} = \frac{1+B}{r_k} \quad (4-19)$$

where

$$h = \frac{r}{r_k}$$

$$B = \sum_{j=1}^{\infty} P_j(\cos \theta) h^j$$

Substitution of the expansion of the numerator  $1/|\bar{\mathbf{R}}_k - \bar{\mathbf{R}}|^3 = 1/r_{kp}^3 = (1+B)^3/r_k^3$  and the relationship  $\bar{\mathbf{R}}_k = \bar{\mathbf{R}} - \bar{\mathbf{R}}_{kp}$  into Equation (4-17) yields

$$\ddot{\bar{\mathbf{R}}}_{PM} = \frac{d^2 \bar{\mathbf{R}}}{dt^2} = -\frac{\mu}{R^3} \bar{\mathbf{R}} + \sum_{\substack{k=1 \\ k \neq j}}^n \mu_k \left( \frac{-\bar{\mathbf{R}}_{kp} (3B + 3B^2 + B^3) - \bar{\mathbf{R}}}{|\bar{\mathbf{R}}_k|^3} \right) \quad (4-20)$$

This procedure eliminates the numerical difficulty. The series in  $h$  is truncated by terminating the series when  $h^n \leq \epsilon_h$ , where  $\epsilon_h$  is a predetermined tolerance.

#### 4.2.2 Associated Partial Derivatives

The associated partial derivatives are given by

$$\frac{\partial \ddot{\bar{\mathbf{R}}}_{PM}}{\partial \bar{\mathbf{R}}} = -\left( \frac{\mu}{R^3} + \sum_{k=1}^n \frac{\mu_k}{|\bar{\mathbf{R}}_k - \bar{\mathbf{R}}|^3} \right) \mathbf{I} + 3 \left( \frac{\mu \bar{\mathbf{R}} \bar{\mathbf{R}}^T}{R^5} + \sum_{k=1}^n \left[ \mu_k \frac{(\bar{\mathbf{R}}_k - \bar{\mathbf{R}})(\bar{\mathbf{R}}_k - \bar{\mathbf{R}}^T)}{|\bar{\mathbf{R}}_k - \bar{\mathbf{R}}|^5} \right] \right) \quad (4-21)$$

$$\frac{\partial \ddot{\bar{\mathbf{R}}}_{PM}}{\partial \dot{\bar{\mathbf{R}}}} = \mathbf{0}_3 \quad (4-22)$$

where  $\mathbf{I}$  is the identity matrix of dimension three.

The associated C-matrix columns for the model parameters  $\mu$  and  $\mu_k$  are given by

$$\frac{\partial \ddot{\bar{\mathbf{R}}}_{PM}}{\partial \mu} = -\frac{\bar{\mathbf{R}}}{R^3} \quad (4-23)$$

$$\frac{\partial \ddot{\bar{\mathbf{R}}}_{PM}}{\partial \mu_k} = \frac{(\bar{\mathbf{R}}_k - \bar{\mathbf{R}})}{|\bar{\mathbf{R}}_k - \bar{\mathbf{R}}|^3} - \frac{\bar{\mathbf{R}}}{R^3} \quad (4-24)$$

### 4.3 NONSPHERICAL GRAVITATIONAL EFFECTS

Most solar system bodies are known to have figures which depart from the spherical model of the particle. The nonsphericity of the gravitational potential may give rise to a significant perturbation of satellite trajectories. Therefore, accurate orbit determination may require the inclusion of nonspherical terms. The gravitational potentials of the earth and moon are the best known of all solar system bodies, because of extensive tracking and analysis of close earth and lunar satellites. The figures of planets with natural satellites are known, although less accurately, through study of the motion of their natural satellites.

#### 4.3.1 Nonspherical Gravitational Perturbation Model

The next perturbation considered is that due to the nonsphericity of a massive body. The method of representing its potential is classical and may be found in numerous publications (References 3, 4, 5). The gravitational field of the body is derived from a scalar potential  $\psi$  that satisfies Poisson's equation

$$\nabla^2 \psi(r, \phi, \lambda) = -4\pi\mu_k \rho(r, \phi, \lambda) \tag{4-25}$$

where  $r \sim$  the magnitude of the vector from the body's center of mass to the satellite

$\phi \sim$  the geocentric, selenocentric, or planetocentric latitude

$\lambda \sim$  the geocentric, selenocentric, or planetocentric longitude (measured east from the prime meridian)

Above the surface of the perturbing body, the mass density,  $\rho$ , is zero; consequently, Equation (4-25) reduces to the Laplacian,  $\nabla^2 \psi = 0$ . Standard separation of variables technique yields the solution

$$\begin{aligned} \psi(r, \phi, \lambda) = & \frac{\mu}{r} + \frac{\mu}{r} \sum_{n=1}^{\infty} C_n^0 \left(\frac{R_e}{r}\right)^n P_n^0(\sin \phi) \\ & + \frac{\mu}{r} \sum_{n=1}^{\infty} \sum_{m=1}^n \left(\frac{R_e}{r}\right)^n P_n^m(\sin \phi) [S_n^m \sin m\lambda + C_n^m \cos m\lambda] \end{aligned} \tag{4-26}$$

where the first term is the point mass potential for Keplerian motion and the second and third terms are the nonspherical potential due to the sum of zonal and tesseral harmonics respectively.

$\mu \sim$  the gravitational parameter of the central body

$R_e \sim$  the radius of the body (usually taken as the equatorial radius)

$P_n^m \sim$  the associated Legendre function

$S_n^m, C_n^m \sim$  harmonic coefficients, i.e.,

- zonal harmonics for  $m = 0$
- sectorial harmonics for  $m = n$
- tesseral harmonics for  $n > m \neq 0$

(note:  $J_n = -C_n^0$ )

The term  $n = 1$  is usually not present when the origin of the coordinate system is placed at the center of mass.

The total gravitational force is the gradient of  $\psi$ ; therefore, the noncentral force acting on the spacecraft due to the attracting body is the gradient of the nonspherical terms in the potential function  $\psi$ .

Expressing the gradient in body-fixed coordinates (Figure 4-2), the following form for the inertial acceleration vector is obtained (see discussion following Equation (4-38)).

$$\bar{a}_b = \begin{bmatrix} a_{x_b} \\ a_{y_b} \\ a_{z_b} \end{bmatrix} = \frac{\partial \psi}{\partial r} \left( \frac{\partial \mathbf{r}}{\partial \bar{r}_b} \right)^T + \frac{\partial \psi}{\partial \phi} \left( \frac{\partial \phi}{\partial \bar{r}_b} \right)^T + \frac{\partial \psi}{\partial \lambda} \left( \frac{\partial \lambda}{\partial \bar{r}_b} \right)^T \quad (4-27)$$

The partial derivatives of the nonspherical portion of the potential with respect to  $r$ ,  $\phi$ , and  $\lambda$  are given by

$$\frac{\partial \psi}{\partial r} = -\frac{1}{r} \frac{\mu}{r} \sum_{n=2}^{\infty} \left( \frac{R_e}{r} \right)^n (n+1) \sum_{m=0}^n (C_n^m \cos m\lambda + S_n^m \sin m\lambda) P_n^m(\sin \phi) \quad (a)$$

$$\frac{\partial \psi}{\partial \phi} = \frac{\mu}{r} \sum_{n=2}^{\infty} \left( \frac{R_e}{r} \right)^n \sum_{m=0}^n (C_n^m \cos m\lambda + S_n^m \sin m\lambda) [P_n^{m+1}(\sin \phi) - m \tan \phi P_n^m(\sin \phi)] \quad (b)(4-28)$$

$$\frac{\partial \psi}{\partial \lambda} = \frac{\mu}{r} \sum_{n=2}^{\infty} \left( \frac{R_e}{r} \right)^n \sum_{m=0}^n m (S_n^m \cos m\lambda - C_n^m \sin m\lambda) P_n^m(\sin \phi). \quad (c)$$

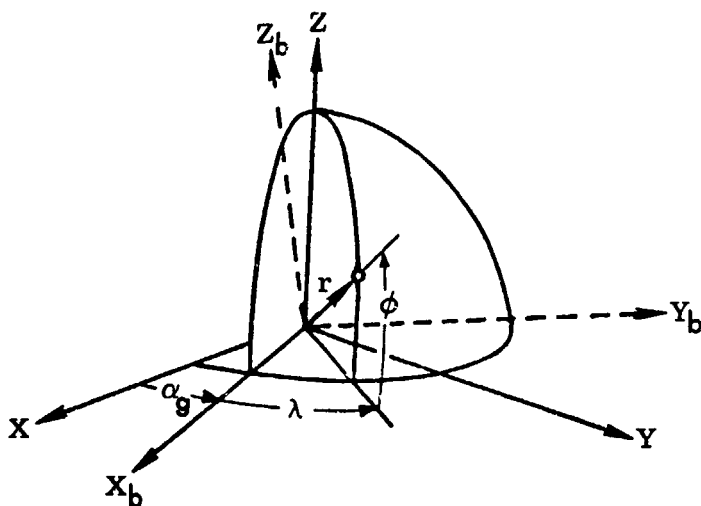


Figure 4-2. Body-Fixed System

The Legendre functions and the terms  $\cos m\lambda$ ,  $\sin m\lambda$ , and  $m \tan \phi$  are computed via recursion formulae:

$$P_n^0(\sin \phi) = [(2n-1) \sin \phi P_{n-1}^0(\sin \phi) - (n-1) P_{n-2}^0(\sin \phi)] / n \quad (4-29)$$

$$P_n^m(\sin \phi) = P_{n-2}^m(\sin \phi) + (2n-1) \cos \phi P_{n-1}^{m-1}(\sin \phi) \quad m \neq 0, m < n \quad (4-30)$$

$$P_n^m(\sin \phi) = (2n-1) \cos \phi P_{n-1}^{m-1}(\sin \phi) \quad m \neq 0, m = n \quad (4-31)$$

where

$$P_0^0(\sin \phi) = 1, \quad P_1^0(\sin \phi) = \sin \phi, \quad P_1^1(\sin \phi) = \cos \phi \quad (4-32)$$

$$\sin m\lambda = 2 \cos \lambda \sin(m-1)\lambda - \sin(m-2)\lambda \quad (a) \quad (4-33)$$

$$\cos m\lambda = 2 \cos \lambda \cos(m-1)\lambda - \cos(m-2)\lambda \quad (b)$$

$$m \tan \phi = [(m-1) \tan \lambda] + \tan \phi \quad (4-34)$$

The recursion relationships above are the most efficient method of computing the complete set of associated Legendre polynomials and spherical harmonics up to a certain order and degree. However, higher degree harmonic terms can cause satellites with repeating ground tracks to undergo large perturbations when the trajectory and the harmonic frequency are synchronized (resonant). The synchronization causes the satellite to sample the gravitational field in such a way that large cumulative perturbations result. Individual resonant harmonics can be computed in GTDS without using the recursive algorithm described above.

Use of a low order recursive harmonic model with nonrecursive computation of high order resonant terms is considerably more efficient than carrying out recursive computation of the total high order harmonic model.

The partial derivatives of  $r$ ,  $\phi$ , and  $\lambda$  with respect to  $x_b$ ,  $y_b$ , and  $z_b$  are computed from the expressions

$$\frac{\partial r}{\partial \bar{r}_b} = \frac{\bar{r}_b^T}{r} \quad (4-35)$$

$$\frac{\partial \phi}{\partial \bar{r}_b} = \frac{1}{\sqrt{x_b^2 + y_b^2}} \left[ -\frac{z_b \bar{r}_b^T}{r^2} + \frac{\partial z_b}{\partial \bar{r}_b} \right] \quad (4-36)$$

$$\frac{\partial \lambda}{\partial \bar{r}_b} = \frac{1}{(x_b^2 + y_b^2)} \left[ x_b \frac{\partial y_b}{\partial \bar{r}_b} - y_b \frac{\partial x_b}{\partial \bar{r}_b} \right] \quad (4-37)$$

where

$$\frac{\partial x_b}{\partial \bar{r}_b}, \quad \frac{\partial y_b}{\partial \bar{r}_b}, \quad \text{and} \quad \frac{\partial z_b}{\partial \bar{r}_b}$$

are the row vectors  $(1, 0, 0)$ ,  $(0, 1, 0)$ , and  $(0, 0, 1)$ , respectively.

Substituting Equations (4-35) through (4-37) into Equation (4-27) yields

$$a_{x_b} = \left( \frac{1}{r} \frac{\partial \psi}{\partial r} - \frac{z_b}{r^2 \sqrt{x_b^2 + y_b^2}} \frac{\partial \psi}{\partial \phi} \right) x_b - \left( \frac{1}{(x_b^2 + y_b^2)} \frac{\partial \psi}{\partial \lambda} \right) x_b \quad (a)$$

$$a_{y_b} = \left( \frac{1}{r} \frac{\partial \psi}{\partial r} - \frac{z_b}{r^2 \sqrt{x_b^2 + y_b^2}} \frac{\partial \psi}{\partial \phi} \right) y_b + \left( \frac{1}{x_b^2 + y_b^2} \frac{\partial \psi}{\partial \lambda} \right) x_b \quad (b) \quad (4-38)$$

$$a_{z_b} = \left( \frac{1}{r} \frac{\partial \psi}{\partial r} \right) z_b + \frac{\sqrt{x_b^2 + y_b^2}}{r^2} \frac{\partial \psi}{\partial \phi} \quad (c)$$

where  $a_{x_b}$ ,  $a_{y_b}$  and  $a_{z_b}$  are the components of the inertial acceleration of the spacecraft expressed in the body-fixed coordinate system, and not the acceleration with respect to the body-fixed coordinate system. Thus, it is necessary to transform these components into an inertial frame before integrating the equations of motion.

Since the numerical computations of the program are calculated in the inertial mean equator and equinox of 1950.0 coordinate system, a series of transformations are made to represent the acceleration vector in this system. For the



case of the earth, there are two options available to accomplish this: the first is the more accurate, whereas the second is computationally faster.

For the more accurate option, the inertial acceleration  $\bar{a}_b$  expressed in body-fixed coordinates is transformed to the inertial mean of 1950.0 axes by means of the transformation

$$\ddot{\bar{R}}_{NS} = C^T B^T \bar{a}_b \quad (4-39)$$

where  $B^T$  transforms from body-fixed to true of date coordinates and  $C^T$  from true of date to inertial mean of 1950.0 coordinates as discussed in Sections 3.3.1 and 3.3.2. The matrix  $B^T$  accounts for polar motion and Greenwich sidereal time.

The simpler option neglects polar motion by assuming the geographic pole  $z_b$  to be aligned with the spin axis  $z$  in the true of date system. This allows the nonspherical gravity components to be expressed directly in true of date coordinates. Thus, by replacing  $(x_b, y_b, z_b)$  in Equations (4-27) and (4-35) through (4-38) by  $(x, y, z)$  the true of date components are calculated directly. The longitude and latitude are calculated as follows

$$\lambda = \alpha - \alpha_g \quad (4-40)$$

$$\phi = \sin^{-1} \left( \frac{z}{r} \right) \quad (4-41)$$

where

$\alpha \sim$  the right ascension of the spacecraft,  $\alpha = \tan^{-1} (y/x)$

$\alpha_g \sim$  the right ascension of Greenwich.

Computation of the acceleration due to the nonspherical moon in 1950.0 coordinates requires some different operations than those used for the earth. The right ascension of the Greenwich meridian has no meaning, so that the step of going from body-fixed coordinates to the true of date system cannot be implemented.

The lunar body-fixed coordinates (also known as selenographic coordinates) are coincident with the principal axes of inertia and are defined in the following way: the  $x'$  axis lies along a direction nearly colinear with the moon to earth vector; the  $z'$  axis lies along the axis of rotation, or polar axis, of the moon; and the  $y'$  axis lies in the equatorial plane of the moon and completes a right-handed coordinate system.

Three rotations are necessary to transform the selenographic acceleration vector to a vector referred to the mean earth equator and equinox of 1950.0 system. The first rotation takes the acceleration vector to the true earth equator and equinox of date coordinate system centered at the moon (selenocentric). The other two rotations involve the precession and nutation effects that are included to express the acceleration in the 1950.0 system. These rotations are discussed in Sections 3.3.1 and 3.3.3.

#### 4.3.2 Associated Partial Derivatives

The partial derivatives of  $\bar{a}_b$  with respect to  $\bar{r}_b$  are obtained by differentiating Equation (4-27) yielding

$$\begin{aligned} \frac{\partial \bar{a}_b}{\partial \bar{r}_b} &= \frac{\partial}{\partial \bar{r}_b} \left( \frac{\partial \psi}{\partial r} \right) \frac{\partial r}{\partial \bar{r}_b} + \frac{\partial}{\partial \bar{r}_b} \left( \frac{\partial \psi}{\partial \phi} \right) \frac{\partial \phi}{\partial \bar{r}_b} + \frac{\partial}{\partial \bar{r}_b} \left( \frac{\partial \psi}{\partial \lambda} \right) \frac{\partial \lambda}{\partial \bar{r}_b} \\ &+ \frac{\partial \psi}{\partial r} \frac{\partial^2 r}{\partial \bar{r}_b^2} + \frac{\partial \psi}{\partial \phi} \frac{\partial^2 \phi}{\partial \bar{r}_b^2} + \frac{\partial \psi}{\partial \lambda} \frac{\partial^2 \lambda}{\partial \bar{r}_b^2} \end{aligned} \quad (4-42)$$

The required partial derivatives of  $\partial \psi / \partial r$ ,  $\partial \psi / \partial \phi$ , and  $\partial \psi / \partial \lambda$  with respect to  $\bar{r}_b$  are obtained by differentiating Equation (4-28) as follows

$$\frac{\partial}{\partial \bar{r}_b} \begin{bmatrix} \frac{\partial \psi}{\partial r} \\ \frac{\partial \psi}{\partial \phi} \\ \frac{\partial \psi}{\partial \lambda} \end{bmatrix} = \begin{bmatrix} \frac{\partial^2 \psi}{\partial r^2} & \frac{\partial^2 \psi}{\partial r \partial \phi} & \frac{\partial^2 \psi}{\partial r \partial \lambda} \\ \frac{\partial^2 \psi}{\partial \phi \partial r} & \frac{\partial^2 \psi}{\partial \phi^2} & \frac{\partial^2 \psi}{\partial \phi \partial \lambda} \\ \frac{\partial^2 \psi}{\partial \lambda \partial r} & \frac{\partial^2 \psi}{\partial \lambda \partial \phi} & \frac{\partial^2 \psi}{\partial \lambda^2} \end{bmatrix} \begin{bmatrix} \frac{\partial r}{\partial \bar{r}_b} \\ \frac{\partial \phi}{\partial \bar{r}_b} \\ \frac{\partial \lambda}{\partial \bar{r}_b} \end{bmatrix} \quad (4-43)$$

In order to minimize computations, the symmetry property of the second partial derivatives of  $\psi$  is utilized as indicated below

$$\frac{\partial^2 \psi}{\partial r^2} = \frac{\mu}{r^3} \sum_{n=2}^{\infty} \left( \frac{R_e}{r} \right)^n (n+2)(n+1) \sum_{m=0}^n (C_n^m \cos m\lambda + S_n^m \sin m\lambda) P_n^m(\sin \phi)$$

$$\frac{\partial^2 \psi}{\partial r \partial \phi} = \frac{\partial^2 \psi}{\partial \phi \partial r} = -\frac{\mu}{r^3} \sum_{n=2}^{\infty} \left( \frac{R_e}{r} \right)^n (n+1) \sum_{m=0}^n (C_n^m \cos m\lambda + S_n^m \sin m\lambda)$$

$$\times [P_n^{m+1}(\sin \phi) - m \tan \phi P_n^m(\sin \phi)]$$

$$\frac{\partial^2 \psi}{\partial r \partial \lambda} = \frac{\partial^2 \psi}{\partial \lambda \partial r} = -\frac{\mu}{r^3} \sum_{n=2}^{\infty} \left( \frac{R_e}{r} \right)^n (n+1) \sum_{m=0}^n m(S_n^m \cos m\lambda - C_n^m \sin m\lambda) P_n^m(\sin \phi)$$

$$\frac{\partial^2 \psi}{\partial \phi^2} = \frac{\mu}{r} \sum_{n=2}^{\infty} \left( \frac{R_e}{r} \right)^n \sum_{m=0}^n (C_n^m \cos m\lambda + S_n^m \sin m\lambda) \{ \tan \phi P_n^{m+1}(\sin \phi) \quad (4-44)$$

$$+ [m^2 \sec^2 \phi - m \tan^2 \phi - n(n+1)] P_n^m(\sin \phi) \}$$

$$\frac{\partial^2 \psi}{\partial \phi \partial \lambda} = \frac{\partial^2 \psi}{\partial \lambda \partial \phi} = \frac{\mu}{r} \sum_{n=2}^{\infty} \left( \frac{R_e}{r} \right)^n \sum_{m=0}^n m(S_n^m \cos m\lambda - C_n^m \sin m\lambda) (P_n^{m+1}(\sin \phi)$$

$$- m \tan \phi P_n^m(\sin \phi))$$

$$\frac{\partial^2 \psi}{\partial \lambda^2} = -\frac{\mu}{r} \sum_{n=2}^{\infty} \left( \frac{R_e}{r} \right)^n \sum_{m=0}^n m^2 (C_n^m \cos m\lambda + S_n^m \sin m\lambda) P_n^m(\sin \phi).$$

The partial derivatives of  $r$ ,  $\phi$ , and  $\lambda$  with respect to  $\bar{r}_b$  are given in Equations (4-35) through (4-37). The required second partial derivatives of  $r$ ,  $\phi$ , and  $\lambda$  with respect to  $\bar{r}_b$  are obtained by differentiating Equations (4-35) through (4-37) with respect to  $\bar{r}_b$ , yielding

$$\frac{\partial^2 r}{\partial \bar{r}_b^2} = \frac{1}{r} \left[ \mathbf{I} - \frac{\bar{r}_b \bar{r}_b^T}{r^2} \right] \quad (4-45)$$

$$\frac{\partial^2 \psi}{\partial \bar{r}_b^2} = - \frac{1}{(x_b^2 + y_b^2)^{3/2}} \left[ \left( \frac{\partial z_b}{\partial \bar{r}_b} \right)^T - \frac{z_b \bar{r}_b}{r^2} \right] \left[ x_b \left( \frac{\partial x_b}{\partial \bar{r}_b} \right) + y_b \left( \frac{\partial y_b}{\partial \bar{r}_b} \right) \right] \quad (4-46)$$

$$- \frac{1}{r^2, x_b^2 + y_b^2} \left[ \bar{r}_b \left( \frac{\partial z_b}{\partial \bar{r}_b} \right) + z_b I - \frac{2z_b}{r^2} \bar{r}_b \bar{r}_b^T \right]$$

$$\frac{\partial^2 \lambda}{\partial \bar{r}_b^2} = - \frac{2}{(x_b^2 + y_b^2)} \begin{bmatrix} -y_b \\ x_b \\ 0 \end{bmatrix} \left[ x_b \left( \frac{\partial x_b}{\partial \bar{r}_b} \right) + y_b \left( \frac{\partial y_b}{\partial \bar{r}_b} \right) \right] + \frac{1}{(x_b^2 + y_b^2)} \begin{bmatrix} 0 & -1 & 0 \\ 1 & 0 & 0 \\ 0 & 0 & 0 \end{bmatrix} \quad (4-47)$$

where  $\partial x_b / \partial \bar{r}_b$ ,  $\partial y_b / \partial \bar{r}_b$ , and  $\partial z_b / \partial \bar{r}_b$  are (1, 0, 0), (0, 1, 0), and (0, 0, 1), respectively.

The symmetry properties of the second partial derivatives of  $r$ ,  $\psi$ , and  $\lambda$  yield

$$\frac{\partial^2}{\partial x_b \partial y_b} = \frac{\partial^2}{\partial y_b \partial x_b}, \quad \frac{\partial^2}{\partial x_b \partial z_b} = \frac{\partial^2}{\partial z_b \partial x_b}, \quad \frac{\partial^2}{\partial y_b \partial z_b} = \frac{\partial^2}{\partial z_b \partial y_b}. \quad (4-48)$$

As noted previously, the potential function  $\psi$  satisfies Laplace's equation,  $\Delta^2 \psi = 0$ . Therefore,

$$\frac{\partial^2 \psi}{\partial x_b^2} = - \left( \frac{\partial^2 \psi}{\partial y_b^2} + \frac{\partial^2 \psi}{\partial z_b^2} \right) \quad (4-49)$$

In view of this and the symmetry of the matrix in Equation (4-43), it is necessary to compute only the three elements above the principal diagonal and two elements on the principal diagonal.

The equations for computing the elements of the C-matrix appearing in the variational equations (Equation (4-7)) are obtained by differentiation of Equation (4-27) with respect to  $C_n^m$  and  $S_n^m$

$$\frac{\partial \bar{a}_b}{\partial C_n^m} = \frac{\partial}{\partial C_n^m} \left( \frac{\partial \psi}{\partial r} \right) \frac{\partial r}{\partial \bar{r}_b} + \frac{\partial}{\partial C_n^m} \left( \frac{\partial \psi}{\partial \lambda} \right) \frac{\partial \lambda}{\partial \bar{r}_b} + \frac{\partial}{\partial C_n^m} \left( \frac{\partial \psi}{\partial \lambda} \right) \frac{\partial \lambda}{\partial \bar{r}_b} \quad (4-50)$$

$$\frac{\partial \bar{a}_b}{\partial S_n^m} = \frac{\partial}{\partial S_n^m} \left( \frac{\partial \psi}{\partial r} \right) \frac{\partial r}{\partial \bar{r}_b} + \frac{\partial}{\partial S_n^m} \left( \frac{\partial \psi}{\partial \phi} \right) \frac{\partial \phi}{\partial \bar{r}_b} + \frac{\partial}{\partial S_n^m} \left( \frac{\partial \psi}{\partial \lambda} \right) \frac{\partial \lambda}{\partial \bar{r}_b} \quad (4-51)$$

where the second partial derivatives of  $\psi$  are obtained by differentiating Equation (4-28) with respect to  $C_n^m$  and  $S_n^m$

$$\frac{\partial}{\partial C_n^m} \begin{bmatrix} \partial \psi / \partial r \\ \partial \psi / \partial \phi \\ \partial \psi / \partial \lambda \end{bmatrix} = \left( \frac{\mu}{r} \right) \left( \frac{R_e}{r} \right)^n \begin{bmatrix} -\frac{1}{r} (n+1) \cos m\lambda P_n^m(\sin \phi) \\ \cos m\lambda [P_n^{m+1}(\sin \phi) - m \tan \phi P_n^m(\sin \phi)] \\ -m \sin m\lambda P_n^m(\sin \phi) \end{bmatrix} \quad (4-52)$$

$$\frac{\partial}{\partial S_n^m} \begin{bmatrix} \partial \psi / \partial r \\ \partial \psi / \partial \phi \\ \partial \psi / \partial \lambda \end{bmatrix} = \left( \frac{\mu}{r} \right) \left( \frac{R_e}{r} \right)^n \begin{bmatrix} -\frac{1}{r} (n+1) \sin m\lambda P_n^m(\sin \phi) \\ \sin m\lambda [P_n^{m+1}(\sin \phi) - m \tan \phi P_n^m(\sin \phi)] \\ m \cos m\lambda P_n^m(\sin \phi) \end{bmatrix} \quad (4-53)$$

As in the case of the accelerations due to nonsphericity that were developed in Section 4.3.1, the partial derivatives for use in the variational equations must be transformed from the body-fixed axes to the inertial mean of 1950.0 coordinates. As discussed previously, these transformations can be determined to high precision, or by a simpler and faster method in which polar motion is neglected.

In the more accurate option, where polar motion is accounted for, the transformations of the partial derivatives of  $\bar{R}_{NS}$  with respect to  $\bar{R}$  are determined by taking partial derivatives of Equation (4-39) as follows

$$\frac{\partial \bar{R}_{NS}}{\partial \bar{R}} = (BC)^T \frac{\partial \bar{a}_b}{\partial \bar{r}_b} \frac{\partial \bar{r}_b}{\partial \bar{R}} = (BC)^T \frac{\partial \bar{a}_b}{\partial \bar{r}_b} BC \quad (4-54)$$

The matrices  $C$  and  $B$  are presented in Sections 3.3.1 and 3.3.2, respectively.

In the simpler option, polar motion is neglected and  $\bar{a}_b$ , as well as its partial derivatives, are calculated with respect to the true of date coordinates. This is accomplished by replacing  $(r_b, x_b, y_b, z_b)$  in Equations (4-39), (4-42), (4-43), and (4-45) through (4-49) by  $(r, x, y, z)$ , the true of date coordinates, and by replacing the matrix  $B$  with the identity matrix  $I$  in Equations (4-39) and (4-54).

The partial derivatives of  $\ddot{\mathbf{R}}_{NS}$  with respect to model parameters  $C_n^m$  and  $S_n^m$  are obtained for the more accurate option as follows

$$\frac{\partial \ddot{\mathbf{R}}_{NS}}{\partial C_n^m} = (BC)^T \frac{\partial \bar{a}_b}{\partial C_n^m} \quad (4-55)$$

$$\frac{\partial \ddot{\mathbf{R}}_{NS}}{\partial S_n^m} = (BC)^T \frac{\partial \bar{a}_b}{\partial S_n^m} \quad (4-56)$$

For the simpler option,  $(r_b, x_b, y_b, z_b)$  is replaced by  $(r, x, y, z)$  in Equations (4-50) and (4-51), and the matrix  $B$  is replaced by the identity matrix  $I$  in Equations (4-55) and (4-56).

#### 4.4 INDIRECT OBLATION PERTURBATION MODEL

Up to this point two types of gravitational accelerations acting on the spacecraft have been considered: the acceleration due to  $n$ -point masses, measured relative to one of the point masses, called the reference body; and the acceleration arising from the nonspherical portion of the gravitational potentials of one or more of the  $n$  bodies which directly influence the spacecraft motion. These nonspherical attractions also affect the inertial acceleration of the reference body, resulting in an indirect acceleration of the spacecraft relative to the reference body (Reference 6). The two bodies of most concern are the earth and moon.

Inspection of Equation (4-26) reveals the rapid attenuation of the gravitational attraction with increasing order of the spherical harmonics and increasing distance from the body. For the earth,  $C_2^0$  (or  $-J_2$ ) is of order  $10^{-3}$  of the Keplerian term, while all the other harmonic coefficients are of order  $10^{-6}$  or less. In the moon's gravitational potential, the size of the higher order terms relative to the central term is larger than in the case of the earth, but the  $C_2^0$  is dominant. Consequently, the only nonspherical potential terms considered for the mutual interaction of the earth and moon are the second zonal harmonics of each, and the resulting effects are referred to as indirect oblation effects.

The complex motions of the earth-moon system, including lunisolar precession and nutation, physical libration of the moon, and perturbations in the lunar orbit, are accounted for in GTDS. Thus, any significant indirect oblateness effects are

due to the use of a relative coordinate system (Equation (4-16)) in place of an inertial coordinate system, and not to errors in the lunar ephemeris.

Considering the moon to be the spacecraft, the force acting on the point mass moon due to the nonsphericity of the earth is (Section 4.3)

$$\mu_M \ddot{\mathbf{R}}_M(\mathbf{E}) = f(C_i^j, S_i^j, \bar{\mathbf{r}}_{EM}, t) \quad (4-57)$$

where  $C_i^j$  and  $S_i^j$  are the harmonic coefficients of the earth's nonspherical potential,  $\bar{\mathbf{r}}_{EM}$  is the moon's position vector in geocentric coordinates, and  $t$  is the time argument used to determine the orientation of the inertial and geocentric axes.

Similarly, the force acting on the point mass earth due to the nonsphericity of the moon is

$$\mu_E \ddot{\mathbf{R}}_E(\mathbf{M}) = f(c_i^j, s_i^j, \bar{\mathbf{r}}_{ME}, t) \quad (4-58)$$

where  $c_i^j$  and  $s_i^j$  are the harmonic coefficients of the moon's nonspherical potential,  $\bar{\mathbf{r}}_{ME}$  is the earth's position vector in selenocentric coordinates, and  $t$  is the time argument used to determine the orientation of the inertial and selenographic axes.

The force acting on the point mass moon due to the earth's oblateness,  $\mu_M \ddot{\mathbf{R}}_M(\mathbf{E})$ , produces an equal and opposite force acting on the earth. Therefore, the inertial acceleration of the earth due to the force of attraction between the earth and moon due to the oblateness of the earth and the point mass moon is

$$\ddot{\mathbf{R}}_E(\mathbf{E}) = -\frac{\mu_M}{\mu_E} \ddot{\mathbf{R}}_M(\mathbf{E}) \quad (4-59)$$

Similarly, the force of attraction between the earth and moon due to the oblateness of the moon and the point mass earth produces an inertial acceleration of the moon given by

$$\ddot{\mathbf{R}}_M(\mathbf{M}) = -\frac{\mu_E}{\mu_M} \ddot{\mathbf{R}}_E(\mathbf{M}) \quad (4-60)$$

Therefore, the inertial acceleration of the earth due to the oblateness of the earth and moon is

$$\ddot{\vec{R}}_E = \ddot{\vec{R}}_E(M) + \ddot{\vec{R}}_E(E) = -\mu_M \left[ \frac{1}{\mu_E} \ddot{\vec{R}}_M(E) - \frac{1}{\mu_M} \ddot{\vec{R}}_E(M) \right] \quad (4-61)$$

and the inertial acceleration of the moon due to the oblateness of the earth and moon is

$$\ddot{\vec{R}}_M = \ddot{\vec{R}}_M(E) + \ddot{\vec{R}}_M(M) = \mu_E \left[ \frac{1}{\mu_E} \ddot{\vec{R}}_M(E) - \frac{1}{\mu_M} \ddot{\vec{R}}_E(M) \right] \quad (4-62)$$

The resulting indirect acceleration of the spacecraft is equal and opposite to the acceleration of the reference body; consequently,

$$\ddot{\vec{R}}_{IO} = \begin{cases} -\ddot{\vec{R}}_E = \mu_M \left[ \frac{1}{\mu_E} \ddot{\vec{R}}_M(E) - \frac{1}{\mu_M} \ddot{\vec{R}}_E(M) \right] & \text{when the earth is} \\ & \text{the reference body} \\ -\ddot{\vec{R}}_M = -\mu_E \left[ \frac{1}{\mu_E} \ddot{\vec{R}}_M(E) - \frac{1}{\mu_M} \ddot{\vec{R}}_E(M) \right] & \text{when the moon is} \\ & \text{the reference body} \end{cases} \quad (4-63)$$

The method for determining the inertial acceleration of the point-mass moon due to an oblate earth,  $\ddot{\vec{R}}_M(E)$ , and the inertial acceleration of the point-mass earth due to an oblate moon,  $\ddot{\vec{R}}_E(M)$ , are presented in Section 4.3. However, since the effects of the higher harmonic terms can be neglected for this application and only the second zonal harmonics considered, the gravitational potential in Equation (4-26) reduces to

$$\psi(r, \phi) = \frac{\mu}{2r} C_2^0 \left( \frac{R_e}{r} \right)^2 (3 \sin^2 \phi - 1) \quad (4-64)$$

The partial derivatives of  $\psi$  with respect to  $r$  and  $\phi$  are

$$\begin{aligned} \frac{\partial \psi}{\partial r} &= -\frac{3}{2} \frac{\mu}{r^4} R_e C_2^0 (3 \sin^2 \phi - 1) \\ \frac{\partial \psi}{\partial \phi} &= \frac{\mu}{r^3} R_e C_2^0 3 \sin \phi \cos \phi \end{aligned} \quad (4-65)$$



and the partial derivatives of  $r$  and  $\phi$  with respect to  $\bar{r}$  are

$$\frac{\partial r}{\partial \bar{r}} = \frac{\bar{r}^T}{r} \quad \frac{\partial \phi}{\partial \bar{r}} = \frac{1}{r \cos \phi} \begin{bmatrix} -\sin \phi \cos \lambda \\ -\sin \phi \sin \lambda \\ \cos^2 \phi \end{bmatrix} \quad (4-66)$$

Since the oblate potential model is symmetric about the pole, and neglecting polar motion, the inertial acceleration of the point mass moon due to the earth's oblateness can be expressed in geocentric true of date coordinates

$$\begin{aligned} \bar{a}_M(E) &= \frac{\partial \psi}{\partial r_M} \left( \frac{\partial r_M}{\partial \bar{r}_M} \right)^T + \frac{\partial \psi}{\partial \phi_M} \left( \frac{\partial \phi_M}{\partial \bar{r}_M} \right)^T \\ &= -\frac{3}{2} \frac{\mu_E}{r_M^4} R_e C_2^0 (3 \sin^2 \phi_M - 1) \frac{\bar{r}_M}{r_M} + \frac{3\mu_E R_e C_2^0}{r_M^4 \cos \phi_M} \begin{bmatrix} -\sin \phi_M \cos \lambda_M \\ -\sin \phi_M \sin \lambda_M \\ \cos^2 \phi_M \end{bmatrix} \end{aligned} \quad (4-67)$$

- where
- $\mu_E \sim$  the gravitational constant of the earth
  - $R_e \sim$  the equatorial radius of the earth
  - $C_2^0 \sim$  the second zonal harmonic coefficient for the earth
  - $\bar{r}_M \sim$  the lunar position vector in true of date coordinates
  - $\phi_M \sim$  the geocentric latitude of the moon
  - $\lambda_M \sim$  the right ascension of the moon in true of date coordinates

The acceleration vector  $\bar{a}_M(E)$  is transformed to inertial mean of 1950.0 coordinates via the transformation matrix  $C^T$  of Section 3.3.1.3, i.e.,

$$\ddot{\bar{R}}_M(E) = C^T \bar{a}_M(E) \quad (4-68)$$

The inertial acceleration of the point mass earth due to the moon's oblateness is expressed in selenographic coordinates as

$$\bar{a}_E(M) = -\frac{3}{2} \frac{\mu_M}{r_E^4} R_m C_2^0 (3 \sin^2 \phi_E - 1) \frac{\bar{r}_E}{r_E} + \frac{3\mu_M}{r_E^4} \frac{R_m C_2^0}{\cos \phi_E} \begin{bmatrix} -\sin \phi_E \cos \lambda_E \\ -\sin \phi_E \sin \lambda_E \\ \cos^2 \phi_E \end{bmatrix} \quad (4-69)$$

where  $\mu_M \sim$  the gravitational constant of the moon  
 $R_m \sim$  the equatorial radius of the moon  
 $c_2^0 \sim$  the second zonal harmonic coefficient for the moon  
 $\bar{r}_E \sim$  the position vector of the earth in selenographic coordinates  
 $\phi_z \sim$  the selenographic latitude of the earth  
 $\lambda_E \sim$  the selenographic longitude of the earth

Transformation of  $\bar{a}_E(M)$  to inertial mean of 1950.0 coordinates yields

$$\ddot{\bar{R}}_E(M) = C^T M^T \bar{a}_E(M) \quad (4-70)$$

where the  $M^T$  matrix transforms from selenographic to selenocentric true of date coordinates (Section 3.3.3), and the  $C^T$  matrix transforms from true of date to mean of 1950.0 coordinates. If a true of reference date inertial system is being utilized, then the  $C^T$  matrix in Equations (4-68) and (4-70) is set equal to the identity matrix.

## 4.5 AERODYNAMIC FORCES AND ATMOSPHERIC MODELS

### 4.5.1 Introduction

The modeling of the aerodynamic force acting on a spacecraft in a near-earth orbit is difficult from two standpoints. First, the characterization of the density at very high altitudes above the surface is extremely complex. Although the exact natures of the phenomena are not well understood, there is experimental evidence that diurnal and seasonal variations, as well as effects due to changes in solar flux and geomagnetic activity, can be modeled with some degree of success.

Atmospheric density models can be divided into two types. Models of the first type are characterized by their dependence on altitude and their independence of any other parameters. Those of the second type are characterized by their dependence not only on altitude, but also on the position of the sun relative to the earth and the amount of energy emitted from the sun.

Several atmospheric models have been constructed over the past several years (References 7-14) to account for various geomagnetic and solar activities. There are three main types of solar radiation known to affect the atmospheric density. The first type, which is the most important in terms of the effect on the structure of the atmosphere, results from solar ultraviolet radiation impinging on the atmosphere; its effect on temperature and density is maximum two to three hours after local noon. This radiation heats the atmosphere by conduction and thereby increases the density at higher altitudes. The process is known as the diurnal (or day-night) effect and causes a redistribution of density, resulting in a diurnal bulge in the atmosphere. The second type of solar activity affecting the atmosphere results from extreme ultraviolet radiation. The atmospheric oscillations that are in phase with this solar flux are often referred to as the erratic or 27-day variations, since the oscillations sometimes exhibit a semiregular character for intervals of several months, during which a period of 27 days is easily recognizable. It has been found that the decimetric flux from the sun apparently varies in the same manner as the extreme ultraviolet emission, and can therefore be used as a fairly reliable index of short-term solar activity. The decimetric flux, specifically the 10.7 cm radiation, is expressed in units of  $10^{-22}$  watt/m<sup>2</sup>/cps bandwidth and is denoted by the symbol  $F_{10.7}$ . The third type of radiation is corpuscular in nature and is referred to as the solar wind. It is responsible for the changes in intensity and energy spectrum observed in the cosmic radiation and is the largest single factor affecting short-term fluctuations in the atmospheric density. Experiments on board Pioneer V were the first to establish that the 11-year solar (sun spot) cycle is a phenomenon that is not localized near the earth or its immediate environment but rather affects large volumes of the inner solar system. The solar wind is modeled as an interplanetary plasma streaming radially and irregularly outward from the sun, compressing the earth's magnetic field on the sunward side and extending it on the night side.

Atmospheric oscillations connected with geomagnetic storms are of significant amplitude but of very short duration (one or two days). Present-day studies indicate a correlation of atmospheric density with geomagnetic activity.

Apart from the difficulty of accurately representing the environment (density) at the spacecraft location, the second aspect of the problem lies in the complication of rigorously modeling the force itself as a function of spacecraft configuration and attitude.

GTDS provides the user with the choice of two atmospheric density models and three types of force representation. The atmospheric density models available are the Modified Harris-Priester and the Roberts analytic formulation of the Jacchia 1971 model. The Harris-Priester model is the simpler of the two and permits the most rapid computation of density. It does not include effects due to seasonal variations or to changes in solar flux or geomagnetic activity, as does the Jacchia-Roberts model.

The aerodynamic force can be represented, at the specification of the user, as

- a simple drag force acting along the relative wind vector on a spherical spacecraft
- a force with components normal to and along the axis of a cylindrical spacecraft
- a force with components along each of the three spacecraft body axes for a configuration consisting of a cylinder with solar paddles oriented at some angle to the axis of the cylinder.

These modeling options are described in detail in the following sections. The aerodynamic force modeling is discussed in Section 4.5.2, the Jacchia-Roberts atmospheric model in Section 4.5.4, and the Modified Harris-Priester atmospheric model in Section 4.5.6.

#### 4.5.2 Aerodynamic Force Modeling

Rigorous treatment of the aerodynamics of free molecular flow involves the representation of the complex interaction of the atmospheric molecules with the surface molecules of the spacecraft. Under certain conditions, this interaction is characterized as a specular or perfectly elastic reflection of the impinging molecules. The reflection is termed diffuse when the impinging molecules penetrate the surface, experience multiple collisions with the body molecules, and are re-emitted randomly with no memory of their prior history. In the case of specular reflection, there is no momentum transfer, and hence no force, tangential to a local surface element. Diffuse reflection does result in such a component of force, although it is small. In general, both types of phenomena are involved to varying degrees, depending upon the details of surface reflectivity and emissivity, temperature, free-stream constituents and their mean molecular motion. Conditions typical of most actual situations result in forces which can be adequately represented in terms of the specular reflection equations. Therefore, the force modeling in GTDS makes this simplifying assumption, and computes the force acting on a local surface element as the momentum transfer normal to that element.

The forces on all elements of the spacecraft surfaces exposed to the free-stream must be resolved in some coordinate frame and summed in order to obtain the total aerodynamic force acting on the spacecraft. This resolution has been performed for a number of elemental shapes at various orientations. GTDS

makes use of the force coefficients defined in Table 4-1 for spheres, cylinders, and flat plates. A force coefficient,  $C_F$ , is defined as the nondimensional quantity

$$C_F = \frac{F}{\frac{1}{2} \rho V^2 A} \quad (4-71)$$

where

$F$  = the magnitude of the force acting on the object

$\rho$  = the density of the medium through which the object is moving

$V$  = the magnitude of the velocity of the object with respect to the medium producing the force

$A$  = an arbitrary reference area

The velocity of the spacecraft relative to the atmosphere is determined in the inertial coordinate system by subtracting the motion of the atmosphere, assumed to rotate with the earth, from that of the spacecraft

$$\bar{V}_{rel} = \dot{\bar{R}} - \bar{\omega} \times \bar{R} \quad (4-72)$$

The earth rotation vector  $\bar{\omega}$  must be appropriately defined in the inertial frame (mean equator and equinox of 1950.0 or true equator and equinox of reference date).

For the case of a spherical spacecraft, the drag acceleration is computed simply using the general form of Equation (4-71) and  $C_D = 1.0$  from Table 4-1

$$\ddot{\bar{R}}_D = -S_s \rho \bar{V}_{rel} |\bar{V}_{rel}| \quad (4-73)$$

where

$$S_s = \frac{1}{2} C_D \left( \frac{A}{m} \right) = \frac{1}{2} \left( \frac{v_d^2}{4m} \right) \quad (4-74)$$

Table 4-1

## Aerodynamic Force Coefficients for Elementary Surfaces

Surface Shape	Reference Direction for Measurement of Angle $\alpha$ to Relative Velocity Vector	Reference Area	Force Coefficient(s) as Functions of $\alpha$	Direction of Force Component
Sphere	Relative wind velocity	Cross-sectional area of sphere	$C_D = 1.0$	Along relative wind vector
Circular Cylinder (exterior surface only)	Cylinder axis	Length times diameter of the cylinder	$C_{N_C} = \frac{4}{3} \sin^2 \alpha$	Normal to cylinder axis in the plane of the axis and the relative velocity
			$C_{A_C} = 0$	Along cylinder axis
Flat Plate	Normal to plate	Area of plate	$C_{N_P} = 2.0 \cos^2 \alpha$	Normal to the plate
			$C_{T_P} = 0$	Tangent to the plate

d is the spacecraft diameter, and m is the mass. If there is propulsive thrust acting, the mass m is variable and is represented as a polynomial in the burn time. The polynomial coefficients are assumed to be known inputs.

When the spacecraft configuration is more complicated than a sphere, it is necessary to know the attitude, in addition to the orbit, in order to model the aerodynamic force.

It is not necessary to compute the entire direction cosine matrix Q when the spacecraft is a cylinder (with enclosing end plates). Due to the axial symmetry, it is only necessary to know the direction cosines  $q_{11}$ ,  $q_{21}$ ,  $q_{31}$  of the cylinder axis.

The unit vector

$$\hat{\mathbf{x}}_B = q_{11} \bar{\mathbf{i}} + q_{21} \bar{\mathbf{j}} + q_{31} \bar{\mathbf{k}} \quad (4-75)$$

then gives the axis orientation in the inertial coordinate frame. As indicated in Table 4-1, the force component along the axis is proportional to the square of the velocity component normal to the end plates. The normal force component is proportional to the square of the velocity component normal to the cylinder.\* Therefore, the velocity relative to the atmosphere is resolved into normal and axial components in order to obtain the total acceleration for the cylindrical spacecraft as

$$\bar{\mathbf{N}} = S_c \hat{\mathbf{x}}_B \times (\hat{\mathbf{x}}_B \cdot \bar{\mathbf{v}}_{rel}) |\hat{\mathbf{x}}_B \times \bar{\mathbf{v}}_{rel}|$$

$$\bar{\mathbf{A}} = -S_e \hat{\mathbf{x}}_B (\hat{\mathbf{x}}_B \cdot \bar{\mathbf{v}}_{rel}) |\hat{\mathbf{x}}_B \cdot \bar{\mathbf{v}}_{rel}| \quad (4-76)$$

$$\ddot{\bar{\mathbf{R}}}_D = \rho (\bar{\mathbf{N}} + \bar{\mathbf{A}})$$

---

\* This is analogous to the solar radiation case, where the force is proportional to the effective area normal to the incident radiation (Section 4.6), and the determination of this effective area is directly analogous to the determination of the effective area normal to the relative velocity vector.

In these equations

$$S_c = \frac{1}{2} \left( \frac{C_{Nc}}{\sin^2 \alpha} \right) \left( \frac{A}{m} \right) = \frac{1}{2} \left( \frac{4}{3} \right) \left( \frac{LD}{m} \right) = \frac{2LD}{3m} \quad (4-77)$$

$$S_e = \frac{1}{2} \left( \frac{C_{Np}}{\cos^2 \alpha} \right) \left( \frac{A}{m} \right) = \frac{1}{2} (2) \left( \frac{\pi d^2}{4m} \right) = \frac{\pi d^2}{4m}$$

where  $L$  is the length of the cylinder and  $d$  is the diameter. As before,  $m$  is the spacecraft mass, which may be variable.

The third type of spacecraft configuration optionally available in GTDS is a cylinder with solar paddles, mounted on trunnion pivots which are orthogonal to the cylinder axis. The incidence angle  $i_p$  defines the angle between the axis and the paddle surface. The spacecraft axis system is chosen so the  $x$ -axis corresponds with the cylinder axis,  $y$  is the trunnion axis, and  $z$  is orthogonal to  $x$  and  $y$ . The  $y$  axis is directed so that positive  $i_p$  corresponds with positive rotation about  $y$ , according to the right-hand rule.

This configuration is not axisymmetric and therefore requires the calculation of the complete transformation matrix  $Q$  (from body to inertial axes). It is most convenient to transform the relative wind velocity into spacecraft body axes, compute the force components in this frame, and then transform the result back into the inertial coordinate frame. This leads to the following equations for the aerodynamic acceleration:

$$\begin{aligned} \bar{V}_B &= Q^{-1} \bar{V}_{rel} = \dot{x}_B \bar{i}_B + \dot{y}_B \bar{j}_B + \dot{z}_B \bar{k}_B \\ V_N &= \dot{x}_B \sin i_p + \dot{z}_B \cos i_p \\ F_{x_B} &= -S_c \dot{x}_B |\dot{x}_B| - S_p V_N |V_N| \sin i_p \\ F_{y_B} &= -S_c \dot{y}_B \sqrt{\dot{y}_B^2 + \dot{z}_B^2} \\ F_{z_B} &= -S_c \dot{z}_B \sqrt{\dot{y}_B^2 + \dot{z}_B^2} - S_p V_N |V_N| \cos i_p \\ \ddot{\bar{R}}_D &= -\rho Q \bar{F}_B \end{aligned} \quad (4-78)$$



The definitions of  $S_c$  and  $S_a$  are the same as in Equations (4-77). The solar paddle contribution is

$$S_p = \frac{1}{2} \left( \frac{C_{Np}}{\cos^2 \alpha} \right) \left( \frac{A_p}{m} \right) = \frac{1}{2} (C_p) \left( \frac{A_p}{m} \right) = \frac{A_p}{m} \quad (4-79)$$

where the paddle area  $A_p$  is an input constant.

The representation of the aerodynamic forces in Equations (4-79) does not consider the effect of mutual shadowing or shielding from the free-stream flow between the cylindrical and solar paddle surfaces.\* Such effects are geometrically very complex, particularly if multiple interference reflections between cylinder and paddles are considered. The simplifications resulting from the neglect of this phenomenon in Equation (4-78) are thought to be consistent with the original assumption of purely specular reflection in the specification of the individual surface type coefficients.

The factor  $\rho$  in the three expressions for  $\ddot{\bar{R}}_D$  is not simply the atmospheric density  $\rho_a$ . It also includes a scale factor

$$\rho = \rho_a (1 + \rho_1) \quad (4-80)$$

to permit an adjustment of the  $\rho C_F$  product. A default value of  $\rho_1 = 0$  is set in the program. However, this value can be modified by user input, or it can be estimated in the differential correction process. Adjustment of  $\rho_1$  does not alter the instantaneous direction of  $\ddot{\bar{R}}_D$ ; it simply changes the magnitude.

### 4.5.3 Associated Partial Derivatives

When the aerodynamic force option is exercised in GTDS, it is necessary to compute partial derivatives of  $\ddot{\bar{R}}_D$  with respect to variations in the spacecraft local inertial state for use in the variational equations. For all configurations, the portion of the partial derivative which accounts for the effects of density variation is

$$\frac{\partial \ddot{\bar{R}}_D}{\partial \bar{R}} = \frac{\ddot{\bar{R}}_D}{r_a} \frac{\partial r_a}{\partial \bar{R}} \quad (4-81)$$

\* Shadowing of the cylinder end plates by the cylindrical surface itself is considered.

since density depends only upon spacecraft local position and not upon local velocity. The forms for  $\partial \rho_a / \partial \bar{\mathbf{R}}$  will be presented in Sections 4.5.5 and 4.5.7 for the Jacchia-Roberts and Harris-Priester models, respectively.

All three forms for  $\ddot{\bar{\mathbf{R}}}_D$  are expressed in terms of  $\bar{\mathbf{V}}_{rel}$ , which can be written in a slightly different form from that in Equation (4-72)

$$\bar{\mathbf{V}}_{rel} = \dot{\bar{\mathbf{R}}} - \Omega \bar{\mathbf{R}} \quad (4-82)$$

where the matrix

$$\Omega = \begin{bmatrix} 0 & -\omega_3 & \omega_2 \\ \omega_3 & 0 & -\omega_1 \\ -\omega_2 & \omega_1 & 0 \end{bmatrix} \quad (4-83)$$

Thus, the partial derivatives can be computed with respect to  $\bar{\mathbf{V}}_{rel}$ , and these can then be used to compute

$$\left. \begin{aligned} \frac{\partial \ddot{\bar{\mathbf{R}}}_D}{\partial \dot{\bar{\mathbf{R}}}} &= \frac{\partial \ddot{\bar{\mathbf{R}}}_D}{\partial \bar{\mathbf{V}}_{rel}} \\ \frac{\partial \ddot{\bar{\mathbf{R}}}_D}{\partial \bar{\mathbf{R}}} &= \left( \frac{\partial \ddot{\bar{\mathbf{R}}}_D}{\partial \bar{\mathbf{V}}_{rel}} \right) \Omega \end{aligned} \right\} \quad (4-84)$$

The partial derivatives of the three configuration forms with respect to  $\bar{\mathbf{V}}_{rel}$  ( $\dot{x}_1, \dot{x}_2, \dot{x}_3$ ) are

Sphere:

$$\frac{\partial \ddot{\bar{\mathbf{R}}}_D}{\partial \bar{\mathbf{V}}_{rel}} = -S_s \rho \left\{ \frac{\bar{\mathbf{V}}_{rel} \bar{\mathbf{V}}_{rel}^T}{|\bar{\mathbf{V}}_{rel}|} + |\bar{\mathbf{V}}_{rel}| \mathbf{I} \right\} \quad (4-85)$$

Cylinder:

$$M = |\hat{X}_B \times \bar{V}_{rel}|$$

$$M^2 = (\hat{X}_B \times \bar{V}_{rel}) \cdot (\hat{X}_B \times \bar{V}_{rel})$$

$$\sigma = \hat{X}_B \cdot \bar{V}_{rel}$$

$$\bar{W}_1 = (q_{11}^2 - 1) \bar{i} + q_{11}q_{21} \bar{j} + q_{11}q_{31} \bar{k}$$

(4-86)

$$\bar{W}_2 = q_{21}q_{11} \bar{i} + (q_{21}^2 - 1) \bar{j} + q_{21}q_{31} \bar{k}$$

$$\bar{W}_3 = q_{31}q_{11} \bar{i} + q_{31}q_{21} \bar{j} + (q_{31}^2 - 1) \bar{k}$$

$$\frac{\partial \ddot{\bar{R}}_D}{\partial \dot{x}_i} = \rho \left[ S_c M \bar{W}_i - \frac{\bar{N}}{M^2} (\bar{W}_i \cdot \bar{V}_{rel}) + \frac{2\bar{A}}{\sigma} q_{i1} \right]$$

(i = 1, 2, 3)

Cylinder + Paddles:

$$\frac{\partial F_{x_B}}{\partial \dot{x}_B} = -2 \left[ S_e |\dot{x}_B| + S_p |V_N| \sin^2 i_p \right]$$

$$\frac{\partial F_{x_B}}{\partial \dot{y}_B} = 0$$

$$\frac{\partial F_{x_B}}{\partial \dot{z}_B} = -2 S_p |V_N| \cos i_p \sin i_p$$

$$\frac{\partial F_{y_B}}{\partial \dot{x}_B} = 0$$

$$\frac{\partial F_{y_B}}{\partial \dot{y}_B} = \frac{F_{y_B}}{\dot{y}_B} - \frac{S_c \dot{y}_B^2}{\sqrt{\dot{y}_B^2 + \dot{z}_B^2}}$$

(4-87)

$$\frac{\partial F_{y_B}}{\partial \dot{z}_B} = - \frac{S_c \dot{y}_B \dot{z}_B}{\sqrt{\dot{y}_B^2 + \dot{z}_B^2}}$$

$$\frac{\partial F_{z_B}}{\partial \dot{x}_B} = \frac{\partial F_{x_B}}{\partial \dot{z}_B}$$

$$\frac{\partial F_{z_B}}{\partial \dot{y}_B} = \frac{\partial F_{y_B}}{\partial \dot{z}_B}$$

$$\frac{\partial F_{z_B}}{\partial \dot{z}_B} = -S_c \left[ \sqrt{\dot{y}_B^2 + \dot{z}_B^2} + \frac{\dot{z}_B^2}{\sqrt{\dot{y}_B^2 + \dot{z}_B^2}} \right] - 2 S_p |V_N| \cos^2 i_p$$

$$\frac{\partial \ddot{\bar{R}}_D}{\partial \bar{V}_{rel}} = \rho Q \frac{\partial \bar{F}_B}{\partial \bar{V}_B} Q^{-1}$$

#### 4.5.4 Jacchia-Roberts Atmospheric Model

In Reference 13, L. G. Jacchia defined two empirical profiles to represent temperature as a function of altitude and exospheric temperature. One profile is defined for the altitude range from 90 to 125 km and the other for the region above 125 km. Jacchia used these temperature functions in the appropriate thermodynamic differential equations to determine density as a function of altitude and exospheric temperature. He assumed that mixing is predominant between 90 and 100 km, and substituted the low altitude temperature profile into the barometric differential equation for this regime. Diffusive equilibrium was assumed above 100 km, leading to the use of the low altitude temperature profile in the diffusion differential equation for altitudes between 100 and 125 km and the high altitude temperature profile for altitudes above 125 km.

Jacchia solved these differential equations by integrating them numerically over the altitude regions for various constant values of exospheric temperature, assuming fixed boundary conditions at the 90 km lower altitude limit. He then tabulated these numerical results for use in the simulation of aerodynamic drag effects upon satellites. Most mechanizations of this model atmosphere in computer programs have involved some means for storing the tabular data and for interpolating values at altitudes computed by the trajectory integration and at exospheric temperatures calculated by the Jacchia formulas. Although the densities determined by this model are accurate, these mechanizations are generally slow running and/or require large blocks of core storage. In addition, the absence of explicit analytic expressions means that the drag partial derivatives must be calculated numerically.

C. E. Roberts, Jr. presented a method for evaluating the Jacchia model analytically in Reference 14, and this formulation is used in the mechanization in GTDS. Roberts found that the barometric and diffusion differential equations could be integrated by partial fractions, using Jacchia's low altitude temperature profile for the range from 90 to 125 km. Above 125 km, Roberts used a different asymptotic function than the one introduced empirically by Jacchia in order to obtain an integrable form. Apart from difficulties of numerical computations with finite numbers of digits, the Roberts analytic expressions match the Jacchia results exactly from 90 to 125 km and to a close approximation above 125 km. The existence of these analytic expressions makes possible the computation of analytic forms for the drag partial derivatives. Since the Roberts formulas were derived for the Jacchia 1970 model, his constants have been adjusted for the later 1971 model. In addition, an error has been corrected in the function  $W(v)$  given by Roberts in Equations (12) of Reference 14.

The computations begin with equations given in the Jacchia report to determine the exospheric temperature and corrections to the standard density due to various effects.

Before execution of a trajectory generation, GTDS determines the total time span of interest. Then, from a permanent data file, one set of values of geomagnetic activity data and two sets of solar flux data are retrieved. The geomagnetic data set is the 3-hour geomagnetic planetary index  $K_p$ . One set of the solar flux data is the daily average 10.7 cm. solar flux,  $F_{10.7}$ , as observed at the solar observatory at Ottawa, Canada; the other set is the 81-day running average (centered at the day of interest),  $\bar{F}_{10.7}$ , of  $F_{10.7}$ . The solar flux data are substituted into the equation

$$T_c = 379^\circ + 3^\circ 24' \bar{F}_{10.7} + 1^\circ 3' [F_{10.7} - \bar{F}_{10.7}] \quad (4-88)$$

for determining the nighttime minimum global exospheric temperature for zero geomagnetic activity. The preprocessing computation of Equation (4-88) is done for each day of the time span of interest, beginning one day prior to the start of the trajectory. The daily values of  $T_c$  and the 3-hourly values of  $K_p$  (beginning 6<sup>h</sup> prior to trajectory start) are stored in a working file for use in the computation of the trajectory.

At each trajectory integration time point, the value of  $T_c$  is retrieved from the working file for the day before the current time. This accounts for the fact that there is a one-day lag in the temperature variation with respect to solar flux change. This value of  $T_c$  is used to compute the uncorrected exospheric temperature  $T_1$  from the formula

$$T_1 = T_c \left\{ 1 + 0.3 \left[ \sin^{2.2} \theta + (\cos^{2.2} \eta - \sin^{2.2} \theta) \cos^{3.0} \frac{\tau}{2} \right] \right\} \quad (4-89)$$

where

$$\eta = \frac{1}{2} |\phi - \delta_s|$$

$$\theta = \frac{1}{2} |\phi + \delta_s|$$

$$\tau = H - 37^\circ 0' + 6^\circ 0' \sin(H + 43^\circ 0') \quad (-\pi < \tau < \pi)$$

$\delta_s$  is the sun's declination, and

$$\phi = \tan^{-1} \left\{ \frac{1}{(1-f)^2} \left[ \frac{X_3}{(X_1^2 + X_2^2)^{1/2}} \right] \right\} \quad (4-90)$$

is the geodetic latitude. The constant  $f$  is the geodetic flattening and  $X_1, X_2, X_3$  are the components of the unit position vector of the spacecraft in true of date coordinates. The parameter

$$H = 180^\circ - \left\{ \frac{(S_1 X_2 - S_2 X_1)}{\pi |S_1 X_2 - S_2 X_1|} \cos^{-1} \left[ \frac{S_1 X_1 + S_2 X_2}{(S_1^2 + S_2^2)^{1/2} (X_1^2 + X_2^2)^{1/2}} \right] \right\} \quad (4-91)$$

is the local hour angle of the sun (counted from upper culmination). The components  $S_1, S_2, S_3$  comprise the unit vector to the sun in true of date coordinates.

The effect of geomagnetic activity upon atmospheric temperature and density shows a lag behind the geomagnetic disturbance. Thus, the value of  $K_p$  is retrieved from the working file for a time 6.<sup>h</sup>7 earlier than the current integration time point. The correction to exospheric temperature is given by

$$\left. \begin{aligned} \Delta T_\infty &= 28^\circ 0 K_p + 0^\circ 03 e^{K_p} & (Z \geq 200 \text{ km}) \\ \Delta T_\infty &= 14^\circ 0 K_p + 0^\circ 02 e^{K_p} & (Z < 200 \text{ km}) \end{aligned} \right\} \quad (4-92)$$

The corrected exospheric temperature is

$$T_\infty = T_1 + \Delta T_\infty \quad (4-93)$$

and the inflection point temperature is

$$T_x = 371^\circ 6678 + 0.0518806 T_\infty - 294^\circ 3505 e^{-0.00216222 T_\infty} \quad (4-94)$$

These two temperatures together with the spacecraft altitude, are used in the Roberts equations to compute the standard density value. However, a number of corrections must be applied to the standard density values in order to account

for various physical effects. These corrections are given by formulas from Jacchia's paper (Reference 13), and will be presented before proceeding to the Roberts equations.

In addition to the correction to the exospheric temperature, there is another direct geomagnetic effect on the standard density below 200 km

$$(\Delta \log_{10} \rho)_G = 0.012 K_p + 1.2 \times 10^{-5} e^{K_p} \quad (4-95)$$

The semi-annual density variation is given by the following relationships (for altitude Z in km):

$$(\Delta \log_{10} \rho)_{SA} = f(Z) g(t) \quad (4-96)$$

where

$$f(Z) = (5.876 \times 10^{-7} Z^{2.331} + 0.06328) e^{-.002868Z}$$

$$g(t) = 0.02835 + [0.3817 + 0.17829 \sin(2\pi\tau_{SA} + 4.137)]$$

$$\times \sin(4\pi\tau_{SA} + 4.259) \quad (4-97)$$

$$\tau_{SA} = \Phi + 0.09544 \left\{ \left[ \frac{1}{2} + \frac{1}{2} \sin(2\pi\Phi + 6.035) \right]^{1.65} - \frac{1}{2} \right\}$$

$$\Phi = \frac{JD_{1958}}{365.2422}$$

In the last equation  $JD_{1958}$  is the number of Julian Days from January 1, 1958.

The correction for the seasonal latitudinal variation of the lower thermosphere is



$$(\Delta \log_{10} \rho)_{LT} = 0.014(Z - 90) e^{[-0.0013(Z-90)^2]} \quad (4-98)$$

$$\times \sin(2\pi\Phi + 1.72) \sin \phi \mid \sin \phi \mid$$

Finally, the correction for the seasonal latitudinal variation of helium is

$$(\Delta \log_{10} \rho)_{He} = 0.65 \left| \frac{\delta_s}{\epsilon} \right| \left[ \sin^3 \left( \frac{\pi}{4} - \frac{\phi \delta_s}{2|\delta_s|} \right) - 0.35355 \right] \quad (4-99)$$

where  $\epsilon$  is the obliquity of the ecliptic.

As mentioned earlier, for altitudes below 125 km Roberts used the same temperature profile that Jacchia used, i.e.,

$$T(Z) = T_x + \frac{d_1}{35^4} \sum_{n=0}^4 C_n Z^n \quad (4-100)$$

where

$$d_1 = T_x - T_0$$

$$T_0 = 183.0 \text{ K}$$

$$C_0 = -89284375.0$$

$$C_1 = 3542400.0 \quad \text{km}^{-1} \quad (4-101)$$

$$C_2 = -52687.5 \quad \text{km}^{-2}$$

$$C_3 = 340.5 \quad \text{km}^{-3}$$

$$C_4 = -0.8 \quad \text{km}^{-4}$$

and where  $T_x$  is the inflection point temperature (at  $Z_x = 125$  km) given by Equation (4-94). Roberts substituted the temperature profile, given by Equation (4-100), in the barometric differential equation and integrated by partial fractions to obtain

$$\rho_s(Z) = \left( \frac{\rho_0 T_0}{M_0} \right) \frac{M(Z)}{T(Z)} F_1^k \exp(kF_2) \quad (4-102)$$

as the expression for density for  $90 < Z \leq 100$  km, where the subscript "0" refers to conditions at 90 km. The mean molecular weight is given as

$$M(Z) = \sum_{n=0}^6 A_n Z^n \quad (4-103)$$

where

$$\begin{aligned} A_0 &= -435093.363387 \\ A_1 &= 28275.5646391 \quad \text{km}^{-1} \\ A_2 &= -765.33466108 \quad \text{km}^{-2} \\ A_3 &= 11.043387545 \quad \text{km}^{-3} \\ A_4 &= -0.08958790995 \quad \text{km}^{-4} \\ A_5 &= 0.00038737586 \quad \text{km}^{-5} \\ A_6 &= -0.000000697444 \quad \text{km}^{-6} \end{aligned}$$

These constants give a value of  $M(90) = M_0 = 28.82678$ , which is not too different from the sea-level mean molecular mass  $M_s$  of 28.960.

The value of density at the lower limit is assumed to be constant at  $\rho_0 = 3.46 \times 10^{-9}$  gm/cm<sup>3</sup>. The constant  $k$  in Equation (4-102) is

$$k = - \frac{35^4 g_s R_a^2}{R d_1 C_4}$$

where

$$\begin{aligned} g_s &= 9.80665 \text{ m/sec}^2 = \text{sea level acceleration due to gravity} \\ R_a &= 6356.766 \text{ km} \\ R &= 8.31432 \text{ Joules/}^\circ\text{K - mole (universal gas constant)} \end{aligned}$$

The functions  $F_1$  ,  $F_2$  in Equation (4-102) are

$$F_1 = \left( \frac{Z + R_a}{90 + R_a} \right)^{p_1} \left( \frac{Z - r_1}{90 - r_1} \right)^{p_2} \left( \frac{Z - r_2}{90 - r_2} \right)^{p_3} \left( \frac{Z^2 - 2XZ + X^2 + Y^2}{8100 - 180X + X^2 + Y^2} \right)^{p_4} \quad (4-104)$$

$$F_2 = (Z - 90) \left[ A_6 + \frac{p_5}{(Z + R_a)(90 + R_a)} \right] + \frac{p_6}{Y} \tan^{-1} \left[ \frac{Y(Z - 90)}{Y^2 + (Z - X)(90 - X)} \right]$$

In these functions  $r_1$  and  $r_2$  are the two real roots and  $X$  and  $Y$  are the real and imaginary parts ( $Y > 0$ ), respectively, of the complex conjugate roots of the quadratic

$$P(Z) = \sum_{n=0}^4 C_n^* Z^n \quad (4-105)$$

with coefficients

$$C_0^* = \frac{35^4 T_x}{C_4 d_1} + \frac{C_0}{C_4}$$

$$C_n^* = \frac{C_n}{C_4} \quad 1 \leq n \leq 4$$

for values of  $C_n$  given by Equations (4-101). The parameters  $p_i$  in the functions  $F_1$  are

$$p_2 = \frac{S(r_1)}{U(r_1)}$$

$$p_3 = \frac{-S(r_2)}{U(r_2)}$$

$$p_5 = \frac{S(-R_a)}{V}$$

$$p_4 = \{B_0 - r_1 r_2 R_a^2 [B_4 + B_5 (2X + r_1 + r_2 - R_a)] + W(r_1) p_2 \\ - r_1 r_2 B_5 R_a (X^2 + Y^2) + W(r_2) p_3 \\ + r_1 r_2 (R_a^2 - X^2 - Y^2) p_5\} / X^*$$

$$p_6 = B_4 + B_5 (2X + r_1 + r_2 - R_a) - p_5 - 2(X + R_a) p_4 \\ - (r_2 + R_a) p_3 - (r_1 + R_a) p_2$$

$$p_1 = B_5 - 2p_4 - p_3 - p_2$$

In these parameters

$$X^* = -2r_1 r_2 R_a (R_a^2 + 2XR_a + X^2 + Y^2)$$

$$V = (R_a + r_1) (R_a + r_2) (R_a^2 + 2XR_a + X^2 + Y^2) \quad (4-106)$$

$$U(r_i) = (r_i + R_a)^2 (r_i^2 - 2XR_i + X^2 + Y^2) (r_1 - r_2)$$

$$W(r_i) = r_1 r_2 R_a (R_a + r_i) \left( R_a + \frac{X^2 + Y^2}{r_i} \right)$$

The function  $W(r_i)$  is corrected from an erroneous expression given in Reference 14. Finally, the coefficients  $B_n$  and the function  $S(Z)$  are given by

$$B_n = \alpha_n + \beta_n \frac{T_x}{T_x - T_0} \quad (n = 0, 1, \dots, 5)$$

$$S(Z) = \sum_{n=0}^5 B_n Z^n$$

where

$$\begin{array}{ll}
 \alpha_0 = 3144902516.672729 & \beta_0 = -52864482.17910969 \\
 \alpha_1 = -123774885.4832917 & \beta_1 = -16632.50847336828 \\
 \alpha_2 = 1816141.096520398 & \beta_2 = -1.308252378125 \\
 \alpha_3 = -11403.31079489267 & \beta_3 = 0.0 \\
 \alpha_4 = 24.36498612105595 & \beta_4 = 0.0 \\
 \alpha_5 = 0.008957502839707995 & \beta_5 = 0.0
 \end{array}$$

As noted above, Equation (4-102) is valid below  $Z = 100$  km. where mixing is assumed to be predominant. However, diffusive equilibrium is assumed above  $Z = 100$  km; hence, the profile given by Equation (4-100) was substituted into the diffusion differential equations (one for each constituent of the atmosphere) and integrated by partial fractions by Roberts to yield for  $100 < Z \leq 125$  km

$$\rho_s(Z) = \sum_{i=1}^5 \rho_i(Z) \quad (4-107)$$

Rigorously, the density at 100 km,  $\rho(100)$ , should be evaluated by means of Equation (4-102) for the particular exospheric temperature  $T_\infty$  of interest. However, since the evaluation of that equation is computationally expensive, it is preferable to avoid adding that expense to that already necessary to compute Equation (4-107). This is avoided in GTDS by precomputing values of  $\rho(100)$ , using Equation (4-102), for a series of values of  $T_\infty$ . These values have been least-squares curve fitted by the polynomial

$$\frac{\rho(100)}{M_s} = \sum_{n=0}^6 \zeta_n T_\infty^n \quad (4-108)$$

where

$$\begin{array}{ll}
 \zeta_0 = 0.1985549 \times 10^{-10} \\
 \zeta_1 = -0.183349 \times 10^{-14} \\
 \zeta_2 = 0.1711735 \times 10^{-17} \\
 \zeta_3 = -0.1021474 \times 10^{-20} \\
 \zeta_4 = 0.3727894 \times 10^{-24} \\
 \zeta_5 = -0.7734110 \times 10^{-28} \\
 \zeta_6 = 0.7026942 \times 10^{-32}
 \end{array}$$

and  $M_s$  = the sea level mean molecular mass = 28.96 gm/mole.

This approximation is used in Equation (4-107).

The constituent mass densities for altitudes between 100 and 125 km are given by

$$\rho_i(Z) = \rho(100) \frac{M_i}{M_s} \rho_i \left[ \frac{T(100)}{T(Z)} \right]^{1+\alpha_i} F_3^{M_i k} \exp(M_i k F_4) \quad (4-109)$$

The identification of the constituents and the values of the corresponding constants in Equation (4-109) are given in Table 4-2.

Table 4-2

Atmospheric Constituents and Related Constants

Index i	Constituent	Molecular mass $M_i$ (grams/mole)	Thermal diffusion coefficient $\alpha_i$	$\mu_i$ , constituent number density $\times (M_s/\rho(100))$ divided by Avogadro's number
1	N <sub>2</sub>	28.0134	0	0.78110
2	Ar	39.948	0	$0.93432 \times 10^{-2}$
3	He	4.0026	-0.38	$0.61471 \times 10^{-5}$
4	O <sub>2</sub>	31.9988	0	0.161778
5	O	15.9994	0	$0.95544 \times 10^{-1}$
6	H	1.00797	0	—

Hydrogen is an insignificant constituent at altitudes below 125 km; hence, it is not included in Equations (4-107) and (4-109). The temperature at 100 km is given by Equation (4-100) in the form

$$T(100) = T_x + \Omega d_1 \quad (4-110)$$

where

$$\Omega = 35^{-4} \sum_{n=0}^4 C_n (100)^n = -0.94585589$$

is the precomputed value of the polynomial for 100 km. The parameter  $k$  in Equation (4-109) is the same as defined previously, and the functions  $F_3$  and  $F_4$  are given as

$$F_3 = \left( \frac{Z + R_a}{R_a + 100} \right)^{q_1} \left( \frac{Z - r_1}{100 - r_1} \right)^{q_2} \left( \frac{Z - r_2}{100 - r_2} \right)^{q_3} \left( \frac{Z^2 - 2XZ + X^2 + Y^2}{100^2 - 200X + X^2 + Y^2} \right)^{q_4} \quad (4-111)$$

$$F_4 = \frac{q_5 (Z - 100)}{(Z + R_a) (R_a + 100)} + \frac{q_6}{Y} \tan^{-1} \left[ \frac{Y(Z - 100)}{Y^2 + (Z - X) (100 - X)} \right]$$

The parameters  $q_i$  are defined as

$$q_2 = \frac{1}{U(r_1)}$$

$$q_3 = \frac{-1}{U(r_2)}$$

$$q_5 = \frac{1}{V}$$

$$q_4 = \{1 + r_1 r_2 (R_a^2 - X^2 - Y^2) q_5 + W(r_1) q_2 + W(r_2) q_3\} / X^*$$

$$q_6 = -q_5 - 2(X + R_a) q_4 - (r_2 + R_a) q_3 - (r_1 + R_a) q_2$$

$$q_1 = -2q_4 - q_3 - q_2$$

and  $X$ ,  $Y$ ,  $r_1$ ,  $r_2$ ,  $X^*$ ,  $V$ ,  $U(v)$ , and  $W(v)$  are the same as defined previously.

Finally, diffusive equilibrium is still assumed for the region above 125 km, but the temperature profile given by Equation (4-100) is no longer valid. Jacchia defined the temperature for the upper region by the empirical asymptotic function

$$T(Z) = T_x + \frac{2}{\pi} (T_\infty - T_x) \tan^{-1} \left\{ 0.95 \pi \left( \frac{T_x - T_0}{T_\infty - T_x} \right) \left( \frac{Z - 125}{35} \right) \right. \\ \left. [1 + 4.5 \times 10^{-6} (Z - 125)^{2.5}] \right\} \quad (4-112)$$

In order to be able to integrate the diffusion differential equations in closed form, Roberts replaced Jacchia's Equation (4-112) with the function

$$T(Z) = T_x - (T_\infty - T_x) \exp \left[ - \left( \frac{T_x - T_0}{T_\infty - T_x} \right) \left( \frac{Z - 125}{35} \right) \left( \frac{1}{k_a + Z} \right) \right] \quad (4-113)$$

This temperature profile is continuous at  $Z_x = 125$  km regardless of the choice of the parameter  $\hat{z}$ . The slope is continuous at  $Z_x$  if

$$\hat{z} = 1.9 (R_a + Z_x) = 12315.3554 \text{ km}$$

The value of  $\hat{z}$  is not set equal to this constant in GTDS, but is computed by a procedure to be described later.

Integration of the diffusion differential equations for the temperature profile given by Equation (4-113) yields, for the first five constituents ( $i = 1, 2, \dots, 5$ ) in Table 4-2

$$c_i(Z) = c_i(125) \left( \frac{T_x}{T} \right)^{1+\alpha_i+\gamma_i} \left( \frac{T_\infty - T}{T_\infty - T_x} \right)^{\gamma_i} \quad (4-114)$$

where

$$\gamma_i = \frac{M_i p_0 R_n^2}{R \hat{z} T_\infty} \left( \frac{T_\infty - T_x}{T_x - T_0} \right) \left( \frac{35}{6481.766} \right) \quad (4-115)$$

The constituent mass densities at 125 km can be obtained rigorously from Equation (4-109). However, as in the case of the density at 100 km, GTDS makes a curve-fitting approximation to give (for  $i = 1, 2, \dots, 5$ ):

$$\log_{10} d_i(125) = \sum_{j=0}^6 c_{ij} T_\infty^j \quad (4-116)$$



as a function of exospheric temperature, where  $d_i$  is the constituent number density divided by Avogadro's number ( $\rho_i = M_i d_i$ ). The polynomial coefficients  $\delta_{ij}$  in Equation (4-116) have been determined for best fits to the values corresponding to Equation (4-109), and are given in Table 4-3.

The value of the helium density computed by Equation (4-114) must be corrected for the seasonal latitudinal variation as given by Equation (4-99). The specific form is

$$[\rho_3(Z)]_{\text{corrected}} = \rho_3(Z) 10^{(\Delta \log_{10} \rho)_{\text{He}}}$$

Above 500 km the concentration of hydrogen ( $i = 6$  in Table 4-2) becomes sufficiently large that it also must be taken into account

$$\rho_6(Z) = \rho_6(500) \left[ \frac{T(500)}{T(Z)} \right]^{(1 + \alpha_6 + \gamma_6)} \left[ \frac{T_\infty - T(Z)}{T_\infty - T(500)} \right]^{\gamma_6} \quad (4-117)$$

where the hydrogen density at 500 km is

$$\rho_6(500) = \frac{M_6}{A} 10^{[73.13 - (39.4 - 5.5 \log_{10} T_{500}) \log_{10} T_{500}]} \quad (4-118)$$

For exospheric temperatures lower than approximately 600°K, the relative concentration of hydrogen is significant at altitudes lower than 500 km; however, the resulting density error is partially compensated for by the least squares fitting of Roberts' parameter  $\beta$  (Equation 4-122).

In Equation (4-117),  $\gamma_6$  is computed by means of Equation (4-115). The quantity  $A$  in Equation (4-118) is Avogadro's number ( $A = 6.02257 \times 10^{23}$ ). The temperature at 500 km is computed in Equation (4-113). Finally, the constituents are summed to yield

$$\rho_s(Z) = \sum_{i=1}^6 \rho_i(Z) \quad (4-119)$$

as the standard density for the region  $Z > 125$  km.

The standard density, as computed by Equations (4-102), (4-107), or (4-119) must be corrected for geomagnetic activity (by Equation (4-95)), the semi-annual variation (by Equation (4-96)), and the seasonal latitudinal variation of the lower thermosphere (by Equation (4-98)). These effects are summed logarithmically to obtain

Table 4-3

Polynomial Coefficients for Constituent Densities at 125 km

Degree of polynomial term (j)	Constituent (i)				
	(1) N <sub>2</sub>	(2) Ar	(3) He	(4) O <sub>2</sub>	(5) O
0	$0.1093155 \times 10^2$	$0.8049405 \times 10^1$	$0.7646886 \times 10^1$	$0.9924237 \times 10^1$	$0.1097083 \times 10^2$
1	$0.1186783 \times 10^{-2}$	$0.2382822 \times 10^{-2}$	$-0.4383486 \times 10^{-3}$	$0.1600311 \times 10^{-2}$	$0.6118742 \times 10^{-4}$
2	$-0.1677341 \times 10^{-5}$	$-0.3391366 \times 10^{-5}$	$0.4694313 \times 10^{-6}$	$-0.2274761 \times 10^{-5}$	$-0.1165003 \times 10^{-6}$
3	$0.1420228 \times 10^{-8}$	$0.2909714 \times 10^{-8}$	$-0.2894886 \times 10^{-9}$	$0.1938454 \times 10^{-8}$	$0.9239354 \times 10^{-10}$
4	$-0.7139785 \times 10^{-12}$	$-0.1481702 \times 10^{-11}$	$0.9451989 \times 10^{-13}$	$-0.9782183 \times 10^{-12}$	$-0.3490739 \times 10^{-13}$
5	$0.1969715 \times 10^{-15}$	$0.4127600 \times 10^{-15}$	$-0.1270838 \times 10^{-16}$	$0.2698450 \times 10^{-15}$	$0.5116298 \times 10^{-17}$
6	$-0.2296182 \times 10^{-19}$	$-0.4837461 \times 10^{-19}$	0.0	$-0.3131808 \times 10^{-19}$	0.0

$$(\Delta \log_{10} \rho)_{\text{corr}} = (\Delta \log_{10} \rho)_G + (\Delta \log_{10} \rho)_{\text{SA}} + (\Delta \log_{10} \rho)_{\text{LT}} \quad (4-120)$$

Thus, the final corrected density is

$$\rho(Z) = \rho_s(Z) 10^{(\Delta \log_{10} \rho)_{\text{corr}}} \quad (4-121)$$

The standard densities, as computed by Equations (4-102) and (4-107) for the region  $90 < Z \leq 125$  km, agree exactly with values published by Jacchia in Reference 13. Above 125 km however, the values given by Equation (4-119) do not agree exactly with the Jacchia data, due to Roberts' introduction of a different form (Equation 4-113) for the temperature profile at the higher altitudes. Values of the parameter  $\ell$  in Roberts' temperature profile were determined for a series of exospheric temperatures, such that the resulting density profiles versus altitude (from 125 km to 2500 km) gave the best least squares fit to the Jacchia tabulated data. Three sample fits are shown in Figure 4-3 for low, medium, and high values of the exospheric temperature. Note that the maximum deviation from the Jacchia values is less than 6.7%. The best-fit values of  $\ell$  are shown in Figure 4-4 as a function of exospheric temperature  $T_\infty$ . The curve in the figure is the polynomial

$$\ell = \sum_{i=0}^4 \ell_i T_\infty^i \quad (4-122)$$

with coefficients

$$\begin{aligned} \ell_0 &= 0.1031445 \times 10^5 \\ \ell_1 &= 0.2341230 \times 10^1 \\ \ell_2 &= 0.1579202 \times 10^{-2} \\ \ell_3 &= -0.1252487 \times 10^{-5} \\ \ell_4 &= 0.2462708 \times 10^{-9} \end{aligned}$$

computed to best fit the optimum  $\ell$  values. Equation (4-122) is programmed in GTDS to provide the means for selecting  $\ell$  in Equation (4-113). In general, the values of  $\ell_i$  are such that the slope of the temperature profile is discontinuous at  $Z_x = 125$  km, but this is not thought to be of any serious consequence.

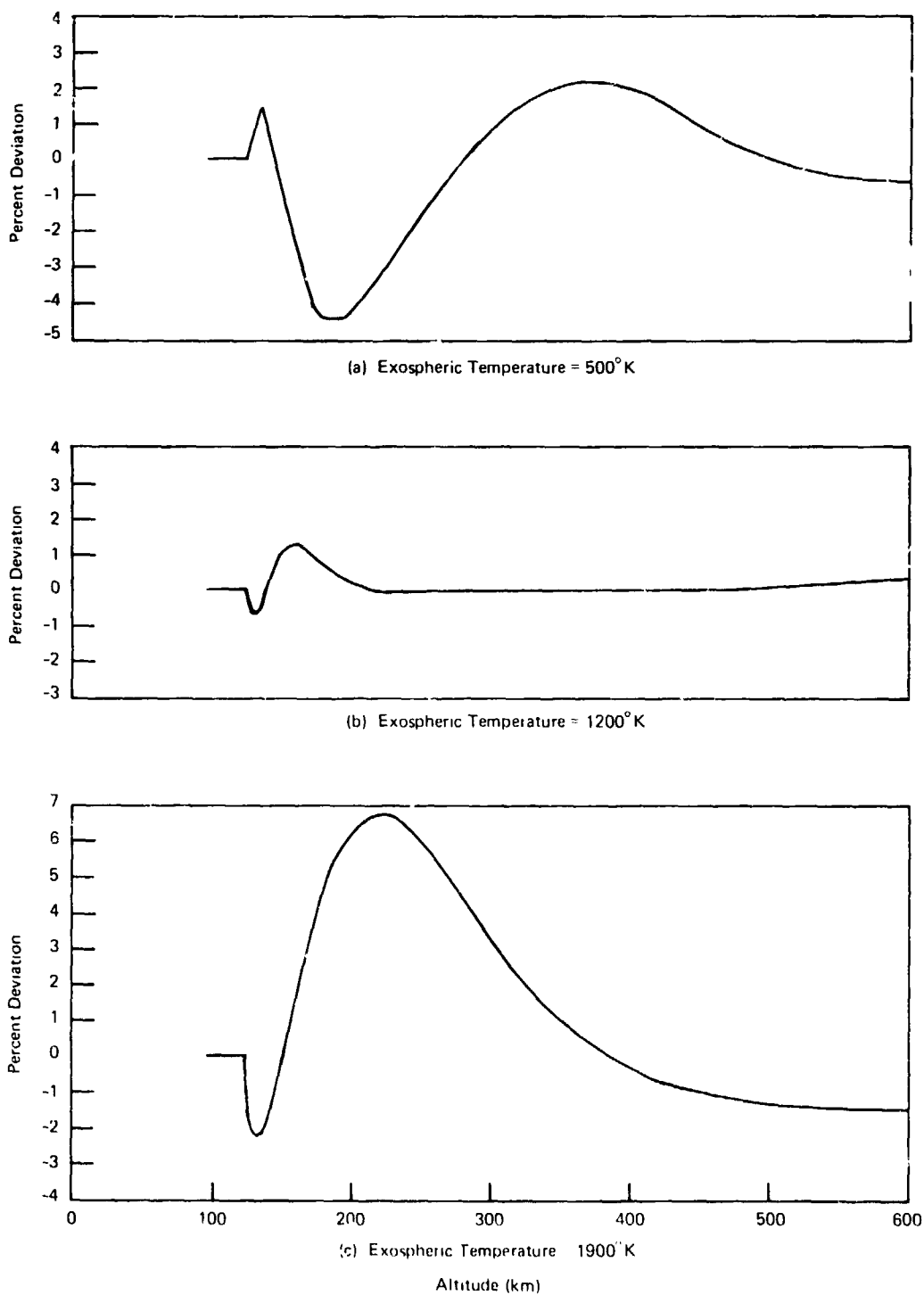


Figure 4-3. Sample Deviations of Jacchia-Roberts Densities from Jacchia 1971 Values.

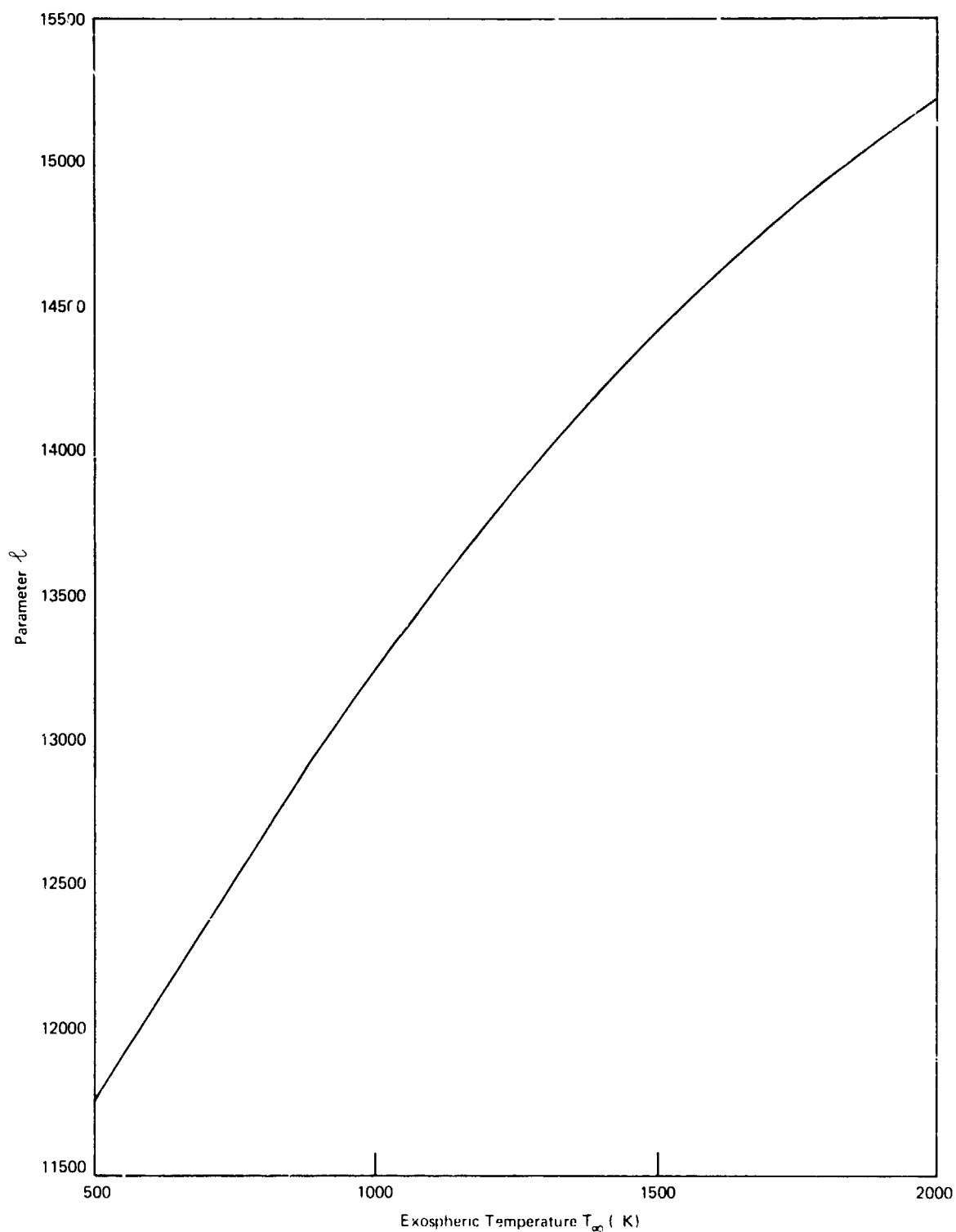


Figure 4-4. Best-fit Values of  $l$  as a Function of the Exospheric Temperature  $T_{\infty}$

#### 4.5.5 Associated Partial Derivatives

The equations for computing the partial derivative  $\partial \rho / \partial \bar{R}$ , which appears in Equation (4-81), are presented in this section for the Jacchia-Roberts model. Equation (4-121) for the density is written in the form

$$\rho(Z) = \rho_s(Z) \Delta \rho_c$$

and the desired partial derivative becomes

$$\frac{\partial \rho}{\partial \bar{R}} = \rho_s \frac{\partial (\Delta \rho_c)}{\partial \bar{R}} + \Delta \rho_c \frac{\partial \rho_s}{\partial \bar{R}} \quad (4-123)$$

The variation of the correction factor is derived from Equations (4-120) and (4-95) through (4-98)

$$\begin{aligned} \frac{\partial (\Delta \rho_c)}{\partial \bar{R}} = & \frac{\Delta \rho_c}{.4342944819} \left\{ g(t) f'(Z) \frac{\partial Z}{\partial \bar{R}} \right. \\ & + .014 \sin(2\pi\Phi + 1.72) e^{-.0013(Z-90)^2} \\ & \times \left[ (1 - .0026 \{Z - 90\}^2) \sin \varphi \left| \sin \varphi \right| \frac{\partial Z}{\partial \bar{R}} \right. \\ & \left. \left. + 2(Z - 90) \left| \sin \varphi \right| \cos \varphi \frac{\partial \varphi}{\partial \bar{R}} \right] \right\} \end{aligned} \quad (4-124)$$

where

$$\begin{aligned} f'(Z) = & -.002868 f(Z) \\ & + 2.331(5.876 \times 10^{-7}) Z^{1.331} e^{-.002868Z} \end{aligned}$$

The variation of altitude with position,  $\partial Z/\partial \bar{R}$ , is computed as shown in Equation (4-150) in Section 4.5.7. Differentiation of Equation (4-90) yields

$$\frac{\partial \phi}{\partial \bar{R}} = \frac{\sin 2\phi}{2} \begin{bmatrix} -\frac{X_1}{X_1^2 + X_2^2} \\ -\frac{X_2}{X_1^2 + X_2^2} \\ \frac{1}{X_3} \end{bmatrix} \quad (4-125)$$

The variation of the standard density is computed directly from the barometric differential equation (Reference 13) for altitudes below 100 km

$$\frac{\partial \rho_s}{\partial \bar{R}} = \rho_s \left\{ \left[ \frac{1}{M} \sum_{n=1}^6 n A_n Z^{n-1} - \frac{Mg}{RT} \right] \frac{\partial Z}{\partial \bar{R}} - \frac{1}{T} \frac{\partial T}{\partial \bar{R}} \right\} \quad (4-126)$$

and from the diffusion differential equation (Reference 13) for altitudes above 100 km

$$\frac{\partial \rho_s}{\partial \bar{R}} = -\frac{1}{T} \left\{ \left[ \frac{\rho'_s g_0 R_a^2}{R(Z + R_a)^2} \right] \frac{\partial Z}{\partial \bar{R}} + (\rho'_s + \alpha_{3\rho'_3}) \frac{\partial T}{\partial \bar{R}} \right\} \quad (4-127)$$

where

$$\rho'_s = \sum_{i=1}^6 \rho'_{s_i} M_i$$

The partial derivatives of the temperature are computed by differentiating Equation (4-100) for altitudes below 125 km

$$\frac{\partial T}{\partial \bar{R}} = \frac{T - T_0}{d_1} \left( \frac{\partial T_x}{\partial T_n} \right) \frac{\partial T_n}{\partial \bar{R}} + \left( \frac{d_1}{35^4} \sum_{n=1}^4 n C_n Z^{n-1} \right) \frac{\partial Z}{\partial \bar{R}} \quad (4-128)$$

or Equation (4-113) for altitudes above 125 km

$$\begin{aligned}
\frac{\partial T}{\partial \bar{R}} = & \frac{\partial T_{\infty}}{\partial \bar{R}} + \left( \frac{T - T_{\infty}}{T_{\infty} - T_x} \right) \left\{ \left( 1 - \frac{\partial T_x}{\partial T_{\infty}} \right) - \left( \frac{Z - Z_x}{R_a + Z} \right) \left( \frac{\ell}{35} \right) \right. \\
& \times \left[ \frac{\partial T_x}{\partial T_{\infty}} - \frac{T_x - T_0}{T_{\infty} - T_x} \left( 1 - \frac{\partial T_x}{\partial T_{\infty}} \right) + \frac{T_x - T_0}{\ell} \sum_{j=1}^4 j \ell_j T_{\infty}^{j-1} \right] \left. \frac{\partial T_{\infty}}{\partial \bar{R}} \right. \\
& \left. - \left( \frac{T - T_{\infty}}{T_{\infty} - T_x} \right) (T_x - T_0) \left[ \frac{R_a + Z_x}{(R_a + Z)^2} \right] \left( \frac{\ell}{35} \right) \frac{\partial Z}{\partial \bar{R}} \right\}
\end{aligned} \quad (4-129)$$

Finally, the derivatives of  $T_x$  and  $T_{\infty}$  are computed by differentiating Equations (4-94) and (4-89), respectively

$$\frac{\partial T_x}{\partial T} = 0.0518806 + (294.3505) (.0021622) e^{-.0021622 T_{\infty}}$$

$$\begin{aligned}
\frac{\partial T_{\infty}}{\partial \bar{R}} = & 0.3 T_c \left\{ 2.2 \sin^{1.2} \theta \cos \theta \left( 1 - \cos^{3.0} \frac{\tau}{2} \right) \frac{\partial \theta}{\partial \bar{R}} \right. \\
& \left. - 2.2 \cos^{1.2} \eta \sin \eta \cos^{2.0} \frac{\tau}{2} \frac{\partial \eta}{\partial \bar{R}} \right. \\
& \left. - \frac{3}{2} \left( \cos^{2.2} \eta - \sin^{2.2} \theta \right) \cos^2 \frac{\tau}{2} \sin \frac{\tau}{2} \frac{\partial \tau}{\partial \bar{R}} \right\}
\end{aligned} \quad (4-130)$$

In the latter expression (from Equations (4-90) and (4-91))



$$\frac{\partial \eta}{\partial \bar{R}} = \frac{1}{2} \frac{\phi - \delta_s}{|\phi - \delta_s|} \frac{\partial \phi}{\partial \bar{R}}$$

$$\frac{\partial \theta}{\partial \bar{R}} = \frac{1}{2} \frac{\phi + \delta_s}{|\phi + \delta_s|} \frac{\partial \phi}{\partial \bar{R}}$$

$$\frac{\partial \tau}{\partial X_i} = \frac{\pi}{180} \left\{ 1 + \frac{\pi}{30} \cos \left[ \frac{\pi(H + 43.0)}{180} \right] \right\} \frac{\partial H}{\partial X_i} \quad (i = 1, 2) \quad (4-131)$$

$$\begin{aligned} \frac{\partial H}{\partial X_i} = & \frac{180}{\pi} \left( \frac{S_1 X_2 - S_2 X_1}{|S_1 X_2 - S_2 X_1|} \right) \left\{ \frac{1}{[(X_1^2 + X_2^2)^{1/2} (S_1^2 + S_2^2) - (S_1 X_1 - S_2 X_2)^2]^{1/2}} \right\} \\ & \times \left[ \frac{(S_1 X_1 - S_2 X_2) X_i}{X_1^2 + X_2^2} - \frac{X_1 X_2}{S_i} \right] \cdot \frac{1 - X_i}{R} \quad (i = 1, 2) \end{aligned}$$

$$\frac{\partial \tau}{\partial X_3} = 0$$

It might be argued that the term in Equation (4-129) involving the derivative  $\partial \ell / \partial T_\infty$  should not be included, since Roberts considered  $\ell$  as a constant in his integration. However,  $T_\infty$  and  $T_x = F(T_\infty)$  were also held constant for the integration over altitude. Therefore, if variations in  $T_\infty$  are taken into account, and  $\ell$  is a function of  $T_\infty$ , then the derivative of  $\ell$  should also be included, and is computed by differentiating Equation (4-122), the best-fitting polynomial to the optimum values of  $\ell$ .

#### 4.5.6 Modified Harris-Priester Atmospheric Model

Harris and Priester determined the physical properties of the upper atmosphere theoretically by solving the heat conduction equation under quasi-hydrostatic conditions (References 10-12). Approximations for fluxes from the extreme ultraviolet and corpuscular heat sources were included, but the model averaged

the semiannual and seasonal-latitudinal variations and did not attempt to account for the extreme ultraviolet 27-day effect. The atmospheric model presently included in GTDS is a modification of the Harris-Priester concept. The modification attempts to account for the diurnal bulge by including a cosine variation between a maximum density profile at the apex of the diurnal bulge (which is located approximately 30° east of the subsolar point) and a minimum density profile at the antapex of the diurnal bulge. Discrete values of the maximum and minimum density-altitude profiles, shown in Table 4-4, correspond to mean solar activity and are stored in tabular form as  $\rho_m(h_i)$  and  $\rho_M(h_i)$ , respectively. Different maximum and minimum profiles can be retrieved from disk storage for different levels of solar activity. Exponential interpolation is used between entries, i.e., the minimum and maximum densities,  $\rho_m$  and  $\rho_M$ , are given by

$$\rho_m(h) = \rho_m(h_i) \exp\left(\frac{h_i - h}{H_m}\right) \tag{a}$$

$$h_i \leq h \leq h_{i+1} \tag{4-132}$$

$$\rho_M(h) = \rho_M(h_i) \exp\left(\frac{h_i - h}{H_M}\right) \tag{b}$$

and the respective scale heights,  $H_m$  and  $H_M$ , by

$$H_m = \frac{h_i - h_{i+1}}{\ln[\rho_m(h_{i+1})/\rho_m(h_i)]} \tag{a}$$

$$\tag{4-133}$$

$$H_M = \frac{h_i - h_{i+1}}{\ln[\rho_M(h_{i+1})/\rho_M(h_i)]} \tag{b}$$

A good approximation (neglecting polar motion) for the height,  $h$ , is given by

$$h = r - r_s \tag{4-134}$$

where  $r_s$  is the radius of the earth given by Equations (3-107) and (3-115) as

$$r_s = \frac{R_e(1 - f)}{\sqrt{1 - (2f - f^2) \cos^2 \delta}} \tag{4-135}$$

and

$r \sim$  the magnitude of the satellite position vector

$R_e \sim$  the equatorial radius of the earth

$f \sim$  the earth's flattening coefficient

$\delta \sim$  the declination of the satellite. It is assumed that  $\delta$  equals the geocentric latitude of the subsatellite point.

Table 4-4

Density Altitude Tables

Height (km)	Min. Density (gm/km <sup>3</sup> )	Max. Density (gm/km <sup>3</sup> )	Height (km)	Min. Density (gm/km <sup>3</sup> )	Max. Density (gm/km <sup>3</sup> )
100	497400.	497400.	420	1.558	5.384
120	24900.	24900.	440	1.091	4.355
130	8377.	8710.	460	.7701	3.362
140	3899.	4059.	480	.5474	2.612
150	2122.	2215.	500	.3916	2.042
160	1263.	1344.	520	.2819	1.605
170	800.8	875.8	540	.2042	1.267
180	528.3	601.0	560	.1488	1.005
190	361.7	429.7	580	.1092	.7997
200	255.7	316.2	600	.08070	.6390
210	183.9	239.6	620	.06012	.5123
220	134.1	185.3	640	.04519	.4121
230	99.49	145.5	660	.03430	.3325
240	74.88	115.7	680	.02632	.2691
250	57.09	93.08	700	.02043	.2185
260	44.03	75.55	720	.01607	.1779
270	34.30	61.82	740	.01281	.1452
280	26.97	50.95	760	.01036	.1190
290	21.39	42.26	780	.008496	.09776
300	17.08	35.26	800	.007069	.08059
320	10.99	25.11	840	.004680	.05741
340	7.214	18.19	880	.003200	.04210
360	4.824	13.37	920	.002210	.03130
380	3.274	9.955	960	.001560	.02360
400	2.249	7.492	1000	.001150	.01810

If the density is assumed to be maximum at the apex of the bulge, then the cosine variation between maximum and minimum density profiles is

$$\rho_0(h) = \rho_m(h) + [\rho_M(h) - \rho_m(h)] \cos^n \left( \frac{\psi}{2} \right) \quad (4-136)$$

where  $\psi$  is the angle between the satellite position vector and the apex of the diurnal bulge. The angle  $\psi$  is given by

$$\cos \psi = \sin \delta \sin \delta_s + \cos \delta \cos \delta_s \cos (\alpha - \alpha_s - \bar{\lambda}) \quad (4-137)$$

where

$\delta_s \sim$  the declination of the sun

$\alpha \sim$  the right ascension of the satellite

$\alpha_s \sim$  the right ascension of the sun

$\bar{\lambda} \sim$  the lag angle between the sun line and the apex of the diurnal bulge (approximately  $30^\circ$ )

It can be calculated in vector notation as

$$\psi = \cos^{-1} \left( \frac{\bar{r} \cdot \bar{U}_B}{r} \right) \quad (4-138)$$

or the cosine function in Equation (4-136) can be determined directly as

$$\cos^n \frac{\psi}{2} = \left[ \frac{1 + \cos \psi}{2} \right]^{n/2} = \left[ \frac{1}{2} + \frac{\bar{r} \cdot \bar{U}_B}{2r} \right]^{n/2} \quad (4-139)$$

where

$\bar{r} \sim$  the satellite position vector expressed in inertial geocentric coordinates

$\bar{U}_B \sim$  the unit vector directed toward the apex of the diurnal bulge expressed in inertial geocentric coordinates.

The vector  $\bar{U}_B$  has the following components

$$U_{B_x} = \cos \delta_s \cos (\alpha_s + \bar{\lambda})$$

$$U_{B_y} = \cos \delta_s \sin (\alpha_s + \bar{\lambda})$$

$$U_{B_z} = \sin \delta_s$$

In the modeling of accelerations in GTDS, the drag coefficient  $C_D$  and atmospheric density  $\rho(h)$  always occur together as a product. The following error model is introduced in order to account for systematic errors in either  $C_D$  or  $\rho$

$$C_D \cdot \rho = C_{D_0} (1 + \rho_1) [1 + \rho_2 (t - t_0)] \left[ 1 + \rho_3 \cos^n \left( \frac{\psi}{2} \right) \right] \rho_0(h) \quad (4-140)$$

where

$C_{D_0} \sim$  a priori specified drag coefficient

$\rho_1 \sim$  scale factor error coefficient on  $C_D \rho$

$\rho_2 \sim$  error coefficient of time variation of  $C_D \rho$

$\rho_3 \sim$  error coefficient accounting for deviations in the diurnal variation of  $\rho(h)$

$t \sim$  the time of the instantaneous satellite position

$t_0 \sim$  the epoch time

The altitude density function,  $\rho_0(h)$ , is determined from Equation (4-133). The quantities  $\rho_1$ ,  $\rho_2$ ,  $\rho_3$ , and  $n$  are adjustable parameters for the error model.

#### 4.5.7 Associated Partial Derivatives

Equation (4-140) for the product of the drag coefficient and the density can be partitioned as follows

$$C_D = C_{D_0} (1 + \rho_1) [1 + \rho_2 (t - t_0)] \quad (4-141)$$

$$\rho(h) = \left(1 + \rho_3 \cos^n \frac{\psi}{2}\right) \left[\rho_m + (\rho_M - \rho_m) \cos^n \frac{\psi}{2}\right] \quad (4-142)$$

Making use of Equations (4-132) and (4-133), the partial derivative of density with respect to position is then given by

$$\frac{\partial \rho}{\partial \bar{R}} = \left( \frac{\partial \rho}{\partial \rho_m} \frac{\partial \rho_m}{\partial h} + \frac{\partial \rho}{\partial \rho_M} \frac{\partial \rho_M}{\partial h} \right) \frac{\partial h}{\partial \bar{R}} + \frac{\partial \rho}{\partial \psi} \frac{\partial \psi}{\partial \bar{R}} \quad (4-143)$$

where

$$\frac{\partial \rho}{\partial \rho_m} = \left(1 - \cos^n \frac{\psi}{2}\right) \left(1 + \rho_3 \cos^n \frac{\psi}{2}\right) \quad (4-144)$$

$$\frac{\partial \rho}{\partial \rho_M} = \cos^n \frac{\psi}{2} \left(1 + \rho_3 \cos^n \frac{\psi}{2}\right) \quad (4-145)$$

$$\frac{\partial \rho_m}{\partial h} = - \frac{\rho_m}{H_m} \quad (4-146)$$

$$\frac{\partial \rho_M}{\partial h} = - \frac{\rho_M}{H_M} \quad (4-147)$$

The partial derivative of density with respect to  $\psi$  and the partial derivative of  $\psi$  with respect to  $\bar{R}$  are obtained from Equations (4-138) and (4-142)

$$\begin{aligned} \frac{\partial \rho}{\partial \psi} = & - \frac{n}{2} \cos^{n-1} \frac{\psi}{2} \sin \frac{\psi}{2} \left\{ (\rho_M - \rho_m) \left(1 + \rho_3 \cos^n \frac{\psi}{2}\right) \right. \\ & \left. + \rho_3 \left[\rho_m + (\rho_M - \rho_m) \cos^n \frac{\psi}{2}\right] \right\} \end{aligned} \quad (4-148)$$

$$\frac{\partial \tau}{\partial \bar{R}} = \frac{1}{\sin \gamma} \left[ \left( \frac{\bar{R} \cdot \bar{U}_B}{R^3} \right) \bar{R} - \frac{\bar{U}_B}{R} \right] \quad (4-149)$$

The partial derivative of the height with respect to  $\bar{R}$  is obtained by differentiating Equation (4-134), yielding

$$\frac{\partial h}{\partial \bar{R}} = \frac{\bar{R}}{R} - R_e \left\{ \frac{(1-f)(2f-f^2)\cos\phi}{[1-(2f-f^2)\cos^2\phi]^{3/2}} \right\} \frac{\partial(\cos\phi)}{\partial \bar{R}} \quad (4-150)$$

where

$$\frac{\partial(\cos\phi)}{\partial \bar{R}} = \frac{1}{R^4 \cos\phi} \begin{bmatrix} XZ^2 \\ YZ^2 \\ -Z(X^2 + Y^2) \end{bmatrix} \quad (4-151)$$

Substitution of Equations (4-144) through (4-151) into Equation (4-143) determines the partial derivative of  $\mu$  with respect to  $\bar{R}$ , as required in Equation (4-81).

The error coefficients  $\epsilon_1$ ,  $\epsilon_2$ , and  $\epsilon_3$  contribute the following partial derivatives to the C matrix appearing in the variational equations

$$\frac{\partial \ddot{\bar{R}}_D}{\partial \epsilon_1} = \frac{\ddot{\bar{R}}_D}{C_D} C_{D_0} [1 + \epsilon_2(t - t_0)] = \frac{\ddot{\bar{R}}_D}{(1 + \epsilon_1)} \quad (a)$$

(4-152)

$$\frac{\partial \ddot{\bar{R}}_D}{\partial \epsilon_2} = \frac{\ddot{\bar{R}}_D}{C_D} C_{D_0} (1 + \epsilon_1) (t - t_0) = \frac{\ddot{\bar{R}}_D (t - t_0)}{[1 + \epsilon_2(t - t_0)]} \quad (b)$$

$$\frac{\partial \ddot{\bar{R}}_D}{\partial \epsilon_3} = \frac{\ddot{\bar{R}}_D}{C_D(h)} \left[ l_m + (\epsilon_M - \epsilon_m) \cos^n \frac{\psi}{2} \right] \cos^n \frac{\psi}{2} = \frac{\ddot{\bar{R}}_D \cos^n \frac{\psi}{2}}{\left( 1 + \epsilon_3 \cos^n \frac{\psi}{2} \right)} \quad (c)$$

#### 4.5.8 Comparison of Atmospheric Models

Only a limited number of comparisons have been made at this time between the results obtained using the Harris-Priester and the Jacchia models. One such comparison evaluated the standard deviation of the weighted residuals in differential correction runs made using data from the San Marco-3 satellite, with a perigee altitude of 213 km and an inclination of 3 degrees. A one day differential correction was performed around the epoch of the element set selected in order to determine the elements at J2000 epoch. When the density parameter  $\rho_1$  (see Equation (4-80)) was not adjusted, both models converged to the same standard deviation, but different elements. When  $\rho_1$  was adjusted, the Jacchia model gave a somewhat lower standard deviation than the Harris-Priester model. If the atmospheric bulge angle used in the Jacchia model was included in the Harris-Priester model, the standard deviation decreased slightly, but was still larger than that for the Jacchia model.

A second comparison was made by generating an ephemeris forward 3 days from the elements obtained in the original differential correction and comparing the satellite's position and velocity with a state vector obtained in a differential correction about the new epoch. The position differences resulting from this procedure were approximately twice as large for the Jacchia model compared with the Harris-Priester model (55 kilometers versus 30 kilometers). Thus, these comparisons were inconclusive since some indicated better results with the Jacchia model, while others indicated better results with the Harris-Priester model.

Clearly, more exhaustive testing is desirable, particularly in light of the fact that the Jacchia-Roberts model is significantly more expensive computationally than the Harris-Priester model. The Atmosphere Explorer satellite series should provide a good opportunity for such testing.

### 4.6 SOLAR RADIATION PRESSURE

#### 4.6.1 Solar Radiation Pressure Perturbation Model

The force due to solar radiation pressure on a vehicle's surface is proportional to the effective area  $A$  of the surface normal to the incident radiation, the surface reflectivity  $\eta$ , and the luminosity  $L_s$  of the sun, and is inversely proportional to the square of the distance  $R_{vs}$  from the sun and the speed of light  $c$ .



The magnitude of the force due to direct solar radiation pressure on an area A is therefore given by\*

$$F = \frac{L_s C_R A}{4\pi R_{vs}^2 c} \quad (4-153)$$

where

$$C_R = 1 + \eta \text{ (e. g., } C_R = 1.95 \text{ for aluminum)} \quad (4-154)$$

The magnitude of the acceleration acting on a spacecraft of mass m and area A, due to direct solar radiation pressure at one astronomical unit from the sun, is

$$\frac{F}{m} = \frac{S}{c} \frac{C_R A}{m} \quad (4-155)$$

where S denotes the mean solar flux at one astronomical unit. The quantities  $C_R$ , A and m are grouped together since they are spacecraft properties and can be determined prior to flight. The magnitude of the acceleration on a spacecraft due to direct solar radiation at the actual distance  $R_{vs}$  from the sun is given by

$$\frac{F}{m} = \frac{S}{c} \frac{R_{sun}^2}{R_{vs}^2} \frac{C_R A}{m} \quad (4-156)$$

where  $R_{sun}$  designates one astronomical unit, i.e., the semimajor axis of the earth's orbit.

All of the above factors except  $R_{vs}$  are constant for a given spacecraft and mission. For computational convenience,  $P_s$  replaces  $S/c$ .  $P_s$  is defined as the force on a perfectly absorbing surface ( $\eta = 0$ ) due to solar radiation pressure at one astronomical unit.

The acceleration due to direct solar radiation is away from the sun, that is, in the direction of

$$\vec{R}_{vs} = \vec{R} - \vec{R}_s \quad (4-157)$$

---

\* The determination of the effective area A of the surface normal to the incident radiation is directly analogous to the determination of the effective area normal to the relative velocity vector for modeling aerodynamic forces, which is discussed in detail in Section 4.5.2.

where

$\bar{\mathbf{R}}$  ~ the position vector of the vehicle in the inertial mean of 1950.0 coordinate system

$\bar{\mathbf{R}}_s$  ~ the position vector of the sun in the inertial mean of 1950.0 coordinate system.

The model for the acceleration  $\ddot{\mathbf{R}}_{SR}$  due to direct solar radiation is

$$\ddot{\mathbf{R}}_{SR} = \nu P_s R_{sun}^2 \frac{C_R A}{m} \frac{\bar{\mathbf{R}}_{vs}}{R_{vs}^3} \quad (4-158)$$

where  $\nu$  is an eclipse factor such that

$$\begin{aligned} \nu &= 0 \text{ if the satellite is in shadow (umbra)} \\ \nu &= 1 \text{ if the satellite is in sunlight} \\ 0 < \nu < 1 &\text{ if the satellite is in penumbra} \end{aligned}$$

A simple cylindrical shadow model is used to determine the eclipse factor. More sophisticated models accounting for penumbral regions and reflected radiation effects may be considered in later versions of the program, as required. From Figure 4-5 it is apparent that the satellite is in sunlight ( $\nu = 1$ ) if

$$D = \bar{\mathbf{R}}' \cdot \bar{\mathbf{U}}_s > 0 \quad (4-159)$$

where

$\bar{\mathbf{R}}'$  ~ the satellite position vector relative to the shadowing body

$\bar{\mathbf{U}}_s$  ~ the solar position unit vector relative to the shadowing body.

If  $D < 0$  and the vector

$$\bar{\mathbf{S}}_c = \bar{\mathbf{R}}' - D\bar{\mathbf{U}}_s \quad (4-160)$$

has a magnitude less than the body radius  $a_n$ , then the spacecraft is in shadow (i.e.,  $\nu = 0$ ); otherwise, it is assumed that the satellite is in sunlight and  $\nu = 1$ .

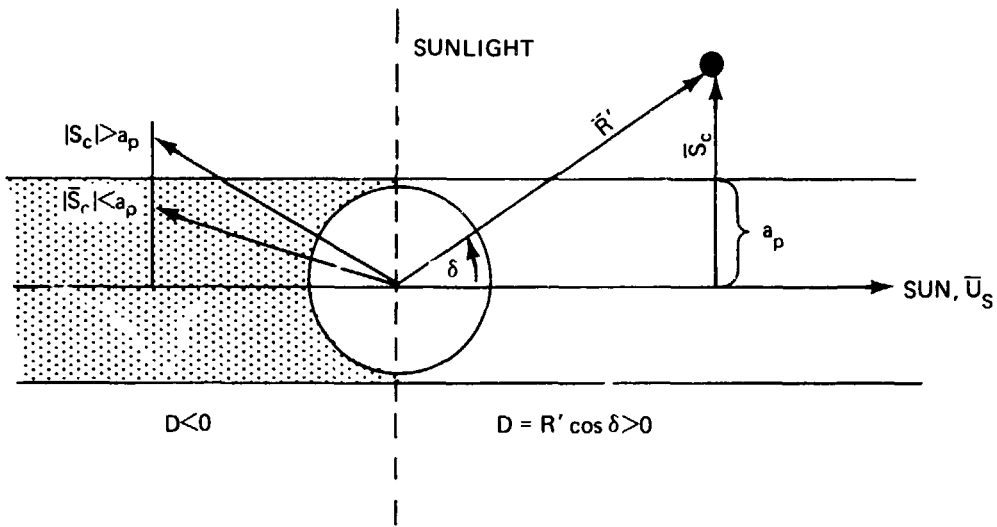


Figure 4-5. Cylindrical Shadow Model

#### 4.6.2 Associated Partial Derivatives

The partial derivative of  $\ddot{\bar{\mathbf{R}}}_{SR}$  with respect to position is

$$\frac{\partial \ddot{\bar{\mathbf{R}}}_{SR}}{\partial \bar{\mathbf{R}}} = \nu \frac{P_s R_{sun}^2 C_R A}{m |\bar{\mathbf{R}} - \bar{\mathbf{R}}_s|^3} \left[ \mathbf{I} - \frac{3 [\bar{\mathbf{R}} - \bar{\mathbf{R}}_s] [\bar{\mathbf{R}} - \bar{\mathbf{R}}_s]^T}{|\bar{\mathbf{R}} - \bar{\mathbf{R}}_s|^2} \right] \quad (4-161)$$

$$\frac{\partial \ddot{\bar{\mathbf{R}}}_{SR}}{\partial \dot{\bar{\mathbf{R}}}} = \mathbf{0}_3 \quad (4-162)$$

and for the solar pressure model parameter

$$k = \frac{P_s A}{m} \quad (4-163)$$

$$\frac{\partial \ddot{\bar{\mathbf{R}}}_{SR}}{\partial k} = \nu R_{sun}^2 C_R \frac{[\bar{\mathbf{R}} - \bar{\mathbf{R}}_s]}{|\bar{\mathbf{R}} - \bar{\mathbf{R}}_s|^3} \quad (4-164)$$

### 4.7 ATTITUDE CONTROL EFFECTS

The function of the attitude control system is related to two modes of operation. During the first mode, commonly known as the acquisition and cruise mode, the attitude control system is used to establish and maintain three-axis stable orientation of the satellite. Such an orientation is obtained during an interplanetary flight, for example, by fixing two directions in space. One direction is always such that the sensitive surface of the solar panels faces the sun and the other direction is determined by pointing an on-board sensor toward a predetermined star. Usually another requirement that must be satisfied during the latter portion of the flight is that the high-gain antenna used for communication should point toward the earth.

In the second mode of operation, applicable during midcourse maneuvers, the attitude control system orients the satellite so that the thrust vector of the vehicle-fixed rocket motor is aligned along a predetermined direction in space. This orientation is maintained by controlling the thrust vector to pass through the center of mass of the satellite. After the maneuver, the attitude control system re-establishes the cruise orientation.

The low-thrust forces, generated by the normal functions of the attitude control system, can produce accelerations of  $1 \times 10^{-7}$  cm/sec<sup>2</sup> to  $3 \times 10^{-7}$  cm/sec<sup>2</sup>. This can result in a target miss of 100 to 300 km at Mars, for example. The translational forces producing the acceleration are the result of thrusters not acting in couples, thruster misalignment and unbalance, or the result of gas leaks through the valves during times that the thrusters are not firing.

#### 4.7.1 Attitude Control Perturbation Model

The model used to account for such accelerations has been constructed from the application of curve-fitting techniques to telemetered data and is defined as follows:

$$\ddot{\mathbf{r}}_{\text{TAC}} = \begin{Bmatrix} a_x + b_x(t - T_{ac1}) + c_x(t - T_{ac1})^2 \\ a_y + b_y(t - T_{ac1}) + c_y(t - T_{ac1})^2 \\ a_z + b_z(t - T_{ac1}) + c_z(t - T_{ac1})^2 \end{Bmatrix} [u(t - T_{ac1}) - u(t - T_{ac2})] \quad (4-165)$$

The coefficients ( $a_x, a_y, a_z \dots c_x, c_y, c_z$ ) are low-thrust polynomial coefficients to be determined. The terms  $T_{ac1}$  and  $T_{ac2}$  are input epochs at which the attitude control acceleration polynomials are turned on and off, respectively. The function  $u$  is defined by

$$u(t - T_{ac1}) = \begin{cases} 1, & t \geq T_{ac1} \\ 0, & t < T_{ac1} \end{cases} \quad (4-166)$$

$$u(t - T_{ac2}) = \begin{cases} 1, & t \geq T_{ac2} \\ 0, & t < T_{ac2} \end{cases} \quad (4-167)$$

The subscript  $x$  denotes the acceleration component along the spacecraft's  $x_v$  (roll) axis; the subscript  $y$  denotes the acceleration component along the spacecraft's  $y_v$  (pitch) axis; and the subscript  $z$  denotes the acceleration component along the spacecraft's  $z_v$  (yaw) axis.

Two transformations are necessary in order to represent this acceleration in the mean of 1950.0 coordinate system: (1) a transformation from the vehicle-fixed coordinate system ( $x_v, y_v, z_v$ ) to the true of date coordinate system and (2) a transformation from the true of date coordinate system to the mean of 1950.0 coordinate system.

The transformation from the vehicle-fixed coordinate system to the true of date coordinate system is described in Section 3.3.12, and is given by

$$\bar{r} = Q\bar{r}_v \quad (4-168)$$

where the transformation matrix  $Q$  is defined in Section 3.3.12. The matrix  $C^T$ , which transforms from the true of date system to the mean of 1950.0 system is described in Section 3.3.1. Thus, the total transformation is given by

$$\ddot{\bar{R}}_{TAC} = C^T Q \ddot{\bar{r}}_{TAC} \quad (4-169)$$

#### 4.7.2 Associated Partial Derivatives

Since  $C$ ,  $Q$ , and  $\ddot{\mathbf{r}}_{TAC}$  are functions of time only, and not of the satellite position or velocity, then

$$\frac{\partial \ddot{\mathbf{r}}_{TAC}}{\partial \dot{\mathbf{R}}} = \frac{\partial \ddot{\mathbf{r}}_{TAC}}{\partial \dot{\mathbf{R}}} = \mathbf{0}_3. \quad (4-170)$$

The contributions to the variational equations (Equation (4-7)) of the control system acceleration parameters  $a_x, a_y, a_z, \dots, c_z$  are

$$\frac{\partial \ddot{\mathbf{r}}_{TAC}}{\partial \bar{\mathbf{a}}} = \mathbf{C}^T \mathbf{Q} [u(t - T_{ac1}) - u(t - T_{ac2})] \quad (4-171)$$

$$\frac{\partial \ddot{\mathbf{r}}_{TAC}}{\partial \bar{\mathbf{b}}} = (t - T_{ac1}) \frac{\partial \ddot{\mathbf{r}}_{TAC}}{\partial \bar{\mathbf{a}}} \quad (4-172)$$

$$\frac{\partial \ddot{\mathbf{r}}_{TAC}}{\partial \bar{\mathbf{c}}} = (t - T_{ac1})^2 \frac{\partial \ddot{\mathbf{r}}_{TAC}}{\partial \bar{\mathbf{a}}} \quad (4-173)$$

where  $\bar{\mathbf{a}}$ ,  $\bar{\mathbf{b}}$ , and  $\bar{\mathbf{c}}$  denote the vectors

$$\bar{\mathbf{a}} = \begin{bmatrix} a_x \\ a_y \\ a_z \end{bmatrix} \quad \bar{\mathbf{b}} = \begin{bmatrix} b_x \\ b_y \\ b_z \end{bmatrix} \quad \bar{\mathbf{c}} = \begin{bmatrix} c_x \\ c_y \\ c_z \end{bmatrix} \quad (4-174)$$

#### 4.8 THRUST EFFECTS

There are many forces acting on a spacecraft during the transfer phase and during the orbiting phase of its trajectory. Even though such forces have been modeled, the state of the vehicle is still uncertain, primarily because of the imprecision associated with the injection conditions and the physical parameters

appearing in the mathematical models. Very small errors in the thrust magnitude and/or thrust direction at injection magnify into very large errors in position and velocity near the target body. In order to avoid such errors and attain pre-assigned terminal conditions, spacecraft are designed with the capability to perform multiple propulsive maneuvers during the interplanetary phase of a mission. Furthermore, if the spacecraft is to orbit a distant planet, maneuvering capability must be available to inject into orbit.

#### 4.8.1 Thrust Acceleration Model

The model describing the acceleration during such corrective maneuvers is based on the reduction of data taken during the motor burn testing procedures and is represented in an inertial true of date system by

$$\ddot{\mathbf{r}}_T = a \{u(t - T_0) - u(t - T_f)\} \bar{\mathbf{U}}_T \quad (4-175)$$

where

$a \sim$  magnitude of the thrust acceleration

$\mathbf{U}_T \sim$  unit vector in the direction of the thrust acceleration

$T_0 \sim$  effective initiation time of the motor burn (ET)

$T_f \sim$  effective termination time of the motor burn (ET)

and  $u$  is defined as in Equations (4-166) and (4-167).

The motor's effective burn time is

$$T_b = T_f - T_0. \quad (4-176)$$

The propulsive acceleration is modeled as follows

$$a = a_0 + a_1 \tau + a_2 \tau^2 + a_3 \tau^3 + a_4 \tau^4 \quad (4-177)$$

where

$$\tau = t - T_0$$

Equation (4-177) characterizes the thrust acceleration as a fourth degree polynomial in  $\tau$ , the time from effective thrust initiation. The polynomial coefficients  $a_0$ ,  $a_1$ ,  $a_2$ ,  $a_3$ , and  $a_4$  are dynamic model parameters which can optionally be specified or estimated and represent the effective thrust-mass ratio as a function of time.

The unit vector  $\bar{U}_T$  is directed along the spacecraft's thrust axis (assumed to be coincident with the  $x_v$ -axis). The true of date components of the vector  $\bar{U}_T$  are

$$U_T = \begin{bmatrix} \cos \alpha_T \cos \delta_T \\ \sin \alpha_T \cos \delta_T \\ \sin \delta_T \end{bmatrix} \quad (4-178)$$

where

$\alpha_T \sim$  the right ascension of the spacecraft's thrust axis relative to the true equator and equinox of date

$\delta_T \sim$  the declination of the spacecraft's thrust axis relative to the true equator and equinox of date.

The thrust axis orientation is represented by the fourth-degree polynomials in  $\tau$

$$\alpha_T = \alpha_0 + \alpha_1 \tau + \alpha_2 \tau^2 + \alpha_3 \tau^3 + \alpha_4 \tau^4 \quad (4-179a)$$

$$\delta_T = \delta_0 + \delta_1 \tau + \delta_2 \tau^2 + \delta_3 \tau^3 + \delta_4 \tau^4 \quad (4-179b)$$

where  $\alpha_0, \alpha_1, \dots, \alpha_4, \delta_0, \dots, \delta_4$  are dynamic parameters which can optionally be estimated.



The unit vector  $\bar{U}_T$  can also be expressed in the orbital frame system, which is obtained from the orbit plane system (Section 3.2.5) by a translation of the origin to the center of mass of the spacecraft and a redesignation of axes such that

$$\bar{r}_{of} = E_1 \bar{r}_{op} \quad (4-180)$$

where

$$E_1 = \begin{bmatrix} 0 & 1 & 0 \\ 0 & 0 & 1 \\ 1 & 0 & 0 \end{bmatrix}$$

The thrust direction is defined by a rotation of  $Y_T$  (the yaw angle) about the  $z_{of}$  axis, followed by a rotation of  $P_T$  (the pitch angle) about the new  $x$  axis. The components of  $\bar{U}_T$  in the orbital frame system are of the same form as Equation (4-178), with  $\delta_T$  replaced by  $Y_T$  and  $\alpha_T$  replaced by  $P_T$ . The true of date components of  $\bar{U}_T$  are then given by

$$\bar{U}_T = (E_1 E)^T \bar{U}_{T_{of}} = E_{of}^T \bar{U}_{T_{of}} \quad (4-181)$$

where  $E$  is the transformation matrix from the inertial true of date system to the orbit plane system (see Section 3.3.5).

The thrust acceleration is expressed in the true equator and equinox of date coordinate system via the unit vector  $\bar{U}_T$ . The transformation to the mean equator and equinox of 1950.0 system is accomplished as follows

$$\ddot{\bar{R}}_T = C^T \ddot{\bar{R}}_T \quad (4-182)$$

where the transformation matrix  $C^T$  is described in Section 3.3.1.

#### 4.8.2 Associated Partial Derivatives

When the acceleration  $\ddot{\bar{R}}_T$  is modeled in the direction  $\bar{U}_T$  given by Equation (4-178) it is independent of both  $\dot{\bar{R}}$  and  $\ddot{\bar{R}}$ ; therefore

$$\frac{\partial \ddot{\bar{R}}_T}{\partial \dot{\bar{R}}} = \frac{\partial \ddot{\bar{R}}_T}{\partial \ddot{\bar{R}}} = 0 \quad (4-183)$$

However, when the direction of the acceleration  $\bar{\ddot{U}}_T$  is expressed as in Equation (4-181), the following partial derivatives are used.

Using Equations (4-175), (4-181) and (4-182), the thrust acceleration during a thrusting interval can be expressed as

$$\bar{\ddot{R}}_T = a(E_1 E C)^T \bar{U}_{T_{of}} \quad (4-184)$$

Since only the matrix E is a function of position and velocity,

$$\frac{\partial \bar{\ddot{R}}_T}{\partial \bar{R}} = a C^T \frac{\partial E^T}{\partial \bar{R}} E_1^T \bar{U}_{T_{of}} \quad (4-185)$$

and

$$\frac{\partial \bar{\ddot{R}}_T}{\partial \dot{\bar{R}}} = a C^T \frac{\partial E^T}{\partial \dot{\bar{R}}} E_1^T \bar{U}_{T_{of}} \quad (4-186)$$

The rows of the matrix E are defined in Section 3.3.5 to be the unit vectors  $\bar{U}$ ,  $\bar{V}$ , and  $\bar{W}$ . The necessary partial derivatives then may be expressed, using subscript notation, as

$$\frac{\partial U_i}{\partial \dot{x}_j} = 0 \quad (4-187)$$

$$\frac{\partial U_i}{\partial x_j} = \frac{\delta_{ij}}{r} - \frac{x_i \cdot x_j}{r^3} \quad (4-188)$$

$$\frac{\partial W_i}{\partial x_j} = \frac{1}{L} \frac{\partial L_i}{\partial x_j} - \frac{L_i}{L^2} \frac{\partial L}{\partial x_j} \quad (4-189)$$

$$\frac{\partial W_i}{\partial \dot{x}_j} = \frac{1}{L} \frac{\partial L_i}{\partial \dot{x}_j} - \frac{L_i}{L^2} \frac{\partial L}{\partial \dot{x}_j} \quad (4-190)$$

$$\frac{\partial V_i}{\partial p} = \begin{bmatrix} 0 & -W_3 & W_2 \\ W_3 & 0 & -W_1 \\ -W_2 & W_1 & 0 \end{bmatrix} \begin{bmatrix} \frac{\partial U_1}{\partial p} \\ \frac{\partial U_2}{\partial p} \\ \frac{\partial U_3}{\partial p} \end{bmatrix} + \begin{bmatrix} 0 & U_3 & -U_2 \\ -U_3 & 0 & U_1 \\ U_2 & U_1 & 0 \end{bmatrix} \begin{bmatrix} \frac{\partial W_1}{\partial p} \\ \frac{\partial W_2}{\partial p} \\ \frac{\partial W_3}{\partial p} \end{bmatrix} \quad (4-191)$$

where

$\delta_{ij}$  is the Kronecker delta operator

$L_i$  is the angular momentum vector ( $\vec{R} \times \dot{\vec{R}}$ )

$L$  is the magnitude of the angular momentum vector

$p$  is any one of the parameters  $x_1, x_2, x_3, \dot{x}_1, \dot{x}_2, \dot{x}_3$

and

$$\frac{\partial L_i}{\partial x_j} = \begin{bmatrix} 0 & \dot{x}_3 & -\dot{x}_2 \\ -\dot{x}_3 & 0 & \dot{x}_1 \\ \dot{x}_2 & -\dot{x}_1 & 0 \end{bmatrix} \quad (4-192)$$

$$\frac{\partial L_i}{\partial \dot{x}_j} = \begin{bmatrix} 0 & -x_3 & x_2 \\ x_3 & 0 & -x_1 \\ -x_2 & x_1 & 0 \end{bmatrix} \quad (4-193)$$

$$\frac{\partial L}{\partial p} = \frac{1}{L} \sum_{i=1}^3 L_i \frac{\partial L_i}{\partial p} \quad (4-194)$$

The C matrix components resulting from the acceleration model parameters  $a_0, \dots, a_4$  are

$$\frac{\partial \ddot{\mathbf{R}}_T}{\partial \bar{\mathbf{a}}} = \frac{\ddot{\mathbf{R}}_T}{\mathbf{a}} \bar{\Gamma}_4^T \quad (4-195)$$

$$\frac{\partial \ddot{\mathbf{R}}_T}{\partial \bar{\mathbf{a}}} = \mathbf{a} \{u(t - T_0) - u(t - T_f)\} \mathbf{C}^T \bar{\mathbf{U}}_2 \bar{\Gamma}_3^T \quad (4-196)$$

$$\frac{\partial \dot{\mathbf{R}}_1}{\partial \bar{\delta}} = \mathbf{a} \{u(t - T_0) - u(t - T_f)\} \mathbf{C}^T \bar{\mathbf{U}}_6 \bar{\Gamma}_3^T \quad (4-197)$$

where

$$\bar{\mathbf{a}} = \begin{bmatrix} a_0 \\ a_1 \\ \cdot \\ \cdot \\ \cdot \\ a_4 \end{bmatrix}, \quad \bar{\alpha} = \begin{bmatrix} \alpha_0 \\ \alpha_1 \\ \cdot \\ \cdot \\ \cdot \\ \alpha_3 \end{bmatrix}, \quad \bar{\delta} = \begin{bmatrix} \delta_0 \\ \delta_1 \\ \cdot \\ \cdot \\ \cdot \\ \delta_3 \end{bmatrix} \quad (4-198)$$

$$\bar{\Gamma}_r^T = [1, \tau, \tau^2, \dots, \tau^r] \quad (4-199)$$

$$\bar{\mathbf{U}}_2 = \frac{\partial \bar{\mathbf{U}}_T}{\partial \alpha_T} = \begin{bmatrix} -\sin \alpha_T \cos \delta_T \\ \cos \alpha_T \cos \delta_T \\ 0 \end{bmatrix} \quad (4-200)$$

$$\bar{\mathbf{U}}_6 = \frac{\partial \bar{\mathbf{U}}_T}{\partial \delta_T} = \begin{bmatrix} -\cos \alpha_T \sin \delta_T \\ -\sin \alpha_T \sin \delta_T \\ \cos \delta_T \end{bmatrix} \quad (4-201)$$

## 4.9 REPLACEMENT ACCELERATION

### 4.9.1 Replacement Acceleration Model

When accelerometer data is available from a spacecraft, this data, when properly converted, may be used to replace the model of all nonpotential accelerations (i. e., atmospheric drag, solar radiation pressure, thrust, and attitude control system accelerations). Letting  $\ddot{\bar{R}}_A$  represent the total acceleration as measured by an on-board accelerometer, and letting

$$\ddot{\bar{R}}_A = \ddot{\bar{R}}_D + \ddot{\bar{R}}_{SR} + \ddot{\bar{R}}_{TAC} + \ddot{\bar{R}}_T \quad (4-202)$$

then Equation (4-1) reduces to

$$\ddot{\bar{R}} = \ddot{\bar{R}}_{PM} + \ddot{\bar{R}}_{NS} + \ddot{\bar{R}}_{IO} + \ddot{\bar{R}}_A \quad (4-203)$$

It is understood, of course, that the accelerations measured by the accelerometers at any instant of time need not represent all of the accelerations on the right hand side of Equation (4-202).

The acceleration  $\ddot{\bar{R}}_A$  is computed from the following relationship

$$\ddot{\bar{R}}_A = Q [K \bar{A} + \bar{B}] \quad (4-204)$$

where  $Q$  is a  $3 \times 3$  transformation matrix from the accelerometer axes to the coordinate system of integration,  $K$  is a diagonal matrix of accelerometer scale factor corrections (in addition to those scale factors used during the pre-processing of the telemetered accelerometer data),  $\bar{B}$  is a  $3 \times 1$  vector of bias corrections (in addition to those biases, such as zero sets, employed in the pre-processing), and  $\bar{A}$  is the  $3 \times 1$  vector of external accelerations expressed in the accelerometer coordinate system.

The matrix  $Q$  is comprised of a number of rotations:  $Q_A$ , the transformation matrix from the accelerometer axes to the vehicle-fixed axes;  $Q_B$ , the transformation matrix from the vehicle-fixed axes to the inertial true of date system; and, if necessary,  $Q_C$ , the transformation matrix from the inertial true of date system to the user selected coordinate system of integration. Thus,  $Q$  is determined by

$$Q = Q_C Q_B Q_A \quad (4-205)$$

where  $Q_A$  is a constant matrix, and  $Q_B$  is determined from

$$Q_B = f(\theta_1, \theta_2, \theta_3) \quad (4-206)$$

and  $\theta_1$ ,  $\theta_2$ , and  $\theta_3$  are the attitude orientation angles which relate the spacecraft vehicle-fixed coordinate system to the true of date coordinate system, as described in Section 3.3.12.

#### 4.9.2 Associated Partial Derivatives

$$\frac{\partial \ddot{\bar{R}}_A}{\partial \theta_i} = Q \frac{\partial}{\partial \theta_i} [K\bar{A} + \bar{B}] \text{ where } i = 1, 2, 3$$

$$\frac{\partial \ddot{\bar{R}}_A}{\partial k_{11}} = q_{(i, 1)} a_1$$

$$\frac{\partial \ddot{\bar{R}}_A}{\partial k_{22}} = q_{(i, 2)} a_2$$

$$\frac{\partial \ddot{\bar{R}}_A}{\partial k_{33}} = q_{(i, 3)} a_3 \quad (4-207)$$

$$\frac{\partial \ddot{\bar{R}}_A}{\partial b_1} = q_{(i, 1)}$$

$$\frac{\partial \ddot{\bar{R}}_A}{\partial b_2} = q_{(i, 2)}$$

$$\frac{\partial \ddot{\bar{R}}_A}{\partial b_3} = q_{(i, 3)}$$

where  $q_{(i,j)}$  is the element in the  $i^{\text{th}}$  row and  $j^{\text{th}}$  column of  $[Q]$ , and  $a_i$  and  $b_i$  are the elements in the  $i^{\text{th}}$  row of the vectors  $\bar{A}$  and  $\bar{B}$ , respectively.

#### 4.10 ANALYTIC PARTIAL DERIVATIVES

The differential correction process requires the development of a set of partial derivatives called the matrizant, or state transition matrix. These partial derivatives give the relationships between perturbations in the spacecraft state at observation times to perturbations in the state at the epoch. Analytic expressions for these partial derivatives which were developed originally for the Brouwer-Lyddane method (References 15 and 16) are available for use with all of the orbit generators utilized in GTDS. The perturbation variables utilized in the analytic partial derivatives are defined in such a way as to couple the perturbation propagation process with the differential correction process. These variables are referred to as the DODS variables.

##### 4.10.1 Definition of the Perturbation Variables

In the statistical estimation process, the spacecraft dynamic state variables in  $\bar{x}$  are normally expressed in an inertial Cartesian coordinate system. As a result, the estimator algorithm solves for the differential correction,  $\delta \bar{x}_{i+1}$ , to be added to the epoch state on the  $i$ th iteration,  $\bar{x}_i$ , to yield an improved estimate  $\bar{x}_{i+1}$ . Note that the unknowns that are solved for are corrections to the Cartesian state variables. The variables for the Brouwer-Lyddane theory are also state corrections, but are defined as follows:

$$\begin{aligned}
 x_1 &= \frac{\delta a}{a} && (\text{semimajor axis}) \\
 x_2 &= \delta e && (\text{eccentricity}) \\
 x_3 &= e \delta f && (\text{true anomaly}) \\
 x_4 &= \delta \sigma && (\text{rotation about } \hat{c}) \\
 x_5 &= \delta \beta && (\text{rotation about } \hat{\beta}) \\
 x_6 &= \delta \gamma && (\text{rotation about } \hat{\gamma}) \\
 x_7 &= \frac{a}{r^2} \delta r && (\text{radial distance})
 \end{aligned} \tag{4-208}$$

$$x_8 = \frac{2}{na \sqrt{1 - e^2 \cos E}} \delta v \quad (\text{velocity}) \quad (4-208)$$

$$x_9 = \delta \theta \quad (\text{flight path angle}) \quad (\text{cont'd})$$

$$x_{19} = \delta \Omega + \delta \omega \quad (\text{longitude of periapsis})$$

Variables  $x_1$ ,  $x_2$ , and  $x_3$  account for in-plane perturbations of the orbit, i.e., perturbations in the semimajor axis  $a$ , the eccentricity  $e$ , and the true anomaly  $f$ , respectively. The variable  $x_3$  can also be related to a perturbation in the mean anomaly  $M$  as follows

$$x_3 = \frac{e\sqrt{1 - e^2}}{(1 - e \cos E)^2} \delta M \quad (4-209)$$

Variables  $x_4$ ,  $x_5$  and  $x_6$  account for angular rotations of the orbit plane. Figure 4-6 illustrates an orbit around a planet. The unit vector  $\hat{a}$  is normal to the orbit plane; the unit vector  $\hat{\beta}$  lies in the orbit plane and is displaced from the ascending node by the angle  $\delta_a$ . The unit vector  $\hat{\gamma}$  forms a right hand system with  $\hat{a}$  and  $\hat{\beta}$ , i.e.,  $\hat{\gamma} = \hat{a} \times \hat{\beta}$ . Variable  $x_4$  accounts for the rotational perturbation  $\delta \alpha$  about  $\hat{a}$ ,  $x_5$  accounts for the rotational perturbation  $\delta \beta$  about  $\hat{\beta}$ , and  $x_6$  accounts

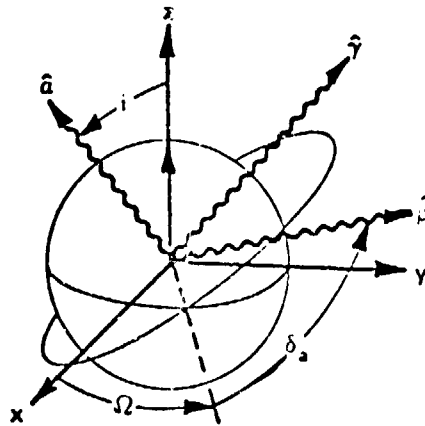


Figure 4-6. Orbital Geometry



for the rotational perturbation  $\delta\gamma$  about  $\hat{\gamma}$ . Variables  $x_4, x_5$  and  $x_6$  can be related to the orbit inclination  $i$ , the right ascension of the ascending node  $\Omega$ , and the argument of periapsis  $\omega$  as follows

$$\delta i = x_5 \cos \delta_a - x_6 \sin \delta_a$$

$$\delta \Omega = \frac{x_5 \sin \delta_a + x_6 \cos \delta_a}{\sin i} \quad (4-210)$$

$$\delta \omega = x_4 - \frac{x_3}{e} - (x_5 \sin \delta_a + x_6 \cos \delta_a) \cot i$$

The angle  $\delta_a$  between the line of nodes and the  $\hat{\beta}$  vector defines the  $\hat{\beta}$  and  $\hat{\gamma}$  directions. This angle can be  $\omega_0$ ,  $\omega_0 + f_0$ ,  $\omega + f$ , or some other specified angle. In the equations that follow,  $\delta_a$  is assumed to be  $\omega + f$ , i.e.,  $\hat{\beta}$  is directed towards the spacecraft.

Only six of the ten variables in Equations (4-208) are independent. Therefore, any six can be selected to be solved for in any orbit determination problem. The selection criteria are dependent upon the sensitivity of the variables to pertinent characteristics of the orbit being determined. Experience has shown that variables  $x_1, x_2, x_3, x_5, x_6$  and  $x_{19}$  are usually a reliable set of variables to use in a variety of earth orbital missions. The dependence of the variables on orbital characteristics is shown in Table 4-5.

Table 4-5

DODS Variable Dependency

	a	e	i	$\Omega$	$\omega$	M	E	f	r	$\theta$	$\delta_a$	V
$x_1$	✓											
$x_2$		✓										
$x_3$					✓	✓	✓	✓				
$x_4$					✓						✓	
$x_5$			✓	✓	✓						✓	
$x_6$			✓	✓	✓						✓	
$x_7$	✓	✓			✓	✓	✓	✓	✓			
$x_8$	✓	✓			✓	✓	✓	✓				✓
$x_9$		✓			✓	✓	✓	✓		✓		
$x_{19}$						✓	✓	✓			✓	

The Brouwer-Lyddane theory was developed for use with drag-free orbits. However, for high altitude, small eccentricity orbits the primary effect of drag is a secular change in the mean anomaly. This effect is relatively small and is noticeable only over a long period of time. Consequently, an optional first order correction to the mean anomaly is included of the form

$$\Delta M_{\text{DRAG}} = \sum_{q=0}^m \sum_{p=2}^3 N_{pq} (t - t_q)^p \quad (4-211)$$

$$m = 0, 1, 2, \dots, 19$$

where

$N_{pq} \sim$  the Brouwer drag parameters

$t_q \sim$  the reference time associated with the  
Brouwer drag parameters

The correction is applied to the mean motion as follows

$$M'' = n_0 \Delta t + \dot{M} \Delta t + M_0'' + \Delta M_{\text{DRAG}} \quad (4-212)$$

Forty DODS variables which account for the forty drag parameters  $N_{pq}$  in Equation (4-211) are defined as

$$x_{20+q} = \frac{N_{2q}}{n^2}$$

$$q = 0, 1, \dots, 19 \quad (4-213)$$

$$x_{40+q} = \frac{N_{3q}}{n^2}$$

These variables are estimated by means of the differential correction process in order to determine the secular corrections to the mean anomaly.

#### 4.10.2 State Transition Matrix Elements

The statistical estimation algorithm requires the matrix of partial derivatives of the observations  $f(t_i)$  at time  $t_i$  with respect to the solve-for state variables  $x_j$  at the epoch time  $t_0$ . These partial derivatives are computed as follows

$$\frac{\partial f(t_i)}{\partial x_j} = \frac{\partial f(t_i)}{\partial \bar{r}(t_i)} \frac{\partial \bar{r}(t_i)}{\partial x_j} \quad j = 1, 2, \dots, 19 \quad (4-214)$$

The partial derivative of the observation model  $f(t_i)$  with respect to the osculating Cartesian state vector  $\bar{r}(t_i)$  is modeled as described in Chapter 7. However, the partial derivatives of the osculating Cartesian state with respect to the DODS variables must be determined. When the Brouwer or Brouwer-Lyddane theory is being utilized,  $\partial \bar{r}(t_i) / \partial x_j$  is obtained analytically, where the solve-for variables  $x_j$  are the DODS variables. When one of the other GTDS orbit generators is used, requiring numerical integration of the orbital equations, two options are available: (1) the required partial derivatives can be obtained from numerical solution of the variational equations or (2) the above analytic partial

derivatives can be used by replacing, via the chain rule, the required partial derivative in Equation (4-214) with

$$\frac{\partial \bar{r}(t_i)}{\partial x_j} = \frac{\partial \bar{r}(t_i)}{\partial x_k} \frac{\partial x_k}{\partial x_j} \quad (4-215)$$

where, in this case, the  $x_k$ 's are the DODS variables, the first term on the right represents the analytic partial derivatives of the osculating Cartesian state with respect to the DODS variables, and the second term represents the partial derivatives of the DODS variables with respect to the appropriate solve-for variables, depending on the orbit generator being used.

The analytic partial derivatives of the osculating Cartesian state with respect to the DODS variables are approximated by two-body Keplerian partial derivatives evaluated using the osculating Keplerian elements at  $t_i$  and  $t_0$ . This approach neglects the higher order effects of the Brouwer secular variation, as well as the partial derivatives of the osculating position and velocity with respect to the Brouwer mean position and velocity. These partial derivatives, which are developed in Reference 17, are presented below.

$$\frac{\partial \bar{r}}{\partial x_1} = \bar{r} - \frac{3}{2} (t - t_0) \dot{\bar{r}} \quad (4-216a)$$

$$\frac{\partial \dot{\bar{r}}}{\partial x_1} = -\frac{\dot{\bar{r}}}{2} + \frac{3}{2} \frac{\mu \bar{r} (t - t_0)}{r^3}$$

$$\frac{\partial \bar{r}}{\partial x_2} = -\frac{1}{(1 - e^2)} \left[ (\cos E_0 + e) \bar{r} - \frac{1}{n} (2 - e^2 - e \cos E) \sin E \dot{\bar{r}} \right] \quad (4-216b)$$

$$\frac{\partial \dot{\bar{r}}}{\partial x_2} = \frac{1}{(1 - e^2)} \left[ \cos E \dot{\bar{r}} - \frac{\dot{\mu} \sin E}{nr^2} (1 + e \cos E - e^2 - e^2 \cos^2 E) \bar{r} \right]$$

$$\frac{\partial \bar{\mathbf{r}}}{\partial \mathbf{x}_3} = \frac{a^2}{r} \left\{ \frac{\sin E}{\sqrt{1-e^2}} [2 \cos E_0 + e \sin^2 E_0 - 2e - (1-e^2) \cos E] \hat{\mathbf{p}} \right. \\ \left. + [1 - (2 \cos E_0 + e \sin^2 E_0 - \cos E) \cos E] \hat{\mathbf{q}} \right\}$$

$$\frac{\partial \dot{\bar{\mathbf{r}}}}{\partial \mathbf{x}_3} = \frac{na^4}{\sqrt{1-e^2}r^3} \{ [1 + 2 \cos E (\cos E_0 - \cos E) \\ - e (\cos E (\sin^2 E + \cos^2 E_0) - 2 \cos E_0) \\ + e^2 (2 \cos^2 E + \cos^2 E_0) - e^3 \cos^3 E] \hat{\mathbf{p}} \\ - \sqrt{1-e^2} \sin E \{ (\cos E_0 - \cos E) [e (\cos E + \cos E_0) - 2] \} \hat{\mathbf{q}} \} \quad (4-216c)$$

$$\frac{\partial \bar{\mathbf{r}}}{\partial \mathbf{x}_4} = \hat{\mathbf{a}} \times \bar{\mathbf{r}} \quad (4-216d)$$

$$\frac{\partial \dot{\bar{\mathbf{r}}}}{\partial \mathbf{x}_4} = \hat{\mathbf{a}} \times \dot{\bar{\mathbf{r}}}$$

$$\frac{\partial \bar{\mathbf{r}}}{\partial \mathbf{x}_5} = \hat{\beta} \times \bar{\mathbf{r}} \quad (4-216e)$$

$$\frac{\partial \dot{\bar{\mathbf{r}}}}{\partial \mathbf{x}_5} = \hat{\beta} \times \dot{\bar{\mathbf{r}}}$$

$$\frac{\partial \bar{\mathbf{r}}}{\partial \mathbf{x}_6} = \hat{\gamma} \times \bar{\mathbf{r}} \quad (4-216f)$$

$$\frac{\partial \dot{\bar{\mathbf{r}}}}{\partial \mathbf{x}_6} = \hat{\gamma} \times \dot{\bar{\mathbf{r}}}$$

$$\frac{\partial \bar{r}}{\partial x_7} = 2 \frac{\partial \bar{r}}{\partial x_1} + (1 - e^2) \cos E \frac{\partial \bar{r}}{\partial x_2} - \sqrt{1 - e^2} \sin E_0 \frac{\partial \bar{r}}{\partial x_3} \quad (4-216g)$$

$$\frac{\partial \dot{\bar{r}}}{\partial x_7} = 2 \frac{\partial \dot{\bar{r}}}{\partial x_1} + (1 - e^2) \cos E \frac{\partial \dot{\bar{r}}}{\partial x_2} - \sqrt{1 - e^2} \sin E_0 \frac{\partial \dot{\bar{r}}}{\partial x_3}$$

$$\frac{\partial \bar{r}}{\partial x_8} = (1 - e \cos E_0) \frac{\partial \bar{r}}{\partial x_1} + (1 - e^2) \cos E_0 \frac{\partial \bar{r}}{\partial x_2} - \sqrt{1 - e^2} \sin E_0 \frac{\partial \bar{r}}{\partial x_3} \quad (4-216h)$$

$$\frac{\partial \dot{\bar{r}}}{\partial x_8} = (1 - e \cos E_0) \frac{\partial \dot{\bar{r}}}{\partial x_1} + (1 - e^2) \cos E_0 \frac{\partial \dot{\bar{r}}}{\partial x_2} - \sqrt{1 - e^2} \sin E_0 \frac{\partial \dot{\bar{r}}}{\partial x_3}$$

$$\frac{\partial \bar{r}}{\partial x_9} = -\sqrt{1 - e^2} \sin E_0 \frac{\partial \bar{r}}{\partial x_2} - (e + \cos E_0) \frac{\partial \bar{r}}{\partial x_3} \quad (4-216i)$$

$$\frac{\partial \dot{\bar{r}}}{\partial x_9} = -\sqrt{1 - e^2} \sin E_0 \frac{\partial \dot{\bar{r}}}{\partial x_2} - (e + \cos E_0) \frac{\partial \dot{\bar{r}}}{\partial x_3}$$

$$\frac{\partial \bar{r}}{\partial x_{19}} = \frac{a(1 - e \cos E_0)^2}{(1 - e^2)(1 - e \cos E)} [-\sqrt{1 - e^2} \sin E \hat{p} + (1 - e^2) \cos E \hat{q}] \quad (4-216j)$$

$$\frac{\partial \dot{\bar{r}}}{\partial x_{19}} = \frac{a^4 n (1 - e \cos E)^2}{r^3 \sqrt{1 - e^2}} [(e - \cos E) \hat{p} - \sqrt{1 - e^2} \sin E \hat{q}]$$

where  $\hat{p}$  and  $\hat{q}$  are unit vectors in the orbit plane, with  $\hat{p}$  directed toward perigee and  $\hat{q}$  advanced 90 degrees in the direction of motion from perigee, i.e.,  $\hat{q} = \hat{a} \times \hat{p}$ . The parameter  $n$  is the mean motion.

The Brouwer mean elements are utilized when the above equations are used for determining the partial derivatives at time  $t$ . Although the Brouwer mean elements at time  $t$  are not determined from two-body relationships, the above equations still provide a good approximation for the state transition matrix elements

for the mean motion.

The partial derivatives of the position and velocity with respect to the DODS drag parameters  $x_{20}, \dots, x_{59}$  are

$$\frac{\partial \bar{r}}{\partial x_{20+q}} = n_0 \dot{\bar{r}} (t - t_q)^2 \quad (4-217)$$

$$\frac{\partial \dot{\bar{r}}}{\partial x_{20+q}} = - \frac{(t - t_q)^2}{\sqrt{a_0} r^3} \{ (\csc E - e_0) \hat{p} + \sqrt{1 - e_0^2} \sin E \hat{q} \}$$

$$q = 0, 1, \dots, 19$$

and

$$\frac{\partial \bar{r}}{\partial x_{40+q}} = n_0 (t - t_q) \frac{\partial \bar{r}}{\partial x_{20+q}} \quad (4-218)$$

$$\frac{\partial \dot{\bar{r}}}{\partial x_{40+q}} = n_0 (t - t_q) \frac{\partial \dot{\bar{r}}}{\partial x_{20+q}}$$

$$q = 0, 1, \dots, 19$$

#### 4.10.3 Conversion of Differential Corrections

Use of the preceding partial derivatives results in the expression of the state perturbations at epoch time in terms of DODS variables. Consequently, the weighted least-squares estimator algorithm yields the differential corrections in terms of DODS variables. These corrections must then be converted into more meaningful variables, such as Keplerian elements or Cartesian components. Specifically, GTDS converts the DODS corrections  $x_1, x_2, \dots, x_{10}$  into corrections of the Brouwer mean elements, i.e., Keplerian elements. The reference mean elements at epoch are then updated to begin the next iteration.

As described in Section 4.10.2, when analytical partial derivatives are used in GTDS with orbit generators other than the Brouwer or Brouwer-Lyddane techniques, the statistical estimation algorithm is modified by introducing the partial derivatives of the DODS variables with respect to the solve-for state variables appropriate for the orbit generator in use. The estimation algorithm then yields the differential corrections in terms of these solve-for state variables.

Only six of the DODS variables described in Section 4.10.1 are independent. The user has the option of selecting which elements are to be corrected. The following conversion equations show the dependency of the mean Keplerian element corrections on all the DODS variables; however, only the six independent variables selected for inclusion in the differential correction process should be included. All the other DODS variables should be set equal to zero. The following equations also include the conversion relationships for the related variables  $E$ ,  $f$ ,  $r$ ,  $\theta$ ,  $\delta_a$  and  $V$ .

$$\Delta a = ax_1 + 2ax_7 + a^3\zeta_5x_8$$

$$\Delta e = x_2 + \zeta_1x_7 + \zeta_5\zeta_6x_8 + r\zeta_8x_9$$

$$\Delta i = x_5 \cos \delta_a - x_6 \sin \delta_a$$

$$\Delta \Omega = \frac{1}{\sin i} (x_5 \sin \delta_a + x_6 \cos \delta_a)$$

(4-219)

$$\Delta \omega = -\frac{1}{e}x_3 + x_4 - \zeta_{12}x_5 - \zeta_{13}x_6 - \zeta_3x_7 - \zeta_7x_8 - \zeta_9x_9$$

$$\Delta M = \frac{1}{e} \zeta_{11}x_3 + \zeta_3\zeta_{11}x_7 + \zeta_7\zeta_{11}x_8 + \zeta_9\zeta_{11}x_9 + \zeta_{11}x_{19}$$

$$\Delta E = \frac{1}{e} \zeta_{10}x_3 + \zeta_3\zeta_{10}x_7 + \zeta_7\zeta_{10}x_8 + \zeta_9\zeta_{10}x_9 + \zeta_{10}x_{19}$$



$$\Delta f = \frac{1}{e} x_3 + \zeta_3 x_7 + \zeta_7 x_8 + \zeta_9 x_9 + x_{19}$$

$$\Delta r = \zeta_2 x_7$$

(4-219)

$$\Delta \theta = x_9$$

(cont'd)

$$\Delta \delta_a = x_4 - \zeta_{12} x_5 - \zeta_{13} x_6 + x_{19}$$

$$\Delta V = \frac{a}{2} \zeta_4 x_8$$

where

$$\zeta_1 = \frac{1 - e^2 - r^3 v^3 \cos \theta}{\mu a^2 e}$$

$$\zeta_2 = \frac{r^2}{a}$$

(4-220)

$$\zeta_3 = \frac{\zeta_1 (2ae + r \cos f) + \zeta_2 (1 + e \cos f) - 2a(1 - e^2)}{re \sin f}$$

$$\zeta_4 = n \sqrt{1 - e^2 \cos^2 E}$$

$$\zeta_5 = \frac{v}{\mu} \zeta_4$$

$$\zeta_6 = \frac{(1 - e^2) a^2 - r^2 \cos^2 \theta}{2e}$$

$$\zeta_7 = \frac{\zeta_5 \zeta_6 (2ae + re + r \cos f) - a^3 (1 - e^2)}{re \sin f}$$

$$\zeta_8 = \frac{rV^2}{\mu ae} \sin \theta \cos \theta$$

$$\zeta_9 = \frac{\zeta_8 (2ae + r \cos f)}{e \sin f}$$

(4-220)

(cont'd)

$$\zeta_{10} = \frac{1 - e \cos E}{\sqrt{1 - e^2}}$$

$$\zeta_{11} = \frac{(1 - e \cos E)^2}{\sqrt{1 - e^2}}$$

$$\zeta_{12} = \frac{\cos i \sin \delta_a}{\sin i}$$

$$\zeta_{13} = \frac{\cos i \cos \delta_a}{\sin i}$$

REPRODUCIBILITY OF THE  
ORIGINAL PAGE IS POOR

#### 4.11 REFERENCES

1. Brouwer, D. and Clemence, G. M.: 1961, Methods of Celestial Mechanics, Academic Press, New York.
2. Danby, J. M. A.: 1962, Fundamentals of Celestial Mechanics, Macmillan, New York.
3. Escobal, P. R.: 1965, Methods of Orbit Determination, John Wiley & Sons, New York.
4. Kaula, W. M.: 1966, Theory of Satellite Geodesy, Blaisdell Press, Los Angeles, California.
5. Sturms, F. M.: Equations of Motion for a Double Precision Trajectory Program, Volume IV, Jet Propulsion Laboratory Report SPS 37-29.
6. Moyer, T. D.: 1971, Mathematical Formulation of the Double-Precision Orbit Determination Program (DPODP), Jet Propulsion Laboratory Technical Report 32-1527, May 1971.
7. Jacchia, L. G.: 1960, "A Variable Atmospheric-Density Model from Satellite Accelerations," Journal of Geophysical Research, 65(9), pp. 2775-82.
8. Jacchia, L. G.: 1963, "Variations in the Earth's Upper Atmosphere as Revealed by Satellite Drag," Rev. Mod. Phys., 35(4), October 1963, pp. 973-91.
9. Jacchia, L. G.: 1964, The Temperature above the Thermopause, Smithsonian Astrophysical Observatory Special Report No. 150, Cambridge, Massachusetts April 1964.
10. Harris, I. and Priester, W.: 1952, "Time Dependent Structure of the Upper Atmosphere," Jour. Atmos. Sciences, 19(4), July 1952, also NASA TN D-1443.
11. Harris, I. and Priester, W.: 1962, Theoretical Models for the Solar Cycle Variation of the Upper Atmosphere, Goddard Space Flight Center Report NASA-TN-D-144, August 1962.
12. Harris, I. and Priester, W.: 1965, "Atmospheric Structure and Its Variations in the Region from 120 to 80 KM," COSPAR International Reference Atmosphere (CIRA) 1965, Space Research IV, North Holland Publishing Co., Amsterdam.

13. Jacchia, L. G.: 1971, Revised Static Models of the Thermosphere and Exosphere with Empirical Temperature Profiles, Smithsonian Astrophysical Observatory Special Report No. 332, Cambridge, Massachusetts, May 1971.
14. Roberts, E. R., Jr.: 1971, "An Analytic Model for Upper Atmosphere Densities Based upon Jacchia's 1970 Models," Celestial Mechanics, 4(3/4), December 1971, pp. 368-377.
15. Brouwer, D.: 1959, "Solution of the Problem of Artificial Satellite Theory without Drag," The Astronomical Journal, 64(1274), October 1959, pp. 378-397.
16. Lyddane, R. H.: 1963, "Small Eccentricities or Inclinations in the Brouwer Theory of the Artificial Satellite," The Astronomical Journal, 68(8), October 1963, pp. 555-558.
17. Goddard Space Flight Center: 1971, Definitive Orbit Determination Operating System Description, Edition II, Goddard Space Flight Center Report X-544-71-35, January 1971.

## CHAPTER 5

## FORMULATION OF THE ORBITAL EQUATIONS OF MOTION

## 5.1 INTRODUCTION

Direct analytical solution of the differential equations describing the motion of a satellite perturbed by the total acceleration vector (Equation (4-1)) is not possible. Historically, solutions to this problem have been obtained using two principal approaches. In one approach, known as the General Perturbation Method, the perturbation model is limited such that an analytical solution is possible. Brouwer theory is a well known orbit generation technique which falls in this category. Brouwer formulated the problem of an earth satellite, perturbed by point mass and zonal gravitational effects, in terms of canonical variables and analytically solved the resulting Hamilton-Jacobi differential equations to first order in a small parameter, using the Von Zeipel method. The resulting orbit generation method is extremely efficient, but its accuracy is limited by the restricted perturbation model and the truncated small-parameter expansions (Reference 1).

In a second approach, known as the Special Perturbation Method, the entire perturbation model can be included in the differential equations (also known as the equations of motion). The differential equations are solved by the numerical integration techniques described in Chapter 6. The Cowell method is the best known orbit generation technique which falls in this category. In the Cowell approach, the equations of motion are expressed in terms of the total acceleration vector (i.e., point mass central body effects plus perturbing accelerations) and solved directly for the position and velocity vectors.

Recently, considerable research has focused on improving the accuracy and efficiency of orbit generation methods. This research indicates that there is no best orbit generation procedure for all orbit types. For this reason, several orbit generation formulations are included in GTDS; taken together, these formulations are suited to a broad range of accuracy and efficiency requirements for the various classes of satellite orbits supported by GSFC.

In general, development of optimum methods for orbit prediction consists of reformulating the equations of motion in terms of a new set of variables such that the resulting equations are more amenable to solution. The principal guidelines used in these reformulations are the following:

1. Choose a dependent variable set which is appropriate for the numerical method of solution.

General Perturbation Methods usually require the use of canonical variables, which are amenable to the use of averaging transformation techniques such as the Von Zeipel method; similarly, in the Special Perturbation Methods selection of appropriate variables may be dictated by the numerical method of solution. For example, the accuracy of numerical integration formulas increases with order. However, each integration formula has a numerical stability region, outside of which the error growth is exponential (see References 2 and 3 for a more complete discussion of numerical stability). For a given set of differential equations, this stability region dictates the allowable stepsizes. As a result, changing dependent variables may affect the stability characteristics of the process.

Reformulations of the Class II equations of motion\* in terms of other dependent variables usually results in a set of Class I equations of motion\*, e.g., the Variation of Parameters equations (Section 5.7). In general, Class I multistep numerical integration formulas (Equations (6-21) and (6-26)) have smaller regions of numerical stability than the Class II multistep methods (Equations (6-22) and (6-27)). Consequently, the numerical stability characteristics of the transformed equations of motion are a very important consideration.

"Well-behaved" equations of motion, i.e., those which change only slightly due to a small change in the elements, will yield large regions of numerical stability in terms of stepsize, thus allowing the use of the accurate high order formulas. For example, element sets which are constants, or vary linearly with time in the unperturbed problem, yield equations of motion which are more numerically stable than the corresponding set of equations expressed in terms of the position and velocity coordinates.

2. Choose an independent variable so as to achieve uniformization of local error over the entire orbit.

Efficient numerical integration can be achieved by adjusting the stepsize to obtain uniformization of the local error over the entire orbit. For near-circular orbits, fixed step integration produces uniformization when time is the independent variable. To achieve uniformization for eccentric orbits, a mechanism is required for using a small time step in the region of large perturbations, and a large time step in the region of small perturbations. A variable stepsize

---

\* Class I differential equations are of the form  $dy/dx = f(x, y)$ ; Class II differential equations are of the form  $d^2y/dx^2 = f(x, y)$ .

integration algorithm is available in GTDS (see Section 6.9); however, frequent stepsize changes are costly and usually introduce error. For this reason, formulations have been developed which achieve uniformization through analytic stepsize regulation, accomplished through the use of an independent variable other than time. A new independent variable  $s$ , related to the time  $t$  by

$$ds = \frac{\sqrt{\mu}}{r^n} dt \quad (5-1)$$

is available in GTDS, where  $r$  is the magnitude of the satellite's position vector and  $n$  is known as the uniformization constant. The effect of such a transformation is that fixed steps in  $s$  yield smaller steps in time for small  $r$  (where the perturbations are usually larger) than for large  $r$ .

The appropriate choice for the uniformization constant depends on both the dependent variable set and the local error source. In the Cowell method the primary source of local error is inaccurate integration of the point mass and  $J_2$  gravitational effects of the earth. A uniformization constant of  $3/2$  is appropriate for these perturbations and is used in the Time Regularized Cowell orbit generator (Section 5.3). The Delaunay-Similar (DS) equations of motion (Section 5.5) are uniformized for the  $J_2$  oblateness perturbation through the choice of a uniformization constant of 2. The Kustaanheimo-Stiefel (KS) formulation (Section 5.4) uses a uniformization constant of 1, which removes the singularity at collision from the equations of motion. In the Intermediate Orbit formulation (Section 5.11), the uniformization constant can be adjusted to produce uniformization with respect to the dominant source of local error. It should be noted that uniformization of local error cannot be achieved through analytic stepsize regulation alone for highly elliptic, long period orbits, for which both the nonspherical effects of the earth and lunar effects are equally important. In such cases, a variable stepsize algorithm is also needed.

3. Choose a dependent variable set in terms of which the solutions to the unperturbed problem are closed, explicit expressions in the independent variable.

In General Perturbation applications, the need for such dependent variable sets is clear. However, such variable sets also are advantageous for use in Special Perturbation Methods. Differential equations for quantities which vary slowly and smoothly with time are known to be more amenable to numerical integration methods (i.e., more numerically stable) than those for quantities which vary rapidly. In the case of satellite motion, the acceleration caused by the attraction

of the primary body is usually much greater than the perturbing accelerations arising from other bodies, nonspherical effects, etc. Since dependent variable sets exist which yield closed, explicit solutions to the unperturbed problem, it is logical to remove the point mass effects of the primary body from the differential equation by considering the relative elliptic orbit described about the primary as a first approximation to the motion. Thus, the equations of motion of such dependent variables include motion arising only from the perturbing acceleration vector. Methods which employ this approach are known as Variation of Parameters (VOP) methods (Section 5.7). GTDS includes VOP orbit generators which use Keplerian, equinoctial, rectangular, Delaunay-Similar (DS), and Kustaanheimo-Stiefel (KS) element sets. The resultant formulations vary with respect to regularity of the dependent variables and the choice of independent variables. GTDS also includes the Intermediate Orbit formulation, in which the equations of motion represent the variation, arising from other perturbations, about the solution to the point mass earth plus  $J_2$  problem.

#### 4. Choose a completely regular dependent variable set.

It is desirable, from the standpoint of generality, to use a set of dependent variables which is well defined, or regular, for the full range of possible orbital conditions. For example, the Keplerian and Delaunay variables are not well defined for small eccentricities or for small or near 180-degree inclinations. Unfortunately, regularity and the requirement for tractable canonical formulations of General Perturbation Methods appear to be mutually exclusive. For this reason, the Brouwer-Lyddane formulation was developed in terms of Poincaré rather than Delaunay variables for use with small eccentricity and small inclination satellites. For Special Perturbation applications, the KS and rectangular variables are completely regular. The equinoctial elements consist of two variable sets which together yield a completely regular set except at collision.

#### 5. Choose a dependent variable set for which the equations of motion are completely regular.

The practical effect of singularities in the equations of motion is to cause rapid oscillations in some of the orbital elements when the orbit is in a near-singular condition. This condition is not desirable from the standpoint of efficiency in numerical integration. Accurate integration of such equations requires extremely small stepsizes in the near-singular region. The rectangular variables and equinoctial elements yield completely regular equations of motion except at collision. The KS equations of motion are completely regular, while the VOP equations of motion are singular for the Kepler and Delaunay elements at small eccentricities and at small and near 180-degree inclinations.



6. Choose a dependent variable set such that the equations of motion have dynamically stable solutions for the unperturbed problem.

A solution is dynamically stable if small variations of the initial values produce a variation of the solution which remains small for any value of the independent variable greater than zero. Dynamic stability is one of the primary motivations for the KS transformation. This characteristic should be particularly advantageous when the solution is obtained via numerical integration.

7. Choose an element set for which the equations of motion do not contain short periodic effects.

As mentioned previously, the efficiency of numerical integration is optimal for the integration of variables which vary smoothly and slowly. Elimination of short periodic effects from the equations of motion significantly smooths the dependent variable motion, thus allowing the use of very large stepsizes. The Intermediate Orbit elements and the Method of Averages (Section 5.8) use this approach. The equations of motion of an averaged element set are integrated. The resulting orbit generation method is extremely efficient, but is limited to average element accuracy rather than the osculating element accuracy achieved in high precision methods.

It should be noted that several of the guidelines stated above are mutually exclusive. The requirements of the specific application dictate which of the guidelines are most important. The characteristics of the orbit generation methods available in GTDS are summarized in Tables 5.1 and 5.2.

The choice of an optimum orbit generation method is dependent on orbit type, accuracy, and efficiency requirements. In general, the reformulated high precision methods are more accurate than the Cowell method. However, the transformations required in these formulations increase computational time; therefore, these methods should be used only for orbits for which they yield improved accuracy at larger stepsizes as compared with the Cowell method, or where these methods have a more appropriate method of analytic stepsize control than does Time Regularized Cowell.

For circular orbits, analytic stepsize regulation is not necessary. In fact, integration of the time equation increases computational time and may introduce errors into the solution. For orbits with eccentricity greater than 0.1, analytic stepsize regulation is usually beneficial. The independent variable is therefore an important consideration in the choice of the orbit generation formulation. As the uniformization constant is increased, the size of the time step at perigee decreases and that at apogee increases. This constant should be chosen so that the local error is uniformized over the entire orbit.

**Table 5-1**  
**Characteristics of High Precision Orbit Generators**

ORBIT GENERATOR	METHOD OF SOLUTION	COMPUTATIONAL SPEED	ANALYTIC STEPSIZE CONTROL	TIME REGULARIZATION CONSTANT	LIMITATIONS	COMMENTS
Cowell	Multistep Numerical Integration Using Störmer-Cowell Formulas	Medium	No		None	
Time Reg. Cowell	Multistep Numerical Integration Using Störmer-Cowell Formulas	Medium	Yes	3/2	None	
VOP - Keplerian	Multistep Numerical Integration Using Adams Formulas	Medium	No		Singularities for $e=0; i=0, 180^\circ$ Elliptic motion only	Provides closed form solution to unperturbed problem
VOP - Equinoctial	Multistep Numerical Integration Using Adams Formulas	Medium	No		Elliptic motion only	Provides closed form solution to unperturbed problem
VOP - Rectangular	Multistep Numerical Integration Using Adams Formulas	Medium	No		None	Provides closed form solution to unperturbed problem
Intermediate Orbit	Multistep Numerical Integration Using Adams Formulas	Medium	Yes	2	Singularities for $e=0; i=0, 63.4^\circ$ Elliptic motion only	Provides closed form solution to $J_2$ through $J_5$ problem
KS	Multistep Numerical Integration Using Adams Formulas	Medium	Yes	1	Elliptic motion only	Provides closed form, stable oscillator, solution to unperturbed problem
DS	Multistep Numerical Integration Using Adams Formulas	Medium	Yes	2	Singularities for $e=0; i=0, 180^\circ$ Elliptic motion only	Provides closed form, dynamically stable, solution to unperturbed problem
Chebyshev Series	Picard Iteration	Low	N/A		None	

**Table 5-2**  
**Characteristics of Approximate Orbit Generators**

ORBIT GENERATOR	METHOD OF SOLUTION	COMPUTATIONAL SPEED	ANALYTIC STEPSIZE CONTROL	TIME REGULARIZATION CONSTANT	LIMITATIONS	COMMENTS
Brouwer	Analytic	High	N/A		Singularities for $e=0, i=0, 63.4^\circ$ Elliptic motion only	Solution includes only $J_2$ through $J_5$ effects
Brouwer-Lyddane	Analytic	High	N/A		Singularities for $i=63.4^\circ$ Elliptic motion only	Solution includes only $J_2$ through $J_5$ effects
Vinti	Analytic	High	N/A		Elliptic motion only	Solution includes $J_2$ through $J_4$ effects
Averaged Kepler	Multistep Numerical Integration Using Adams Formulas	High	No		Singularities for $e=0, i=0, 180^\circ$ Elliptic motion only	Solution does not include short-period effects
Averaged Equinoctial	Multistep Numerical Integration Using Adams Formulas	High	No		Elliptic motion only	Solution does not include short-period effects

For applications which require high efficiency, it is important to consider the number of output points which are required. Using analytic methods such as Brouwer theory, the computational cost is directly proportional to the number of output points. However, when numerical integration is used, the cost is mainly dependent on the arc length and not the number of intermediate output points. For DC applications, the computational cost of the averaged orbit generation methods is often competitive with that of Brouwer theory and offers considerably greater flexibility with respect to the perturbation model.

## 5.2 COWELL METHOD

The Cowell equations of motion of a satellite are expressed by the general formula

$$\frac{d^2 \bar{\mathbf{r}}}{dt^2} = - \frac{\mu \bar{\mathbf{r}}}{|\bar{\mathbf{r}}|^3} + \bar{\mathbf{P}} \quad (5-2)$$

where  $\bar{\mathbf{r}} \sim$  the position vector in an inertial Cartesian coordinate system  
 $t \sim$  the physical time  
 $\mu \sim$  the gravitational constant  
 $\bar{\mathbf{P}} \sim$  the total perturbing acceleration

$\bar{\mathbf{P}}$  can include any of the perturbing accelerations discussed in Chapter 4.

This set of three Class II differential equations is solved directly for the position vector using the Störmer-Cowell numerical integration formulas (Equations (6-22) and (6-27)). The three Class I equations for the velocity vector  $\dot{\bar{\mathbf{r}}}$

$$\frac{d\dot{\bar{\mathbf{r}}}}{dt} = - \frac{\mu \bar{\mathbf{r}}}{|\bar{\mathbf{r}}|^3} + \bar{\mathbf{P}} \quad (5-3)$$

are integrated using the Adams numerical integration formulas (Equations (6-21) and (6-26)) in the case of velocity dependent perturbations, such as atmospheric drag.

The Cartesian coordinates and the equations of motion are regular, except at collision. This method can be used for elliptic, parabolic and hyperbolic orbits. The point mass gravitational attraction of the primary body appears explicitly in the equations of motion, and is usually the dominant acceleration which must be integrated.

For circular orbits, the choice of time as the independent variable produces uniformization of the local error with respect to the integration of the two-body acceleration. The Time Regularized Cowell formulation (Section 5.3) was developed to achieve uniformization of local error in the case of noncircular orbits.

### 5.3 TIME REGULARIZED COWELL

Efficient numerical integration is aided by uniformization of the local error at each integration step. To achieve uniformization of local error using the Cowell method, the equations of motion (5-2) and (5-3) must be uniformized with respect to the dominant local error source, which is generally the point mass and  $J_2$  gravitational accelerations. These equations are already uniformized for circular orbits. For noncircular orbits, however, uniformization is achieved by reformulating the Cowell equations in terms of a new independent variable  $s$ , defined by the relationship

$$\frac{ds}{dt} = \frac{\sqrt{\mu}}{r^n} \quad (5-4)$$

where  $n$  is the uniformization constant. The resulting equations of motion are called the Time Regularized Cowell equations. The choice of  $3/2$  for  $n$  uniformizes the local error with respect to the point mass and  $J_2$  gravitational effects.

Under this general transformation, the Time Regularized Cowell equations of motion become

$$\ddot{\mathbf{r}} = n \left( \frac{\mathbf{r}' \cdot \mathbf{r}'}{r} \right) - r^{(2n-3)} \mathbf{r} + \frac{r^{2n}}{\mu} \mathbf{P} \left( t, \mathbf{r}, \frac{\sqrt{\mu}}{r^n} \mathbf{r}' \right) \quad (5-5)$$

where the prime notation refers to differentiation with respect to the independent variable  $s$ . This equation involves derivatives with respect to the variable  $s$  only. The position vector is obtained by integrating Equation (5-5) using the Class II Störmer-Cowell formulas (Equations (6-22) and (6-27)). The velocity vector is obtained by integrating Equation (5-5) using the Class I Adams formulas (Equations (6-21) and (6-26)). Since the velocity appears explicitly in the equations of motion, the velocity equation must be integrated even in the case of velocity free perturbations. In addition, the following Class II equation is integrated for the time

$$t'' = \frac{n r^{2n-1} \dot{r}}{\mu} \quad (5-6)$$

Comparison of the Time Regularized Cowell and the Cowell integration schemes indicates that the favorable properties of simplicity, precision and adaptability are shared by both methods, while for highly eccentric or drag perturbed orbits the analytic stepsize regulation afforded by the Time Regularized Cowell is superior.

#### 5.4 KUSTAANHEIMO - STEIFEL (KS) FORMULATION

By means of the KS transformation, the nonlinear equations of two-body motion are transformed to a set of linear, dynamically stable differential equations, similar to those of an unperturbed harmonic oscillator (see Reference 4 for a complete derivation). This transformation consists of choosing a set of regular dependent variables such that the resulting differential equations are regular, i.e., have no singularities. Regularization of the differential equations requires the extension of the position and velocity vectors from three dimensional to four dimensional vectors. The singularity at collision is removed by choosing the generalized eccentric anomaly  $E$  as the independent variable such that

$$\frac{dE}{dt} = \frac{2\omega}{r} \quad (5-7)$$

where the frequency  $\omega$  is related to the negative of the total energy  $\omega = \sqrt{h/2}$ . In addition, this transformation produces analytic stepsize regulation with a uniformization constant of 1. Therefore, a time equation must also be integrated. A time element  $\tau$  is introduced such that

$$t = \tau - \frac{1}{\omega} (\bar{u}, \bar{u}') \quad (5-8)$$

where  $\bar{u}$  and  $\bar{u}'$  are the transformed position and velocity vectors ( $\bar{u}' = d\bar{u}/dE$ ), and the notation  $(\bar{u}, \bar{u}')$  denotes the scalar product of the two vectors. This time element varies linearly with the independent variable for unperturbed motion and is therefore more amenable to numerical integration than the time equation. (See Appendix B for a more detailed discussion of time elements.)

Regularized equations of motion behave considerably better with respect to numerical integration than the corresponding nonregularized equations. For unperturbed two-body motion, every solution to the regularized differential equations is dynamically stable. This means that small variations of the initial values produce a variation of the solution which remains small for any positive value of the independent variable. Dynamic stabilization of the KS equations of

motion is accomplished by using a time element and by including as a dependent variable the frequency  $\omega$ , which is related to the total energy, and taking advantage of the fact that it is a constant of the motion for conservative forces. Consequently, a total of ten equations of motion are integrated.

The KS equations of motion are formulated as VOP equations in terms of regular elements: The frequency  $\omega$ , the time element  $\tau$ , and the two 4-vectors  $\bar{\alpha}$  and  $\bar{\beta}$ . Elements are quantities which, during unperturbed two-body motion, are constants or linear functions of the independent variable. The advantage of introducing elements is that they vary almost linearly if the motion is subjected to weak perturbations.

#### 5.4.1 The KS Variation of Parameters (VOP) Equations of Motion

The KS equations of motion are VOP equations in Lagrangian form. The equations for the 4-vector elements  $\bar{\alpha}$  and  $\bar{\beta}$  are

$$\frac{d\bar{\alpha}}{dE} = \left\{ \frac{1}{2\omega^2} \left[ \frac{\bar{V}}{2} \bar{u} + \frac{r}{4} \left( \frac{\partial V}{\partial \bar{u}} - 2L^T \bar{P} \right) \right] + \frac{2}{\omega} \frac{d\omega}{dE} \bar{u}' \right\} \sin \frac{E}{2} \quad (a)$$

(5-9)

$$\frac{d\bar{\beta}}{dE} = - \left\{ \frac{1}{2\omega^2} \left[ \frac{\bar{V}}{2} \bar{u} + \frac{r}{4} \left( \frac{\partial V}{\partial \bar{u}} - 2L^T \bar{P} \right) \right] + \frac{2}{\omega} \frac{d\omega}{dE} \bar{u}' \right\} \cos \frac{E}{2} \quad (b)$$

while the equations of motion for the time element  $\tau$  and the frequency  $\omega$  are

$$\frac{d\tau}{dE} = \frac{1}{8\omega^3} (\mu - 2rV) - \frac{r}{16\omega^3} \left( \bar{u}, \frac{\partial V}{\partial \bar{u}} - 2L^T \bar{P} \right) - \frac{2}{\omega^2} \frac{d\omega}{dE} (\bar{u}, \bar{u}') \quad (a)$$

(5-10)

$$\frac{d\omega}{dE} = - \frac{r}{8\omega^2} \frac{\partial V}{\partial t} - \frac{1}{2\omega} (\bar{u}', L^T \bar{P}) \quad (b)$$

In the above equations

$V \sim$  perturbing potential function

$\bar{P} \sim$  additional perturbing accelerations

$\mu \sim$  gravitational constant

$L \sim$  KS transformation matrix defined by Equation (5-21)

In GTDS, the perturbing potential  $V$  which is used is the potential arising from the  $J_2$  nonspherical effects

$$V = \frac{3}{2} \mu R_e^2 J_2 \left[ \frac{z^2}{r^5} - \frac{1}{3r^3} \right] \quad (5-11)$$

where  $R_e$  is the radius of the central body. The quantity  $\bar{P}$  represents the perturbing accelerations due to higher harmonics, drag, radiation pressure, etc.

The components of  $\bar{u}$ , the transformed position vector, and  $\bar{u}'$ , the transformed velocity vector, are obtained from the elements as follows

$$\bar{u} = \bar{\alpha} \cos \frac{E}{2} + \bar{\beta} \sin \frac{E}{2} \quad (5-12)$$

$$\bar{u}' = -\frac{1}{2} \bar{\alpha} \sin \frac{E}{2} + \frac{1}{2} \bar{\beta} \cos \frac{E}{2} \quad (5-13)$$

The magnitude of the position vector is

$$r = u_1^2 + u_2^2 + u_3^2 + u_4^2 \quad (5-14)$$

The position vector  $\bar{r}$  of the satellite is computed for use in the evaluation of the perturbing accelerations using Equations (5-37) through (5-39). The velocity  $\dot{\bar{r}}$  is also computed in the case of velocity dependent accelerations, using Equations (5-40) through (5-42). The physical time is computed from

$$t = \tau - \frac{1}{\omega} (\bar{u}, \bar{u}') \quad (5-15)$$

The notation  $(\bar{u}, \bar{u}')$  denotes the scalar product of the two vectors.

The transformed components of the perturbing accelerations are computed as

$$(L^T P)_1 = u_1 P_1 + u_2 P_2 + u_3 P_3 \quad (5-16)$$



$$(L^T P)_2 = -u_2 P_1 + u_1 P_2 + u_4 P_3 \quad (5-17)$$

$$(L^T P)_3 = -u_3 P_1 - u_4 P_2 + u_1 P_3 \quad (5-18)$$

$$(L^T P)_4 = u_4 P_1 - u_3 P_2 + u_2 P_3 \quad (5-19)$$

#### 5.4.2 Transformation from Cartesian Position and Velocity to KS Parametric Values

The KS transformation is defined as

$$\bar{\mathbf{x}} = L(u) \cdot \bar{\mathbf{u}} \quad (5-20)$$

where  $\bar{\mathbf{x}}$  is a vector whose first three components are the Cartesian position coordinates and the fourth component  $x_4$  is always zero, i.e.,  $\bar{\mathbf{x}} = (x, y, z, 0)$ .

The matrix  $L(u)$  is the KS matrix with components given by

$$L = \begin{pmatrix} u_1 & -u_2 & -u_3 & u_4 \\ u_2 & u_1 & -u_4 & -u_3 \\ u_3 & u_4 & u_1 & u_2 \\ u_4 & -u_3 & u_2 & -u_1 \end{pmatrix} \quad (5-21)$$

The elements of this matrix are computed as follows.

Assuming that  $\bar{\mathbf{r}}$  and  $\dot{\bar{\mathbf{r}}}$  are given at the instant  $t = t_0$ , the radial distance is computed from

$$r = \sqrt{x^2 + y^2 + z^2} \quad (5-22)$$

and the frequency from

$$2\omega^2 = \frac{\mu}{r} - \frac{1}{2} |\dot{\bar{\mathbf{r}}}|^2 - V \quad (5-23)$$

where  $V$  represents the perturbing potential, which is the  $J_2$  potential in GTDS (see Equation (5-11)).

If  $x \geq 0$ , the parametric state vector is found from

$$u_1^2 + u_4^2 = \frac{1}{2} (r + x) \quad (5-24)$$

$$u_2 = \frac{yu_1 + zu_4}{r + x} \quad (5-25)$$

$$u_3 = \frac{zu_1 - yu_4}{r + x} \quad (5-26)$$

or, if  $x \leq 0$ , from

$$u_2^2 + u_3^2 = \frac{1}{2} (r - x) \quad (5-27)$$

$$u_1 = \frac{yu_2 + zu_3}{r - x} \quad (5-28)$$

$$u_4 = \frac{zu_2 - yu_3}{r - x} \quad (5-29)$$

The derivatives of the transformed position vector with respect to  $E$  are

$$u'_1 = \frac{1}{4\omega} (u_1 \dot{x} + u_2 \dot{y} + u_3 \dot{z}) \quad (5-30)$$

$$u'_2 = \frac{1}{4\omega} (-u_2 \dot{x} + u_1 \dot{y} + u_4 \dot{z}) \quad (5-31)$$

$$u'_3 = \frac{1}{4\omega} (-u_3 \dot{x} - u_4 \dot{y} + u_1 \dot{z}) \quad (5-32)$$

$$u'_4 = \frac{1}{4\omega} (u_4 \dot{x} - u_3 \dot{y} + u_2 \dot{z}) \quad (5-33)$$

The initial value of the time element is

$$\tau = \frac{1}{\omega} (\bar{u}, \bar{u}') \quad (5-34)$$

If  $E = 0$  is adopted as the initial value of the eccentric anomaly, then

$$\bar{\alpha} = \bar{u} \quad (5-35)$$

and

$$\bar{\beta} = 2\bar{u}' \quad (5-36)$$

#### 5.4.3 Transformation from KS Parametric Variables to Cartesian Position and Velocity.

Using Equation (5-20), the Cartesian components of position are calculated from

$$x = u_1^2 - u_2^2 - u_3^2 + u_4^2 \quad (5-37)$$

$$y = 2(u_1 u_2 - u_3 u_4) \quad (5-38)$$

$$z = 2(u_1 u_3 + u_2 u_4) \quad (5-39)$$

and the Cartesian velocity components are determined from

$$\dot{x} = \frac{4\omega}{r} (u_1 u'_1 - u_2 u'_2 - u_3 u'_3 + u_4 u'_4) \quad (5-40)$$

$$\dot{y} = \frac{4\omega}{r} (u_2 u'_1 + u_1 u'_2 - u_4 u'_3 - u_3 u'_4) \quad (5-41)$$

$$\dot{z} = \frac{4\omega}{r} (u_3 u'_1 + u_4 u'_2 + u_1 u'_3 + u_2 u'_4) \quad (5-42)$$

## 5.5 DELAUNAY - SIMILAR (DS) ELEMENTS

The DS method is a VOP formulation which was developed using the generalized true anomaly as the independent variable, such that

$$\frac{dt}{ds} = \frac{r^2}{G - \frac{1}{2} \left[ \Phi - \frac{\mu}{\sqrt{2L}} \right]} \quad (5-43)$$

where  $L$ ,  $G$  and  $\Phi$  are defined later in this section (see References 5, 6, and 7 for a more complete discussion).

This choice for the independent variable is particularly appropriate for numerical integration of the oblateness perturbation. The dependent variables are a generalization of the classical Delaunay elements and are singular for  $e = 0$ ,  $i = 0$  and at collision. The transformation of the equations of motion is carried out in terms of canonical variables. This approach leads to the requirement for a canonical variable, conjugate to the physical time, which is the negative of the total energy. The resulting set of equations of motion is uniformized with respect to integration of the  $J_2$  nonspherical perturbation.

The geometrical and physical interpretations of the eight DS elements for the unperturbed problem are:

$\psi \sim$  the true anomaly

$g \sim$  the argument of pericenter

$h \sim$  the longitude of the ascending node

$\ell \sim$  the "mean" mean anomaly

$\Phi \sim$  a measure of the perturbing energy, which vanishes in unperturbed motion

$G \sim$  the total angular momentum

$H \sim$  the z-component of the angular momentum

$L \sim$  the total energy

where  $L_0$  is the initial value of the total energy.

This set of DS elements contains one fast variable, the generalized true anomaly  $\psi$ . The element  $\ell$  has been defined such that it is a constant in the case of unperturbed motion.

For the two-body problem, the DS elements yield closed and explicit solutions in terms of the independent variable. Not all of the DS elements are osculating. The reason is that the orbits are situated on the energy surface

$$F = F_0 + r^2 V = 0 \quad (5-44)$$

where  $F_0$  is the unperturbed Hamiltonian.

This energy manifold depends on the perturbing potential  $V$ . To compute the osculating elements at a certain time, the potential  $V$  must be set equal to zero since, by definition, osculating elements represent the Keplerian position and velocity with respect to the moving coordinate system inherent in the VOP equations of motion.

The DS elements vector is denoted by

$$(\alpha_1, \alpha_2, \alpha_3, \alpha_4, \alpha_5, \alpha_6, \alpha_7, \alpha_8) = (\psi, g, h, \ell, \Phi, G, H, L) \quad (5-45)$$

in the following sections.

### 5.5.1 The DS Variation of Parameters (VOP) Equations of Motion

The DS equations of motion, which are VOP equations in canonical form, are as follows

$$\frac{d\alpha_i}{ds} = \frac{\partial F_0}{\partial \alpha_{i+4}} + V \frac{\partial}{\partial \alpha_{i+4}} \left( \frac{r^2}{q} \right) + \frac{r^2}{q} \sum_{j=1}^4 (D_{i+4,j}) \left( \frac{\partial V}{\partial x_j} - P_j \right) \quad (5-46)$$

$$i = 1, \dots, 4$$

$$\frac{da_{i+4}}{ds} = -V \frac{\partial}{\partial \alpha_i} \left( \frac{r^2}{q} \right) - \frac{r^2}{q} \sum_{j=1}^4 D_{ij} \left( \frac{\partial V}{\partial x_j} - P_j \right) \quad (5-47)$$

$$i = 1, \dots, 4$$

where  $x_1, x_2$ , and  $x_3$  are the three components of  $\bar{r}$  and  $x_4$  is the time.  $V$  is the perturbing potential given in Equation (5-11), and the scaling factor  $q$  defining the time transformation in Equation (5-43) is given by

$$q = \alpha_6 - \frac{1}{2} \left( \alpha_5 - \frac{\mu}{\sqrt{2\alpha_8}} \right) \quad (5-48)$$

The unperturbed Hamiltonian  $F_0$  is given by

$$F_0 = \alpha_5 - \frac{\mu}{\sqrt{2\alpha_8}} \quad (5-49)$$

and its derivatives by

$$\frac{\partial F_0}{\partial \alpha_5} = 1 \quad (5-50)$$

$$\frac{\partial F_0}{\partial \alpha_6} = 0 \quad (5-51)$$

$$\frac{\partial F_0}{\partial \alpha_7} = 0 \quad (5-52)$$

$$\frac{\partial F_0}{\partial \alpha_8} = -\frac{\mu}{(2\alpha_8)^{3/2}} \quad (5-53)$$

$\bar{P}$  is the additional perturbing acceleration vector expressed in rectangular coordinates. The extension of phase space by the inclusion of time and total energy as variables results in the introduction of an additional canonical force

$$P_4 = - \frac{\partial F_0}{\partial \dot{r}} \cdot \bar{P} \quad (5-54)$$

The elements of the  $8 \times 4$  matrix D,

$$D = \frac{\partial(x_1, x_2, x_3, x_4)}{\partial(a_1, a_2, \dots, a_8)} \quad (5-55)$$

are computed by the following relationship

$$\frac{\partial x_i}{\partial a_j} = \frac{\partial r}{\partial a_j} \tau_i + r \frac{\partial \tau_i}{\partial a_j} \quad \begin{matrix} i = 1, \dots, 3 \\ j = 1, \dots, 8 \end{matrix} \quad (5-56)$$

where

$$\tau_1 = \cos(a_1 + a_2) \cos a_3 - \sin(a_1 + a_2) \sin a_3 \cos I \quad (5-57)$$

$$\tau_2 = \cos(a_1 + a_2) \sin a_3 + \sin(a_1 + a_2) \cos a_3 \cos I \quad (5-58)$$

$$\tau_3 = \sin(a_1 + a_2) \sin I \quad (5-59)$$

and

$$\cos I = \frac{|x_7|}{a_6} \quad (5-60)$$

$$\sin I = \text{sign}(x_7) \sqrt{1 - \frac{a_7^2}{a_6^2}} \quad (5-61)$$

$$r = \frac{p}{1 + e \cos a_1} \quad (5-62)$$

$$p = \frac{1}{\mu} \left( a_6 - a_5 + \frac{\mu}{\sqrt{2a_8}} \right)^2 \quad (5-63)$$

$$e = \sqrt{1 - \frac{2a_8 p}{\mu}} \quad (5-64)$$

The partial derivatives of  $\tau_1, \tau_2, \tau_3$ , and  $x_4$  are given in Table 5.3. The partial derivatives of  $r, p, q$ , and  $e$  are given in Table 5.4. The vector  $\partial(r^2/q)/\partial a$  is evaluated using the relationship

$$\frac{\partial}{\partial a_i} \left( \frac{r^2}{q} \right) = \frac{2r}{q} \frac{\partial r}{\partial a_i} - \frac{r^2}{q^2} \frac{\partial q}{\partial a_i} \tag{5-65}$$

The conservative accelerations present in  $V$  give rise to a differential equation for  $L$ , the total energy of the orbit,

$$\frac{dL}{ds} = \frac{r^2}{q} \left( \frac{\partial V}{\partial x_4} - P_4 \right) \tag{5-66}$$

where

$$\frac{\partial V}{\partial x_4} - P_4 = 0 \tag{5-67}$$

Therefore,  $L$  is a constant in this case. This fact is exploited in GTDS by not integrating the equation for  $L$  numerically when only conservative forces are present. This avoids cumulative magnified errors in other elements which are driven by small numerical errors in  $L$ .

5.5.2 Transformation from Cartesian Position and Velocity to DS Elements

It is assumed that  $\bar{r}, \dot{\bar{r}}$ , and  $t$  are given. In order to numerically integrate the DS equations of motion, the initial values of the DS variables are computed. The total angular momentum  $G$  is computed from

$$G = \sqrt{G_1^2 + G_2^2 + G_3^2} \tag{5-68}$$

where

$$\bar{G} = \bar{r} \times \dot{\bar{r}} \tag{5-69}$$

The  $z$ -component of the angular momentum  $\bar{G}$  is given by

$$H = G_3 \tag{5-70}$$



Table 5-3  
Partial Derivatives of the Auxiliary Parameters  $\tau_1, \tau_2, \tau_3, x_4$

	$\tau_1$	$\tau_2$	$\tau_3$	$x_4$	$\tau_5$	$\tau_6$	$\tau_7$	$\tau_8$
$\tau_1$	$-\sin(\alpha_1 + \alpha_2) \cos \alpha_3$ $-\cos(\alpha_1 + \alpha_2) \sin \alpha_3 \cos I$	$\frac{\partial \tau_1}{\partial \alpha_1}$	$-\cos(\alpha_1 + \alpha_2) \sin \alpha_3$ $-\sin(\alpha_1 + \alpha_2) \cos \alpha_3 \cos I$	0	0	$\frac{1}{\alpha_3} \sin(\alpha_1 + \alpha_2) \sin \alpha_3 \cos I$	$-\frac{1}{\alpha_3} \sin(\alpha_1 + \alpha_2) \sin \alpha_3$	0
$\tau_2$	$-\sin(\alpha_1 + \alpha_2) \sin \alpha_3$ $+\cos(\alpha_1 + \alpha_2) \cos \alpha_3 \cos I$	$\frac{\partial \tau_2}{\partial \alpha_1}$	$\cos(\alpha_1 + \alpha_2) \cos \alpha_3$ $-\sin(\alpha_1 + \alpha_2) \sin \alpha_3 \cos I$	0	0	$-\frac{1}{\alpha_3} \sin(\alpha_1 + \alpha_2) \cos \alpha_3 \cos I$	$\frac{1}{\alpha_3} \sin(\alpha_1 + \alpha_2) \cos \alpha_3$	0
$\tau_3$	$\cos(\alpha_1 + \alpha_2) \sin I$	$\frac{\partial \tau_3}{\partial \alpha_1}$	0	1	0	$\frac{1}{\alpha_3} \frac{\cos^2 I}{\sin I} \sin(\alpha_1 + \alpha_2)$	$-\frac{1}{\alpha_3} \frac{\cos I}{\sin I} \sin(\alpha_1 + \alpha_2)$	0
$x_4$	$\frac{\mu}{(2\alpha_8)^{3/2}} \left[ \frac{r^2}{\rho^2} (1 - e^2)^{3/2} - 1 \right]$	0	0	0	$-\frac{\mu}{(2\alpha_8)^{3/2}} \frac{1 - e^2}{p} \frac{r}{p}$ $+\sin \alpha_1 \left( \frac{r}{p} + 1 \right) \frac{\partial e}{\partial \alpha_5}$	$-\frac{\partial x_4}{\partial \alpha_5}$	0	$\frac{3}{2\alpha_8} (x_4 - x_8) - \frac{\mu}{(2\alpha_8)^{3/2}} \frac{r}{p}$ $+\sqrt{1 - e^2} \sin \alpha_1 \left( \frac{r}{p} + 1 \right) \frac{\partial e}{\partial \alpha_8}$

**Table 5-4**  
**Partial Derivatives of the Auxiliary Parameters q, p, e, r**

	$/\partial a_1$	$/\partial a_2$	$/\partial a_3$	$/\partial a_4$	$/\partial a_5$	$/\partial a_6$	$/\partial a_7$	$/\partial a_8$
$\partial q/$	0	0	0	0	$-\frac{1}{2}$	1	0	$\frac{-\mu}{2(2a_8)^{3/2}}$
$\partial p/$	0	0	0	0	$-2\sqrt{\frac{p}{\mu}}$	$-\frac{\partial p}{\partial a_5}$	0	$\frac{\mu}{(2a_8)^{3/2}} \frac{\partial p}{\partial a_5}$
$\partial e/$	0	0	0	0	$\frac{-a_8}{e\mu} \frac{\partial p}{\partial a_5}$	$\frac{-a_8}{e\mu} \frac{\partial p}{\partial a_6}$	0	$\frac{-1}{\mu e} \left[ p + a_8 \frac{\partial p}{\partial a_8} \right]$
$\partial r/$	$\frac{er^2}{p} \sin a_1$	0	0	0	$\frac{r}{p} \left[ \frac{\partial p}{\partial a_5} - r \frac{\partial e}{\partial a_5} \cos a_1 \right]$	$\frac{r}{p} \left[ \frac{\partial p}{\partial a_6} - r \frac{\partial e}{\partial a_6} \cos a_1 \right]$	0	$\frac{r}{p} \left[ \frac{\partial p}{\partial a_8} - r \frac{\partial e}{\partial a_8} \cos a_1 \right]$

The total energy  $L$  is computed as

$$\dot{L} = -\frac{1}{2} v^2 + \frac{\mu}{r} - V \quad (5-71)$$

where

$$r = \sqrt{x^2 + y^2 + z^2} \quad (5-72)$$

$$v = \sqrt{\dot{x}^2 + \dot{y}^2 + \dot{z}^2} \quad (5-73)$$

and  $V$  is given by Equation (5-11).

The perturbing energy  $\Phi$  is

$$\Phi = G - \sqrt{G^2 + 2r^2V} + \frac{\mu}{\sqrt{2L}} \quad (5-74)$$

The generalized true anomaly is computed as

$$\psi = \tan^{-1}(\sin \psi / \cos \psi) \quad (5-75)$$

where

$$\cos \psi = \frac{1}{e} \left( \frac{p}{r} - 1 \right) \quad (5-76)$$

$$\sin \psi = \frac{p\dot{r}}{er^2} \left[ \dot{\psi} + \frac{4rV}{\sqrt{\mu p}} \left( \frac{1}{r} + \frac{L \cos \psi}{\mu e} \right) \right]^{-1} \quad (5-77)$$

$$\dot{r} = \frac{(\bar{r} \cdot \dot{\bar{r}})}{r} \quad (5-78)$$

$$p = \frac{1}{\mu} \left( G + \frac{\mu}{\sqrt{2L}} - \Phi \right)^2 \quad (5-79)$$

$$e = \sqrt{1 - \frac{2L}{\mu} p} \quad (5-80)$$

and

$$\dot{\psi} = \frac{q}{r^2} \left[ 1 + V \frac{\partial(r^2/q)}{\partial \Phi} \right] \quad (5-81)$$

This last derivative, given by Equations (5-48) and (5-65), depends only on  $L$ ,  $G$ , and  $\Phi$  given above.

The longitude of the ascending node  $h$  is given by

$$h = \tan^{-1} \left( \frac{G_1}{-G_2} \right) \quad (5-82)$$

and the argument of pericenter  $g$  by

$$g = u - \psi \quad (-\pi \leq g \leq \pi) \quad (5-83)$$

where

$$u = \tan^{-1} \left[ \frac{z(G_1^2 + G_2^2) - G_3(xG_1 + yG_2)}{G(yG_1 - xG_2)} \right] \quad (5-84)$$

The eccentric anomaly  $E$  is computed as

$$E = 2 \tan^{-1} \left[ \sqrt{\frac{1-e}{1+e}} \tan \frac{\psi}{2} \right] \quad (-\pi \leq E \leq \pi) \quad (5-85)$$

and the variable  $\ell$  is given by

$$\ell = t - \frac{\mu}{(2L)^{3/2}} \left[ E - \psi - e \sqrt{1-e^2} \frac{r}{p} \sin \psi \right] \quad (5-86)$$

### 5.5.3 Transformation from DS Elements to Cartesian Position and Velocity

Predicted values of the DS variables obtained from the numerical integration must be transformed to physical Cartesian position, velocity and time in order to evaluate the perturbing forces and for computation of observations. The following equations yield the Cartesian state.

$$\bar{r} = \bar{c}x_1 + \bar{d}x_2 \quad (5-87)$$

$$\dot{\bar{r}} = \bar{c}\dot{x}_1 + \bar{d}\dot{x}_2 + \dot{\bar{c}}x_1 + \dot{\bar{d}}x_2 \quad (5-88)$$

where  $\bar{c}$  and  $\bar{d}$  are the vectors

$$\bar{c} = \begin{pmatrix} \cos g \cos h - \sin g \sin h \cos I \\ \cos g \sin h + \sin g \cos h \cos I \\ \sin g \sin I \end{pmatrix} \quad (5-89)$$

$$\bar{d} = \begin{pmatrix} -\sin g \cos h - \cos g \sin h \cos I \\ -\sin g \sin h + \cos g \cos h \cos I \\ \cos g \sin I \end{pmatrix} \quad (5-90)$$

and

$$\begin{aligned} x_1 &= r \cos \psi \\ x_2 &= r \sin \psi \end{aligned} \quad (5-91)$$

The required derivatives for the velocities are given by

$$\dot{\bar{c}} = \bar{d} \dot{g} \quad (5-92a)$$

$$\dot{\bar{d}} = -\bar{c} \dot{g} \quad (5-92b)$$

$$\dot{x}_1 = \dot{r} \cos \psi - r \dot{\psi} \sin \psi \quad (5-93a)$$

$$\dot{x}_2 = \dot{r} \sin \psi + r \dot{\psi} \cos \psi \quad (5-93b)$$

The quantity  $\dot{r}$  can be expressed directly in terms of DS elements as

$$\dot{r} = \frac{er^2 \sin \psi}{p} \left[ \dot{\psi} + \frac{4rV}{\sqrt{\mu p}} \left( \frac{1}{r} + \frac{L \cos \psi}{\mu e} \right) \right] \quad (5-94)$$

and  $\dot{\psi}$  is given by Equation (5-81).

The physical time is computed from

$$t = \ell + \frac{\mu}{(2L)^{3/2}} \left( E - \psi - r \frac{e}{p} \sqrt{1 - e^2} \sin \psi \right) \quad (5-95)$$

where

$$E = 2 \tan^{-1} \left( \sqrt{\frac{1-e}{1+e}} \tan \frac{\psi}{2} \right) \quad (5-96)$$

## 5.6 PICARD ITERATION USING CHEBYSHEV SERIES

The Picard iteration method used in GTDS (derived in Reference 8) can be used to integrate the Class I Cowell equations of motion

$$\frac{d\vec{r}}{dt} = \frac{-\mu\vec{r}}{r^3} + \vec{P} \quad (5-97)$$

$$\frac{d\vec{r}}{dt} = \dot{\vec{r}} \quad (5-98)$$

using the following iterative process (Reference 9)

$$\dot{\vec{r}}_{n+1}(t) = \dot{\vec{r}}(t_0) + \int_{t_0}^t \ddot{\vec{r}}(t', \vec{r}_n, \dot{\vec{r}}_n) dt' \quad (5-99)$$

$$\vec{r}_{n+1}(t) = \vec{r}(t_0) + \int_{t_0}^t \dot{\vec{r}}_{n+1} dt' \quad (5-100)$$

The starting values  $\vec{r}_0(t)$ ,  $\dot{\vec{r}}_0(t)$  are arbitrary continuous vector functions on the interval  $[t_0, t]$  which satisfy the given initial conditions

$$\vec{r}_0(t_0) = \vec{r}(t_0) \quad (5-101)$$

$$\dot{\vec{r}}_0(t_0) = \dot{\vec{r}}(t_0) \quad (5-102)$$

In the present version of GTDS,  $\bar{\mathbf{r}}_0(t)$  and  $\dot{\bar{\mathbf{r}}}_0(t)$  are solutions to the unperturbed problem ( $\bar{\mathbf{D}} = 0$  in Equation 5-97)). Since the sequence converges to a close approximation of the exact solution, the method can be used to generate very accurate solutions. Except at collision, the Cartesian coordinates and equations of motion are regular, which means that the method can be used for elliptic, parabolic and hyperbolic orbits.

In order to solve Equations (5-97) and (5-98) for a given value of  $n$  (i.e., to accomplish one iteration), the Chebyshev series is used as follows. The position and velocity vectors available from the  $(n-1)^{\text{st}}$  iteration,  $\bar{\mathbf{r}}_{n-1}$  and  $\dot{\bar{\mathbf{r}}}_{n-1}$ , are evaluated at the Chebyshev points in time. (The precise location of the Chebyshev points are given in the next section.) The forces (per unit mass) are then evaluated at each of these points in time (using the values of  $\bar{\mathbf{r}}_{n-1}$  and  $\dot{\bar{\mathbf{r}}}_{n-1}$ ). These special values of the acceleration vector are then used to determine the interpolating polynomial in time in the form of a Chebyshev series. The coefficients of the Chebyshev series are determined directly from the special values in a rather simple way due to the orthogonality of the Chebyshev polynomials (as described later in this section). The Chebyshev series representation of the acceleration is then integrated in order to obtain the Chebyshev series representation of the velocity to within an arbitrary constant of integration. The constant of integration is determined by requiring that the initial velocity  $\dot{\bar{\mathbf{r}}}(t_0)$  agree with the series for the velocity evaluated at  $t_0$ . The result is an approximation to  $\dot{\bar{\mathbf{r}}}_n$ . Similarly, the series representation of the velocity is then integrated in order to obtain the series representation of the position, where now the initial position  $\bar{\mathbf{r}}(t_0)$  is used to determine the constant of integration. The result is an approximation to  $\bar{\mathbf{r}}_n$ , thus completing one step of the Picard Iteration procedure.

The preceding set of operations are repeated until two successive approximate solutions agree to within a tolerance that may be specified by the user. This completes one step of the integration and the process is continued stepwise until the final time is attained.

A finite Chebyshev series fitted to a function has the significant property of making the least possible maximum error of all the common interpolating orthogonal polynomial series. The maximum error committed, as well as the overall truncation error, diminishes as the number of points used in the fitting increases. Since the error in the fitting of the accelerations oscillates with an amplitude less than or equal to the maximum error, the errors partially cancel each other during integration.

The Chebyshev series solution is derived in the following manner. The interval of time  $(t_0, t_f)$  is mapped linearly onto the interval  $(-1, 1)$  by means of the expression

$$\xi = 1 - 2 \left( \frac{t - t_0}{t_f - t_0} \right) \quad (5-103)$$

where

$\xi \sim$  the normalized time

$t_0 \sim$  the initial time

$t_f \sim$  the final time

$t_f - t_0 \sim$  the interval of time for which the orbit is to be integrated by Chebyshev series

The normalized time  $\xi = 1$  corresponds to  $t = t_0$ . The time points for which the Chebyshev series is to be fitted are the zeroes of the  $(N + 1)^{\text{st}}$  Chebyshev polynomial. At these points, the Chebyshev polynomials have an orthogonality property with respect to summation. The Chebyshev polynomials  $T_j$  are defined as

$$T_j(\xi) = \cos j(\cos^{-1} \xi) \quad -1 \leq \xi \leq 1 \quad (5-104)$$

and the  $N + 1$  Chebyshev points are given by

$$\xi_k = \cos \left( \frac{k\pi}{N} \right) \quad \text{for } k = 0, 1, \dots, N \quad (N \leq 48) \quad (5-105)$$

An interpolating polynomial  $p_M(\xi)$ , representing the  $i^{\text{th}}$  component of acceleration as a function of the normalized time  $\xi$ , is expressed as a finite series in Chebyshev polynomials

$$p_M(\xi) = \sum_{j=0}^{M'} c_j T_j(\xi) \quad (5-106)$$

where  $M$  is the degree of the polynomial ( $M \leq N$ ) and the prime denotes that the first term is factored by one-half (if  $M = N$ , the last term should also be factored by one-half). The  $c_j$ 's are numerical coefficients which are determined from the  $i^{\text{th}}$  acceleration components  $\ddot{r}_i(\xi_k)$  at the Chebyshev points by means of the relationship



$$c_j = \frac{2}{N} \sum_{k=0}^{N''} \ddot{r}_i(\xi_k) T_j(\xi_k) \quad (5-107)$$

where the double prime indicates that the first and last terms (for  $j = 0$  and  $j = M$ ) are factored by one-half.

The integration with respect to time is carried out using the following formula

$$\int T_j(\xi) d\xi = \frac{1}{2} \left\{ \left( \frac{1}{j+1} \right) T_{j+1}(\xi) - \left( \frac{1}{j-1} \right) T_{j-1}(\xi) \right\} \quad j > 1 \quad (5-108)$$

Special cases hold for  $j = 0$  and  $j = 1$ , i.e.,

$$\int T_0(\xi) d\xi = T_1(\xi) \quad (5-109)$$

$$\int T_1(\xi) d\xi = \frac{1}{4} \{T_0(\xi) + T_2(\xi)\} \quad (5-110)$$

The coefficients for the integral of the series for  $p_M(\xi)$  are represented by  $b_j$ , i.e.,

$$\int_{-1}^{\xi} p_M(x) dx = \sum_{j=0}^{M+1} b_j T_j(\xi) \quad (5-111)$$

At  $\xi = 1$ , this expression for the  $i^{\text{th}}$  velocity component is set equal to the initial value of that component of velocity by adjusting the constant  $b_0$  to satisfy this condition. A similar adjustment is made after the integration of velocity components in order to match the series evaluated at  $\xi = 1$  with the initial component of position.

The integration formulas lead to a simple relationship between the  $b_j$ 's and  $c_j$ 's, given by

$$b_j = \frac{1}{2j} [c_{j-1} - c_{j+1}] \quad 1 \leq j \leq (M+1) \quad (5-112)$$

where  $c_{M+1} = c_{M+2} = 0$  by definition, and  $b_0$  is obtained as described above.

Once the  $c_j$  's are known, the summations required to evaluate  $p_M(\xi)$  for any value of time can be done more efficiently by use of a backward recurrence relationship. Intermediate quantities  $d_j$  are computed using the algorithm

$$d_j(\xi) = 2\xi d_{j+1}(\xi) - d_{j+2}(\xi) + c_j \tag{5-113}$$

for  $j = M, M-1, \dots, 0$ , starting with  $d_{M+1}(\xi) = d_{M+2}(\xi) = 0$ . The value  $p_M(\xi)$  is then computed from

$$p_M(\xi) = \frac{1}{2} [d_0(\xi) - d_2(\xi)] \tag{5-114}$$

### 5.7 GAUSSIAN VARIATION OF PARAMETERS FORMULATIONS

In real space, the unperturbed satellite orbit is a conic section lying in a plane which has a constant orientation, shape, and size relative to an inertial frame. For a perturbing acceleration which is small compared with the central attraction, the characteristics of the conic section (e.g., semimajor axis, eccentricity) vary slowly with time. To a lesser extent, the attitude of the orbital plane with respect to the inertial frame is a continuous function of time. However, the satellite's position along its orbit changes rapidly with time.

The numerical integration process is improved by introducing state variables which take advantage of this disparity of effect. The introduction of such variables allows comparison of the motion within the plane to a reference orbit and treatment of the motion of the plane as a slight correction. The method of Variation of Parameters (VOP) uses this approach.

In this section, three orbit generators are discussed which are based on the Gaussian form of the VOP equations

$$\frac{\partial \alpha}{\partial t} = \frac{\partial \alpha}{\partial \dot{\mathbf{r}}} \bar{\mathbf{P}} \tag{5-115}$$

- where  $\alpha \sim$  a slow element
- $\dot{\mathbf{r}} \sim$  the velocity vector
- $\bar{\mathbf{P}} \sim$  the perturbing acceleration vector

and

$$\frac{\partial \beta}{\partial t} = \beta' + \frac{\partial \beta}{\partial \dot{\mathbf{x}}} \bar{\mathbf{P}} \tag{5-116}$$

where  $\beta \sim$  a fast element

$\beta' \sim$  the derivative of  $\beta$  for unperturbed two-body motion

These three orbit generators differ in the choice of dependent variables, i.e., either Keplerian, equinoctial, or rectangular elements. Some of the Keplerian elements become undefined when the inclination is zero or near  $180^\circ$ , when the eccentricity is zero, and at collision. The equinoctial elements (discussed in Section 3.2.6) and rectangular elements are selected to eliminate all singularities except for collision. All three generators use time as the independent variable and are therefore well suited to the accurate integration of circular orbits. The Keplerian, equinoctial, and rectangular VOP formulations are discussed in Sections 5.7.1, 5.7.2, and 5.7.3, respectively.

### 5.7.1 Keplerian Elements

The input initial conditions for an orbit in GTDS may be expressed as rectangular components of position and velocity at a given time  $t$ . The equations used in GTDS for the conversion of rectangular position and velocity components to Keplerian elements are discussed in Section 3.3.8.3. For calculation of disturbing forces and for printout, GTDS converts instantaneous values of the Keplerian elements to rectangular components of position and velocity. The formulation used for these conversions is discussed in Section 3.3.8.1. Although all three classes of Keplerian orbits (elliptic, parabolic, and hyperbolic) are treated in the conversions, the VOP methods of GTDS apply only to the elliptic case.

The VOP equations of motion for Keplerian elements are taken in the form of the Gaussian planetary equations

$$\frac{da}{dt} = \frac{2\dot{\bar{r}}}{n^2 a} \cdot \bar{\mathbf{p}} \quad (5-117a)$$

$$\frac{de}{dt} = \frac{\sqrt{1-e^2}}{na^2 e} \left[ y_p \hat{x}_p - x_p \hat{y}_p + \frac{\sqrt{1-e^2}}{n} \dot{\bar{r}} \right] \cdot \bar{\mathbf{p}} \quad (5-117b)$$

$$\frac{di}{dt} = \frac{- \left[ (y_p \hat{x}_p - x_p \hat{y}_p) \cos i + \frac{\partial \bar{r}}{\partial \Omega} \right] \cdot \bar{\mathbf{p}}}{na^2 \sqrt{1-e^2} \sin i} \quad (5-117c)$$

$$\frac{d\Omega}{dt} = \frac{1}{na^2 \sqrt{1-e^2} \sin i} \frac{\partial \bar{r}}{\partial i} \cdot \bar{P} \quad (5-117d)$$

$$\frac{d\omega}{dt} = -\frac{1}{na^2} \left[ \frac{-\sqrt{1-e^2}}{e} (L\hat{x}_p + N\hat{y}_p) + \frac{\cot i}{\sqrt{1-e^2}} \frac{\partial \bar{r}}{\partial i} \right] \cdot \bar{P} \quad (5-117e)$$

$$\frac{dM}{dt} = n + \frac{1}{na^2} \left[ -2\bar{r} - \frac{1-e^2}{e} (L\hat{x}_p + N\hat{y}_p) \right] \cdot \bar{P} \quad (5-117f)$$

where  $x_p$  and  $y_p$  are the orbit plane coordinates given in Equation (3-145),  $\hat{x}_p$  and  $\hat{y}_p$  are Keplerian unit vectors defined in Section 3.2.5 and given by the inverse of Equation (3-159), and  $\bar{P}$  is the perturbing acceleration vector. The following auxiliary quantities are also defined

$$n = \sqrt{\frac{\mu}{a^3}} \quad (5-118a)$$

$$\frac{\partial \bar{r}}{\partial \Omega} = \begin{pmatrix} -y \\ x \\ 0 \end{pmatrix} \quad (5-118b)$$

$$\frac{\partial \bar{r}}{\partial i} = \begin{pmatrix} z \sin \Omega \\ -z \cos \Omega \\ (x_p \sin \omega + y_p \cos \omega) \cos i \end{pmatrix} \quad (5-118c)$$

$$L = \frac{a^2}{r} [e \cos E - 1 - \sin^2 E] \quad (5-118d)$$

$$N = \frac{a^2 \sin E}{r \sqrt{1-e^2}} (\cos E - e) \quad (5-118e)$$

The eccentric anomaly is obtained by solving Kepler's equation according to the method described in Section 3.3.8.1.

### 5.7.2 Equinoctial Elements

Since disturbing forces are calculated as rectangular components, and initial values may be rectangular components of position and velocity, GTDS has a capacity for converting Cartesian coordinates to equinoctial elements (see Section 3.3.9.2). The transformation from equinoctial elements to Cartesian coordinates is discussed in Section 3.3.9.1. The Gaussian equations in equinoctial elements are given by the following expressions (References 10 and 11)

$$\frac{da}{dt} = \frac{2\dot{\bar{r}}}{n^2 a} \cdot \bar{\mathbf{P}} \quad (5-119a)$$

$$\frac{dh}{dt} = \left[ \frac{1}{\mu} [(2\dot{X}_1 Y_1 - X_1 \dot{Y}_1) \hat{f} - X_1 \dot{X}_1 \hat{g}] + \frac{k}{G} (q I Y_1 - p X_1) \hat{w} \right] \cdot \bar{\mathbf{P}} \quad (5-119b)$$

$$\frac{dk}{dt} = \left[ -\frac{1}{\mu} [Y_1 \dot{Y}_1 \hat{f} - (2X_1 \dot{Y}_1 - \dot{X}_1 Y_1) \hat{g}] - \frac{h}{G} (q I Y_1 - p X_1) \hat{w} \right] \cdot \bar{\mathbf{P}} \quad (5-119c)$$

$$\frac{d\lambda}{dt} = \left[ n - \frac{2}{na^2} \bar{r} + \beta \left( k \frac{\partial h}{\partial \bar{r}} - h \frac{\partial k}{\partial \bar{r}} \right) + \frac{1}{na^2} (q I Y_1 - p X_1) \hat{w} \right] \cdot \bar{\mathbf{P}} \quad (5-119d)$$

$$\frac{dp}{dt} = \left[ \frac{1 + p^2 + q^2}{2G} Y_1 \hat{w} \right] \cdot \bar{\mathbf{P}} \quad (5-119e)$$

$$\frac{dq}{dt} = \left[ \frac{(1 + p^2 + q^2) I}{2G} X_1 \hat{w} \right] \cdot \bar{\mathbf{P}} \quad (5-119f)$$

where

$$G = na^2 \sqrt{1 - h^2 - k^2} \quad (5-119g)$$

The  $\hat{f}$ ,  $\hat{g}$ , and  $\hat{w}$  unit vectors are defined in Sections 3.2.5 and 3.3.9.1, while the components of the position and velocity vectors in the orbit plane  $X_1$ ,  $Y_1$ ,  $\dot{X}_1$ ,  $\dot{Y}_1$ , and  $\beta$  are defined in Section 3.3.9.1.

### 5.7.3 Rectangular Formulation

The initial Cartesian components of position and velocity completely define any orbit whether it be elliptic, parabolic, hyperbolic, or any degenerate rectilinear orbit. From the initial position and velocity a completely general closed-form solution of the two-body problem is available for determining coordinates and velocities at any other time (Reference 12). The closed form solution avoids the singularities associated with different types of two-body motion. In the rectangular VOP formulation, the dependent variables  $\bar{r}_0$  and  $\dot{\bar{r}}_0$  are the initial conditions at the time  $t_0$  on an osculating two-body trajectory which yields the same state  $\bar{r}$  and  $\dot{\bar{r}}$  at time  $t$  as that of the perturbed trajectory. The dependent variable is the time. The osculating position and velocity at time  $t$  are obtained by inserting the perturbed initial conditions for the time of interest in the standard closed formulas for two-body motion.

The dependent variables, or perturbed initial conditions, are all slow variables, i.e., their time derivatives are all zero when the perturbing accelerations are set to zero. Therefore, all the equations of motion are in the form given in Equation (5-115).

$$\frac{d\dot{\bar{r}}_0}{dt} = \frac{\partial \dot{\bar{r}}_0}{\partial \bar{r}} \bar{P} \quad (5-120a)$$

$$\frac{d\dot{\bar{r}}_0}{dt} = \frac{\partial \dot{\bar{r}}_0}{\partial \dot{\bar{r}}} \bar{P} \quad (5-120b)$$

where the partial derivative matrices are as follows

$$\begin{bmatrix} \partial \dot{\bar{x}}_0 / \partial \dot{\bar{x}} & \partial \dot{\bar{x}}_0 / \partial \dot{\bar{y}} & \partial \dot{\bar{x}}_0 / \partial \dot{\bar{z}} \\ \partial \dot{\bar{y}}_0 / \partial \dot{\bar{x}} & \partial \dot{\bar{y}}_0 / \partial \dot{\bar{y}} & \partial \dot{\bar{y}}_0 / \partial \dot{\bar{z}} \\ \partial \dot{\bar{z}}_0 / \partial \dot{\bar{x}} & \partial \dot{\bar{z}}_0 / \partial \dot{\bar{y}} & \partial \dot{\bar{z}}_0 / \partial \dot{\bar{z}} \end{bmatrix} = - \begin{bmatrix} g & 0 & 0 \\ 0 & g & 0 \\ 0 & 0 & g \end{bmatrix} + U \begin{bmatrix} \dot{\bar{x}}_0 \\ \dot{\bar{y}}_0 \\ \dot{\bar{z}}_0 \end{bmatrix} [\dot{\bar{x}} \ \dot{\bar{y}} \ \dot{\bar{z}}] \quad (5-121a)$$

$$+ \begin{bmatrix} \dot{\bar{x}}_0 & \dot{\bar{x}}_0 \\ \dot{\bar{y}}_0 & \dot{\bar{y}}_0 \\ \dot{\bar{z}}_0 & \dot{\bar{z}}_0 \end{bmatrix} \begin{bmatrix} f s_2 & -(f-1) s_2 \\ (\dot{g}-1) s_2 & -g s_2 \end{bmatrix} \begin{bmatrix} x & y & z \\ \dot{x} & \dot{y} & \dot{z} \end{bmatrix}$$

$$\begin{bmatrix} \partial \ddot{x}_0 / \partial \dot{x} & \partial \ddot{x}_0 / \partial \dot{y} & \partial \ddot{x}_0 / \partial \dot{z} \\ \partial \ddot{y}_0 / \partial \dot{x} & \partial \ddot{y}_0 / \partial \dot{y} & \partial \ddot{y}_0 / \partial \dot{z} \\ \partial \ddot{z}_0 / \partial \dot{x} & \partial \ddot{z}_0 / \partial \dot{y} & \partial \ddot{z}_0 / \partial \dot{z} \end{bmatrix} = \begin{bmatrix} f & 0 & 0 \\ 0 & f & 0 \\ 0 & 0 & f \end{bmatrix} + U \begin{bmatrix} \ddot{x}_0 \\ \ddot{y}_0 \\ \ddot{z}_0 \end{bmatrix} \begin{bmatrix} \dot{x} & \dot{y} & \dot{z} \end{bmatrix} \quad (5-121b)$$

$$+ \begin{bmatrix} \dot{x}_0 & \dot{x}_0 \\ \dot{y}_0 & \dot{y}_0 \\ \dot{z}_0 & \dot{z}_0 \end{bmatrix} \begin{bmatrix} -\frac{\dot{f}s_1 + (f-1)/r_0}{r_0} & \frac{(f-1)s_1}{r_0} \\ -\dot{f}s_1 & (f-1)s_1 \end{bmatrix} \begin{bmatrix} x & y & z \\ \dot{x} & \dot{y} & \dot{z} \end{bmatrix}$$

The position and velocity are computed as follows

$$\bar{r} = f\bar{r}_0 + g\dot{\bar{r}}_0 \quad (5-122a)$$

$$\dot{\bar{r}} = \dot{f}\bar{r}_0 + \dot{g}\dot{\bar{r}}_0 \quad (5-122b)$$

where

$$f = 1 - \mu s_2 / r_0 \quad (5-123a)$$

$$g = (t - t_0) - \mu s_3 \quad (5-123b)$$

$$\dot{f} = -\mu s_1 / (r r_0) \quad (5-123c)$$

$$\dot{g} = 1 - \mu s_2 / r \quad (5-123d)$$

In the above formulas,  $\mu$  is the gravitational constant and

$$r_0 = (x_0^2 + y_0^2 + z_0^2)^{1/2} \quad (5-124a)$$

$$r = r_0 s_0 + \sigma_0 s_1 + \mu s_2 \quad (5-124b)$$

$$s_0 = 1 + \alpha^2 \psi^2 / 2! + \alpha^4 \psi^4 / 4! + \alpha^6 \psi^6 / 6! + \dots \quad (5-124c)$$

$$s_1 = \psi + \alpha^1 \psi^3 / 3! + \alpha^3 \psi^5 / 5! + \alpha^5 \psi^7 / 7! + \dots \quad (5-124d)$$

$$s_2 = \psi^2/2! + \alpha' \psi^4/4! + \alpha'^2 \psi^6/6! + \alpha'^3 \psi^8/8! + \dots \quad (5-124e)$$

$$s_3 = \psi^3/3! + \alpha' \psi^5/5! + \alpha'^2 \psi^7/7! + \alpha'^3 \psi^9/9! + \dots \quad (5-124f)$$

where the parameter  $\psi$  satisfies the following modified form of Kepler's equation

$$t = t_0 + r_0' s_1 + \sigma_0' s_2 + \mu s_3 \quad (5-125)$$

The equation is solved for  $\psi$  using a Newton-Raphson iteration process. In this equation

$$\sigma_0' = x_0' \dot{x}_0' + y_0' \dot{y}_0' + z_0' \dot{z}_0' \quad (5-126a)$$

$$\alpha' = \dot{x}_0'^2 + \dot{y}_0'^2 + \dot{z}_0'^2 - \frac{2\mu}{r} \quad (5-126b)$$

The parameter  $U$  is evaluated as follows

$$U = \mu(\psi s_4 - 3s_5) \quad (5-127)$$

where

$$s_4 = \psi^4/4! + \alpha' \psi^6/6! + \alpha'^2 \psi^8/8! + \alpha'^3 \psi^{10}/10! + \dots \quad (5-128a)$$

$$s_5 = \psi^5/5! + \alpha' \psi^7/7! + \alpha'^2 \psi^9/9! + \alpha'^3 \psi^{11}/11! + \dots \quad (5-128b)$$

The following accelerations at time  $t_0$  on the osculating trajectory are also used

$$\ddot{x}_0' = -\mu x_0' / r_0'^3 \quad (5-129a)$$

$$\ddot{y}_0' = -\mu y_0' / r_0'^3 \quad (5-129b)$$

$$\ddot{z}_0' = -\mu z_0' / r_0'^3 \quad (5-129c)$$

Initial conditions are specified by the values  $x_0, y_0, z_0, \dot{x}_0, \dot{y}_0, \dot{z}_0$  of the coordinates at a given reference time  $t_0$ . At time  $t_0$ ,



$$\begin{bmatrix} \dot{x}_0 \\ \dot{y}_0 \\ \dot{z}_0 \\ \dot{\dot{x}}_0 \\ \dot{\dot{y}}_0 \\ \dot{\dot{z}}_0 \end{bmatrix} = \begin{bmatrix} x_0 \\ y_0 \\ z_0 \\ \dot{x}_0 \\ \dot{y}_0 \\ \dot{z}_0 \end{bmatrix}$$

## 5.8 NUMERICAL AVERAGING FORMULATIONS

The efficiency of numerical integration methods can be increased by eliminating short period effects (i.e., those with a period less than or equal to the satellite's period) from the equations of motion. The Method of Averages uses this approach, wherein the equations of motion for an average element set are integrated. The resulting orbit generation method is extremely efficient, but is limited to average element accuracy rather than the osculating element accuracy achieved in high precision methods.

The averaging methods are particularly useful for orbit determination problems for which the cost of precision orbit calculations is prohibitively expensive, or where high accuracy is not essential. Mission design, for example, is based on the consideration of both the scientific objectives of the mission and the engineering constraints. Optimum mission design usually requires a large number of orbit calculations to determine the characteristics of the proposed orbits. An averaging orbit prediction process is well suited to the preliminary stages of mission planning where long-term trends, not local fluctuations, are of primary interest. The averaging methods may also be useful for differential correction problems involving large quantities of data. The only assumption required for application of the averaging method is that the orbital elements remain reasonably constant throughout one period.

The averaging process can be handled either analytically or numerically (Reference 13). The analytic method averages the effect of each perturbation (drag, oblateness, third-body effects, etc.) separately. The resulting closed-form expressions for the averaged rates can be used to construct a very efficient orbit generator. The numerical averaging technique combines many of the advantages of analytic averaging with the ability to simulate the effect of any small perturbations which can be deterministically modeled. These effects are included by averaging out

the short-period oscillations in the perturbations by means of a mechanical quadrature technique. By using the Gaussian form of the Variation of Parameters equations in conjunction with the GTDS force model, the long-term effect of any combination of perturbations can be computed. Consequently, the numerical technique is more flexible than the analytic method.

### 5.8.1 The Averaged Equations of Motion

The averaging methods in GTDS use either the equinoctial or the Keplerian formulation (Section 5.7) of the Variation of Parameters equations of motion. The precision Variation of Parameters equations can be written in the form

$$\begin{aligned}\dot{\bar{\mathbf{x}}} &= \epsilon \mathbf{f}(\bar{\mathbf{x}}, \mathbf{y}) \\ \dot{\mathbf{y}} &= \mathbf{h}(\bar{\mathbf{x}}) + \epsilon \mathbf{g}(\bar{\mathbf{x}}, \mathbf{y})\end{aligned}\tag{5-131}$$

where  $\bar{\mathbf{x}} \sim$  the vector of slow osculating orbital elements

$\mathbf{y} \sim$  the fast osculating orbital element (e.g., mean or eccentric anomaly)

$\epsilon \sim$  a small parameter which is proportional to the perturbing acceleration

and  $\mathbf{f}$ ,  $\mathbf{g}$ , and  $\mathbf{h}$  are sufficiently smooth functions which are periodic in  $\mathbf{y}$  with period  $2\pi$ . The averaged solution to these equations is defined by (Reference 14)

$$\begin{aligned}\bar{\mathbf{x}}_A(t) &= \frac{1}{2\pi} \int_{y_A(t)-\pi}^{y_A(t)+\pi} \bar{\mathbf{x}}(t') dy_A(t') \\ y_A(t) &= \frac{1}{2\pi} \int_{y_A(t)-\pi}^{y_A(t)+\pi} y(t') dy_A(t')\end{aligned}\tag{5-132}$$

Differentiating Equations (5-132) and substituting the results into Equations (5-131) yields the averaged equations of motion

$$\dot{\bar{x}}_A(t) = \frac{\epsilon}{2\pi} \int_{y_A(t)-\pi}^{y_A(t)+\pi} [f(\bar{x}(t'), y(t'))] dy_A(t') \quad (5-133)$$

$$\dot{y}_A(t) = \frac{1}{2\pi} \int_{y_A(t)-\pi}^{y_A(t)+\pi} \{h[\bar{x}(t'), y(t')] + \epsilon g[\bar{x}(t'), y(t')]\} dy_A(t')$$

When  $\bar{x}_A(t')$  and  $y_A(t')$  are used in the evaluation of the arguments of the  $f$ ,  $g$ , and  $h$  functions, the standard first order averaged equations of motion are obtained (Reference 15). In GTDS, the integrals in Equation (5-133) are evaluated numerically using a Gaussian quadrature method.

### 5.8.2 Numerical Evaluation of the Averaged Equations of Motion

Four different approximations are currently available for evaluation of the arguments of the  $f$ ,  $g$ , and  $h$  functions in Equations (5-133):

#### 1. Traditional mean element behavior

$$\begin{aligned} \bar{x}(t') &= \bar{x}_A(t) \\ \bar{y}(t') &= y_A(t') \end{aligned} \quad (5-134)$$

#### 2. Traditional mean element behavior plus mean long-period effects

$$\begin{aligned} \bar{x}(t') &= \bar{x}_A(t) + \dot{\bar{x}}_A(t) [t' - t] \\ y(t') &= y_A(t') \end{aligned} \quad (5-135)$$

where  $\dot{\bar{x}}_A$  is the averaged rate computed in the previous evaluation

#### 3. Traditional mean element behavior plus short-period effects arising from $J_2$

$$\begin{aligned} \bar{x}(t') &= \bar{x}_A(t) + \Delta \bar{x}_{J_2} \\ y(t') &= y_A(t') + \Delta y_{J_2} \end{aligned} \quad (5-136)$$

The short-period corrections are obtained using Brower theory.

#### 4. Traditional mean element, mean long-period and short-period effects

$$\begin{aligned}\bar{\mathbf{x}}(t') &= \bar{\mathbf{x}}_A(t) + \dot{\bar{\mathbf{x}}}_A(t) [t' - t] + \Delta \bar{\mathbf{x}}_{J_2} \\ y(t') &= y_A(t') + \Delta y_{J_2}\end{aligned}\tag{5-137}$$

Currently, only Equation (5-134) is available for evaluation of the argument in Equations (5-137).

#### 5.8.3 Averaged Equinoctial Variation of Parameters Formulation

The averaged equinoctial formulation (Section 5.7.2) uses a slow element vector  $\bar{\mathbf{x}} = (a, h, k, p, q)$  and a fast variable equal to the mean longitude  $\lambda$ . To uniformize the integrand in Equation (5-133) and to reduce computational time, the integration variable is transformed from mean to eccentric longitude  $F$ , using the relationship

$$\frac{dF_A}{d\lambda_A} = [1 - \kappa_A \cos F_A - h_A \sin F_A]^{-1}\tag{5-138}$$

#### 5.8.4 Averaged Keplerian Variation of Parameters Formulation

The averaged Keplerian formulation uses a slow element vector  $\bar{\mathbf{x}} = (a, e, i, \Omega, \omega)$  and a fast variable equal to the mean anomaly  $M$ . All four methods outlined in Section 5.8.2 are available for evaluation of the equations of motion. When methods 3 and 4 are used, the integration variable is transformed to the true anomaly  $f$ , using the relationship

$$\frac{df_A}{dM_A} = \frac{a_A^2 \sqrt{1 - e_A^2}}{r_A^2}\tag{5-139}$$

where  $r_A$  is the magnitude of the position vector computed using the averaged elements.

#### 5.8.5 Transformation from Osculating Orbital Elements to Averaged Elements

The accuracy of predictions obtained using the averaged orbit generator are improved if initial average elements are used instead of osculating elements. In GTDS, this transformation is accomplished by solving the integral equation for the average semimajor axis

$$a_A(t) = \frac{1}{T_A} \int_{t-T_A/2}^{t+T_A/2} a(t') dt' \quad (5-140)$$

using the following Newton-Raphson iterative procedure

$$F_n = [a_A(t)]_n - \frac{1}{\langle T_A \rangle_n} \int_{t-(T_A/2)_n}^{t+(T_A/2)_n} a(t') dt' \quad (5-141a)$$

$$D_n = \frac{dF_n}{d[a_A(t)]_n} \quad (5-141b)$$

$$[a_A(t)]_{n+1} = [a_A(t)]_n - \frac{F_n}{D_n} \quad (5-141c)$$

where

$[a_A(t)]_0 = a \sim$  the osculating semimajor axis

and where  $T_A$ , the average period, is

$$T_A = 2\pi \sqrt{\frac{a_A^3}{\mu}} \quad (5-142)$$

The average equinoctial element set is then computed by averaging the osculating elements over the average period, i.e.,

$$\bar{x}_A(t) = \frac{1}{T_A} \int_{t-T_A/2}^{t+T_A/2} \bar{x}(t') dt' \quad (5-143a)$$

$$y_A(t) = \frac{1}{T_A} \int_{t-T_A/2}^{t+T_A/2} y(t') dt' \quad (5-143b)$$

The average equinoctial elements are transformed to average position and velocity vectors, Keplerian elements, and spherical coordinates.

## 5.9 BROUWER THEORY

GTDS includes two analytical solutions of satellite motion for a simplified disturbing potential field limited to zonal harmonic coefficients for  $J_2$  through  $J_5$  (see Section 4.3). Brouwer's first order solution of this problem is obtained by applying the Von Zeipel method in Delaunay canonical variables (Reference 1). The resulting solution contains singularities for small inclinations and eccentricities and at a critical inclination of  $63^\circ 26'$ .

It was shown in Reference 15 that the first order Brouwer solution for secular and long period effects is identical to that obtained using first order numerical averaging (Section 5.8) with the same perturbing force model. Thus, Brouwer theory is equivalent to the first order averaging solution plus short period effects for the  $J_2$  through  $J_5$  perturbing acceleration. For applications which require more complete perturbation models, averaging methods are more accurate than Brouwer theory.

Brouwer theory provides a rapid means of determining a satellite ephemeris. Its precision is related to the error committed in omitting all perturbations except the low order zonal harmonics. The orbit from the Brouwer theory can also be used as an intermediate orbit in the semianalytic techniques discussed in Section 5.11.

For applications which require high efficiency, it is important to consider the number of output points which are required. For Brouwer theory, the computational cost is directly proportional to the number of output points. However, when averaged numerical integration is used, the cost is mainly dependent on the arc length instead of the number of intermediate output points. For differential correction applications, the computational cost of the averaged orbit generation methods is often competitive with that of Brouwer theory and offers considerably greater flexibility with respect to the perturbation model.

Computationally, the Brouwer solution is divided into secular, long period, and short period terms. The solution consists of a secular motion, upon which is superimposed a number of long period terms. Superimposed on the sum of the secular and long period terms are a number of more rapid oscillations or short period terms. The periodic terms of both long and short period are developed to order  $(J_2)$ , while secular terms are developed to order  $(J_2)^2$ . The harmonic coefficients  $J_3$ ,  $J_4$ , and  $J_5$  are considered to be of order  $(J_2)^2$  in the derivations.

The Delaunay elements are related to the classical elements in the following way

$$L = (\mu a)^{1/2} \quad \ell = \text{the mean anomaly} = M$$

$$G = L (1 - e^2)^{1/2} \quad g = \text{the argument of pericenter} = \omega$$

$$H = G \cos i \quad h = \text{the longitude of the ascending node} = \Omega$$

However, the solution is written here in terms of classical elements  $(a, e, i, \ell, g, h) = (a, e, i, M, \omega, \Omega)$ . In the formulas that follow, double primed variables refer to secular or mean motion, single primed variables refer to secular plus long period terms, and unprimed variables refer to secular plus long and short period terms. The unprimed variables are osculating elements.

Only the elements  $\ell, g$ , and  $h$  undergo secular motions. Mean elements at epoch are denoted by a subscript "0" and the time elapsed from epoch by  $\Delta t$ . Mean elements are usually obtained from osculating elements by the procedure outlined in Section 5.9.1. The first order solutions to the mean element equations of motion are

$$a'' = a_0'' + \Delta a \quad (5-144a)$$

$$e'' = e_0'' + \Delta e \quad (5-144b)$$

$$i'' = i_0'' + \Delta i \quad (5-144c)$$

$$\ell'' = n_0 \Delta t + \dot{\ell} \Delta t + \ell_0'' + \Delta \ell + \Delta \ell_{\text{DRAG}} \quad (0 \leq \ell'' < 2\pi) \quad (5-144d)$$

$$g'' = \dot{g} \Delta t + g_0'' + \Delta g \quad (0 \leq g'' < 2\pi) \quad (5-144e)$$

$$h'' = \dot{h} \Delta t + h_0'' + \Delta h \quad (0 \leq h'' < 2\pi) \quad (5-144f)$$

where  $\Delta a, \Delta e, \Delta i, \Delta \ell, \Delta g$ , and  $\Delta h$  are user-provided perturbations not accounted for in the Brouwer-Lyddane model, and

$$\Delta \ell_{\text{DRAG}} = \sum_{q=0}^{19} \sum_{p=2}^3 N_{p,q} (t - t_q)^p \quad (5-145)$$

where  $N_{p,q}$  are the Brouwer drag coefficients, and  $t_q$  is the reference time of the  $q^{\text{th}}$   $N_{p,q}$ . This model is based on the premise that drag is a minor component of the total perturbation force.

The restricted perturbation model and first order approximation, which are used in the derivation of these equations, may lead to errors which increase with time. The element rates of change are given by

$$\dot{l} = n_0 \eta \left\{ \gamma'_2 \left[ \frac{3}{2} (3\theta^2 - 1) + \frac{3}{32} \gamma'_2 (25\eta^2 + 16\eta - 15 + (30 - 96\eta - 90\eta^2) \theta^2 + (105 + 144\eta + 25\eta^2) \theta^4) \right] + \frac{15}{16} \gamma'_4 e''^2 (3 - 30\theta^2 + 35\theta^4) \right\} \quad (5-146)$$

$$\begin{aligned} \dot{g} = n_0 \left\{ \gamma'_2 \left[ \frac{3}{2} (5\theta^2 - 1) + \frac{3}{32} \gamma'_2 (25\eta^2 + 24\eta - 35 \right. \right. \\ \left. \left. + (90 - 192\eta - 126\eta^2) \theta^2 + (385 + 360\eta + 45\eta^2) \theta^4) \right] \right. \\ \left. + \frac{5}{16} \gamma'_4 [21 - 9\eta^2 + (126\eta^2 - 270) \theta^2 + (385 - 189\eta^2) \theta^4] \right\} \quad (5-147) \end{aligned}$$

$$\begin{aligned} \dot{h} = n_0 \left\{ \gamma'_2 \left[ \frac{3}{8} \gamma'_2 ((9\eta^2 + 12\eta - 5) \theta - (35 + 36\eta + 5\eta^2) \theta^3) - 3\theta \right] \right. \\ \left. + \frac{5}{4} \gamma'_4 \theta (5 - 3\eta^2) (3 - 7\theta^2) \right\} \quad (5-148) \end{aligned}$$

The following substitutions have been made in order to abbreviate the preceding expressions.

$$n_0 = \sqrt{\frac{\mu}{a^3}}$$

$$\eta = \sqrt{1 - e'^2}$$

$$\theta = \cos i''$$

$$k_2 = \frac{J_2 R_e^2}{2}$$

$$\gamma_2 = \frac{k_2}{a'^2}$$

$$\gamma'_2 = \frac{\gamma_2}{\eta^4}$$

$$k_3 = -J_3 R_e^3$$

$$\gamma_3 = \frac{k_3}{a'^3}$$

$$\gamma'_3 = \frac{\gamma_3}{\eta^6}$$

$$k_4 = -\frac{3J_4 R_e^4}{8}$$

$$\gamma_4 = \frac{k_4}{a'^4}$$

$$\gamma'_4 = \frac{\gamma_4}{\eta^8}$$



$$k_5 = -J_5 R_e^5$$

$$\gamma_5 = \frac{k_5}{a''^5}$$

$$\gamma'_5 = \frac{\gamma_5}{\eta^{10}}$$

The secular terms depend only on the even zonal harmonic coefficients  $J_2$  and  $J_4$ .

The mean value of the eccentric anomaly  $E''$  is obtained iteratively from Kepler's equation

$$E'' - e'' \sin E'' = \ell'' \quad (5-149)$$

The mean true anomaly  $f''$  and mean radial distance  $r''$  are

$$f'' = \tan^{-1} \left[ \frac{\sqrt{1 - e''^2} \sin E''}{\cos E'' - e''} \right] \quad (5-150)$$

$$r'' = a''(1 - e'' \cos E'') \quad (5-151)$$

#### 5.9.1 Transformation from Osculating Orbital Elements to Brouwer Mean Elements

The iterative algorithm used for conversion of osculating Keplerian elements to Brouwer mean elements is described here (see References 16 and 17). This algorithm is useful in two situations. Since Brouwer or Brouwer-Lyddane theories require Brouwer mean elements as an initial state, the first application consists of converting osculating elements to mean elements for use with the Brouwer and Brouwer-Lyddane orbit generators. Secondly, osculating elements may be converted to Brouwer mean elements for reporting purposes. Such mean elements are also useful as initial data for the integration of orbits by the Method of Averaging and for other purposes.

Singular points for zero eccentricity, zero inclination, and at inclination  $63^\circ 26'$  do not permit calculation of mean elements there. Only Keplerian elliptic motion can be treated, which requires  $0 \leq e \leq 1$ .

The iterative process is executed according to the equation

$$x_i^{(s+1)} = x_i^{(s)} + (y_i - y_i^{(s)}) \quad (5-152)$$

$$i = 1, 2, \dots, 6$$

where  $x_i^{(s)} \sim$  the  $i^{\text{th}}$  mean classical Keplerian element obtained from the  $s^{\text{th}}$  iteration

$y_i \sim$  the initial osculating Keplerian element

$y_i^{(s)} \sim$  the osculating Keplerian element estimated from the  $s^{\text{th}}$  iteration

Double primes denote mean elements at the time of conversion. This algorithm ignores correlations between the elements of the order of  $10^{-3}$ , which are of no practical importance in the calculations.

A convergence criteria limits the number of iterations. The sum of the squares of the differences between estimated and initially given osculating elements are compared with a prescribed tolerance; when the sum is less than the tolerance, the calculation is terminated.

The following method for obtaining mean elements at a given time is more exact than those methods which propagate mean elements from some previous time using Equations (5-144) and (5-145), since the propagated mean elements deteriorate with time due to perturbations not included in the solution. The values of the mean elements on the  $s^{\text{th}}$  iteration are used to compute estimates of the osculating elements. As shown by Equation (5-152), the difference between the  $s^{\text{th}}$  estimated value and the initial known value of the osculating elements is used to correct the  $s^{\text{th}}$  estimate of the mean elements. The starting approximation for the mean elements is the set of initially known osculating elements.

### 5.9.2 Transformation from Brouwer Mean Elements to Osculating Keplerian Elements

The osculating elements include the secular, long period, and short period terms. The osculating elements are expressed by

$$a = a'' \left\{ 1 + \gamma_2 \left[ (-1 + 3\epsilon^2) \left( \frac{a''^3}{r'^3} - \eta^{-3} \right) + 3(1 - \epsilon^2) \frac{a''^3}{r'^3} \cos(2g' + 2f') \right] \right\} \quad (5-153)$$

$$\begin{aligned} e = e'' + \gamma_1 e'' + \frac{\eta^2}{2e''} \left\{ \gamma_2 \left[ (-1 + 3\epsilon^2) \left( \frac{a''^3}{r'^3} - \eta^{-3} \right) \right. \right. \\ \left. \left. + 3(1 - \epsilon^2) \left( \frac{a''^3}{r'^3} - \eta^{-4} \right) \cos(2g' + 2f') \right] \right. \\ \left. - \gamma_2' (1 - \epsilon^2) [3e'' \cos(2g' + f') + e'' \cos(2g' + 3f')] \right\} \end{aligned} \quad (5-154)$$

$$\begin{aligned} i = i'' + \delta_1 i + \frac{1}{2} \gamma_2' \theta (1 - \theta^2)^{1/2} [3 \cos(2g' + 2f') \\ + 3e'' \cos(2g' + f') + e'' \cos(2g' + 3f')] \end{aligned} \quad (5-155)$$

$$\begin{aligned} \ell = \ell'' + \delta_1 \ell - \frac{\eta^3}{4e''} \gamma_2' \left\{ 2(-1 + 3\theta^2) \left( \frac{a''^2}{r'^2} \eta^2 + \frac{a''}{r'} + 1 \right) \sin f' \right. \\ + 3(1 - \theta^2) \left[ \left( -\frac{a''^2}{r'^2} \eta^2 - \frac{a''}{r'} + 1 \right) \sin(2g' + f') \right. \\ \left. \left. + \left( \frac{a''^2}{r'^2} \eta^2 + \frac{a''}{r'} + \frac{1}{3} \right) \sin(2g' + 3f') \right] \right\} \end{aligned} \quad (5-156)$$

$$\begin{aligned} g = g'' + \delta_1 g + \frac{\eta^2}{4e''} \gamma_2' \left\{ 2(-1 + 3\theta^2) \left( \frac{a''^2}{r'^2} \eta^2 + \frac{a''}{r'} + 1 \right) \sin f' \right. \\ + 3(1 - \theta^2) \left[ \left( -\frac{a''^2}{r'^2} \eta^2 - \frac{a''}{r'} + 1 \right) \sin(2g' + f') \right. \\ \left. \left. + \left( \frac{a''^2}{r'^2} \eta^2 + \frac{a''}{r'} + \frac{1}{3} \right) \sin(2g' + 3f') \right] \right\} \\ + \frac{1}{4} \gamma_2' \{ 6(-1 + 5\theta^2) (f' - \ell' + e'' \sin f') \\ + (3 - 5\theta^2) [3 \sin(2g' + 2f') + 3e'' \sin(2g' + f') \\ + e'' \sin(2g' + 3f')] \} \end{aligned} \quad (5-157)$$

$$\begin{aligned} h = h'' + \delta_1 h - \frac{1}{2} \gamma_2' \{ [6(f' - \ell' + e'' \sin f') - 3 \sin(2g' + 2f') \\ - 3e'' \sin(2g' + f') - e'' \sin(2g' + 3f')] \} \end{aligned} \quad (5-158)$$

where the long period effects (denoted by  $\delta_1$ ) affect the elements  $e, i, \ell, g$ , and  $h$ , but **not the semimajor axis  $a$** , and are given by the following equations

$$\begin{aligned} \delta_1 e = & \left\{ \frac{1}{8} \gamma'_2 e'' \eta^2 [1 - 11\theta^2 - 40\theta^4(1 - 5\theta^2)^{-1}] \right. \\ & \left. - \frac{5}{12} \frac{\gamma'_4}{\gamma'_2} e'' \eta^2 [1 - 3\theta^2 - 8\theta^4(1 - 5\theta^2)^{-1}] \right\} \cos 2g'' \\ & + \left\{ \frac{1}{4} \frac{\gamma'_3}{\gamma'_2} \eta^2 \sin i'' + \frac{5}{64} \frac{\gamma'_5}{\gamma'_2} \eta^2 \sin i'' (4 + 3e''^2) \right. \\ & \times [1 - 9\theta^2 - 24\theta^4(1 - 5\theta^2)^{-1}] \left. \right\} \sin g'' \\ & - \frac{35}{384} \frac{\gamma'_5}{\gamma'_2} e''^2 \eta^2 \sin i'' [1 - 5\theta^2 - 16\theta^4(1 - 5\theta^2)^{-1}] \sin 3g'' \end{aligned} \quad (5-159)$$

$$\delta_1 i = - \frac{e'' \delta_1 e}{\eta^2 \tan i''} \quad (5-160)$$

$$\begin{aligned} \delta_1 \ell = & \left\{ \frac{1}{8} \gamma'_2 \eta^3 [1 - 11\theta^2 - 40\theta^4(1 - 5\theta^2)^{-1}] \right. \\ & \left. - \frac{5}{12} \frac{\gamma'_4}{\gamma'_2} \eta^3 [1 - 3\theta^2 - 8\theta^4(1 - 5\theta^2)^{-1}] \right\} \sin 2g'' \\ & + \left\{ - \frac{1}{4} \frac{\gamma'_3}{\gamma'_2} \frac{\eta^3}{e''} \sin i'' - \frac{5}{64} \frac{\gamma'_5}{\gamma'_2} \frac{\eta^3}{e''} \sin i'' (4 + 9e''^2) \right. \\ & \times [1 - 9\theta^2 - 24\theta^4(1 - 5\theta^2)^{-1}] \left. \right\} \cos g'' \\ & + \frac{35}{384} \frac{\gamma'_5}{\gamma'_2} \eta^3 e'' \sin i'' [1 - 5\theta^2 - 16\theta^4(1 - 5\theta^2)^{-1}] \cos 3g'' \end{aligned} \quad (5-161)$$

$$\begin{aligned}
\delta_{1g} = & \left\{ -\frac{1}{16} \gamma'_2 [(2 + e''^2) - 11(2 + 3e''^2) \theta^2 - 40(2 + 5e''^2) \theta^4 (1 - 5\theta^2)^{-1} \right. \\
& - 400 e''^2 \theta^6 (1 - 5\theta^2)^{-2}] + \frac{5}{24} \frac{\gamma'_4}{\gamma'_2} [2 + e''^2 - 3(2 + 3e''^2) \theta^2 \\
& \left. - 8(2 + 5e''^2) \theta^4 (1 - 5\theta^2)^{-1} - 80 e''^2 \theta^6 (1 - 5\theta^2)^{-2}] \right\} \sin 2g'' \\
& + \left\{ \frac{1}{4} \frac{\gamma'_3}{\gamma'_2} \left( \frac{\sin i''}{e''} - \frac{e'' \theta^2}{\sin i''} \right) + \frac{5}{64} \frac{\gamma'_5}{\gamma'_2} \right. \\
& \times \left[ \left( \frac{\eta^2 \sin i''}{e''} - \frac{e'' \theta^2}{\sin i''} \right) (4 + 3e''^2) + e'' \sin i'' (26 + 9e''^2) \right] \quad (5-162) \\
& \times [1 - 9\theta^2 - 24\theta^4 (1 - 5\theta^2)^{-1}] \\
& - \frac{15}{32} \frac{\gamma'_5}{\gamma'_2} e'' \theta^2 \sin i'' (4 + 3e''^2) [3 + 16\theta^2 (1 - 5\theta^2)^{-1} \\
& \left. + 40\theta^4 (1 - 5\theta^2)^{-2}] \right\} \cos g'' + \left\{ -\frac{35}{1152} \frac{\gamma'_5}{\gamma'_2} \left[ e'' \sin i'' (3 + 2e''^2) \right. \right. \\
& \left. \left. - \frac{e''^3 \theta^2}{\sin i''} \right] [1 - 5\theta^2 - 16\theta^4 (1 - 5\theta^2)^{-1}] \right. \\
& + \frac{35}{576} \frac{\gamma'_5}{\gamma'_2} e''^2 \theta^2 \sin i'' [5 + 32\theta^2 (1 - 5\theta^2)^{-1} \\
& \left. \left. + 80\theta^4 (1 - 5\theta^2)^{-2}] \right\} \cos 3g''
\end{aligned}$$

$$\begin{aligned}
\delta_1 h = & \left\{ -\frac{1}{8} \gamma_2' e''^2 \theta [11 + 80 \theta^2 (1 - 5 \theta^2)^{-1} + 200 \theta^4 (1 - 5 \theta^2)^{-2}] \right. \\
& + \frac{5}{12} \frac{\gamma_4'}{\gamma_2'} e''^2 \theta [3 + 16 \theta^2 (1 - 5 \theta^2)^{-1} + 40 \theta^4 (1 - 5 \theta^2)^{-2}] \left. \right\} \sin 2g'' \\
& + \left\{ \frac{1}{4} \frac{\gamma_3'}{\gamma_2'} \frac{e' \theta}{\sin i''} + \frac{5}{64} \frac{\gamma_5'}{\gamma_2'} \frac{e'' \theta}{\sin i''} (4 + 3e''^2) \right. \\
& \times [1 - 9 \theta^2 - 24 \theta^4 (1 - 5 \theta^2)^{-1}] \\
& + \frac{15}{32} \frac{\gamma_5'}{\gamma_2'} e' \theta \sin i'' (4 + 3e''^2) [3 + 16 \theta^2 (1 - 5 \theta^2)^{-1} \\
& + 40 \theta^4 (1 - 5 \theta^2)^{-2}] \left. \right\} \cos g'' \\
& + \left\{ -\frac{35}{1152} \frac{\gamma_5'}{\gamma_2'} \frac{e''^3 \theta}{\sin i''} [1 - 5 \theta^2 - 16 \theta^4 (1 - 5 \theta^2)^{-1}] \right. \\
& - \frac{35}{576} \frac{\gamma_5'}{\gamma_2'} e''^3 \theta \sin i'' [5 + 32 \theta^2 (1 - 5 \theta^2)^{-1} \\
& + 80 \theta^4 (1 - 5 \theta^2)^{-2}] \left. \right\} \cos 3g''
\end{aligned} \tag{5-163}$$

In these formulas,  $f'$  and  $r'$  are computed from

$$E' - e'' \sin E' = \vartheta' \tag{5-164}$$

and

$$\tan \frac{1}{2} f' = \left( \frac{1 + e''}{1 - e''} \right)^{1/2} \tan \frac{1}{2} E' \tag{5-165}$$

$$\frac{a''}{r'} = \frac{1 + e'' \cos f'}{1 - e''^2}$$

or

$$\begin{aligned}\frac{r'}{a''} \sin f' &= (1 - e''^2)^{1/2} \sin E' \\ \frac{r'}{a''} \cos f' &= \cos E' - e'' \\ \frac{r'}{a''} &= 1 - e'' \cos E'\end{aligned}\tag{5-166}$$

For the calculation of the coordinates at any time, the complete values of  $e$  and  $\ell$  should be used for the solution of Kepler's equation

$$E - e \sin E = \ell \tag{5-167}$$

The conversion of osculating Keplerian elements to rectangular components of position and velocity is discussed in Section 3.3.8.

## 5.10 BROUWER-LYDDANE THEORY

Lyddane modified Brouwer's formulation to obtain algorithms applicable for zero eccentricity and zero inclination (Reference 18). He reformulated the orbital equations in terms of Poincaré variables rather than the Delaunay variables used by Brouwer. The solution, carried out by the Von Zeipel method, accounts for up to fifth order zonal harmonics of the gravitational potential. The results are written here in classical elements rather than Poincaré elements.

The Brouwer formulas are suitable for the computation of the classical elements with one exception. In computing short period terms, Lyddane uses  $\ell''$  and  $g''$  instead of  $\ell'$  and  $g'$ . Brouwer remarked that either is satisfactory, but in the Lyddane theory,  $\ell'$  and  $g'$  may be ill defined. In addition, the relationships

$$\begin{aligned}(1 - e'') [(a''/r'')^3 - \eta^{-3}] &= \eta^{-6} [\alpha'' + e'' (1 + \eta)^{-1} \\ &\quad + 3 \cos f'' + 3e'' \cos^2 f'' + e''^2 \cos^3 f'']\end{aligned}\tag{5-168a}$$

and

$$(1 - e'') [(a''/r'')^3 - \eta^{-4}] = \eta^{-6} [\alpha'' + 3 \cos f'' + 3e'' \cos^2 f'' + e''^2 \cos^3 f''] \tag{5-168b}$$

are used in the computation of  $\delta e$  to avoid roundoff problems, where  $\eta$  is defined following Equation (5-148).

### 5.10.1 Transformation from Osculating Orbital Elements to Brouwer Mean Elements

The mean motions due to secular terms are calculated by Equations (5-144) through (5-148) of Section 5.9.

### 5.10.2 Transformation from Brouwer Mean Elements to Osculating Keplerian Elements

The osculating elements are computed using Equations (5-169) through (5-185) (Reference 19). Since the periodic terms are somewhat lengthy, a number of substitutions have been made in these equations.

#### Semimajor Axis

$$a = a'' \left\{ 1 + \gamma_2 \left[ (3e''^2 - 1) \frac{e''}{\eta^6} \left( e'' \eta + \frac{e''}{1 + \eta} + \cos f'' (3 + 3e'' \cos f'' + e'' - \cos^2 f'') \right) + 3(1 - e''^2) \left( \frac{a''}{r''} \right)^3 \cos(2f'' + 2g'') \right] \right\} \quad (5-169)$$

#### Eccentricity

$$e = \sqrt{(e'' + \delta e)^2 + (e'' \delta \ell)^2} \quad (5-170)$$

where

$$\begin{aligned} \delta e = \delta_1 e - \frac{\eta^2}{2} \left\{ \gamma_2' (1 - e''^2) [3 \cos(2g'' + f'') + \cos(3f'' + 2g'')] \right. \\ \left. - 3\gamma_2 \frac{1}{\eta^6} (1 - e''^2) \cos(2g'' + 2f'') (3e'' \cos^2 f'' + 3 \cos f'' + e''^2 \cos^3 f'' + e'') - \gamma_2 \frac{1}{\eta^6} (3e''^2 - 1) \right. \\ \left. \times \left[ e'' \eta + \frac{e''}{1 + \eta} + 3e'' \cos^2 f'' + 3 \cos f'' + e''^2 \cos^3 f'' \right] \right\} \end{aligned} \quad (5-171)$$



$$e'' \delta \ell = B_4 \sin 2g'' - B_5 \cos g'' + B_6 \cos 3g''$$

$$- \frac{1}{4} \gamma_2' \gamma_2' \left\{ 2(3\theta^2 - 1) \left[ \gamma^2 \left( \frac{a''}{r''} \right)^2 + \frac{a''}{r''} + 1 \right] \sin f'' \right. \\ \left. + 3(1 - \theta^2) \left[ \left( -\gamma^2 \left( \frac{e''}{r''} \right)^2 - \frac{a''}{r''} + 1 \right) \sin(2g'' + f'') \right. \right. \\ \left. \left. + \left( \gamma^2 \left( \frac{a''}{r''} \right)^2 + \frac{a''}{r''} + \frac{1}{3} \right) \sin(3f'' + 2g'') \right] \right\} \quad (5-172)$$

and  $\delta_1 e = B_{13} \cos 2g'' + B_{14} \sin g'' - B_{15} \sin 3g'' \quad (5-173)$

### Inclination

$$i = 2 \sin^{-1} \left\{ \left[ \sin \left( \frac{i''}{2} \right) \delta h \right]^2 + \left[ \frac{1}{2} \delta i \cos \left( \frac{i''}{2} \right) + \sin \left( \frac{i''}{2} \right) \right]^2 \right\}^{1/2} \quad (5-174)$$

where

$$\delta i = \frac{1}{2} \gamma_2' \gamma_2' \sin i'' \{ e'' \cos(3f'' + 2g'') \\ + 3[e'' \cos(2g'' + f'') + \cos(2f'' + 2g'')] \} \quad (5-175)$$

$$- \frac{A_{20}}{\gamma^2} (B_7 \cos 2g'' + B_8 \sin g'' - B_9 \sin 3g'')$$

and

$$\sin \left( \frac{i''}{2} \right) \delta h = \frac{1}{2 \cos(i''/2)} \left\{ B_{10} \sin 2g'' + B_{11} \cos g'' + B_{12} \cos 3g'' \right. \\ - \frac{1}{2} \gamma_2' \gamma_2' \sin i'' [6(e'' \sin f'' - e'' + f'') \\ - 3(\sin(2g'' + 2f'') + e'' \sin(2g'' + f'')) \\ \left. - e'' \sin(3f'' + 2g'') \right] \} \quad (5-176)$$

Mean Anomaly  $\ell$ , Argument of Perigee  $g$ , and Right Ascension of Ascending Node  $h$

$$\ell = \tan^{-1} \left\{ \frac{e'' \delta \ell \cos \ell'' + (e'' + \delta e) \sin \ell''}{(e'' + \delta e) \cos \ell'' - e'' \delta \ell \sin \ell''} \right\} \quad \text{if } e \neq 0 \quad (5-177)$$

$$\ell = 0 \quad \text{if } e = 0 \quad (5-178)$$

$$h = \tan^{-1} \left\{ \frac{\sin\left(\frac{i''}{2}\right) \delta h \cos h'' + \sinh'' \left[ \frac{1}{2} \delta i \cos\left(\frac{i''}{2}\right) + \sin\left(\frac{i''}{2}\right) \right]}{\cos h'' \left[ \frac{1}{2} \delta i \cos\left(\frac{i''}{2}\right) + \sin\left(\frac{i''}{2}\right) \right] - \sin\left(\frac{i''}{2}\right) \delta h \sinh''} \right\} \quad \text{if } i \neq 0 \quad (5-179)$$

$$h = 0 \quad \text{if } i = 0 \quad (5-180)$$

$$g = (\ell + g + h) - \ell - h \quad (5-181)$$

where

$$\begin{aligned} \ell + g + h = & (\ell' + g' + h') + \left\{ \frac{1}{4} \left( \frac{\eta^2}{\eta + 1} \right) e'' \gamma'_2 \left[ 3(1 - e^2) \left( \sin(3f'' + 2g'') \right) \right. \right. \\ & \times \left( \frac{1}{3} + \left( \frac{a''}{r''} \right)^2 \eta'' + \frac{a''}{r''} \right) + \sin(2g'' + f'') \left( 1 - \left( \frac{a''}{r''} \right)^2 \eta^2 - \frac{a''}{r''} \right) \\ & \left. \left. + 2 \sin f'' (3e^2 - 1) \left( 1 + \left( \frac{a''}{r''} \right)^2 \eta^2 + \frac{a''}{r''} \right) \right] \right\} \\ & + \frac{3}{2} \gamma'_2 [(5e^2 - 2e - 1) (e'' \sin f'' + f'' - \ell'') + (3 + 4e - 5e^2) \\ & \times \left\{ \frac{1}{4} \gamma'_2 [e'' \sin(3f'' + 2g'') + 3(\sin(2g'' + 2f'') + e'' \sin(2g'' + f''))] \right\} \end{aligned} \quad (5-182)$$

where

$$(\ell' + g' - h') = (\ell'' + g'' + h'') + B_3 \cos 3g'' + B_1 \sin 2g'' + B_2 \cos g'' \quad (5-183)$$

The quantity  $\theta$  is defined following Equation (5-148). The following abbreviations are introduced to shorten the written formulas.

$$A'_1 = \frac{1}{(1 - 5\theta^2)} \quad A_{13} = (5e''^2 + 2) \theta^4 A'_1$$

$$A_1 = \frac{1}{8} \gamma'_2 \eta^2 (1 - 11 \theta^2 - 40 \theta^4 A'_1) \quad A_{14} = e''^2 \theta^6 A_1'^2$$

$$A'_2 = 3\theta^2 + 8\theta^4 A'_1 \quad A_{15} = \theta^2 A'_1$$

$$A_2 = \frac{5}{12} \frac{\gamma'_4}{\gamma'_2} \eta^2 (1 - A'_2) \quad A_{16} = A_{15}^2$$

$$A_3 = \frac{\gamma'_5}{\gamma'_2} (3e''^2 + 4) \quad A_{17} = e'' \sin i'$$

$$A_4 = \frac{\gamma'_5}{\gamma'_2} (1 - 3A'_2) \quad A_{18} = \frac{A_{17}}{1 + \eta} \quad (5-184)$$

$$A_5 = A_3(1 - 3A'_2) \quad A_{19} = (1 + \eta) \sin i''$$

$$A_6 = \frac{1}{4} \frac{\gamma'_3}{\gamma'_2} \quad A_{20} = e'' \eta$$

$$A_7 = A_6 \eta^2 \sin i'' \quad A_{21} = e'' A_{20}$$

$$A_8 = \frac{\gamma'_5}{\gamma'_2} e''^2 (1 - 5c'^2 - 16c'^4 A'_1) \quad A_{22} = A_{20} \tan \left( \frac{i''}{2} \right)$$

$$A_9 = \eta'^2 \sin i'' \quad A_{23} = \eta'^2 A_{17}$$

$$A_{10} = 2 + e''^2 \quad A_{24} = A_{11} + 2 \quad (5-184) \text{ cont'd}$$

$$A_{11} = 3e''^2 + 2 \quad A_{25} = 16A_{15} + 40A_{16} + 3$$

$$A_{12} = A_{11} c'^2 \quad A_{26} = \frac{1}{8} A_{21} (11 + 200A_{16} + 80A_{15})$$

and

$$B_1 = \eta (A_1 - A_2) - \left[ \frac{1}{16} (A_{10} - 400A_{14} - 40A_{13} - 11A_{12}) + \frac{1}{8} A_{21} (11 + 200A_{16} + 80A_{15}) \right] \gamma'_2 + \frac{5}{24} \left[ -80A_{14} - 8A_{13} - 3A_{12} + 2A_{25}A_{21} + A_{10} \right] \frac{\gamma'_4}{\gamma'_2}$$

$$B_2 = A_6 A_{18} (2 + \eta - e''^2) + \frac{5}{64} A_5 A_{18} \eta'^2 - \frac{15}{32} A_4 A_{17} \eta'^3 + A_{20} \tan \left( \frac{i''}{2} \right) \times \left[ \frac{5}{64} A_5 + A_6 \right] + \frac{5}{64} A_4 A_{17} [9e''^2 + 26] + \frac{15}{32} A_3 A_{20} A_{25} \sin i'' (1 - c') \quad (5-185)$$

$$B_3 = \frac{35}{576} \frac{\gamma'_5}{\gamma'_2} e'' \sin i'' (c' - 1) A_{21} [80A_{16} + 5 + 32A_{15}]$$

$$- \frac{35}{1152} \frac{A_8}{c''} \left\{ A_{21} \tan \left( \frac{i''}{2} \right) + [2e''^2 + 3(1 - \eta'^3)] \sin i'' \right\}$$

$$B_4 = \eta' c'' (A_1 - A_2)$$

$$B_5 = \eta \left[ \frac{5}{64} A_4 A_9 (\mathcal{G} e''^2 + 4) + A_7 \right]$$

$$B_6 = \frac{35}{384} \eta^3 A_8 \sin i''$$

$$B_7 = \eta^2 A_{17} A_1' \left[ \frac{1}{8} \gamma_2' (1 - 15\theta^2) - \frac{5}{12} \frac{\gamma_4'}{\gamma_2'} (1 - 7\theta^2) \right]$$

$$B_8 = \frac{5}{64} A_3 \eta^2 (1 - 9\theta^2 - 24\theta^4 A_1') + \eta^2 A_6$$

$$B_9 = \frac{35}{384} \eta^2 A_8$$

$$B_{10} = \sin i'' \left[ \frac{5}{12} \frac{\gamma_4'}{\gamma_2'} A_{21} A_{25} - A_{26} \gamma_2' \right] \quad \begin{array}{l} (5-185) \\ \text{cont'd} \end{array}$$

$$B_{11} = A_{21} \left[ \frac{5}{64} A_5 + A_6 + \frac{15}{32} A_3 A_{25} \sin^2 i'' \right]$$

$$B_{12} = - \left[ (80A_{16} + 32A_{15} + 5) \left( \frac{35}{576} \frac{\gamma_5'}{\gamma_2'} e'' \sin^2 i'' A_{21} \right) + \frac{35}{1152} A_8 A_{20} \right]$$

$$B_{13} = e'' (A_1 - A_2)$$

$$B_{14} = \frac{5}{64} A_5 \eta^2 \sin i'' + A_7$$

$$B_{15} = \frac{35}{384} A_8 \eta^2 \sin i''$$

The mean value of the eccentric anomaly  $E''$  is obtained iteratively from Kepler's equation

$$E'' - e'' \sin E'' = \mathcal{L}'' \quad (5-186)$$

The mean true anomaly  $f''$ , the mean radial distance  $r''$ , and the ratio of the mean semimajor axis and the mean radial distance are given by

$$f'' = \tan^{-1} \left[ \frac{\sqrt{1 - e''^2} \sin E''}{\cos E'' - e''} \right] \quad (5-187)$$

$$r'' = a'' (1 - e'' \cos E'') \quad (5-188)$$

$$\frac{a''}{r''} = \frac{1}{(1 - e'' \cos E'')} \quad (5-189)$$

## 5.11 INTERMEDIATE ORBIT

The Intermediate Orbit methods used in GTDS (Reference 20) are semianalytic methods which combine analytic theory and numerical integration. The solution to a simpler problem obtained by means of an analytic theory is used as a reference solution, and the difference in the time rate of change between the true solution and this reference solution is integrated to obtain the true solution. Either a Variation of Parameters or an Encke approach can be used in the development of these methods. Using Intermediate Orbit methods causes the quantities on the right hand side of the resulting differential equations to vary slowly and smoothly with time, making them more amenable to numerical integration methods (i.e., more numerically stable) than the original differential equations.

Intermediate Orbit methods can be developed for any analytical theory; however, only two intermediate orbits have been considered for implementation in GTDS. The first is an orbit in which short period effects due to  $J_2$  have been eliminated using the Brouwer theory. The second is the orbit resulting from  $J_2$  perturbations using the complete Brouwer theory for secular, long period, and short period perturbations. The equations of motion are better conditioned for numerical integration when they are smoothed by removal of fast varying short period  $J_2$  effects or when made slower and smoother varying by using the complete Brouwer theory to remove secular, long period, and short period perturbations

arising from  $J_2$ . Orbits of small eccentricity and low inclination can be considered by an option which uses the same intermediary orbits as above, but which are expressed in Poincaré rather than Delaunay variables.

Efficient numerical integration is achieved through minimizing local error by an appropriate choice of a uniformization constant  $n$ . This involves selection of a new independent variable  $s$ , related to the time  $t$  by

$$ds = \frac{\sqrt{\mu}}{r^n} dt$$

where  $r$  is the magnitude of the satellite's position vector,  $\mu$  is the gravitational constant, and  $n$  is known as the uniformization constant. To a considerable extent, the optimum choice of  $n$  depends on the dominant perturbation affecting the orbit under consideration. Thus, for the Intermediate Orbit method based on short period  $J_2$  perturbations, the main portion of  $J_2$  must be modeled, leading to a choice of  $n = 2$ ; however, the Intermediate Orbit method using the full Brouwer theory may still require a selection of  $n = 2$  (or higher for an elliptic orbit) if the orbit is significantly perturbed by drag. If the intermediary orbit is out of the high drag region, then the choice of  $n$  depends upon the ellipticity of the orbit and whether or not third body perturbations are significant.

GTDS's full Brouwer intermediary is an osculating Keplerian orbit which changes due to  $J_2$ , the coefficient of the second zonal harmonic. Perturbations due to  $J_2$  dominate those caused by other gravitational harmonics, third bodies, drag, etc., for many close earth satellites. While other secular perturbations eventually cause the intermediary and true orbit to become widely separated, the GTDS intermediary stays near the true orbit much longer than the two-body solution.

## 5.12 VINTI THEORY

Vinti theory is a General Perturbation Method. In an approach similar to that of Brouwer, the dependent variable set is chosen such that the Hamilton-Jacobi equations of motion are separable. Of the eleven coordinate systems which have this property, oblate spheroidal coordinates  $\rho, \eta, \phi$ , are chosen since they are most appropriate for describing motion about an oblate earth. These coordinates are related to the rectangular position coordinates as follows

$$x + iy = (\rho^2 + c^2) (1 - \eta^2)^{1/2} e^{i\phi} \quad (5-190)$$

$$z = \rho\eta \quad (5-191)$$

where

$$c^2 = R_e^2 J_2 \left( 1 - \frac{1}{4} J_3^2 J_2^{-3} \right) \quad (5-192)$$

and where  $R_e$  is the mean equatorial radius of the earth and  $J_2$  and  $J_3$  are coefficients of the zonal harmonics (see Section 4.3.1). On the other hand, Brouwer theory was developed in terms of elliptic coordinates, which are most appropriate for describing motion about a point mass body.

Vinti obtains an analytic solution for perturbed satellite motion arising from a potential of the form

$$V = -\mu(\rho^2 + c^2\eta^2)^{-1}(\rho + \eta\delta) \quad (5-193)$$

where

$$\delta = -\frac{1}{2}R_e J_2^{-1} J_3 \quad (5-194)$$

The above potential leads to a fit of the gravitational potential

$$V = -\frac{\mu}{r} \left[ 1 - \sum_{n=2}^{\infty} \left\{ \left( \frac{R_e}{r} \right)^n J_n P_n(\sin \pi) \right\} \right] \quad (5-195)$$

exactly for the second zonal harmonic and about two-thirds of the fourth zonal harmonic.

The resulting solution gives the periodic terms correctly to order  $J_2^2$  and the secular terms for the intermediate orbit to arbitrarily high order. The mathematical details are given in Reference 21. This method for treating the effects of  $J_3$  eliminates singularities for small eccentricities and for small or 180 degree inclinations which usually occur in perturbation theories. Thus, Vinti theory is particularly appropriate for computation of polar and circular equatorial orbits.



### 5.13 REFERENCES

1. Brouwer, D.: 1959, "Solution of the Problem of Artificial Satellite Theory without Drag," Astronomical Journal, 64(1274), November 1959, pp. 378-397.
2. Henrici, P.: 1962, Discrete Variable Methods in Ordinary Differential Equations, John Wiley & Sons, Inc., New York.
3. Lapidus, L. and Sanfeld, J.: 1971, Numerical Solution of Ordinary Differential Equations, Academic Press, Inc., New York.
4. Stiefel, E. L. and Scheifele, G.: 1971, Linear and Regular Celestial Mechanics, Springer-Verlag, New York.
5. Scheifele, G. and Stiefel, E.: 1972, Canonical Satellite Theory, Report to ESRO, prepared under ESOC Contract No. 219/70/AR, February 1972.
6. Scheifele, G.: 1973, Numerical Orbit Computation Based on a Canonical Intermediate Orbit, Report to ESRO, prepared under ESOC Contract No. 490/72/AR, September 1973, with Appendix by S. Samway.
7. Samway, R. C.: 1973, A Special Perturbation Method Based on Canonical Delaunay-Similar Elements with the True Anomaly as the Independent Variable, Applied Mechanics Research Laboratory Report 1054, July 1973.
8. Petrovski, I. G.: 1973, Ordinary Differential Equations, (R. A. Silverman, ed. and transl.), Dover Publications, Inc., New York.
9. Feagin, T.: 1973, Description of the Numerical Integration of the Equations of Motion of a Space Vehicle Using Chebyshev Series, Goddard Space Flight Center Report X582-73-176, June 1973.
10. Long, A. C., Nimitz, K. S., and Cefola, P.J.: 1973, The Next Generation of Orbit Prediction Formulations for Artificial Satellites II, Computer Sciences Corporation Report 9101-14600-01TR, March 1973.
11. Broucke, R. A.: 1970, "On the Matrizant of the Two-Body Problem," Astronomy and Astrophysics, 6(2), pp. 173-182.
12. Goodyear, W. H.: 1965, "Completely General Closed-Form Solution for Coordinates and Partial Derivatives of the Two-Body Problem," Astronomical Journal, 70(3), April 1965, pp. 189-192.

13. Cefola, P. J., Long, A. C., and Holloway, G., Jr.: 1974, "The Long-Term Prediction of Artificial Satellite Orbits," AIAA Paper No. 74-170, presented at the AIAA 12th Aerospace Sciences Meeting, Washington, D. C., January 30 - February 1, 1974.
14. Velez, C. E. and Fuchs, A. J.: 1974, "A Review of Averaging Techniques and Their Application to Orbit Determination Systems," AIAA Paper No. 74-171, presented at AIAA 12th Aerospace Sciences Meeting, Washington, D. C., January 30 - February 1, 1974.
15. Morrison, J. A.: 1966, "Generalized Method of Averaging and the Von Zeipel Method," in Progress in Astronautics and Aeronautics, Vol. 17: Methods in Astrodynamics and Celestial Mechanics, (R. L. Duncombe and V. G. Szebehely, eds.), Academic Press, New York, pp. 117-138.
16. Cain, B. J.: 1967, "Determination of Mean Elements for Brouwer's Satellite Theory," Astronomical Journal, 67(6), August 1962, pp. 391-392.
17. Walter, H. G.: 1967, "Conversion of Osculating Orbital Elements into Mean Elements," Astronomical Journal, 72(8), October 1967, pp. 994-997.
18. Lyddane, R. H.: 1963, "Small Eccentricities or Inclinations in the Brouwer Theory of the Artificial Satellite," Astronomical Journal, 68(8), October 1963, pp. 555-558.
19. Leech, H. W.: 1974, Evaluation of Brouwer Differential Correction and Complementary Perturbation Capability in the Definitive Orbit Determination System, Computer Sciences Corporation Report 3000-07000-01TM, April 1974.
20. Alfried, K. T. and Velez, C. E.: 1975, "The Application of General Perturbation Theories to the Artificial Satellite Problem," Acta Astronautica, Vol. 2, pp. 577-591.
21. Vinti, J. P.: 1969, "Improvement of the Spheroidal Method for Artificial Satellites," Astronomical Journal, 74(1), February 1969, pp. 25-34.

## CHAPTER 6

NUMERICAL INTEGRATION OF THE EQUATIONS OF  
MOTION AND VARIATIONAL EQUATIONS

This chapter describes the Störmer-Cowell/Adams integration processes available in GTDS for the integration of the Cowell and various VOP (Chapter 5) formulations of the equations of motion. These processes were selected on the basis of several efficiency studies (References 1, 2) comparing various classes of popular integration algorithms as applied to special perturbation techniques. This chapter also describes a single step integration method, the Runge-Kutta method, which is used in GTDS in connection with sequential estimation and as a starter for certain multi-step processes.

Multi-step methods of the type described below were found to minimize the number of derivative evaluations required to produce a given accuracy at the end of the requested interval of integration. Since, in general, the major cost in computing an orbit is the evaluation of the complex force function (Chapter 4), this implies multi-step algorithms are most efficient.

Within the class of multistep methods one must still select options such as:

(1) Type of formulation - i.e., methods may be used which solve second order systems directly (Class II), such as Störmer's method, or which normalize the second order system into a higher dimensional first order system and use a Class I formula such as Adams-Bashforth:

(2) Type of algorithm - several algorithms may be selected within the multistep predictor-corrector schemes ranging from PE (prediction only) to  $P(EC)^n$ ,  $PE(CE)^n$  and  $PECE^*$ , where P = predict, E = evaluate derivative, C = correct, and  $E^*$  = pseudo-evaluate, i.e., correct or re-correct only part of the total derivative;

(3) Order of process - various order formulas may be selected to use in the algorithm, recognizing the fact that higher order formulas are more accurate but less stable;

(4) Stepsize control - since the orbit dynamics may undergo large variations during a revolution, e.g., high eccentricity orbits, an algorithm must be selected to allow stepsize variations. This can be done either by numerical monitoring of local errors or by analytic transformations of the independent variable (Time-regularization).

Most of the above mentioned degrees of freedom are available in the GTDS system and have been studied for various problems (References 3, 4). Some general conclusions reached are:

(1) For formulations involving second-order equations, Class II integrators should be used to solve the system directly, utilizing a Class I method to obtain first derivatives if required;

(2) The highest possible order formula, subject only to the constraints of numerical stability, should be used;

(3) Pseudo-evaluate algorithms significantly increase the stability regions of predictor-corrector schemes at little or no cost in efficiency;

(4) Efficiency dictates the use of stepsize control for moderate and high eccentricity orbits; analytic stepsize control is more efficient and reliable than numerical stepsize control;

(5) The choice of the "best" integrator and independent variable is highly dependent on the choice of formulation of the equations of motion. Formulation characteristics such as regularity, or "smoothness" of dependent variables, and dynamic stability influence parameters such as numerical stability regions, choice of order, etc. As new formulations are introduced, careful "matching" of appropriate numerical schemes is required.

In the following sections the multi-step methods based on Newton's interpolating polynomial are derived and the basic algorithms for iteration, starting, interpolation and stepsize control are discussed.

## 6.1 ADAMS-COWELL ORDINATE SECOND SUM FORMULAS

The formulas for the integration and interpolation of the equations of motion and the variational equations are basically of the Newtonian type derivable from standard difference operator techniques. For the integration, these formulas define the well-known predictor-corrector Adams method for first-order equations and Cowell method for second-order systems. Formulas of the same class may be used to perform the required interpolations to determine values not given in the integration process and to form the starting set of solution values required by the predictor-corrector process.

In the following discussion, an outline of the derivations of the required formulas is given. In addition, a detailed description of the computational algorithms necessary to perform the integrations is presented.

Let  $s$  and  $h$  denote real numbers, and consider the linear operators  $\nabla$ ,  $E^s$ ,  $D$ , and  $I$ , which are defined as

$$\nabla f(t) = f(t) - f(t-h) \quad \left\{ \begin{array}{l} \text{Backward} \\ \text{Difference} \\ \text{Operator} \end{array} \right\} \quad (6-1)$$

$$E^s f(t) = f(t+sh) \quad \left\{ \begin{array}{l} \text{Shifting} \\ \text{Operator} \end{array} \right\} \quad (6-2)$$

$$D f(t) = \frac{d}{dt} f(t) = \dot{f}(t) \quad \left\{ \begin{array}{l} \text{Differentiation} \\ \text{Operator} \end{array} \right\} \quad (6-3)$$

$$I f(t) = f(t). \quad \left\{ \begin{array}{l} \text{Identity} \\ \text{Operator} \end{array} \right\} \quad (6-4)$$

Two well-known relations among these operators are

$$E^s = (I - \nabla)^{-s} \quad (6-5)$$

and

$$h D = -\ln(I - \nabla) \quad (6-6)$$

Utilizing Equations (6-5) and (6-6), the following operator identities can be derived

$$E^s = h \left[ \frac{(I - \nabla)^{-s}}{-\ln(I - \nabla)} \right] D$$

$$E^s = h^2 \left[ \frac{(I - \nabla)^{-s}}{[\ln(I - \nabla)]^2} \right] D^2$$

Expanding the bracketed terms in a  $\nabla$  series yields

$$E^s = h \left[ \nabla^{-1} + \sum_{i=0}^{\infty} \gamma'_{i+1}(s, \nabla^i) \right] D \quad (6-7)$$

$$E^s = h^2 \left[ \nabla^{-2} + (s-1) \nabla^{-1} + \sum_{i=0}^{\infty} \gamma_{i+2}''(s) \nabla^i \right] D^2 \quad (6-8)$$

where the  $\gamma_i'(s)$  and  $\gamma_i''(s)$  are given by the following recursive formulas in  $s$  (see Reference 5)

$$\gamma_0(s) = \gamma_0'(s) = \gamma_0''(s) = 1 \quad (6-9)$$

$$\gamma_i'(s) = \sum_{j=0}^i \gamma_j'(0) \gamma_{i-j}(s) \quad (6-10)$$

$$\gamma_i''(s) = \sum_{j=0}^i \gamma_j''(0) \gamma_{i-j}(s) \quad i = 0, 1, 2, \dots, k \quad (6-11)$$

where

$$\gamma_i(s) = \frac{s+i-1}{i} \gamma_{i-1}(s) \quad (6-12)$$

and

$$\gamma_i'(0) = - \sum_{j=0}^{i-1} \frac{1}{i-j+1} \gamma_j'(0) \quad (6-13)$$

$$\gamma_i''(0) = \sum_{j=0}^i \gamma_j'(0) \gamma_{i-j}'(0) \quad (6-14)$$

Applying the operators (6-7) and (6-8) to the functions  $\dot{x}(t)$  and  $x(t)$ , respectively, and truncating after  $k$  terms, gives

$$\dot{x}(t+sh) = h \left[ \nabla^{-1} \ddot{x}(t) + \sum_{i=0}^k \gamma_{i+1}'(s) \nabla^i \ddot{x}(t) \right] \quad (6-15)$$

$$x(t + sh) = h^2 \left[ \nabla^{-2} \ddot{x}(t) + (s-1) \nabla^{-1} \dot{x}(t) + \sum_{i=0}^k \gamma_{i+2}''(s) \nabla^i \ddot{x}(t) \right] \quad (6-16)$$

The quantities  $\nabla^{-1} \dot{x}(t)$  and  $\nabla^{-2} \ddot{x}(t)$  are called the first and second sums of  $\ddot{x}(t)$ , and satisfy the relationships

$$\nabla^{-1} \dot{x}(t) - \nabla^{-1} \dot{x}(t-h) = \ddot{x}(t) \quad (6-17)$$

and

$$\nabla^{-2} \ddot{x}(t) - \nabla^{-2} \ddot{x}(t-h) = \nabla^{-1} \dot{x}(t). \quad (6-18)$$

By varying the value for  $s$ , Equations (6-15) and (6-16) define the Adams-Cowell predictor-corrector formulas, as well as the Newtonian interpolation and starting formulas (Reference 6). For example, the Adams-Cowell predictor formulas are obtained by setting  $s = 1$  and  $x_n = x(t_n) = x(t_0 + nh)$  to give

$$\dot{x}_{n+1} = h \left[ \nabla^{-1} \ddot{x}_n + \sum_{i=0}^k \gamma_{i+1}'(1) \nabla^i \ddot{x}_n \right] \quad (6-19)$$

and

$$x_{n+1} = h^2 \left[ \nabla^{-2} \ddot{x}_n + \sum_{i=0}^k \gamma_{i+2}''(1) \nabla^i \ddot{x}_n \right] \quad (6-20)$$

The preceding equations may be expressed in ordinate form as

$$\dot{x}_{n+1} = h \left[ z S_n + \sum_{i=0}^k \beta_i \ddot{x}_{n-i} \right] \quad (6-21)$$

$$x_{n+1} = h^2 \left[ w S_n + \sum_{i=0}^k \alpha_i \ddot{x}_{n-i} \right] \quad (6-22)$$

where

$$IS_n = \nabla^{-1} \ddot{x}_n \quad (6-23)$$

$$IIS_n = \nabla^{-2} \ddot{x}_n \quad (6-24)$$

The coefficients  $\alpha_i$  and  $\beta_i$  can be expressed as functions of  $\gamma'_i$  and  $\gamma''_i$  from the recursive relations given by Equations (6-9) through (6-14), e. g.,

$$\alpha_i = (-1)^i \sum_{m=i}^k \binom{m}{i} \gamma''_{m+2} \quad (1) \quad (6-25)$$

$$i = 0, 1, 2, \dots, k$$

The Adams-Cowell corrector formulas are obtained from Equations (6-15) and (6-16) by setting  $s = 0$  and  $t = t_{n+1}$  yielding

$$\dot{x}_{n+1} = h \left[ IS_{n+1} + \sum_{i=0}^k \beta_i^* \ddot{x}_{n+1-i} \right] \quad (6-26)$$

and

$$x_{n+1} = h^2 \left[ IIS_n + \sum_{i=0}^k \alpha_i^* \ddot{x}_{n+1-i} \right] \quad (6-27)$$

where  $\alpha_i^*$  and  $\beta_i^*$  are computed analogously to  $\alpha_i$  and  $\beta_i$  but using  $\gamma''_i(0)$  and  $\gamma'_i(0)$ . The  $\beta_i$  and  $\beta_i^*$  are called the summed ordinate Adams-Moulton predictor-corrector coefficients and  $\alpha_i$  and  $\alpha_i^*$  the corresponding Störmer-Cowell coefficients.

These coefficients are tabulated in rational form in Reference 5 for formulas of order 4 through 15.



## 6.2 PREDICT-PSEUDO CORRECT ALGORITHM FOR EQUATIONS OF MOTION

The concept of pseudo-evaluation is introduced as a device which helps stabilize the numerical integration at little or no cost in computation. It is recognized that

(1) In a predictor-corrector scheme, the numerical stability region is proportional to the number of derivative evaluations within a given step (Reference 7);

(2) For systems of the form

$$\dot{\mathbf{x}} = \mathbf{f}(\mathbf{x}) + \epsilon \mathbf{g}(\mathbf{x})$$

where  $\epsilon$  is a small parameter, the stability region is mainly influenced by the  $\mathbf{f}(\mathbf{x})$  term.

The idea, then, is to introduce into a predictor-corrector algorithm designed to solve the above system a "pseudo-evaluation", i.e., a partial evaluation of  $\dot{\mathbf{x}}$ , where  $\mathbf{f}(\mathbf{x})$  is recomputed using the latest corrected value of  $\mathbf{x}$ , and  $\mathbf{g}(\mathbf{x})$  is re-evaluated based on a previous value of  $\mathbf{x}$ . For example, assume that the equations to be integrated have the form

$$\ddot{\bar{\mathbf{R}}} = \frac{-\mu \bar{\mathbf{R}}}{R^3} + \bar{\mathbf{P}}(t, \bar{\mathbf{R}}, \dot{\bar{\mathbf{R}}}) \quad (6-28)$$

where the first term represents the primary attracting body acting on the satellite. Assuming the accelerations and sums

$$\ddot{\bar{\mathbf{R}}}(t_{n-i}), \quad {}^i\mathbf{S}_n = \nabla^{-1} \ddot{\bar{\mathbf{R}}}_n, \quad {}^{ii}\mathbf{S}_n = \nabla^{-2} \ddot{\bar{\mathbf{R}}}_n, \quad i = 0, 1, 2, \dots, k \quad (6-29)$$

are known, then the iterative algorithm to advance to time  $t_{n+1}$  is

(A) Predict: Using Equations (6-21) and (6-22), predict values (denoted by superscript  $p$ )

$$\bar{\mathbf{R}}^{(p)}(t_{n+1}) = [\mathbf{X}_{n+1}^{(p)}, \mathbf{Y}_{n+1}^{(p)}, \mathbf{Z}_{n+1}^{(p)}] \quad (6-30)$$

$$\dot{\bar{\mathbf{R}}}^{(p)}(t_{n+1}) = [\dot{\mathbf{X}}_{n+1}^{(p)}, \dot{\mathbf{Y}}_{n+1}^{(p)}, \dot{\mathbf{Z}}_{n+1}^{(p)}] \quad (6-31)$$

(B) Evaluate: Using Equation (6-28), evaluate

$$\ddot{\bar{R}}(t_{n+1}) = \frac{-\mu \bar{R}_{n+1}^{(p)}}{R_{n+1}^{(p)3}} + P(t_{n+1}, \bar{R}_{n+1}^{(p)}, \dot{\bar{R}}_{n+1}^{(p)}) \quad (6-32)$$

(C) Correct: Using Equations (6-26) and (6-27), obtain improved values, (denoted by the superscript c)  $\bar{R}_{n+1}^{(c)}$  and  $\dot{\bar{R}}_{n+1}^{(c)}$ .

(D) Test: Compare the magnitude of the vector  $[\bar{R}^{(p)}(t_{n+1}) - \bar{R}^{(c)}(t_{n+1})]$  against a prescribed tolerance. If this quantity is sufficiently small, proceed to Step (E); otherwise, replace the values  $\bar{R}^{(p)}$  and  $\dot{\bar{R}}^{(p)}$  with  $\bar{R}^{(c)}$  and  $\dot{\bar{R}}^{(c)}$  and repeat Steps (B), (C), and (D).

(E) Pseudo Correct: Compute the acceleration

$$\ddot{\bar{R}}(t_{n+1}) = \frac{-\mu \bar{R}_{n+1}^{(c)}}{R_{n+1}^{(c)3}} + P(t_{n+1}, \bar{R}_{n+1}^{(p)}, \dot{\bar{R}}_{n+1}^{(p)}) \quad (6-33)$$

where the P term is obtained from Step B.

(F) Update Sums: Compute the updated sums

$$IS_{n+1} = IS_n + \ddot{\bar{R}}(t_{n+1}) \quad (6-34)$$

$$IIS_{n+1} = IIS_n + IS_{n+1} \quad (6-35)$$

The computational cycle (A) → (F) may then be repeated with  $n = n + 1$ .

In n-body or earth-moon trajectory computations, the equations of motion will frequently be independent of the velocity term  $\dot{\bar{R}}$ , i. e., the acceleration is of the form

$$\ddot{\bar{R}} = \frac{-\mu \bar{R}}{R^3} + P(t, \bar{R}) \quad (6-36)$$

For trajectory segments possessing this characteristic, the preceding computational cycle may be simplified. Particularly in Step (A), the predicted  $\dot{\bar{R}}^{(p)}$  need not be computed, and in Step (C), the provisional corrected values  $\dot{\bar{R}}^{(c)}$  are not required. After the test in Step (D) is satisfied,  $\dot{\bar{R}}^{(c)}$  may be obtained by one application of the corrector formula in Equation (6-26).

For the case of the integration of VOP type formulations, the concept of pseudo-evaluation should be extended to include the major perturbation beyond the central force, in particular,  $J_2$  for near-earth satellites (Reference 7). This is due to the fact that in these formulations the stability is governed by the principal perturbations; the central force contribution is analytically integrated and hence does not influence numerical stability.

### 6.3 CORRECTOR-ONLY COWELL INTEGRATION FOR LINEAR SYSTEMS

From the Adams-Cowell corrector equations

$$y_{n+1} = h^2 \left[ I^1 S_n + \sum_{i=0}^k \alpha_i^* \ddot{y}_{n+1-i} \right] \quad (6-37)$$

and

$$\dot{y}_{n+1} = h \left[ I S_n + \sum_{i=0}^k \beta_i^* \ddot{y}_{n+1-i} \right] \quad (6-38)$$

closed form equations can be derived when the equation being integrated is linear. Such a linear equation is

$$\ddot{y} = a(t) y + b(t) \dot{y} + f(t) \quad (6-39)$$

where  $a(t)$ ,  $b(t)$  and  $f(t)$  are known time varying functions.

Equations (6-37) and (6-38) can be written as

$$y_{n+1} = h^2 \left[ I^1 S_n + \alpha_0^* \ddot{y}_{n+1} + \sum_{i=1}^k \alpha_i^* \ddot{y}_{n+1-i} \right] \quad (6-40)$$

$$\dot{y}_{n+1} = h \left[ I S_n + \beta_0^* \ddot{y}_{n+1} + \sum_{i=1}^k \beta_i^* \ddot{y}_{n+1-i} \right] \quad (6-41)$$

By expanding the derivative  $\ddot{y}_{n+1}$ , we obtain

$$y_{n+1} = h^2 \left[ I I S_n + a_0^* a_{n+1} y_{n+1} + a_0^* b_{n+1} \dot{y}_{n+1} + a_0^* f_{n+1} + \sum_{i=1}^k a_i^* \ddot{y}_{n+1-i} \right] \quad (6-42)$$

$$\dot{y}_{n+1} = h \left[ I S_n + \beta_0^* a_{n+1} y_{n+1} + \beta_0^* b_{n+1} \dot{y}_{n+1} + \beta_0^* f_{n+1} + \sum_{i=1}^k \beta_i^* \ddot{y}_{n+1-i} \right] \quad (6-43)$$

Defining the known quantities

$$x_n = h^2 \left[ I I S_n + a_0^* f_{n+1} + \sum_{i=1}^k a_i^* \ddot{y}_{n+1-i} \right] \quad (6-44)$$

$$v_n = h \left[ I S_n + \beta_0^* f_{n+1} + \sum_{i=1}^k \beta_i^* \ddot{y}_{n+1-i} \right] \quad (6-45)$$

and the matrix

$$H = \begin{bmatrix} h^2 a_0^* a_{n+1} & h^2 a_0^* b_{n+1} \\ h \beta_0^* a_{n+1} & h \beta_0^* b_{n+1} \end{bmatrix} \quad (6-46)$$

then Equations (6-42) and (6-43) may be written as

$$\begin{bmatrix} y_{n+1} \\ \dot{y}_{n+1} \end{bmatrix} = H \begin{bmatrix} y_{n+1} \\ \dot{y}_{n+1} \end{bmatrix} + \begin{bmatrix} x_n \\ v_n \end{bmatrix} \quad (6-47)$$

The solution to Equation (6-47) is

$$\begin{bmatrix} y_{n+1} \\ \dot{y}_{n+1} \end{bmatrix} = [I - H]^{-1} \begin{bmatrix} x_n \\ v_n \end{bmatrix} \quad (6-48)$$

It should be noted that the inverse in the preceding equation will always exist if  $h$  is sufficiently small. The inverse depends only on the coefficients  $a$  and  $b$ , and need be computed only once when solving equations of the form of Equation (6-39) with different nonhomogeneous terms  $f(t)$ .

#### 6.4 CORRECTOR-ONLY ALGORITHM FOR VARIATIONAL EQUATIONS

In the Cowell formulation, the position and velocity partial derivatives of the satellite motion with respect to any parameter appearing in the acceleration model in Equation (6-28) or state (dynamic parameters) may be obtained by the numerical integration of a system of equations of the form

$$\ddot{Y} = A(t) Y + B(t) \dot{Y} + C(t) \quad (6-49)$$

from initial conditions at  $t_0$  given by

$$Y(t_0) = \frac{\partial \bar{R}(t_0)}{\partial \bar{p}} \quad \dot{Y}(t_0) = \frac{\partial \dot{\bar{R}}(t_0)}{\partial \bar{p}} \quad (6-50)$$

where

$$A(t) = \left[ \frac{\partial \ddot{\bar{\mathbf{R}}}(t)}{\partial \bar{\mathbf{p}}} \right]_{3 \times 3} \quad (6-51)$$

$$B(t) = \left[ \frac{\partial \dot{\bar{\mathbf{R}}}(t)}{\partial \bar{\mathbf{p}}} \right]_{3 \times 3} \quad (6-52)$$

$$C(t) = \left[ \frac{\partial \ddot{\bar{\mathbf{R}}}(t)}{\partial \bar{\mathbf{p}}} \right] \quad \left\{ \begin{array}{l} 3 \times \ell \text{ matrix of} \\ \text{acceleration partial derivatives} \end{array} \right\} \quad (6-53)$$

$$Y(t) = \left[ \frac{\partial \bar{\mathbf{R}}(t)}{\partial \bar{\mathbf{p}}} \right] \quad \left\{ \begin{array}{l} 3 \times \ell \text{ matrix of} \\ \text{position partial derivatives} \end{array} \right\} \quad (6-54)$$

and

$$\dot{\mathbf{Y}}(t) = \left[ \frac{\partial \dot{\bar{\mathbf{R}}}(t)}{\partial \bar{\mathbf{p}}} \right] \quad \left\{ \begin{array}{l} 3 \times \ell \text{ matrix of} \\ \text{velocity partial derivatives} \end{array} \right\} \quad (6-55)$$

The vector  $\bar{\mathbf{p}}$  contains the parameters in the acceleration model to be estimated.

The components of the matrices A, B, and C were developed in Chapter 4.

Optionally, the components of  $\bar{\mathbf{p}}$  correspond to the spacecraft's position and velocity at epoch and can be expressed in mean of 1950.0 Cartesian coordinates, true of date Cartesian coordinates, classical Keplerian orbital elements, spherical coordinates, or DODS variables. The initial conditions for the variational equations, Equation (6-49), are dependent upon the coordinate systems selected. The partial derivatives of  $\bar{\mathbf{R}}$  and  $\dot{\bar{\mathbf{R}}}$  with respect to Keplerian elements and spherical coordinates can be obtained from Sections 3.3.8 and 3.3.4, respectively. Since the first six elements of  $\bar{\mathbf{p}}$  are the state vector, the first six columns of C are zero. Most model parameters such as thrust, drag, harmonic coefficients, etc. enter into  $\mathbf{P}(t, \bar{\mathbf{R}}, \dot{\bar{\mathbf{R}}})$  of Equation (6-28) linearly, so that the computation of C(t) may be simplified by retaining many of the quantities used in the computation of  $\ddot{\bar{\mathbf{R}}}(t)$ .

The integration of system Equation (6-49) may be performed by the utilization of the corrector-only formula Equation (6-48) as follows. Assuming that the satellite position and velocity,  $\bar{R}(t_{n+1})$  and  $\dot{\bar{R}}(t_{n+1})$ , the matrices  $\ddot{Y}_{n+1-i}$   $i = 0, 1, 2, \dots, k$  and summation matrices  ${}^I P_n$  and  ${}^{II} P_n$  ( $3 \times \ell$ ) are known, then the algorithm to advance  $Y$  to time  $t_{n+1}$  is:

(A) Compute the matrices  $A(t_{n+1})$ ,  $B(t_{n+1})$ , and  $C(t_{n+1})$ , which depend only on  $t_{n+1}$ ,  $\bar{R}_{n+1}$ , and  $\dot{\bar{R}}_{n+1}$ .

(B) Compute the  $6 \times 6$  matrix  $[I - H]^{-1}$  where

$$H = \begin{bmatrix} h^2 \alpha_0^* A_{n+1} & h^2 \alpha_0^* C_{n+1} \\ h \beta_0^* A_{n+1} & h \beta_0^* C_{n+1} \end{bmatrix} \quad (6-56)$$

$\alpha_0^*$  and  $\beta_0^*$  are the corrector coefficients of Equations (6-26) and (6-27), and  $h$  is the stepsize.

(C) Form the  $3 \times \ell$  matrices,  $X_n$  and  $V_n$ .

$$X_n = h^2 \left[ {}^I P_n + \sum_{i=1}^k \alpha_i^* \ddot{Y}_{n+1-i} + \alpha_0^* C_{n+1} \right] \quad (6-57)$$

$$V_n = h \left[ {}^I P_n + \sum_{i=1}^k \beta_i^* \ddot{Y}_{n+1-i} + \beta_0^* C_{n+1} \right] \quad (6-58)$$

(D) Compute the required position and velocity partial derivatives,  $Y_{n+1}$  and  $\dot{Y}_{n+1}$ , by the matrix equation

$$\begin{bmatrix} Y_{n+1} \\ \dot{Y}_{n+1} \end{bmatrix}_{6 \times \ell} = [I - H]_{6 \times 6}^{-1} \begin{bmatrix} X_n \\ V_n \end{bmatrix}_{6 \times \ell} \quad (6-59)$$

(E) Update acceleration and sums by

$$\ddot{Y}_{n+1} = A_{n+1} Y_{n+1} + B_{n+1} \dot{Y}_{n+1} + C_{n+1} \quad (6-60)$$

$${}^I P_{n+1} = {}^I P_n + \ddot{Y}_{n+1} \quad (6-61)$$

$${}^{II} P_{n+1} = {}^{II} P_n + {}^I P_{n+1} \quad (6-62)$$

completing the cycle. After computing  $\bar{R}_{n+2}$  and  $\dot{\bar{R}}_{n+2}$ , Steps (A) → (E) may be repeated with  $n = n + 1$ .

At points along the trajectory where the equations of motion are velocity-free, i. e., of the form of Equation (5-36), the matrix B in Equation (6-49) is zero, so that it is necessary to solve a system of the form

$$\ddot{Y} = A(t) Y + C(t) \quad (6-63)$$

As in the case of the equations of motion, the computational algorithm can then be simplified. In particular, in Step (A) only the matrices A and C are required, and in Step B, H becomes the  $3 \times 3$  matrix

$$H = h^2 \alpha_0^* A_{n+1} \quad (6-64)$$

The required partial derivatives are then given by

$$Y_{n+1} = [I - H]^{-1} X_n \quad (6-65)$$

$$\dot{Y}_{n+1} = h \beta_0^* A_{n+1} Y_{n+1} + V_n \quad (6-66)$$

The order and stepsize used in the integration of the variational equations may differ from that used in the integration of the equations of motion without any significant difficulty.



## 6.5 MAPPING OF POSITION PARTIAL DERIVATIVES

It is well known from the theory of linear differential equations that the solution of the  $n$ -dimensional linear system

$$\dot{\bar{x}} = D(t) \bar{x} \quad (6-67)$$

satisfying the initial condition

$$\bar{x}(t_0) = \bar{x}_0 \quad (6-68)$$

is given by

$$\bar{x}(t) = \Phi(t, t_0) \bar{x}_0 \quad (6-69)$$

where  $\Phi$  is a fundamental matrix solution of Equation (6-67), i. e., an  $n \times n$  matrix satisfying

$$\dot{\Phi} = D(t) \Phi \quad (6-70)$$

with initial condition

$$\Phi(t_0, t_0) = I \quad (6-71)$$

In our context,  $\Phi(t, t_0)$  is called the state transition matrix. The properties of  $\Phi$  can be used to enhance the computational algorithm for position and velocity partial derivatives as follows: during the integration of a trajectory, a column of  $C(t)$  corresponding to a dynamic parameter may become zero. For example, when leaving the sphere of influence of the earth, the acceleration partial derivative with respect to a geopotential coefficient of the earth will become effectively zero. If we denote this time by  $T$ , then the position partial derivative with respect to this parameter, which we denote by  $x_j(t)$ , will satisfy an equation of the form of Equation (6-67) for  $t > T$  where

$$D(t) = \begin{bmatrix} 0 & I \\ A(t) & B(t) \end{bmatrix}_{6 \times 6} \quad (6-72)$$

with an initial condition  $\bar{x}(T)$ . Let  $\Phi(t, T)$  be the state transition matrix satisfying  $\Phi(T, T) = I$ . Then, the required position partial derivative may be obtained for any  $t > T$  by

$$\bar{x}(t) = \Phi(t, T) \bar{x}(T) \quad (6-73)$$

The overall state transition matrix  $\Phi(t, t_0)$  for  $t > T$  may be computed by

$$\Phi(t, t_0) = \Phi(t, T) \Phi(T, t_0) \quad (6-74)$$

where the elements of the matrix  $\Phi(T, t_0)$  are

$$\Phi(T, t_0) = \begin{bmatrix} \frac{\partial \bar{K}(T)}{\partial \bar{R}_0} & \frac{\partial \bar{R}(T)}{\partial \dot{\bar{R}}_0} \\ \frac{\partial \dot{\bar{R}}(T)}{\partial \bar{R}_0} & \frac{\partial \dot{\bar{R}}(T)}{\partial \dot{\bar{R}}_0} \end{bmatrix} \quad (6-75)$$

which are contained in the  $Y$  and  $\dot{Y}$  matrices when  $t = T$  (assuming  $\bar{p}$  contains the state). The computational strategy for the computation of the partial derivative of  $\bar{x}(t)$  is to use the method of Section 6.3 up to  $t = T$ . At that point the matrix  $\Phi(T, t_0)$  is stored,  $\Phi(T, T)$  is initialized, and for any  $t > T$ ,  $\bar{x}(t)$  is computed using Equation (6-73), and  $\Phi(t, t_0)$  is computed using Equation (6-74). A similar process may be used for multiple event times  $T_1, T_2, \dots, T_r$  at which various columns of  $C(t)$  become zero. Assuming  $T_1 \leq T_2 \leq \dots \leq T_r \leq t$ , Equation (6-74) becomes

$$\Phi(t, t_0) = \Phi(t, T_r) \Phi(T_r, T_{r-1}) \dots \Phi(T_1, t_0) \quad (6-76)$$

## 6.6 THE RUNGE-KUTTA INTEGRATION METHOD

The Runge-Kutta method is a numerical integration technique by means of which the value of the dependent variable at some future time can be calculated from a weighted summation formula, similar to a numerical quadrature. This method is equivalent to a Taylor series solution of the equations of motion up to a certain power of the integration stepsize in the independent variable. Taylor series

24  
 solutions require differentiation of a given function a number of times, followed by evaluation of these derivatives at the point of interest. However, the Runge-Kutta method bypasses these differentiations by evaluating the derivative on the right hand side of the first order equation at a number of selected points. For example, in the equations of motion the acceleration per unit mass is evaluated a number of times at each integration step in order to proceed to the next integration step.

Runge-Kutta methods have the advantage that the interval of integration can be readily changed. The formulas are single step; thus, they do not require any past history of values. In common with other special perturbation methods, the Runge-Kutta method is extremely flexible. The acceleration models in GTDS may be changed without affecting the implementation of the Runge-Kutta formulation.

The Runge-Kutta formula used in GTDS is an eighth order formulation requiring ten function evaluations (Reference 8). The expression  $f(x, y)$  is the derivative on the right hand side of the first order differential equation  $dx/dy = f(x, y)$  which is to be evaluated. This function arises from the equations of motion or from the variational equations. The Shanks eighth order Runge-Kutta algorithm is computed in the following manner. The following formulas apply to a single component of the vector of the quantities being integrated where the vector of dependent variables is denoted by  $\bar{x}$  and the independent variable is denoted by  $y$ .

$$f_0 = f(\bar{x}_0, y_0)$$

$$f_1 = f(\bar{x}_0 + k_1, y_0 + a_1 h)$$

.

.

.

$$f_9 = f(\bar{x}_0 + k_9, y_0 + a_9 h)$$

where

$$k_1 = a_1 h b_{1,0} f_0$$

$$k_2 = a_2 h \sum_{j=0}^1 b_{2,j} f_j$$

.

.

.

$$k_9 = a_9 h \sum_{j=0}^9 b_{9,j} f_j$$

The next value of the component  $x$  is computed from the present value  $x_0$  and the Shanks coefficients  $a_i, b_{ij}, c_i$

$$x = \bar{x}_0 + \sum_{i=0}^9 c_i f_i$$

In these formulas, the Runge-Kutta stepsize in the independent variable is denoted by  $h$ , and the subscript "0" designates current values. Table 6-1 contains the coefficients for the eighth order Runge-Kutta scheme; the coefficients are presented in a form convenient for calculating the summations required to determine the  $k_i$ 's.

TABLE 6-1

$i$	$a_i$	$a_i \sum_{j=0}^{i-1} b_{ij}$
1	$\frac{4}{27}$	$\frac{4}{27}$
2	$\frac{2}{9}$	$\frac{1}{18} (1 + 3)$
3	$\frac{1}{3}$	$\frac{1}{12} (1 + 0 + 3)$
4	$\frac{1}{2}$	$\frac{1}{8} (1 + 0 + 0 + 3)$
5	$\frac{2}{3}$	$\frac{1}{54} (13 + 0 - 27 + 42 + 8)$
6	$\frac{1}{6}$	$\frac{1}{4320} (389 + 0 - 54 + 966 - 824 + 243)$
7	1	$\frac{1}{20} (-231 + 0 + 81 - 1164 + 656 - 122 + 800)$
8	$\frac{5}{6}$	$\frac{1}{288} (-127 + 0 + 18 - 678 + 456 - 9 + 576 + 4)$
9	1	$\frac{1}{820} (1481 + 0 - 81 + 7104 - 3376 + 72 - 5040 - 60 + 720)$

$$(c_0+c_1+c_2+c_3+c_4+c_5+c_6+c_7+c_8+c_9) = \frac{1}{840} (41 + 0 + 0 + 27 + 272 + 27 + 216 + 0 + 216 + 41)$$

## 6.7 THE STARTING PROCEDURE

Two starting procedures are available in GTDS, an iterative method and a Runge-Kutta method. The iterative starter is generally used; however, the Runge-Kutta method may optionally be used as a starter for multi-step integration methods.

### 6.7.1 Iterative Starter

The starting arrays

$$\ddot{\bar{R}}_{n-i}, \ddot{Y}_{n-i}, i = 0, 1, 2, \dots k \quad (6-77)$$

and the associated first and second sums required by the integration process may be computed by an iterative process based on Equations (6-15) and (6-16) using varying values for  $s$ . Let  $m = [(k+1)/2]$ , where the brackets indicate the greatest integer function, and  $\bar{R}_0$ ,  $\dot{\bar{R}}_0$ , and  $\ddot{\bar{R}}_0$  be the given initial values at  $t = t_0$  of Equation (6-28) (the process is analogous for Equation (6-49)). The values

$$\bar{R}_i, \dot{\bar{R}}_i, \ddot{\bar{R}}_i, i = \pm 1, \pm 2, \dots \pm m$$

can then be computed by successive approximations, yielding the required starting values.

Let  $\delta_i'(s)$  and  $\delta_i''(s)$  be the coefficients of the ordinate forms of Equations (6-15) and (6-16) with  $k = 2m$

$$\dot{x}(t_n + sh) = h \left[ {}^I S_n + \sum_{i=0}^{2m} \delta_i'(s) \ddot{x}_{n-i} \right] \quad (6-78)$$

$$x(t_n + sh) = h^2 \left[ {}^{II} S_n + (s-1) {}^I S_n + \sum_{i=0}^{2m} \delta_i''(s) \ddot{x}_{n-i} \right] \quad (6-79)$$

Then letting  $\bar{R}^{(j)}$  denote the  $j^{\text{th}}$  approximation, the  $(j+1)^{\text{st}}$  approximation is given by the following procedure

(A) Compute the sums  ${}^I S_m$  and  ${}^{II} S_m$  using

$${}^I S_m = \frac{\dot{\bar{R}}_0}{h} - \sum_{i=0}^{2m} \delta_i'(-m) \ddot{\bar{R}}_{m-i}^{(j)} \quad (6-80)$$

$${}^I\dot{S}_m = \frac{\bar{R}_0}{h^2} + (m+1) {}^I\dot{S}_m - \sum_{i=0}^{2m} \delta_i'' (-m) \ddot{R}_{m-i}^{(j)} \quad (6-81)$$

(B) Compute the corrected position and velocity vectors using Equations (6-79) and (6-78) with  $n = m$  and  $s = (i-m)$

$$\bar{R}_i^{(j+1)} = h^2 \left[ {}^I\dot{S}_m + (i-m-1) {}^I\dot{S}_m + \sum_{\ell=0}^{2m} \delta_\ell'' (i-m) \ddot{R}_{m-\ell}^{(j)} \right] \quad (6-80)$$

$$\dot{\bar{R}}_i^{(j+1)} = h \left[ {}^I\dot{S}_m + \sum_{\ell=0}^{2m} \delta_\ell' (i-m) \ddot{R}_{m-\ell}^{(j)} \right] \quad (6-81)$$

$i = \pm 1, \pm 2, \dots, \pm m$

(C) Compute the acceleration  $\ddot{R}_i^{(j+1)}$  using the force model. This completes the iteration. Steps (A) - (C) are repeated until the successive values of  $\bar{R}_i$  and  $\dot{\bar{R}}_i$  converge.

As in the process described in Section 6.2, if the accelerations are velocity-free, simplifications in the computational algorithm may be made. In particular, in Step (B) the computation of  $\dot{\bar{R}}_i^{(j+1)}$  may be omitted until convergence on the positions  $\bar{R}_i$ .

The first approximation ( $j = 1$ ) may be obtained by a variety of methods: Near a primary, two-body analysis may be used effectively, either in the form of orbital elements or  $f$  and  $g$  series; between two primaries, either a single step low-order method or the use of a prestored ephemeris should be used.

### 6.7.2 Runge-Kutta Starter

The multi-step methods avoid the multiple function evaluations at each integration step which are characteristic of the Runge-Kutta method, but they are not self-starting. Starting from an initial position and velocity, the Runge-Kutta method can be used to build the required starting array for the Cowell and Time Regularized Cowell equations of motion and variational equations.

## 6.8 INTERPOLATION

Interpolation for values of  $\bar{R}(t)$  and  $\dot{\bar{R}}(t)$  for  $t_{n-1} < t < t_n$  may be obtained from Equations (6-79) and (6-78) using  $s = (t - t_{n-1})/h$ . The accuracy of this interpolation is consistent with that of the integration.

## 6.9 LOCAL ERROR CONTROL

Local error control is performed by a variable stepsize process automatically and semiautomatically (see References 9 and 10). In the automatic mode, step-sizes are selected based on the magnitude of the local error,  $\epsilon_n$ , computed on a step-by-step basis by the Milne formula

$$\epsilon_n = \frac{C |\bar{R}_n^{(p)} - \bar{R}_n^{(c)}|}{|\bar{R}_n^{(c)}|} \quad (6-84)$$

where  $C$  is a constant depending on the order of Equations (6-22) and (6-27).  $\bar{R}_n^{(p)}$  and  $\bar{R}_n^{(c)}$  are the predicted and finally accepted position vectors, respectively, computed at time  $t = t_n$ . The stepsizes are selected so that  $\epsilon_n$  at each step satisfies the constraint equation

$$T_2 \leq \epsilon_n \leq T_1 \quad (6-85)$$

where  $T_1$  and  $T_2$  are specified upper and lower bounds on the local error.

The variable stepsize integration algorithm is as follows: at each step  $n$ , the test in Equation (6-85) is performed. There are three cases:

- (A)  $\epsilon_n > T_1$ ; the stepsize is decreased, and the  $n^{\text{th}}$  computed point is rejected and recomputed with the new stepsize, where the required back values are obtained by interpolation.
- (B)  $\epsilon_n < T_2$ ; the stepsize is increased, the  $n^{\text{th}}$  computed point is accepted and the integration proceeds with the new stepsize, where the required back values are obtained by using every other point from a saved array of points if  $h_{\text{new}} = 2h$  or by interpolation if  $h < h_{\text{new}} < 2h$ . A maximum increase of  $2h$  is allowed.

(C)  $\epsilon_n$  satisfies Equation (6-85); the integration proceeds uninterrupted.  
 In either case (A) or (B),  $h_{new}$  is computed by the formula

$$h_{new} = h \left[ \frac{T_3}{\epsilon_n} \right]^{1/k} \quad (6-86)$$

where  $T_3$  is a specified "allowable" local error satisfying  $T_2 \leq T_3 \leq T_1$ .

In the semiautomatic mode, stepsizes are specified as a function of radial distances from the primary (Reference 10). The required stepsizes and radial distances may be determined by an integration calibration process using the automatic variable stepsize integrator. Since the stepsize distribution over the orbit generally depends on the orbital elements, particularly the semimajor axis and eccentricity, such a calibration would be repeated only if these elements changed considerably. This model of integration is generally less sensitive to the numerical difficulties associated with variable stepsize integration. The use of a regularized time variable also proves useful for this problem. This technique is described in the next section.

The same stepsizes are used for integration of the variational equations and the equations of motion.

## 6.10 TIME REGULARIZATION

For orbits that are highly eccentric or that connect regions with significantly different gravitational force magnitudes, accurate direct integration of Equation (6-28) or (6-49), with time as the independent variable, usually requires either a very small fixed stepsize, or many stepsize changes in a variable stepsize scheme. Frequent stepsize changes are costly and result in errors propagating due to the interpolation procedure used to restart.

To improve this situation, the classical approach is to transform the independent variable to a new variable, denoted by  $\tau$ , defined by the relation (Reference 11)

$$\frac{dt}{d\tau} = \frac{R^n}{\sqrt{\mu}} \quad 1 \leq n \leq 2 \quad (6-87)$$



For  $n = 1$  or  $2$ , this variable corresponds to the use of eccentric anomaly or true anomaly as the independent variable in the integration of elliptic motion. The use of regularization in the computation of free-flight earth-moon trajectories is investigated in Reference 12. This study indicates increased computational accuracy and a significant reduction in computation time due to regularization.

To express Equation (6-28) or (6-49) in terms of the new independent variable  $\tau$ , the following notation is employed

$$D g = \frac{d g}{d \tau} = \frac{R^n}{\sqrt{\mu}} \dot{g} \quad (6-88)$$

$$D^2 g = \frac{d^2 g}{d \tau^2} = \frac{R^n}{\mu} [n R^{n-1} \dot{R} \dot{g} + R^n \ddot{g}] \quad (6-89)$$

where

$$\dot{R} = \frac{\bar{R} \cdot \dot{\bar{R}}}{R} \quad (6-90)$$

and  $g(t)$  is any arbitrary vector-valued function in the  $t$  system. Similarly,

$$D^{-1} g = \dot{g} = \frac{\sqrt{\mu}}{R^n} g' \quad (6-91)$$

$$D^{-2} g = \ddot{g} = \frac{\mu}{R^n} \left[ R^{-n} g'' - \frac{n R'}{R^{n+1}} g' \right] \quad (6-92)$$

where the prime indicates differentiation with respect to  $\tau$ , and

$$R' = \frac{R^{n-1}}{\sqrt{\mu}} (\bar{R} \cdot \dot{\bar{R}}) \quad (6-93)$$

The transformed Equation (6-28) may then be expressed as

$$\bar{R}'' = D^2 \bar{R}(\tau) \quad (6-94)$$

$$t'' = \frac{n R^{2n-1} \dot{R}}{\mu} \quad (6-95)$$

The integration of Equation (6-95) is required to compute the time  $t$  as a function of the new independent variable  $\tau$ .

The integration of Equations (6-94) and (6-95) may be carried out with essentially the same procedures outlined in the previous sections. The additional remarks required are:

- (A) Given  $t(\tau)$ ,  $\bar{R}(\tau)$ , and  $\bar{R}'(\tau)$ , a corresponding  $\bar{R}''(\tau)$  is computed by first computing the time derivatives

$$\dot{\bar{R}}(\tau) = D^{-1} \bar{R}' = \frac{\sqrt{\mu}}{R^n(\tau)} \bar{R}'(\tau) \quad (6-96)$$

and

$$\ddot{\bar{R}}(\tau) = \frac{-\mu \bar{R}(\tau)}{R^3(\tau)} + P[t(\tau), \bar{R}(\tau), \dot{\bar{R}}(\tau)] \quad (6-97)$$

yielding

$$\bar{R}''(\tau) = \frac{n R' \bar{R}'}{R} - R^{2n-3} \bar{R} + \frac{R^{2n}}{\mu} P\left(t, \bar{R}, \frac{\sqrt{\mu}}{R^n} R'\right) \quad (6-98)$$

- (B) The value of the independent variable  $\tau$  corresponding to an output request time or observation time  $t_r$  may be obtained by inverse interpolation in the  $t_i$  array obtained by the integration of Equation (6-95). This value of  $\tau$  may then be used to compute the required  $\bar{R}$  and  $\bar{R}'$  by the usual interpolation procedure indicated in Section 6.8.

Analogous regularization procedures may be used for Equation (6-49). The regularized variational equations are of the form

$$Y'' = \left[ \frac{R^{2n}}{\mu} A(t) \right] Y + \frac{R^n}{\sqrt{\mu}} \left[ B(t) + \frac{n \dot{R}}{R} \right] Y' + \frac{R^{2n}}{\mu} C(t) \quad (6-99)$$

An additional advantage of using regularized time is that the initial (fixed) step-size may be conveniently selected as a fraction of the regularized period  $S$ , where, if  $T$  is the satellite period,

$$S = \int_0^T \frac{\sqrt{\mu}}{R^n} dt \quad (6-100)$$

The integral may be evaluated by quadrature for the two-body problem by a change of variable from  $t$  to true anomaly,  $f$ , resulting in the formula

$$S = \frac{1}{p^{(n-2+1/2)}} \int_0^{2\pi} (1 + e \cos f)^{n-2} df \quad (6-101)$$

where  $p$  is the semilatus rectum of the ellipse. Frequently, a fraction of this period (of the order 1/100) will serve as an adequate stepsize for the integration of Equations (6-92) and (6-93).

A drawback of the method is that the equations of motion in the  $\tau$  system (Equation (6-94)) always contain explicit first derivatives, regardless of the situation in the  $t$  system, (see Equation (6-92)); thus, the computational simplifications possible for velocity-free accelerations do not apply. Hence, the trade-off between the advantages and disadvantages of the regularized time integration depend upon the stepsize, length of arc, efficiency requirements, and eccentricity magnitude.

Experience has shown that regularized time integration considerably improves the efficiency of variable stepsize integration for moderate to high eccentricities ( $e \geq .2$ ). For the Cowell formulation, the value  $n = 3/2$  seems to give best results, whereas, for orbital element formulations, the optimum value of  $n$  appears to be 2 (Reference 13). Improvements in the accuracy of the integration of the time equation (Equation (6-95)) may also be obtained through use of a time element (see Appendix B).

## 11 REFERENCES

1. Moore, W. and Beaudet, P.: 1973, "The Testing of Fixed-Step Numerical Integration Processes for the Cowell Method of Special Perturbations," Proceedings of the Conference on the Numerical Solution of Ordinary Differential Equations, Springer Lecture Notes in Mathematics, Vol. 362.
2. Velez, C. E., Cefola, P., et al.: 1973, "Calculation of Precision Satellite Orbits with Non-Singular Elements," Proceedings of the Conference on the Numerical Solution of Ordinary Differential Equations, Springer Lecture Notes in Mathematics, Vol. 362.
3. Long, A., and Wei, S.: 1973, "Evaluation of GTDS Orbit Generators for the AE-C Mission," Computer Sciences Corporation Report No. 3000-07400-01TM, November 1973.
4. Beaudet, P.: 1974, "The Testing and Comparison of Various Methods of Special Perturbations," Computer Sciences Corporation Report No. 3000-08600-01TM, March 1974.
5. Maury, J. L., and Brodsky, G. P.: 1969, "Cowell Type Numerical Integration as Applied to Satellite Orbit Computation," Goddard Space Flight Center Report X-553-69-46, also NASA Report NASA-TM-X-63542, December 1969.
6. Peabody, P. R.: 1967, "DODS Mod-N Design," Computer Sciences Corporation Report No. ND-9758-104-2-1, August 1967.
7. Velez, C. E., and Dixon, B.: 1974, "On the Choice of Numerical Integration Methods in the Computation of Orbits," Goddard Space Flight Center Report X-582-74-97, April 1974.
8. Shanks, E. B.: 1966, "Solution of Differential Equations by Evaluation of Functions," Math. of Computation, Vol. 20, pp. 21-38.
9. Velez, C. E., and Brodsky, G. P.: 1969, "GEOSTAR-I, A Geopotential and Station Position Recovery System," Goddard Space Flight Center Report X-553-69-544, also NASA Report NASA-TM-X-63979, November 1969.
0. Jet Propulsion Laboratory: 1966, DPODP System Documentation, Vol. I, November 1966.
1. Tapley, B. D., Szebehely, V. and Lewallen, J. M.: 1969, "Trajectory Optimization Using Regularized Variables," AIAA Journal 7(6), September 1969, pp. 1010-1017.

12. Szebehely, V., Pierce, D. A., and Standish, E. M.: 1971, "A Group of Earth-to-Moon Trajectories with Consecutive Collisions," in Celestial Mechanics and Astrodynamics, (V. G. Szebehely, ed.), New York, Academic Press, p. 35.
13. Peñas, A.: 1973, "Accurate Integration of Orbits Using Delaunay-Similar Elements," Goddard Space Flight Center Report X-582-73-375, December 1973.

## OBSERVATION MODELS

Spacecraft tracking observations involve the measurement of some physical property of electromagnetic wave propagation between the tracking station and the spacecraft. The process of analytically relating the measurement quantities to the spacecraft state vector is referred to as observation modeling. This chapter presents the models and associated equations for computing observations within GTDS. The models consist of kinematic equations which yield the "ideal" values of the observations in trajectory-related units (e.g., range, range rate, azimuth, and elevation). Therefore, the modeled observations are functions of the spacecraft's best estimated position and velocity, as well as specified model parameters (e.g., tracking station location and timing errors). "Actual" data are usually preprocessed in a separate computer program which calibrates, time-corrects, smoothes, compact, and converts the raw tracking data into units compatible with the calculated observations. However, the preprocessor program does not correct for the effects of atmospheric refraction and may not correct for propagation times, transponder delays, or antenna mount errors. As a result, corrections for these systematic errors are computed in GTDS and applied to the "actual" data. Systematic errors may still be present, however, due to the preprocessor smoothing and compact.

The procedures and formulations presented in this chapter describe all data types which are implemented in GTDS. Section 7.1 presents a general description of the forms of the computed observations and their partial derivatives. Section 7.2 presents equations and transformations for modeling ideal observations and their partial derivatives for ground-based tracking systems. Sections 7.3, 7.4, and 7.5 discuss satellite-to-satellite tracking, radar altimeter tracking, and very long baseline interferometer tracking, respectively. Atmospheric effects are discussed in Section 7.6, and other corrections (light time delay, transponder delay, and antenna mount corrections) are presented in Section 7.7. Finally, the interrelationship between the observation models and the estimation process is summarized in Section 7.8.

## 7.1 GENERAL DESCRIPTION

The basic orbit determination process consists of differentially correcting estimates for a set of parameters from an observational model to minimize the sum of squares of the weighted differences between the measured observations and the corresponding quantities computed from the model. In GTDS, this model is assumed to be of the form

$$O_c = f_0 [\bar{r}_{1t}(t + \delta t, \bar{p}, \bar{r}_s), \dot{\bar{r}}_{1t}(t + \delta t, \bar{p}, \bar{r}_s)] + b + RF_c \quad (7-1)$$

where

$t \sim$  time tag of the observation.

$\delta t \sim$  timing bias.

$O_c \sim$  computed observation at corrected time  $t + \delta t$ .

$\bar{r}_{1t}, \dot{\bar{r}}_{1t} \sim$  vehicle position and velocity at an appropriate time related to  $t = t + \delta t$ . For most observations modeled in GTDS, the position and velocity are expressed in local tangent coordinates with respect to a station position  $\bar{r}_s$ . Other observations are modeled in terms of the vehicle inertial state vector. In either case, the state vector is dependent on the dynamic parameter vector  $\bar{p}$ .

$b \sim$  measurement bias or offset.

$f_0 \sim$  geometric relationship defined by the observation type at time  $t + \delta t$ .

$RF_c \sim$  correction to the observation due to atmospheric refraction, light time, transponder delay, antenna mount errors, etc.

The observational model parameters which may be estimated are:

$\bar{p} \sim$  dynamic parameters in the equations of motion which can be estimated. These include variables related to the position and velocity, gravitational harmonic coefficients, drag parameters, etc.

$\bar{r}_s \sim$  station location in earth-fixed coordinates.

$b \sim$  measurement bias, which depends on the measurement type and the tracking station.

$\delta t \sim$  timing bias, which is both station and pass dependent.

The observation models simulate the following tracking system data types:

- Goddard Range and Range Rate (GRARR) System, Applications Technology Satellite Range and Range Rate (ATSR) System, and Unified S-Band (USB) System

- (1) Range
  - (2) Range rate or range difference
  - (3) X angle or azimuth
  - (4) Y angle or elevation
- C-Band Radar
  - (1) Range
  - (2) Azimuth
  - (3) Elevation
- Minitrack Interferometer System
  - (1) Direction cosine  $\ell$
  - (2) Direction cosine  $m$
- Satellite-to-Satellite Tracking (SST)
  - (1) Round trip light time
  - (2) Round trip light time difference
- Radar Altimeter (RA)
  - (1) Altitude
- Very Long Baseline Interferometer (VLBI) System
  - (1) Time difference
  - (2) Time-rate difference

After preprocessing, some observations are converted to metric form while others are in the form of time intervals. In general, the time tag on each observation is converted to Universal Time Coordinated (UTC), which is derived from Atomic Time A.1 so as to be a close approximation to UT2 (Chapter 3).

The differential correction process requires the computation of the "computed" measurements and the systematic error corrections which are applied to the actual observation data. The process also requires computation of partial derivatives of the measurements with respect to the model parameters  $\bar{p}$ ,  $\bar{r}_s$ ,  $b$ , and  $\delta t$ . These partial derivatives can be expressed as follows



$$\frac{\partial O_c}{\partial \bar{p}} = \frac{\partial f_0}{\partial \bar{p}}$$

$$\frac{\partial O_c}{\partial \bar{r}_s} = \frac{\partial f_0}{\partial \bar{r}_s}$$

(7-2)

$$\frac{\partial O_c}{\partial b} = 1$$

$$\frac{\partial O_c}{\partial (\delta t)} = \frac{\partial f_0}{\partial (\delta t)} = \dot{f}_0$$

It is assumed that the partial derivatives of the systematic error correction terms  $RF_c$  with respect to  $\bar{p}$ ,  $\bar{r}_s$ ,  $b$  and  $\delta t$  are either zero or negligible.

## 7.2 GROUND BASED TRACKER MODELS

This section presents the transformations and equations for computing the ideal measurements (i.e., no systematic errors  $b$ ,  $RF_c$ , or  $\delta t$  present). The measurements correspond to those from the GRARR, ATSR, USB, C-Band, and Minitrack Systems. Since many of the measurements are common to more than one of these systems (e.g., range rate  $\dot{\rho}$  is common to GRARR, ATSR, and USB), the section is organized by measurement type rather than by measurement system.

### 7.2.1 Tracking Process

For all systems except the Minitrack system, the electromagnetic signal is transmitted from the ground station at time  $t_T$  and is received at the satellite at time  $t_v$ . The signal is retransmitted by the satellite transponder at time  $t_v + \Delta\tau$ , where  $\Delta\tau$  is the transponder delay. The return signal is received at the ground station at time  $t_R$ . Thus, precise modeling requires that the tracking system be treated as a dynamic process, since both the satellite and the tracking station are moving relative to inertial space during the time it takes the signal to traverse the round trip from the ground station to the satellite and return.

The tracking instruments measure three basic quantities: The time interval required for the signal to traverse the path from the ground transmitter to the

satellite and back to the ground receiver, the direction of the received signal at the ground station as measured by the receiver antenna gimbal angles, and the Doppler frequency shift of the received signal compared with the transmitted signal. Preprocessor programs multiply the round-trip time interval by the signal propagation speed, thereby converting it to the geometric distance. The GTDS measurement model then relates the station-to-spacecraft range vector to the geometric distance and its direction angles at the receiver. The Doppler frequency shift data is related to the station-to-spacecraft range rate as described in Appendix A, Sections A.1.2.3 and A.3.2, and in Appendix C.

### 7.2.2 Local Tangent Plane Coordinates

The ground based tracking measurement models are most conveniently expressed in station-centered local tangent plane coordinates except for the USB and SST range and range-rate measurements. At the time of the measurement computation, the spacecraft state vector is available in either mean of 1950.0 or true of reference date inertial coordinates. The inertial state vector must first be transformed to body-fixed coordinates using the appropriate transformation matrices from Section 3.3. The transformation from mean of 1950.0 coordinates to body-fixed coordinates is expressed as

$$\bar{\mathbf{r}}_b(t) = \mathbf{B}(t) \mathbf{C}(t) \bar{\mathbf{R}}(t) \quad (7-3)$$

$$\dot{\bar{\mathbf{r}}}_b(t) = \dot{\mathbf{B}}(t) \mathbf{C}(t) \bar{\mathbf{R}}(t) + \mathbf{B}(t) \mathbf{C}(t) \dot{\bar{\mathbf{R}}}(t)$$

where  $\mathbf{C}$  and  $\mathbf{B}$  are the transformation matrices from mean of 1950.0 to true of date coordinates (Section 3.3.1) and from true of date to body-fixed coordinates (Section 3.3.2), respectively;  $\bar{\mathbf{R}}$  and  $\bar{\mathbf{r}}_b$  are the spacecraft position vectors in mean of 1950.0 and body-fixed coordinates, respectively; and  $\dot{\bar{\mathbf{R}}}$  and  $\dot{\bar{\mathbf{r}}}_b$  are the spacecraft velocity vectors in mean of 1950.0 and body-fixed coordinates, respectively. The tracking station position vector  $\bar{\mathbf{r}}_s$ , expressed in body-fixed coordinates, is given in Section 3.3.7 as

$$\bar{\mathbf{r}}_s = \begin{bmatrix} (N_s + h_s) \cos \phi_s \cos \lambda_s \\ (N_s + h_s) \cos \phi_s \sin \lambda_s \\ [N_s(1 - e^2) + h_s] \sin \phi_s \end{bmatrix} \quad (7-4)$$

where  $e^2 = 2f - f^2$ ,  $f$  is the flattening coefficient of the earth, and

$$N_s = \frac{R_e}{\sqrt{1 - (2f - f^2) \sin^2 \phi_s}} \quad (7-5)$$

The spacecraft position and velocity vectors, expressed in local tangent plane coordinates, are given in Section 3.3.7 as

$$\bar{\mathbf{r}}_{1t}(t) = \mathbf{M}_{1t}(\bar{\mathbf{r}}_b(t) - \bar{\mathbf{r}}_s) \quad (7-6)$$

$$\dot{\bar{\mathbf{r}}}_{1t}(t) = \mathbf{M}_{1t} \dot{\bar{\mathbf{r}}}_b(t)$$

Substituting Equations (7-3) into Equations (7-6) relates the local tangent coordinates to the inertial coordinates

$$\begin{aligned} \bar{\mathbf{r}}_{1t} &= \mathbf{M}_{1t} [\mathbf{BC}\bar{\mathbf{R}}(t) - \bar{\mathbf{r}}_s] \\ \dot{\bar{\mathbf{r}}}_{1t} &= \mathbf{M}_{1t} [\dot{\mathbf{B}}\mathbf{C}\bar{\mathbf{R}}(t) + \mathbf{BC}\dot{\bar{\mathbf{R}}}(t)] \end{aligned} \quad (7-7)$$

The vectors  $\bar{\mathbf{r}}_{1t}$  and  $\dot{\bar{\mathbf{r}}}_{1t}$  are used to model the tracking measurements.

The partial derivatives of the calculated measurement are computed using local tangent coordinates as the intermediate system (except for the USB and SST ranges and range rates) as follows

$$\frac{\partial \mathbf{O}_c}{\partial \bar{\mathbf{p}}} \approx \frac{\partial f_0}{\partial \bar{\mathbf{p}}} = \frac{\partial f_0}{\partial \bar{\mathbf{r}}_{1t}} \frac{\partial \bar{\mathbf{r}}_{1t}}{\partial \bar{\mathbf{R}}} \frac{\partial \bar{\mathbf{R}}}{\partial \bar{\mathbf{p}}} + \frac{\partial f_0}{\partial \dot{\bar{\mathbf{r}}}_{1t}} \left[ \frac{\partial \dot{\bar{\mathbf{r}}}_{1t}}{\partial \bar{\mathbf{R}}} \frac{\partial \bar{\mathbf{R}}}{\partial \bar{\mathbf{p}}} + \frac{\partial \dot{\bar{\mathbf{r}}}_{1t}}{\partial \dot{\bar{\mathbf{R}}}} \frac{\partial \dot{\bar{\mathbf{R}}}}{\partial \bar{\mathbf{p}}} \right] \quad (7-8)$$

From Equations (7-7)

$$\frac{\partial \bar{\mathbf{r}}_{1t}}{\partial \bar{\mathbf{R}}} = \mathbf{M}_{1t} \mathbf{BC}, \quad \frac{\partial \dot{\bar{\mathbf{r}}}_{1t}}{\partial \bar{\mathbf{R}}} = \mathbf{M}_{1t} \dot{\mathbf{B}}\mathbf{C}, \quad \frac{\partial \dot{\bar{\mathbf{r}}}_{1t}}{\partial \dot{\bar{\mathbf{R}}}} = \mathbf{M}_{1t} \mathbf{BC} \quad (7-9)$$

Substituting Equations (7-9) into Equation (7-8) yields

$$\frac{\partial \mathbf{O}_c}{\partial \bar{\mathbf{p}}} \approx \frac{\partial f_0}{\partial \bar{\mathbf{r}}_{1t}} \mathbf{M}_{1t} \mathbf{BC} \frac{\partial \bar{\mathbf{R}}}{\partial \bar{\mathbf{p}}} + \frac{\partial f_0}{\partial \dot{\bar{\mathbf{r}}}_{1t}} \left[ \mathbf{M}_{1t} \dot{\mathbf{B}}\mathbf{C} \frac{\partial \bar{\mathbf{R}}}{\partial \bar{\mathbf{p}}} + \mathbf{M}_{1t} \mathbf{BC} \frac{\partial \dot{\bar{\mathbf{R}}}}{\partial \bar{\mathbf{p}}} \right] \quad (7-10)$$

The matrices  $\partial \bar{\mathbf{R}}/\partial \bar{\mathbf{p}}$  and  $\partial \dot{\bar{\mathbf{R}}}/\partial \bar{\mathbf{p}}$  are obtained from the variational equations described in Chapter 4. The partial derivatives of the vacuum measurements,  $\partial f_j/\partial \bar{\mathbf{r}}_{1t}$  and  $\partial f_0/\partial \dot{\bar{\mathbf{r}}}_{1t}$ , are presented in the following subsections.

### 7.2.3 Measurement Equations and Partial Derivatives

In the absence of an atmosphere, electromagnetic signals follow a straight line path between the station and the spacecraft, traveling at the vacuum speed of light. Equations describing vacuum signal propagation are presented below along with pertinent partial derivatives required for the orbit determination and error analysis processes. Corrections for atmospheric effects are presented in Section 7.6. A functional description of each trajectory sensor system, as well as a description of the data preprocessing, can be found in Appendix A.

#### 7.2.3.1 Gimbal Angles

The gimbal angles provide the direction of the received downlink signal at the ground station. For rotatable dish antennas the direction angles are measured from the antenna gimbaling system. For the fixed antennas in the Minitrack system, however, the signal direction is determined from principles of interferometry.

Assuming no atmospheric refraction, the signal direction at the ground receiver is determined from the straight line propagation path from the spacecraft at time  $t_v$  to the receiving station antenna at time  $t_r$ . GTDS approximates this direction by the instantaneous straight line path from the spacecraft to the station at time  $t_v$ . This approximation introduces negligible error in the signal direction angles because of the relatively small distance (relative to inertial space) traversed by the station during the downlink propagation time interval.

The following sections describe the various gimbal angle models included in GTDS.

##### 7.2.3.1.1 Gimbal Angles $X_{30}$ and $Y_{30}$ (GRARR, ATSR, USB)

The gimbal angles for the 30-foot antennas in the GRARR, ATSR, and USB systems are denoted  $X_{30}$  and  $Y_{30}$ . The  $X_{30}$ -axis is aligned north-south in the local horizon (tangent) plane at the tracking station. The reference plane for the angular measurements is the vertical plane which is aligned east-west and includes the tracking station zenith. The angle  $X_{30}$  is measured from the vertical axis (zenith) to the projection of the station-to-spacecraft vector onto the reference plane. This angle is positive when the spacecraft is east of the station, i.e.,

$$X_{30} = \tan^{-1} \left( \frac{x_{1t}}{z_{1t}} \right) \quad -\frac{\pi}{2} \leq X_{30} \leq \frac{\pi}{2} \quad (7-11)$$

The angle  $Y_{30}$  is measured from the projection of the station-to-spacecraft vector onto the reference plane to the vector itself. This angle is positive when the spacecraft is north of the station, i.e.,

$$Y_{30} = \tan^{-1} \left( \frac{y_{1t}}{\sqrt{x_{1t}^2 + z_{1t}^2}} \right) \quad -\frac{\pi}{2} \leq Y_{30} \leq \frac{\pi}{2} \quad (7-12)$$

The partial derivatives of  $X_{30}$  and  $Y_{30}$  with respect to the local tangent plane coordinates are

$$\begin{aligned} \frac{\partial X_{30}}{\partial \bar{r}_{1t}} &= \frac{1}{(x_{1t}^2 + z_{1t}^2)} [z_{1t}, 0, -x_{1t}] \\ \frac{\partial X_{30}}{\partial \bar{r}_{1t}} &= 0 \end{aligned} \quad (7-13)$$

and

$$\begin{aligned} \frac{\partial Y_{30}}{\partial \bar{r}_{1t}} &= \frac{1}{\rho^2} \left[ \frac{-x_{1t} y_{1t}}{\sqrt{x_{1t}^2 + z_{1t}^2}}, \sqrt{x_{1t}^2 + z_{1t}^2}, \frac{-y_{1t} z_{1t}}{\sqrt{x_{1t}^2 + z_{1t}^2}} \right] \\ \frac{\partial Y_{30}}{\partial \bar{r}_{1t}} &= 0 \end{aligned} \quad (7-14)$$

where

$$\rho = \sqrt{x_{1t}^2 + y_{1t}^2 + z_{1t}^2}$$

#### 7.2.3.1.2 Gimbal Angles $X_{85}$ and $Y_{85}$ (USB)

The gimbal angles associated with the USB 85-foot antennas are denoted  $X_{85}$  and  $Y_{85}$ . The  $X_{85}$ -axis is aligned east-west in the local horizon (tangent) plane at the tracking station. The reference plane for the angular measurements is the vertical plane which is aligned north-south and includes the tracking station zenith. The angle  $X_{85}$  is measured from the vertical axis (zenith) to the projection of the station-to-spacecraft vector onto the reference plane. This angle is positive when the spacecraft is south of the station, i.e.,

$$X_{85} = \tan^{-1} \left( -\frac{y_{1t}}{z_{1t}} \right) \quad -\frac{\pi}{2} \leq X_{85} \leq \frac{\pi}{2} \quad (7-15)$$

The angle  $Y_{85}$  is measured from the projection of the station-to-spacecraft vector onto the reference plane to the vector itself. This angle is positive when the spacecraft is east of the station, i.e.,

$$Y_{85} = \tan^{-1} \left( \frac{x_{1t}}{\sqrt{y_{1t}^2 + z_{1t}^2}} \right) \quad -\frac{\pi}{2} \leq Y_{85} \leq \frac{\pi}{2} \quad (7-16)$$

The partial derivatives of  $X_{85}$  and  $Y_{85}$  with respect to the local tangent plane coordinates are

$$\frac{\partial X_{85}}{\partial \bar{r}_{1t}} = \frac{1}{(y_{1t}^2 + z_{1t}^2)} [0, -z_{1t}, y_{1t}] \quad (7-17)$$

$$\frac{\partial X_{85}}{\partial \dot{\bar{r}}_{1t}} = 0$$

and

$$\frac{\partial Y_{85}}{\partial \bar{r}_{1t}} = \frac{1}{\rho^2} \left[ \sqrt{y_{1t}^2 + z_{1t}^2}, \frac{-x_{1t} y_{1t}}{\sqrt{y_{1t}^2 + z_{1t}^2}}, \frac{-x_{1t} z_{1t}}{\sqrt{y_{1t}^2 + z_{1t}^2}} \right]$$

$$\frac{\partial Y_{85}}{\partial \dot{\bar{r}}_{1t}} = 0 \quad (7-18)$$

#### 7.2.3.1.3 Gimbal Angles A and E (ATSR, C-Band)

The azimuth angle A is measured in the local tangent (horizon) plane, clockwise from north to the projection of the station-to-spacecraft vector onto the local tangent plane. This angle is positive when measured eastward (clockwise) from north, i.e.,

$$A = \sin^{-1} \left( \frac{x_{1t}}{\sqrt{x_{1t}^2 + y_{1t}^2}} \right)$$

$$0 \leq A \leq 2\pi \quad (7-19)$$

$$A = \cos^{-1} \left( \frac{y_{1t}}{\sqrt{x_{1t}^2 + y_{1t}^2}} \right)$$

The elevation angle E is measured from the projection of the station-to-spacecraft vector onto the local tangent plane to the vector itself. This angle is positive whenever the spacecraft is above the horizon, i.e.,

$$E = \tan^{-1} \left( \frac{z_{1t}}{\sqrt{x_{1t}^2 + y_{1t}^2}} \right) \quad (7-20)$$

The partial derivatives of A and E with respect to the local tangent plane co-ordinates are

$$\frac{\partial A}{\partial \bar{r}_{1t}} = \frac{1}{(x_{1t}^2 + y_{1t}^2)} [y_{1t}, -x_{1t}, 0] \quad (7-21)$$

$$\frac{\partial A}{\partial \bar{r}_{1t}} = 0$$

and

$$\frac{\partial E}{\partial \bar{r}_{1t}} = \frac{1}{\rho^2} \left[ \frac{-x_{1t} z_{1t}}{\sqrt{x_{1t}^2 + y_{1t}^2}}, \frac{-y_{1t} z_{1t}}{\sqrt{x_{1t}^2 + y_{1t}^2}}, \sqrt{x_{1t}^2 + y_{1t}^2} \right]$$

$$\frac{\partial E}{\partial \bar{r}_{1t}} = 0 \quad (7-22)$$

#### 7.2.3.1.4 Direction Cosines $\ell$ and $m$ (Minitrack)

The direction cosine  $\ell$  is the cosine of the angle between the station-to-spacecraft vector and the axis pointing toward the east in the local tangent system (the  $x_{1t}$ -axis). This direction cosine is positive when the spacecraft is east of the station, i.e.,

$$\ell = \frac{x_{1t}}{\rho} \quad (7-23)$$

The direction cosine  $m$  is the cosine of the angle between the station-to-spacecraft vector and the axis pointing toward the north in the local tangent system (the  $y_{1t}$ -axis). This direction cosine is positive when the spacecraft is north of the station, i.e.,

$$m = \frac{y_{1t}}{\rho} \quad (7-24)$$

The partial derivatives of  $\ell$  and  $m$  with respect to the local tangent plane coordinates are

$$\frac{\partial \ell}{\partial \vec{r}_{1t}} = \frac{1}{\rho^3} [(y_{1t}^2 + z_{1t}^2), -x_{1t}y_{1t}, -x_{1t}z_{1t}] \quad (7-25)$$

$$\frac{\partial \ell}{\partial \dot{\vec{r}}_{1t}} = 0$$

and

$$\frac{\partial m}{\partial \vec{r}_{1t}} = \frac{1}{\rho^3} [-x_{1t}y_{1t}, (x_{1t}^2 + z_{1t}^2), -y_{1t}z_{1t}] \quad (7-26)$$

$$\frac{\partial m}{\partial \dot{\vec{r}}_{1t}} = 0$$

#### 7.2.3.2 Range (GRARR, ATSR, USB, C-Band Systems)

From the description of the tracking process in Section 7.2.1, it is seen that all trackers provide the user with the round trip light time delay from the transmitter through the satellite to the ground receiver, and an associated time tag. The round trip range is seen to be



$$\rho_{RT} = |\bar{r}_v(t_v) - \bar{r}_T(t_T)| + |\bar{r}_R(t_R) - \bar{r}_v(t_v + \Delta\tau)| \quad (7-27)$$

where

$\rho_{RT} \sim$  round trip range

$\bar{r}_v \sim$  satellite position vector in inertial Cartesian coordinates

$\bar{r}_T \sim$  ground transmitter position vector in inertial Cartesian coordinates

$\bar{r}_R \sim$  ground receiver position vector in inertial Cartesian coordinates

$\Delta\tau \sim$  transponder delay

$t_T \sim$  time signal is transmitted from the ground station

$t_v \sim$  time signal is received at the satellite

$t_R \sim$  time signal is received at the ground station

In the case of USB and C-Band, the time tag on the raw data corresponds to the time  $t_R$  at which the measured signal arrives at the ground receiver; for GRARR and ATSR, the time tag on the raw data corresponds to the ground receive time  $t_R$  less the measured value of the round trip light time delay. For all systems, the preprocessor provides GTDS with  $\rho(t_R)$ , the average of the uplink and downlink propagation distances. The value  $\rho(t_R)$  is generated by multiplying the observed round trip propagation delay by  $c/2$ . The preprocessor also provides  $t_R$  by making the appropriate modifications to the raw time tag for GRARR and ATSR data.

For the greatest accuracy, the expected value of the range should be calculated by determining the uplink and downlink path of the signal as defined in Equation (7-27). This method requires an iterative process to determine the uplink and downlink light time delays. A second, less accurate, method is to approximate the range by calculating the instantaneous range at the spacecraft turnaround time. The iterative method is used to calculate the expected range for USB, C-Band, and ATSR, while the instantaneous method is used for VHF GRARR.

#### 7.2.3.2.1 Iterative Method for Expected Range

The expected value of  $\rho(t_R)$  is computed from ephemeris information and station coordinates using the following equation

$$\rho(t_R) = \frac{1}{2} \{ |\bar{r}_v(t_v) - \bar{r}_T(t_T)| + |\bar{r}_v(t_v) - \bar{r}_R(t_R)| \} \quad (7-28)$$

For simplicity, this equation is presented in an inertial reference frame, where

$\bar{r}_v \sim$  spacecraft inertial position vector

$\bar{r}_T \sim$  transmitting site inertial position vector

$\bar{r}_R \sim$  receiving site inertial position vector

$t_T \sim$  time at which the measured signal left the ground transmitter

$t_v \sim$  time at which the measured signal was received and retransmitted by the spacecraft. The assumption of instantaneous turnaround is used; the constant bias in the observed range caused by the spacecraft electronic delay is accounted for as a measurement error elsewhere in GTDS.

$t_R \sim$  time tag of the reduced observed range (that is, the time at which the measured signal arrived at the ground receiver).

The algorithm used in GTDS to compute  $\rho(t_R)$  proceeds as follows:

1. Calculate  $\bar{r}_R(t_R)$
2. Calculate iteratively the downlink propagation distance  $\rho_d(t_R)$  using the following equations

$$\begin{aligned}
 (a) \quad \rho_d(t_R) &= |\bar{r}_v(t_v) - \bar{r}_R(t_R)| \\
 (b) \quad \delta_d(t_R) &= \rho_d(t_R)/c \\
 (c) \quad t_v &= t_R - \delta_d(t_R)
 \end{aligned}
 \tag{7-29}$$

The iteration process is initiated by assuming that  $t_v = t_R$ , and is terminated when successive values of  $\delta_d(t_R)$  agree to within  $10^{-8}$  seconds.

3. Calculate iteratively the uplink propagation distance  $\rho_u(t_R)$  using the following equations

$$\begin{aligned}
 (a) \quad \rho_u(t_R) &= |\bar{r}(t_v) - \bar{r}_T(t_T)| \\
 (b) \quad \delta_u(t_R) &= \rho_u(t_R)/c \\
 (c) \quad t_T &= t_v - \delta_u(t_R)
 \end{aligned}
 \tag{7-30}$$

Iteration is initiated by assuming that  $\delta_u(t_R) = \delta_d(t_R)$ , and is terminated when successive values of  $\delta_u(t_R)$  agree to within  $10^{-8}$  seconds.

The following geometrically exact equation is used to compute the expected value of the range  $\rho(t_R)$  for the USB, C-Band and ATSR systems.

$$\rho(t_R) = [\rho_u(t_R) + \rho_d(t_R)] / 2 \quad (7-31)$$

#### 7.2.3.2.2 Instantaneous Method for Expected Range

Range data produced by the GRARR-VHF system is less accurate than that produced by the other tracking systems; therefore, it does not warrant the application of the iterative solution described above. Instead, the following more efficient algorithm is used to determine an instantaneous approximation for  $\rho(t_R)$  using GRARR range data

$$\begin{aligned} \rho(t_R) &= |\bar{r}_v(t_v) - \bar{r}_T(t_v)| = |\bar{r}_{1t}(t_v)| \\ &= \sqrt{x_{1t}^2 + y_{1t}^2 + z_{1t}^2} \end{aligned} \quad (7-32)$$

where

$$t_v = t_R - \rho(t_R)/c$$

and  $\bar{r}_{1t}$  is the spacecraft position vector in local tangent plane coordinates.

#### 7.2.3.2.3 Range Partial Derivatives

The partial derivatives of the expected range (Equation (7-28)) in inertial coordinates (USB system) are

$$\begin{aligned} \frac{\partial \rho(t_R)}{\partial \bar{r}_v(t_v)} &= \frac{1}{2\rho_u \rho_d} \{ \rho_d [\bar{r}_v^T(t_v) - \bar{r}_T^T(t_T)] \\ &\quad + \rho_u [\bar{r}_v^T(t_v) - \bar{r}_R^T(t_R)] \} \end{aligned} \quad (7-33)$$

$$\frac{\partial \rho(t_R)}{\partial \dot{\bar{r}}_v(t_v)} = 0 \quad (7-34)$$

If it is assumed that  $\rho_u = \rho_d = \rho(t_R)$ , Equation (7-33) reduces to

$$\frac{\partial \rho(t_R)}{\partial \bar{r}_v(t_v)} = \frac{1}{2\rho(t_R)} \{ 2\bar{r}_v^T(t_v) - [\bar{r}_T^T(t_T) + \bar{r}_R^T(t_R)] \} \quad (7-35)$$

The partial derivatives of the expected range in local tangent plane coordinates (for the remaining systems) are

$$\frac{\partial \rho(t_R)}{\partial \bar{r}_{1t}(t_v)} = \frac{\bar{r}_{1t}^T(t_v)}{\rho(t_R)} \quad (7-36)$$

$$\frac{\partial \rho(t_R)}{\partial \dot{\bar{r}}_{1t}(t_v)} = 0 \quad (7-37)$$

### 7.2.3.3 Range Rate (GRARR, ATSR, USB)

The range rate of a spacecraft is determined by measuring the Doppler shift of a signal resulting from the relative motion between the station and the spacecraft. This can be done either by measuring the time required to count a fixed number of Doppler-plus-bias cycles, as with GRARR and ATSR, or by counting the Doppler-plus-bias cycles over a fixed time interval, as with USB. For all tracking systems, the preprocessor converts the raw Doppler information transmitted from the stations to range rate and a time tag.

There are three modes of calculating the expected value of the range rate for each of these tracking systems. In the first method, the range rate is obtained by computing the time difference quotient of ranges calculated at the beginning and at the end of the Doppler count interval, iteratively correcting for the light time delays. The second method uses the instantaneous ranges at the beginning and at the end of the count interval, with no corrections for the light time delays. The third and least accurate method is to calculate an instantaneous range rate at the midpoint of the Doppler count interval as seen at the spacecraft. The first method is used to compute the expected value of the range rate for the USB system, while the other two methods are used (optionally) for the GRARR and ATSR systems.

### 7.2.3.3.1 Iterative Range Difference Method

The modeling of the expected value of the range rate which is most precise is to difference the average range at the beginning and end of the count interval as shown below (Reference 1).

$$\dot{\rho}(t_R) = \frac{[\rho_u(t_R) + \rho_d(t_R)] - [\rho_u(t_R - \Delta t_{RR}) + \rho_d(t_R - \Delta t_{RR})]}{2\Delta t_{RR}} \quad (7-38)$$

where

$\rho_u(t_R) \sim$  uplink propagation path of a signal arriving at the receiver at  $t_R$

$\rho_d(t_R) \sim$  downlink propagation path of a signal arriving at the receiver at  $t_R$

$\Delta t_{RR} \sim$  Doppler count time interval

The calculations for these uplink and downlink ranges are iteratively corrected for the light time delay in exactly the same manner as the expected ranges modeled in Section 7.2.3.2.1. This method is used for USB measurements where the time tag on the observed data is  $t_R$  (corresponding to the end of the count interval) and the count interval  $\Delta t_{RR}$  corresponds to the sample interval. This method is accurate for both two-way and three-way Doppler measurements using the USB system. Two-way Doppler measurements are obtained when the transmitting and receiving antennas are the same, while three-way Doppler measurements are obtained when the transmitting and receiving antennas are different.

The range-rate partial derivatives with respect to the epoch state elements  $\bar{R}$  and  $\dot{R}$  are computed most efficiently by using the algorithms for the range partial derivatives

$$\frac{\partial \dot{\rho}(t_R)}{\partial \bar{R}} = \frac{\frac{\partial \rho(t_R)}{\partial \bar{R}} - \frac{\partial \rho(t_R - \Delta t_{RR})}{\partial \bar{R}}}{\Delta t_{RR}} \quad (7-39)$$

$$\frac{\partial \dot{\rho}(t_R)}{\partial \dot{R}} = \frac{\frac{\partial \rho(t_R)}{\partial \dot{R}} - \frac{\partial \rho(t_R - \Delta t_{RR})}{\partial \dot{R}}}{\Delta t_{RR}} \quad (7-40)$$

### 7.2.3.3.2 Instantaneous Range Difference

A less accurate but more efficient range difference formulation is available in GTDS for GRARR and ATSR. It is assumed in this model that propagation delays are negligible compared with the Doppler count time interval. The resulting equation is

$$\dot{\rho} = \frac{\rho(t_v + \Delta t_{RR}) - \rho(t_v)}{\Delta t_{RR}} = \frac{|\bar{r}_{1t}(t_v + \Delta t_{RR})| - |\bar{r}_{1t}(t_v)|}{\Delta t_{RR}} \quad (7-41)$$

The two range vectors  $\bar{r}_{1t}(t_v + \Delta t_{RR})$  and  $\bar{r}_{1t}(t_v)$  are computed in the same manner as those for the range computations (Section 7.2.3.2.2). In order to use this method in GTDS, the preprocessor must provide  $t_R$ , the time of the received signal at the beginning of the Doppler count interval, and  $\Delta t_{RR}$ , the count interval. The partial derivatives of  $\dot{\rho}$  with respect to local tangent coordinates are

$$\frac{\partial \dot{\rho}}{\partial \bar{r}_{1t}} = \frac{1}{\Delta t_{RR}} \left\{ \frac{\bar{r}_{1t}^T(t_v + \Delta t_{RR})}{|\bar{r}_{1t}(t_v + \Delta t_{RR})|} - \frac{\bar{r}_{1t}^T(t_v)}{|\bar{r}_{1t}(t_v)|} \right\} \quad (7-42)$$

$$\frac{\partial \dot{\rho}}{\partial \dot{\bar{r}}_{1t}} = 0 \quad (7-43)$$

### 7.2.3.3.3 Average Range Rate

A third method, which is the least accurate but most efficient, calculates the instantaneous range rate at the midpoint of the Doppler count interval as seen at the spacecraft. This value is used to approximate the average range rate over the uplink and downlink paths, and is therefore denoted  $\dot{\rho}_{avg}$ . It is computed as

$$\dot{\rho}_{avg} = \frac{\bar{r}_{1t}(t_v) \cdot \dot{\bar{r}}_{1t}(t_v)}{|\bar{r}_{1t}(t_v)|} \quad (7-44)$$

The position and velocity vectors are expressed in station-centered local tangent plane coordinates evaluated at the vehicle turnaround time  $t_v$ .

This method is used for the GRARR and ATSR range-rate models. When this method is used the preprocessor modifies the time tag on the GRARR data according to the relationship

$$t_v = t_R + \frac{\Delta t_{RR}}{2} - \frac{|\bar{r}_{1t}(t_v)|}{c} \quad (7-45)$$

The partial derivatives of  $\dot{\rho}_{avg}$  with respect to local tangent plane coordinates are

$$\frac{\partial \dot{\rho}_{avg}}{\partial \dot{\bar{r}}_{1t}} = \frac{1}{\rho} \left[ \dot{\bar{r}}_{1t}^T - \frac{\dot{\rho}}{\rho} \bar{r}_{1t}^T \right] \quad (7-46)$$

$$\frac{\partial \dot{\rho}_{avg}}{\partial \dot{\bar{r}}_{1t}} = \frac{\bar{r}_{1t}^T}{\rho} \quad (7-47)$$

### 7.3 SATELLITE-TO-SATELLITE TRACKING (SST) MODEL

The formulation is presented in this section for the satellite-to-satellite range sum and range sum rate (Doppler) model. Partial derivatives of the range sum and range sum rate models are developed with respect to dynamical parameters, such as the epoch state vectors, for use in the statistical estimation process. It is assumed that the tracking is accomplished by the modified ATSR system and that the relay satellite is in a near-synchronous orbit.

#### 7.3.1 Introduction

The Applications Technology Satellite-6 (ATS-6) is an advanced synchronous orbit communication satellite. It is the first satellite in the ATS series which does not employ spin stabilization. This feature, coupled with an onboard digital computer, enables ATS-6 to function as a relay satellite in a satellite tracking network, tracking other satellites such as Nimbus-F, GEOS-C, and the Apollo-Soyuz Test Project (ASTP). The ATS-6 satellite includes a multi-frequency transponder system containing six receivers and nine transmitters capable of operating on about 17 frequencies. A key feature of these transponders for satellite-to-satellite tracking (SST) is the maintenance of coherence of the phase relationships between various radio frequency signals. The range sum and Doppler measurements are dependent on phase measurements of the returning

signals, and as such are sensitive to any phase delay originating in the transmission equipment. Since no onboard frequency source is absolutely accurate, signal coherence is maintained in order to avoid introducing any additional bias into these two measurements. Angle measurements, on the other hand, are not affected by coherence.

The range and Doppler measurements are functions of the positions and velocities of the ground transmitter, the relay satellite, and the target (ground transponder or satellite). The same techniques can also be used to make range and Doppler measurements for the relay satellite alone.

Three main tracking modes are considered: The coherent mode, the phase-locked loop (PLL) mode, and the crystal (XTAL) mode. The relay-only tracking mode is referred to as the coherent mode, even though all of the relay modes are coherent. The phase-locked loop mode is the relay mode used to track phase-locked loop transponders, such as GEOS and ASTP. The crystal mode is used to track crystal oscillator transponders, such as Nimbus-F. A detailed description of these tracking modes can be found in Reference 2.

The ground transmitter broadcasts two uplink C-Band tones, a pilot tone and a carrier tone. The carrier tone is modulated by the range tones and is the signal used to generate the Doppler data. There are three uplink pilot frequency options: 5950, 6150, and 6350 MHz. The carrier frequency can be varied to lock the target transponder circuits onto the signal. The S-Band frequency which the relay satellite transmits to the target is determined by the difference between the pilot and carrier frequencies. When switching from one uplink option to another, both frequencies are shifted so as to keep the frequency difference constant. The two uplink signals are generated by a set of two fixed and two variable frequency synthesizers, along with a frequency multiplier and adders.

The measurement geometry is illustrated in Figure 7-1. The transmitting station transmits a signal at time  $t_0$  which is received by the relay satellite at  $t_1$  and transmitted to the target satellite at  $t_1 + \Delta\tau_1$ , where  $\Delta\tau_1$  is the transponder time delay. The target satellite receives the signal at  $t_2$  and transmits it back to the relay satellite at  $t_2 + \Delta\tau_2$ . The relay satellite receives the signal at  $t_3$  and, after a transponder delay of  $\Delta\tau_3$ , sends it back to the ground station, which receives it at  $t_4$ . The ground station records the data and tags it with the UTC time tag  $t_R$ . The range sum measurement is the time that an RF signal takes to traverse the four-legged path from the transmitter to the relay satellite, to the target, back to the relay satellite, and then to the transmitter. In the coherent tracking mode (relay only) the range sum observation is the light time for the two legs from the transmitter to the relay satellite and back to the transmitter.

The range sum measurement is accomplished through sidetone ranging techniques



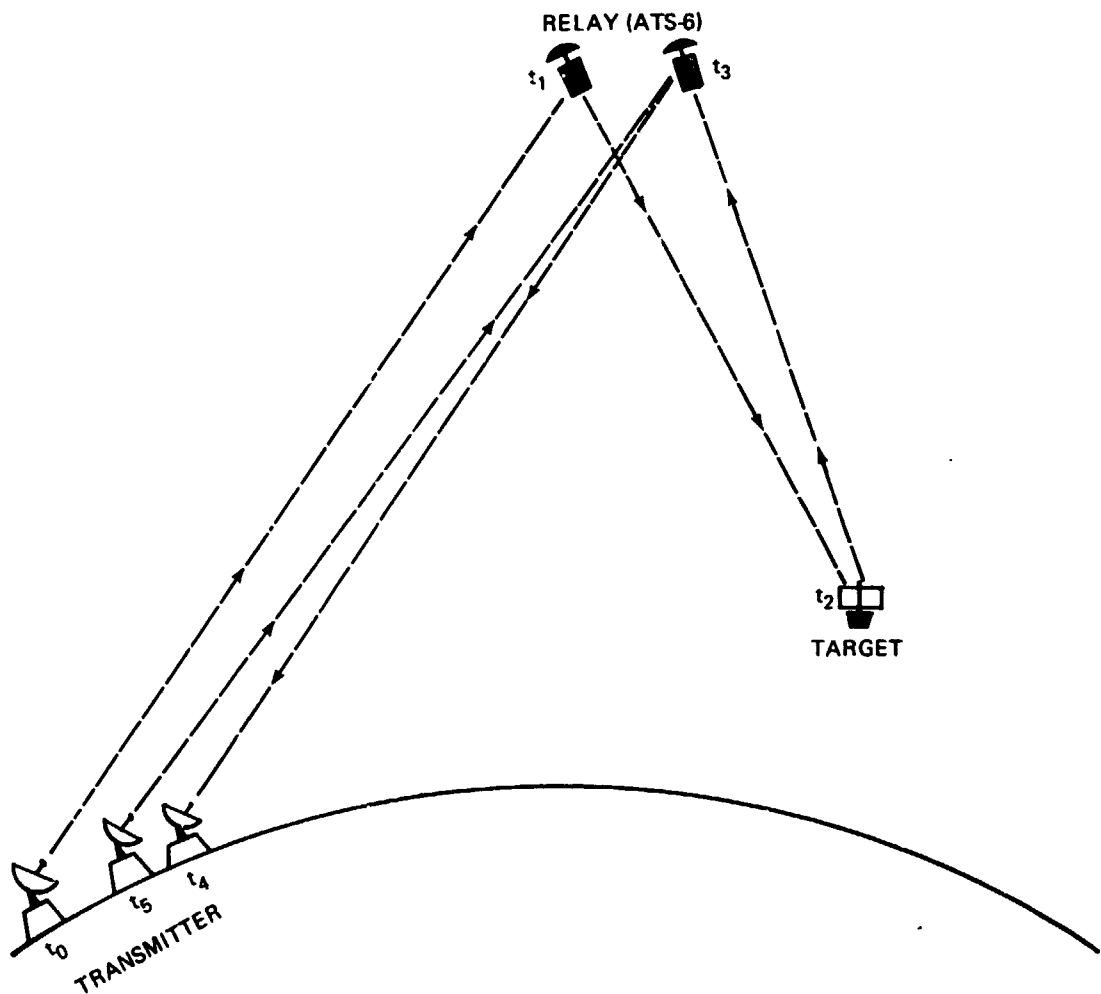


Figure 7-1. SST Tracking Geometry

The Doppler measurements are a function of a two-component signal. The first component originates from the transmitter at  $t_0$ , follows the four-leg path, and is frequency shifted by the motion of both the relay satellite and the target. The second component originates at the ground transmitter at  $t_5$ , travels to the relay satellite, where it is mixed with the signal arriving at  $t_3$  from the target, and is rebroadcast to the transmitter, which receives it at  $t_4$ . The latter component is frequency shifted only by the motion of the relay satellite. The incoming carrier signal is converted into a Doppler-plus-bias signal which is the input to an N-cycle counter.

### 7.3.2 Light Time Modeling

In the formulation of the modeling procedures used in the computation of the range and range-rate measurements, an inertial reference frame was selected since most orbit integrators use an inertial frame and less computation is required to transform a single station location than to transform two satellite state vectors. An inertial frame also makes it unnecessary to consider any rotational effects on the radar signal. All signal paths are straight lines traversed at a constant speed  $c$ , except as affected by atmospheric refraction. All of the internal calculations are carried out in terms of time, i.e., the light time for the range and the time required for a given number of cycles of the Doppler frequency to be counted. The light time calculations are performed by means of a backward tracing of the light path (see Figure 7-1). The first step is to compute the transmitter location at time  $t_4$ . Next, the state vectors of the relay satellite at time  $t_3$ , the target at time  $t_2$ , the relay satellite at time  $t_1$ , and the transmitter at time  $t_0$  are solved for successively, using an iterative procedure. For Doppler or coherent mode data, the location of the transmitter at  $t_5$  is also determined. If a forward solution were used, it would begin at  $t_0$  and solve for the appropriate state vectors at  $t_1$ ,  $t_2$ ,  $t_3$ , and  $t_4$  in succession. The advantage of a forward method is that the Doppler-shifted carrier frequency is known for each leg and the transponder delay can be calculated, giving the exact time of retransmission. However, for the C-Band and S-Band frequency ranges involved in the ATSR satellite-to-satellite system, the transponder delays are virtually constant and sufficiently small that the motion of the relay satellite and the target during the delay can be ignored in the light time solution. Since the transmitter location at  $t_5$  is a function of the relay satellite orbit and the coordinates of the transmitter at  $t_4$ , it can be solved for most efficiently using the backward tracing method. Large ambiguities in the range measurements and Doppler measurements can be resolved using either method, since the high resolution correction can be derived from any solution which is in the neighborhood of the true time. The most important reason for favoring the backward solution is the simplicity of the calculation of the Doppler count interval.

Since the Doppler count is made over the time interval between two positive-directed zero crossings of the received downlink (Doppler plus bias) signal, it is more convenient to trace the light path backward from the two known reception times. As the observation is time tagged within  $10^{-5}$  seconds of the beginning of the Doppler count, the first of these reception times is set equal to the time tag.

### 7.3.3 The Range Observation

The range observation measures the phase shift in the range tone corresponding to the time required for a specified phase to travel from the transmitter to the

relay satellite, to the target, back to the relay satellite, and then back to the station (for the coherent mode the path is simply from the transmitter to the relay satellite and back). The range tones are transmitted as a modulation on the carrier signal; they return modulated on the carrier (or, in the crystal mode, on the subcarrier). In practice, the time delay is measured from the zero phase of a 500 kHz, 100 kHz, or 20 kHz transmitted range tone to the next zero phase in the received signal, which gives the round trip time minus a whole number of range-tone cycles. This ambiguity is partially accounted for through use of low-frequency tones, down to a minimum of 8 Hz. In effect, the signal which stops the timing clock is disabled until the return of the zero phase of the lowest frequency range tone which was transmitted simultaneously with the high-frequency tone. For satellites at near-synchronous altitudes, an ambiguity still remains in the number of 8 Hz cycles which should be added to the range time; this ambiguity must be resolved in the orbit determination program based on an a priori estimate of the orbit. The total range of the signal propagation path is

$$\begin{aligned} \rho_L = & |\bar{r}_1(t_1) - \bar{r}_s(t_0)| + |\bar{r}_2(t_2) - \bar{r}_1(t_1 + \Delta\tau_1)| \\ & + |\bar{r}_1(t_3) - \bar{r}_2(t_2 + \Delta\tau_2)| + |\bar{r}_s(t_4) - \bar{r}_1(t_3 + \Delta\tau_3)| \end{aligned} \quad (7-48)$$

for four-way ranging, and

$$\rho_S = |\bar{r}_s(t_5) - \bar{r}_1(t_3)| + |\bar{r}_s(t_4) - \bar{r}_1(t_3 + \Delta\tau_3)| \quad (7-49)$$

for two-way ranging (used for coherent mode tracking only), where

$\bar{r}_1 \sim$  inertial position vector of the relay satellite

$\bar{r}_2 \sim$  inertial position vector of the target satellite

$\bar{r}_s \sim$  inertial position vector of the ground station

$\rho_L \sim$  four-leg round trip range

$\rho_S \sim$  two-leg round trip range

$\Delta\tau_1 \sim$  transponder delay during first pass through the relay satellite

$\Delta\tau_2 \sim$  transponder delay at the target satellite

$\Delta\tau_3 \sim$  transponder delay during second pass through the relay satellite

From Equation (7-46) the four-way signal propagation time is

$$\Delta t_R = \frac{\rho_L}{c} + \Delta t_{A_1} + \Delta t_{A_4} + \Delta \tau_1 + \Delta \tau_2 + \Delta \tau_3 \quad (7-50)$$

where

$\Delta t_{A_1} \sim$  atmospheric delay during leg 1

$\Delta t_{A_4} \sim$  atmospheric delay during leg 4

$c \sim$  vacuum speed of light

The role of the target may be filled by a ground transponder, in which case there are two additional atmospheric delays

$\Delta t_{A_2} \sim$  atmospheric delay during leg 2

$\Delta t_{A_3} \sim$  atmospheric delay during leg 3

and Equation (7-50) becomes

$$\Delta t_R = \frac{\rho_L}{c} + \Delta t_{A_1} + \Delta t_{A_2} + \Delta t_{A_3} + \Delta t_{A_4} + \Delta \tau_1 + \Delta \tau_2 + \Delta \tau_3 \quad (7-51)$$

However, the atmospheric delays, which are of the same order as the uncertainties in the system biases, are not included in the GTDS satellite-to-satellite tracking implementation, reducing Equations (7-50) and (7-51) to

$$\Delta t_R = \frac{\rho_L}{c} + \Delta \tau_1 + \Delta \tau_2 + \Delta \tau_3 \quad (7-52)$$

The satellite transponder time delays are functions of the frequency of the signal received by the transponder, i.e.,

$$\Delta \tau_1 = f_1(\nu_1)$$

$$\Delta \tau_2 = f_2(\nu_2) \quad (7-53)$$

$$\Delta \tau_3 = f_3(\nu_3)$$

The functions  $f_1$  and  $f_2$  are determined by bench calibration of the individual transponders prior to the launch of each satellite, and are entered in GTDS as tables of transponder delay versus frequency. Delays for intermediate frequencies are then obtained by interpolation. In the absence of tables, a nominal (default) constant delay can be used.

### 7.3.3.1 Range Sum Calculation

The actual observations are not corrected for transponder delays in the pre-processor since Doppler corrections to the frequency-dependent transponder delays are not available until the ground transmitter-to-relay satellite leg has been solved. Thus, the transponder delay is added to the computed observation at the end of the light time solution. This does not invalidate the light time solution itself, however, because during a typical one-microsecond transponder delay a satellite will only have traveled a distance of the order of a few millimeters. The light time for each transmission leg is (neglecting atmospheric delays)

$$\begin{aligned}\Delta t_1 &= \frac{|\bar{r}_1(t_1) - \bar{r}_s(t_0)|}{c} \\ \Delta t_2 &= \frac{|\bar{r}_2(t_2) - \bar{r}_1(t_1 + \Delta\tau_1)|}{c} \\ \Delta t_3 &= \frac{|\bar{r}_1(t_3) - \bar{r}_2(t_2 + \Delta\tau_2)|}{c} \\ \Delta t_4 &= \frac{|\bar{r}_s(t_4) - \bar{r}_1(t_3 + \Delta\tau_3)|}{c}\end{aligned}\tag{7-54}$$

For Doppler or coherent mode measurements, a fifth leg is required, i.e.,

$$\Delta t_5 = \frac{|\bar{r}_s(t_5) - \bar{r}_1(t_3)|}{c}\tag{7-55}$$

Each leg of the light path is solved for using the following algorithm:

- (1) Assume that  $t_3 = t_4$ , i.e., that  $\Delta t_4 = 0$ , and calculate the state of the receiving station and the relay satellite at  $t_4$ .
- (2) Calculate the time required for light to traverse the path  $\bar{r}_s(t_4) - \bar{r}_1(t_4)$

$$\Delta t_4 = \frac{|\bar{r}_s(t_4) - \bar{r}_1(t_4)|}{c} \quad (7-56)$$

- (3) Estimate  $t_3$  as  $t_4 - \Delta t_4$  and solve for the state of the relay satellite at this new estimate of  $t_3$ .
- (4) Refine the estimate of  $t_3$  using the formula

$$t'_3 = t_3 + \left\{ \frac{c \cdot (t_4 - t_3) - |\bar{r}_s(t_4) - \bar{r}_1(t_3)|}{c - \frac{[\bar{r}_s(t_4) - \bar{r}_1(t_3)]}{|\bar{r}_s(t_4) - \bar{r}_1(t_3)|} \cdot \dot{\bar{r}}_1(t_3)} \right\} \quad (7-57)$$

This formula is derived from the Newton-Raphson method, which converges quadratically.

- (5) Repeat steps 3 and 4 until convergence is obtained.
- (6) Proceed in the same manner to determine  $\Delta t_3, \Delta t_2$ , and  $\Delta t_1$ .

The desired observables are modeled from the exact geometry calculated in this fashion.

### 7.3.3.2 Partial Derivatives of the Range Observation

The range observation, without corrections for transponder delays and atmospheric delays, can be written as

$$\Delta t_R = \frac{1}{c} \left[ |\bar{r}_1(t_1) - \bar{r}_s(t_0)| + |\bar{r}_2(t_2) - \bar{r}_1(t_1)| \right. \\ \left. + |\bar{r}_1(t_3) - \bar{r}_2(t_2)| + |\bar{r}_s(t_4) - \bar{r}_1(t_3)| \right] \quad (7-58)$$

where

$\bar{r}_s \sim$  ground station position vector

$\bar{r}_1 \sim$  relay satellite position vector

$\bar{r}_2 \sim$  target position vector

The partial derivatives of the range observation with respect to the target position and velocity vectors are then

$$\frac{\partial \Delta t_R}{\partial \bar{r}_2(t_2)} = \frac{1}{c} \left[ \frac{\bar{r}_2(t_2) - \bar{r}_1(t_1)}{|\bar{r}_2(t_2) - \bar{r}_1(t_1)|} - \frac{\bar{r}_1(t_3) - \bar{r}_2(t_2)}{|\bar{r}_1(t_3) - \bar{r}_2(t_2)|} \right] = \frac{1}{c} (\hat{U}_2 - \hat{U}_3) \quad (7-59)$$

$$\frac{\partial \Delta t_R}{\partial \dot{\bar{r}}_2(t_2)} = 0 \quad (7-60)$$

where  $\hat{U}_2$  and  $\hat{U}_3$  are unit vectors directed along legs 2 and 3, respectively. Similarly, the partial derivatives of the range observation with respect to the relay satellite position and velocity vectors are

$$\frac{\partial \Delta t_R}{\partial \bar{r}_1} = \frac{1}{c} (\hat{U}_1 - \hat{U}_2 + \hat{U}_3 - \hat{U}_4) \quad (7-61)$$

$$\frac{\partial \Delta t_R}{\partial \dot{\bar{r}}_1} = 0 \quad (7-62)$$

where  $\hat{U}_1$  and  $\hat{U}_4$  are unit vectors directed along legs 1 and 4, respectively.

For differentiation purposes,  $\bar{r}_1(t_1)$  and  $\bar{r}_1(t_3)$  have been replaced by  $\bar{r}_1$ , which represents a mean position vector lying between  $\bar{r}_1(t_1)$  and  $\bar{r}_1(t_3)$ ; the variations of this mean vector closely approximate those of  $\bar{r}_1(t_1)$  and  $\bar{r}_1(t_3)$ . Similarly,  $\dot{\bar{r}}_1(t_1)$  and  $\dot{\bar{r}}_1(t_3)$  have been replaced with  $\dot{\bar{r}}_1$ .

The partial derivatives with respect to the relay satellite coordinates or with respect to target satellite coordinates are related to the epoch coordinates via

the appropriate state transition matrix. This matrix can be used to link the epoch time with any convenient time within the observation time span; however, for practical purposes, it can be considered constant for the duration of the observation, which is only about half a second.

Partial derivatives with respect to the coordinates of the ground station or a target transponder located on the ground are chained back to earth-fixed geodetic coordinates, using Equation (7-10). The partial derivatives of the range observation with respect to station coordinates at the time of observation are

$$\frac{\partial \Delta t_R}{\partial \bar{r}_s} = \frac{1}{c} (\hat{U}_4 - \hat{U}_1) \quad (7-63)$$

where  $\bar{r}_s(t_0)$  and  $\bar{r}_s(t_4)$  have been replaced with a mean station location vector  $\bar{r}_s$ .

In the coherent mode, the second and third legs are missing from the expression for  $\Delta t_R$ , so that

$$\frac{\partial \Delta t_R}{\partial \bar{r}_1} = \frac{1}{c} (\hat{U}_5 - \hat{U}_4) \quad (7-64)$$

and

$$\frac{\partial \Delta t_R}{\partial \bar{r}_s} = - \frac{\partial \Delta t_R}{\partial \bar{r}_1} = \frac{1}{c} (\hat{U}_4 - \hat{U}_5) \quad (7-65)$$

where  $\hat{U}_5$  is a unit vector directed along leg 5.

#### 7.3.4 The Doppler Observation

The Doppler observation involves the counting of a number of cycles of a frequency returned from the relay satellite to determine its Doppler shift due to the motion of the relay and target satellites relative to the ground station and to one another. The actual frequency counting can be done by one of two methods, the destruct mode or the nondestruct mode.

In the destruct mode, the counter input frequency  $\nu_{in}$  is the sum of a bias frequency  $\nu_b$  plus one-fifth the Doppler frequency. This counter input frequency, nominally 0.1 MHz, is counted up to a fixed number of cycles  $N$ . The time required to count these  $N_0$  cycles is measured by  $C_0$ , the number of 100 MHz cycles



counted in the same time period. The counter is then reset to zero, giving rise to the nondestruct mode. The observation is the average Doppler frequency  $\bar{\nu}_d$ , which is related to the average value  $\bar{\nu}_{in}$  of the counter input frequency over the time interval by

$$\bar{\nu}_d = 5(\bar{\nu}_{in} - \nu_b) = 5 \left( \frac{N_0}{\Delta t_{RR}} - \nu_b \right) \quad (7-66)$$

In the nondestruct mode, the counter input frequency is the sum of a bias frequency plus 100 times the Doppler frequency. It is nominally 20 MHz, and is to be counted over a fixed time interval  $\Delta t_{RR}$ . The resulting count  $N_0$  is cumulative, since the counter is not reset to zero between measurements (hence the name nondestruct). The time interval  $\Delta t_{RR}$  over which each count is taken is the same as the time between measurements. The measurement is the cumulative count  $N_0$ . The average value of the Doppler frequency can be calculated from the raw measurement via the relationship

$$\bar{\nu}_d = \frac{\bar{\nu}_{in} - \nu_b}{100} = \frac{1}{100} \left( \frac{\Delta N}{\Delta t_{RR}} - \nu_b \right) \quad (7-67)$$

where  $\Delta N$  is the increase in the N-count since the previous measurement, after accounting for any counter overflows.

#### 7.3.4.1 Formulation of the Doppler Observation

In all three tracking modes considered, the counter input frequency  $\nu_{in}$  can be expressed in the form

$$\nu_{in} = \nu_{R_2} [A\alpha_1\alpha_2\beta_1\beta_2 + B\alpha_3\alpha_2 - C] \quad (7-68)$$

where  $\nu_{R_2}$  is the system reference frequency, the  $\alpha$ 's and  $\beta$ 's are the Doppler factors for individual transmission legs, and the coefficients A, B, and C are constants which depend only on the tracking mode counting method and the frequency options used ( $A = 0$  for the coherent mode). If the Lorentz factor (which is approximately  $1 + 10^{-12}$ ) affecting the timing of clocks moving with the tracking station is assumed to be unity, the Doppler-factor products in Equation (7-68) can be expressed as

$$\alpha_1\alpha_2\beta_1\beta_2 = 1 - \frac{\dot{\rho}_L}{c} \quad (7-69a)$$

and

$$\alpha_3 \alpha_2 = 1 - \frac{\dot{\rho}_S}{c} \quad (7-65b)$$

where  $\dot{\rho}_L$  is the time rate of change of the four-leg round trip range (ground station-to-relay-to-target-to-relay-to-ground station) and  $\dot{\rho}_S$  is the time rate of change of the two-leg round trip range (ground station-to-relay-to-ground station). These relationships are derived in detail in Reference 2.

The average Doppler frequency can then be expressed as

$$\begin{aligned} \bar{\nu}_d &= k(\bar{\nu}_{in} - \nu_b) = k\nu_R \left[ A \left( 1 - \frac{\dot{\rho}_L}{c} \right) + B \left( 1 - \frac{\dot{\rho}_S}{c} \right) - C \right] - k\nu_b \\ &= k \left[ \nu_R (A + B - C) - \nu_R \left( A \frac{\dot{\rho}_L}{c} + B \frac{\dot{\rho}_S}{c} \right) \right] - k\nu_b \quad (7-70) \\ &= -k\nu_R \left( A \frac{\dot{\rho}_L}{c} + B \frac{\dot{\rho}_S}{c} \right) \end{aligned}$$

where  $k$  is 5 or 0.01, depending on whether the destruct or nondestruct mode is being used, and  $\nu_R$  is the 5 MHz system reference frequency. For a particular tracking configuration, the bias term  $(A + B - C)$  and the coefficients  $A$  and  $B$  can be determined in advance, so that only the range rates  $\dot{\rho}_L$  and  $\dot{\rho}_S$  need to be modeled for observation.

The count obtained over a time interval  $\Delta t_{RR}$  in a destruct mode Doppler count is

$$\begin{aligned} N &= \int_{t_R}^{t_R + \Delta t_{RR}} \nu_{in} dt \\ &= \nu_b \Delta t_{RR} - \frac{\nu_R A}{c} \int_{t_R}^{t_R + \Delta t_{RR}} \dot{\rho}_L dt - \frac{\nu_R B}{c} \int_{t_R}^{t_R + \Delta t_{RR}} \dot{\rho}_S dt \quad (7-71) \\ &= \nu_b \Delta t_{RR} - \frac{\nu_R}{c} (A \Delta \rho_L + B \Delta \rho_S) \end{aligned}$$

where  $\Delta\rho_L$  and  $\Delta\rho_S$  are the changes in the four-leg and two-leg round trip ranges, respectively, during the time  $\Delta t_{RR}$ . The same equation applies in the nondestruct mode. These relationships permit modeling of the Doppler measurement using a backward light-time solution algorithm. For either destruct or nondestruct data, a light-time solution is performed at the time tag, yielding values of  $\rho_L$  and  $\rho_S$ . A second light-time solution is performed at the time tag plus  $\Delta t_{RR}$  for the destruct mode or at the time tag minus  $\Delta t_{RR}$  for the nondestruct mode. Values for  $\Delta\rho_L$  and  $\Delta\rho_S$  are obtained from these solutions, and a value of  $\Delta N$  is computed. The average Doppler frequency is set equal to  $k(\Delta N/\Delta t_{RR} - \nu_b)$ . Iterative calculations may be performed in the destruct mode, using a Newton-Raphson method with  $\Delta t_{RR}$  as the independent variable, until the calculated  $\Delta N$  is within a specified margin of the preset count  $N$ . Corrections, such as transponder delays, are not required, since only the differences are used in the Doppler light-time solutions.

#### 7.3.4.2 Partial Derivatives of the Doppler Measurement

Since the dimension of the Doppler measurement varies according to whether the destruct or nondestruct mode is being used, and since preprocessing of the data will often change the dimensions of the measured observations, GTDS converts all of the observations and expresses the partial derivatives in terms of the average Doppler frequency  $\bar{\nu}_d$ , i.e.,

$$\frac{\partial O_c}{\partial \bar{s}} = \frac{\partial \bar{\nu}_d}{\partial \bar{s}} \quad (7-72)$$

In this equation,  $\bar{s}$  is the total state vector, which includes both the position and velocity vectors. When  $\Delta t$  is modeled in the destruct mode

$$\Delta t = \frac{N_0}{\nu_b + \frac{\bar{\nu}_d}{5}} \quad (7-73)$$

and

$$\frac{\partial \Delta t}{\partial \bar{s}_0} = \frac{-N_0}{5 \left( \frac{\bar{\nu}_d}{5} + \nu_b \right)^2} \frac{\partial \bar{\nu}_d}{\partial \bar{s}_0} = \frac{-(\Delta t)^2}{5N_0} \frac{\partial \bar{\nu}_d}{\partial \bar{s}_0} \quad (7-74)$$

where  $\bar{s}_0$  is the state vector at epoch.

In the nondestruct mode

$$\Delta N = \Delta t_0 (100 \bar{\nu}_d + \nu_b) \quad (7-75)$$

and

$$\frac{\partial \Delta N}{\partial \bar{s}_0} = 100 \Delta t_0 \frac{\partial \bar{\nu}_d}{\partial \bar{s}_0} \quad (7-76)$$

Now,

$$\begin{aligned} \frac{\partial \bar{\nu}_d}{\partial \bar{s}_0} &= \frac{\partial}{\partial \bar{s}_0} \left[ -\frac{k \nu_R}{c} (A \bar{\dot{\rho}}_L + B \bar{\dot{\rho}}_S) \right] \\ &= -\frac{k \nu_R}{c} \left( A \frac{\partial \bar{\dot{\rho}}_L}{\partial \bar{s}_0} + B \frac{\partial \bar{\dot{\rho}}_S}{\partial \bar{s}_0} \right) \end{aligned} \quad (7-77)$$

where  $\bar{\dot{\rho}}_L$  and  $\bar{\dot{\rho}}_S$  represent the average range rates over the time interval  $\Delta t_{RR}$ . The average range rate is given by

$$\bar{\dot{\rho}} = \frac{\int_t^{t+\Delta t_{RR}} \dot{\rho} dt}{\int_t^{t+\Delta t_{RR}} dt} = \frac{\rho(t + \Delta t_{RR}) - \rho(t)}{\Delta t_{RR}} \quad (7-78)$$

and

$$\begin{aligned} \frac{\partial \bar{\dot{\rho}}}{\partial \bar{s}_0} &= \frac{1}{\Delta t_{RR}} \left\{ \frac{\partial \rho(t + \Delta t_{RR})}{\partial \bar{s}_0} - \frac{\partial \rho(t)}{\partial \bar{s}_0} \right\} \\ &= \frac{1}{\Delta t_{RR}} \left\{ \frac{\partial \rho(t + \Delta t_{RR})}{\partial \bar{s}(t + \Delta t_{RR})} \frac{\partial \bar{s}(t + \Delta t_{RR})}{\partial \bar{s}_0} - \frac{\partial \rho(t)}{\partial \bar{s}(t)} \frac{\partial \bar{s}(t)}{\partial \bar{s}_0} \right\} \\ &= \frac{1}{\Delta t_{RR}} \left\{ \frac{\partial \rho(t + \Delta t_{RR})}{\partial \bar{s}(t + \Delta t_{RR})} \Phi(t + \Delta t_{RR}, t_0) - \frac{\partial \rho(t)}{\partial \bar{s}(t)} \Phi(t, t_0) \right\} \end{aligned} \quad (7-79)$$

where  $\rho$  represents  $\rho_L$  or  $\rho_S$ , and  $\Phi(t, t_0)$  is the state transition matrix (see Section 6.5) from epoch time  $t_0$  to time  $t$ . As indicated in Section 7.3.3, the partial derivatives of the range with respect to any of the velocity components are zero. Thus, Equation (7-79) reduces to

$$\frac{\partial \bar{\rho}}{\partial \bar{s}_0} = \frac{1}{\Delta t_{RR}} \left\{ \frac{\partial \rho(t + \Delta t_{RR})}{\partial \bar{r}(t + \Delta t_{RR})} \tilde{\Phi}(t + \Delta t_{RR}, t_0) - \frac{\partial \rho(t)}{\partial \bar{r}(t)} \tilde{\Phi}(t, t_0) \right\} \quad (7-80)$$

where  $\tilde{\Phi}$  represents a modified state transition matrix, consisting of the first three rows of the state transition matrix, i.e.,

$$\tilde{\Phi}(t, t_0) = \frac{\partial \bar{r}(t)}{\partial \bar{s}(t_0)} \quad (7-81)$$

where  $\bar{r}$  represents the position vector of the relay satellite, the target satellite, or the ground station.

The partial derivatives of the average range rates  $\bar{\rho}_L$  and  $\bar{\rho}_S$  with respect to the relay satellite state at epoch can be expressed as

$$\begin{aligned} \frac{\partial \bar{\rho}_L}{\partial \bar{s}_1(t_0)} &= \frac{1}{\Delta t_{RR}} \left\{ \frac{\partial \rho_L(t + \Delta t_{RR})}{\partial \bar{r}_1(t + \Delta t_{RR})} \tilde{\Phi}_1(t + \Delta t_{RR}, t_0) - \frac{\partial \rho_L(t)}{\partial \bar{r}_1(t)} \tilde{\Phi}_1(t, t_0) \right\} \\ &= \frac{1}{\Delta t_{RR}} \left\{ (\hat{U}_1 - \hat{U}_2 + \hat{U}_3 - \hat{U}_4) \Big|_{t+\Delta t_{RR}} \tilde{\Phi}_1(t + \Delta t_{RR}, t_0) \right. \\ &\quad \left. - (\hat{U}_1 - \hat{U}_2 + \hat{U}_3 - \hat{U}_4) \Big|_t \tilde{\Phi}_1(t, t_0) \right\} \end{aligned} \quad (7-82)$$

$$\begin{aligned} \frac{\partial \bar{\rho}_S}{\partial \bar{s}_1(t_0)} &= \frac{1}{\Delta t_{RR}} \left\{ (\hat{U}_5 - \hat{U}_4) \Big|_{t+\Delta t_{RR}} \tilde{\Phi}_1(t + \Delta t_{RR}, t_0) \right. \\ &\quad \left. - (\hat{U}_5 - \hat{U}_4) \Big|_t \tilde{\Phi}_1(t, t_0) \right\} \end{aligned} \quad (7-83)$$

The partial derivatives with respect to the target satellite state are given by

$$\frac{\partial \bar{\rho}_L}{\partial \bar{s}_2(t_0)} = \frac{1}{\Delta t_{RR}} \left\{ (\hat{U}_2 - \hat{U}_3)|_{t+\Delta t_{RR}} \tilde{\Phi}_2(t + \Delta t_{RR}, t_0) - (\hat{U}_2 - \hat{U}_3)|_t \tilde{\Phi}_2(t, t_0) \right\} \quad (7-84)$$

and

$$\frac{\partial \bar{\rho}_S}{\partial \bar{s}_2(t_0)} = 0 \quad (7-85)$$

Finally, the partial derivatives with respect to the ground station state are

$$\frac{\partial \bar{\rho}_L}{\partial \bar{s}_S(t_0)} = \frac{1}{\Delta t_{RR}} \left\{ (\hat{U}_4 - \hat{U}_1)|_{t+\Delta t_{RR}} \tilde{\Phi}_S(t + \Delta t_{RR}, t_0) - (\hat{U}_4 - \hat{U}_1)|_t \tilde{\Phi}_S(t, t_0) \right\} \quad (7-86)$$

and

$$\frac{\partial \bar{\rho}_S}{\partial \bar{s}_S(t_0)} = \frac{1}{\Delta t_{RR}} \left\{ (\hat{U}_4 - \hat{U}_5)|_{t+\Delta t_{RR}} \tilde{\Phi}_S(t + \Delta t_{RR}, t_0) - (\hat{U}_4 - \hat{U}_5)|_t \tilde{\Phi}_S(t, t_0) \right\} \quad (7-87)$$

After the range-rate partial derivatives have been determined, an appropriate transformation must be applied to obtain the partial derivative of the input measurement. For example, the partial derivative of the Doppler count interval is given by

$$\frac{\partial \Delta t}{\partial \bar{s}_0} = \frac{-(\Delta t)^2}{N_0} \frac{\partial \bar{\nu}_d}{\partial \bar{s}_0} = \frac{(\Delta t)^2 \nu_R}{N_0 c} \left( A \frac{\partial \bar{\rho}_L}{\partial \bar{s}_0} + B \frac{\partial \bar{\rho}_S}{\partial \bar{s}_0} \right) \quad (7-88)$$

where A, B, and  $\nu_R$  are defined in Section 7.3.4.1.

The state vectors of the relay and target satellites may also depend on dynamic parameters (e.g., solar radiation, geopotential coefficients, etc.) which are to be solved for. If both state vectors have a common variable, the partial derivative is the sum of the two independent partial derivatives. For example, the partial derivative of the four-leg average range rate with respect to a gravitational constant G is

$$\begin{aligned}
\frac{\partial \bar{\rho}_L}{\partial G} &= \frac{1}{\Delta t_{RR}} \left\{ \frac{\partial \rho_L(t + \Delta t_{RR})}{\partial G} - \frac{\partial \rho_L(t)}{\partial G} \right\} \\
&= \frac{1}{\Delta t_{RR}} \left\{ \left( \frac{\partial \rho_L(t + \Delta t_{RR})}{\partial \bar{r}_1(t + \Delta t_{RR})} \frac{\partial \bar{r}_1(t + \Delta t_{RR})}{\partial G} \right. \right. \\
&\quad \left. \left. + \frac{\partial \rho_L(t + \Delta t_{RR})}{\partial \bar{r}_2(t + \Delta t_{RR})} \frac{\partial \bar{r}_2(t + \Delta t_{RR})}{\partial G} \right) \right. \\
&\quad \left. - \left( \frac{\partial \rho_L(t)}{\partial \bar{r}_1(t)} \frac{\partial \bar{r}_1(t)}{\partial G} + \frac{\partial \rho_L(t)}{\partial \bar{r}_2(t)} \frac{\partial \bar{r}_2(t)}{\partial G} \right) \right\} \\
&= \frac{1}{\Delta t_{RR}} \left\{ \left( \frac{\partial \rho_L(t + \Delta t_{RR})}{\partial \bar{r}_1(t + \Delta t_{RR})} \frac{\partial \bar{r}_1(t + \Delta t_{RR})}{\partial G} - \frac{\partial \rho_L(t)}{\partial \bar{r}_1(t)} \frac{\partial \bar{r}_1(t)}{\partial G} \right) \right. \\
&\quad \left. + \left( \frac{\partial \rho_L(t + \Delta t_{RR})}{\partial \bar{r}_2(t + \Delta t_{RR})} \frac{\partial \bar{r}_2(t + \Delta t_{RR})}{\partial G} - \frac{\partial \rho_L(t)}{\partial \bar{r}_2(t)} \frac{\partial \bar{r}_2(t)}{\partial G} \right) \right\}
\end{aligned}
\tag{7-89}$$

## 7.4 RADAR ALTIMETER MODEL

GTDS models the satellite's orbital state vector in inertial coordinates. However, the radar altimeter measures the height of the satellite relative to the actual sea surface at the subsatellite point. Thus, the observation modeling must relate the inertial coordinates to the actual sea surface height. This is accomplished by expressing both the satellite's position and the sea surface in body-fixed coordinates  $x_b$ ,  $y_b$  and  $z_b$ .

### 7.4.1 Surface Model

The sea surface is primarily determined by the earth's gravity potential, which is the sum of the gravitational potential and the potential of the centrifugal force resulting from the earth's rotation. A particular equipotential surface of the earth's geopotential field, called a geoid, passes through the mean sea level surface and is nearly spherical, with flattening at the poles and a pear-shaped bulge in the southern hemisphere. The geoid approximates very closely (within a meter

or two) the real sea surface in ocean areas. Small static and dynamic differences between the instantaneous sea surface and the geoid are caused by currents, tides, and weather phenomena. Typical magnitudes of these deviations (References 3 and 4) are presented in Table 7-1.

Table 7-1.  
Sea Surface – Geoid Deviation Sources

Source	Typical Magnitude
Sea swell	1 meter
Wind waves	1 meter
Storm surges	10 centimeters
Barotropic depressions	10 centimeters
Currents	1 meter
Tides	1 meter

Since complete information is unavailable for modeling these small effects, they are neglected in the radar altimeter model.

A reference surface is utilized which is conveniently chosen to be a rotationally symmetric ellipsoid that best fits the geoid in a least squares sense. The maximum distance between this ellipsoid and the geoid is approximately 100 meters. This ellipsoidal surface also represents an equipotential surface of the normal geopotential, which includes (in addition to the point-mass term) even zonal harmonic coefficients, of which only  $C_2^0$  and  $C_4^0$  are significant. As a result, the sum of the additional terms needed to fully describe the geopotential (i.e., the disturbing potential) is small (Reference 5).

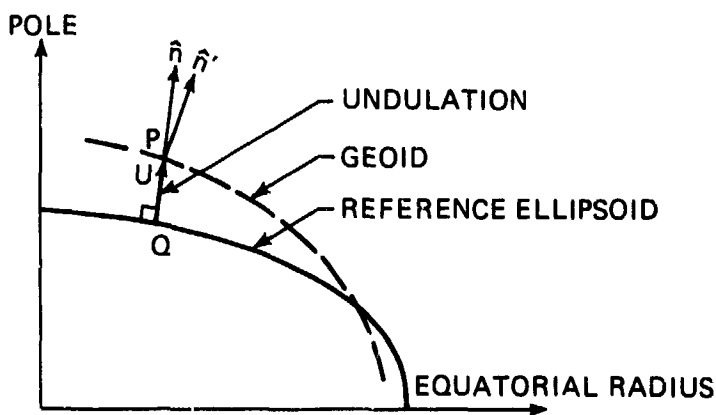


Figure 7-2. Geoid Undulation



Figure 7-2 shows an exaggerated cross section of the geoid and the reference ellipsoid. The distance measured along the normal to the reference ellipsoid from point Q to the point P on the geoid is called the geoidal undulation and is designated by U. Expressing the geopotential function  $\psi$  as the sum of the normal geopotential  $\psi_N$  and the disturbing potential  $\psi_D$  yields

$$\psi(r, \phi', \lambda) = \psi_N(r, \phi', \lambda) + \psi_D(r, \phi', \lambda) \quad (7-92)$$

where, from Section 4.3,

$$\psi_N(r, \phi', \lambda) = \frac{\mu}{r} + \frac{\mu}{r} \left[ C_2^0 \left( \frac{R_e}{r} \right)^2 P_2^0(\sin \phi') + C_4^0 \left( \frac{R_e}{r} \right)^4 P_4^0(\sin \phi') \right] \quad (7-93)$$

and

$$\begin{aligned} \psi_D(r, \phi', \lambda) = & \frac{\mu}{r} \left[ \Delta C_2^0 \left( \frac{R_e}{r} \right)^2 P_2^0(\sin \phi') + \Delta C_4^0 \left( \frac{R_e}{r} \right)^4 P_4^0(\sin \phi') \right] \\ & + \frac{\mu}{r} \sum_{\substack{n=2 \\ n \neq 2,4}}^{\infty} C_n^0 \left( \frac{R_e}{r} \right)^n P_n^0(\sin \phi') \\ & + \frac{\mu}{r} \sum_{n=2}^{\infty} \sum_{m=1}^n \left( \frac{R_e}{r} \right)^n P_n^m(\sin \phi') [S_n^m \sin m\lambda + C_n^m \cos m\lambda] \end{aligned} \quad (7-94)$$

In these equations,  $r$  is the geocentric radius,  $\phi'$  is the geocentric latitude,  $\lambda$  is the longitude, and  $R_e$  is the earth's equatorial radius. The geopotential function (the sum of the normal geopotential and the disturbing potential) differs from the gravitational potential in that it includes a term which represents the centrifugal potential due to the earth's rotation. This term is included in the second zonal harmonic coefficient. Furthermore, the  $C_4^0$  term in the normal geopotential is a function of  $C_2^0$ , whereas  $C_2^0$  and  $C_4^0$  are not functionally related in the gravitational potential. Consequently,  $\Delta C_2^0$  and  $\Delta C_4^0$  are included in Equation (7-94) to account for these differences.

In order to evaluate the magnitude of the geoidal undulations, the geoid of potential  $\psi_0$  is compared with the reference ellipsoid of the same potential  $\psi_N(Q) = \psi_0$ . The normal potential  $\psi_N(P)$  at P can be approximated by the linear relationship

$$\psi_N(P) = \psi_N(Q) + \left( \frac{\partial \psi_N}{\partial \hat{n}} \right)_Q U = \psi_N(Q) - \gamma(Q) U \quad (7-95)$$

where  $\gamma(Q)$  is normal gravity, i.e., the magnitude of the gradient of the normal geopotential on the reference ellipsoid at the point Q, where the algebraic sign is consistent with geodetic convention.

By definition

$$\psi(P) = \psi_N(P) + \psi_D(P) \quad (7-96)$$

and

$$\psi(P) = \psi_0 = \psi_N(Q) \quad (7-97)$$

Substituting Equations (7-96) and (7-97) into Equation (7-95) yields Brun's Formula (Reference 5) for the geoidal undulation

$$U = \frac{\psi_D(P)}{\gamma(Q)} \quad (7-98)$$

The geoidal undulation  $U$  is a function of the disturbing potential at the point  $P$  and normal gravity  $\gamma$  at the point  $Q$ . However, frequently the coordinates of the point  $Q$  are known, but not those of point  $P$ . In this case, evaluation of the disturbing potential  $\psi_D$  at  $Q$  instead of  $P$  will cause only a small error in the calculation of  $U$ .

A better approximation for the disturbing potential  $\psi_D(P)$  can be obtained by correcting the geocentric radius  $r$  by the undulation  $U$ , calculated as described above. This value can then be used in Equation (7-98) to obtain a better value of  $U$ . Standard (normal) gravity, which is the gradient of the normal potential  $\psi_N$ , is derived as a function of geodetic latitude and equatorial gravity in Reference 3, yielding

$$\gamma = \gamma_e (1 - f_2 \sin \phi + f_4 \sin^4 \phi) \quad (7-99)$$

where

$$f_2 = -f + \frac{5}{2}m + \frac{1}{2}f^2 - \frac{26}{7}fm + \frac{15}{4}m^2 \quad (7-100a)$$

$$f_4 = -\frac{1}{2}f^2 + \frac{5}{2}fm \quad (7-100b)$$

$$m + \frac{3}{2}m^2 = \frac{\omega^2 R_e}{\gamma_e} \quad (7-100c)$$

and

$\gamma_e \sim$  normal equatorial gravity, which is  $978.049 \text{ cm/sec}^2$  for the International Ellipsoid

$\omega \sim$  earth's rotation rate  $= 0.72921151 \times 10^{-4} \text{ rad/sec}$

$\phi \sim$  geodetic latitude

$f \sim$  flattening of the reference ellipsoid;  $f = (a - b)/c$ , where  $a$  and  $b$  are the semimajor and semiminor axes, respectively, of the reference ellipsoid.

The value of  $m$  is obtained iteratively from the expression

$$m_n = \frac{\Omega^2 R_e}{\gamma_e} - \frac{3}{2} m_{n-1}^2 \quad (7-101)$$

starting from  $m_0 = 0.00344986$ .

The normal geopotential field and the normal gravity field of the reference ellipsoid are determined by four constants, usually chosen to be

$a \sim$  semimajor axis of the reference ellipsoid

$f \sim$  flattening of the reference ellipsoid

$\gamma_e \sim$  equatorial gravity

$\omega \sim$  earth's angular speed of rotation.

The flattening  $f$  of the reference ellipsoid of revolution and the values of  $C_2^0$  for the spherical harmonic expansion of the normal potential are directly related. Thus,  $C_2^0$  can be used instead of  $f$  as one of the four constants.

#### 7.4.2 Measurement Equation

Ideally, the radar altimeter measure the minimum distance from the spacecraft to the sea surface, which is equivalent to the distance from the sea surface to the spacecraft measured normal to the sea surface. Since the sea surface is closely approximated by the geoid, the geoid is a convenient reference surface for altimetry; however, the present global mathematical models of the geoid are

not accurate in fine detail. In the remainder of this section, the term geoid will denote the mathematical model of the geoid represented by means of a spherical harmonic expansion.

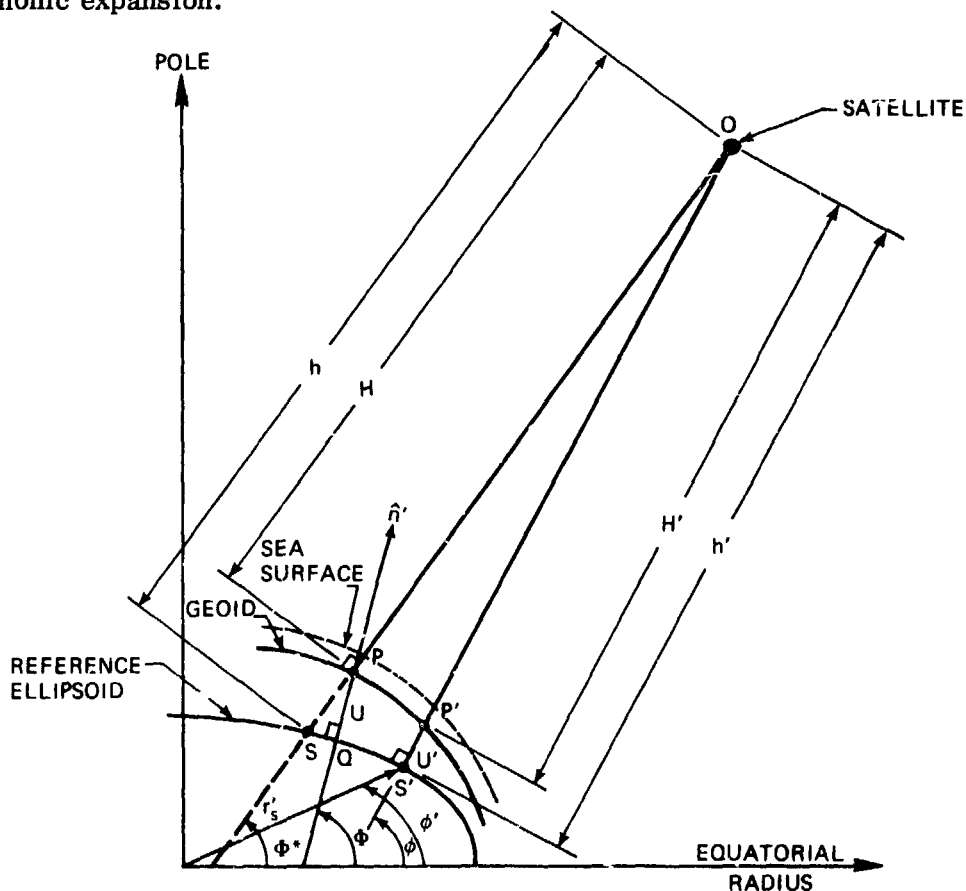


Figure 7-3. Geoid Geometry

The minimum distance from the geoid to the spacecraft is indicated by the line segment  $OP$  in Figure 7-3. Solving for this distance is difficult because of the complicated form of the equations for the geopotential. Therefore, an approximation to the distance  $H$  is made by using the length  $H'$  of the line segment  $OP'$  along the normal to the reference ellipsoid passing through the spacecraft.

The spacecraft position is assumed to be known in earth-fixed Cartesian coordinates  $x_b$ ,  $y_b$ , and  $z_b$  by transforming from inertial to body-fixed coordinates using the methods of Section 3.3.1. The geocentric latitude  $\phi'$ , the longitude  $\lambda$ , and the magnitude  $r_b$  of the position vector to the spacecraft are given by

$$\phi' = \tan^{-1} \left[ \frac{z_b}{\sqrt{x_b^2 + y_b^2}} \right] \quad (7-102)$$

$$\lambda = \tan^{-1} \left[ \frac{y_b}{x_b} \right] \quad (7-103)$$

and

$$r_b = \sqrt{x_b^2 + y_b^2 + z_b^2} \quad (7-104)$$

The geodetic latitude  $\phi$  and altitude  $h'$  to the subsatellite point  $S'$  on the reference ellipsoid are obtained from Section 3.3.6 as

$$\tan \phi = \frac{z_b}{\sqrt{x_b^2 + y_b^2}} \left[ 1 - \frac{N}{(N + h')} (2f - f^2) \right]^{-1} \quad (7-105)$$

where

$$N = \frac{R_e}{\sqrt{1 - (2f - f^2) \sin^2 \phi}} \quad (7-106)$$

and

$$h' = \frac{\sqrt{x_b^2 + y_b^2}}{\cos \phi} - N \quad (7-107)$$

Equations (7-105), (7-106), and (7-107) must be solved iteratively.

The geoid undulation  $U'$  at  $S'$  is obtained from Brun's Equation, Equation (7-98), (where  $\psi_D(P)$  is given in Equation (7-94) and  $\gamma(S')$  is given in Equation (7-99)) and, if necessary, using the procedure described in Section 7.4.1 to obtain the required precision.

Therefore, the resulting approximation for  $H$  is

$$H \cong H' = h' - u' \quad (7-108)$$

### 7.4.3 Partial Derivatives

Partial derivatives of the observation are determined by transforming the observation partial derivatives with respect to body-fixed coordinates to partial derivatives with respect to inertial Cartesian coordinates as described in Section 7.2.2. The partial derivative of  $H$  with respect to  $\bar{r}_b$  is transformed to a partial derivative with respect to  $\bar{R}$  as follows

$\frac{\partial}{\partial \bar{R}}$

$$\frac{\partial H}{\partial \bar{R}} = \frac{\partial H}{\partial \bar{r}_b} \frac{\partial \bar{r}_b}{\partial \bar{R}} = \frac{\partial H}{\partial \bar{r}_b} \quad (7-109)$$

The partial derivative of  $H$  in Equation (7-109) involves numerous higher order terms because of the dependence of the location of  $P'$  (Figure 7-3) on the undulation  $U'$  and the coordinates  $x_b$ ,  $y_b$ , and  $z_b$ . However, these effects can be neglected to first order. The partial derivative of  $H$  with respect to  $\bar{r}_b$  is therefore approximated as

$$\frac{\partial H}{\partial \bar{r}_b} = \frac{\partial h'}{\partial \bar{r}_b} = \frac{\bar{h}'^T}{h'} \quad (7-110)$$

where

$$\bar{h}' = \begin{bmatrix} x_b - x' \\ y_b - y' \\ z_b - z' \end{bmatrix} \quad (7-111)$$

Equation (7-110) is exact for a spherical geoid.

## 7.5 VERY LONG BASELINE INTERFEROMETER (VLBI) MODEL

The Very Long Baseline Interferometer (VLBI) system records signals transmitted by a satellite, along with timing signals from a local atomic clock, at two or more ground stations. The presence at each station of accurate atomic clocks, which can be coordinated by comparison with portable clocks dispatched between stations, means that the signals from the satellite recorded at each station can be time correlated with great precision. The ground stations measure phase differences between simultaneously received signals transmitted by the spacecraft. The observables are a phase difference time interval  $\tau$  and its time derivative  $\dot{\tau}$ . The time difference  $\tau$  is the difference in the spacecraft range as measured from each of the ground stations on a given baseline, divided by the speed of light  $c$ . Neglecting atmospheric effects, the time difference between reception of the same wavefront or phase at the first and second stations is

$$\tau = \frac{1}{c} (\rho_1 - \rho_2) = \frac{1}{c} \left\{ |\bar{r}_{1t_1}(t)| - |\bar{r}_{1t_2}(t + \tau)| \right\} \quad (7-112)$$

where  $\rho_1$  and  $\rho_2$  are the ranges from the first and second stations to the satellite, respectively. The range vectors  $\bar{r}_{1t_1}$  and  $\bar{r}_{1t_2}$  are evaluated in the local tangent plane system centered at the first and second stations, respectively. An iterative procedure is required to determine  $\tau$ , since the actual light time between the satellite and the station is not known initially. The iteration is initiated by assuming that  $\tau$  is zero on the right-hand side of Equation (7-112).

The time-rate (Doppler) difference  $\dot{\tau}$  is the difference in spacecraft range rate as measured from each station and divided by  $c$ , i.e.,

$$\dot{\tau} = \frac{1}{c} (\dot{\rho}_1 - \dot{\rho}_2) = \frac{1}{c} \left[ \left( \frac{\bar{r}_{1t_1}(t) \cdot \dot{\bar{r}}_{1t_1}(t)}{\rho_1} \right) - \left( \frac{\bar{r}_{1t_2}(t + \tau) \cdot \dot{\bar{r}}_{1t_2}(t + \tau)}{\rho_2} \right) \right] \quad (7-113)$$

The partial derivatives of  $\tau$  and  $\dot{\tau}$  with respect to the epoch state vector components and dynamic model parameters are given by

$$\begin{aligned} \frac{\partial \tau}{\partial \bar{p}} = \frac{1}{c} \left\{ \frac{\partial \rho_1(t)}{\partial \bar{r}_{1t}(t)} \frac{\partial \bar{r}_{1t}(t)}{\partial \bar{R}(t)} \frac{\partial \bar{R}(t)}{\partial \bar{p}} \right. \\ \left. + \frac{\partial \rho_2(t')}{\partial \bar{r}_{1t}(t')} \frac{\partial \bar{r}_{1t}(t')}{\partial \bar{R}(t')} \frac{\partial \bar{R}(t')}{\partial \bar{p}} \right\} \end{aligned} \quad (7-114a)$$

$$\begin{aligned} \frac{\partial \dot{\tau}}{\partial \bar{p}} = \frac{1}{c} \left\{ \frac{\partial \dot{\rho}_1(t)}{\partial \bar{r}_{1t}(t)} \frac{\partial \bar{r}_{1t}(t)}{\partial \bar{R}(t)} \frac{\partial \bar{R}(t)}{\partial \bar{p}} \right. \\ + \frac{\partial \dot{\rho}_1(t)}{\partial \dot{\bar{r}}_{1t}(t)} \left( \frac{\partial \dot{\bar{r}}_{1t_1}(t)}{\partial \bar{R}(t)} \frac{\partial \bar{R}(t)}{\partial \bar{p}} + \frac{\partial \dot{\bar{r}}_{1t_1}(t)}{\partial \dot{\bar{R}}(t)} \frac{\partial \dot{\bar{R}}(t)}{\partial \bar{p}} \right) \\ - \frac{\partial \dot{\rho}_2(t')}{\partial \bar{r}_{1t_2}(t')} \frac{\partial \bar{r}_{1t}(t')}{\partial \bar{R}(t')} \frac{\partial \bar{R}(t')}{\partial \bar{p}} \\ \left. + \frac{\partial \dot{\rho}_2(t')}{\partial \dot{\bar{r}}_{1t_2}(t')} \left( \frac{\partial \dot{\bar{r}}_{1t_2}(t')}{\partial \bar{R}(t')} \frac{\partial \bar{R}(t')}{\partial \bar{p}} + \frac{\partial \dot{\bar{r}}_{1t_2}(t')}{\partial \dot{\bar{R}}(t')} \frac{\partial \dot{\bar{R}}(t')}{\partial \bar{p}} \right) \right\} \end{aligned} \quad (7-114b)$$

where  $t' = t + \tau$ .

The partial derivatives  $\partial \bar{R}(t)/\partial \bar{p}$  and  $\partial \dot{\bar{R}}(t)/\partial \bar{p}$  are obtained from solutions to the variational equations; the partial derivatives  $\partial \bar{r}_{1t}(t)/\partial \bar{R}(t)$ ,  $\partial \dot{\bar{r}}_{1t}(t)/\partial \bar{R}(t)$ , and  $\partial \dot{\bar{r}}_{1t}(t)/\partial \dot{\bar{R}}(t)$  are presented in Section 7.2.2; and the partial derivatives of the  $\rho$ 's and  $\dot{\rho}$ 's with respect to their respective station-centered local tangent plane coordinates are given in Sections 7.2.3.2 and 7.2.3.3.

## 7.6 ATMOSPHERIC EFFECTS

All satellite radar tracking observations from ground tracking stations are affected by the propagation characteristics of electromagnetic radiation through the earth's atmosphere. The bending, or refraction, of the rays means that a measurement of the direction of the signal propagation at the ground does not correspond to the direction of the relative position vector between the spacecraft and the tracking station. This ray bending also requires that the interpretation of the Doppler-shift measurement must be based on the projection of the appropriate velocity along the local propagation path direction, not along the relative position vector. Since the local propagation speed in the atmosphere is different from the vacuum speed, the interpretation of time-delay measurements must account for this effect.

In principle, the refraction effects may be characterized in terms of the variable local index of refraction  $n$  of the medium through which the signal is propagated. It is assumed in the correction algorithms that locally the atmosphere is spherically symmetric with respect to the center of the earth; therefore,  $n$  varies only with the altitude  $h$  (measured radially) at each tracking station. However, the  $n$  versus  $h$  profile is determined as a function of the station location and the variations in solar flux. The nature of these dependencies is discussed in the following sections, which present the mathematical algorithms characterizing the three basic refraction effects considered.

### 7.6.1 Troposphere Model (References 6 and 7)

The troposphere is the familiar gaseous atmosphere, which extends from the earth's surface upward to a sensible limit of about 30 kilometers. For the microwave frequencies of interest in spacecraft tracking, the troposphere is essentially a nondispersive medium, i.e., the index of refraction  $n$  is independent of the frequency of the signal transmitted through it. Within this region,  $n$  is expressed as

$$n = 1 + N_T \quad (7-115)$$

where the tropospheric refractivity  $N_T$  depends only on the thermodynamic properties of the air. Since temperature and pressure data are not readily available at altitude, surface data are used to compute the surface refractivity  $N_s$ , and an exponential decay with altitude is assumed

$$N_T = N_s e^{-(h-h_s)/H_T} \quad (7-116)$$



where  $h_s$  and  $N_s$  are the altitude and refractivity at the tracking site, respectively, and  $H_T$  is the tropospheric scale height, i.e.,

$$H_T = \frac{1}{N_s} \int_{h_s}^{\infty} N_T(h) dh$$

The National Bureau of Standards Central Radio Propagation Laboratory (NBS CRPL) gives values of the scale height for different values of the surface refractivity. Reference 6 stresses the importance of using corresponding values of  $H_T$  and  $N_s$ . (Some formulations have fixed  $H_T$  at a standard value, allowing only  $N_s$  to vary.)

### 7.6.2 Ionosphere Models (References 8 through 12)

Above the troposphere is another "atmosphere" called the ionosphere, consisting of ionized particles and extending from about 80 kilometers to beyond 1000 kilometers. The index of refraction  $n$  is less than 1 in this dispersive medium and it is expressed rigorously in terms of the ionospheric refractivity  $N_I$ . For the sign convention chosen, the ionospheric refractivity  $N_I > 0$  and

$$n^2 = 1 - 2N_I \quad (7-117)$$

The difference from unity is small, and to first order in the refractivity  $N_I$ ,  $n$  can be written in a form analogous to that for the troposphere

$$n = 1 - N_I \quad (7-118)$$

The refractivity depends on the electron density  $N_e$  (in electrons/m<sup>3</sup>) and the signal frequency  $\nu$  (in Hz) according to

$$N_I = \frac{40.3 N_e}{\nu^2} \quad (7-119)$$

The electron density profile for the ionosphere reaches a maximum value  $N_m$  at altitude  $h_m$ , decaying to zero very rapidly below, and very slowly above, this altitude (Figure 7-4). The exact shape of the profile and the values of  $N_m$  and  $h_m$  are highly variable functions of geographical location, time of day, season, and sunspot activity. If sufficient ionospheric sounding data are measured (with an

ionosonde or a backscattering radar) at a given location and time, a reasonably accurate construction can be made of the electron density profile. From these data, interpolated to the time and geographic location of interest, the values of  $N_m$  and  $h_m$  can be estimated.

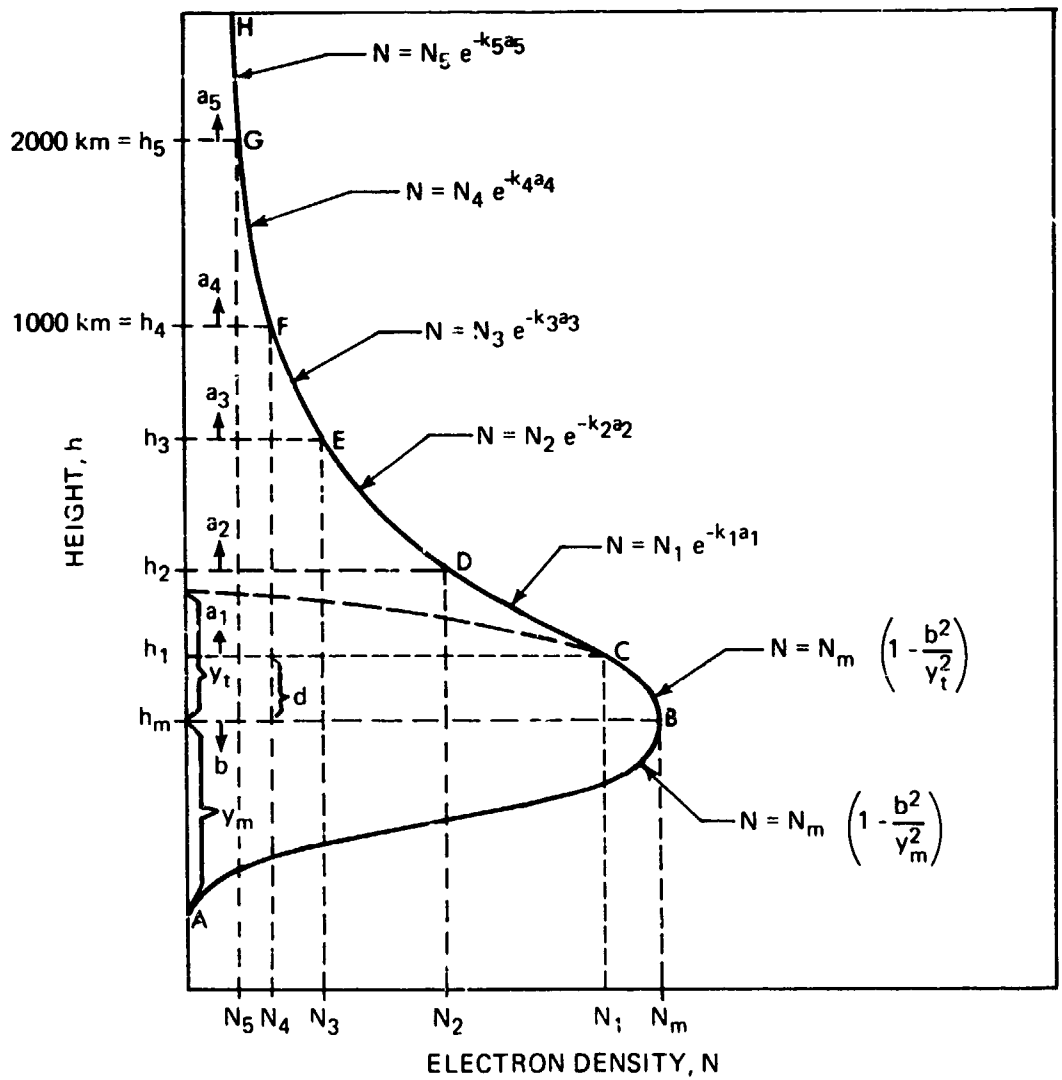


Figure 7-4. Empirical Worldwide Electron Density Profile

7.6.2.1 Modified Chapman Profile

The quantities  $N_m$  and  $h_m$  define only one point on the electron density versus altitude profile. The other points can be assumed to lie on a modified Chapman profile in the form (Reference 8)

$$N_e = N_m e^{(1-z-e^{-z})} \tag{7-120}$$

$$z = \frac{h - h_m}{H_I} \tag{7-121}$$

where  $h$  is the altitude and  $H_I$  is the ionospheric scale height.

Substituting the modified Chapman profile (Equation (7-120)) into Equation (7-119) gives

$$N_I = \frac{40.3 N_m}{\nu^2} e^{(1-z-e^{-z})} \tag{7-122}$$

as the altitude variation of the ionospheric refractivity.

It is generally conceded that the modified Chapman profile does not represent the best possible normalized profile. The fixed ratio of the total electron content above the maximum point to that below tends to be too large, on the average, compared with the observed diurnal variation. However, the theoretical foundation upon which Chapman based the derivation (Reference 9) and the susceptibility of the function to treatment of refraction effects in a closed analytical form argue for its continued use.

In GTDS, the maximum electron density  $N_m$  and its associated altitude  $h_m$  are determined as functions of the tracking station location and the variations in solar flux. The method of characterizing and determining these variables is described in Section 7.6.2.3. The ionospheric scale height is given in Reference 8 as

$$H_I = \frac{5}{3} [30 + 0.2(h_m - 200)] \text{ (km)} \tag{7-123}$$

### 7.6.2.2 Empirical Worldwide Profile

The electron density profile is modeled as consisting of a bi-parabolic bottomside layer, a parabolic topside layer, and a five-sectioned topside exponential layer, as shown in Figure 7-4. This profile is defined by the following equations

#### Bottomside

$$N_I = N_m \left( 1 - \frac{b^2}{y_m^2} \right)^2 \quad (\text{Segment A-B}) \quad (7-124)$$

#### Topside

$$N_I = N_m \left( 1 - \frac{b^2}{y_t^2} \right) \quad (\text{Segment B-C}) \quad (7-125a)$$

$$N_I = N_1 e^{-k_1 a_1} \quad (\text{Segment C-D}) \quad (7-125b)$$

$$N_I = N_2 e^{-k_2 a_2} \quad (\text{Segment D-E}) \quad (7-125c)$$

$$N_I = N_3 e^{-k_3 a_3} \quad (\text{Segment E-F}) \quad (7-126d)$$

$$N_I = N_4 e^{-k_4 a_4} \quad (\text{Segment F-G}) \quad (7-125e)$$

$$N_I = N_5 e^{-k_5 a_5} \quad (\text{Segment G-H}) \quad (7-125f)$$

where

$$y_t = \alpha y_m \quad (7-126a)$$

$$\alpha = \begin{cases} 1 & \text{for } f_0 F_2 \leq 10.5 \text{ MHz} \\ 1 + .1333 (f_0 F_2 - 10.5) & \text{for } f_0 F_2 > 10.5 \text{ MHz} \end{cases} \quad (7-126b)$$

$$b = h - h_m \quad (7-126c)$$

$$a_1 = h - h_1 \quad (7-126d)$$

$$a_2 = h - h_2 \quad (7-126e)$$

$$a_3 = h - h_3 \quad (7-126f)$$

$$a_4 = h - h_4 \quad (7-126g)$$

$$a_5 = h - h_5 \quad (7-126h)$$

The empirical profile is completely defined by the parameters  $h_m$ ,  $N_m$ , and  $y_m$  for the bottomside segment, and  $N_1$ ,  $N_2$ ,  $N_3$ ,  $N_4$ ,  $N_5$ ,  $k_1$ ,  $k_2$ ,  $k_3$ ,  $k_4$ ,  $k_5$ ,  $h_1$ ,  $h_2$ ,  $h_3$ ,  $h_4$ , and  $h_5$  for the topside segment. The maximum electron density point ( $h_m$ ,  $N_m$ ) is determined as a function of the location and the variations of the solar flux as described in Section 7.6.2.3. The parameters  $h_1$  through  $h_5$  are defined as follows

$$h_1 = h_m + d \quad (7-127a)$$

$$h_2 = h_1 + \frac{1}{3} (1.0 \times 10^3 - h_1) \quad (7-127b)$$

$$h_3 = h_1 + \frac{2}{3} (1.0 \times 10^3 - h_1) \quad (7-127c)$$

$$h_4 = 1000 \text{ km} \quad (7-127d)$$

$$h_5 = 2000 \text{ km} \quad (7-127e)$$

and  $d$  can be determined from

$$d = \frac{\sqrt{1 + k_1^2 y_t^2} - 1}{k_1} \quad (7-128)$$

The values of  $N_1$  through  $N_5$  are determined sequentially for the adjacent lower profile segments so as to maintain continuity of  $N_f$  at the segment interfaces

$$N_1 = \left(1 - \frac{d^2}{y_t^2}\right) N_m \quad (7-129a)$$

$$N_2 = N_1 e^{-k_1(h_2 - h_1)} \quad (7-129b)$$

$$N_3 = N_2 e^{-k_2(h_3 - h_2)} \quad (7-129c)$$

$$N_4 = N_3 e^{-k_3(h_4 - h_3)} \quad (7-129d)$$

$$N_5 = N_4 e^{-k_4(h_5 - h_4)} \quad (7-129e)$$

The final independent variables for the segmented  $N_I$  versus  $h$  profile are the maximum electron density  $N_m$ , its associated altitude  $h_m$ , the half-thickness of the bottomside layer  $y_m$ , and the decay constants  $k_1$  through  $k_5$  for the five topside exponential layers, respectively. The method for determining these variables in GTDS is described in Section 7.6.2.3.

### 7.6.2.3 Electron Density Profile Parameters

Both the Chapman and the empirical profiles require the maximum electron density  $N_m$  and its associated altitude  $h_m$ . These variables are determined (References 10 and 12) as functions of the critical frequency of the  $F_2$  layer,  $f_o F_2$ , and the M-factor, which is the ratio of  $MUF(3000)F_2$  (the highest frequency usable for a 3000 kilometer single hop propagation via the  $F_2$  layer) to the critical frequency  $f_o F_2$ , i.e.,

$$\begin{aligned} h_m &= [1346.92 - 526.40 \times (M\text{-factor}) + 59.825 \times (M\text{-factor})^2] \\ N_m &= 1.24 \times 10^{-2} \times (f_o F_2)^2 \end{aligned} \quad (7-130)$$

where  $N_m$  is in electrons/ $m^3$ ,  $h_m$  is in kilometers, and  $f_o F_2$  is in Hertz. The critical frequency and the M-factor are functions of location and the variations of the solar flux.

The critical frequency  $f_o F_2$  and the M-factor (also denoted  $M(3000)F_2$ ), required for the profile calculation, are computed from monthly  $U_{s,k}$  coefficient sets using equations based on Fourier series expansions and spherical harmonic analysis, which were developed by the Institute for Telecommunication Sciences (ITS) in Boulder (now National Oceanic and Atmospheric Administration - Boulder).

The values of  $f_o F_2$  and  $M(3000)F_2$  are functions  $\Omega(\phi, \lambda, T)$  of geodetic latitude  $\phi$ , longitude  $\lambda$ , and time  $T$ . The function  $\Omega(\phi, \lambda, T)$  can be expressed by a series of products of time-dependent functions  $D(T)$  and position-dependent geodetic functions  $G(\phi, \lambda)$ :

$$\Omega(\phi, \lambda, T) = \Omega[D(T), G(\phi, \lambda)] = \sum_{k=0}^K D_k(T) G_k(\phi, \lambda) \quad (7-131)$$

where  $K$  is the cutoff point for the approximate representation of  $\Omega$ ;  $K = 75$  when  $\Omega = f_o F_2$ , and  $K = 48$  when  $\Omega = M(3000)F_2$ . These cutoff points were originally determined using a Student's  $t$  test.

The time-dependent functions can be expanded in their Fourier series representation with the coefficients  $A_j^{(k)}$  and  $B_j^{(k)}$

$$D_k(T) = A_0^{(k)} + \sum_{j=1}^H (A_j^{(k)} \cos jT + B_j^{(k)} \sin jT) \quad (7-132)$$

The number of harmonics retained in the series is  $H$ ; higher harmonics are not considered since they are produced more by noise than by real physical variation. It is sufficient to use  $H = 6$  for the  $f_0 F_2$  computation and  $H = 4$  for the  $M(3000)F_2$  computation.

The Fourier coefficients  $A_j^{(k)}$  and  $B_j^{(k)}$  are numerically mapped as predicted, or final, coefficients  $U_{j,k}$ , which are the  $f_0 F_2$  or  $M(3000)F_2$  coefficient sets used for the  $f_0 F_2$  and  $M(3000)F_2$  computations, respectively.

$$\begin{aligned} A_j^{(k)} &= U_{2j,k} & j &= 0, 1, \dots, H \\ B_j^{(k)} &= U_{2j-1,k} & j &= 1, 2, \dots, H \end{aligned} \quad (7-133)$$

Thus,

$$\begin{aligned} \Omega(\phi, \lambda, T) &= \sum_{k=0}^K U_{0,k} G_k(\phi, \lambda) + \sum_{j=1}^H \left[ \cos jT \cdot \sum_{k=0}^K U_{2j,k} G_k(\phi, \lambda) \right. \\ &\quad \left. + \sin jT \cdot \sum_{k=0}^K U_{2j-1,k} G_k(\phi, \lambda) \right] \end{aligned} \quad (7-134)$$

The geodetic functions  $G_k(\phi, \lambda)$  are linear combinations of the surface spherical harmonics. Extensive investigations to find the best arguments for the harmonic functions resulted in the use of the modified magnetic dip  $x = x(\phi, \lambda)$ , since smaller residuals between the measured and computed test data values for  $f_0 F_2$  were obtained for this case than for any other case. Thus,  $G_k(\phi, \lambda)$  is both an explicit and an implicit function of latitude  $\phi$  and longitude  $\lambda$ , i.e.,

$$G_0(\phi, \lambda) = \sin^{q_0} x \quad (7-135)$$

$$G_k(\phi, \lambda) = \sin^{q_k} x \cdot \cos^k \phi \cdot \sin k\lambda$$

$$k = 1, 2, \dots, K$$

where  $q_k$  denotes the highest power of  $\sin x$  for the  $k^{\text{th}}$  order harmonic in longitude.

The modified magnetic dip  $x$  is an explicit function of latitude and the magnetic dip  $\ell$ , where  $\ell$  is computed from the magnetic field components  $X(\phi, \lambda)$ ,  $Y(\phi, \lambda)$ ,  $Z(\phi, \lambda)$ , i.e.,

$$\sin x = \frac{1}{\sqrt{\ell^2 + \cos \phi}}, \quad \ell = \tan^{-1} \left[ \frac{-Z}{\sqrt{X^2 + Y^2}} \right] \quad (7-136)$$

where  $X$ ,  $Y$ , and  $Z$  are the north, east, and vertical components of the magnetic field vector. They are computed following the spherical harmonic analysis of the magnetic field by Chapman and Bartels, as discussed in detail in Reference 11. Defining

$$\theta = 90^\circ - \phi \quad \text{and} \quad R = \frac{R_e}{R_e + h_m}$$

where  $R_e \sim$  equatorial radius of the earth

$h_m \sim$  height of the  $F_2$  layer

the following expressions for  $X$ ,  $Y$ , and  $Z$  result

$$\begin{aligned} X &= \sum_{n=1}^6 \sum_{m=0}^n \frac{d}{d\theta} P_{n,m}(\cos \theta) [g_n^m \cos m\lambda + h_n^m \sin m\lambda] R^{n+2} \\ Y &= \sum_{n=1}^6 \sum_{m=0}^n \frac{m P_{n,m}(\cos \theta)}{\sin \theta} [g_n^m \sin m\lambda - h_n^m \cos m\lambda] R^{n+2} \\ Z &= \sum_{n=1}^6 \sum_{m=0}^n -(n+1) P_{n,m}(\cos \theta) [g_n^m \cos m\lambda + h_n^m \sin m\lambda] R^{n+2} \end{aligned} \quad (7-137)$$



Values tabulated from the analysis of the magnetic field for Epoch 1960 are used for the coefficients  $g_n^m$  and  $h_n^m$ . The quantity  $P_{n,m}(\cos \theta)$  is a multiple of the associated Legendre function.

In addition to the maximum electron density, the empirical electron density profile also requires the half-thickness of the bottomside layer  $y_m$ , and the five topside decay constants  $k_1$  through  $k_5$ . The bottomside layer half-thickness is interpolated from tables in which  $y_m$  is modeled as a function of  $f_0 F_2$  and local time. The five topside decay constants are interpolated from tables as functions of  $f_0 F_2$ , magnetic latitude, and daily solar flux. Adjustments for seasonal effects are then made for  $y_m$  and the lower three exponential decay constants. The magnetic latitude is given by

$$\phi_m = \sin^{-1} [\sin \phi \sin \phi_p + \cos \phi \cos \phi_p \cos(\lambda - \lambda_p)] \quad (7-138)$$

where  $(\phi_p, \lambda_p)$  are the geodetic latitude and longitude of the magnetic north pole.

### 7.6.3 Chapman Profile Refraction Corrections

The refraction correction formulas described in this section assume a spherically symmetric atmosphere. The tropospheric correction terms utilize an exponential refractivity profile and the ionospheric correction terms utilize a modified Chapman electron density profile. Approximations in the derivation limit the application at very small elevation angles. The values for  $N_m$  and  $h_m$  used in the following equations are determined as functions of the location of the tracking station and the time as described in Section 7.6.2.3. The scale height  $H_1$  is calculated from Equation (7-123).

#### 7.6.3.1 Range Correction

There are two speeds associated with electromagnetic signal propagation through a medium of index of refraction  $n$

$$c_p = \text{phase speed} = \frac{c}{n} \quad (7-139)$$

$$c_g = \text{group speed} = \frac{c}{n + \nu \frac{dn}{d\nu}} \quad (7-140)$$

where  $c$  is the vacuum speed of light.

The phase speed  $c_p$  is the speed associated with a phenomenon sensed by a phase measurement. The group speed  $c_g$  is the speed associated with a measurement of the transmission time of an energy pulse. In a nondispersive medium, such as the troposphere,  $dn/d\nu = 0$  by definition; therefore, the phase and group speeds are the same

$$c_p = c_g = \frac{c}{n} = \frac{c}{1 + N_T} \quad (7-141)$$

in terms of the refractivity given by Equation (7-115). The ionosphere, however, is dispersive and the two speeds are different. Appropriate differentiations and substitutions of Equations (7-117), (7-118), and (7-119) into Equations (7-139) and (7-140) show that, to first order in  $N_I$

$$c_p = \frac{c}{n} \approx \frac{c}{1 - N_I} \quad (7-142)$$

$$c_g = nc \approx (1 - N_I) c \approx \frac{c}{1 + N_I} \quad (7-143)$$

The phase speed is greater than the vacuum speed of light. The time associated with the transmission of a signal over a path from the tracking station to the spacecraft is written as

$$\Delta t_p = \int_{\text{total path}} ds/c_p = \frac{1}{c} \int_{\text{troposphere}} (1 + N_T) ds + \frac{1}{c} \int_{\text{ionosphere}} (1 - N_I) ds \quad (7-144)$$

$$\Delta t_g = \int_{\text{total path}} ds/c_g = \frac{1}{c} \int_{\text{troposphere}} (1 + N_T) ds + \frac{1}{c} \int_{\text{ionosphere}} (1 + N_I) ds$$

depending on whether or not the measurement is of a phase or a group transmission property. In these expressions,  $ds$  is the increment of length along the signal propagation path.

The first terms in Equations (7-144) (unity in the integrands) represent the vacuum transmission times, and the second terms (the refractivities) represent

the time corrections  $\Delta t_c$  caused by the atmosphere. The evaluation of Equations (7-144), by substituting for the refractivities from Equations (7-116) and (7-122), yields the total atmospheric range correction in the form

$$\Delta \rho = c \Delta t_c = \csc E [Q + U - (P + V) \cot^2 E] \quad (7-145)$$

The ionospheric terms are

$$Q = \pm \frac{40.3 N_m e H_I}{\nu^2} \left[ e^{-e^{-z}} - e^{-e^{\{(h_m - h_L)/H_I\}}} \right]$$

$$P = \pm \frac{40.3 N_m e H_I}{\nu^2 r_s} \left\{ h \left[ e^{-e^{-z}} - e^{-e^{\{(h_m - h_L)/H_I\}}} \right] \right. \quad (7-146)$$

$$\left. - (h - h_L) - H_I [S(Z) - S_L] \right\}$$

where the positive sign denotes the range increment due to a group delay, and where the negative sign corresponds to the phase range decrement. The tropospheric delay terms are

$$U = H_I N_s \quad (7-147)$$

$$V = \frac{H_I^2 N_s}{r_s}$$

In Equations (7-145) through (7-147)

$E \sim$  elevation of the straight line relative position vector from tracking station to spacecraft

$h \sim$  spacecraft altitude

$r_s \sim$  tracking station radius from the center of the earth

$\nu \sim$  frequency of signal transmission

$h_L \sim$  lower altitude limit for the ionosphere (set at 80 kilometers in GTDS)

$$S(z) = e^{-z} - \frac{e^{-2z}}{2 \cdot 2!} + \frac{e^{-3z}}{3 \cdot 3!} - \frac{e^{-4z}}{4 \cdot 4!} + \dots \quad (7-148)$$

$$S_L = 0.5772156649 + \left( \frac{h_m - h_L}{H_I} \right) \quad (7-149)$$

where

$$z = \frac{h - h_m}{H_I} \quad (7-150)$$

The expression  $S_L$  is used as the evaluation of the series  $S(z)$  at the lower limit because of convergence difficulties with the expression given by Equation (7-148).

The approximations made in the evaluation of the integrals in Equations (7-144) limit the validity of the form of the solution given by Equation (7-145). In particular, the error increases as the elevation angle decreases. Hence, the algorithm which is implemented in GTDS modifies this basic form (Equation (7-145)) in order to minimize the erroneous excursions at low elevation angles.

Typically, the true range refraction correction increases monotonically as the elevation angle decreases. Equation (7-145), however, can exhibit a maximum value at some angle and then decrease (even to negative values) for smaller angles. The maximum value is found by setting the derivative

$$\frac{d\Delta\rho}{dE} = -(\cot E) \Delta\rho + 2(P + V) \cot E \csc^3 E$$

to zero and solving for  $E = E_M$

$$\cot^2 E_M = \frac{Q + U - 2(P + V)}{3(P + V)} \quad (7-151)$$

In an example computed for typical troposphere and ionosphere profiles and for a VHF frequency of 136 MHz, the maximum value given by Equation (7-151) occurred at roughly  $E_M = 22^\circ$ . Thus, it would not be a good approximation to truncate the range corrections to this same maximum value for all elevations  $E < 22^\circ$ . Accordingly, the algorithm in GTDS simply replaces the true  $\cot^2 E$  term in Equation (7-145) with the limiting value given by Equation (7-151) when  $\cot^2 E > \cot^2 E_M$ . The  $\csc E$  factor in Equation (7-145) causes the range correction

to continue to increase as  $E$  decreases below  $E_m$ . In fact, it is necessary to truncate this factor (and hence the range correction) at a small elevation angle to prevent the values from becoming unrealistically large. On the basis of comparisons with ray traces computed through a typical ionospheric profile, it was determined that the csc  $E$  cutoff should be made for  $\sin E < 0.225$ . The comparison of the ray trace results with the GTDS algorithm is shown in Figure 7-5. The ionosphere was represented as a modified Chapman profile given by Equation (7-120), with

$$N_m = 1.0 \times 10^{12} \text{ electrons/m}^3$$

$$h_m = 300 \text{ km}$$

$$H_f = 65 \text{ km}$$

$$\nu = 136 \text{ MHz}$$

For  $E \geq 35^\circ$ , the corrections given by Equation (7-14) are essentially the same as the exact ray trace results. Below this angle the errors are less than 20%. Since uncertainties in the knowledge of the ionospheric characteristics can exceed 50%, it is not worthwhile from a practical standpoint to insist on greater accuracy in the algorithm at lower elevation angles.

#### 7.6.3.2 Elevation Angle-Dependent Corrections

Bouguer's Formula, the analogue to Snell's Law for a spherically stratified medium, gives

$$nr \sin i = \text{constant} \quad (7-152)$$

along any ray through the medium. Here  $i$  is the local incidence angle between the ray and the radius vector of magnitude  $r$ . Substituting  $r_s + h$  for  $r$  in this formula and evaluating at two points on a ray yields a relationship for the two incidence angles as functions of the altitudes and indices of refraction

$$\frac{\sin i_0}{\sin i} = \frac{n}{n_0} \left( \frac{r_s + h}{r_s + h_0} \right) \quad (7-153)$$

If the initial point is taken at the tracking station, the apparent elevation angle of the ray is  $E_s$ . The initial point yields

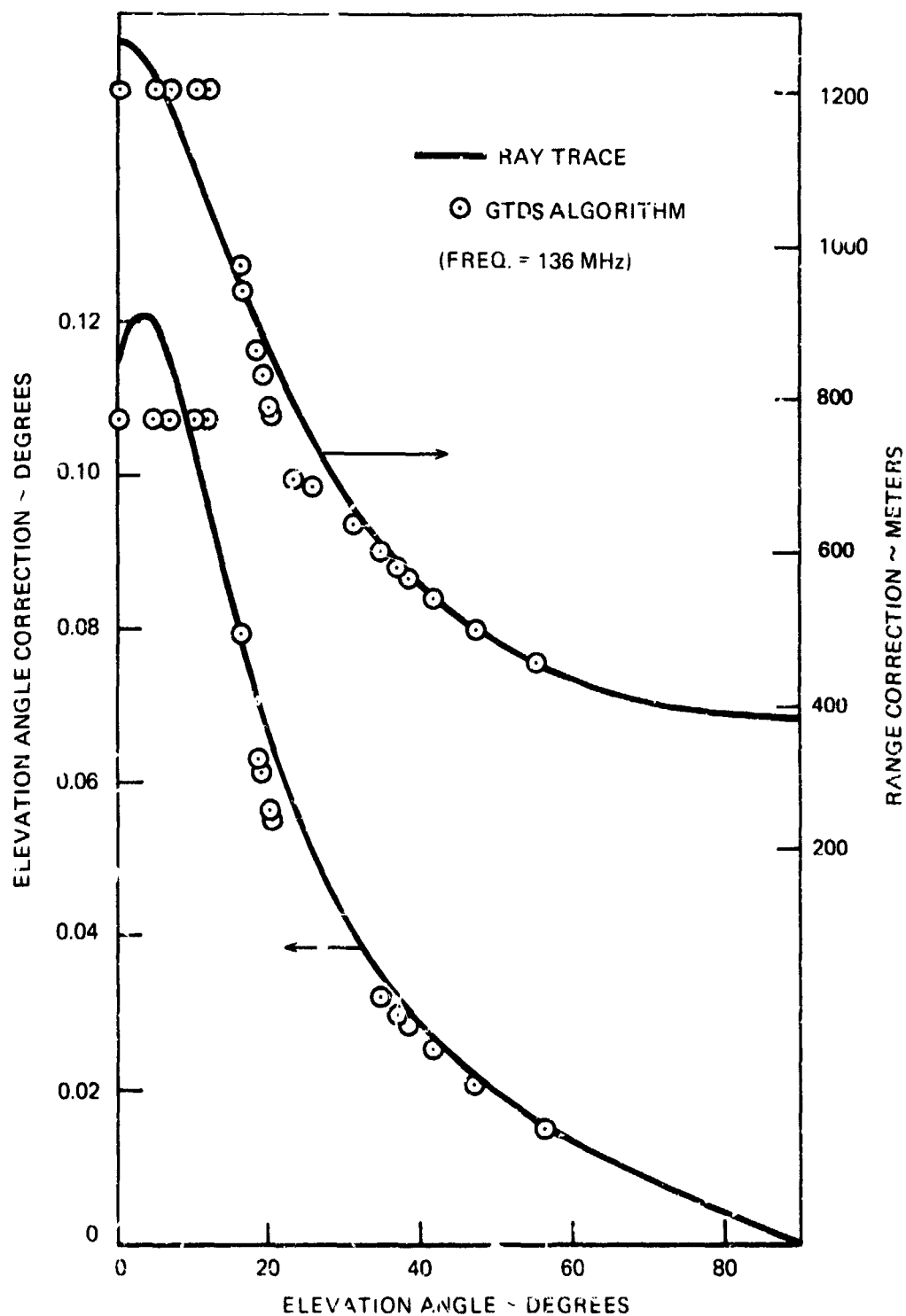


Figure 7-5. Refraction Correction Comparison of Ray Trace vs. GTDS Algorithms (CSC model)

$$h_0 = 0$$

$$n_0 = 1 + N_s \quad (7-154)$$

$$\sin i_0 = \cos E_a$$

Substituting Equations (7-154) into Equation (7-153) yields

$$\cos E_a = \frac{n(r_s + h)}{(1 + N_s) r_s} \sin i \quad (7-155)$$

If  $i$  were known a priori at the spacecraft position, Equation (7-155) could be used to compute the apparent elevation angle at the ground station. However,  $i$  is not known and Equation (7-155) must be modified to reformulate the desired solution in terms of quantities which are known. An approximation is made to an integration along the ray, resulting in

$$\cos E_a = \frac{\cos E}{(1 + N_s)(1 + I)} \quad (7-156)$$

where

$$I = \frac{\cot E}{r_s \delta} [Q - U - (P - V)(2 + \cot^2 E)] \quad (7-157)$$

$$\delta = \cos^{-1} \left( \frac{r_s \cos E}{r_s + h} \right) - E \quad (7-158)$$

Equation (7-156) is used as given for the correction of Minitrack data, since the direction cosines with respect to the station horizontal base line both involve the factor  $E_a$ . The correction for the elevation angle is determined (via the tangent of the difference of two angles) to give

$$E_a - E = \tan^{-1} \left\{ \frac{\cos E [\sqrt{(1 + N_s)^2 (1 + I)^2 - \cos^2 E} - \sin E]}{\cos^2 E + \sin E \sqrt{(1 + N_s)^2 (1 + I)^2 - \cos^2 E}} \right\} \quad (7-159)$$

The refraction corrections to the X and Y gimbal angles (for both the 30' and the 85' antennas) enter through the dependence of these angles on the elevation angle of the propagation path. The appropriate corrections are

$$(X_A - X)_{30} = \tan^{-1} \left\{ \frac{\sin A \cos E [\sin E - \sqrt{(1 + N_s)^2 (1 + I)^2 - \cos^2 E}]}{\sin E \sqrt{(1 + N_s)^2 (1 + I)^2 - \cos^2 E} + \sin^2 A \cos^2 E} \right\}$$

$$(Y_A - Y)_{30} = \sin^{-1} \left\{ \frac{\cos A \cos E}{(1 + N_s)(1 + I)} \left[ \sqrt{1 - \cos^2 A \cos^2 E} - \sqrt{(1 + N_s)^2 (1 + I)^2 - \cos^2 A \cos^2 E} \right] \right\} \quad (7-160)$$

$$(X_A - X)_{85} = \tan^{-1} \left\{ \frac{\cos A \cos E \sqrt{(1 + N_s)^2 (1 + I)^2 \cos^2 E} - \sin E}{\sin E \sqrt{(1 + N_s)^2 (1 + I)^2 - \cos^2 E} + \cos^2 A \cos^2 E} \right\}$$

$$(Y_A - Y)_{85} = \sin^{-1} \left\{ \frac{\sin A \cos E}{(1 + N_s)(1 + I)} \left[ \sqrt{1 - \sin^2 A \cos^2 E} - \sqrt{(1 + N_s)^2 (1 + I)^2 - \sin^2 A \cos^2 E} \right] \right\}$$

where A is the azimuth angle.

### 7.6.3.3 Doppler Corrections

The effects of atmospheric refraction on USB Doppler measurements are expressed in Appendix C in terms of difference vectors  $\Delta \bar{u}$  and  $\Delta \bar{d}$  between unit vectors along the actual (uplink and downlink) propagation paths and the straight lines characterizing the hypothetical vacuum propagation paths. Figure C-1 depicts the geometry of the two- or three-way Doppler signal transmission. From this figure, the four equations which define the conditions at each end of the uplink and downlink paths are (Equations (C-12) and (C-14))

$$\begin{aligned} \bar{u}_T &= \bar{u} + \Delta \bar{u}_T \\ \bar{u}_v &= \bar{u} + \Delta \bar{u}_v \\ \bar{d}_v &= \bar{d} + \Delta \bar{d}_v \\ \bar{d}_R &= \bar{d} + \Delta \bar{d}_R \end{aligned} \quad (7-161)$$



where

$$\bar{u} = \frac{\bar{r}_v - \bar{r}_T}{|\bar{r}_v - \bar{r}_T|}$$

and

(7-162)

$$\bar{d} = \frac{\bar{r}_R - \bar{r}_v}{|\bar{r}_R - \bar{r}_v|}$$

are unit vectors pointing up along the uplink path and down along the downlink path (both paths are characterized as straight line relative position vectors) and

$\bar{r}_v \sim$  satellite position vector

$\bar{r}_T \sim$  ground transmitter position vector

$\bar{r}_R \sim$  ground receiver position vector

An equation was derived in Appendix C for the Doppler-plus-bias cycle count  $N$  for the two-way or three-way measurement made by the USB system. The atmospheric refraction effect is the term (Equation (C-34))

$$\Delta \dot{\rho}_{avg} / 2$$

The quantity

$$\Delta \dot{\rho}_{avg} = \frac{\Delta \dot{\rho}(t + \Delta t_{RR}) + \Delta \dot{\rho}(t)}{2} \quad (7-163)$$

is the average of the quantities obtained by evaluating

$$\Delta \dot{\rho} = \Delta \bar{u}_T \cdot \dot{\bar{r}}_T + \Delta \bar{d}_v \cdot \dot{\bar{r}}_v - \Delta \bar{u}_v \cdot \dot{\bar{r}}_v - \Delta \bar{d}_R \cdot \dot{\bar{r}}_R \quad (7-164)$$

at the beginning and at the end of the Doppler-plus-bias counting interval.

The computation of the USB Doppler refraction effect, therefore, requires a means for computing the correction vectors  $\Delta \bar{u}_T$ ,  $\Delta \bar{u}_v$ ,  $\Delta \bar{d}_v$ , and  $\Delta \bar{d}_R$  at the appropriate times.

The correction vector  $\Delta \bar{u}_T$  for the uplink path at an instant when the ground station transmits a signal to the spacecraft is the difference between the unit vectors  $\bar{u}_T$  and  $\bar{u}$  along the actual and the hypothetical vacuum propagation paths. It must lie in the plane defined by  $\bar{u}$  and the local vertical  $\bar{v}_T$  at the station, if it is assumed that the refractive medium is a spherically layered atmosphere. Therefore,  $\Delta \bar{u}_T$  is expressed as a linear combination\* of  $\bar{u}$  and  $\bar{v}_T$

$$\Delta \bar{u}_T = A\bar{u} + B\bar{v}_T \quad (7-165)$$

In terms of the apparent elevation angle  $E_a$  of the actual propagation path and the straight-line relative position vector elevation angle  $E$

$$\bar{u}_T \cdot \bar{u} = \cos (E_a - E) \quad (7-166)$$

$$\bar{u}_T \cdot \bar{v}_T = \sin E_a$$

Substituting from Equations (7-161) and (7-165) into Equations (7-166) and solving explicitly for A and B yields

$$A = \frac{\cos E_a}{\cos E} - 1 \quad (7-167)$$

$$B = \sin E_a - \tan E \cos E_a$$

Equation (7-156) can then be used to eliminate  $E_a$ , giving finally

$$A = \frac{1}{(1 + N_s)(1 + I)} - 1 \quad (7-168)$$

$$B = \frac{1}{(1 + N_s)(1 + I)} \left[ \sqrt{(1 + N_s)^2 (1 + I)^2 - \cos^2 E} - \sin E \right]$$

where I is as defined in Equation (7-157) and  $N_s$  is the tropospheric surface refractivity at the transmitter.

---

\* The vectors  $\bar{u}$  and  $\bar{v}_T$  coincide in the exceptional case of a direct overhead alignment. However, this case works out correctly, since  $A = -B$ , giving  $\Delta \bar{u}_T = 0$ .

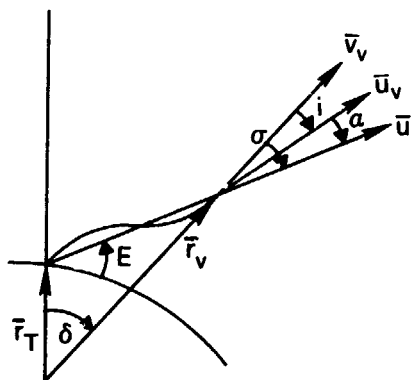


Figure 7-6. Uplink Path Geometry at Spacecraft Signal Reception.

Similar considerations apply in the determination of the correction vector  $\Delta \bar{u}_v$  for the uplink path at the instant when the signal is received at the spacecraft. The geometry and notation are presented in Figure 7-6. Here again, the correction vector is expressed as a linear combination

$$\Delta \bar{u}_v = C \bar{u} + D \bar{v}_v \quad (7-169)$$

The following relationships are obtained from Figure 7-6

$$\bar{u} \cdot \bar{v}_v = \cos \sigma$$

$$\bar{u}_v \cdot \bar{u} = \cos \alpha$$

$$\bar{u}_v \cdot \bar{v}_v = \cos i$$

$$\cos \alpha = \cos \sigma \cos i + \sin \sigma \sin i$$

Straightforward manipulation of these relationships, using Equations (7-169) and (7-161), yields a system of two simultaneous equations in the unknown coefficients C and D. The solutions for C and D in terms of i and  $\sigma$  are

$$C = \frac{\sin i}{\sin \sigma} - 1 \quad (7-170)$$

$$D = \cos i - \cot \sigma \sin i$$

Equating the right-hand sides of Equations (7-155) and (7-156), making use of Equation (7-118), and solving explicitly for  $\sin i$  yields

$$\sin i = \frac{r_T}{r_v} \frac{\cos E}{(1 - N_I)(1 + I)} \quad (7-171)$$

Examination of the triangle in Figure 7-6 shows that

$$E + \frac{\pi}{2} + \delta + \sigma = \pi$$

or

$$E + \delta = \frac{\pi}{2} - \sigma$$

Therefore

$$\sin \sigma = \cos (E + \delta)$$

and from Equation (7-158) this can be reduced to

$$\sin \sigma = \cos (E + \delta) = \frac{r_T}{r_v} \cos E \quad (7-172)$$

Substituting Equations (7-171) and (7-172) into Equation (7-170) finally yields

$$C = \frac{1}{(1 - N_I)(1 + I)} - 1 \quad (7-173)$$

$$D = \frac{1}{(1 - N_I)(1 + I)} \left[ \sqrt{(1 - N_I)^2 (1 + I)^2 - \frac{r_T^2 \cos^2 E}{r_v^2}} - \sqrt{1 - \frac{r_T^2 \cos^2 E}{r_v^2}} \right]$$

If the same procedure is repeated for the downlink path to solve for the correction vectors  $\Delta \vec{d}_v$  and  $\Delta \vec{d}_R$ , the result is

$$\begin{aligned}\Delta \bar{d}_v &= C' \bar{d} + D' \bar{v}_v \\ \Delta \bar{d}_R &= A' \bar{d} + B' \bar{v}_R\end{aligned}\tag{7-174}$$

The solutions for  $C'$  and  $A'$  are identical with those for  $C$  and  $A$ , whereas the solutions for  $D'$  and  $B'$  are the negatives of those for  $D$  and  $B$  (Equations (7-173) and (7-168)).

The quantities  $I$  and  $N_I$  appear in the expressions for the primed and unprimed values of  $A$ ,  $B$ ,  $C$ , and  $D$ . Equations (7-122), (7-146), and (7-157) show the dependence of these quantities on the signal transmission frequency. The uplink carrier frequency should be used to compute the unprimed quantities, while the downlink carrier frequency should be used for the primed quantities.

The Doppler refraction correction for GRARR VHF and for sidetone ATSR data is shown in Appendix C (Equation (C-42)) to be of the form

$$-\Delta \bar{u}_v \cdot \dot{\bar{r}}_v$$

where the spacecraft velocity  $\dot{\bar{r}}_v$  is taken at the signal turnaround time corresponding to the midpoint of the Doppler count interval. This time is the observation time tag (the preprocessor-determined midpoint of the Doppler count interval) corrected in the orbit determination processing for the light time from the spacecraft to the station. The light-path bending term  $\Delta \bar{u}_v$  is computed according to Equations (7-169), (7-170) and (7-173). The vector  $\bar{u}$  is defined (Equation (C-12)) as the unit vector directed along the instantaneous relative position vector from the station to the spacecraft. All other parameters in Equations (7-170) and (7-173) are defined in terms of this instantaneous relative geometry.

#### 7.6.4 Segmented Profile Refraction Corrections

The refraction correction formulas, described in Reference 10, assume that the total refraction correction is the sum of the tropospheric and ionospheric corrections as follows

$$\begin{aligned}\Delta \rho &= \Delta \rho_T + \Delta \rho_I \\ \Delta E &= \Delta E_T + \Delta E_I \\ \Delta \dot{\rho} &= \Delta \dot{\rho}_T + \Delta \dot{\rho}_I\end{aligned}\tag{7-175}$$

where  $\Delta\rho_T$ ,  $\Delta E_T$ , and  $\Delta\dot{\rho}_T$  are due to the troposphere, and  $\Delta\rho_I$ ,  $\Delta E_I$ , and  $\Delta\dot{\rho}_I$  are due to the ionosphere. These individual corrections are presented below.

#### 7.6.4.1 Tropospheric Correction

The tropospheric corrections are obtained from Reference 7 and assume that the atmosphere has spherical symmetry and an exponential refractivity function as described by Equation (7-116). The equations are applicable over the entire range of elevation angle (0-90°).

Using monthly mean values of the refractivity  $N_s$ , the scale height  $H_T$ , and the local earth radius  $r_s$  at the tracking station, the following parameters are calculated

$$p = \sqrt{2H_T/r_s} \quad (7-176)$$

$$q = 10^{-6} N_s r_s / H_T \quad (7-177)$$

The range and elevation angle corrections are

$$\Delta\rho_T = 10^{-6} N_s H_T \left( M - \frac{1}{2} 10^{-6} N_s r_s^2 \cos^2 E_a L^2 / H_T \right) \text{ (km)} \quad (7-178)$$

$$\Delta E_T = 10^{-6} N_s \cos E_a (i - r_s L / \rho) \text{ (radians)} \quad (7-179)$$

where

$E_a \sim$  apparent elevation angle of the received signal

$\rho \sim$  slant range to the satellite

The quantity  $L$  is given by

$$L = 1 - i \sin E_a + \frac{1}{2} 10^{-6} N_s i^2 \quad (7-180)$$

and the quantities  $i$  (bending integral) and  $m$  are complex integral functions of the refractivity function and the elevation angle. Reference 7 presents the following approximations for  $i$  and  $m$  which are accurate over the entire range of elevation angle

$$i = F(\sin E_s, p^2 I_1, p^4 I_2, i_0/p, i_1/p^2) \quad (7-181)$$

$$m = F(\sin E_s, p^2 M, p^4 M_2, m_0/p, m_1/p^2) \quad (7-182)$$

where the function  $F$  is given by

$$F(\alpha, F_1, F_2, f_0, f_1) = \frac{1}{\alpha + \frac{g_1}{\alpha + \frac{g_2 \times 1.08885}{\alpha + \frac{g_3 \times 1.320903}{\alpha + g_4 \times 1.21313}}}} \quad (7-183)$$

with

$$\begin{aligned} g_1 &= F_1 \\ g_2 &= (F_2/g_1) - g_1 \end{aligned} \quad (7-184)$$

$$g_3 = g_2 / \left[ f_0^2 g_1 \left( 1 - \frac{g_1}{g_2} \right) - (1 + f_1 g_1) \right]$$

$$g_4 = f_0 g_1 g_3 / g_2$$

The variables  $I_1$ ,  $I_2$ ,  $i_0$  and  $i_1$  are

$$\begin{aligned} I_1 &= \frac{1}{2} \left( 1 - \frac{1}{2} q \right) \\ I_2 &= \frac{3}{4} \left( 1 - \frac{3}{4} q + \frac{1}{6} q^2 \right) \end{aligned} \quad (7-185)$$

$$i_0 = \sqrt{\pi} (1 - 0.9206 q)^{-0.4468}$$

$$i_1 = 2/(1 - q)$$

and the variables  $M_1$ ,  $M_2$ ,  $m_0$  and  $m_1$  are

$$M_1 = \frac{1}{2} \left( 1 - \frac{3}{4} q \right)$$

$$M_2 = \frac{3}{4} \left( 1 - \frac{25}{24} q + \frac{11}{36} q^2 \right)$$
(7-186)

$$m_0 = i_0 \left( 1 + q + \frac{1}{12} q^2 i_0^2 \right) - \frac{1}{2} q k_0$$

$$m_1 = 2 \left( 1 + \frac{1}{4} q i_0^2 \right) (1 - q)$$

with

$$k_0 = \sqrt{2\pi} (1 - 0.9408 q)^{-0.4759}$$
(7-187)

The range-rate correction is given by

$$\Delta \dot{\rho}_T = -10^{-6} \dot{E}_a N_s H_T \cos E_a \left[ n^2 - \frac{r_s}{\rho} q L \cos^2 E_a \right.$$

$$\left. \times (i + 10^{-6} N_s i j - j \sin E_a) \right]$$
(7-188)

where

$$j = F(\sin E_a, p^2 J_1, p^4 J_2, j_0/p, j_1/p^2)$$
(7-189)

$$n = F(\sin E_a, p^2 N_1, p^4 N_2, n_0/p^2, n_1/p^2)$$
(7-190)

The variables  $J_1$ ,  $J_2$ ,  $j_0$ , and  $j_1$  are

$$J_1 = \frac{3}{2} I_1$$
(7-191)

$$J_2 = \frac{1}{2} (5I_2 - J_1)$$



$$j_0 = \sqrt{i_1} \quad (7-191)$$

(cont'd)

$$j_1 = i_2 / j_0$$

where

$$i_2 = \sqrt{\pi} / (1 - 1.023 q)^{1.8} \quad (7-192)$$

The variables  $N_1$ ,  $N_2$ ,  $n_0$ , and  $n_1$  are

$$N_1 = \frac{3}{2} M_1$$

$$N_2 = \frac{1}{2} (5 M_2 - N_1^2) \quad (7-193)$$

$$n_0 = \sqrt{m_1}$$

$$n_1 = \left[ \frac{i_0}{(1 - q)^2} + i_2 q + \frac{1}{4} i_2 (i_0 q)^2 \right] / n_0$$

#### 7.6.4.2 Ionospheric Correction

Ionospheric refraction corrections are computed from the empirical electron density profile, described in Section 7.6.2.2, and its integrated electron content. The profile is computed for the latitude  $\phi$  and longitude  $\lambda$  where the radio wave from the observing station to the satellite penetrates the ionosphere. This is called the subionospheric point and is computed as a function of the station latitude  $\phi_s$  and longitude  $\lambda_s$ , and the elevation angle  $E$  and azimuth angle  $A$  from the station to the satellite

$$\phi = \sin^{-1} (\sin \phi_s \cos \alpha + \cos \phi_s \sin \alpha \cos A) \quad (7-194)$$

$$\lambda = \lambda_s + \sin^{-1} \left( \frac{\sin A \sin \alpha}{\cos \phi} \right) \quad (7-195)$$

where  $\alpha$  is the geocentric angle between the station and the subionospheric point

$$\alpha = \frac{\pi}{2} - E - \sin^{-1} \left( \frac{R_e \cos E}{R_e + h_m} \right) \quad (7-196)$$

and  $h_m$  is the height of the ionosphere at the maximum electron density above the surface of the earth. On the first iteration,  $h_m$  is estimated to be 300 kilometers. After computing  $h_m$  via Equation (7-130), the difference between the computed and estimated values of  $h_m$  is determined. If this difference is less than 1 kilometer, its effect is negligible; if it is greater than or equal to 1 kilometer, Equations (7-194) through (7-196) are iterated upon to obtain a new value of  $h_m$ .

The total vertical electron content  $N_I$  required by the correction algorithm is obtained by integrating the electron density profile in Equations (7-124) and (7-125) from zero to the height of the satellite  $h$ . For a satellite below the biparabolic layer of the ionosphere

$$\bar{N}_I = 0 \quad (7-197)$$

For a satellite in the bottomside biparabolic layer

$$\bar{N}_I = \int_0^h N_I dh = N_m \left[ \frac{8}{15} y_m - (h_m - h) + \frac{2}{3} \frac{(h_m - h)^3}{y_m^2} - \frac{1}{5} \frac{(h_m - h)^5}{y_m^4} \right] \quad (7-198)$$

where  $y_m$  is the half-thickness of the bottomside layer of the segmented electron density profile.

For a satellite in the topside parabolic layer

$$N_I = N_m \left[ \frac{9}{15} y_m - (h_m - h) + \frac{(h_m - h)^3}{3y_t^2} \right] \quad (7-199)$$

where  $y_t$  is the thickness of the topside parabolic layer (see Figure 7-4) and is given by

$$y_t = \alpha y_m \quad (7-200)$$

where

$$\sigma = \begin{cases} 1 & \text{for } f_0 F_2 \leq 10.5 \text{ MHz} \\ 1 + .1333 (f_0 F_2 - 10.5) & \text{for } f_0 F_2 > 10.5 \text{ MHz} \end{cases}$$

For a satellite in the first exponential layer

$$\bar{N}_I = N_m \left( \frac{8}{15} y_m + d - \frac{d^3}{3y_t^2} \right) + N_m \left( 1 - \frac{d^2}{y_t^2} \right) \left( \frac{1 - e^{-k_1(h-h_1)}}{k_1} \right) \quad (7-201)$$

where

$$d = \frac{\sqrt{1 + k_1^2 y_t^2} - 1}{k_1}$$

For a satellite in the second exponential layer

$$\begin{aligned} \bar{N}_I = N_m \left( \frac{8}{15} y_m + d - \frac{d^3}{3y_t^2} \right) + N_m \left( 1 - \frac{d^2}{y_t^2} \right) \\ \times \left( \frac{1 - e^{-k_1(h_2-h_1)}}{k_1} + \frac{e^{-k_1(h_2-h_1)} - e^{-[k_1(h_2-h_1) + k_2(h-h_2)]}}{k_2} \right) \end{aligned} \quad (7-202)$$

For a satellite in the third exponential layer

$$\begin{aligned} \bar{N}_I = N_m \left( \frac{8}{15} y_m + d - \frac{d^3}{3y_t^2} \right) + N_m \left( 1 - \frac{d^2}{y_t^2} \right) \\ \times \left\{ \frac{1 - e^{-k_1(h_2-h_1)}}{k_1} + \frac{e^{-k_1(h_2-h_1)} [1 - e^{-k_2(h_3-h_2)}]}{k_2} \right. \\ \left. + \frac{e^{-[k_1(h_2-h_1) + k_2(h_3-h_2)]} [1 - e^{-k_3(h-h_3)}]}{k_3} \right\} \end{aligned} \quad (7-203)$$

For a satellite in the fourth exponential layer

$$\begin{aligned}
 \bar{N}_I = N_m \left( \frac{8}{15} y_m + d - \frac{d^3}{3y_t^2} \right) + N_m \left( 1 - \frac{d^2}{y_t^2} \right) \\
 \times \left\{ \frac{1 - e^{-k_1(h_2-h_1)}}{k_1} + \frac{e^{-k_1(h_2-h_1)} [1 - e^{-k_2(h_3-h_2)}]}{k_2} \right. \\
 + \frac{e^{-[k_1(h_2-h_1)+k_2(h_3-h_2)]} [1 - e^{-k_3(h_4-h_3)}]}{k_3} \\
 \left. + \frac{e^{-[k_1(h_2-h_1)+k_2(h_3-h_2)+k_3(h_4-h_3)]} [1 - e^{-k_4(h-h_4)}]}{k_4} \right\}
 \end{aligned} \tag{7-204}$$

Finally, for a satellite in or above the fifth exponential layer

$$\begin{aligned}
 \bar{N}_I = N_m \left( \frac{8}{15} y_m + d - \frac{d^3}{3y_t^2} \right) + N_m \left( 1 - \frac{d^2}{y_t^2} \right) \\
 \times \left\{ \frac{1 - e^{-k_1(h_2-h_1)}}{k_1} + \frac{e^{-k_1(h_2-h_1)} [1 - e^{-k_2(h_3-h_2)}]}{k_2} \right. \\
 + \frac{e^{-[k_1(h_2-h_1)+k_2(h_3-h_2)]} [1 - e^{-k_3(h_4-h_3)}]}{k_3} \\
 + \frac{e^{-[k_1(h_2-h_1)+k_2(h_3-h_2)+k_3(h_4-h_3)]} [1 - e^{-k_4(h_5-h_4)}]}{k_4} \\
 \left. + \frac{e^{-[k_1(h_2-h_1)+k_2(h_3-h_2)+k_3(h_4-h_3)+k_4(h_5-h_4)]} [1 - e^{-k_5(h-h_5)}]}{k_5} \right\}
 \end{aligned} \tag{7-205}$$

The range correction  $\Delta \rho_I$  is computed from the vertical electron content and the elevation angle at which the radiowave passes through the ionosphere

$$\Delta \rho_I = \frac{40.3 \bar{N}_I}{f^2 \sqrt{1 - \left( \frac{R_e}{R_e + h_{\text{mean}}} \right)^2 \cos^2 E_s}} \quad (7-206)$$

where the height of the mean of the electron distribution  $h_{\text{mean}}$  is

$$h_{\text{mean}} = h_m + \frac{1}{2} \frac{N_I}{N_m} - \frac{8}{15} y_m \quad (7-207)$$

the quantity  $f$  is the transmission frequency, and

$$\frac{1}{f} = \left( \frac{1}{2f_u^2} + \frac{1}{2f_d^2} \right)^{1/2} \quad (7-208)$$

where  $f_u$  and  $f_d$  are the uplink and downlink frequencies, respectively.

The range-rate correction  $\Delta \dot{\rho}_I$  is obtained by differencing two successive range corrections in the following form

$$\Delta \dot{\rho}_I = - \frac{\Delta \rho_I(t) - \Delta \rho_I(t - \Delta t)}{\Delta t} \quad (7-209)$$

At the start of a data span for which no previous range correction exists,  $\Delta \dot{\rho}_I$  assumes one of the following forms:

#### Satellites Below the Lower Biparabolic Layer

$$\Delta \dot{\rho}_I = 0 \quad (7-210)$$

### Satellites Within the Lower Biparabolic Layer

$$\Delta \dot{\rho}_I = -\frac{d\Delta\rho_I}{dt} = -\left(\frac{f_0 F_2}{f}\right)^2 \times \frac{(40.3 \times 1.24 \times 10^{-2}) \left[1 - \left(\frac{h_m - h}{y_m}\right)^2\right]^2}{\left[1 - \left(\frac{R_e}{R_e + h_{mean}} \cos E_a\right)^2\right]^{1/2}} \times \dot{h}$$

(7-211)

$$+ \frac{\Delta\rho_I \left(\frac{R_e}{R_e + h_{mean}}\right)^2 \sin E_a \cos E_a}{1 - \left(\frac{R_e}{R_e + h_{mean}} \cos E_a\right)^2} \times \dot{E}$$

where  $\dot{h}$  is the altitude rate and  $\dot{E}$  is the elevation rate of the satellite.

### Satellites in the Topside Parabolic Layer

$$\Delta \dot{\rho}_I = -\frac{d\Delta\rho_I}{dt} = -\left(\frac{f_0 F_2}{f}\right)^2 \times \frac{(40.3 \times 1.24 \times 10^{-2}) \left[1 - \frac{(h_m - h)^2}{y_t^2}\right]}{\left[1 - \left(\frac{R_e}{R_e + h_{mean}} \cos E_a\right)^2\right]^{1/2}} \times \dot{h}$$

(7-212)

$$+ \frac{\Delta\rho_I \left(\frac{R_e}{R_e + h_{mean}}\right)^2 \sin E_a \cos E_a}{1 - \left(\frac{R_e}{R_e + h_{mean}} \cos E_a\right)^2} \times \dot{E}$$

## Satellites in the Exponential Layers

$$\Delta \dot{\rho}_I = - \frac{d\Delta \rho_I}{dt} = - \left( \frac{f_0 F_2}{f} \right)^2 \times \frac{(40.3 \times 1.24 \times 10^{-2}) \left[ 1 - \frac{d^2}{y_t^2} \right] \times \dot{h} \times em}{\left[ 1 - \left( \frac{R_e}{R_e + h_{mean}} \cos E_a \right)^2 \right]^{1/2}} \quad (7-213)$$

$$+ \frac{\Delta \rho_I \left( \frac{R_e}{R_e + h_{mean}} \right)^2 \sin E_a \cos E_a}{1 - \left( \frac{R_e}{R_e + h_{mean}} \cos E_a \right)^2} \times \dot{E}$$

The exponential multiplier  $em$  of the  $\dot{h}$  term can take on five different forms.  
For a satellite in the first exponential layer

$$em = e^{-k_1(h-h_1)} \quad (7-214a)$$

For a satellite in the second exponential layer

$$em = e^{-k_1(h_2-h_1)} e^{-k_2(h-h_2)} \quad (7-214b)$$

For a satellite in the third exponential layer

$$em = e^{-k_1(h_2-h_1)} e^{-k_2(h_3-h_2)} e^{-k_3(h-h_3)} \quad (7-124c)$$

For a satellite in the fourth exponential layer

$$em = e^{-k_1(h_2-h_1)} e^{-k_2(h_3-h_2)} e^{-k_3(h_4-h_3)} e^{-k_4(h-h_4)} \quad (7-124d)$$

Finally, for a satellite in or above the fifth exponential layer

$$em = e^{-k_1(h_2-h_1)} e^{-k_2(h_3-h_2)} e^{-k_3(h_4-h_3)} e^{-k_4(h_5-h_4)} e^{-k_5(h-h_5)} \quad (7-124e)$$

The elevation angle correction  $\Delta E_a$  is given by

$$\cos (\Delta E_a) = \frac{X_1 \cos \alpha - X_2}{(X_1^2 + X_2^2 - 2X_1 X_2 \cos \alpha)^{1/2}} \quad (7-215)$$

where

$$X_1 = [(R_e + h)^2 - R_e^2 \cos^2 E_a]^{1/2} + R_e \cos E_a \tan \frac{a}{2} \quad (7-216)$$

$$X_2 = R_e \sin E_a - R_e \cos E_a \tan \frac{a}{2} \quad (7-217)$$

$$\alpha = \frac{1}{2} \left( \frac{f_0 F_2}{f} \right)^2 \xi \frac{\tan \phi_0 \sec^2 \phi_0}{r_0} \frac{\bar{N}_I}{N_m} \quad (\text{deviation angle}) \quad (7-218)$$

$$r_0 = R_e + h_{\text{mean}} \quad (7-219)$$

$$h_{\text{mean}} = h_m + \frac{1}{2} \frac{\bar{N}_I}{N_m} - \frac{8}{15} y_{\text{in}} \quad (7-220)$$

$$\sin \phi_0 = \frac{R_e}{r_0} \cos E_a \quad (7-221)$$

The variable  $\xi$  is tabulated as a function of

$$\left( \frac{f_0 F_2}{f} \right) \sec^2 \phi_m$$

where

$$\sin \phi_m = \frac{R_e}{r_m} \cos E_a \quad (7-222)$$

and

$$r_m = R_e + h_m \quad (7-223)$$



## 7.7 ADDITIONAL CORRECTIONS

### 7.7.1 Light-Time Correction

GTDS provides for a light time correction which can be applied to GRARR, C-Band, and Minitrack observations for greater accuracy of modeling. All of these observation types are modeled (Section 7.2.3) in terms of the instantaneous relative position vector from the tracking station to the spacecraft, computed in the local tangent coordinate system (Section 7.2.2). Since the spacecraft is the only object which is moving in this coordinate system, the appropriate time for calculating the instantaneous relative position vector is the time  $t_v$  when the vehicle transponder turns the tracking signal around. (For the one-way Minitrack signal,  $t_v$  corresponds to the time when the signal was transmitted by the spacecraft.) The actual observation is time-tagged at the time  $t_R$  when the signal is received at the ground station. The light-time correction consists of making an approximation to  $t_v$  by changing the observation time tag to

$$t_v = t_R - \frac{\Delta\rho}{c} \quad (7-224)$$

where  $\Delta\rho$  is the one-way relative range from the spacecraft to the tracking station. A first approximation to  $\Delta\rho$  is determined in GTDS by computing the relative range vector at the actual observation time  $t_R$ , utilizing the spacecraft position vector at  $t_R$ . The difference between this relative range and the correct relative range corresponding to  $t_v$  could be corrected by means of an iterative estimation algorithm. However, this is not done in GTDS, since the very small improvement in accuracy is insignificant compared with the degree of the approximation implicit in the basic observation model. Thus, the first estimate for  $\Delta\rho$  is used in computing the light-time correction to the observation time tag.

### 7.7.2 Antenna Mount Corrections

For X and Y antennas, a correction is performed on range and range-rate measurements, since the electrical phase center of the antenna moves with the antenna and is displaced from the geodetic point of reference which is the center of the fixed axis. The correction  $\Delta R$  applied for range is

$$\Delta R = D \cos(Y) \quad (7-225)$$

which, by differentiation with respect to time, gives the correction for range rate

$$\dot{\Delta R} = -D \sin(Y) \dot{Y} \quad (7-226)$$

In these expressions,  $Y$  is the observed  $Y$  angle and  $D$  is the nominal distance from the electrical phase center to the center of the fixed axis. The correction to  $\Delta R$  and  $\Delta \dot{R}$  due to the  $X$  angle and the corrections to the  $X$  and  $Y$  angles due to the displacement of the electrical phase center are ignored.

### 7.7.3 Transponder Delay Correction

For those tracking systems which use a transponder on-board the satellite to receive and then retransmit a signal, the transponder delay, i.e., the time interval between reception and transmission of a given signal, must be taken into consideration. These satellite transponder time delays are functions of the frequency of the signal received by the transponder, i.e.,

$$\Delta\tau = f(\nu_R) \quad (7-227)$$

The characteristics of the function  $f$  for a specific transponder must be determined experimentally by calibration of the transponder on the ground before launch. The function obtained in this manner can then be entered in GTDS as a table of transponder delay time versus frequency, from which the delay for any intermediate value of frequency can be obtained by interpolation. As an alternative, provision is made in GTDS to use nominal (default) tables or constant delay times.

## 7.8 ESTIMATION MODEL

The deviation between the actual observation and the predicted observation is modeled as a first-order Taylor series expansion around the predicted observation. This expansion relates deviations in the observation residuals to deviations in dynamic parameters, station locations, observation biases, and time biases, and establishes the required set of linear regression equations. The estimation model for any observable may then be written as

$$O_0 - O_c = \frac{\partial O_c}{\partial \bar{q}} \Delta \bar{q} + n \quad (7-228)$$

where

$O_0 \sim$  the actual observation with time tag  $t$

$O_c \sim$  the predicted observation based on a previous estimate of the parameter vector  $\bar{q}$

$\Delta \bar{q} \sim$  the correction to the parameter vector  $\bar{q}$

$n \sim$  the observation noise

The parameter vector  $\bar{q}$  may consist of dynamic parameters  $\bar{p}$  (those parameters involved in the equations of motion); station locations  $\bar{r}_s$ ; observation biases  $b$ ; and observation time biases  $\delta t$ . The total parameter vector may then be written as

$$\bar{q} = \begin{bmatrix} \bar{p} \\ \bar{r}_s \\ b \\ \delta t \end{bmatrix} \quad (7-229)$$

The modeled observation can be written functionally as

$$O_c = f(\bar{q}, t) = f(\bar{p}, \bar{r}_s, b, \delta t, t) \quad (7-230)$$

Substituting the appropriate partial derivatives of Equation (7-230) into Equation (7-228) yields

$$O_0 - O_c = \left( \frac{\partial O_c}{\partial \bar{p}} \right) \Delta \bar{p} + \left( \frac{\partial O_c}{\partial \bar{r}_s} \right) \Delta \bar{r}_s + \left( \frac{\partial O_c}{\partial b} \right) \Delta b + \left( \frac{\partial O_c}{\partial (\delta t)} \right) \Delta (\delta t) + n \quad (7-231)$$

which may be written in a more compact form as

$$O_0 - O_c = \begin{bmatrix} \frac{\partial O_c}{\partial \bar{p}} & \frac{\partial O_c}{\partial \bar{r}_s} & \frac{\partial O_c}{\partial b} & \frac{\partial O_c}{\partial (\delta t)} \end{bmatrix} \begin{bmatrix} \Delta \bar{p} \\ \Delta \bar{r}_s \\ \Delta b \\ \Delta (\delta t) \end{bmatrix} + n \quad (7-232)$$

or

$$O_0 - O_c = F \Delta \bar{q} + n \quad (7-233)$$

Equation (7-233) defines the linear regression equations that are solved by the iterative classical or sequential weighted least squares methods described in

Chapter 8. The formulation, as shown in Equation (7-233), describes  $m$  equations (for  $m$  observations) in  $p$  unknowns (the number of  $q$  parameters). The matrix  $F$  in Equation (7-233) is of dimension  $(m \times p)$ . Chapter 8 derives the required solution to the normal equations in terms of  $F$  and the weighting matrix  $W$  under the assumption that  $W$  is a diagonal matrix, that is, the observations are uncorrelated. Under this assumption, the terms in the normal equations requiring  $F$  can be developed on an observation-by-observation basis, thus yielding the solution of the normal equations without explicitly forming the full  $(m \times p)$   $F$  matrix. This is a standard method for all existing least squares orbit determination programs and is discussed in more detail in Chapter 8.

## 7.9 REFERENCES

1. Ryan, J.: 1968, Apollo Unified S-Band Range Rate Data Utilization Techniques, Goddard Space Flight Center Report X-830-68-431, November 1968.
2. Ayres, C. L., Stull, H.E., and Teles, J.: 1975, Tracking Data Relay Range and Range Rate Observation Modeling via the Applications Technology Satellite - 6 (ATS-6), Goddard Space Flight Center Report X-570-75-53, March 1975.
3. Greenwood, J. A., et al.: 1967, Radar Altimetry from a Spacecraft and Its Potential Application to Geodesy and Oceanography, New York University School of Engineering and Science, Department of Meteorology and Oceanography, Report on Contract N62306-1589, U. S. Naval Oceanographic Office, May 1967.
4. Brown, R. D., and Fury, R. J.: 1972, Determination of the Geoid from Satellite Altimeter Data, Computer Sciences Corporation Report 5035-21000-01TM, April 1972.
5. Heiskanen, W. A., and Moritz, H.: 1967, Physical Geodesy, W. H. Freeman and Company, 1967.
6. Berbert, J. H., and Parker, H. C.: 1970, GEOS Satellite Tracking Corrections for Refraction in the Troposphere, Goddard Space Flight Center Report X-514-70-55, February 1970.
7. Marini, J. W.: 1971, Closed Form Satellite Tracking Data Corrections for an Arbitrary Tropospheric Profile, Goddard Space Flight Center Report X-551-71-122 (Preprint), March 1971.
8. Freeman, J. J.: 1965, Final Report on Ionospheric Correction to Tracking Parameters, Goddard Space Flight Center Report NAS 5-9782, November 3, 1965.
9. Davies, K.: 1965, Ionospheric Radio Propagation, National Bureau of Standards Monograph 80, April 1, 1965.
10. DBA Systems, Inc.: 1972, Ionospheric and Tropospheric Refraction Corrections in GTDS, DBA Systems, Inc. Final Report, prepared for Goddard Space Flight Center under Contract No. NAS 5-11730, September 1972.

11. Jones, W. B., Graham, R. P., and Leftin, M.: 1969, Advances in Ionospheric Mapping by Numerical Methods, ESSA Research Laboratories Technical Report ERL 107-ITS-75, Boulder, Colorado, May 1969.
12. Schmid, P. E., et. al.; 1973, NASA-GSFC Ionospheric Corrections to Satellite Tracking Data, Goddard Space Flight Center Report X-591-73-281, December 1973.

## CHAPTER 8

## ESTIMATION

The basic orbit estimation problem involves solving for values of a set of parameters from an observational model (described in Chapter 7) so as to minimize, in the sense of weighted least squares, the differences between a computed and an observed trajectory. The model parameters include the trajectory of the vehicle (initial conditions and differential equation parameters), the locations of the observing stations, and the bias errors in their instruments or clocks (these errors may vary as a function of the pass over a station). In practice, values are determined for only a selected subset of the model parameters.

Since the observations made by a tracking system are imperfect, no trajectory fits these observations exactly. At best, only an estimate of the actual trajectory can be obtained from the data. GTDS uses either a classical weighted least squares estimator (derived in Section 8.2) or a sequential estimator (derived in Section 8.4.1). For a theoretical discussion of estimation, see References 1 through 6.

## 8.1 DESCRIPTION OF THE PROBLEM

Let a set of  $m$  observations, denoted by an  $m$ -dimensional vector  $\bar{y}$ , be given. These observations are assumed to be equal to a known vector function  $\bar{f}$  of a set of  $p$  parameters, denoted by a  $p$ -dimensional vector  $\bar{x}$  plus additive random noise, denoted by a vector  $\bar{n}$

$$\bar{y} = \bar{f}(\bar{x}) + \bar{n} \quad (8-1)$$

The above equation is called a nonlinear regression equation. The trajectory determination problem is to estimate  $\bar{x}$  given  $\bar{y}$ , the functional form of  $\bar{f}$ , and the statistical properties of  $\bar{n}$ .

The estimation process attempts to deduce a value for  $\bar{x}$  that minimizes the weighted sum of the squares of the observation residuals  $[\bar{y} - \bar{f}(\bar{x})]$  between the actual observations and the observations computed using the mathematical model. More precisely,

$$Q(\bar{x}) = [\bar{y} - \bar{f}(\bar{x})]^T W [\bar{y} - \bar{f}(\bar{x})] \quad (8-2)$$

is minimized, where  $W$  is the  $m \times m$  weighting matrix. This scalar quantity is called the loss function. An a priori estimate of the state  $\bar{x}_0$  is assumed to be available for use in the minimization. The deviation of  $\bar{x}_0$  from the true value of the state is assumed to have zero mean and covariance  $P_{\Delta x_0}$  in order to make the subsequent statistical evaluation more amenable to interpretation.

A necessary condition for the loss function to be minimum with respect to  $\bar{x}$  is that  $\partial Q / \partial \bar{x} = 0$ . Therefore, the value of  $\bar{x}$  which minimizes  $Q$  is a root of the equation

$$\frac{\partial Q}{\partial \bar{x}} = -2 [\bar{y} - \bar{f}(\bar{x})]^T W \left( \frac{\partial \bar{f}}{\partial \bar{x}} \right) = 0 \quad (8-3)$$

The method of solving this nonlinear minimization is to linearize Equation (8-3) and then apply a standard Newton-Raphson procedure to iteratively solve the nonlinear problem. Expanding  $\bar{f}(\bar{x})$  in a truncated Taylor series about the a priori estimate  $\bar{x}_0$  yields

$$\bar{f}(\bar{x}) = \bar{f}(\bar{x}_0) + F \overline{\Delta x} \quad (8-4)$$

where

$$\overline{\Delta x} = \bar{x} - \bar{x}_0 \quad (8-5)$$

and

$$F = \left( \frac{\partial \bar{f}}{\partial \bar{x}} \right)_{(\bar{x} = \bar{x}_0)} \cdot \left\{ \begin{array}{l} \text{the } m \times p \text{ matrix of} \\ \text{partial derivatives of} \\ \bar{f}(\bar{x}) \text{ with respect to } \bar{x} \\ \text{evaluated at } \bar{x} = \bar{x}_0 \end{array} \right\} \quad (8-6)$$

The linearized observation vector becomes

$$\overline{\Delta y} = F \overline{\Delta x} + \bar{n} \quad (8-7)$$



where

$$\overline{\Delta y} = \bar{y} - \bar{f}(\bar{x}_0) \quad (8-8)$$

Substituting Equations (8-4) and (8-7) into Equation (8-3), the linearized partial derivative of the loss function in Equation (8-3) becomes

$$-2 (\overline{\Delta y} - F \overline{\Delta x})^T W F = 0 \quad (8-9)$$

which can immediately be solved for  $\overline{\Delta x}$ , yielding the classic equation for the best estimate  $\hat{\Delta x}$

$$\hat{\Delta x} = (F^T W F)^{-1} F^T W \overline{\Delta y} \quad (8-10)$$

The value of  $\hat{x}$ , the estimate derived from the linearized system, is therefore,

$$\hat{x} = \bar{x}_0 + \hat{\Delta x} \quad (8-11)$$

The symmetric matrix  $(F^T W F)$  is called the normal matrix.

As a result of the linearization performed in Equation (8-4), the correction  $\hat{\Delta x}$  must be small so as not to violate linearity. This means that the a priori estimate  $\bar{x}_0$  must be reasonably close to the true extremal solution of Equation (8-2). If such is not the case, the process is iteratively repeated in a standard Newton-Raphson procedure, each time using the last best estimate  $\hat{x}$  as a reference for the linearization. The iterations continue until the differential correction vector  $\hat{\Delta x}$  is truly small (i.e., approaching zero), which is equivalent to minimizing the original nonlinear loss function  $Q(x)$ .

The inverse of the  $p \times p$  normal matrix  $(F^T W F)$  is the covariance matrix of the error in the weighted least squares estimate  $\hat{x}$  after convergence is achieved, and the following statistical assumptions of the measurement process are satisfied:

- (a) The observation noise is unbiased, i.e.,  $E\{\bar{n}\} = 0$ .
- (b) The covariance of the observation noise vector is known and its inverse is the weighting matrix  $W$ . Let  $\sigma_1^2$  be the variance of the measurement noise component  $n_1$ , which corresponds to measurement  $y_1$ ;  $\sigma_2^2$  the variance of component  $n_2$ , which corresponds to  $y_2$ ; and so on. The weighting matrix is then

$$W = \begin{bmatrix} \sigma_1^{-2} & & & \\ & \sigma_2^{-2} & & 0 \\ & & \ddots & \\ 0 & & & \sigma_m^{-2} \end{bmatrix} \quad (8-12)$$

Equating the inverse of  $W$  to the covariance matrix of the measurement errors implies that multicomponent observations at a given time (e.g., range, azimuth, elevation) are not spatially correlated and that measurements at different times are not time correlated.

- (c) The mathematical models of the trajectory and observations characterize exactly the physics governing the observation process. All parameters such as biases, tracking station locations, and physical constants that are not being estimated are known exactly.

The above criteria can never be met precisely in real spacecraft applications. As a result, the covariance matrix  $(F^T W F)^{-1}$  must be realistically interpreted with regard to the specific application. In orbit estimation applications using radar tracking data, the covariance (off-diagonal) elements of the measurement error are rarely available. In fact, for sensors that measure multicomponent vectors, the differing circuitry involved in the independent components frequently yields different time corrections for each component. This results in a measurement vector having components at different times. As a result, GTDS considers the observations to be uncorrelated scalar measurements so that the weighting matrix  $W$  is always diagonal and contains only the variances as shown in Equation (8-12).

The variance for each observation is formed from the relationship

$$\sigma_k^2 = k_1 \tilde{\sigma}_k^2 + k_2 \bar{\sigma}_k^2 \quad (8-13)$$

where

$\tilde{\sigma}_k$  ~ the a priori standard deviation of the observation noise.

$\bar{\sigma}_k$  ~ the standard deviation of the data reduction curve fit obtained during preprocessing of the observation data. The curve fit is assumed to be polynomial in form.

$k_1$  ~ a specified gain constant applied to  $\tilde{\sigma}_k$ .

$k_2$  ~ a specified gain constant applied to  $\bar{\sigma}_k$ .

Typical a priori weighting schemes for observations processed in GTDS are presented in Appendix D.

There is another, more subtle, qualification for identifying  $(F^T W F)^{-1}$  with the covariance matrix of uncertainty. In nonlinear regression problems such as trajectory estimation, the true covariance matrix is equal to  $(F^T W F)^{-1}$  plus terms involving higher order partial derivatives of the computed observations with respect to the variables solved for. These higher order terms were neglected during linearization. So long as large deviations are not obtained, the linearity assumption is reasonably well satisfied.

In the following sections the specific estimator algorithms implemented in GTDS and their associated covariance matrices are derived and discussed, and details concerning the application of the estimation process are described. Much of the material is taken from References 4, 5, and 6.

## 8.2 THE BATCH ESTIMATOR ALGORITHM

In order to facilitate the derivation of an iterative weighted least squares solution, the various quantities that are iteration dependent will be subscripted with an  $i$ . Thus,  $\bar{\Delta x}$  in Equation (8-5) is written  $\bar{\Delta x}_i = \bar{x} - \hat{x}_i$ , where  $\hat{x}_i$  is the best estimate of  $\bar{x}$ , the extended state, obtained from the  $i^{\text{th}}$  iteration. At the

beginning of the process ( $0^{\text{th}}$  iteration),  $\hat{x}_0 = \bar{x}_0$  is the a priori value of these solve-for variables. The objective is to determine  $\hat{x}_{i+1}$  from  $\hat{x}_i$  so as to minimize the loss function.

The initial assumption that the measurement vector  $\bar{y}$  can be related to the state and model parameters at epoch time  $t_0$  is given as

$$\bar{y} = \bar{f}(\bar{x}, \bar{z}) + \bar{n} \quad (8-14)$$

where two classes of variables are included. The  $p$ -dimensional vector  $\bar{x}$ , designated the solve-for vector, contains as components the state and model parameters whose values are known with limited certainty and are to be estimated. The  $q$ -dimensional vector  $\bar{z}$ , designated the consider vector, contains as components all model parameters whose values are known with limited certainty but are not to be estimated. Nevertheless, the uncertainty of  $\bar{z}$  is to be considered. A priori values of  $\bar{x}$  and  $\bar{z}$  are specified as  $\bar{x}_0$  and  $\bar{z}_0$  with respective covariance matrices  $P_{\Delta x_0}$  and  $P_{\Delta z_0}$ , i.e.,

$$\mathcal{E}\{\bar{x}_0\} = \bar{x}, \quad \text{cov}\{\bar{x}_0 - \bar{x}\} = P_{\Delta x_0} \quad (8-15)$$

$$\mathcal{E}\{\bar{z}_0\} = \bar{z}, \quad \text{cov}\{\bar{z}_0 - \bar{z}\} = P_{\Delta z_0} \quad (8-16)$$

On the  $i^{\text{th}}$  iteration the loss function is defined to be

$$Q(\bar{x}) = [\bar{y} - \bar{f}(\bar{x}, \bar{z}_0)]^T W [\bar{y} - \bar{f}(\bar{x}, \bar{z}_0)] + (\bar{x} - \bar{x}_0)^T P_{\Delta x_0}^{-1} (\bar{x} - \bar{x}_0) \quad (8-17)$$

The second term on the right has been added to the loss function to constrain the best estimate to the a priori specified  $\bar{x}_0$ , with the degree of constraint dependent upon the uncertainty  $P_{\Delta x_0}$ . This term accounts for the fact that  $\bar{x}_0$  is known to be accurate to a confidence level given by  $P_{\Delta x_0}$ . Therefore, any solution is constrained to satisfy the a priori realization  $\bar{x}_c$  to within the limits of its uncertainty.

To obtain the weighted least squares solution that minimizes  $Q(\bar{x})$  in Equation (8-17), the same procedure is followed as is used in Section 8.1. First,  $\partial Q / \partial \bar{x}$  is linearized; then, a Newton-Raphson procedure is iteratively applied to solve the nonlinear minimization problem. For convenience, the value of  $\hat{x}_i$  for the  $i^{\text{th}}$  iteration is considered first, and the nonlinear regression equation is linearized as follows.

$$\bar{f}(\bar{x}, \bar{z}) = \bar{f}(\hat{x}_i, \bar{z}_0) + F_i \bar{\Delta x}_i + E_i \bar{\Delta z}_i \quad (8-18)$$

where

$$\bar{\Delta x}_i = \bar{x} - \hat{x}_i \quad (8-19)$$

$$\bar{\Delta z}_i = \bar{z} - \bar{z}_0 \quad (8-20)$$

and

$$F_i = \left( \frac{\partial \bar{f}}{\partial \bar{x}} \right)_{(\bar{x}, \bar{z} = \hat{x}_i, \bar{z}_0)} \quad (8-21a)$$

$$E_i = \left( \frac{\partial \bar{f}}{\partial \bar{z}} \right)_{(\bar{x}, \bar{z} = \hat{x}_i, \bar{z}_0)} \quad (8-21b)$$

Since the consider variables  $\bar{z}$  are not being estimated, their values remain equal to  $\bar{z}_0$ .

Substituting terms with nonzero mean from Equation (8-18) into Equation (8-17) yields the linearized loss function

$$\begin{aligned} Q'(\bar{\Delta x}_i) &= [\bar{\Delta y}_i - F_i \bar{\Delta x}_i]^T W [\bar{\Delta y}_i - F_i \bar{\Delta x}_i] \\ &+ (\bar{\Delta x}_i - \tilde{\Delta x}_i)^T P_{\Delta x_0}^{-1} (\bar{\Delta x}_i - \tilde{\Delta x}_i) \end{aligned} \quad (8-22)$$

where the measurement residuals are

$$\bar{\Delta y}_i = \bar{y} - \bar{f}(\hat{x}_i, \bar{z}_0) \quad (8-23)$$

and the deviation of the a priori estimate from the  $i^{\text{th}}$  iterative estimate is

$$\tilde{\Delta x}_i = \bar{x}_0 - \hat{x}_i \quad (8-24)$$

The value of  $\overline{\Delta x_i}$  that minimizes  $Q'$ , denoted by  $\hat{\Delta x_{i+1}}$ , is therefore

$$\hat{\Delta x_{i+1}} = (F_i^T W F_i + P_{\Delta x_0}^{-1})^{-1} [F_i^T W \overline{\Delta y_i} + P_{\Delta x_0}^{-1} \hat{\Delta x_i}] \quad (8-25)$$

and the best estimate of the solve-for variables is

$$\hat{x}_{i+1} = \overline{x_0} + \sum_{k=1}^{i+1} \hat{\Delta x_k} = \hat{x_i} + \hat{\Delta x_{i+1}} \quad (8-26)$$

This estimation process is iteratively applied until the convergence criteria (discussed in Section 8.6.3) are satisfied.

Equation (8-25) is the estimator algorithm used in GTDS. It requires the inversion of a  $p \times p$  matrix, the same dimension as the vector of solve-for variables. Insofar as the estimator algorithm is concerned, it makes no difference whether consider variables are included. Equation (8-25) depends only on the values  $\overline{z_0}$ , not on the uncertainty  $P_{\Delta z_0}$ . This might be expected, since the uncertainty resulting from the inclusion of consider variables affects only the second order statistics or covariances (i. e., the ensemble properties). The last term on the right in Equation (8-25) can only be included subsequent to the initial iteration, since on the initial iteration  $\hat{\Delta x} = 0$ .

The estimator algorithm in Equation (8-25) differs slightly from the classical weighted least squares algorithm (Equation (8-10)). This difference results from the addition of the second term on the right in the loss function (Equation (8-17)).

### 8.2.1 Mean and Covariance of Estimate

The best estimate  $\hat{x}$  which results from convergence of the estimator algorithm will next be examined to determine its statistical properties. Two quantities are of concern, the expected (mean) value and the covariance of the estimate. The expected value of the deviation  $\hat{\Delta x}$  yields the amount of bias in the estimate, while the covariance indicates the amount of dispersion or uncertainty. Obviously, zero bias and minimum dispersion are the qualities sought.

In the following discussion, it is assumed that the iterations have converged and that the unsubscripted variables  $\bar{x}, \bar{\Delta x}, \bar{\Delta y}$ , etc., correspond to the converged solution and perturbations about it.

The expected value and covariance of the measurement noise vector  $\bar{n}$  are assumed to be

$$\mathcal{E}\{\bar{n}\} = 0 \quad (8-27a)$$

$$\text{cov}\{\bar{n}\} = W^{-1} \quad (8-27b)$$

and the linearized vector of observation residuals can be written as

$$\bar{\Delta y} = F \bar{\Delta x} + E \bar{\Delta z} + \bar{n} \quad (8-28)$$

Therefore, the expected value of  $\bar{\Delta y}$  is

$$\mathcal{E}\{\bar{\Delta y}\} = \mathcal{E}\{F\bar{\Delta x}\} \quad (8-29)$$

since  $\mathcal{E}\{\bar{n}\} = \mathcal{E}\{\bar{\Delta z}\} = 0$ . The covariance of  $\bar{\Delta y}$  is

$$\begin{aligned} \text{cov}\{\bar{\Delta y}\} &= \mathcal{E}\{[\bar{\Delta y} - \mathcal{E}(\bar{\Delta y})][\bar{\Delta y} - \mathcal{E}(\bar{\Delta y})]^T\} \\ &= E \mathcal{E}\{\bar{\Delta z} \bar{\Delta z}^T\} E^T + E \mathcal{E}\{\bar{\Delta z} \bar{n}^T\} + \mathcal{E}\{\bar{n} \bar{\Delta z}^T\} E^T + \mathcal{E}\{\bar{n} \bar{n}^T\} \quad (8-30) \\ &= E P_{\Delta z_0} E^T + W^{-1} \end{aligned}$$

where the correlation between the consider variable errors and the measurement noise is assumed zero, i.e.,

$$\mathcal{E}\{\bar{\Delta z} \bar{n}^T\} = 0 \quad (8-31)$$

The mean of the best estimate  $\hat{x}_{i+1}$  is

$$\begin{aligned}
 \mathcal{E} \{ \hat{x}_{i+1} - \bar{x} \} &= \mathcal{E} \{ \hat{\Delta x}_{i+1} - \overline{\Delta x}_i \} \\
 &= \left( F^T W F + P_{\Delta x_0}^{-1} \right)^{-1} \left[ F^T W \mathcal{E} \{ \overline{\Delta y} \} + P_{\Delta x_0}^{-1} \mathcal{E} \{ \tilde{\Delta x} \} - \left( F^T W F \right. \right. \\
 &\quad \left. \left. + P_{\Delta x_0}^{-1} \right) \mathcal{E} \{ \overline{\Delta x} \} \right] \\
 &= \left( F^T W F + P_{\Delta x_0}^{-1} \right)^{-1} P_{\Delta x_0}^{-1} \mathcal{E} \{ \bar{x}_0 - \bar{x} \}
 \end{aligned} \tag{8-32}$$

However,  $\bar{x}_0$  was defined to have an expected value equal to  $\bar{x}$  (see Equation (8-15)). Therefore

$$\mathcal{E} \{ \hat{x} - \bar{x} \} = 0 \quad \text{and} \quad \mathcal{E} \{ \hat{x} \} = \bar{x} \tag{8-33}$$

Equation (8-33) shows that the best estimate is unbiased. The covariance of the error in the estimate is

$$\begin{aligned}
 P_{\Delta x} &= \mathcal{E} \{ [\hat{x}_{i+1} - \bar{x}] [\hat{x}_{i+1} - \bar{x}]^T \} = \mathcal{E} \{ [\hat{\Delta x}_{i+1} - \overline{\Delta x}_i] [\hat{\Delta x}_{i+1} - \overline{\Delta x}_i]^T \} \\
 &= \psi \left\{ F^T W E P_{\Delta z_0} E^T W F + F^T W F + P_{\Delta x_0}^{-1} \right. \\
 &\quad \left. + F^T W \left[ E \mathcal{E} \{ \overline{\Delta z} (\overline{\Delta x} - \tilde{\Delta x})^T \} P_{\Delta x_0}^{-1} + E \mathcal{E} \{ \overline{\Delta z} \bar{n}^T \} W F \right] \right. \\
 &\quad \left. + \left[ P_{\Delta x_0}^{-1} \mathcal{E} \{ (\overline{\Delta x} - \tilde{\Delta x}) \overline{\Delta z}^T \} E^T + F^T W \mathcal{E} \{ \bar{n} \overline{\Delta z}^T \} E \right] W F \right. \\
 &\quad \left. + P_{\Delta x_0}^{-1} \mathcal{E} \{ (\overline{\Delta x} - \tilde{\Delta x}) \bar{n}^T \} W F + F^T W \mathcal{E} \{ \bar{n} (\overline{\Delta x} - \tilde{\Delta x})^T \} P_{\Delta x_0} \right\} \psi^T
 \end{aligned} \tag{8-34}$$

where

$$\psi = \left( F^T W F + P_{\Delta x_0}^{-1} \right)^{-1} \tag{8-35}$$



To simplify Equation (8-34) the following definitions are made

$$\begin{aligned}
 C_{\Delta x_0 \Delta z} &= E \{ (\overline{\Delta x} - \tilde{\Delta x}) \overline{\Delta z}^T \} = E \{ (\bar{x} - \bar{x}_0) (\bar{z} - \bar{z}_0)^T \} \\
 &= E \{ (\bar{x}_0 - \bar{x}) (\bar{z}_0 - \bar{z})^T \} \\
 C_{\Delta x_0 \Delta z}^T &= E \{ \overline{\Delta z} (\overline{\Delta x} - \tilde{\Delta x})^T \} = E \{ (\bar{z} - \bar{z}_0) (\bar{x} - \bar{x}_0)^T \} \\
 &= E \{ (\bar{z}_0 - \bar{z}) (\bar{x}_0 - \bar{x})^T \}
 \end{aligned} \tag{8-36}$$

$$C_{\Delta z n} = E \{ \overline{\Delta z} \bar{n}^T \} = E \{ (\bar{z} - \bar{z}_0) \bar{n}^T \} = 0 \tag{8-37}$$

$$C_{\Delta z n}^T = E \{ \bar{n} \overline{\Delta z}^T \} = E \{ \bar{n} (\bar{z} - \bar{z}_0)^T \} = 0$$

$$C_{\Delta x_0 n} = E \{ (\overline{\Delta x} - \tilde{\Delta x}) \bar{n}^T \} = E \{ (\bar{x} - \bar{x}_0) \bar{n}^T \} = 0 \tag{8-38}$$

$$C_{\Delta x_0 n}^T = E \{ \bar{n} (\overline{\Delta x} - \tilde{\Delta x})^T \} = E \{ \bar{n} (\bar{x} - \bar{x}_0)^T \} = 0$$

Therefore, Equation (8-34) becomes

$$\begin{aligned}
 P_{\Delta x} &= \psi \{ F^T W E P_{\Delta z_0} E^T W F + \psi^{-1} \\
 &\quad + F^T W E C_{\Delta x_0 \Delta z}^T P_{\Delta x_0}^{-1} + P_{\Delta x_0}^{-1} C_{\Delta x_0 \Delta z} E^T W F \} \psi^T
 \end{aligned} \tag{8-39}$$

In Equations (8-37) and (8-38) it is assumed that no statistical correlation exists between the measurement noise and the error in the solve-for or consider variables. The correlation between errors in the a priori solve-for and consider variables  $C_{\Delta x_0 \Delta z}$  is neglected in GTDS, primarily because a priori values of this correlation matrix are usually unavailable. The terms are maintained in Equation (8-39) for completeness and for possible use in the error analysis application discussed later. In the event that no consider variables are included, Equation (8-39) reduces to

$$P_{\Delta x} = \psi \{ (F^T W F + P_{\Delta x_0}^{-1})^{-1} \} \tag{8-40}$$

which is the gain matrix in the estimator algorithm (Equation (8-25)).

It was stated previously that a desirable quality of an estimate is small dispersions. It is evident from Equation (8-40) that the covariance matrix of error in the estimate  $P_{\Delta_x}$  varies with the measurement uncertainty  $W$  and the a priori covariance matrix of the solve-for variable uncertainty  $P_{\Delta_{x_0}}$ . Equation (8-39) shows that  $P_{\Delta_x}$  also varies with the covariance matrix of uncertainty in the consider variables  $P_{\Delta_{z_0}}$ . Therefore, minimizing the measurement noise, as well as the a priori uncertainty in the solve-for and consider variables, will result in reducing the dispersion or uncertainty in the estimated variables.

The correlation between errors in the solve-for and consider variables, which results from the processing, is

$$C_{\Delta_x \Delta_z} = E \{ (\hat{x} - \bar{x}) (\bar{z}_0 - \bar{z})^T \} \quad (8-41)$$

$$= \psi \left\{ P_{\Delta_{x_0}}^{-1} C_{\Delta_{x_0} \Delta_z} - F^T W E P_{\Delta_{z_0}} \right\}$$

Even if the a priori correlation  $C_{\Delta_{x_0} \Delta_z}$  is assumed to be zero, a correlation between errors in the solve-for and consider variables will result because of their dependency in the processing model.

### 8.2.2 Observation Partial Derivatives

Throughout Sections 8.2 and 8.2.1, the components of the solve-for and consider vectors  $\bar{x}$  and  $\bar{z}$  have been ignored along with the way the components and their error covariances  $P_{\Delta_x}$  and  $P_{\Delta_z}$  are associated with a specific time or epoch. Furthermore, it has been assumed in Equation (8-14) that the calculated measurements at various times ( $t_1, t_2, \dots, t_m$ ) can be related to the solve-for and consider variables at the epoch time  $t_0$ . In Equation (8-18) it is assumed that the time varying matrices  $F_i$  and  $E_i$  can be calculated which linearly relate the calculated measurements to variables at the epoch time. In the following section, attention will be focused upon the solve-for and consider vector components, the manner in which the time dependency is accomplished, and the properties of the normal matrix which are utilized in its formation.

The general estimation (solve-for) vector  $\bar{x}$  in the regression equation (Equation (8-14)) and the estimator equation (Equation (8-25)) contains variables from  $\bar{q}$  in Equation (7-221), i.e.,

$$\bar{\mathbf{x}} - \bar{\mathbf{q}} = \begin{bmatrix} \bar{\mathbf{p}} \\ \bar{\mathbf{r}}_s \\ b \\ \delta t \end{bmatrix} = \{\text{solve-for vector}\} \quad (8-42)$$

where

$\bar{\mathbf{p}} \sim$  dynamic parameters, consisting of the vehicle's state components at epoch and model parameters in the acceleration model (Equation (4-1)). These parameters include gravity constants, the drag parameter, the solar radiation constant, thrust, and attitude parameters.

$\bar{\mathbf{r}}_s \sim$  tracking station locations in earth-fixed coordinates.

$b \sim$  measurement biases.

$\delta t \sim$  measurement timing bias.

The specified components of the solve-for vector are ordered as follows:

- six (or fewer) position and velocity components,  $\bar{\mathbf{R}}_0$  and  $\dot{\bar{\mathbf{R}}}_0$ , or equivalent elements
- drag parameter  $\mu_1$
- solar radiation parameter  $k = P_s A/m_0$
- gravitational potential constants  $\mu$ ,  $\mu_k$ ,  $C_n^m$ , and  $S_n^m$
- thrust acceleration parameters  $a_0, \dots, a_4$ ;  $\alpha_0, \dots, \alpha_3$ ; and  $\delta_0, \dots, \delta_3$
- attitude control parameters  $a_x, a_y, a_z$ ;  $b_x, b_y, b_z$ ; and  $c_x, c_y, c_z$
- tracking station locations  $\bar{\mathbf{r}}_s$
- observation biases  $b$  and  $\delta t$

Either of the five optional characterizations of the epoch position and velocity, described in Section 1.6, can be solved for. The mean of 1950.0 Cartesian coordinates  $\bar{\mathbf{R}}_0$  and  $\dot{\bar{\mathbf{R}}}_0$  are used for the purpose of describing the method.

Each row of the  $F(t)$  matrix in Equation (8-21a) contains partial derivatives of the computed observation with respect to  $\bar{R}_0$ ,  $\dot{\bar{R}}_0$ , and the other specified components of  $\bar{p}$ ,  $\bar{r}_s$ ,  $b$ , and  $\delta t$ . The dynamic variables  $\bar{p}$  must be related to the epoch time through the state transition matrix  $\Phi(t_i, t_0)$  as discussed in Chapters 4 and 6. Partial derivatives with respect to  $\bar{r}_s$ ,  $b$ , and  $\delta t$  are not dependent upon an epoch and can be obtained by differentiating the observation equation explicitly.

The nonlinear observation equation is written in Equation (7-1) as

$$O_c = \bar{f}_0 [\bar{r}_{1t} (t + \delta t, \bar{p}, \bar{r}_s), \dot{\bar{r}}_{1t} (t + \delta t, \bar{p}, \bar{r}_s)] + b + RF_c \quad (8-43)$$

where

$\bar{r}_{1t}, \dot{\bar{r}}_{1t} \sim$  vehicle position and velocity vectors expressed in local tangent coordinates with respect to a tracking station located at  $\bar{r}_s$

$RF_c \sim$  systematic error correction to observation due to atmospheric refraction, light time, transponder delay, antenna mount errors, etc.

The partial derivatives of an observation  $O_c$ , at time  $t_j$ , with respect to the solve-for variables  $\bar{x}$  are

$$\bar{a}_j = \frac{\partial O_c}{\partial \bar{x}} = \begin{bmatrix} \frac{\partial \bar{f}_0(t_j)}{\partial \bar{R}(t_j)} & \frac{\partial \bar{f}_0(t_j)}{\partial \dot{\bar{R}}(t_j)} & \frac{\partial \bar{f}_0(t_j)}{\partial \bar{r}_s} & \frac{\partial \bar{f}_0(t_j)}{\partial b} & \frac{\partial \bar{f}_0(t_j)}{\partial \delta t} \end{bmatrix} \begin{bmatrix} \frac{\partial \bar{R}(t_j)}{\partial \bar{p}(t_0)} \\ \frac{\partial \dot{\bar{R}}(t_j)}{\partial \bar{p}(t_0)} \\ 1 \\ 1 \\ 1 \end{bmatrix} \quad (8-44)$$

The first matrix on the right is explicitly determined from the observation equations in Chapter 7. The second matrix on the right must be obtained by integrating the variational equations (or approximations of these equations) as described in Chapter 6. Equation (8-44) constitutes a single row  $\bar{a}$  of the  $F$  matrix.

On each iteration, the  $m$  observations are sequentially processed to form the normal matrix  $F^T W F$ . Since the weighting matrix  $W$  is diagonal, the recursive relation for accumulating the normal matrix is

$$F^T W F = \sum_{j=1}^m \frac{\bar{a}_j^T \bar{a}_j}{\sigma_j^2} \quad (8-45)$$

where

$$\bar{a}_j = \frac{\partial \bar{f} [\hat{x}_i(t_j), \bar{z}_0]}{\partial \bar{z}} = \{j^{\text{th}} \text{ row of } F \text{ matrix given by Equation (8-44)}\}$$

and  $\sigma_j$  is the standard deviation of the  $j^{\text{th}}$  observation.

By forming  $F^T W F$  row-by-row instead of manipulating the full  $(m \times p)$   $F$  matrix, a saving in storage and computation time is realized. Since the matrix  $F^T W F$  is symmetric, elements below the main diagonal need not be computed or stored.

The general consider vector  $\bar{z}$  in the regression equation (Equation (8-14)) can have as components any model parameters in  $\bar{p}$ ,  $\bar{r}_s$ ,  $b$ , or  $\delta t$ .

Each row of the  $E(t)$  matrix in Equation (8-21b) contains partial derivatives of the computed observations with respect to the specified components of  $\bar{z}$ . The partial derivatives with respect to the dynamic variables  $\bar{p}$ , specified in  $\bar{z}$ , can be calculated simultaneously with the dynamic partial derivatives in  $F(t)$  as described in Chapter 6. However, the partial derivatives in  $E(t)$  need only be computed on the final converged iteration, since the estimator equation (Equation (8-25)) is not dependent upon  $E(t)$ .

In GTDS the components of the vectors  $\bar{x}$  and  $\bar{z}$  are merged on the final iteration to an expanded state vector  $\bar{u}$ . The elements of  $\bar{u}$  are ordered as described above. The observation partial derivatives are then calculated with respect to  $\bar{u}$ , and a  $(p+q) \times (p+q)$  expanded state normal matrix  $\tilde{F}^T W \tilde{F}$  is sequentially accumulated as described above. When all  $m$  observations have been processed, selected elements of  $\tilde{F}^T W \tilde{F}$  are extracted to form  $F^T W F$ ,  $E^T W E$ , and  $E^T W F$ , which are required to compute the covariance and correlation matrices in Equations (8-39) through (8-41). It should be noted that only elements on and above the main diagonal of  $\tilde{F}^T W \tilde{F}$  need be calculated and stored.

### 8.2.3 Covariance Matrix Transformations

The converged estimate  $\hat{x}$ , covariance matrix  $P_{\Delta x}$ , and correlation matrix  $C_{\Delta x \Delta z}$  resulting from the differential correction process correspond to the epoch time  $t_0$ . Since GTDS can estimate the state in any of five subsets, the first six components of  $\hat{x}$  can correspond to Cartesian coordinates in mean of 1950.0 or

true of date axes, classical Keplerian orbital elements, spherical coordinates, or DODS variables. For discussion purposes, the first six components (the state components) of  $\hat{\mathbf{x}}$  are denoted by  $\bar{\mathbf{s}}$ . The vector  $\bar{\mathbf{s}}$  can optionally be

$$\bar{\mathbf{s}} = \begin{bmatrix} X \\ Y \\ Z \\ \dot{X} \\ \dot{Y} \\ \dot{Z} \end{bmatrix} \text{ Mean of } 1950.0 = \begin{bmatrix} x \\ y \\ z \\ \dot{x} \\ \dot{y} \\ \dot{z} \end{bmatrix} \text{ True of Epoch} = \begin{bmatrix} a \\ e \\ i \\ \Omega \\ \omega \\ M \end{bmatrix} \text{ Keplerian Elements} = \begin{bmatrix} r \\ \alpha \\ \delta \\ V \\ A \\ \beta \end{bmatrix} \text{ Spherical Elements} = \begin{bmatrix} x_1 \\ x_2 \\ x_3 \\ x_4 \\ x_5 \\ x_6 \end{bmatrix} \text{ DODS Variables}$$

depending on the variable set used in the differential correction process. The upper left  $6 \times 6$  submatrix of  $P_{\Delta x}$ , denoted  $P_{\Delta s}$ , also corresponds to the variables used in the differential correction process.

GTDS transforms the estimated state  $\bar{\mathbf{s}}$  and its covariance matrix  $P_{\Delta s}$  to any of the other variable sets shown above. The constant solve-for parameters and consider parameters in  $\hat{\mathbf{x}}$  and  $\bar{\mathbf{z}}$  of the original differential correction problem are not coordinate dependent. Only the state (position and velocity) depends upon the coordinate system utilized. Therefore, only the subset  $\bar{\mathbf{s}}$  of  $\hat{\mathbf{x}}$  and submatrix  $P_{\Delta s}$  of  $P_{\Delta x}$  need be considered in the coordinate transformation.

If the sets to which  $\bar{\mathbf{s}}$  and  $P_{\Delta s}$  are being transformed are denoted by  $\bar{\mathbf{s}}'$  and  $P_{\Delta s}'$ , the nonlinear transformation can be written as

$$\bar{\mathbf{s}}'(t_0) = h[\bar{\mathbf{s}}(t_0)] \tag{8-46}$$

Transformations of this type between Cartesian and spherical coordinates are presented in Section 3.3.4, and between Cartesian and Keplerian elements in Section 3.3.8.

To transform the covariance matrix  $P_{\Delta s}$ , Equation (8-46) is linearized, yielding

$$\overline{\Delta \mathbf{s}}'(t_0) = H(t_0) \overline{\Delta \mathbf{s}}(t_0) \tag{8-47a}$$

where

$$H(t_0) = \left( \frac{d\bar{\mathbf{s}}'}{d\bar{\mathbf{s}}} \right)_{t=t_0} \tag{8-47b}$$

These partial derivatives between Cartesian and spherical coordinates and Cartesian and Keplerian elements are presented in Sections 3.3.4 and 3.3.8, respectively. The covariance matrix  $P_{\Delta_s}$  is defined as

$$P_{\Delta_s}(t_0) = \mathcal{E} \{ [\hat{\Delta s}(t_0) - \overline{\Delta s}(t_0)] [\hat{\Delta s}(t_0) - \overline{\Delta s}(t_0)]^T \} \quad (8-48)$$

where  $\hat{\Delta s}$  and  $\overline{\Delta s}$  correspond to the first six components of  $\hat{\Delta x}$  and  $\overline{\Delta x}$ , defined previously. The covariance matrix of transformed variables  $P_{\Delta_s'}$  is defined as

$$P_{\Delta_s'}(t_0) = \mathcal{E} \{ [\hat{\Delta s}'(t_0) - \overline{\Delta s}'(t_0)] [\hat{\Delta s}'(t_0) - \overline{\Delta s}'(t_0)]^T \} \quad (8-49)$$

Substituting Equation (8-47a) into Equation (8-49) yields

$$P_{\Delta_s'}(t_0) = H(t_0) P_{\Delta_s}(t_0) H^T(t_0) \quad (8-50)$$

A second type of transformation occasionally encountered concerns the timewise propagation of the estimate  $\hat{x}$  and the covariance matrix  $P_{\Delta_x}$ . The estimate  $\hat{x}(t_0)$  is transformed timewise by merely integrating the equations of motion from initial conditions  $\hat{x}(t_0)$  to other times of interest. The best estimate of all model parameters is used in this integration.

The timewise propagation of the covariance matrix of state and model parameters is slightly more complicated. First, the propagation is separate from the differential correction process, and model parameters other than those estimated (solved for) can be considered as uncertain in the propagation process. The a priori values of the uncertain state and model parameters (whether solved for or considered) at epoch time  $t_0$  are denoted by  $\hat{u}(t_0)$  and their covariance matrix by  $P_{\Delta_u}(t_0)$ . At any later time  $t$ , they are given by

$$\hat{u} = \begin{bmatrix} \hat{x} \\ \overline{z}_0 \end{bmatrix} \quad \text{and} \quad P_{\Delta_u} = \begin{bmatrix} P_{\Delta_x} & C_{\Delta_x \Delta z} \\ \text{---} & \text{---} \\ C_{\Delta_x \Delta z}^T & P_{\Delta z_0} \end{bmatrix}$$

It is assumed that  $\hat{u}$  and  $P_{\Delta u}$  are composed of state components  $\bar{s}$  and uncertain model parameters  $\bar{u}^*$ . Perturbations about  $\bar{u}(t)$  are related to perturbations about the a priori values as follows

$$\bar{\Delta u}(t) = \varphi(t, t_0) \bar{\Delta u}(t_0) \quad (8-51a)$$

where the transition matrix  $\varphi$  is given by

$$\varphi(t, t_0) = \begin{bmatrix} \Phi(t, t_0) & \psi(t, t_0) \\ \text{-----} & \text{-----} \\ 0 & I \end{bmatrix} \quad (8-51b)$$

with

$$\Phi(t, t_0) = \left( \frac{\partial \bar{s}(t)}{\partial \bar{s}(t_0)} \right) \quad \text{and} \quad \psi(t, t_0) = \left( \frac{\partial \bar{s}(t)}{\partial \bar{u}^*(t_0)} \right) \quad (8-51c)$$

By definition, the covariance matrix of  $\hat{u}$  at time  $t$  is

$$P_{\Delta u}(t) = E\{ [\hat{\Delta u}(t) - \bar{\Delta u}(t)] [\hat{\Delta u}(t) - \bar{\Delta u}(t)]^T \} \quad (8-52)$$

Substituting Equation (8-51a) into Equation (8-52) yields

$$P_{\Delta u}(t) = \varphi(t, t_0) P_{\Delta u}(t_0) \varphi^T(t, t_0) \quad (8-53)$$

The covariance matrix of state (upper left  $6 \times 6$  submatrix of  $P_{\Delta u}$ ) is obtained by partitioning  $\varphi$  and  $P_{\Delta u}$  into their  $\bar{s}$  and  $\bar{u}^*$  subparts as follows

$$\begin{aligned} P_{\Delta s}(t) = & \Phi(t, t_0) P_{\Delta s}(t_0) \Phi^T(t, t_0) + \psi(t, t_0) C_{\Delta s \Delta u^*}^T \Phi^T(t, t_0) \\ & + \Phi(t, t_0) C_{\Delta s \Delta u^*} \psi^T(t, t_0) + \psi(t, t_0) P_{\Delta u^*} \psi^T(t, t_0) \end{aligned} \quad (8-54a)$$

If no uncertain model parameters are included in the propagation, Equation (8-54a) reduces to

$$P_{\Delta s}(t) = \Phi(t, t_0) P_{\Delta s}(t_0) \Phi^T(t, t_0) \quad (8-54b)$$



From the same partitioning, the correlation between the state  $\bar{s}$  and  $\bar{u}^*$  is given by

$$C_{\Delta_s \Delta_{u^*}}(t) = \Phi(t, t_0) C_{\Delta_s \Delta_{u^*}} + \theta(t, t_0) P_{\Delta_{u^*}} \quad (8-54c)$$

## 8.2.4 Computational Procedure for the Differential Correction Program

This section describes conceptually how the estimator and covariance equations are solved in GTDS. Figure 8-1, the computational flow schematic, will aid in the discussion. The figure is divided into functional blocks and the discussion is similarly organized. The logic shown in Figure 8-1 is not the same as the specific source logic in GTDS, but is presented in order to characterize the concepts.

### 8.2.4.1 A Priori Input

The process is initialized by specifying all necessary input data at (A). This includes the estimated and considered variables and their covariances, as well as measurement time spans and times to which the best estimates of the state and covariances are to be propagated. The state input is optionally expressed in any of several convenient coordinate systems. It is transformed to the basic coordinate system used in GTDS (i.e., mean equator and equinox of 1950.0 or true equator and equinox of a given epoch) for subsequent processing. These transformations are described in Chapter 3.

### 8.2.4.2 Data Management

The next step is the preparation of the observation data for processing at (B). This encompasses relocating the data within the specified measurement span from the original input device (cards, single or multiple tapes, disk, or keyboard) to a working file convenient for subsequent retrieval during processing. During this relocation function, the data sequence can optionally be edited considering the type of observation, the source of the data, the tracking station, and the time span between adjacent points. The data on the working file are chronologically numbered, and the number of the data point which bounds the initial epoch time  $t_0$  from below is recorded. The data management function also includes the determination of whether the initial epoch time is less than the first data time, between the first and last data time, or larger than the last data time. For the first case, the data are processed sequentially from the first point at  $t_1$  to the last point at  $t_m$ . For the second case, the processing starts backward

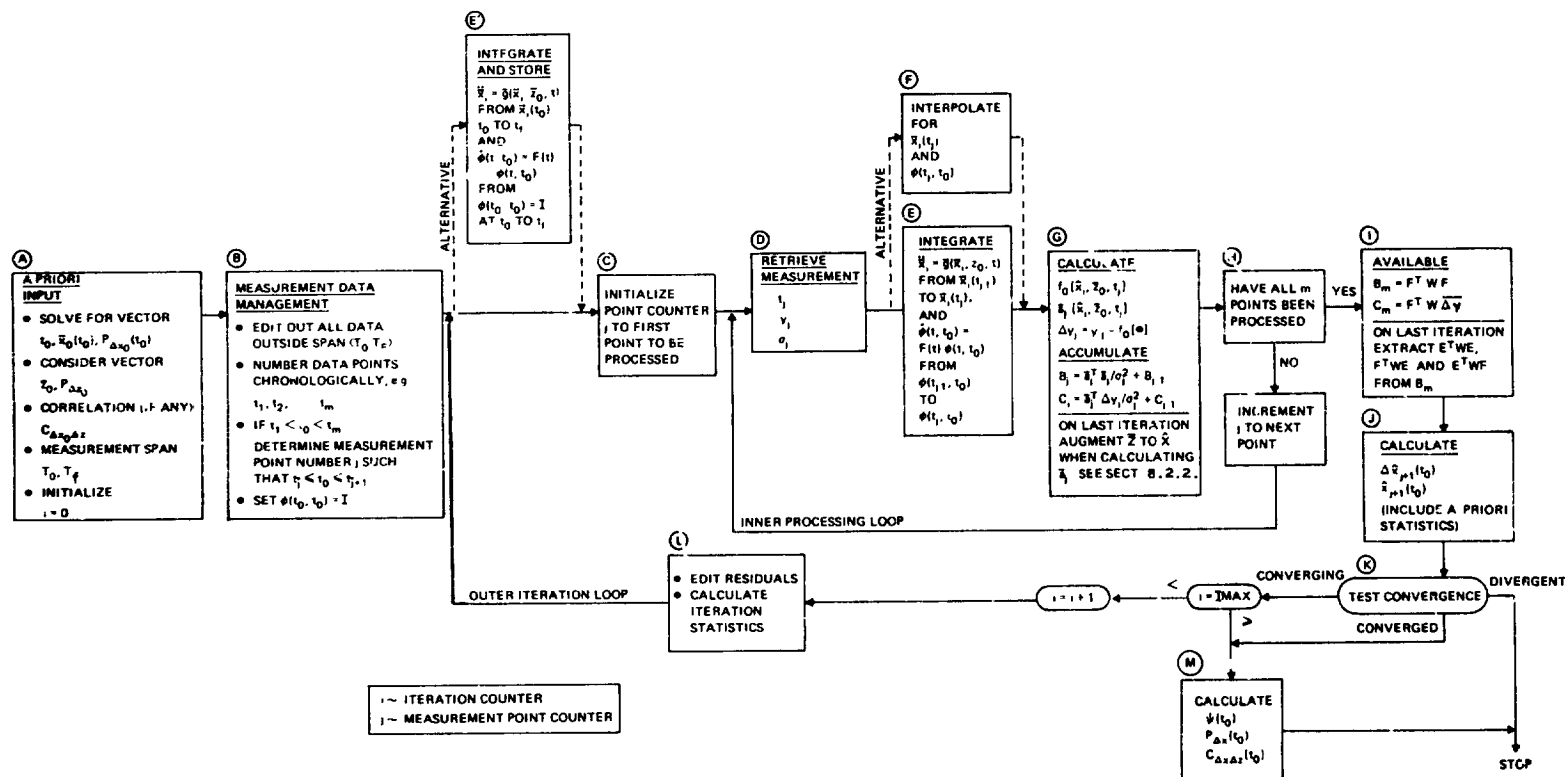


Figure 8-1. Computational Sequence for the Differential Correction Program

in time from the initial epoch to the first data point. It then switches back to the initial epoch and proceeds forward in time to the last data point. In the third case, the data are processed backward in time from the last (chronological) data point to the first data point.

#### 8.2.4.3 Outer Iteration Loop

The outer iteration loop begins at (E)' or (C). Normal GTDS operation starts at (C) with initialization of the inner processing loop point counter  $j$  and subsequent integration of the ephemeris from observation point to observation point within the inner loop (at (E)). An alternative scheme, planned for the standalone DC Program, begins the outer loop at (E)' by calculating and storing the ephemeris and state transition matrix over the entire DC time span ( $T_0$  to  $T_f$ ). Later, in the inner loop, the state and state transition matrix are obtained by interpolation of the stored data (at (F)).

#### 8.2.4.4 Inner Processing Loop

The inner processing loop starts by retrieving the first data point to be processed from the working file at (D). Under normal operation, the nonlinear equations of motion (see Chapter 5) and associated variational equations (see Chapter 4) are numerically integrated (see Chapter 6) to the data time at (E). Alternatively, if the ephemeris and state transition matrix are generated and stored at (E)', their values are interpolated to the observation time at (F). The best estimate of the measurement and its related residual  $\overline{\Delta y_j}$  are calculated (see Chapter 7) along with the single row  $\overline{a_j}$  of the F matrix corresponding to the measurement at (G). To minimize core storage, the matrix products  $F^T W \overline{\Delta y}$  and  $F^T W F$  are accumulated as each row of F is calculated, as described in Section 8.2.2. It is apparent from Equation (8-25) that only these matrix products are required for determining the estimate. All symmetric matrices (e.g.,  $F^T W F$ ) are stored in upper triangular form. On the last iteration the matrix products  $F^T W F$ ,  $E^T W E$ ,  $F^T W E$ , and  $E^T W F$  are accumulated for subsequent use in computing the covariance and correlation matrices. At (H) tests are performed to determine if all  $m$  data points have been processed. If they have not, the measurement point counter  $j$  is incremented or decremented, depending on whether the data is being processed forward or backward in time. The logic then returns to the beginning of the processing loop to retrieve the next point to be processed.

#### 8.2.4.5 Estimation Computation

When all  $m$  data points have been processed, the complete matrix products  $F^T W$  and  $F^T W F$  are available at (I) as is the measurement residual vector  $\overline{\Delta y}$ . On the last iteration  $F^T W E$ ,  $E^T W F$ , and  $E^T W E$  are also available. The best estimate of the perturbations  $\Delta \hat{x}_{i+1}$  and variables  $\hat{x}_{i+1}$  are then calculated via Equations (8-25) and (8-26) at (J).

#### 8.2.4.6 Termination of Outer Iteration Loop

After determining an estimate at (J), the iteration is complete and convergence tests are performed at (K). The convergence criteria are described in Section 8.6.3. If the iterations are converging, the iteration counter  $i$  is tested against the maximum number of iterations allowable. If the maximum has not been reached, the iteration counter is incremented and logic proceeds through (L) to begin the next iteration at (D). At (L) the measurement residual vector can be used to edit the data as discussed in Section 8.6.2, as well as to determine iteration statistics as discussed in Section 8.6.4. If the convergence test at (K) determines that divergence is occurring, the problem can be terminated. If the iteration has converged, or the maximum number of iterations has been reached, then the covariance and correlation matrices at epoch  $t_0$  are calculated at (M). Finally, the state vector, the covariance matrix, and the correlation matrix can be transformed to other space and time sets as described in Section 8.2.3.

### 8.3 ERROR ANALYSIS APPLICATION

The weighted least squares estimator algorithm and the associated covariance and correlation matrices, derived in Sections 8.2 and 8.2.1, are summarized as follows.

#### Estimator

$$\Delta \hat{x}_{i+1} = \left[ F_i^T W F_i + P_{\Delta x_0}^{-1} \right]^{-1} \left( F_i^T W \overline{\Delta y}_i + P_{\Delta x_0}^{-1} \Delta \hat{x}_i \right) \quad (8-55)$$

## Covariance of Estimate

$$\begin{aligned}
 P_{\Delta x} = \psi & \left[ F^T W E P_{\Delta z_0} E^T W F + F^T W E C_{\Delta x_0 \Delta z}^T P_{\Delta x_0}^{-1} \right. \\
 & \left. + P_{\Delta x_0}^{-1} C_{\Delta x_0 \Delta z} E^T W F + F^T W F + P_{\Delta x_0}^{-1} \right] \psi^T
 \end{aligned}
 \tag{8-56}$$

## Correlation of Estimate and Consider Variables

$$C_{\Delta x \Delta z} = \psi \left[ P_{\Delta x_0}^{-1} C_{\Delta x_0 \Delta z} - F^T W E P_{\Delta z_0} \right] \tag{8-57}$$

where

$$\psi = [F^T W F + P_{\Delta x_0}^{-1}]^{-1} \tag{8-58a}$$

$$P_{\Delta x_0} = \mathcal{E} \{(\bar{x}_0 - \bar{x})(\bar{x}_0 - \bar{x})^T\} \tag{8-58b}$$

$$P_{\Delta x} = \mathcal{E} \{(\hat{x} - \bar{x})(\hat{x} - \bar{x})^T\} \tag{8-58c}$$

$$P_{\Delta z_0} = \mathcal{E} \{(\bar{z}_0 - \bar{z})(\bar{z}_0 - \bar{z})^T\} \tag{8-58d}$$

$$C_{\Delta x_0 \Delta z} = \mathcal{E} \{(\bar{x}_0 - \bar{x})(\bar{z}_0 - \bar{z})^T\} \tag{8-58e}$$

$$C_{\Delta x \Delta z} = \mathcal{E} \{(\hat{x} - \bar{x})(\bar{z}_0 - \bar{z})^T\} \tag{8-58f}$$

( $\hat{x}$  is the converged  $\hat{x}_i$ )

In Equations (8-55) through (8-57), only the estimator requires measurement data. The equations for the covariance and correlation matrices require only the statistics  $W$  of the observations, which are usually known for specific classes of trackers and sensors. Therefore, if it is assumed that the a priori reference trajectory  $\bar{x}_0$  is the best estimate, the estimator equation can be omitted and the covariance and correlation matrices can be determined for specific mission sensors and observation profiles. It must also be assumed that the mathematical models in the program accurately characterize the physical situation. Since actual measurements are not required, these operations can be performed during preflight studies to determine:

- the effect of measurement data errors (random and systematic), measurement time spans, and sampling rates on the accuracy of the estimated state and model parameters
- the effect of the trajectory dynamics and the trajectory/sensor relative geometry on the accuracy of the estimated state and model parameters
- the relative effects of different types of measurements on the accuracy of the estimated state and model parameters

Such problems are referred to as error analysis problems, since they are solely concerned with the influence that errors in problem variables have on the accuracy of the estimate. This type of analysis can strongly influence the design and enhancement of spacecraft missions, as well as establish requirements for observation sensor accuracies, sampling rates, tracking times, and sensor locations.

The method for evaluating Equations (8-56) and (8-57) in GTDS is nearly identical to that for estimating applications. An a priori estimate of the solve-for and consider variables  $\bar{x}_0$  and  $\bar{z}_0$ , along with their covariance and correlation matrices  $P_{\Delta x_0}$ ,  $P_{\Delta z_0}$  and  $C_{\Delta x_0 \Delta z_0}$  is specified. The measurement schedule and measurement uncertainty  $W$  is also specified a priori. The program then proceeds to integrate the nonlinear differential equations of motion and their corresponding variational equations to the measurement times and compute the measurement partial derivatives. The rows of the matrices  $F$  and  $E$  in Equations (8-56) and (8-57) are accumulated as the measurement statistics are processed. Ultimately, the covariance and correlation matrices  $P_{\Delta x}$  and  $C_{\Delta x \Delta z}$  are calculated at the epoch time. The covariance and correlation matrices are then propagated to specified times  $T_1, T_2, \dots, T_S$  by means of Equations (8-51) and (8-54). Analogously to the transformations presented in Equations (8-46) through (8-50), the time transformed covariance matrix  $P_{\Delta s}(T_i)$ , which is a submatrix of  $P_{\Delta x}(T_i)$ , is itself transformed to the  $\bar{s}'$  system. From the nonlinear transformation

$$\bar{s}'(T_i) = h[\bar{s}(T_i)] \quad (8-59)$$

a linearization yields

$$\Delta s'(T_i) = H(T_i) \bar{\Delta s}(T_i) \quad (8-60)$$

where

$$H(T_i) = \left( \frac{\partial \bar{s}'}{\partial \bar{s}} \right)_{t=T_i} \quad (8-61)$$

The covariance matrix of  $\hat{s}'(T_i)$  is thus formed by appropriate substitution as

$$\begin{aligned} P_{\Delta s}(T_i) &= E\{[\hat{\Delta s}'(T_i) - \overline{\Delta s}'(T_i)][\hat{\Delta s}'(T_i) - \overline{\Delta s}'(T_i)]^T\} \\ &= H(T_i) P_{\Delta s}(T_i) H^T(T_i) \end{aligned} \quad (8-62)$$

The correlation  $C_{\Delta s \Delta z}(T_i)$  is transformed to  $C_{\Delta s' \Delta z}(T_i)$  as follows

$$\begin{aligned} C_{\Delta s' \Delta z}(T_i) &= E\{[\hat{s}'(T_i) - \overline{s}'(T_i)][\bar{z}_0 - \bar{z}]^T\} \\ &= E\{[\hat{\Delta s}'(T_i) - \overline{\Delta s}'(T_i)][\bar{z}_0 - \bar{z}]^T\} \\ &= E\{H(T_i)[\hat{\Delta s}(T_i) - \overline{\Delta s}(T_i)][\bar{z}_0 - \bar{z}]^T\} \\ &= H(T_i) C_{\Delta s \Delta z}(T_i) \end{aligned} \quad (8-63)$$

Since the estimation equation is not being solved, iteration is unnecessary.

Differentiating Equation (8-25) with respect to  $\bar{z}$  and ignoring both the iteration notation and the  $\bar{z}$  dependence on the matrix of observation partial derivatives, the variation of the least squares estimator with respect to the consider parameters is

$$\frac{\partial \hat{\Delta x}}{\partial \bar{z}} = - (F^T W F + P_{\Delta z_0}^{-1})^{-1} F^T W E \quad (8-64)$$

Within the bounds of linearity, the responsiveness of the components of  $\hat{\Delta x}$  to perturbations in the components of  $\bar{z}$  are given in the epoch sensitivity matrix

$$S = \left( \frac{\partial \hat{\Delta x}_i}{\partial z_j} \Delta z_j \right) \quad (8-65)$$

From Equations (8-51) for the state vector  $\bar{s}$ , the perturbation about a given value of  $s$  is

$$\hat{\Delta s}(t) = \Phi(t, t_0) \hat{\Delta s}(t_0) + \theta(t, t_0) \bar{\Delta u}^* \quad (8-66)$$

Differentiating  $\hat{\Delta s}(t)$  with respect to  $\bar{u}^*$ , the variation of the state components with respect to the consider dynamic parameters is obtained

$$\frac{\partial \hat{\Delta s}(t)}{\partial \bar{u}^*} = \Phi(t, t_0) \left[ \frac{\partial \hat{\Delta s}}{\partial \bar{u}^*} \right] + \theta(t, t_0) \quad (8-67)$$

Then the time propagation of the matrix of functional sensitivities is

$$S(t) = \left( \frac{\partial \hat{s}(t)}{\partial \bar{u}_j^*} \bar{\Delta u}_j^* \right) \quad (8-68)$$

As in the transformation of the covariance matrix from  $P_{\Delta s}$  to  $P_{\Delta s'}$ , a simple chain rule calculation yields the variation of the transformed state with respect to the consider variables

$$\left( \frac{\partial \hat{s}'(t)}{\partial \bar{z}} \right) = \left( \frac{\partial \hat{s}'(t)}{\partial \bar{s}(t)} \right) \left( \frac{\partial \bar{s}(t)}{\partial \bar{z}} \right) \quad (8-69)$$

To give more insight into the applicability of the sensitivity quantities, the  $i^{\text{th}}$  component of the least squares estimator  $\hat{\Delta s}$  is written in nonlinear functional form as

$$\hat{\Delta s}_i = \bar{g}_i(\bar{z}) \quad (8-70)$$

By expanding  $\bar{g}_i(\bar{z})$  in a Taylor series about  $\bar{z} = \bar{z}_0$ , the following first-order approximation is obtained

$$\hat{\Delta s}_i = \bar{g}_i(\bar{z}) = \bar{g}_i(\bar{z}_0) + \sum_j \left( \frac{\partial \hat{\Delta s}_i}{\partial \bar{z}_j} \right) \Delta \bar{z}_j \quad (8-71)$$

If the errors in the  $\bar{z}$  parameters are uncorrelated in a Bayesian sense (as they are assumed to be in GTDS), and if the linearity assumption is valid, an estimate of the variance of  $\hat{\Delta s}_i$  due solely to the variability in  $\bar{z}$  is obtained. In particular, this variance estimate is given by invoking the variance operator on both sides of the above expression for  $\hat{\Delta s}_i$  and noting that  $\bar{g}_i(\bar{z}_0)$  is a constant and that the  $\Delta \bar{z}_j$ 's are uncorrelated. Therefore,

$$\sigma_{\hat{\Delta s}_i}^2(\bar{z}) = \sum_j \left( \frac{\partial \hat{\Delta s}_i}{\partial \bar{z}_j} \right)^2 \sigma_{\Delta \bar{z}_j}^2 \quad (8-72)$$

Assuming the linearization is valid, it is easily seen that  $\Delta z_j = \sigma_{\Delta \bar{z}_j}$  in the sensitivity analysis. Hence, the sum of squares of the sensitivities for a given state component over all consider parameters plus the excess of the  $(i, i)$  element of the consider covariance of  $\hat{\Delta s}$  over  $\sigma_{\hat{\Delta s}_i}^2(\bar{z})$  yields the total variation observed in  $\hat{\Delta s}_i$ . This excess quantity is the  $(i, i)$  element of the normal matrix (measurement noise variance component) since the covariance equations were derived under the assumption that  $\bar{n}$  and  $\bar{z}_0$  are uncorrelated, thus uncoupling their effects on variance estimation.



It would appear that since an estimate is not actually being determined, it should make little difference whether model parameters are associated with the solve-for vector  $\bar{x}$  or the consider vector  $\bar{z}$ . A subtle difference does exist, however. Components of the consider vector  $\bar{z}$  are maintained at their a priori specified values throughout the processing, and therefore have no possibility for modification through estimation. As a result, their covariances never differ from those initially specified, i.e.,  $P_{\Delta z_0}$  in Equation (8-56). The solve-for variables  $\bar{x}$  have their values continually modified through the estimation process, which is reflected through the changes in the variance elements in  $P_{\Delta x}$ . Because of the coupling, the uncertainty of the state components is affected differently if the same model parameter is associated with  $\bar{x}$  rather than with  $\bar{z}$ .

## 8.4 SEQUENTIAL ESTIMATION

In the approach taken to the basic orbit estimation problem in the preceding sections of this chapter, the observations are processed by classical least squares methods, i.e., by processing the data in batches. The solution to the problem is the state vector (the system parameters or unknown constants) which is estimated from a set of measured data. Since the problem is nonlinear, the solution is linearized about the a priori state estimate and then iterated to minimize the loss function. This approach requires considerable computation time and cannot be applied to real-time situations.

An alternative approach is to perform the data reduction and parameter estimation in a sequential or recursive manner. The process is begun by making an initial estimate of the state vector from a minimum data set or from a judicious guess. Each new data point is combined with the previous parameter estimate by appropriately weighting the data point to give an improved estimate of the state. This process is repeated as each new data point is reduced. Hence, the procedure can be interrupted at any time and the best estimates of the system parameters and their uncertainties based on all accumulated data to that time are known. Other advantages of sequential weighted least squares estimators are that at each step the calculations are fixed in size and format and that the need for storing previous data points is eliminated. Under certain assumptions the sequential weighted least squares estimator is identical to the "Kalman" minimum variance estimator. Additional discussion of sequential weighted least squares and minimum variance estimation can be found in Reference 2.

The Extended Kalman Filter is the basic sequential estimator in GTDS. Its derivation from recursive weighted least squares is discussed in Section 8.4.1. Because of the sensitivity of Kalman filters to dynamic model errors associated

with orbit generation, filters have been designed to adaptively estimate the true value of the unmodeled acceleration along with the state. This approach, dynamic model compensation, is discussed in Section 8.4.2. In Section 8.4.3, statistical adaptive filtering, which eliminates the need to specify a priori noise statistics, is discussed.

#### 8.4.1 Derivation and Applications of the Extended Kalman Filter

In reconsidering the weighted least squares problem described in Section 8.1, an m-component observation vector  $\bar{y}$  is assumed. The nonlinear regression equation (Equation (8-1)) is linearized about a reference state  $\bar{x}_0$  as shown in Equation (8-7). The best estimate  $\hat{x}$ , in the classical weighted least squares sense, is given by Equations (8-10) and (8-11) as

$$\hat{x}_m = \bar{x}_0 + \Delta \hat{x}_m \quad (8-73)$$

where

$$\Delta \hat{x}_m = (F^T W F)^{-1} F^T W \bar{\Delta y} \quad (8-74)$$

The subscript m indicates that the solution is based on an m-component observation vector, and the quantities F, W, and  $\bar{\Delta y}$  are defined by Equations (8-6), (8-12), and (8-8), respectively. If one more observation is included, the correction has exactly the same form,

$$\Delta \hat{x}_{m+1} = (F'^T W' F')^{-1} F'^T W' \bar{\Delta y}' \quad (8-75)$$

where  $F'$ ,  $W'$ , and  $\bar{\Delta y}'$  are related to F, W, and  $\bar{\Delta y}$  as follows

$$F' = \begin{bmatrix} F \\ \text{---} \\ F_{m+1} \end{bmatrix}, \quad W' = \begin{bmatrix} W & \vdots & 0 \\ \text{---} & \vdots & \text{---} \\ 0 & \vdots & w_{m+1} \end{bmatrix}, \quad \bar{\Delta y}' = \begin{bmatrix} \bar{\Delta y} \\ \text{---} \\ \Delta y_{m+1} \end{bmatrix} \quad (8-76)$$

and  $F_{m+1}$ ,  $w_{m+1}$ , and  $\Delta y_{m+1}$  correspond to the  $(m+1)^{\text{st}}$  observation. In other words, the original matrices and vectors are augmented to include the next observation.

Substituting Equation (8-76) into Equation (8-75) gives

$$\Delta \hat{x}_{m+1} = \left( [F^T; F_{m+1}^T] \begin{bmatrix} W & \vdots & 0 \\ \text{---} & \vdots & \text{---} \\ 0 & \vdots & w_{m+1} \end{bmatrix} \begin{bmatrix} F \\ \text{---} \\ F_{m+1} \end{bmatrix} \right)^{-1} [F^T; F_{m+1}^T] \begin{bmatrix} W & \vdots & 0 \\ \text{---} & \vdots & \text{---} \\ 0 & \vdots & w_{m+1} \end{bmatrix} \begin{bmatrix} \bar{\Delta y} \\ \text{---} \\ \Delta y_{m+1} \end{bmatrix} \quad (8-77)$$

The quantity in parentheses in Equation (8-77) is the inverse of the covariance matrix of error  $P_{\Delta x_{m+1}}$  for the weighted least squares estimate  $\hat{\Delta x}_{m+1}$ , i.e.,

$$P_{\Delta x_{m+1}} = (F^T W F + F_{m+1}^T w_{m+1} F_{m+1})^{-1} \quad (8-78)$$

However,  $F^T W F$  is the inverse of the covariance matrix  $P_{\Delta x_m}$ , which is based on  $m$  observations. Therefore,

$$P_{\Delta x_{m+1}} = (P_{\Delta x_m}^{-1} + F_{m+1}^T w_{m+1} F_{m+1})^{-1} \quad (8-79)$$

Equations (8-77) and (8-79) are expressions for the state correction estimate and the covariance of the error in the estimate obtained by processing  $(m+1)$  observations. These expressions can be written more conveniently in the following recursive form

$$\hat{\Delta x}_{m+1} = \hat{\Delta x}_m + \overline{\Delta x} \quad (8-80a)$$

$$P_{\Delta x_{m+1}} = P_{\Delta x_m} + \Delta P \quad (8-80b)$$

where  $\overline{\Delta x}$  and  $\Delta P$  represent the changes in  $\hat{\Delta x}_m$  and  $P_{\Delta x_m}$  caused by the  $(m+1)^{st}$  observation. This form allows the state vector and covariance matrix to be determined as each observation is sequentially processed.

As shown in Appendix E, Equation (8-80b) can be written as

$$P_{\Delta x_{m+1}} = P_{\Delta x_m} - P_{\Delta x_m} F_{m+1}^T [w_{m+1}^{-1} + F_{m+1} P_{\Delta x_m} F_{m+1}^T]^{-1} F_{m+1} P_{\Delta x_m} \quad (8-81a)$$

or

$$P_{\Delta x_{m+1}} = P_{\Delta x_m} - K F_{m+1} P_{\Delta x_m} = (I - K F_{m+1}) P_{\Delta x_m} \quad (8-81b)$$

where

$$K \equiv P_{\Delta x_m} F_{m+1}^T [w_{m+1}^{-1} + F_{m+1} P_{\Delta x_m} F_{m+1}^T]^{-1} \quad (8-81c)$$

Substituting  $P_{\Delta x_{m+1}}$  from Equation (8-81b) into the first term on the right of Equation (8-77) yields

$$\hat{\Delta x}_{m+1} = (I - K F_{m+1}) P_{\Delta x_m} [F^T W \overline{\Delta y} + F_{m+1}^T w_{m+1} \Delta y_{m+1}] \quad (8-82)$$

Substituting Equations (8-74) and (8-81b) into Equation (8-82) yields

$$\hat{\Delta x}_{m+1} = (I - K F_{m+1}) \hat{\Delta x}_m + P_{\Delta x_{m+1}} F_{m+1}^T w_{m+1} \Delta y_{m+1} \quad (8-83)$$

In Appendix E it is shown that

$$K = P_{\Delta x_{m+1}} F_{m+1}^T W_{m+1}^{-1} \quad (8-84)$$

Therefore, Equation (8-83) can be written as

$$\hat{\Delta x}_{m+1} = \hat{\Delta x}_m + K [\Delta y_{m+1} - F_{m+1} \hat{\Delta x}_m] \quad (8-85)$$

Summarizing the above results,

$$\hat{x}_{m+1} = \bar{x}_0 + \hat{\Delta x}_{m+1} \quad (a)$$

$$\hat{\Delta x}_{m+1} = \hat{\Delta x}_m + K [\Delta y_{m+1} - F_{m+1} \hat{\Delta x}_m] \quad (b)$$

$$P_{\Delta x_{m+1}} = P_{\Delta x_m} - K F_{m+1} P_{\Delta x_m} = (I - K F_{m+1}) P_{\Delta x_m} \quad (c)$$

$$K = P_{\Delta x_m} F_{m+1}^T [W_{m+1}^{-1} + F_{m+1} P_{\Delta x_m} F_{m+1}^T]^{-1} \quad (d)$$

where

$$F_{m+1} \sim \left( \frac{\partial \bar{f}_{m+1}}{\partial \bar{x}} \right)_{(\bar{x} = \bar{x}_0)}$$

and

$\Delta y_{m+1} \sim$  the linearized (m+1)<sup>st</sup> observation (see Equation (8-8))

$W_{m+1}^{-1} \sim$  the variance of the (m+1)<sup>st</sup> observation, e.g.,  $\sigma_{m+1}^2$

The preceding recursive form of the weighted least squares estimate yields the update equations for the Extended Kalman Filter in GTDS. The weighted least squares estimate is a minimum variance estimate because the observations are weighted with  $W = 1/\sigma^2$ . This is the condition necessary for Equation (8-78) to be the covariance matrix of error. The matrix  $K$  is defined as the Kalman gain. For additional discussion of Kalman filter theory, see References 6, 7, and 8.

Assuming that  $F_{m+1}^T$  in Equation (8-84) is a matrix whose elements are all unity, then each element of the gain matrix  $K$  is a ratio between the statistical measure of uncertainty in the state estimate  $P_{\Delta x_{m+1}}$  and the uncertainty in the measurement  $\sigma_{m+1}^2$ .

From the fundamental definition of the covariance matrix given in Equation (8-34), a more convenient form for  $P_{\Delta x_{m+1}}$  can be derived using Equation (8-86b)

$$\begin{aligned}
P_{\Delta x_{m+1}} &= \mathcal{E} \{ \widehat{\Delta x}_{m+1} \widehat{\Delta x}_{m+1}^T \} = \mathcal{E} \{ [(I - KF_{m+1}) \widehat{\Delta x}_m + K \Delta y_{m+1}] \\
&\quad \times [(I - KF_{m+1}) \widehat{\Delta x}_m + K \Delta y_{m+1}]^T \} \\
&= \mathcal{E} \{ [(I - KF_{m+1}) \widehat{\Delta x}_m + K \Delta y_{m+1}] \widehat{\Delta x}_m^T (I - KF_{m+1})^T \\
&\quad + [(I - KF_{m+1}) \widehat{\Delta x}_m + K \Delta y_{m+1}] \Delta y_{m+1}^T K^T \} \quad (8-87) \\
&= (I - KF_{m+1}) \mathcal{E} \{ \widehat{\Delta x}_m \widehat{\Delta x}_m^T \} (I - KF_{m+1})^T + K \mathcal{E} \{ \Delta y_{m+1} \widehat{\Delta x}_m^T \} \\
&\quad \times (I - KF_{m+1})^T + (I - KF_{m+1}) \mathcal{E} \{ \widehat{\Delta x}_m \Delta y_{m+1}^T \} K^T \\
&\quad + K \mathcal{E} \{ \Delta y_{m+1} \Delta y_{m+1}^T \} K^T
\end{aligned}$$

Assuming uncorrelated measurement errors, then

$$\mathcal{E} \{ \Delta y_{m+1} \widehat{\Delta x}_m^T \} = \mathcal{E} \{ \widehat{\Delta x}_m \Delta y_{m+1}^T \} = 0 \quad (8-88)$$

By definition

$$\mathcal{E} \{ \widehat{\Delta x}_m \widehat{\Delta x}_m^T \} = P_{\Delta x_m} \quad (a)$$

and

$$\mathcal{E} \{ \Delta y_{m+1} \Delta y_{m+1}^T \} = w_{m+1}^{-1} \quad (b)$$

Substituting Equations (8-88) and (8-89) into Equation (8-87) yields

$$P_{\Delta x_{m+1}} = (I - KF_{m+1}) P_{\Delta x_m} (I - KF_{m+1})^T + K w_{m+1}^{-1} K^T \quad (8-90)$$

Equation (8-90) is preferred over Equation (8-86c) for the following reasons: To first order, it is insensitive to errors in the filter gain, and it is better conditioned for numerical computations, since it is the sum of two symmetric non-negative definite matrices.

Up to this point the effect of adding one more observation to a set of  $m$  observations has been considered. These results will next be generalized to indicate sequential estimates without dependence on the size of the observation vector, that is,  $j$  will represent the observation counter, replacing  $m$  in the subscripts.

The prediction formulas for the Extended Kalman Filter follow from the discussion in Section 8.2.3 concerning the timewise propagation of state perturbations (Equation (8-51)). Including the state noise  $\bar{\omega}$  with zero mean and covariance  $Q$ , the prediction equation can be written

$$\hat{\Delta x}(t_{j+1}|t_j) = \Phi(t_{j+1}|t_j) \hat{\Delta x}(t_j|t_j) + \bar{w}_{j+1}, \quad (8-91)$$

where  $\hat{\Delta x}(t_{j+1}|t_j)$  denotes the best estimate of the correction at time  $t_{j+1}$  based on processing data through time  $t_j$ , and  $\Phi(t_{j+1}|t_j)$  is the state transition matrix. For prediction purposes, the state noise  $\bar{w}_{j+1}$  in Equation (8-91) is set equal to zero. The predicted covariance matrix at time  $t_{j+1}$  is obtained from Equation (8-91) as follows

$$\begin{aligned} P_{\Delta x}(t_{j+1}|t_j) &= E\{\hat{\Delta x}(t_{j+1}|t_j) \hat{\Delta x}^T(t_{j+1}|t_j)\} \\ &= E\{[\Phi \hat{\Delta x}(t_j|t_j) + \bar{w}_{j+1}] [\Phi \hat{\Delta x}(t_j|t_j) + \bar{w}_{j+1}]^T\} \\ &= E\{[\Phi \hat{\Delta x}(t_j|t_j) + \bar{w}_{j+1}] \hat{\Delta x}^T(t_j|t_j) \Phi^T + [\Phi \hat{\Delta x}(t_j|t_j) + \bar{w}_{j+1}] \bar{w}_{j+1}^T\} \\ &= \Phi E\{\hat{\Delta x}(t_j|t_j) \hat{\Delta x}^T(t_j|t_j)\} \Phi^T + E\{\bar{w}_{j+1} \hat{\Delta x}^T(t_j|t_j)\} \Phi^T \\ &\quad + \Phi E\{\hat{\Delta x}(t_j|t_j) \bar{w}_{j+1}^T\} + E\{\bar{w}_{j+1} \bar{w}_{j+1}^T\} \end{aligned} \quad (8-92a)$$

Assuming that the noise  $\bar{w}$  and the state  $\hat{\Delta x}$  are uncorrelated, Equation (8-92a) becomes

$$P_{\Delta x}(t_{j+1}|t_j) = \Phi P_{\Delta x}(t_j|t_j) \Phi^T + Q_{j+1} \quad (8-92b)$$

where  $Q_{j+1}$  is the covariance of the state noise, i.e.,

$$Q_{j+1} = E\{\bar{w}_{j+1} \bar{w}_{j+1}^T\} \quad (8-93)$$

In order to use this formulation of the Extended Kalman Filter, a reference trajectory must be generated. This is done by numerically integrating a nonlinear second-order differential equation (see Equation (5-2)) of the form

$$\ddot{\bar{x}}_{ref}(t) = \bar{g}(\bar{x}, t) \quad (8-94)$$

where  $\bar{g}$  is a known function of the state variables,  $\bar{x}$  is an  $n$ -dimensional state vector,  $\bar{x}(t_0) = \bar{x}_0$ , and  $t \geq t_0$ .

The predicted measurement residual error  $r(t_{j+1}|t_j)$  is

$$r(t_{j+1}|t_j) = y(t_{j+1}) - F_{j+1} \hat{x}(t_{j+1}|t_j) \quad (8-95)$$

where  $\hat{x}(t_{j+1}|t_j)$  is obtained from the integration of Equation (8-94) with the initial state for the integration obtained from the previous state updated by Equation (8-91), and the predicted measurement residual uncertainty  $Y(t_{j+1}|t_j)$  is

$$Y(t_{j+1}|t_j) = \mathcal{E}\{r(t_{j+1}|t_j) r^T(t_{j+1}|t_j)\} = F_{j+1} P_{\Delta x}(t_{j+1}|t_j) F_{j+1}^T + w_{j+1}^{-1} \quad (8-96)$$

A comparison of these residuals with their theoretical statistical properties provides a means of judging the performance of the filter (cf. Section 8.6.4).

Equations (8-91) and (8-92b) are used to predict the state correction and covariance matrices at a future time  $t_{j+1}$ , based on the best estimate at the last observation at time  $t_j$ . The next measurement  $y_{j+1}$  is then used to update the state correction and covariance matrices (Equation (8-85)). These steps are repeated until all the observations have been processed. The advantage of this recursive estimator is that the estimate of the state and covariance based on processing  $m+1$  observations uses the information contained in the  $(m+1)^{\text{st}}$  observation plus the state and covariance based on  $m$  observations. The entire process of accumulating sums and inverting matrices does not have to be repeated when a new observation is processed. The error covariance of the filter is inversely proportional to the measurement noise from Equation (8-79). Large measurement noise implies that  $w_m$  is small, and hence  $P_{m+1}$  decreases by only a small amount. Small measurement noise implies a large  $w_{m+1}$ , and consequently a relatively large decrease in  $P_{m+1}$ .

The recursive equations can be applied from the first point on. In that case, the reference trajectory is chosen as  $\hat{x}(t_0) = \bar{x}_0$ , the a priori state; hence  $\hat{\Delta x}(t_0|t_0) = 0$ . There are two ways in which the Extended Kalman Filter may be used, with an updated or a nonupdated reference trajectory. In the nonupdated reference approach, the corrections  $\hat{\Delta x}$  are accumulated, and the a priori reference state  $\bar{x}_0$  is corrected only once, at the final time after all data are processed.

The updated state vector at the final time, based on processing all the data, is then smoothed back to the initial time to obtain the best estimate of the state at all intervening times. The covariance matrix can also be propagated backward in time via Equation (8-92b) to obtain the timewise variation of the uncertainty of the state based on processing all data.

If the batch of observations is sufficiently large, a new initial reference state can be determined from the following equation

$$\bar{x}'(t_0) = \bar{x}(t_0) + \hat{\Delta x}(t_0|t_f) \quad (8-97)$$

where

$\hat{\Delta x}(t_0|t_f) \sim$  the new best estimate of the state at  $t_0$  based on processing all observations

$t_f \sim$  the time of the final observation

This reference state will be closer to the "true" initial state than will  $\bar{x}(t_0)$ . Using the new state, the data are reprocessed, i.e., the solution is linearized about  $\bar{x}'(t_0)$ , and the filtering process is repeated over the same batch of observations. This process is repetitively applied until there is no change in the initial reference state. At that time, convergence to the best estimate of the state has been achieved, i.e., a solution has been found which is as close to the "true" solution as the neglected nonlinear effects will allow. These "global iterations" involve the same procedure as that which is followed in the batch processor (iterated weighted least squares). This mode is used when the signal-to-noise ratio is small, and a good initial estimate of the state is available. The nonupdated reference approach is not presently available in GTDS.

Another approach (used primarily when the signal-to-noise ratio is large or when a good estimate of the state is unavailable) is to update the reference trajectory after processing each subset of the data vector  $\bar{y}$ . This allows large errors in the a priori state  $\bar{x}_0$  to be corrected early in the process, thereby assuring that the processing of later data satisfies linearity. This, in turn, improves the outer loop (global iteration) convergence. Linearization about  $\hat{x}(t_0)$  results in  $\Delta x(t_0|t_0) = 0$ . Hence, using Equation (8-91) and relinearizing about each point yields

$$\hat{\Delta x}(t|t_j) = 0, \quad t_j \leq t \leq t_{j+1}, \quad \text{for all } j \quad (8-98)$$

Since, due to the relinearization,

$$\hat{\Delta x}(t_{j+1}|t_{j+1}) = \hat{x}(t_{j+1}|t_{j+1}) - \hat{x}(t_{j+1}|t_j) \quad (8-99)$$

substitution of Equations (8-8), (8-98), and (8-99) into Equation (8-86b) gives

$$\hat{x}(t_{j+1}|t_{j+1}) = \hat{x}(t_{j+1}|t_j) + K(t_{j+1}) [y(t_{j+1}) - f(\hat{x}(t_{j+1}|t_j); t_{j+1})] \quad (8-100)$$

The preceding result is used for updating the state vector. The updated reference mode is ideally suited to real-time applications.

The Extended Kalman Filter for continuous-discrete systems described above is the result of the application of the linear Kalman filter to a linearized non-linear system, which is relinearized after each observation. To summarize, the procedure for the updated reference mode in GTDS is as follows:

1. Store the reference state  $\hat{x}(t_j|t_j)$  and the covariance matrix  $P_{\Delta x}(t_j|t_j)$ .
2. Compute the predicted state at time  $t_{j+1}$  by numerically integrating Equation (8-94), i.e., obtain  $\hat{x}(t_{j+1}|t_j)$  given  $\hat{x}(t_j|t_j)$ .



3. Calculate the state transition matrix from time  $t_j$  to time  $t_{j+1}$ , either analytically or numerically, as discussed in Section 4.10.2.

$$\Phi(t_{j+1}, t_j; \hat{\mathbf{x}}(t_j | t_j)) = \left[ \frac{\partial \bar{\mathbf{x}}(t_{j+1})}{\partial \bar{\mathbf{x}}(t_j)} \right]_{\bar{\mathbf{x}}(t_j) = \hat{\mathbf{x}}(t_j | t_j)}$$

4. Compute the predicted error covariance matrix at time  $t_{j+1}$  via Equation (8-92b).

$$\mathbf{P}_{\Delta \mathbf{x}}(t_{j+1} | t_j) = \Phi(t_{j+1}, t_j) \mathbf{P}_{\Delta \mathbf{x}}(t_j | t_j) \Phi^T(t_{j+1}, t_j) + \mathbf{Q}_{j+1}$$

5. Compute the observation via Equation (8-1) assuming no noise.

$$\mathbf{y}(t_{j+1}) = \bar{\mathbf{f}}(\hat{\mathbf{x}}(t_{j+1} | t_j); t_{j+1})$$

6. Compute the partial derivative of the observation via Equation (8-6).

$$\mathbf{F}_{j+1} = \left( \frac{\partial \bar{\mathbf{f}}}{\partial \bar{\mathbf{x}}} \right)_{\bar{\mathbf{x}} = \hat{\mathbf{x}}(t_{j+1} | t_j)}$$

7. Test whether this is an acceptable observation, i.e., is the absolute value of the residual (observed minus computed value) less than the RMS multiplier times the square root of the predicted measurement residual uncertainty  $\mathbf{Y}(t_{j+1} | t_j)$  in Equation (8-96)? If not, reject the observation, increment  $j$ , and return to Step 1.

8. Calculate the filter gain matrix via Equation (8-86d)

$$\mathbf{K}(t_{j+1}) = \mathbf{P}_{\Delta \mathbf{x}}(t_{j+1} | t_j) \mathbf{F}_{j+1}^T [\mathbf{F}_{j+1} \mathbf{P}_{\Delta \mathbf{x}}(t_{j+1} | t_j) \mathbf{F}_{j+1}^T + \mathbf{w}_{j+1}^{-1}]^{-1}$$

9. Process the observation  $\mathbf{y}(t_{j+1})$  to obtain the updated state via Equation (8-100)

$$\hat{\mathbf{x}}(t_{j+1} | t_{j+1}) = \hat{\mathbf{x}}(t_{j+1} | t_j) + \mathbf{K}(t_{j+1}) [\mathbf{y}(t_{j+1}) - \bar{\mathbf{f}}(\hat{\mathbf{x}}(t_{j+1} | t_j); t_{j+1})]$$

10. Compute the updated error covariance matrix at time  $t_{j+1}$  via Equation (8-90)

$$\begin{aligned} \mathbf{P}_{\Delta \mathbf{x}}(t_{j+1} | t_{j+1}) &= [\mathbf{I} - \mathbf{K}(t_{j+1}) \mathbf{F}_{j+1}] \mathbf{P}_{\Delta \mathbf{x}}(t_{j+1} | t_j) [\mathbf{I} - \mathbf{K}(t_{j+1}) \mathbf{F}_{j+1}]^T \\ &\quad + \mathbf{K}(t_{j+1}) \mathbf{w}_{j+1}^{-1} \mathbf{K}^T(t_{j+1}) \end{aligned}$$

11. Increment  $j$  and return to Step 1 to repeat the cycle for the next observation.
12. Continue the cycle between Step 1 and Step 12 until a specified set of observation data is processed.
13. Integrate back to epoch and output the results utilizing data to time  $t_f$ , e.g.,  $\hat{x}(t_0 | t_f)$  and  $P_{\Delta x}(t_0 | t_f)$ , where  $t_f$  represents the time of the final data point in the set of observations processed.
14. Continue the cycle between Step 1 and Step 14 until all the data are processed.
15. Make a final pass through the observation data to compute residual statistics and print final reports.

One of the main difficulties associated with the filtering approach to orbit determination is filter divergence, i.e., the estimated (filtered) state diverges from the actual state. It can occur when estimates of the state become more accurate and hence the covariance becomes smaller. As a result, the Kalman gain decreases and new observations exert less influence on the solution. The observations, which are a realization of the true state, have a smaller effect than the "learned" dynamical model. Therefore, successive estimates of the state tend to follow the erroneous "learned" dynamical model and to diverge from the true state which is reflected in the observations. Consequently, the estimated covariance fails to represent the true estimation error.

Divergence can arise from the following sources:

1. Linearization errors (e.g., measurement linearization)
2. Computational errors (e.g.,  $P_{\Delta x}$  loses its positive semidefiniteness)
3. Modeling errors
4. Unknown noise statistics

Generally, the first source can be minimized by iterating the solution (updated reference trajectory). Computational errors can be minimized by square root filtering algorithms (Reference 9) and program coding techniques (Reference 10). Modeling errors can be handled in either a nonadaptive or an adaptive manner. The nonadaptive methods modify the filter structure in order to maintain the Kalman gain at some suitable level for sustained filter operation. The Modified Extended Kalman Filter (MEKF) by Torroglosa (Reference 11) implemented in GTDS is a filter of this type. The adaptive techniques can be divided into structural and statistical methods. The structural or dynamic model compensation methods are designed to adaptively estimate the true value of the unmodeled

acceleration along with the state. Tapley and his associates (References 12, 13 and 14) have followed this approach, which will be discussed in Section 8.4.2. The statistical methods are designed to correct the basic filter to accommodate the combined effects of all error sources, e.g., the neglected nonlinearities, unknown noise statistics, and computational error effects, in addition to the model errors. The Jazwinski Filter (Reference 15) in GTDS is a filter of this type. Statistical adaptive filtering is discussed in Section 8.4.3.

#### 8.4.2 Dynamic Model Compensation Filtering

The dynamic model compensation (DMC) techniques are designed to adaptively estimate the true value of the unmodeled acceleration along with the state. A sequential estimation method has been developed (References 12, 13, and 14) which compensates for unmodeled effects in the differential equations which define the dynamical process. The advantages of this method are: (1) It can be used to obtain an improved estimate of the state vector in real-time applications, and (2) it yields information which can be used in post-flight analysis to improve the basic dynamical model. The unmodeled accelerations are assumed to be a first order Gauss-Markov process, i.e., they consist of the superposition of a time-correlated component and a purely random component. Because this type of filter is not implemented in GTDS at the present time, the discussion of the mathematical model follows that of Reference 12. There the technique is applied to estimate the state of a lunar orbiting spacecraft acted upon by unmodeled forces due to venting, water dumps, or translational forces due to unbalanced attitude control reactions.

The equations of motion of the nonlinear dynamical system are given by

$$\dot{\bar{\mathbf{r}}} = \bar{\mathbf{v}} \quad (a) \quad (8-101)$$

$$\dot{\bar{\mathbf{v}}} = \bar{\mathbf{a}}_m(\bar{\mathbf{r}}, \bar{\mathbf{v}}, t) + \bar{\mathbf{a}}_u(t) \quad (b)$$

where  $\bar{\mathbf{r}}$  and  $\bar{\mathbf{v}}$  are the position and velocity components,  $\bar{\mathbf{a}}_m$  is the three-component acceleration vector used in the filter-world or nominal dynamical model, and  $\bar{\mathbf{a}}_u$  is the three-component vector of all unknown and/or unmodeled accelerations.

The unmodeled acceleration  $\bar{\mathbf{a}}_u(t)$  is represented as a first-order Gauss-Markov process  $\bar{\boldsymbol{\epsilon}}(t)$  which satisfies the differential equation

$$\dot{\bar{\boldsymbol{\epsilon}}}(t) = \mathbf{A}(t) \bar{\boldsymbol{\epsilon}}(t) + \mathbf{B}(t) \bar{\mathbf{u}}(t) \quad (8-102)$$

where  $A(t)$  and  $B(t)$  are coefficient matrices,  $\bar{\epsilon}(t)$  is a three-component vector, and  $\bar{u}(t)$  is a three-component vector of Gaussian noise whose components satisfy the a priori statistics

$$\mathcal{E}\{\bar{u}(t)\} = 0, \quad \mathcal{E}\{\bar{u}(t) \bar{u}^T(\tau)\} = I \delta(t - \tau) \quad (8-103)$$

The matrix  $I$  is a  $3 \times 3$  identity matrix and  $\delta(t - \tau)$  is the Dirac delta function. The quantity  $A(t)$  is a  $3 \times 3$  diagonal matrix of the time correlation coefficients

$$A(t) = \begin{bmatrix} -1/T_1 & 0 & 0 \\ 0 & -1/T_2 & 0 \\ 0 & 0 & -1/T_3 \end{bmatrix} \quad (8-104)$$

where  $T_1$ ,  $T_2$ , and  $T_3$  are the correlation times, which are unknown parameters to be estimated by including the vector  $\bar{T}$

$$\bar{T}^T = [T_1 T_2 T_3] \quad (8-105)$$

in the set of parameters to be estimated.

The quantity  $B(t)$  is a  $3 \times 3$  diagonal matrix

$$B(t) = \begin{bmatrix} b_1 & 0 & 0 \\ 0 & b_2 & 0 \\ 0 & 0 & b_3 \end{bmatrix} \quad (8-106)$$

where the  $b_j$  are treated as specified constants.

When Equations (8-101) and (8-102) are combined with  $\dot{T} = 0$ , the dynamical system is described by the following set of first-order differential equations

$$\begin{aligned} \dot{\bar{r}} &= \bar{v} \\ \dot{\bar{v}} &= \bar{a}_m(\bar{r}, \bar{v}, t) + \bar{\epsilon}(t) \\ \dot{\bar{\epsilon}} &= A\bar{\epsilon} + B\bar{u}(t) \\ \dot{\bar{T}} &= 0 \end{aligned} \quad (8-107)$$

If the state vector  $\bar{x}$  is augmented as

$$\bar{x}^T = [\bar{r}^T | \bar{v}^T | \bar{\epsilon}^T | \bar{T}^T] \quad (8-108)$$

the dynamical system in Equation (8-107) can be written as

$$\dot{\bar{\mathbf{x}}} = \bar{\mathbf{g}}(\bar{\mathbf{x}}, \bar{\mathbf{u}}, t), \quad \bar{\mathbf{x}}(t_0) = \bar{\mathbf{x}}_0 \quad (8-109a)$$

where

$$\bar{\mathbf{g}}^T = [\bar{\mathbf{v}}^T \{ (\bar{\mathbf{a}}_m + \bar{\boldsymbol{\varepsilon}})^T \} (A\bar{\boldsymbol{\varepsilon}} + B\bar{\mathbf{u}})^T \mid 0] \quad (8-109b)$$

and the initial conditions  $\bar{\mathbf{x}}_0$  are unknown.

For  $t > t_j$ , where  $t_j$  is a reference epoch, the solutions to Equation (8-107) in integral form are

$$\bar{\mathbf{r}}(t) = \bar{\mathbf{r}}(t_j) + \bar{\mathbf{v}}(t_j) \Delta t + \int_{t_j}^t \bar{\mathbf{a}}(\bar{\mathbf{r}}, \bar{\mathbf{v}}, \bar{\boldsymbol{\varepsilon}}, t) [t - \tau] d\tau \quad (a)$$

$$\bar{\mathbf{v}}(t) = \bar{\mathbf{v}}(t_j) + \int_{t_j}^t \bar{\mathbf{a}}(\bar{\mathbf{r}}, \bar{\mathbf{v}}, \bar{\boldsymbol{\varepsilon}}, t) d\tau \quad (b)$$

(8-110)

$$\bar{\boldsymbol{\varepsilon}}(t) = \mathbf{E}(t) \bar{\boldsymbol{\varepsilon}}(t_j) + \bar{\boldsymbol{\ell}}(t_j) \quad (c)$$

$$\bar{\mathbf{T}}(t) = \bar{\mathbf{T}}(t_j) \quad (d)$$

where  $\Delta t = t - t_j$  and  $\bar{\mathbf{a}}(\bar{\mathbf{r}}, \bar{\mathbf{v}}, \bar{\boldsymbol{\varepsilon}}, t) = \bar{\mathbf{a}}_m(\bar{\mathbf{r}}, \bar{\mathbf{v}}, t) + \bar{\boldsymbol{\varepsilon}}(t)$

The matrices  $\mathbf{E}(t)$  and  $\bar{\boldsymbol{\ell}}(t_j)$  are defined as

$$\mathbf{E}(t) = \begin{bmatrix} a_1 & 0 & 0 \\ 0 & a_2 & 0 \\ 0 & 0 & a_3 \end{bmatrix} \quad (a)$$

(8-111)

$$\bar{\boldsymbol{\ell}}^T(t_j) = [\sigma_1(1 - \alpha_1^2)^{1/2} u_1 \mid \sigma_2(1 - \alpha_2^2)^{1/2} u_2 \mid \sigma_3(1 - \alpha_3^2)^{1/2} u_3] \quad (b)$$

where

$$\alpha_k = \exp[-(t - t_j)/T_k] \quad (a)$$

and

$$k = 1, 2, 3 \quad (8-112)$$

$$\sigma_k = b_k(2/T_k)^{1/2} \quad (b)$$

Equation (8-110) can also be written as

$$\bar{x}(t, t_j) = \bar{G}(\bar{x}(t_j), t_j, t) + \bar{w}_j, \quad t \geq t_j \quad (8-113)$$

where

$$\bar{w}^T = [\omega_r^T; \omega_v^T; \omega_e^T; 0]$$

is the state noise matrix which is due to the purely random components of the unmodeled accelerations

$$\bar{w}_j = \begin{bmatrix} \int_{t_j}^t \bar{\ell}(t_j) [t - \tau] d\tau \\ \int_{t_j}^t \bar{\ell}(t_j) d\tau \\ \bar{\ell}(t_j) \\ 0 \end{bmatrix} \quad (8-114)$$

The statistics of  $\bar{w}$  are

$$E[\bar{w}] = 0, \quad E[\bar{w}\bar{w}^T] = Q_j \delta_{ij} = \begin{bmatrix} Q_{rr} & Q_{rv} & Q_{re} & 0 \\ Q_{rv} & Q_{vv} & Q_{ve} & 0 \\ Q_{re} & Q_{ev} & Q_{ee} & 0 \\ 0 & 0 & 0 & 0 \end{bmatrix} \delta_{ij} \quad (8-115)$$

where  $\delta_{ij}$  is the Kronecker delta function, and

$$\begin{aligned} Q_{rr} &= S_j (\Delta t)^4 / 4 \\ Q_{rv} &= Q_{vr} = S_j (\Delta t)^3 / 2 \\ Q_{re} &= Q_{er} = S_j (\Delta t)^2 / 2 \\ Q_{vv} &= S_j (\Delta t)^2 \\ Q_{ve} &= Q_{ev} = S_j \Delta t \\ Q_{ee} &= S_j \end{aligned} \quad (8-116)$$

and

$$S_j = \begin{bmatrix} \sigma_1^2(1 - \alpha_1^2) & 0 & 0 \\ 0 & \sigma_2^2(1 - \alpha_2^2) & 0 \\ 0 & 0 & \sigma_3^2(1 - \alpha_3^2) \end{bmatrix} \quad (8-117)$$

The observation equation for the  $j^{\text{th}}$  observation is

$$\bar{y}_j = \bar{f}(\bar{x}(t_j), t_j) + \bar{n}_j \quad (8-118a)$$

where  $\bar{n}_j$  is the observation noise which satisfies the following conditions

$$\mathcal{E}[\bar{n}] = 0, \quad \mathcal{E}[\bar{n}\bar{n}^T] = R_j \delta_{ij} \quad (8-118b)$$

and where  $R$  is the covariance matrix of the observation noise.

The procedure then follows that of the Extended Kalman Filter described in Section 8.4.1, with the following modifications:

1. The state is predicted via Equation (8-113) with  $\bar{w} \equiv 0$ .
2. Equation (8-115) is used for  $Q_{j+1}$  in the predicted covariance matrix of error.
3. In the filter gain matrix  $K$ ,  $R$  from Equation (8-118b) replaces  $w^{-1}$ .
4. The updated covariance matrix is computed via Equation (8-86c) rather than Equation (8-90).

The algorithm requires a priori values for the augmented state  $\bar{x}_0$ , along with the a priori covariance matrices  $P_{\Delta x_0}$ ,  $Q_j$ , and  $R_j$ .

When applied to the Apollo 10 and 11 missions, the DMC method gave the following results:

1. Its accuracy was limited by the observation noise rather than by the model inaccuracies.
2. The unmodeled accelerations were primarily due to neglected effects in the lunar potential, and the magnitude of the unmodeled accelerations was dominated by the radial component.
3. The estimated values of unmodeled accelerations were repeatable from orbit to orbit and from mission to mission.

4. The magnitude of the radial component of the unmodeled acceleration was highly correlated with the location of lunar surface mascons.

The obvious drawback of the preceding filtering theories is that the noise statistics must be supplied a priori. A remedy for this difficulty is discussed in the following section.

#### 8.4.3 Statistical Adaptive Filtering

Statistical adaptive filtering techniques are designed to correct the basic filter to account for the combined effects of all error sources, e.g., neglected nonlinearities, unknown noise statistics, computational errors, and model errors. One of the difficulties with filtering is the determination of the proper value of  $Q$ , the state noise covariance. Additional problems arise in determining the statistics associated with the observation noise. Effects such as atmospheric refraction variation and random disturbances in the radar instrumentation are unpredictable. The assumptions that have been made are that  $\bar{n}$ , the measurement noise (Equation (8-1)), and  $\bar{w}$ , the state noise (Equation (8-91)), have zero mean. However, due to model errors and nonlinearities, this is rarely true. The goal of statistical adaptive filtering is to determine the actual mean and covariance of both the state and observation noise so that better estimates of the state can be obtained.

Numerous investigators have developed adaptive sequential estimation techniques based on the recursive Kalman filter equations (References 15 and 16). The J-adaptive filter in GTDS is discussed as an example of statistical adaptive filters. Jazwinski developed a sequential adaptive estimator having the capability to track system state and model errors in the presence of large and unpredictable system or environmental variations. The approach is to add a low frequency random forcing function, representing the model errors, to the differential equation representing the system model. The filter then estimates this function as well as the state. The model chosen for this random forcing function is a polynomial with time-varying coefficients. This particular approach is especially useful in parameter identification problems.

It is assumed that the estimator system model is

$$\dot{\bar{x}} = \bar{g}_1(\bar{x}, t) + \bar{g}_2\bar{u}(t) \quad (8-119)$$

where  $\bar{g}_1$  includes the accelerations that are well known,

$\bar{g}_2$  includes possible unknown accelerations and model errors in  $\bar{g}_1$ .

and  $\bar{u}(t)$  is a random forcing function.



If  $\bar{u}(t)$  is a linear polynomial in time, the discrete form of the system model over the time interval  $[t_j, t_{j+1}]$  is

$$\bar{x}(t_{j+1}) = \bar{G}[\bar{x}(t_j), \bar{u}(t)] \quad (8-120a)$$

$$\bar{u}(t) = \bar{u}(t_j) + \dot{\bar{u}}(t_j) [t - t_j] \quad (8-120b)$$

where  $\dot{\bar{u}}$  is modeled as a random constant to be estimated.

The measurement model is the same as in previous sections, i.e.,

$$\bar{y}(t_j) = \bar{F}(\bar{x}(t_j); t_j) + \bar{n} \quad (8-121a)$$

where  $\bar{n}$  is measurement noise with

$$\mathcal{E}\{\bar{n}\bar{n}^T\} = R \quad (8-121b)$$

Hence, the complete dynamical system model is

$$\hat{\bar{x}}(t_{j+1}|t_j) = \bar{G}[\hat{\bar{x}}(t_j|t_j), \bar{u}(t_{j+1}|t_j)] + \bar{w} \quad (8-122a)$$

$$\bar{u}(t_{j+1}|t_j) = \bar{u}(t_j|t_j) + \dot{\bar{u}}(t_{j+1}|t_j) \tau; \quad \tau = t_{j+1} - t_j \quad (8-122b)$$

$$\dot{\bar{u}}(t_{j+1}|t_j) = \dot{\bar{u}}(t_j|t_j) \quad (8-122c)$$

In order to describe the system, the covariance and correlation matrices are defined as follows

$$\mathcal{E}\{\hat{\Delta x}(t_j) \hat{\Delta x}^T(t_j)\} = P(t_j|t_j) \quad (8-123a)$$

$$\mathcal{E}\{\hat{\Delta x}(t_j) \hat{\Delta u}^T(t_j)\} = C_{u,x}(t_j|t_j) \quad (8-123b)$$

$$\mathcal{E}\{\hat{\Delta x}(t_j) \hat{\Delta u}^T(t_j)\} = C_{u,x}(t_j|t_j) \quad (8-123c)$$

$$\mathcal{E}\{\hat{\Delta u}(t_j) \hat{\Delta u}^T(t_j)\} = U_{uu}(t_j|t_j) \quad (8-123d)$$

$$\mathcal{E}\{\hat{\Delta u}(t_j) \hat{\Delta u}^T(t_j)\} = U_{uu}(t_j|t_j) \quad (8-123e)$$

$$\mathcal{E}\{\hat{\Delta u}(t_j) \hat{\Delta u}^T(t_j)\} = U_{uu}(t_j|t_j) \quad (8-123f)$$

where

$$\hat{\Delta \mathbf{x}}(t_j) = \bar{\mathbf{x}}(t_j) - \hat{\mathbf{x}}(t_j) \quad (8-124a)$$

$$\hat{\Delta \mathbf{u}}(t_j) = \bar{\mathbf{u}}(t_j) - \hat{\mathbf{u}}(t_j) \quad (8-124b)$$

$$\hat{\Delta \dot{\mathbf{u}}}(t_j) = \dot{\bar{\mathbf{u}}}(t_j) - \dot{\hat{\mathbf{u}}}(t_j) \quad (8-124c)$$

Let

$$\bar{\mathbf{x}}(t_{j+1}|t_j) = \phi \bar{\mathbf{x}}(t_j) + \psi \bar{\mathbf{u}}(t_j) + \psi_d \dot{\bar{\mathbf{u}}}(t_j) \quad (8-125)$$

where

$$\phi(t_{j+1}|t_j) = \frac{\partial \bar{\mathbf{x}}(t_{j+1})}{\partial \bar{\mathbf{x}}(t_j)} \quad (8-126a)$$

$$\psi(t_{j+1}|t_j) = \frac{\partial \bar{\mathbf{x}}(t_{j+1})}{\partial \bar{\mathbf{u}}(t_j)} \quad (8-126b)$$

$$\psi_d(t_{j+1}|t_j) = \frac{\partial \bar{\mathbf{x}}(t_{j+1})}{\partial \dot{\bar{\mathbf{u}}}(t_j)} \quad (8-126c)$$

The Jazwinski Filter is derived by augmenting the state  $\bar{\mathbf{x}}$  with the vectors  $\bar{\mathbf{u}}$  and  $\dot{\bar{\mathbf{u}}}$  and using the Extended Kalman Filter in augmented form.

Equations (8-122b), (8-122c), and (8-125) can be combined to yield an augmented transition matrix

$$\Phi = \begin{bmatrix} \phi & \psi & \psi_d \\ 0 & \mathbf{I} & \tau \\ 0 & 0 & \mathbf{I} \end{bmatrix} \quad (8-127)$$

The augmented form of the error covariance matrix is

$$\mathcal{P}(t_j | t_j) = \begin{bmatrix} \mathbf{P} & \mathbf{C}_{ux} & \mathbf{C}_{\dot{u}x} \\ \mathbf{C}_{ux}^T & \mathbf{U}_{uu} & \mathbf{U}_{u\dot{u}} \\ \mathbf{C}_{\dot{u}x}^T & \mathbf{U}_{u\dot{u}}^T & \mathbf{U}_{\dot{u}\dot{u}} \end{bmatrix} \quad (8-128)$$

The augmented state, gain, and observation matrices are

$$\mathcal{X} = \begin{bmatrix} \bar{x} \\ \bar{u} \\ \dot{\bar{u}} \end{bmatrix} \quad \mathcal{K} = \begin{bmatrix} K_x \\ K_u \\ K_{\dot{u}} \end{bmatrix} \quad \mathcal{Z} = [F \mid 0 \mid 0] \quad (8-129)$$

Substituting Equations (8-127) and (8-128) into Equation (8-92b) and ignoring the state noise yields

$$\mathcal{P}(t_{j+1}|t_j) = \begin{bmatrix} \phi & \psi & \psi_d \\ 0 & I & \tau \\ 0 & 0 & I \end{bmatrix} \begin{bmatrix} P & C_{ux} & C_{ux}^T \\ C_{ux}^T & U_{uu} & U_{u\dot{u}} \\ C_{ux}^T & U_{u\dot{u}}^T & U_{\dot{u}\dot{u}} \end{bmatrix} \begin{bmatrix} \phi^T & 0 & 0 \\ \psi^T & I & 0 \\ \psi_d^T & \tau & I \end{bmatrix} \quad (8-130)$$

Expanding the right-hand side, the upper triangular elements of  $\mathcal{P}(t_{j+1}|t_j)$  are

$$\begin{aligned} P(t_{j+1}|t_j) &= \phi P \phi^T + \psi C_{ux}^T \phi^T + \psi_d C_{ux}^T \phi^T + \phi C_{ux} \psi^T + \psi U_{uu} \psi^T \\ &\quad + \psi_d U_{u\dot{u}}^T \psi^T + \phi C_{ux} \psi_d^T + \psi U_{u\dot{u}} \psi_d^T + \psi_d U_{\dot{u}\dot{u}} \psi_d^T \end{aligned} \quad (8-131a)$$

$$C_{ux}(t_{j+1}|t_j) = \phi C_{ux} + \psi U_{uu} + \psi_d U_{u\dot{u}}^T + \tau(\phi C_{ux} + \psi U_{u\dot{u}} + \psi_d U_{\dot{u}\dot{u}}) \quad (8-131b)$$

$$C_{ux}^T(t_{j+1}|t_j) = \phi C_{ux}^T + \psi U_{uu} + \psi_d U_{\dot{u}\dot{u}} \quad (8-131c)$$

$$U_{uu}(t_{j+1}|t_j) = U_{uu} + \tau U_{u\dot{u}}^T + \tau(U_{u\dot{u}} + \tau U_{\dot{u}\dot{u}}) \quad (8-131d)$$

$$U_{u\dot{u}}(t_{j+1}|t_j) = U_{u\dot{u}} + \tau U_{\dot{u}\dot{u}} \quad (8-131e)$$

$$U_{\dot{u}\dot{u}}(t_{j+1}|t_j) = U_{\dot{u}\dot{u}} \quad (8-131f)$$

where all the terms on the right-hand sides of Equations (8-131a) through (8-131f) are evaluated at  $(t_j|t_j)$ .

Substituting Equations (8-128) and (8-129) into Equation (8-86d) yields

$$\begin{bmatrix} K_x \\ K_u \\ K_{\dot{u}} \end{bmatrix} = \begin{bmatrix} P & C_{ux} & C_{\dot{u}x} \\ C_{ux}^T & U_{uu} & U_{u\dot{u}} \\ C_{\dot{u}x}^T & U_{u\dot{u}}^T & U_{\dot{u}\dot{u}} \end{bmatrix} \begin{bmatrix} F^T \\ 0 \\ 0 \end{bmatrix} \quad (8-132)$$

$$\times \left\{ w_{j+1}^{-1} + [F^T \ 0 \ 0] \begin{bmatrix} P & C_{ux} & C_{\dot{u}x} \\ C_{ux}^T & U_{uu} & U_{u\dot{u}} \\ C_{\dot{u}x}^T & U_{u\dot{u}}^T & U_{\dot{u}\dot{u}} \end{bmatrix} \begin{bmatrix} F^T \\ 0 \\ 0 \end{bmatrix} \right\}^{-1}$$

Carrying out the indicated matrix multiplications,

$$\begin{bmatrix} K_x \\ K_u \\ K_{\dot{u}} \end{bmatrix} = \begin{bmatrix} PF^T(FPF^T + w_{j+1}^{-1})^{-1} \\ C_{ux}^T F^T(FPF^T + w_{j+1}^{-1})^{-1} \\ C_{\dot{u}x}^T F^T(FPF^T + w_{j+1}^{-1})^{-1} \end{bmatrix} \quad (8-133)$$

Substituting Equations (8-128) and (8-129) into Equation (8-86c) yields

$$P(t_{j+1}|t_{j+1}) = \left( I - \begin{bmatrix} K_x \\ K_u \\ K_{\dot{u}} \end{bmatrix} [F^T \ 0 \ 0] \right) \begin{bmatrix} P & C_{ux} & C_{\dot{u}x} \\ C_{ux}^T & U_{uu} & U_{u\dot{u}} \\ C_{\dot{u}x}^T & U_{u\dot{u}}^T & U_{\dot{u}\dot{u}} \end{bmatrix} \quad (8-134)$$

$$= \begin{bmatrix} I - K_x F & 0 & 0 \\ -K_u F & I & 0 \\ -K_{\dot{u}} F & 0 & I \end{bmatrix} \begin{bmatrix} P & C_{ux} & C_{\dot{u}x} \\ C_{ux}^T & U_{uu} & U_{u\dot{u}} \\ C_{\dot{u}x}^T & U_{u\dot{u}}^T & U_{\dot{u}\dot{u}} \end{bmatrix}$$

Hence, the upper triangular elements of  $P(t_{j+1}|t_{j+1})$  are

$$P(t_{j+1}|t_{j+1}) = (I - K_x F) P(t_{j+1}|t_j) \quad (8-135a)$$

$$C_{ux}(t_{j+1}|t_{j+1}) = (I - K_x F) C_{ux}(t_{j+1}|t_j) \quad (8-135b)$$

$$C_{ux}^*(t_{j+1}|t_{j+1}) = (I - K_x F) C_{ux}^*(t_{j+1}|t_j) \quad (8-135c)$$

$$U_{uu}(t_{j+1}|t_{j+1}) = U_{uu}(t_{j+1}|t_j) - K_u F C_{ux}(t_{j+1}|t_j) \quad (8-135d)$$

$$U_{uu}^*(t_{j+1}|t_{j+1}) = U_{uu}^*(t_{j+1}|t_j) - K_u F C_{ux}^*(t_{j+1}|t_j) \quad (8-135e)$$

$$U_{uu}^{\dagger}(t_{j+1}|t_{j+1}) = U_{uu}^{\dagger}(t_{j+1}|t_j) - K_u F C_{ux}^{\dagger}(t_{j+1}|t_j) \quad (8-135f)$$

Substituting Equation (8-129) into Equation (8-100) gives the update equation for the augmented state

$$\begin{bmatrix} \bar{x} \\ \bar{u} \\ \dot{\bar{u}} \end{bmatrix}_{(t_{j+1}|t_{j+1})} = \begin{bmatrix} \bar{x} \\ \bar{u} \\ \dot{\bar{u}} \end{bmatrix}_{(t_{j+1}|t_j)} + \begin{bmatrix} K_x \\ K_u \\ K_u^* \end{bmatrix} [\bar{y}(t_{j+1}) - \bar{f}(\hat{x}(t_{j+1}|t_j); t_{j+1})] \quad (8-136)$$

or

$$\hat{x}(t_{j+1}|t_{j+1}) = \hat{x}(t_{j+1}|t_j) + K_x [\bar{y}(t_{j+1}) - \bar{f}(\hat{x}(t_{j+1}|t_j)))] \quad (8-137a)$$

$$\bar{u}(t_{j+1}|t_{j+1}) = \bar{u}(t_{j+1}|t_j) + K_u [\bar{y}(t_{j+1}) - \bar{f}(\hat{x}(t_{j+1}|t_j)))] \quad (8-137b)$$

$$\dot{\bar{u}}(t_{j+1}|t_j) = \dot{\bar{u}}(t_{j+1}|t_j) + K_u^* [\bar{y}(t_{j+1}) - \bar{f}(\hat{x}(t_{j+1}|t_j)))] \quad (8-137c)$$

Equations (8-125) and (8-130) are the prediction equations for the Jazwinski Filter, and Equations (8-133), (8-134), and (8-137) are the update equations. The inclusion of Equation (8-135f) is a modification by Torroglosa which keeps the covariance matrix of the state from becoming nonpositive definite. In the original Jazwinski Filter, the uncertainty in  $u$  was maintained constant and hence,  $U_{uu}^{\dagger}(t_{j+1}|t_j) = \bar{U}_{uu}^{\dagger}$ . The initial conditions  $\hat{x}(0|0)$ ,  $P_{\Delta x}(0|0)$ ,  $U_{uu}(0|0)$ , and  $U_{uu}^*(0|0)$  must be specified. The correlation terms  $C_{ux}(0|0)$ ,  $C_{ux}^*(0|0)$ ,  $U_{ux}^{\dagger}(0|0)$ , and the initial values of  $\hat{u}(0|0)$  and  $\dot{\hat{u}}(0|0)$  are set equal to zero externally.

#### 8.4.4 Computational Procedure for the Filter Program

The computational sequence for the Filter Program is similar to that for the Differential Correction Program (see Section 8.2.4). The computational flow

schematic is shown in Figure 8-2. Both the figure and the accompanying discussion are divided into functional blocks.

#### 8.4.4.1 A Priori Input

All necessary input data are specified at (A). This includes the estimated variables and their covariances, the measurement time spans, and the number of observations per set. The state input can be expressed optionally in any of several convenient coordinate systems as in the DC Program. For subsequent processing, the state is transformed into the mean equator and equinox of 1950.0 system or into the true equator and equinox of a given epoch system. The transformations are given in Chapter 3.

#### 8.4.4.2 Data Management

The observation data are prepared for processing at (B) and (C). This encompasses relocating the data for the specified measurement span from the original input device (cards, single or multiple tapes, disk, or keyboard) to a working file convenient for subsequent retrieval during processing. During this relocation function, the data sequence can optionally be edited considering the type of observation, the source of the data, the tracking station, and the time span between adjacent points. The data on the working file are chronologically numbered, and the number of the data point which bounds the initial epoch time  $t_0$  from below is recorded. The data management function also includes the determination of whether the initial epoch time is less than the first data time, between the first and last data time, or larger than the last data time. For the first case, the data are processed sequentially from the first point at  $t_1$  to the last point at  $t_m$ . For the second case, the processing starts backwards in time from the initial epoch to the first data point, and it then switches back to the initial epoch and proceeds forward in time to the last data point. In the third case, the data are processed backwards in time from the last (chronological) data point to the first.

#### 8.4.4.3 Processing Loop

The processing loop begins by retrieving the first data point to be processed from the working file at (D). A test is made to determine the optimal integrator to be used considering the time span between observations at  $t_j$  and  $t_{j-1}$ . A predicted covariance for the observation is calculated. The observation, its residual, and the partial derivatives of the measurements with respect to

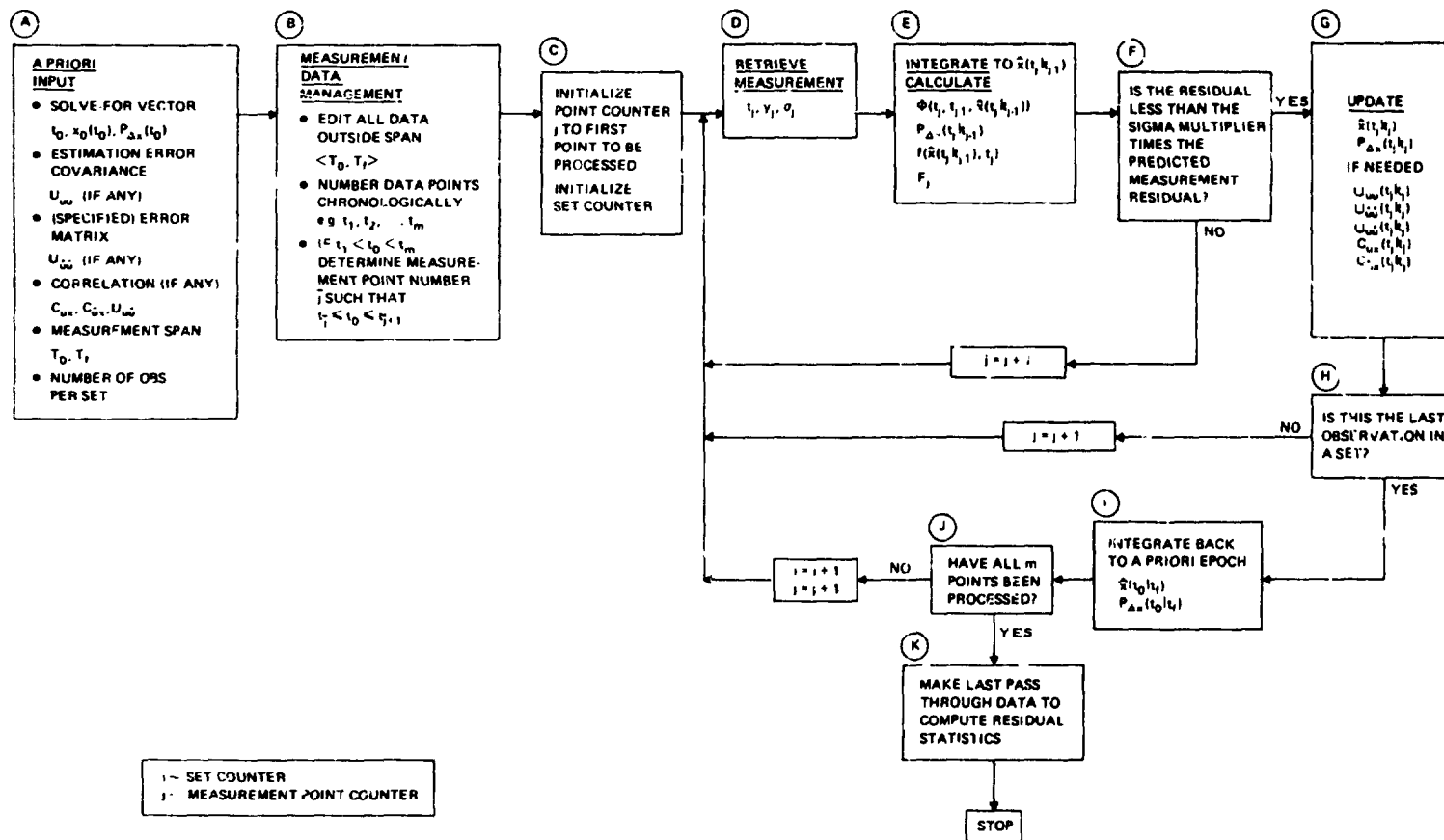


Figure 8-2. Computational Sequence for the Filter Program

parameters being estimated are computed at (E), determining whether to accept or reject the observation at (F). If the observation is accepted, the Kalman gain is calculated, the state, state covariance matrix, and correlation matrices are updated, and the processed observation is output at (G).

#### 3.4.4.4 Data Set Loop

If it has been determined at (H) that the last observation of a set has been processed, the updated state at the last observation time and its covariance matrix are printed; the updated state is then integrated backwards to the a priori epoch time; and the Current Elements Report, the Solve-for Parameters Report, and the End-of-Set Summary Report are printed, all at (I). After it has been determined at (J) that all the observations have been processed, a last pass is made through the observation data to compute residual statistics and print final reports at (K).

### 8.5 COVARIANCE MATRIX INTERPRETATION

In the previous sections, equations have been presented for calculating the mean  $\hat{x}$  and the covariance matrix  $P_{\Delta x}$  of the errors in the estimated state and model parameters. There is little difficulty in recognizing the value of the mean, or estimated value, but interpretation of the covariance and correlation matrices in terms of the uncertainty of the variables is not as clear. Yet, the covariance matrix yields a great deal of information on the statistical character of the variables. Some of these characteristics are described in the following sections.

#### 8.5.1 Augmented Vector and Covariance

The estimation process yields the mean  $\hat{x}$  and covariance of errors  $P_{\Delta x}$  of the solve-for variables, and the matrix  $C_{\Delta x \Delta z}$  relating errors in solve-for and consider variables. The mean  $\bar{z}_0$  and covariance  $P_{\Delta z_0}$  of the consider variables are known a priori. As an aid in understanding the role of each of the matrices, the augmented, or expanded, state vector  $\bar{u}$  is defined as  $(\bar{x} \mid \bar{z})^T$ . The best estimate (or expected value) of  $u$  is  $(\hat{x} \mid \bar{z}_0)^T$ . The covariance matrix of errors of  $\bar{u}$  is  $P_{\Delta u}$ , which can be partitioned into the following components

$$P_{\Delta u} = \begin{bmatrix} P_{\Delta x} & C_{\Delta x \Delta z} \\ \text{---} & \text{---} \\ C_{\Delta z \Delta x} & P_{\Delta z_0} \end{bmatrix}$$



where  $P_{\Delta u}$  is a positive definite symmetric matrix. Therefore

$$C_{\Delta z \Delta x} = C_{\Delta x \Delta z}^T$$

The submatrix  $P_{\Delta z_0}$  remains constant throughout the processing, since the consider variable uncertainty cannot be improved through estimation.

The following sections present a geometric heuristic interpretation of the covariance matrices  $P_{\Delta u}$ ,  $P_{\Delta x}$ , and/or  $P_{\Delta z_0}$  in terms of hyperdimensional volumes of constant probability in the  $(p + q)$ -,  $p$ -, and/or  $q$ -dimensional Euclidean space of the vector components.

### 8.5.2 Hyperellipse Probabilities

In the following discussion, the random vector  $\bar{x}$  with uncertainty  $P_{\Delta x}$  is considered. The discussion is equally applicable to the random variables  $\bar{u}$  and  $\bar{z}$ . Assuming that the random vector  $\bar{x}(t)$  is normally distributed, it can be completely described by its mean and covariance. The assumption that  $\bar{x}(t)$  is normally distributed is partially justified as a result of an analogue of the Central Limit Theorem which states: "If a large number of random variables are combined in a reasonably complicated fashion to form a single multivariate random variable, then this random variable will have a nearly normal distribution."

For the following discussion, it is assumed that the random vector of errors  $\Delta x$  about the mean  $\hat{x}$  is composed of six components. It is normally distributed with zero mean and covariance  $P_{\Delta x}$ . Its probability density function can be written as

$$p_x(\Delta x) = \frac{1}{(2\pi)^3 |P_{\Delta x}|^{1/2}} \exp \left[ -\frac{1}{2} \Delta x^T P_{\Delta x}^{-1} \Delta x \right] \quad (8-138)$$

If  $P_{\Delta x}$  is a diagonal matrix, then  $\bar{x}$  has components that are statistically independent (uncorrelated), and  $p_x(\Delta x)$  can then be factored into a product of six univariate functions of  $x_1, x_2, \dots, x_6$  (the one-dimensional marginal probability density functions of the six components of the state). This constitutes a sufficient condition for independence of the marginal random variables  $x_1, \dots, x_6$ .

By virtue of its definition,  $P_{\Delta x}$  is a nonnegative definite matrix so that it has nonnegative eigenvalues. Hence, a similarity transformation

$$\overline{\Delta y} = S \overline{\Delta x} \quad (8-139)$$

which diagonalizes  $P_{\Delta x}$  is always possible since the hypersurface of constant likelihood (constant value of probability density) in six-dimensional space is a hyperellipsoid, and by a rotation of axes it is possible to use the principal axes of the hyperellipsoid as coordinate axes (i.e., to transform to another random variable space having uncorrelated or independent components). The  $\overline{\Delta y}$  in Equation (8-139) represents space coordinates and is unrelated to the observations.

Of interest is the probability that  $x_1, x_2, \dots, x_6$  lie within the hyperellipsoid

$$\overline{\Delta x}^T P_{\Delta x}^{-1} \overline{\Delta x} = \ell^2 \quad (8-140)$$

where  $\ell$  is constant. By transforming to principal axes, this expression becomes

$$\frac{\Delta y_1^2}{\sigma_1^2} + \frac{\Delta y_2^2}{\sigma_2^2} + \dots + \frac{\Delta y_6^2}{\sigma_6^2} = \ell^2 \quad (8-141)$$

where  $\sigma_1, \sigma_2, \dots, \sigma_6$  are the eigenvalues of  $P_{\Delta x}$ . The transformation matrix from  $\overline{\Delta x}$  to  $\overline{\Delta y}$  space is accomplished by the matrix of eigenvectors  $S$ . By a second transformation,  $\Delta z_i = \Delta y_i / \sigma_i$ , the expression in Equation (8-141) becomes the equation for a hypersphere in six dimensions

$$\Delta z_1^2 + \Delta z_2^2 + \dots + \Delta z_6^2 = \ell^2 \quad (8-142)$$

The probability of finding  $\overline{\Delta z}$  inside this hypersphere is

$$\iiint \dots \int_{\text{volume}} \frac{1}{(2\pi)^3} \exp \left\{ -\frac{1}{2} (\Delta z_1^2 + \dots + \Delta z_6^2) \right\} d\Delta z_1 d\Delta z_2 \dots d\Delta z_6 \quad (8-143)$$

where the integration is carried out over the volume of the hypersphere of radius  $\Delta r$ , where

$$\Delta r^2 = \Delta z_1^2 + \Delta z_2^2 + \dots + \Delta z_6^2 \tag{8-144}$$

Thus, the probability of finding  $\Delta x_1, \Delta x_2, \dots, \Delta x_6$  inside the hyperellipsoid  $\frac{\Delta x^T}{\Delta x} P_{\Delta x}^{-1} \frac{\Delta x}{\Delta x} = \ell^2$  is

$$P_r = \frac{1}{(2 \pi)^3} \int_0^\ell e^{-1/2 \Delta r^2} f(\Delta r) d \Delta r \tag{8-145}$$

where  $f(\Delta r)$  is the spherically symmetric differential volume element.

In six-dimensional space, Equation (8-145) is

$$P_r = \frac{1}{(2 \pi)^3} \int_0^\ell e^{-1/2 \Delta r^2} (\pi^3 \Delta r^5) d \Delta r = \left[ 1 - \frac{1}{2} e^{-1/2 \ell^2} \left( \frac{\ell^4}{4} + \ell^2 + 2 \right) \right] \tag{8-146}$$

For  $\ell = 1, 2$ , and  $3$ , the probability is  $0.014, 0.332$ , and  $0.826$ , respectively. Also of interest are hyperellipsoids of other dimensions. Considering an  $m$ -dimensional random vector where  $m = 1$  through  $7$ , the probabilities corresponding to  $\ell = 1$  through  $4$  (often called  $1, 2, 3$ , and  $4\sigma$  probabilities) are as shown in Table 8-1.

Table 8-1  
Hyperellipse Probabilities

$m \backslash \ell$	1	2	3	4
1	0.683	0.955	0.997	1.00
2	0.394	0.865	0.989	1.00
3	0.200	0.739	0.971	0.999
4	0.090	0.594	0.939	0.997
5	0.037	0.450	0.891	0.993
6	0.014	0.323	0.826	0.986
7	0.005	0.220	0.747	0.975

The problem of evaluating the hyperellipsoid, however, remains very difficult since it cannot be visualized. The equation for the ellipsoid can be transformed to its principal axes by means of the eigenvector transformation. The resulting diagonal matrix of eigenvalues yields the maximum excursions of the state variables. However, these excursions are in the transformed (principal) axes and therefore are maximum excursions for combinations of  $\Delta x_1, \Delta x_2, \dots, \Delta x_6$  and still difficult to visualize.

### 8.5.3 Hyperrectangle Probabilities

Another method of interpreting the confidence regions of state variable uncertainty is by means of hyperrectangles instead of hyperellipses. Consider a two-dimensional case where  $P_{\Delta x}$  is the covariance matrix

$$P_{\Delta x} = \begin{bmatrix} \sigma_{\Delta x_1}^2 & \sigma_{\Delta x_1 \Delta x_2} \\ \sigma_{\Delta x_1 \Delta x_2} & \sigma_{\Delta x_2}^2 \end{bmatrix} \tag{8-147}$$

The quadratic form  $\overline{\Delta x}^T P_{\Delta x}^{-1} \overline{\Delta x} = \ell^2$  is

$$\sigma_{\Delta x_2}^2 \Delta x_1^2 - 2 \sigma_{\Delta x_1 \Delta x_2} \Delta x_1 \Delta x_2 + \sigma_{\Delta x_1}^2 \Delta x_2^2 = \ell^2 |P_{\Delta x}| \tag{8-148}$$

This quadratic equation represents an ellipse such as that in Figure 8.3.

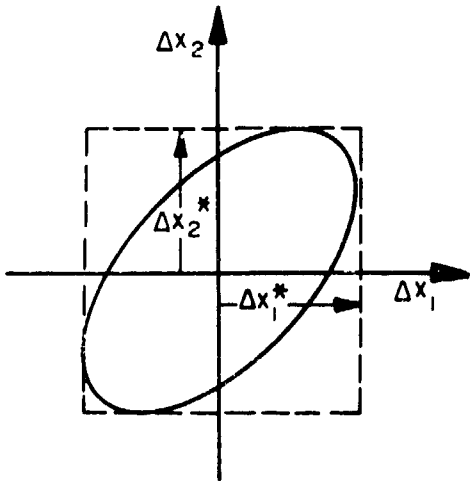


Figure 8-3. Error Ellipse and Rectangle

The width  $\Delta x_1^*$  and height  $\Delta x_2^*$  of the rectangle enclosing the ellipse are determined from Equation (8-148) for the condition that  $d\Delta x_2/d\Delta x_1 = 0$  and  $d\Delta x_1/d\Delta x_2 = 0$ , respectively, yielding

$$\begin{aligned}\Delta x_2^* &= \ell \sigma_{\Delta x_2} \\ \Delta x_1^* &= \ell \sigma_{\Delta x_1}\end{aligned}\tag{8-149}$$

Thus, the probability that  $\Delta x_1$  lies within the region  $-3\sigma_{\Delta x_1} \leq \Delta x_1 \leq 3\sigma_{\Delta x_1}$  is 0.997,  $\Delta x_2$  falling wherever it may. The probability that  $\Delta x_2$  lies within the region  $-3\sigma_{\Delta x_2} \leq \Delta x_2 \leq 3\sigma_{\Delta x_2}$  is also 0.997,  $\Delta x_1$  falling wherever it may. Assuming no significant correlations, the probability that  $\Delta x_1$  and  $\Delta x_2$  simultaneously lie with the respective regions  $-3\sigma_{\Delta x_1} \leq \Delta x_1 \leq 3\sigma_{\Delta x_1}$  and  $-3\sigma_{\Delta x_2} \leq \Delta x_2 \leq 3\sigma_{\Delta x_2}$  is therefore  $(0.997)^2$  or 0.994. The probability that  $\Delta x_1$  and  $\Delta x_2$  lie within the  $3\sigma$  ellipse is 0.989, slightly less than that for the rectangle due to the lesser area.

Extending this interpretation to six dimensions, the probability that  $\Delta x_1, \Delta x_2, \dots, \Delta x_6$  simultaneously lie within their  $3\sigma$  hyperrectangles is  $(0.997)^6$  or 0.982. The probability that they lie within the six-dimensional hyperellipsoid is 0.826, significantly lower because of the smaller volume. The hyperrectangle probabilities corresponding to  $\ell = 1, 2, 3$ , and 4 and  $m = 1$  through 7 are presented in Table 8-2.

Table 8-2  
Hyperrectangle Probabilities

m \ $\ell$	1	2	3	4
1	0.683	0.955	0.997	1.00
2	0.466	0.912	0.994	1.00
3	0.319	0.872	0.991	1.00
4	0.218	0.832	0.988	1.00
5	0.149	0.794	0.985	1.00
6	0.102	0.759	0.982	1.00
7	0.069	0.724	0.979	1.00

The hyperrectangle probabilities are much easier to analyze since the various sides of the hyperrectangles are multiples of the square root of the variances. However, it is important to be aware of the fact that the boundary of the hyperrectangle merely encloses a volume of space and in no way can be regarded as a boundary of constant probability as is the case with hyperellipses.

The hyperrectangle probabilities are particularly convenient during program checkout. By processing simulated data having Gaussian random error with zero mean and known variances, the residuals of the estimated vector can be compared with the calculated standard deviations. The distribution of residuals should satisfy the 1, 2, 3, and 4 $\sigma$  probabilities in Table 3-2.

#### 8.5.4 Correlation Coefficient

It has been shown that the off-diagonal covariance elements of a covariance matrix determine the deviation between the random vector coordinate axes and the principal axes of the hyperellipse of constant probability. When the covariance elements are zero, the principal axes are aligned with the coordinate axes and the components are independent of each other. Furthermore, the normal density function (Equation (8-138)) can then be factored into a product of  $n$  univariate functions of  $\Delta x_1, \Delta x_2, \dots, \Delta x_n$ .

Another measure of the dependence of two random vectors  $\overline{\Delta x}$  and  $\overline{\Delta z}$ , having a  $(p \times q)$  correlation matrix

$$C_{\Delta x \Delta z} = \begin{bmatrix} \text{cov}(\Delta x_1, \Delta z_1) & \text{cov}(\Delta x_1, \Delta z_2) & \cdots & \text{cov}(\Delta x_1, \Delta z_q) \\ \text{cov}(\Delta x_2, \Delta z_1) & & & \\ & \cdot & & \\ & & \cdot & \\ & & & \cdot \\ \text{cov}(\Delta x_p, \Delta z_1) & \text{cov}(\Delta x_p, \Delta z_2) & \cdots & \text{cov}(\Delta x_p, \Delta z_q) \end{bmatrix} \quad (8-150)$$

is the correlation coefficient, defined as

$$\rho_{ij} = \rho(\Delta x_i, \Delta z_j) = \frac{\text{cov}(\Delta x_i, \Delta z_j)}{\sqrt{\text{var}(\Delta x_i) \text{var}(\Delta z_j)}} \quad (8-151)$$

The variance elements are the squares of the standard deviations for  $\Delta x_i$  and  $\Delta z_j$ , respectively, and lie along the main diagonal of  $P_{\Delta x}$  and  $P_{\Delta z}$ , respectively. The correlation coefficient satisfies the following conditions:

- $\rho = 0$  if and only if  $\Delta x_i$  and  $\Delta z_j$  (and therefore  $x_i$  and  $z_j$ ) are uncorrelated
- $|\rho| \leq 1$
- $\rho = \pm 1$ , if and only if

$$\left\{ \frac{\Delta x_i}{\sigma_{\Delta x_j}} \right\} = \pm \left\{ \frac{\Delta z_j}{\sigma_{\Delta z_j}} \right\} \quad (8-152)$$

where

$\sigma_{\Delta x_i}, \sigma_{\Delta z_j} \sim$  the standard deviations of the errors  $x_i$  and  $z_j$ , respectively.

## 8.6 ESTIMATION RELATED TECHNIQUES

Specific techniques required in the estimation process include matrix inversion, editing of residuals, iteration control, residual statistics, and hypothesis tests.

### 8.6.1 Matrix Inversion

The normal matrix is inverted by recursively inverting smaller matrices and by the use of the Schur identity. The symmetrical properties of the normal matrix are utilized during the inversion process. The Schur identity method is developed by assuming that the matrix to be inverted is of the form

$$[M] = \begin{bmatrix} [M_{11}] & [M_{12}] \\ \text{---} & \text{---} \\ [M_{21}] & [M_{22}] \end{bmatrix} \quad (8-153)$$

with the inverse given by

$$[M]^{-1} = \begin{bmatrix} [H_{11}] & [H_{12}] \\ \text{---} & \text{---} \\ [H_{21}] & [H_{22}] \end{bmatrix} \quad (8-154)$$

Since

$$[M] \quad [M]^{-1} = \begin{pmatrix} [I] & \vdots & [O] \\ \vdots & & \vdots \\ [O] & \vdots & [I] \end{pmatrix} \quad (8-155)$$

then

$$[M_{11}] [H_{11}] + [M_{12}] [H_{21}] = [I] \quad (8-156)$$

$$[M_{21}] [H_{11}] - [M_{22}] [H_{21}] = [O]$$

Eliminating  $[H_{21}]$  from Equation (8-156) and solving for  $[H_{11}]$  gives

$$[M_{11}] [H_{11}] + [M_{12}] [M_{22}]^{-1} [M_{21}] [H_{11}] = [I] \quad (8-157)$$

or

$$[H_{11}] = [M_{11}]^{-1} - [M_{11}]^{-1} [M_{12}] [M_{22}]^{-1} ([M_{21}] [H_{11}]). \quad (8-158)$$

Premultiplying Equation (8-157) by  $[M_{21}] [M_{11}]^{-1}$  gives

$$[M_{21}] [H_{11}] + [M_{21}] [M_{11}]^{-1} [M_{12}] [M_{22}]^{-1} [M_{21}] [H_{11}] = [M_{21}] [M_{11}]^{-1} \quad (8-159)$$

or

$$[M_{21}] [H_{11}] = \left[ [I] + [M_{21}] [M_{11}]^{-1} [M_{12}] [M_{22}]^{-1} \right]^{-1} [M_{21}] [M_{11}]^{-1} \quad (8-160)$$

Substituting Equation (8-160) into Equation (8-158) gives

$$\begin{aligned} [H_{11}] &= [M_{11}]^{-1} - [M_{11}]^{-1} [M_{12}] [M_{22}]^{-1} \\ &\quad \times \left[ [I] + [M_{21}] [M_{11}]^{-1} [M_{12}] [M_{22}]^{-1} \right]^{-1} [M_{21}] [M_{11}]^{-1} \end{aligned} \quad (8-161)$$



The matrices  $[H_{22}]$ ,  $[H_{12}]$ , and  $[H_{21}]$  may be derived in a similar manner, yielding

$$\begin{aligned} [H_{22}] &= - \left[ [M_{21}] [M_{11}]^{-1} [M_{12}] + [M_{22}] \right]^{-1} \\ [H_{12}] &= - [M_{11}]^{-1} [M_{12}] [H_{22}] \\ [H_{21}] &= [M_{22}]^{-1} [M_{21}] [H_{11}] \end{aligned} \quad (8-162)$$

It is assumed that the inverse of  $[M_{11}]$  is known and that  $[M_{22}]$  is in all cases a (1x1) matrix. The matrix inversions required in Equations (8-161) and (8-162) are simply the reciprocals of the elements of the respective matrices. The inversion begins by setting  $[M_{11}]$  as

$$[M_{11}]^{-1} = \frac{1}{m_{11}} \quad (8-163)$$

and

$$-[M_{22}]^{-1} = -\frac{1}{m_{22}}. \quad (8-164)$$

Equations (8-161) and (8-162) are then employed to determine the inverse of

$$\begin{bmatrix} m_{11} & m_{12} \\ m_{21} & m_{22} \end{bmatrix} \quad (8-165)$$

The result is called  $[M_{11}]$  and the diagonal element following (in this case  $m_{33}$ ) is used to form a new  $[M_{22}]$ . The process is continued along the diagonal until the required matrix is inverted. GTDS takes full advantage of the symmetry of the normal matrix by computing and storing only the upper triangle of the matrix. The inversion process is designed to invert a matrix in upper triangular form and store the result in the same manner.

### 8.6.2 Editing of Observation Residuals

The observation residual, as computed by GTDS, is defined as the actual observation minus the computed observation that is based on the trajectory specified by the current state vector solution. Deletion of an observation from the differential correction or filter computation may be accomplished by one or more of the following tests that are made on each iteration or filter set for each observation:

- By number. After examination of a previous run's residual printout, the user may elect to delete some residuals by sequence number.
- By time. The observation is rejected if it falls outside a specified time span.
- By type. The observation type is among those to be rejected.
- By station. The identifier of the station making the observation is among those to be rejected.
- By  $n^{\text{th}}$  observation. Every  $n^{\text{th}}$  observation of this type is to be processed; all other observations are rejected.
- By deviation. The observation is rejected when the deviation from the orbit established by the previous iteration is greater than a specified value, or, in a filter run, when the residual differs from the predicted measurement residual, by more than a specified amount.
- By geometry. The observation is rejected when the elevation angle of the line of sight from the tracking station is below a specified minimum value.

If a residual is deleted by any test, then the row of the augmented matrix  $F$  (matrix of partial derivatives of the observations with respect to the estimated parameters) corresponding to the observation is not computed.

### 8.6.3 Iteration Control for the Differential Correction Program

Conditions that may cause termination of the differential correction process are as follows:

- Convergence of the solution
- Maximum number of consecutive divergent iterations reached
- Maximum number of iterations reached

The convergence criteria in GTDS are based on iterative reduction of the square root of the mean square of the observation residuals. This quantity, denoted by RMS, is calculated as follows on the  $i^{\text{th}}$  iteration

$$\text{RMS} = \left\{ \frac{1}{m} (\overline{\Delta y_i})^T W \overline{\Delta y_i} + \tilde{x_i}^T P_{\Delta x_0}^{-1} \tilde{x_i} \right\}^{1/2} \quad (8-166)$$

where  $\overline{\Delta y_i}$  and  $\tilde{x_i}$  are defined in Equations (8-23) and (8-24), and  $m$  is the number of observations. If the value of RMS decreases during two consecutive iterations, the solution is converging. After a prespecified number of consecutive divergent iterations, the problem is terminated. After testing for convergence or divergence, a predicted RMS is calculated through first order in  $\hat{\Delta x}_{i+1}$  for the next iteration as follows

$$\begin{aligned} \text{RMSP} = & \left\{ \frac{1}{m} (\overline{\Delta y_i} - F_i \hat{\Delta x}_{i+1})^T W (\overline{\Delta y_i} - F_i \hat{\Delta x}_{i+1}) \right. \\ & \left. + (\hat{\Delta x}_{i+1} - \tilde{x_i})^T P_{\Delta x_0}^{-1} (\hat{\Delta x}_{i+1} - \tilde{x_i}) \right\}^{1/2} \end{aligned} \quad (8-167)$$

where  $\hat{\Delta x}_{i+1}$ ,  $\tilde{x_i}$ , and  $F_i$  are defined in Equations (8-25), (8-24), and (8-21a), respectively. The second term on the right is exactly correct for the  $(i+1)^{\text{st}}$  iteration. The first term on the right linearly corrects the measurement residuals to account for the differential correction  $\hat{\Delta x}_{i+1}$ . If the regression equation (Equation (8-14)) were linear, the predicted RMS (RMSP) would be exactly correct. The iterations are considered converged and the problem terminated when the following criterion is met

$$\left| \frac{\text{RMSB} - \text{RMSP}}{\text{RMSB}} \right| < \epsilon \quad (8-168)$$

where

$\text{RMSB} \sim$  the smallest RMS achieved compared with all previous iterations

$\epsilon \sim$  the improvement ratio criterion specified by input

#### 8.6.4 Weighted Least Squares and Filter Statistics

Upon completion of each iteration of the weighted least squares fit or after a specified set of observations has been filtered, a summary of the observation

residual statistics is calculated and printed. The statistical quantities that comprise the summary are computed for data types and residual groups which contain data from specific tracking stations. The following abbreviations are used in the statistical relationships

$\overline{\Delta y_j} \sim$  the  $j^{\text{th}}$  residual,  $y_j - f[\hat{x}_i(t_j), \bar{z}_0]$

$n_s \sim$  the total number of residuals for a station and data type (group).

- Root Mean Square Error

The total weighted RMS, the predicted total RMSP, and the RMS for each station and data type are calculated from Equations (8-166) and (8-167). It is normally desirable that RMS be small, preferably zero.

- Group Mean

The mean value of each residual group is a measure of the bias in the observation and is calculated as follows

$$\bar{m} = \frac{1}{n_s} \sum_{j=1}^{n_s} \overline{\Delta y_j} \quad (8-169)$$

It is desirable that  $\bar{m}$  for each group be zero to be consistent with the assumption in Equation (8-27a) that the measurement noise has zero mean.

- Sum of Squares About Mean

The sum of the squares of the residuals about the mean of each residual group is

$$S = \sum_{j=1}^{n_s} (\overline{\Delta y_j} - \bar{m})^2 \quad (8-170)$$

- Sample Standard Deviation

The sample standard deviation of each residual group is a measure of the dispersion of the observation data and is calculated as follows

$$\sigma = \left( \frac{1}{n_s - 1} \sum (\bar{\Delta y}_j - \bar{m})^2 \right)^{1/2} = \left( \frac{S}{n_s - 1} \right)^{1/2} \quad (8-171)$$

In GTDS the approximation is made that  $n_s$  is large. Hence,  $n_s - 1$  is replaced by  $n_s$  in the denominator of Equation (8-171). The standard deviation should be consistent with the values used in the a priori weighting matrix  $W$ .

- Confidence Interval for Group Mean

If the observation residual group population is normally distributed with zero mean, then the variable

$$t = \frac{\bar{m}_i}{\sqrt{\sigma^2/n_s}} \quad (8-172)$$

has a t-distribution (Student's) with  $(n_s - 1)$  degrees of freedom. Therefore, confidence intervals for the mean can be constructed from tables of the t-distribution. As  $n_s$  becomes large, the t-distribution approaches the normal distribution.

- Observation Residual Groups

For each iteration of the weighted least squares fit, or after a specified set of observations has been filtered, the following data are printed for each residual group:

- the number of observations  $n_s$
- the number of rejected and accepted observations
- the histograms of observations by true anomaly

## 8.7 REFERENCES

1. Schmidt, S. F.: 1966, "The Application of State Space Methods to Navigation Problems," Advances in Control Systems, Vol. 3, (C. T. Leondes, ed.), Academic Press, New York.
2. Deutsch, R.: 1965, Estimation Theory, Prentice-Hall, Englewood Cliffs, N. J.
3. Doob, J. L.: 1963, Stochastic Processes, John Wiley and Sons, New York.
4. De Salima, T. H.: 1970, Houston Operations Predictor/Estimator (HOPE) Engineering Manual, Goddard Space Flight Center Report 70-FMT-792A, June 1970.
5. Tonies, C. C. et. al.: 1966, TRACE Orbit Determination Program, Version D, Air Force Systems Command Report TP-669(9990)-3, September 1966.
6. Jazwinski, A. H.: 1970, Stochastic Processes and Filtering Theory, Academic Press, New York.
7. Analytic Sciences Corporation: 1971, A Short Course on Kalman Filter Theory and Application, Reading, Massachusetts.
8. Kalman, R. E.: 1960, "New Methods and Results in Linear Prediction and Filtering Theory," Symposium on Engineering Applications of Random Function Theory and Probability, Purdue University, West Lafayette, Indiana, November 1960.
9. Andrews, A.: 1968, "A Square Root Formulation of the Kalman Covariance Equations," AIAA Journal, Vol. 6, June 1968, pp. 1165-1166.
10. Fitzgerald, R. J.: 1971, "Divergence of the Kalman Filter," IEEE Transactions on Automatic Control, Vol. 16, No. 6, December 1971, pp. 736-747.
11. Torroglosa, V.: 1973, Filtering Theory Applied to Orbit Determination, Goddard Space Flight Center Report X-582-73-379, December 1973.
12. Ingram, D. S. and Tapley, B. D.: 1974, "Lunar Orbit Determination in the Presence of Unmodeled Accelerations," Celestial Mechanics, Vol. 9, pp. 191-211.
13. Tapley, B. D. and Ingram, D. S.: 1973, "Orbit Determination in the Presence of Unmodeled Accelerations," IEEE Transactions on Automatic Control, Vol. 18, No. 4 August 1973, pp. 369-373.

14. Tapley, B. D. and Schutz, B. E.: 1974, Estimation of Unmodeled Forces on a Lunar Satellite, Department of Aerospace Engineering and Engineering Mechanics, University of Texas, Austin, Texas.
15. Jazwinski, A. H.: 1973, "Adaptive Sequential Estimation with Applications," Fifth IFAC Symposium on Automatic Control in Space, Genoa, Italy, June 1973; work done under NASA contracts NAS 8-26973 and NAS 5-22011.
16. Sage, A. P. and Husa, G. W.: 1969, "Algorithms for Sequential Adaptive Estimation of Prior Statistics," Information and Control Sciences Center, Southern Methodist University, Dallas, Texas; work done under Air Force Contract F44620-68-C-0023.

## CHAPTER 9

## EARLY ORBIT METHODS

The estimator algorithm in the Goddard Trajectory Determination System (GTDS) requires an a priori estimate of the spacecraft position and velocity in order to initiate the iterative estimation process (see Chapter 8). An accurate estimate is frequently unavailable because of large booster injection errors, maneuver errors, or unknown orbits of tracked satellites. GTDS has been provided with the capability to determine a starting value of position and velocity from a limited number of discrete tracking data samples.

Three techniques are optionally provided to perform this function. They are as follows:

- The Gauss Method and Double r-Iteration Method – These deterministic methods use three sets of chronologically ordered gimbal angle observation pairs to solve for the six Cartesian position and velocity components at an epoch time equal to that of the second observation. The gimbal angle observation sets need not be from the same tracking station. The central angle (from the earth's center) subtended by the three sets of angles should be less than 60 degrees for the Gauss Method and less than 360° for the Double r Method. Either X and Y or A and E gimbal angle data from GRARR, ATSR, USB or C-Band Systems,  $\ell$ - and  $m$ -direction cosines from the Minitrack System, or geocentric right ascension  $\alpha$  and declination  $\delta$  observations can be used.
- The Range and Angles Method – This method uses multiple (more than two) sets of simultaneously measured range and gimbal angle data from the GRARR, ATSR, USB or C-Band radar systems. Two-body equations are regressively fitted to the transformed data to yield epoch values of the spacecraft position and velocity.

## 9.1 ANGLES ONLY METHODS

Both the Gauss Method and the Double r-Iteration Method use three sets of chronologically ordered gimbal angle measurements from up to three separate tracking stations to determine the Cartesian components of position and velocity. The angle data set can be distributed over an orbital arc of less than 60 degrees in mean anomaly for the Gauss Method and up to 360° in mean anomaly for the



Double r-Iteration Method. The epoch for the position and velocity corresponds to the time of the second observation set. The methods are deterministic since the six measurement components yield the six position and velocity components. Additional descriptions of these methods are presented in Reference 1.

### 9.1.1 Transformation of Topocentric Gimbal Angles to Inertial Coordinates

All gimbal angles are initially transformed to topocentric station centered azimuth A and elevation angle E. The  $X_{30}$  and  $Y_{30}$  angles corresponding to the GRARR and USB 30 foot antennas are transformed by

$$\begin{aligned}\sin E &= \cos X_{30} \cos Y_{30} \\ \cos E &= \sqrt{1 - \sin^2 E}\end{aligned}\quad \left(0 \leq E \leq \frac{\pi}{2}\right) \quad (9-1a)$$

and

$$\begin{aligned}\sin A &= \sin X_{30} \cos Y_{30} / \cos E \\ \cos A &= \sin Y_{30} / \cos E\end{aligned}\quad (0 \leq A \leq 2\pi) \quad (9-1b)$$

The  $X_{85}$  and  $Y_{85}$  angles corresponding to the USB 85 foot antennas are transformed by

$$\begin{aligned}\sin E &= \cos Y_{85} \cos X_{85} \\ \cos E &= \sqrt{1 - \sin^2 E}\end{aligned}\quad \left(0 \leq E \leq \frac{\pi}{2}\right) \quad (9-1c)$$

$$\begin{aligned}\sin A &= \sin Y_{85} / \cos E \\ \cos A &= -\cos Y_{85} \sin X_{85} / \cos E\end{aligned}\quad (0 \leq A \leq 2\pi) \quad (9-1d)$$

The direction cosines  $\ell$  and  $m$  are transformed by

$$\cos E = \sqrt{\ell^2 + m^2} \quad \left(0 \leq E \leq \frac{\pi}{2}\right) \quad (9-2a)$$

and

$$\begin{aligned} \sin A &= \ell / \cos E \\ (0 \leq E \leq 2\pi) \\ \cos A &= m / \cos E. \end{aligned} \quad (9-2b)$$

The C-Band radar gimbal angles are directly measured as  $A$  and  $E$ , and the resulting angle sets are denoted by  $(t, A, E)$ . The altitude above the reference earth ellipsoid, the geodetic latitude, and longitude of the tracking station measuring the angle set are denoted by  $(h_s, \phi_s, \lambda_s)$ . The unit vector directed toward the spacecraft can be written in topocentric local tangent coordinates as follows.

$$\hat{L}_{1t} = \begin{bmatrix} \cos E \sin A \\ \cos E \cos A \\ \sin E \end{bmatrix} \quad (9-3)$$

The tracking station coordinates, expressed in body-fixed axes, are presented in Section 3.3.7 as

$$\bar{r}_{s_b} = \begin{bmatrix} (N_s + h_s) \cos \phi_s \cos \lambda_s \\ (N_s + h_s) \cos \phi_s \sin \lambda_s \\ [N_s + h_s - (2f - f^2) N_s] \sin \phi_s \end{bmatrix} \quad (9-4)$$

where

$$N_s = \frac{R_e}{\sqrt{1 - (2f - f^2) \sin^2 \phi_s}} \quad (9-5)$$

and

$R_e \sim$  earth's equatorial radius  
 $f \sim$  earth's flattening coefficient

Both the  $\hat{L}_{1t}$  and  $\hat{r}_{sb}$  vectors are transformed to a common inertial Cartesian axes system, either true of reference date or mean of 1950.0. The transformations, presented in Sections 3.3.1, 3.3.2, and 3.3.7, follow. The matrix  $M_{1t}^T$  from Section 3.3.7 transforms from the topocentric local tangent system to the body-fixed system and is a function of the station's latitude and longitude, i.e.,

$$\hat{L}_b = M_{1t}^T \hat{L}_{1t} \quad (9-6)$$

where

$$M_{1t} = \begin{bmatrix} -\sin \lambda_s & \cos \lambda_s & 0 \\ -\sin \phi_s \cos \lambda_s & -\sin \phi_s \sin \lambda_s & \cos \phi_s \\ \cos \phi_s \cos \lambda_s & \cos \phi_s \sin \lambda_s & \sin \phi_s \end{bmatrix} \quad (9-7)$$

The matrix  $B^T$ , from Section 3.3.2.3, transforms from the body-fixed system to the true of date system and is normally a function of the Greenwich sidereal time and polar motion. Polar motion is neglected for early orbit application (from considerations of precision). The transformation is as follows

$$\hat{L}_T = \begin{bmatrix} \cos \delta_t & \cos \alpha_t \\ \cos \delta_t & \sin \alpha_t \\ \sin \delta_t \end{bmatrix} = B^T(\alpha_g) \hat{L}_b \quad (9-8)$$

and

$$\hat{r}_s = B^T(\alpha_g) \hat{r}_{sb} \quad (9-9)$$

where

$$B^T = \begin{bmatrix} \cos \alpha_g & -\sin \alpha_g & 0 \\ \sin \alpha_g & \cos \alpha_g & 0 \\ 0 & 0 & 1 \end{bmatrix} \quad (9-10)$$

and

- $\alpha_t \sim$  topocentric right ascension of spacecraft from true-of-date equinox
- $\delta_t \sim$  topocentric declination of spacecraft from true-of-date equator
- $\alpha_g \sim$  Greenwich sidereal time at measurement time  $t$  (see Equation (3-19)).

Equations (9-6) and (9-8) can be combined resulting in a single transformation matrix  $M_{1t}$  identical to that in Equation (9-7), with  $\lambda_s$  replaced by  $(\lambda_s + \alpha_g)$ , the longitude measured from the true vernal equinox. The unit vector  $\hat{L}_T$  in Equation (9-8) can be solved for the topocentric right ascension  $\alpha_t$  and declination  $\delta_t$ . Should observations of the topocentric right ascension and declination be available, they can be used to replace the topocentric gimbal angles and determine  $\hat{L}_T$  directly from Equation (9-8). The matrix  $C^T$  from Section 3.3.1.3 transforms from the true of date system to the mean of 1950.0 system and accounts for nutation and precession. The resulting transformation is

$$\hat{L} = C^T \hat{L}_T \quad (9-11)$$

$$\bar{R}_s = C^T \bar{r}_s \quad (9-12)$$

where  $C^T$  is the product of the precession transformation  $A(\zeta_0, \theta_p, \xi_p)$  and the nutation transformation  $N(\delta\epsilon, \delta\psi)$  as follows

$$C^T = (NA)^T \quad (9-13)$$

The elements of the summation matrix  $C^T$  are obtained from an ephemeris file in GTDS as a function of time from 1950.0.

Combining the preceding transformations,

$$\hat{L} = (M_{1t} B C)^T \hat{L}_{1t} \quad (9-14)$$

and

$$\bar{R}_s = (BC)^T \bar{r}_s \quad (9-15)$$

Equations (9-14) and (9-15) present the transformations necessary when the computations are performed in the mean of 1950.0 system. Specifying  $C = I$  permits the vectors to be transformed to the true of reference date system.

In the following sections three sets of gimbal angles, obtained at times  $t_1, t_2$  and  $t_3$ , are available from either the same or different stations. Station vectors and unit vectors directed towards the spacecraft,  $(\bar{R}_{s1}, \hat{L}_1)$ ,  $(\bar{R}_{s2}, \hat{L}_2)$  and  $(\bar{R}_{s3}, \hat{L}_3)$ , can be determined from Equations (9-3), (9-14), and (9-15) for each gimbal angle set.

### 9.1.2 Gauss Method

The Gauss Method utilizes the geometric properties of the station positions and station-to-spacecraft unit vectors, in conjunction with an approximation of the orbital dynamics, to determine an estimate of the spacecraft's position at time  $t_2$ . The orbital dynamics are approximated by the low order terms of the  $f$  and  $g$  series, therefore limiting the orbital arc of the angular observations to be within approximately  $60^\circ$  in mean anomaly. Subsequently, the accuracy of the position vector is iteratively improved, and the velocity vector determined by the method of Gibbs. This method utilizes the approximately known position vectors at the three observation times to determine a velocity vector at time  $t_2$ . Knowing the velocity allows one higher order term to be included in the  $f$  and  $g$  series and thereby improves the spacecraft position determination.

The geocentric inertial position vector  $\bar{R}_i$  can be determined from the known vectors  $\hat{L}_i$  and  $\bar{R}_{s_i}$  and the unknown slant range  $\rho_i$  from the station to the spacecraft as follows (see Figure 9-1).

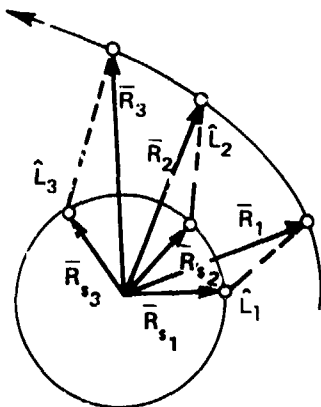


Figure 9-1. Position Vector Geometry

$$\bar{R}_i = \bar{R}_{s_i} + \rho_i \hat{L}_i \quad (i = 1, 2, 3) \quad (9-16)$$

The three vectors  $\bar{R}_1$ ,  $\bar{R}_2$  and  $\bar{R}_3$  are coplanar since they all lie in the same orbit plane. Therefore,  $\bar{R}_2$  can be written as a linear combination of  $\bar{R}_1$  and  $\bar{R}_3$  as follows

$$C_1 \bar{R}_1 + C_2 \bar{R}_2 + C_3 \bar{R}_3 = 0 \quad (9-17)$$

where

$$C_2 = -1 \quad (9-18)$$

Substituting Equation (9-16) into Equation (9-17) yields

$$C_1 \rho_1 \hat{L}_1 + C_2 \rho_2 \hat{L}_2 + C_3 \rho_3 \hat{L}_3 = - (C_1 \bar{R}_{s_1} + C_2 \bar{R}_{s_2} + C_3 \bar{R}_{s_3}) \quad (9-19)$$

or, in matrix form

$$L \begin{bmatrix} C_1 \rho_1 \\ C_2 \rho_2 \\ C_3 \rho_3 \end{bmatrix} = - R_s \begin{bmatrix} C_1 \\ C_2 \\ C_3 \end{bmatrix} \quad (9-20)$$

where

$$L = \begin{bmatrix} \hat{L}_1 & \hat{L}_2 & \hat{L}_3 \end{bmatrix} \quad \text{and} \quad R_s = \begin{bmatrix} \bar{R}_{s_1} & \bar{R}_{s_2} & \bar{R}_{s_3} \end{bmatrix} \quad (9-21)$$

Premultiplying Equation (9-20) by  $L^{-1}$  yields

$$\begin{bmatrix} C_1 \rho_1 \\ C_2 \rho_2 \\ C_3 \rho_3 \end{bmatrix} = -D \begin{bmatrix} C_1 \\ C_2 \\ C_3 \end{bmatrix} \quad (9-22)$$

where

$$D = L^{-1} R_s \quad (9-23)$$

The preceding three scalar equations involve the five unknown variables  $C_1$ ,  $C_2$ ,  $\rho_1$ ,  $\rho_2$  and  $\rho_3$ . Additional conditions must be imposed to determine the slant ranges  $\rho_1$ ,  $\rho_2$  or  $\rho_3$ . Knowing any one of these ranges, a geocentric position vector  $\bar{R}_1$ ,  $\bar{R}_2$  or  $\bar{R}_3$  can be determined from Equation (9-16).

The cross product of  $\bar{R}_1$  and  $\bar{R}_2$  with Equation (9-17) yields

$$\begin{aligned} \bar{R}_1 \times \bar{R}_2 &= C_3 \bar{R}_1 \times \bar{R}_3 \\ \bar{R}_3 \times \bar{R}_2 &= C_1 \bar{R}_3 \times \bar{R}_1 \end{aligned} \quad (9-24)$$

Dotting  $\hat{k}$ , the unit vector normal to the orbital plane in the direction of the angular momentum, into Equation (9-24) gives

$$C_3 = \frac{\hat{k} \cdot (\bar{R}_1 \times \bar{R}_2)}{\hat{k} \cdot (\bar{R}_1 \times \bar{R}_3)} \quad (9-25)$$

$$C_1 = \frac{\hat{k} \cdot (\bar{R}_2 \times \bar{R}_3)}{\hat{k} \cdot (\bar{R}_1 \times \bar{R}_3)}$$

The position vectors can next be expressed in terms of the f and g series representation for two-body motion (Reference 2). The series is expanded about  $t_2$ , the time of the second observation, as follows

$$\bar{R}_i = f_i \bar{R}_2 + g_i \bar{R}_2 \quad (9-26)$$

where

$$f_i \equiv 1 - \frac{1}{2} u_2 \tau_i^2 - \frac{1}{6} \dot{u}_2 \tau_i^3 - \frac{1}{24} (\ddot{u}_2 - u_2^2) \tau_i^4 - \frac{1}{120} (\dddot{u}_2 - 4u_2 \dot{u}_2) \tau_i^5 - \dots \quad (9-27a)$$

$$g_i \equiv \tau_i - \frac{1}{6} u_2 \tau_i^3 - \frac{1}{12} \dot{u}_2 \tau_i^4 - \frac{1}{120} (3\ddot{u}_2 - u_2^2) \tau_i^5 - \dots \quad (9-27b)$$

and

$$\tau_i = t_i - t_2 \quad (9-28)$$

$$u_2 = \frac{\mu}{R_2^3} \quad (9-29)$$

where

$\mu \sim$  gravitational parameter for the earth

Substituting  $\bar{R}_1$  and  $\bar{R}_3$  from Equation (9-26) into Equation (9-25) yields

$$C_1 = \frac{g_3}{f_1 g_3 - f_3 g_1} \quad (9-30)$$

$$C_3 = \frac{-g_1}{f_1 g_3 - f_3 g_1}$$

Approximating  $f_1, f_3, g_1$  and  $g_3$  by

$$f_i = 1 - \frac{1}{2} u_2 \tau_i^2 + O(\tau_i^3) \quad (9-31)$$

$$g_i = \tau_i - \frac{1}{6} u_2 \tau_i^3 + O(\tau_i^4) \quad (i = 1, 3)$$



Equation (9-30) becomes

$$\begin{aligned} C_1 &= a_1 + b_1 u_2 \\ C_3 &= a_3 + b_3 u_2 \end{aligned} \quad (9-32)$$

where

$$a_1 = \frac{\tau_3}{\tau_3 - \tau_1} \quad b_1 = \frac{\tau_3}{6(\tau_3 - \tau_1)} [(\tau_3 - \tau_1)^2 - \tau_3^2] \quad (9-33)$$

$$a_3 = -\frac{\tau_1}{\tau_3 - \tau_1} \quad b_3 = -\frac{\tau_1}{5(\tau_3 - \tau_1)} [(\tau_3 - \tau_1)^2 - \tau_1^2]$$

Substituting Equation (9-32) into (9-22) gives

$$\begin{bmatrix} (a_1 + b_1 u_2) \rho_1 \\ -\rho_2 \\ (a_3 + b_3 u_2) \rho_3 \end{bmatrix} = -D \left\{ \begin{bmatrix} a_1 \\ -1 \\ a_3 \end{bmatrix} + \begin{bmatrix} b_1 \\ 0 \\ b_3 \end{bmatrix} u_2 \right\} \quad (9-34)$$

The preceding three scalar equations involve the four unknown variables  $\rho_1$ ,  $\rho_2$ ,  $\rho_3$  and  $u_2$ .

Dotting Equation (9-16) with itself (for  $i = 2$ ) yields

$$R_2^2 = \rho_2^2 + \rho_2 C_\psi + R_{s_2}^2 \quad (9-35)$$

where

$$C_\psi = 2 \hat{L}_2 \cdot \bar{R}_{s_2} \quad (9-36)$$

is known. The second scalar equation of Equation (9-34) is

$$\rho_2 = d_1^* + d_2^* \frac{\mu}{R_2^3} \quad (9-37)$$

where

$$\begin{aligned} d_1^* &= d_{21} a_1 - d_{22} + d_{23} u_3 \\ d_2^* &= d_{21} b_1 + d_{23} b_3 \end{aligned} \quad (9-38)$$

and the matrix D contains the elements  $(d_{ij})$ .

Substituting Equation (9-37) into (9-35) gives

$$R_2^2 = \left( d_1^* + d_2^* \frac{\mu}{R_2^3} \right)^2 + \left( d_1^* + d_2^* \frac{\mu}{R_2^3} \right) C_\psi + R_{s_2}^2 \quad (9-39)$$

or

$$R_2^8 - (d_1^2 + d_1 C_\psi + R_{s_2}^2) R_2^6 - \mu (d_2^* C_\psi + 2d_1^* d_2^*) R_2^3 - \mu^2 d_2^{*2} = 0 \quad (9-40)$$

Solving the preceding equation for its real positive root yields  $R_2$ , which, from Equation (9-29), determines  $u_2$ . Equation (9-34) can then be solved for  $\rho_1$ ,  $\rho_2$  and  $\rho_3$ , and, finally, Equation (9-16) can be solved for  $\bar{R}_1$ ,  $\bar{R}_2$  and  $\bar{R}_3$ . This sequence of computations is summarized in Figure 9-2. The resulting position vectors are only approximately correct because of the truncation of the f and g series to get Equations (9-31).

The accuracy of the position can be improved and the velocity vector computed by the method of Gibbs (Reference 1). This method utilizes the three approximately known position vectors  $\bar{R}_1$ ,  $\bar{R}_2$  and  $\bar{R}_3$  to determine the velocity  $\dot{\bar{R}}_2$ . This allows an additional term to be retained in the f and g series.

The position vectors  $\bar{R}_1$  and  $\bar{R}_3$  can be obtained from a Taylor series expansion about  $\bar{R}_2$  as follows

$$\bar{R}_i = \bar{R}_2 + \dot{\bar{R}}_2 \tau_i + \ddot{\bar{R}}_2 \frac{\tau_i^2}{2} + \dddot{\bar{R}}_2 \frac{\tau_i^3}{6} \quad (9-41)$$

The vector differences  $(\bar{R}_1 - \bar{R}_2)$  and  $(\bar{R}_3 - \bar{R}_2)$  can be obtained from Equation (9-41). Multiplying  $(\bar{R}_1 - \bar{R}_2)$  by  $-\tau_3^2$  and adding to  $(\bar{R}_3 - \bar{R}_2)$  multiplied by  $\tau_1^2$  yields

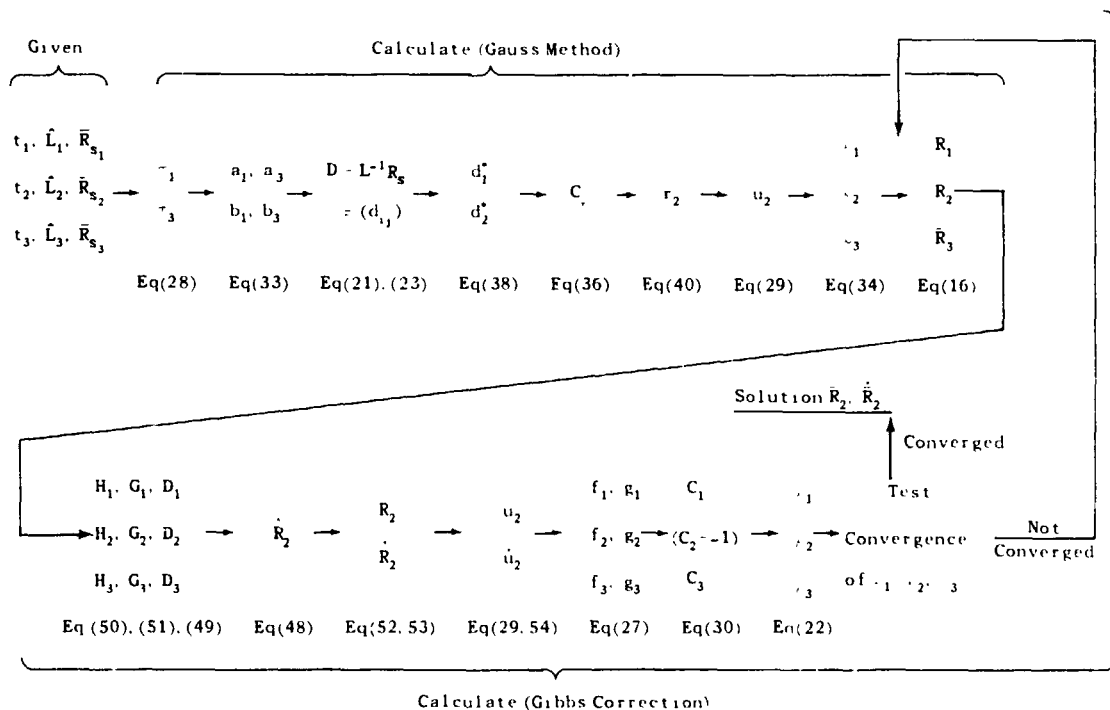


Figure 9-2. Gauss Method Computational Sequence

$$\begin{aligned}
 & -\tau_3^2 \bar{R}_1 + (\tau_3^2 - \tau_1^2) \bar{R}_2 + \tau_2^2 \bar{R}_3 \\
 & = -\tau_1 \tau_2 \tau_{13} \left[ \ddot{\bar{R}}_2 - \tau_2 \tau_3 \frac{\ddot{\bar{R}}_2}{6} - \tau_1 \tau_3 (\tau_3 + \tau_1) \frac{\bar{R}_2^{(IV)}}{24} + \dots \right] \quad (9-42)
 \end{aligned}$$

where

$$\tau_{13} = \tau_3 - \tau_1 \quad (9-43)$$

Differentiating twice gives

$$-\tau_3^2 \ddot{\bar{R}}_1 + (\tau_3^2 - \tau_1^2) \ddot{\bar{R}}_2 + \tau_1^2 \ddot{\bar{R}}_3 = -\tau_1 \tau_3 \tau_{13} \ddot{\bar{R}}_2 + 0 (\bar{R}_2^{(IV)}) \quad (9-44)$$

Multiplying  $(\bar{R}_1 - \bar{R}_2)$  by  $\tau_3$  and  $(\bar{R}_3 - \bar{R}_2)$  by  $-\tau_1$ , adding the results and differentiating twice yields

REPRODUCIBILITY OF THE  
ORIGINAL PAGE IS POOR

$$\tau_3 \ddot{\bar{R}}_1 - \tau_{13} \ddot{\bar{R}}_2 - \tau_1 \ddot{\bar{R}}_3 = -\tau_1 \tau_3 \tau_{13} \frac{\bar{R}_2^{(IV)}}{2} + O(\bar{R}_2^{(IV)}) \quad (9-45)$$

Solving Equations (9-44) and (9-45) for  $\ddot{\bar{R}}_2$  and  $\bar{R}_2^{(IV)}$  and substituting them into Equation (9-42) gives

$$\begin{aligned} & -\tau_3^2 \bar{R}_1 + (\tau_3^2 - \tau_1^2) \bar{R}_2 + \tau_1^2 \bar{R}_3 \\ & = -\tau_1 \tau_2 \tau_{13} \left[ \dot{\bar{R}}_2 - \tau_3 \frac{\ddot{\bar{R}}_1}{12} + (\tau_3 - \tau_1) \frac{\ddot{\bar{R}}_2}{12} - \tau_1 \frac{\ddot{\bar{R}}_3}{12} \right] \end{aligned} \quad (9-46)$$

Substituting the inverse-square law

$$\ddot{\bar{R}}_i = -\mu \frac{\bar{R}_i}{R_i^3} \quad (i = 1, 2, 3) \quad (9-47)$$

into Equation (9-46) and rearranging terms yields

$$\dot{\bar{R}}_2 = -D_1 \bar{R}_1 + D_2 \bar{R}_2 + D_3 \bar{R}_3 \quad (9-48)$$

where

$$D_i = G_i + \frac{H_i}{R_i^3} \quad (i = 1, 2, 3) \quad (9-49)$$

with

$$H_1 = \frac{\mu \tau_3}{12}, \quad H_3 = -\frac{\mu \tau_1}{12}, \quad H_2 = H_1 - H_3 \quad (9-50)$$

$$G_1 = -\frac{\tau_3}{\tau_1 \tau_{13}}, \quad G_3 = -\frac{\tau_1}{\tau_3 \tau_{13}}, \quad G_2 = G_1 - G_3 \quad (9-51)$$

Knowing  $\bar{R}_2$  and  $\dot{\bar{R}}_2$  from Equations (9-40) and (9-48),  $R_2$  and its time derivative  $\dot{R}_2$  are obtained from

$$R_2 = \sqrt{\bar{R}_2 \cdot \dot{\bar{R}}_2} \quad (9-52)$$

and

$$\dot{R}_2 = \frac{\bar{R}_2 \cdot \dot{\bar{R}}_2}{R_2} \quad (9-53)$$

Then  $u_2$  can be determined from Equation (9-29), and  $\dot{u}_2$  can be determined as follows

$$\dot{u}_2 = -\frac{3\mu}{R_2^2} \dot{R}_2 \quad (9-54)$$

Knowing  $\dot{u}_2$  from the preceding equation permits one higher order term to be included in the  $f$  and  $g$  series in Equation (9-27). An improved determination of  $\bar{R}_2$  is thereby obtained by iteratively solving Equation (9-27) for  $f_i$  and  $g_i$  (including the higher order term); Equation (9-30) for  $C_1$  and  $C_3$ ; and Equation (9-22) for  $\rho_1$ ,  $\rho_2$  and  $\rho_3$ . After converging on  $\rho_1$ ,  $\rho_2$  and  $\rho_3$ , Equation (9-16) is solved for  $\bar{R}_2$  and Equation (9-48) is solved for  $\dot{\bar{R}}_2$ . The computation sequence is shown schematically in Figure 9-2.

### 9.1.3 Double r-Iteration Method

The Double r-Iteration method requires an initial guess of the magnitudes  $R_1$  and  $R_2$ . Then the geometric relations of the three station positions and station-to-spacecraft unit vectors are used in conjunction with the orbital dynamics to determine the time intervals  $\tau'_1$  (between the first and second observations) and  $\tau'_3$  (between the third and second observations). A standard Newton-Raphson successive approximation scheme is then used to correct  $R_1$  and  $R_2$  to match  $\tau'_1$  and  $\tau'_3$  to the known intervals  $\tau_1$  and  $\tau_3$ .

The Double r-Iteration method can be used when the angle data is spread out over a considerable arc in eccentric anomaly whereas the Gauss method is unreliable and may not converge over large arcs.

From Figure 9-1 and Equation (9-16), the slant range vector from the station to the spacecraft is

$$\bar{\rho}_i = \bar{R}_i - \bar{R}_{s_i} \quad (i = 1, 2, 3) \quad (9-55)$$

Dotting Equation (9-16) with itself yields Equation (9-35) rewritten for the  $i^{\text{th}}$  observation as follows

$$\rho_i^2 + \rho_i C_{\psi_i} + (R_{s_i}^2 - R_i^2) = 0 \quad (i = 1, 2, 3) \quad (9-56)$$

where

$$C_{\psi_i} = 2\hat{L}_i \cdot \bar{R}_{s_i} \quad (i = 1, 2, 3) \quad (9-57)$$

Solving Equation (9-56) for  $\rho_1$  and  $\rho_2$  by means of the Binominal Theorem gives

$$\rho_i = \frac{1}{2} \{-C_{\psi_i} + \sqrt{C_{\psi_i}^2 - 4(R_{s_i}^2 - R_i^2)}\} \quad (9-58)$$

where the positive sign on the radical is known to yield the correct root from physical considerations. Initially estimating  $R_1$  and  $R_2$ , Equation (9-58) can be solved for  $\rho_1$  and  $\rho_2$ , and Equation (9-16) for  $\bar{R}_1$  and  $\bar{R}_2$ . Knowing  $\bar{R}_1$  and  $\bar{R}_2$  merely defines the orbit plane (in terms of  $\Omega$  and  $i$ ) and two position vectors in this plane. However, there are numerous orbits (in terms of  $a$  and  $e$ ) which satisfy the two position vectors  $\bar{R}_1$  and  $\bar{R}_2$ . Therefore, a third position vector, along with orbital dynamics relationships, are necessary to uniquely determine the orbit being observed.

The quantity  $\hat{k}$  is defined as the unit vector perpendicular to the orbit plane, i.e.,

$$\hat{k} = \frac{\bar{R}_1 \times \bar{R}_2}{R_1 R_2} \quad (9-59)$$

Then, since the third position vector  $\bar{R}_3$  must lie in the orbital plane,

$$\bar{R}_3 \cdot \hat{k} = 0 \quad (9-60)$$

Substituting Equation (9-16) into Equation (9-60) yields

$$\rho_3 = \frac{\bar{R}_3 \cdot \hat{k}}{\hat{L}_3 \cdot \hat{k}} \quad (9-61)$$

Knowing  $\rho_3$ , the geocentric vector  $\bar{R}_3$  can be obtained from Equation (9-16). Note that when  $\bar{\rho}_3$  lies in the orbit plane,  $\bar{R}_3$  and  $\hat{L}_3$  are perpendicular to  $\hat{k}$  and Equation (9-61) is singular. Should such a singularity occur, a different observation time  $t_3$  must be used. Thus the vectors  $\bar{R}_1$ ,  $\bar{R}_2$  and  $\bar{R}_3$  have to be determined as functions of the estimated vector magnitudes  $R_1$  and  $R_2$ .

The difference in the true anomalies can be determined as follows

$$\cos(f_j - f_k) = \frac{\bar{R}_j \cdot \bar{R}_k}{R_j R_k} \quad (9-62a)$$

$$\sin(f_j - f_k) = m \sqrt{1 - \cos^2(f_j - f_k)} \quad (j, k = 1, 2, 3) \quad (9-62b)$$

where  $f$  denotes the true anomaly and

$$m = \pm \frac{X_k Y_j - X_j Y_k}{|X_k Y_j - X_j Y_k|} \quad (9-63)$$

where  $X_k$ ,  $Y_k$ ,  $Z_k$  are the components of  $\bar{R}_k$ ; the positive sign is used for direct orbits and the negative sign for retrograde orbits. In order to correct the estimated values of  $R_1$  and  $R_2$ , it is necessary to compute the resulting time intervals between  $(\bar{R}_3, \bar{R}_2)$  and  $(\bar{R}_1, \bar{R}_2)$  to obtain residuals as actual time differences. The semilatus rectum obtained from Gaussian sector to triangle theorem (Reference 1) is

$$p = \frac{R_1 + C_{r3} R_3 - C_{r1} R_2}{1 + C_{r3} - C_{r1}} \quad (9-64)$$

or, dividing the numerator and denominator by  $C_1$

$$p = \frac{C_1 R_1 + C_3 R_3 - R_2}{C_1 + C_3 - 1} \quad (9-65)$$

where

$$C_1 = \frac{R_2 \sin(f_3 - f_2)}{R_1 \sin(f_3 - f_1)} \quad C_3 = \frac{R_2 \sin(f_2 - f_1)}{R_3 \sin(f_3 - f_1)} \quad (9-66)$$

$$C_{r1} = \frac{R_1 \sin(f_3 - f_1)}{R_2 \sin(f_3 - f_2)} \quad C_{r3} = \frac{R_1 \sin(f_2 - f_1)}{R_3 \sin(f_3 - f_2)}$$

For very short observational arcs, both Equation (9-64) and Equation (9-65) are poorly determined, and the Gauss Method (Section 9.1.2) should be used. The singularity inherent in Equation (9-64) when  $f_3 - f_1 = \pi$  can be avoided, along with other numerical difficulties, by using Equation (9-65) when  $f_3 - f_1 \leq \pi$  and Equation (9-64) whenever  $f_3 - f_1 > \pi$ .

From Equation (3-183) the conic equation for true anomaly is

$$e \cos f_i = \frac{p}{R_i} - 1 \quad (i = 1, 2, 3) \quad (9-67)$$

Expanding factors of the form  $\sin(f_1 + f_2 + f_3)$  gives

$$e \sin f_1 = \frac{e \cos f_1 \cos(f_2 - f_1) - e \cos f_2}{\sin(f_2 - f_1)} \quad (9-68)$$

$$e \sin f_2 = \frac{-e \cos f_2 \cos(f_2 - f_1) + e \cos f_1}{\sin(f_2 - f_1)}$$

for  $(f_2 - f_1) \neq \pi$ , and

$$e \sin f_2 = \frac{e \cos f_2 \cos(f_3 - f_2) - e \cos f_3}{\sin(f_3 - f_1)} \quad (9-69)$$

$$e \sin f_3 = \frac{-e \cos f_3 \cos(f_3 - f_2) + e \cos f_2}{\sin(f_3 - f_1)}$$



for  $(f_3 - f_1) \neq \pi$ . From Equations (9-67) thru (9-69) the eccentricity can be determined as

$$e^2 = (e \cos f_2)^2 + (e \sin f_2)^2 \quad (9-70)$$

and the semimajor axis as

$$a = \frac{p}{(1 - e^2)} \quad (9-71)$$

For an elliptical orbit ( $e < 1$ ) the mean motion  $n$  is

$$n = \frac{1}{a} \sqrt{\frac{\mu}{a}} \quad (9-72)$$

and the eccentric anomaly  $E_i$  is

$$\sin E_i = \frac{R_i}{p} \sqrt{1 - e^2} \sin f_i \quad (9-73)$$

$$\cos E_i = \frac{R_i}{p} (e + \cos f_i) \quad (i = 1, 2, 3)$$

The preceding equation can be written as follows for the second observation point

$$S_e = [e \sin E_2] = \frac{R_2}{p} \sqrt{1 - e^2} [e \sin f_2] \quad (9-74)$$

$$C_e = [e \cos E_2] = \frac{R_2}{p} (e^2 + [e \cos f_2])$$

The following equations for differences in eccentric anomalies expressed as functions of true anomaly differences can be obtained by expanding Equation (9-73).

$$\sin(E_3 - E_2) = \frac{R_3}{\sqrt{ap}} \sin(f_3 - f_2) - \frac{R_3}{p} [1 - \cos(f_3 - f_2)] S_e \quad (9-75)$$

$$\cos(E_3 - E_2) = 1 - \frac{R_3 R_1}{ap} [1 - \cos(f_3 - f_2)]$$

$$\sin(E_2 - E_1) = \frac{R_1}{\sqrt{ap}} \sin(f_2 - f_1) - \frac{R_1}{p} [1 - \cos(f_2 - f_1)] S_e \quad (9-76)$$

$$\cos(E_2 - E_1) = 1 - \frac{R_2 R_1}{ap} [1 - \cos(f_2 - f_1)]$$

Kepler's equation (Equation (3-147)) is written as

$$M = E - e \sin E \quad (9-77)$$

where  $M$  is the mean anomaly. Mean anomaly differences about the second point can be written

$$M_3 - M_2 = E_3 - E_2 + 2 S_e \sin^2 \left( \frac{E_3 - E_2}{2} \right) - C_e \sin(E_3 - E_2) \quad (9-78)$$

$$M_1 - M_2 = E_1 - E_2 + 2 S_e \sin^2 \left( \frac{E_2 - E_1}{2} \right) + C_e \sin(E_2 - E_1)$$

The mean anomaly can also be written in terms of the mean motion as

$$M_i - M_2 = n(t_i - t_2) \quad (i = 1, 2, 3) \quad (9-79)$$

Rewriting the preceding equation for the time differences yields

$$\tau'_3 = \frac{M_3 - M_2}{n}, \quad \tau'_1 = \frac{M_1 - M_2}{n} \quad (9-80)$$

where  $\tau'_3$  and  $\tau'_1$  are defined by Equation (9-28). Equation (9-80) expresses the time differences between points 3 and 2 and between points 1 and 2 as functions of the geocentric position vector magnitudes  $R_1$  and  $R_2$ . This process is summarized in Figure 9-3.

The calculated time differences  $\tau'_1$  and  $\tau'_3$  will, in general, not agree with the ephemeris time differences  $\tau_1$  and  $\tau_3$  corresponding to the station observations. Thus  $R_1$  and  $R_2$  must be adjusted to obtain agreement between the calculated and actual time differences. A standard Newton-Raphson successive approximation procedure performs this adjustment as shown in Figure 9-3.

If the functions  $F_1$  and  $F_2$  are defined as follows,

$$F_1(R_1, R_2) = \tau_1 - \frac{M_1 - M_2}{n} \quad (9-81)$$

$$F_2(R_1, R_2) = \tau_3 - \frac{M_3 - M_2}{n}$$

the calculated and actual time differences will agree when  $F_1$  and  $F_2$  are zero. The algorithm for successively driving  $F_1$  and  $F_2$  to zero is obtained by linearizing Equations (9-81) about the estimated values of  $R_1$  and  $R_2$ , denoted  $R_{1i}$  and  $R_{2i}$ .

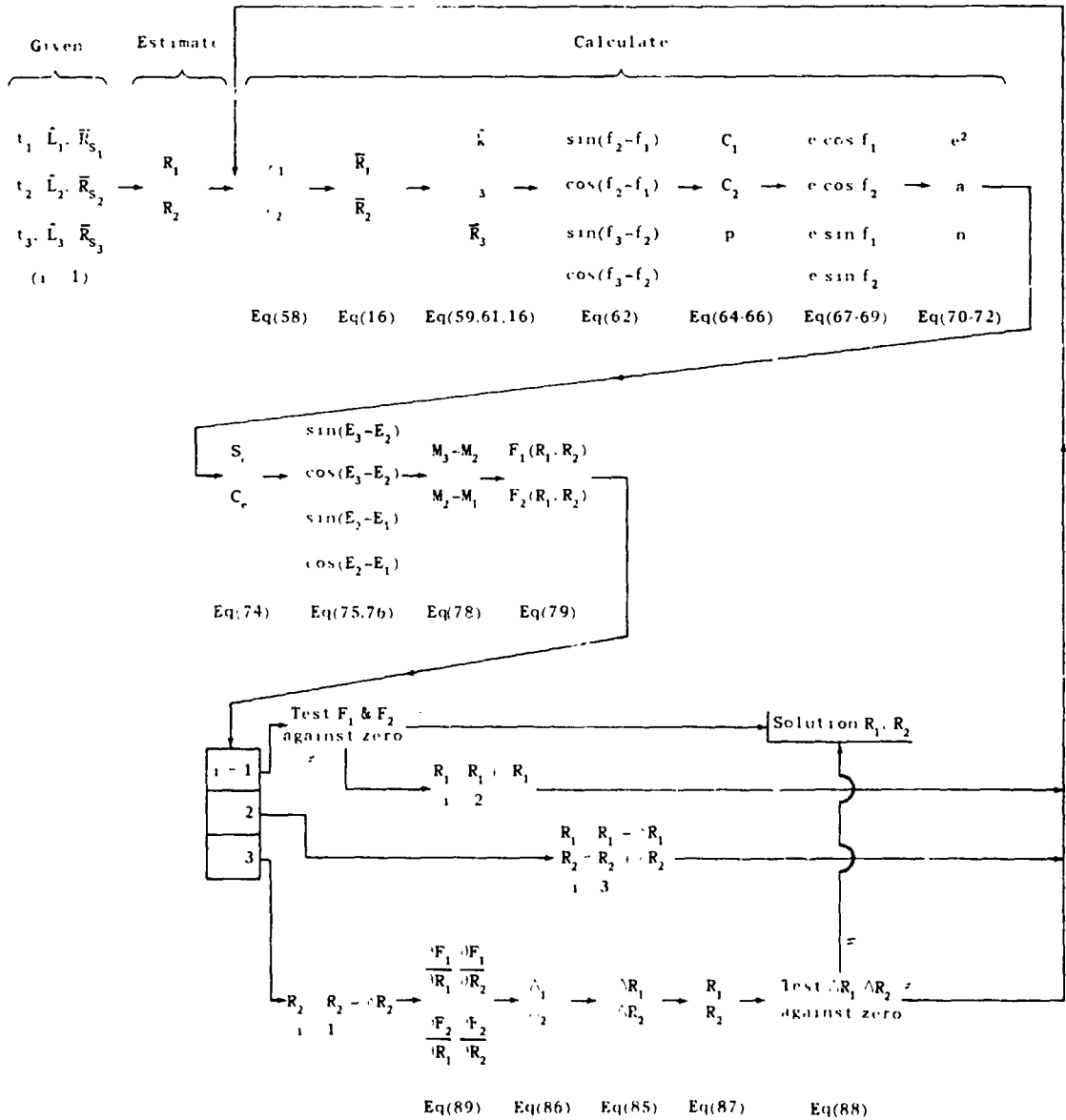


Figure 9-3. Double r-Iteration Computation Sequence

This linearization yields

$$\Delta F_1 = \frac{\partial F_1}{\partial R_1} \Delta R_1 + \frac{\partial F_1}{\partial R_2} \Delta R_2 \quad (9-82)$$

$$\Delta F_2 = \frac{\partial F_2}{\partial R_1} \Delta R_1 + \frac{\partial F_2}{\partial R_2} \Delta R_2$$

where

$$\Delta F_1 = F_{1_{i+1}} - F_{1_i} = F_{1_i} \quad (9-83)$$

$$\Delta F_2 = F_{2_{i+1}} - F_{2_i} = F_{2_i}$$

and

$$\Delta R_1 = R_{1_{i+1}} - R_{1_i} \quad (9-84)$$

$$\Delta R_2 = R_{2_{i+1}} - R_{2_i}$$

Solving Equation (9-82) simultaneously for  $\Delta R_1$  and  $\Delta R_2$ ,

$$\Delta R_1 = \frac{\Delta_1}{\Delta} \quad (9-85)$$

$$\Delta R_2 = \frac{\Delta_2}{\Delta}$$

where

$$\Delta_1 = \left( \frac{\partial F_1}{\partial R_2} \right) F_{2_i} - \left( \frac{\partial F_2}{\partial R_2} \right) F_{1_i} \quad (9-86)$$

$$\Delta_2 = \left( \frac{\partial F_2}{\partial R_1} \right) F_{1_i} - \left( \frac{\partial F_1}{\partial R_1} \right) F_{2_i}$$

and

$$\Delta = \left( \frac{\partial F_1}{\partial R_1} \right) \left( \frac{\partial F_2}{\partial R_2} \right) - \left( \frac{\partial F_1}{\partial R_2} \right) \left( \frac{\partial F_2}{\partial R_1} \right)$$

The corrections  $\Delta R_1$  and  $\Delta R_2$  are added to  $R_{1_i}$  and  $R_{2_i}$  to yield the  $i + 1^{\text{th}}$  approximation

$$R_{1_{i+1}} = R_{1_i} + \Delta R_1 \quad (9-87)$$

$$R_{2_{i+1}} = R_{2_i} + \Delta R_2$$

This process is repeated successively, incrementing  $i$  each time, until convergence is obtained. The convergence criteria are satisfied when the absolute values of the corrections are less than a prespecified tolerance  $\epsilon$ , i.e.,

$$|\Delta R_1| < \epsilon \quad (9-88)$$

$$|\Delta R_2| < \epsilon.$$

The partial derivatives required in Equations (9-86) are approximated by the one-sided finite difference approximations

$$\begin{aligned} \frac{\partial F_1}{\partial R_1} &\approx \frac{F_1(R_1 + \delta R_1, R_2) - F_1(R_1, R_2)}{\delta R_1} \\ \frac{\partial F_1}{\partial R_2} &\approx \frac{F_1(R_1, R_2 + \delta R_2) - F_1(R_1, R_2)}{\delta R_2} \\ \frac{\partial F_2}{\partial R_1} &\approx \frac{F_2(R_1 + \delta R_1, R_2) - F_2(R_1, R_2)}{\delta R_1} \\ \frac{\partial F_2}{\partial R_2} &\approx \frac{F_2(R_1, R_2 + \delta R_2) - F_2(R_1, R_2)}{\delta R_2} \end{aligned} \quad (9-89)$$

The converged solution for  $R_1$  and  $R_2$  yields the position vectors  $\bar{R}_1$ ,  $\bar{R}_2$ ,  $\bar{R}_3$  and all related variables in Figure (9-3). Therefore, the closed-form  $f$  and  $g$  coefficients (Reference 1) are

$$f = 1 - \frac{a}{R_2} [1 - \cos(E_3 - E_2)] \quad (9-90)$$

$$g = \tau_3 - \frac{1}{n} [E_3 - E_2 - \sin(E_3 - E_2)],$$

which yields the velocity vector

$$\dot{\bar{r}}_2 = \frac{\bar{r}_3 - f R_2}{g} \quad (9-91)$$

## 9.2 RANGE AND ANGLES METHOD

The Range and Angles Method determines spacecraft position and velocity by fitting two-body orbit relations to GRARR, C-Band or USB range and gimbal angle data in a regression manner.

A set of  $m$  chronologically ordered radar data vectors are available from the GRARR, C-Band and/or USB systems. Each vector consists of a range measurement and two gimbal angle measurements. The measurement vectors are first transformed to the station centered topocentric local tangent Cartesian coordinate system. The GRARR and USB angles,  $X$  and  $Y$ , are transformed to azimuth  $A$  and elevation angle  $E$ , as shown in Equation (9-1). The C-band data vectors and transformed GRARR and USB data vectors are then transformed to local tangent coordinates as follows

$$\bar{\rho}_{1t_i} = \begin{bmatrix} x_{1t} \\ y_{1t} \\ z_{1t} \end{bmatrix} = \rho_i \begin{bmatrix} \cos E_i \sin A_i \\ \cos E_i \cos A_i \\ \sin E_i \end{bmatrix} \quad (i = 1, 2, \dots, m) \quad (9-92)$$

The local tangent vectors are then transformed to true of reference date or mean of 1950.0 inertial coordinate systems as described in Section 9.1.1, i.e.,

$$\bar{\rho}_i = (M_{1t} \ BC)^T \bar{\rho}_{1t_i} \quad (9-93)$$

The station position vector in geocentric inertial Cartesian coordinates, given in Equation (9-15), is

$$\bar{R}_{s_i} = (BC)^T \bar{r}_{s_{b_i}} \quad (9-94)$$

where the station coordinates in body-fixed axes are given in Equations (9-4) and (9-5). Vectorially adding the station vectors  $\bar{R}_{s_i}$  and topocentric spacecraft vectors  $\bar{\rho}_i$  yields the geocentric spacecraft position vector

$$\bar{R}_i = \bar{R}_{s_i} + \bar{\rho}_i \quad (i = 1, 2, \dots, m) \quad (9-95)$$

A two-body orbit is then fitted to the  $m$  position vectors by using the  $f$  and  $g$  series, expanded about a desired epoch time

$$R_i = f_i \bar{R}_0 + g_i \dot{\bar{R}}_0 \quad (i = 1, 2, \dots, m) \quad (9-96)$$

Multiplying the preceding equation by  $f_i$  and then summing on  $i$  yields

$$\sum_{i=1}^m f_i \bar{R}_i = \sum_{i=1}^m f_i^2 \bar{R}_0 + \sum_{i=1}^m f_i g_i \dot{\bar{R}}_0 \quad (9-97a)$$



Multiplying Equation (9-96) by  $g_i$  and summing on  $i$  yields

$$\sum_{i=1}^m g_i \bar{R}_i = \sum_{i=1}^m f_i g_i \bar{R}_0 + \sum_{i=1}^m g_i^2 \dot{\bar{R}}_0 \quad (9-97b)$$

Solving Equations (9-97a and b) simultaneously for  $\bar{R}_0$  and  $\dot{\bar{R}}_0$  yields the desired inertial geocentric position and velocity at epoch.

$$\bar{R}_0 = \frac{\sum_{i=1}^m g_i^2 \sum_{i=1}^m f_i \bar{R}_i - \sum_{i=1}^m f_i g_i \sum_{i=1}^m g_i \bar{R}_i}{\sum_{i=1}^m f_i^2 \sum_{i=1}^m g_i^2 - \left( \sum_{i=1}^m f_i g_i \right)^2} \quad (9-98)$$

$$\dot{\bar{R}}_0 = \frac{\sum_{i=1}^m f_i^2 \sum_{i=1}^m g_i \bar{R}_i - \sum_{i=1}^m f_i g_i \sum_{i=1}^m f_i \bar{R}_i}{\sum_{i=1}^m f_i^2 \sum_{i=1}^m g_i^2 - \left( \sum_{i=1}^m f_i g_i \right)^2} \quad (9-99)$$

Equations (9-98) and (9-99) are solved iteratively by successively improved approximations for  $f_i$  and  $g_i$ .

The orbit is initially approximated by a circular orbit with the semi-major axis  $a$  obtained by averaging the  $m$  position vectors

$$a = \frac{1}{m} \sum_{i=1}^m |R_i| \quad (9-100)$$

The mean motion  $n$  is

$$n = \sqrt{\frac{\mu}{a^3}} \quad (9-101)$$

and the mean anomaly measured from epoch is

$$M_i - M_0 = n(t_i - t_0) \quad (9-102)$$

The coefficients  $f$  and  $g$  for the two-body circular orbit, corresponding to each measurement vector, are (Reference 1)

$$\begin{aligned} f_i &= \cos(M_i - M_0) \\ g_i &= \frac{1}{n} \sin(M_i - M_0) \end{aligned} \quad (9-103)$$

Substituting the preceding  $f_i$  and  $g_i$  into Equations (9-98) and (9-99) yields the first approximation for  $\bar{R}_0$  and  $\dot{\bar{R}}_0$ . After the initial iteration the coefficients  $f_i$  and  $g_i$  are calculated from the following procedure.

Reference 2 presents a general method for computing  $f_i$  and  $g_i$  as functions of  $\bar{R}_0$  and  $\dot{\bar{R}}_0$ . The Sundman transformation is used to obtain a new independent variable  $\psi$  defined by

$$\dot{\psi} = \frac{1}{\bar{R}} \quad (9-104)$$

The coefficients  $f_i$  and  $g_i$  are determined from the relations

$$\begin{aligned} f_i &= 1 - \mu S_2(\psi_i) / \bar{R}_0 \\ g_i &= \bar{R}_0 S_1(\psi_i) + \sigma_0 S_2(\psi_i). \end{aligned} \quad (9-105)$$

The velocity  $\dot{\bar{R}}_i$  can be determined by

$$\dot{\bar{R}}_i = \dot{f}_i \bar{R}_0 + \dot{g}_i \dot{\bar{R}}_0 \quad (9-106)$$

where

$$\begin{aligned}\dot{\bar{f}}_i &= -\mu S_1(\psi_i) / (R_i R_0) \\ \dot{\bar{g}}_i &= 1 - \mu S_2(\psi_i) / R_i\end{aligned}\tag{9-107}$$

and the time difference between  $\bar{R}_i$  and  $\bar{R}_c$  is

$$\tau_i = t_i - t_0 = R_0 S_1(\psi_i) + \sigma_0 S_2(\psi_i) + \mu S_3(\psi_i)\tag{9-108}$$

The parameter  $\sigma_0$  is

$$\sigma_0 = \bar{R}_0 \cdot \dot{\bar{R}}_0\tag{9-109}$$

and the parameters  $S_1$ ,  $S_2$  and  $S_3$  are obtained by solving Kepler's equation by successively approximating  $\psi_i$  to satisfy Equation (9-108). The method, described in Reference 2, is summarized below.

After initially estimating a value of  $\psi$ , the quantity  $\lambda$  is calculated from

$$\lambda = \alpha \psi^2\tag{9-110}$$

where

$$\alpha = \dot{\bar{R}}_0 \cdot \dot{\bar{R}}_0 - 2\mu / R_0\tag{9-111}$$

The parameters  $C_0$ ,  $C_1$  ...,  $C_5$  are next computed as functions of  $\lambda$

$$3C_5 = (1 + (1 + (1 + (1 + (1 + (1 + (1 + \frac{\lambda}{19 \cdot 18}) \frac{\lambda}{17 \cdot 16}) \frac{\lambda}{15 \cdot 14}) \frac{\lambda}{13 \cdot 12}) \frac{\lambda}{11 \cdot 10}) \frac{\lambda}{9 \cdot 8}) \frac{\lambda}{7 \cdot 6})) / 40$$

$$C_4 = (1 + (1 + (1 + (1 + (1 + (1 + (1 + \frac{\lambda}{18 \cdot 17}) \frac{\lambda}{16 \cdot 15}) \frac{\lambda}{14 \cdot 13}) \frac{\lambda}{12 \cdot 11}) \frac{\lambda}{10 \cdot 9}) \frac{\lambda}{8 \cdot 7}) \frac{\lambda}{6 \cdot 5}) / 24$$

$$C_3 = \left[ \frac{1}{2} + \lambda(3C_5) \right] / 3$$

(9-112)

$$C_2 = \frac{1}{2} + \lambda C_4$$

$$C_1 = 1 + \lambda C_3$$

$$C_0 = 1 + \lambda C_2$$

and  $S_1$ ,  $S_2$  and  $S_3$  are calculated as functions of  $C_1$ ,  $C_2$ ,  $C_3$  and  $\psi$

$$S_1 = C_1 \psi$$

$$S_2 = C_2 \psi \quad (9-113)$$

$$S_3 = C_3 \psi$$

The time interval between the point corresponding to  $\psi$  and the reference epoch  $t_0$  is determined from Equation (9-108) to be

$$\tau(\psi) = R_0 S_1 + \sigma_0 S_2 + \mu S_3, \quad (9-114)$$

and the geocentric radius corresponding to  $\psi$  is

$$R(\psi) = |R_0 C_0 + \sigma_0 S_1 + \mu S_2| \quad (9-115)$$



The difference between the desired time increment  $\tau_i$  and  $\tau(\psi)$  is

$$\Delta\tau = \tau_i - r_0 S_1(\psi) - \sigma_0 S_2(\psi) - \mu S_3(\psi) \quad (9-116)$$

The successive approximation scheme involves correcting  $\psi$  in order to cause  $\Delta\tau$  to vanish. The finite difference form of Equation (9-104)

$$\psi_i = \frac{t_i - t_0}{R} \quad (\text{where } \psi \equiv 0 \text{ at } t = t_0) \quad (9-117)$$

aids in determining the iterative correction algorithm

$$\psi_{k+1} = \psi_k + \frac{\Delta\tau}{R(\psi_k)} \quad (9-118)$$

When the solution has converged, the value  $\psi_i$  which yields  $\tau_i$  is obtained. Values of  $S_1(\psi_i)$  and  $S_2(\psi_i)$  are a by-product and are used to determine  $f_i$  and  $g_i$  by means of Equation (9-105).

Repeating the preceding process for the data times  $t_1, t_2, \dots, t_m$ , the values of  $f_i$  and  $g_i$  for  $i = 1, 2, \dots, m$  are obtained for substitution into Equations (9-98) and (9-99), along with data measurements  $\bar{R}_1, \bar{R}_2, \dots, \bar{R}_m$ . These equations yield new estimates of  $\bar{R}_0$  and  $\dot{\bar{R}}_0$  to commence the next iteration. This computational sequence is shown schematically in Figure 9-4.

### 9.3 REFERENCES

1. Escobal, P. R.: 1965, Method of Orbit Determination, John Wiley and Sons, New York.
2. Goodyear, W. H.: 1966, A General Method for the Computation of Cartesian Coordinates and Partial Derivatives of the Two-Body Problem, NASA Report NASA-CR-522, September 1966.

## APPENDIX A

TRAJECTORY SENSOR SYSTEM FUNCTIONAL  
DESCRIPTIONS AND PREPROCESSING

The trajectory sensor systems measure the various propagation characteristics of electromagnetic or optical signals transmitted between the satellite and tracking stations (or other reference sources). These data are subsequently used to determine the satellite trajectory. The dependence of these measurements upon the relative states of the spacecraft provides the key to the orbit determination process.

This appendix provides a brief functional description of the trajectory sensing systems currently included in GTDS. It also describes the procedures followed in preprocessing the data prior to GTDS processing. These computations are independent of GTDS and are presented primarily for informational purposes. However, they do provide an insight to the condition of the data at the preprocessor/processor interface which is necessary in order to understand the processor measurement model described in Chapter 7.

A.1 GODDARD RANGE AND RANGE-RATE (GRARR) SYSTEM AND  
APPLICATIONS TECHNOLOGY SATELLITE RANGE AND RANGE-  
RATE (ATSR) SYSTEMA.1.1 Functional Description

The GRARR System (References 4 through 6) and the ATSR System (References 4, 5, and 6) determine and record spacecraft range, radial velocity and angular position. GRARR and ATSR Systems are located at the tracking sites shown in Table A-1. These systems transmit a continuous wave signal from the tracking station antenna at a carrier frequency  $\nu_T$ , which is modulated by a low-frequency tone  $\nu_L$ . This signal propagates to the spacecraft's omni-directional antenna, where the received frequency  $\nu_R$  appears to be slightly different from that transmitted ( $\nu_T$ ) because of the uplink Doppler shift. The received signal is modified by the spacecraft transponder electronics and retransmitted back to the ground-tracking station. Again, the signal experiences a downlink Doppler shift so that the frequency  $\nu_R$  received at the ground differs from that transmitted to the spacecraft. The 30-foot diameter ground receiving antenna is automatically steered through two gimbal angles,  $X_{30}$  and  $Y_{30}$  (or A and B shown in Figure A-1), to

Table A-1  
GRARR and ATSR Stations

	Frequency Independent Hardware	Gimbal Angles
<u>GRARR Stations</u>		
Rosman, North Carolina	Yes	$X_{30}, Y_{30}$
Orroral Valley, Canberra, Australia	Yes	$X_{30}, Y_{30}$
Tananarive, Malagasy Republic	Yes	$X_{30}, Y_{30}$
Fairbanks, Alaska	Yes	$X_{30}, Y_{30}$
Santiago, Chile	No	$X_{30}, Y_{30}$
<u>ATSR Stations</u>		
Rosman, North Carolina	No	$X_{30}, Y_{30}$
Mojave, California	No	$X_{30}, Y_{30}$
Toowoomba, Australia	No	A, E
Kashima, Japan	No	A, E

maximize the received signal strength. As the signal is processed through the ground electronics system, the spacecraft transponder modification is undone and the transmitted carrier frequency is subtracted. At the output, the differenced Doppler signal (reflecting the uplink and downlink Doppler shifts) is modified by the addition of a bias signal of known frequency  $\nu_b$ .

Three different types of measurements result from signals received during the "frame" time interval which begins at "frame" time  $t_F$ :

1. The gimbal pickoff angles, X and Y or A and E, defining the direction of the received signal path at the antenna at time  $t_F$ , are recorded in degrees and decimal fractions.
2. The two-way range time delay is measured as a count  $C_L$  of the number of cycles of a reference frequency  $\nu_{R1}$  occurring between positive-directed zero crossings of the low-frequency ranging tone (frequency =  $\nu_L$ ) associated with the transmitted and received signals. The counter is started and the frame time  $t_F$  is signaled simultaneously by a zero crossing of the transmitted signal. The counter is stopped by the next zero crossing of the received signal. Since the lowest sidetone



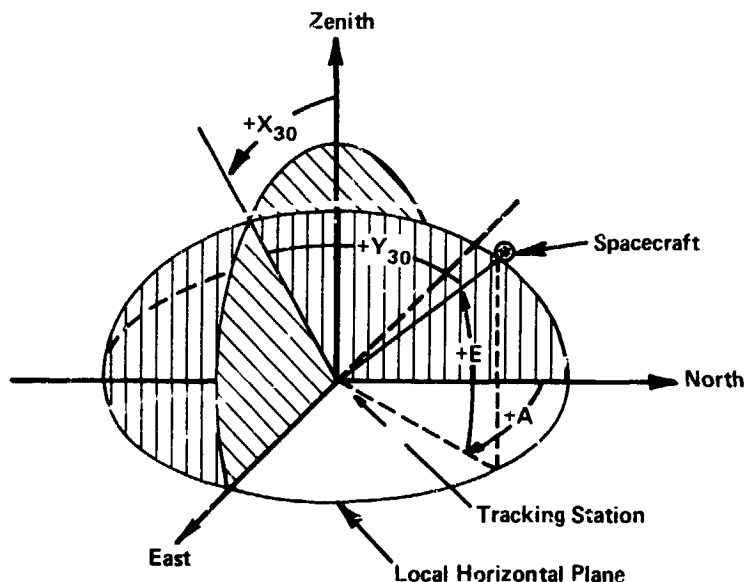


Figure A-1. Schematic of GRARR Gimbal Angles

frequency for the GRARR System is 8 Hz, the maximum unambiguous one-way range measurement corresponds to a distance of approximately 18,737 kilometers. Distances greater than this produce phase shifts larger than one cycle of the  $\nu_L$  signal. When this occurs, the GRARR system utilizes a pseudo-random binary code to determine the range ambiguity number  $\rho_a$ , the number of whole cycles to be added to the counter-measured fractional phase shift. The ATSR System does not require an ambiguity resolving system since it is used only in conjunction with ATS synchronous satellites which remain in the same ambiguity period during a pass.

3. The two-way range-rate measurement is made by counting the number of cycles  $C_0$  of a reference frequency  $\nu_{R2}$  required to count exactly  $N$  cycles of the Doppler-plus-bias signal  $\nu_d + \nu_b$  in the GRARR System and 100 times  $\nu_d + \nu_b$  for the ATSR System. The count also is started at the frame time  $t_F$  and ended after the accumulation of  $N$  cycles of the  $\nu_d + \nu_b$  signal. All GRARR Stations except Santiago have been modified to remove the dependency of  $C_0$  on the independent frequencies  $\nu_b$  and  $\nu_{R2}$ . The modification amounts to deriving the reference and bias frequencies from the same source as the transmitted frequency.

The gimbal angles  $X_{30}$  and  $Y_{30}$  (or  $A$  and  $E$ ) are measured only at the frame time  $t_F$ , but the range and range-rate measurements are made at the frame time and at three subsequent data sample times  $t_s$  within the frame-time

interval. The spacing of these data samples (and hence the time span of a data frame) may be varied to give range and range-rate recording rates of 4, 2, or 1 samples per second or 6 samples per minute. ATSR Stations can also record at a rate of 8 samples per record. The data, one angle sample and four range and range-rate samples for each frame, are punched on paper tape at the tracking station in standard Baudot 5-level teletype code and then transmitted to GSFC via teletype to be preprocessed.

### A.1.2 Preprocessing Description

The GRARR and ATSR data processing procedures and interfaces are obtained from References 1 through 6 and have been revised to reflect subsequent modifications in the software. Emphasis is placed on the preprocessor computations, but the interfaces with the stations and the processor are also included. Figure A-2 summarizes the station/preprocessor/processor interfaces and will aid in the ensuing description.

The data are formatted into frames at the station. Each frame contains four sets of range and range-rate observables  $C_0$  and  $C_1$ , as well as a single set of gimbal angles  $X_{30}$  and  $Y_{30}$  (or A and E). Each frame is time-tagged in station time  $t_R$ . Prior to transmission to the Goddard Space Flight Center, data calibration corrections are applied to the data, and the time tag is corrected for the propagation delay of the WWV signal from transmission to its reception at the tracking station, i.e.,

$$t_F = t_R + \Delta t_{\text{wwv}} \quad (\text{A-1})$$

Thus,  $t_F$  corresponds to the UTC time at initiation of the range counter. Each range observable  $C_1$  is divided by the reference frequency  $\nu_{R1}$ , thereby converting it to a time interval  $\Delta t_R$  with a standard transponder delay  $\Delta\tau$  accounted for as follows

$$\Delta t_R = \frac{C_1}{\nu_{R1}} - \Delta\tau \quad (\text{A-2})$$

where

$$\Delta\tau = \begin{cases} \approx 0 & \text{for S-Band} \\ \approx 17.1 \mu\text{sec} & \text{for VHF} \end{cases}$$

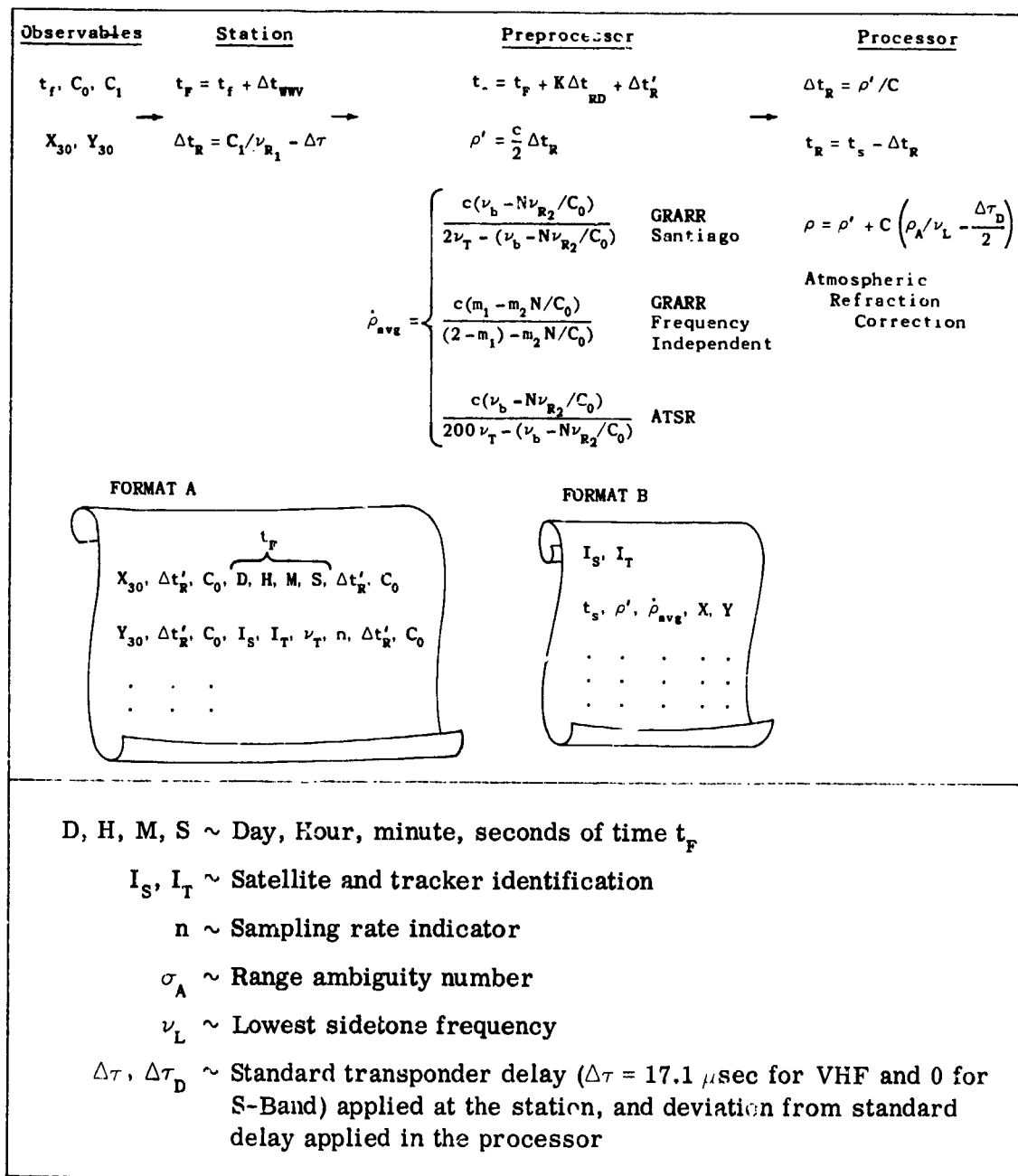


Figure A-2. GRARR and ATSR Data Preprocessor Computations and Interfaces

Each frame of data is received at GSFC in approximately format A in Figure A-2 (data quality, carriage return, line feed, and figure shift indicators are omitted). These data are then preprocessed as described in the following sections.

#### A.1.2.1 Gimbal Angles

The gimbal angles  $X_{30}$  and  $Y_{30}$  ( $\pm 00.00$  to  $\pm 90.00$  degrees) or A ( $000.00$  to  $360.00$  degrees) and E ( $000.00$  to  $090.00$  degrees) are unaltered in the preprocessor. Atmospheric refraction corrections must be applied later in the processor.

#### A.1.2.2 Range

The range observable  $C_1$  is corrected to the two-way propagation time interval  $\Delta t_R$  at the station. In the preprocessor, the interval is converted to one-way distance by multiplying by one-half the velocity  $c$  of the signal propagation as follows

$$\rho' = \frac{c}{2} \Delta t_R \quad (A-3)$$

where

$$c = 2.997925 \times 10^8 \text{ m/sec}$$

The preprocessed range  $\rho'$  always lies in the first ambiguity period and must, therefore, be corrected for range ambiguity in the processor. Furthermore, the transponder delay is a function of the received signal frequency at the spacecraft transponder. Therefore, any deviations from the standard transponder delay deducted in the preprocessor must be accounted for in the processor. The time at each of the four range samples within each frame is

$$t_s = t_r + k \Delta t_{RD} \quad (k = 0, 1, 2, 3) \quad (A-4)$$

where

$\Delta t_{RD} \sim$  the reciprocal of the recording rate

The time  $t_s$  is the ground receive time in UTC, corresponding to each range sample. The range and gimbal angles correspond to the spacecraft's position at the time it retransmits the tracking signal. Therefore, the times must be corrected for the one-way light time in the processor. The gimbal angles correspond to the first time (i.e.,  $k = 0$  in Equation (A-4) on each frame).

### A.1.2.3 Range-Rate

The interpretation of the Doppler cycle count  $C_0$  as a measure of the tracking station-to-spacecraft relative range-rate rests upon the following assumptions:

- (1) The Doppler effect can be adequately represented by the theory of special relativity.
- (2) A simplification can be made in representing the motion of the tracking station.

Assuming the tracking station motion is uniform in inertial space, it is shown in Appendix C that the average range-rate (in the sense of the Theorem of the Mean) over the time interval  $t_s$  and  $t_s + \Delta t_{RR}$  is

$$\dot{\rho}_{avg} = \frac{c(\nu_b - N/\Delta t_{RR})}{2\nu_T - (\nu_b - N/\Delta t_{RR})} \quad (A-5)$$

where the Doppler-plus-bias count time interval  $\Delta t_{RR}$  is

$$\Delta t_{RR} = \frac{C_0}{\nu_{R2}} \quad (A-6)$$

Equation (A-5) is used for the GRARR station at Santiago. Since ATSR stations count  $N$  cycles of 100 times the two-way Doppler-plus-bias frequency, the range-rate equation for the ATSR station data is

$$\dot{\rho}_{avg} = \frac{c(\nu_b - N/\Delta t_{RR})}{200 \nu_T - (\nu_b - N/\Delta t_{RR})} \quad (A-7)$$

The average range rate  $\dot{\rho}_{avg}$  in Equations (A-5) and (A-7) is dependent on the three frequencies  $\nu_T$ ,  $\nu_b$ , and  $\nu_{R2}$ . Four of the GRARR stations were modified by driving  $\nu_b$  and  $\nu_{R2}$  with the transmitted frequency  $\nu_T$ , i.e.,

$$\nu_b = m_1 \nu_T \quad \nu_{R2} = m_2 \nu_T \quad (A-8)$$

where  $m_1$  and  $m_2$  are the following constants.

GRARR Stations		$m_1$	$m_2$
Rosman	} VHF Crystal	1/5000	1/15
Tananarive			
Carnarvon			
Fairbanks			
	S-Band Crystal	1/3600	1/180
	S-Band PLL*	$\sigma$ /4500	$\sigma$ /225

\* $\sigma$  = phase locked transponder multiplication constant (Reference 4).

Substituting Equations (A-8) into (A-5) yields the relation for preprocessing Doppler data from these frequency independent GRARR stations

$$\dot{\rho}_{avg} = \frac{c(m_1 - m_2 N/C_0)}{(2 - m_1) - m_2 N/C_0} \tag{A-9}$$

A more precise modeling of the Doppler data is provided by the range difference formula in Appendix C. In this optional processing mode, the preprocessor computes

$$\dot{\rho} = \frac{c}{2\nu_T \Delta t_{RR}} (\nu_b \Delta t_{RR} - N) \tag{A-10}$$

rather than  $\dot{\rho}_{avg}$ . The processing program compares  $\dot{\rho}$  with the range difference calculated by Equation (7-41).

#### A.1.2.4 Smoothing

The range, range-rate and gimbal angle data are finally smoothed by regressively fitting low order (third or fourth) polynomials to at least 20 samples each of range and range-rate and at least 5 samples each of the gimbal angles. A least squares method is used for the polynomial fits, and a  $2.5\sigma$  data rejection criterion is used to eliminate "wild" data. The midpoint values of the polynomials replace the original data. The smoothed values are stored in a format similar to format B in Figure A-2 for subsequent use in the processor.

## A.2 C-BAND RADAR SYSTEM

### A.2.1 Functional Description

The FPQ-6, FPS-16, TPQ-18, and MPS-26 pulse radars used most frequently to support NASA satellite tracking are listed in Table A-2. These radars measure the two-way light time from the antenna to the spacecraft as well as the antenna pointing angles. The antenna Gimbaling system records the azimuth and elevation angles A and E shown in Figure A-1.

The usual mode of tracking a satellite via a C-Band radar is similar to the GRARR System. The two-way light time of a transmitted pulse and associated gimbal angles are measured and time tagged at the ground receive time of the return pulse. The range measurement is corrected for satellite transponder time delay, and the time tag is corrected for system delays and WWV propagation time delay. The resulting two-way time is converted to units of distance by multiplying by one-half the speed of light. These corrections are performed at the tracking site. There is no range ambiguity or range-rate associated with this type of system.

Table A-2  
C-Band Radar Sites

Station Locations	Type
Bermuda	FPQ-6, FPS-16
Grand Canary Island	MPS-26
Carnarvon, Australia	FPQ-6
Woomera, Australia	FPS-16
Hawaii	FPS-16
Point Arguello, California	FPS-16
Eglin Air Force Base	FPS-16
Patrick Air Force Base	FPQ-6
Cape Kennedy	FPS-16
Grand Bahama	FPS-16, TPQ-18
Grand Turk	TPQ-18
San Salvador Island	FPS-16
Merritt Island	TPQ-18
Ascension Island	FPS-16, TPQ-18

A.2.2 Preprocessing Description

The data received from the C-Band tracking site is calibrated, corrected for transponder delay, and time corrected. The preprocessor converts the range data from yards (received from the station) to kilometers (1 meter equals 3,280,839,895 international feet) and the gimbal angles from mils to degrees (6400 mils equals 360 degrees). The time tag corresponds to the ground receive time.

Capability must be provided in the processor to account for atmospheric refraction and light time correction of the time tag.

A.3 UNIFIED S-BAND (USB) SYSTEM

A.3.1 Functional Description

The USB System (References 2, 5, 6, 7 and 8) determines and records the spacecraft range, range-rate, and antenna gimbal angle positions at the globally located tracking sites listed in Table A-3. The USB System transmits a continuous S-Band carrier signal with a modulated pseudo random code. The nominal up-link signal frequency of 2 GHz is multiplied by a constant ( $k = 240/221$ ) at the coherent spacecraft transponder, and retransmitted to the receiving stations.

Table A-3  
Unified S-Band (USB) Stations

USB Station	Antenna Size, Feet
2-Merritt Island	30, 30
Bermuda	30
Carnarvon, Australia	30
Hawaii	30
Corpus Christi, Texas	30
Guam	30
2-Goldstone, California	85 and a 30 oriented as an 85
Pioneer	85 hr, dec angles
Ascension Island	30
Canberra, Australia	85
Tidbinbilla, Australia	85 hr, dec angles
Madrid, Spain	85
Cerebros, Spain	85 hr, dec angles
Grand Canary Island	30
2-Greenbelt, Maryland	30 and a 30 oriented as an 85
Vanguard Ship	30



The USB System range measurement is made by means of an autocorrelation involving a pseudo random code which is modulated onto the S-Band uplink carrier and coherently turned around by the transponder. The locally generated code at the ground station undergoes a variable delay when compared with the received code, which has undergone a two-way propagation delay. When the inserted ground station delay equals the two-way propagation delay, the autocorrelation has a maximum value and the inserted ground time delay is a measure of the slant range. With the "long code" or normal pseudo random noise code, the USB range measurement is unambiguous to a range of 800,000 km. Normally, only one such "range acquisition" is made over a single tracking station, and subsequent range readouts are obtained by updating the initial measurement by integrating a "clock Doppler" signal. That is, once range acquisition is made, the ranging code is switched off and a clock modulation is switched on. The relative phase change of the clock signal, as relayed via the spacecraft, is then a measure of range change. As presently configured, the clock is not an integral submultiple of the carrier frequency, however, the smallest increment of range change in the tracking format (termed the range unit RU) corresponds to approximately 16 cycles of two-way carrier Doppler change. Thus, whenever the vehicle moves a radial distance of approximately 16 half-wavelengths of the carrier frequency relative to the ground station, one RU is recorded. One RU corresponds to 1.0496936 meters of range. The range update is done at the tracking site and, from an equipment standpoint, is essentially independent of the carrier Doppler tracking information which is also contained in the raw USB data format. Only the receiver radio frequency and intermediate frequency stages are common to the range and range-rate channels.

The raw time tag associated with the range corresponds to UTC ground receive time and includes an on-site correction for WWV propagation time delay. Typically, all USB remote site clocks are synchronized to the Naval Observatory Master clock to within 50 microseconds. The USB dish antennas employ an X-Y gimbal mounting system (see Figure A-1). The 30-foot diameter antennas employ an  $X_{30}$ -axis aligned North-South, whereas the 85-foot antenna  $X_{85}$ -axis is aligned East-West. The X-axis is always contained in the local tangent plane.

The basic measurement of range rate in the USB System is that of carrier frequency Doppler phase change. The down link carrier from the spacecraft is coherently tracked by a phase-locked ground receiver. The essential system functions are:

1. The up-link carrier has a nominal fixed frequency of 2 GHz derived from a cesium clock source.

2. The transponder receiver aboard the spacecraft is phase-locked to the up-link frequency plus the up-link Doppler shift.
3. The transponder transmitter frequency is coherently derived from the up-link carrier plus up-link Doppler shift. A fixed frequency turn-around ratio of 240/221 is used for all USB tracking.
4. The ground receiver is phase locked to the down-link signal which is at the transponder output frequency plus the down-link Doppler frequency shift.
5. In the 2-way mode, a 1 MHz signal is subtracted from the ground receiver signal prior to comparison with a signal which is coherent with the transmitted carrier frequency. The basic output is then the Doppler frequency plus a stable 1 MHz bias.

The raw data consists of whole cycle counts of phase change, which is a direct measure of the spacecraft radial change relative to the station. The basic measurement  $N$  is a nondestruct cycle count of carrier phase shift plus bias over a time period  $\Delta t_{RR}$ . It is termed nondestructive since, although the counter is read out at even time intervals, the accumulated count is not destroyed. Thus, the average frequency is obtained by differencing the count in adjacent frames and dividing by the sample time.

The Doppler count  $N$  is resolved to .01 cycle through the implementation of the Time Increment Resolver (TIR). Cycle resolving gives a precise measure of the time between the start of the data interval and the time at which the last positive-directed zero crossing of the biased Doppler signal is counted. This time duration is measured by counting the cycles of a 100 MHz oscillator. The Doppler count, along with the TIR count, will appear in the same data transmission frame. In the high speed format, the granularity of TIR is 10 nanoseconds, while in the low speed format, the granularity is 40 nanoseconds.

The normal low speed data rates of the USB system are one frame per six seconds and one frame per 10 seconds. This low speed data is derived on-site from the high speed data, which consists of a 240 bit format. High speed data is simultaneously available at a rate of 10 frames per second, 5 frames per second, or 2.5 frames per second, depending on the operator selection at the on-site USB data processor. USB sites are capable of obtaining gimbal angle and range rate data without ranging in contrast to the GRARR system which always provides range data.

### A.3.2 Preprocessing Description

The USB range data is transmitted from the sites in octal with a granularity of 1.0496936 meters. The output of the data handler is the one-way range in kilometers with no data corrections applied.

The N-count and TIR required to compute range rate are transmitted in octal with a granularity of 1 cycle and 40 nanoseconds respectively. The 1-way and 3-way Doppler are converted to range rate in km/sec through the equations

$$FOC = \left[ \frac{N(t) - N^*(t - \Delta t_{RR})}{\Delta t_{RR}} \right] * 4 * C(t) * 10^{-8} \quad (A-11)$$

$$N^*(t) = N(t) - FOC \quad (A-12)$$

$$\dot{\rho}_{avg} = \left[ \frac{N^*(t) - N^*(t - \Delta t_{RR})}{\Delta t_{RR}} - 10^6 \right] * \frac{c}{2K\nu_T} \quad (A-13)$$

where

- FOC = fractions of a cycle
- N(t) = contents of Doppler counter at time t
- N\*(t) = Doppler counter at time t corrected by TIR
- C(t) = contents of TIR counter
- $\Delta t_{RR}$  = sample interval of the Doppler counter
- $\dot{\rho}_{avg}$  = average range rate
- c = speed of light
- K = transponder turnaround ratio (240/221 for USB)
- $\nu_T$  = transmitter frequency.

The angular measurements are the X and Y gimbal angles, with the 85-foot sites having the X-axis aligned East-West and the 30-foot sites having the X-axis aligned North-South. The data are transmitted in octal with a granularity of  $6.8664 \times 10^{-4}$  degrees. The data handler outputs the angles in radians.

The time tag associated with all USB angle data is the ground receive time corrected on-site for WWV propagation delay.

## A.4 MINITRACK SYSTEM

### A.4.1 Functional Description

The Minitrack system, References 5, 6, 9 and 10, is basically a radio direction finder which utilizes the interferometer principle to locate a radiating transmitter carried by a spacecraft. The Minitrack network is composed of seven stations, globally located as shown in Table A-4.

Table A-4  
Minitrack Stations

Quito, Ecuador
Santiago, Chile
Winkfield, England
Johannesburg, South Africa
Fairbanks, Alaska
Orroral Valley, Canberra, Australia
Tananarive, Malagasy Republic

Each system consists of a series of six horizontal baselines at each station, three oriented east-west (EW) and three oriented north-south (NS), as shown in Figure A-3a. A fixed antenna system is located at each end of each baseline to receive a nominal 136 MHz signal transmitted continuously from a spacecraft as it passes within view of each station. The spacecraft transmitter frequency can be preset to any of 2000 frequencies between 136.000 and 137.999 MHz in steps of 1 kHz. Each set of three EW or NS baselines consists of a fine, a medium, and a coarse baseline. The fine baselines are accurately surveyed to be 46 or 57 times the vacuum wavelength of the nominal 136 MHz signal. The medium and coarse baselines are 4.0 and 3.5 nominal wavelengths, respectively.

The principle underlying the Minitrack system is illustrated by the following simplified two-dimensional case (see Figure A-3b). The spacecraft transmitter is assumed to be located at an elevation angle  $\alpha$  and at a very large distance from the station so that received signals appear to be planar wavefronts, e.g., BC and B'C'. The baseline distance AB is a multiple  $N_B$  of the nominal 136 MHz vacuum wavelength. At any given instant, the phase of the signal along the propagation paths AC' and BB' is characterized by the two sinusoids shown in

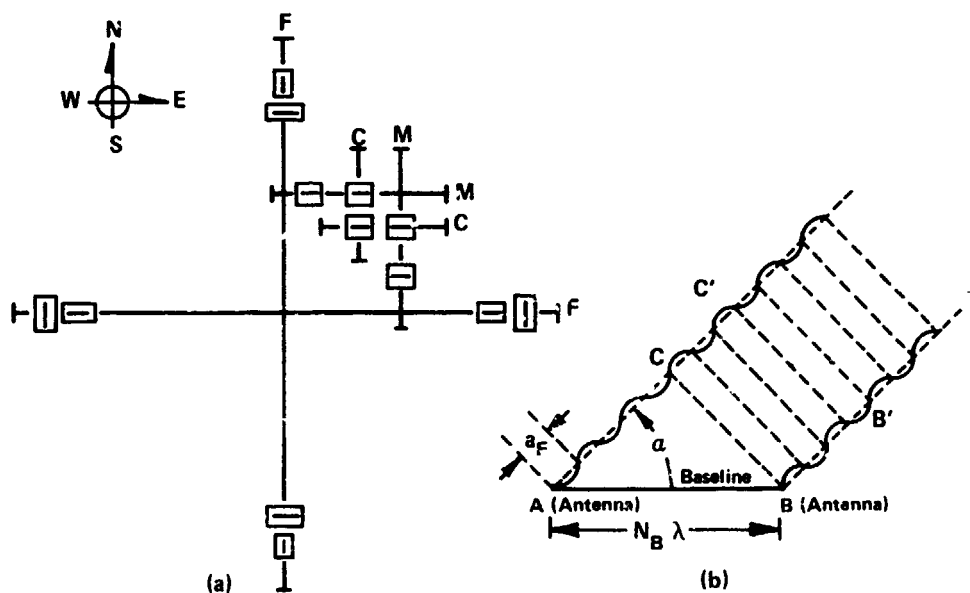


Figure A-3. Minitrack Baseline and Signal Reception Geometry

Figure A-3b. The separate signals received by the two antennas at A and B are fed into a phase counter which measures the phase difference between the two signals, normalized to a fractional part of the received signal wavelength, e.g.,  $a_F$  in the figure. This measurement gives no information concerning the additional number of whole wavelengths which occur between the signal received at antenna A and the signal received at antenna B. This ambiguous integral number, as well as the fractional phase displacement itself, is dependent upon the wavelength of the received signal  $\lambda$ , the length of the baseline  $N_F$ , and the spacecraft angular geometry  $\alpha$ . Thus, the reason for the multiplicity of parallel baselines (i.e., 46 or 57, 4 and 3.5 wavelength bases) is to resolve the integral cycle count ambiguity on the longer (fine) baseline. This resolution is accomplished by synthesizing a 0.5 wavelength measurement by differencing the 4.0 and 3.5 wavelength baseline phase difference measurements, i.e.,

$$\bar{a}_{0.5} = a_{4.0} - a_{3.5} \quad (A-14)$$

where  $\bar{a}$  indicates absolute phase difference.

It would be impractical to build a 0.5 wavelength baseline, since the antennas would physically interfere with each other. The synthesized 0.5 wavelength phase

difference  $\bar{a}_{0.5}$  is unambiguous since the extra path length, corresponding to AC in Figure A-3b, is less than one wavelength. By similarity of triangles in the figure, the absolute length of the path AC may be estimated from the 0.5 wavelength value as follows

$$\bar{a}_F = \frac{N_F}{0.5} \bar{a}_{0.5} \quad (\text{A-15})$$

where  $N_F = 46$  or  $57$ .

In practice  $\bar{a}_{0.5}$  is not precise enough to be used directly to obtain  $\bar{a}_F$ ; therefore, a slightly more complicated process is used to determine the unambiguous fine phase difference  $\bar{a}_F$ . Knowing  $\bar{a}_F$ , the direction cosine is

$$\cos \alpha = \frac{AC}{AB} = \frac{\bar{a}_F}{AB} \quad (\text{A-16})$$

For the three dimensional case, the corresponding ratios obtained from the EW and NS phase difference measurements yield the direction cosines  $l$  and  $m$  of the signal path at the station.

Each fine baseline has its own phase difference counter; hence, two measurements (EW and NS) are recorded simultaneously. The four ambiguity baselines (EW and NS, medium and coarse baselines) share a single counter through a multiplexed digital recording system. Since all measurements cannot be made simultaneously, the sequence of recordings for each data frame occurs according to the schedule of Table A-5. These data may be recorded at the rate of one frame every 1, 2, 10, 20, or 60 seconds. The fine baseline counter registers a decimal number between .000 and .999, and the medium and coarse baseline counter registers a decimal number from .00 to .99.

The frame rate is generally scheduled so that 31 frames give complete coverage of the usable data for a spacecraft pass over a station. A message consisting of up to 31 frames is punched on paper tape at the tracking station in standard Baudot 5-level teletype code and transmitted via teletype to GSFC for preprocessing.

Table A-5  
Minitrack Counter Sequence

Time Registered by Minitrack Data Clock	Initiation of Both Fine Baseline Counters	Initiation of Ambiguity Counter and Baseline Sampled
$t_F^*$	X	E-W Medium
$t_F + 0.2 \text{ sec}$	X	E-W Coarse
$t_F + 0.4 \text{ sec}$	X	N-S Medium
$t_F + 0.6 \text{ sec}$	X	N-S Coarse
$t_F + 0.8 \text{ sec}$	X	

\* $t_F$  = UTC at the beginning of the frame.

#### A.4.2 Preprocessing Description

The Minitrack preprocessing procedures and interfaces are obtained from References 9 and 10 and have been revised to reflect subsequent modifications to the software. Figure A-4 summarizes the station/preprocessor/processor interfaces and will aid in the following description.

At the Minitrack station, the fine, medium, and coarse phase difference measurements are sampled and recorded in frames, as described in Section A.4.1. The time-tag  $t_F$  for each frame is corrected at the station for the propagation delay of the WWV signal from transmission to reception at the tracking station. Thus,  $t_F$  corresponds to UTC time at the beginning of each frame. Each frame of data is transmitted to GSFC in approximately format A of Figure A-4 (the data signal strength indicators are omitted). These data are then preprocessed by rectifying the shift in whole cycle counts between consecutive fine, medium, and coarse phase difference measurements, and then least square fitting low order polynomials to the data. Electronic system filter delays are corrected in the polynomial time variable, and calibration corrections are applied to the data.

The ambiguity correction for the fine phase data is determined from the medium and coarse data. At each output time, a 0.5 wavelength baseline phase difference  $\bar{a}_{0.5}$  is synthesized from the 4.0 wavelength baseline (medium) data  $a_{4.0}$ , and the 3.5 wavelength baseline (coarse) data  $a_{3.5}$ . The medium and coarse data are obtained from the smoothing polynomial previously determined.

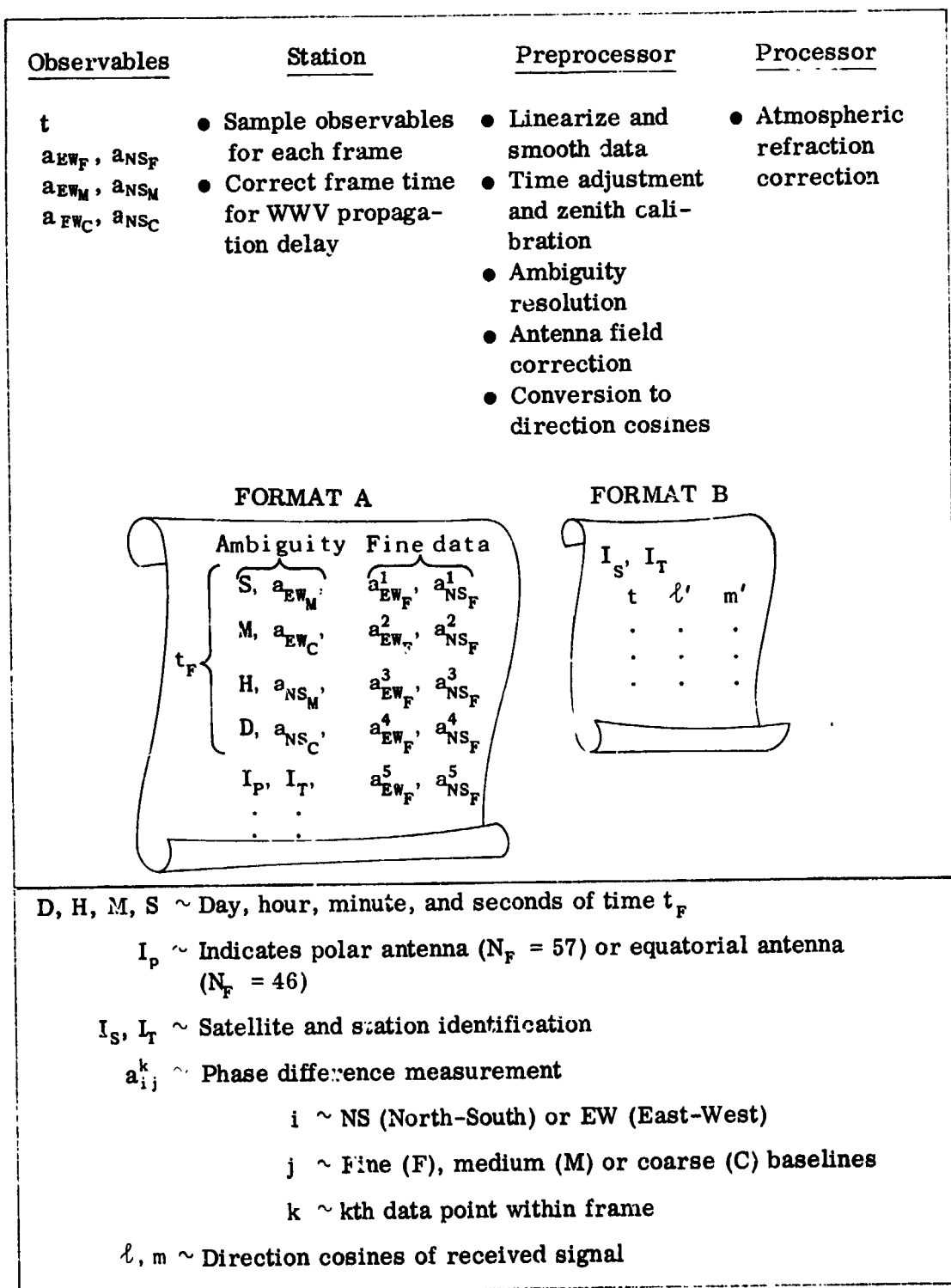


Figure A-4. Minitrack Preprocessor and Interface Schematic



Because of its short baseline, the synthesized 0.5 wavelength baseline data is an absolute (unambiguous) phase difference (the bar denotes absolute phase difference). Were it not for inaccuracies in  $\bar{a}_{0.5}$ , it could be used to determine the ambiguity correction for the fine data. In order to minimize the amplification of these measurement inaccuracies,  $\bar{a}_{0.5}$  is used to correct the ambiguities in  $a_{3.5}$  and  $a_{4.0}$ , which are then used to synthesize  $a_{7.5}$ , corresponding to a fictitious 7.5 wavelength baseline reading. Finally,  $\bar{a}_{7.5}$  is used to correct the ambiguity in the 46 or 57 wavelength baseline fine data. This stepping process is described mathematically in Section A.4.2.3.

At each output time, the absolute fine phase difference data are corrected for antenna field corrections and converted to direction cosines for use in subsequent processing. Data at different output times from the same station are correlated by means of the smoothing polynomials which are used to replace the actual measurements.

The preprocessing steps summarized above are described in more detail in the following sections.

#### A.4.2.1 Data Linearization and Smoothing

As stated in Section A.4.1, up to 31 frames of data are recorded for each spacecraft pass over a station. Each frame of data contains five fine, one medium, and one coarse baseline phase-difference measurements from each East-West (EW) and North-South (NS) baseline set. Thus, up to 155 fine, 31 medium, and 31 coarse baseline measurements are recorded from each of the EW and NS baseline sets for each spacecraft/station pass.

The fine phase difference counters register only from .000 to .999; therefore, it is possible that the absolute value of the difference between consecutive readings may be numerically larger than .500. This is assumed to mean that a new cycle crossing occurred between measurements, and that the measured data should be rectified by adding or subtracting a full cycle count to one of the points. This process of rectifying the data by converting to nonmodular number sets is called linearization.

#### A.4.2.1.1 Ambiguity Data

The ambiguity data (medium and coarse baselines) are linearized first since it is less likely that the phase difference will exceed  $\pm.50$  between consecutive points with these data. The linearization is accomplished as follows:

- (a) Beginning with the first phase difference measurement, the difference between consecutive points is calculated, i.e.,

$$\delta_i = a_{i+1} - a_i \quad (\text{A-17})$$

- (b) If  $\delta_i$  lies within the range  $-.500 < \delta_i < .500$ , no rectification is necessary. If  $\delta_i \geq .500$ , then integer multiples of 1.000 are subtracted from  $a_{i+1}$  until  $\delta_i$  lies within the range  $-.500 < \delta_i < .500$ . If  $\delta_i \leq -.500$ , then integer multiples of 1.000 are added to  $a_{i+1}$  until  $\delta_i$  lies within the range  $-.500 < \delta_i < .500$ .

- (c) The index  $i$  is then updated and steps (a) and (b) are repeated until all phase difference measurements have been rectified.

This linearization process is applied separately to each of the EW and NS medium and coarse baseline data sets. The components of the resulting data vectors  $\bar{b}_{EW_M}$ ,  $\bar{b}_{NS_M}$ ,  $\bar{b}_{EW_C}$ , and  $\bar{b}_{NS_C}$  have the correct relative phase, but the vectors may have an incorrect absolute phase.

After linearizing the medium and coarse baseline data, quadratic smoothing polynomials are least-squares fitted to each of the four data sets. The polynomials are of the form

$$b_n = A_n + B_n \tau + C_n \tau^2 \quad (\text{A-18})$$

$$(n = EW_M, EW_C, NS_M, NS_C)$$

where  $\tau$  is the time measured from  $t_{FM}$ , the frame time of the midframe (middle frame of the data sets), i.e.,  $\tau = t - t_{FM}$ . When determining the polynomial coefficients, the ambiguity data are tagged at their frame times; thus, each of the polynomials is biased in time by the multiplexer time delay. The multiplexer time delay is accounted for later when evaluating the polynomial. Ambiguity data exhibiting unusually large deviations from the smoothing polynomials are rejected during the fitting process.

#### A.4.2.1.2 Fine Data

The linearization procedure for the fine baseline data is somewhat more complicated than for the ambiguity data, since the phase change between data in successive frames can exceed one cycle. Therefore, an approximation to the LW and NS data phase change is estimated as follows, using the fine phase rate  $\dot{\tilde{a}}_F$ .

$$\delta_i = a_{i+1} - a_i - \dot{\tilde{a}}_F(t_{i+1} - t_i) \quad (\text{A-19})$$

The fine phase rate is determined by averaging the ratioed slopes of the medium and coarse smoothing polynomials at the middle frame time  $t_{FM}$

$$\dot{\tilde{a}}_F = \frac{N_F}{2} \left( \frac{B_C}{3.5} + \frac{B_M}{4.0} \right) \quad (N_F = 46 \text{ or } 57) \quad (\text{A-20})$$

The quantities  $B_C$  and  $B_M$  are the coarse and medium phase rates from Equation (A-18) at the middle frame time, i.e.,  $\tau = 0$ .

The fine phase linearization is accomplished as described in Steps (a), (b), and (c) in the preceding section, but using the estimated difference given by Equation (A-19). The components of the resulting data vectors  $\bar{b}_{EW_F}$  and  $\bar{b}_{NS_F}$  have the correct relative phase, but the vectors may have an incorrect absolute phase.

After linearizing the fine baseline data, their time tags  $t_s$  are computed for the appropriate sequential position within each frame by accounting for sequencer delay  $\Delta t_P$  and for the counter delay in the phase readout digitizing equipment  $\Delta t_c$ , as follows

$$t_s = t_F + \Delta t_P + \Delta t_c \quad (\text{A-21})$$

where

$$\Delta t_P = 0, .2, .4, .6, .8$$

depending on the relative position of the data point within its frame (see Table A-5), and

$$\Delta t_c = .01 a_F$$

Cubic smoothing polynomials are then least-squares fitted to the linearized and time corrected EW and NS fine baseline data. The polynomials are of the form

$$b_m = A_m + B_m \tau_m + C_m \tau_m^2 + D_m \tau_m^3 \quad (A-22)$$

$$(m = EW_F, NS_F)$$

where  $\tau_m$  is the time measured from the middle point of each data set. The NS and EW midpoint times  $t_{M_m}$  can differ due to the correction  $\Delta t_c$ . Fine data exhibiting large deviations from the smoothing polynomials are rejected during the fitting process.

#### A.4.2.2 Time Adjustment and Zenith Calibration

The four ambiguity polynomials and two fine baseline polynomials, in Equations (A-18) and (A-22), are inconsistent in terms of their time variables. The ambiguity polynomials neglect sequencer delay and use a reference time equal to the mid-frame time  $t_{FM}$ . The fine polynomials use a reference time equal to the time of the midpoint  $t_{M_m}$  of each data set. Neither of the polynomials accounts for the delays between the time the signal is received at the antennas and the times the phase differences are sampled and tagged, nor do they account for calibrations in the phase difference measurements.

These discrepancies are accounted for by making the following corrections to the fine baseline smoothing polynomials

$$b_m = [A'_m] + B_m \tau_m + C_m \tau_m^2 + D_m \tau_m^3 \quad (A-23)$$

where

$$A'_m = A_m - Z_m \quad (A-24)$$

$$\tau_m = t - t_m^* \quad (A-25)$$

$$t_m^* = t_{M_m} + \frac{KF_m}{1000} + KI - 0.4 \quad (A-26)$$

$$(m = EW_F, NS_F)$$

The correction terms are defined as follows:

$Z_m \sim$  zenith calibration constant which accounts for internal system changes such as aging and maintenance of electronic components, phase shifts caused by antennas and feed lines, and unequal lengths of cable connecting the antenna pairs

$KF_m \sim$  delay of approximately 36 msec caused by the fine filter

$KI \sim$  delay of .120 sec due to the optional 2 Hz bandwidth filter when used

The 0.4 second delay in Equation (A-26) accounts for the difference between the time of the middle point  $t_{m_m}$  and the midframe time  $t_{FM}$ . This term shifts the reference time of the fine polynomials to that of the corrected midframe time. The notation  $[ ]$  denotes that the integer part of the number is truncated leaving only the fractional part. This transforms the phase difference to the first ambiguity period at the reference time.

The ambiguity polynomials are corrected for sequencer and 2 Hz filter delay, their reference times are made equal to those of the fine polynomials, and calibration corrections are applied as shown in the following equations.

$$b_n = [A'_n] + B_n \tau + C_n \tau^2 \quad (A-27)$$

where

$$A'_n = A_n + B_n (t_m^* - t_n^*) + C_n (t_m^* - t_n^*)^2 - Z_n \quad (A-28)$$

$$\tau = t - t_m^* \quad (A-29)$$

$$t_n^* = t_{FM} + \Delta t_{ci} \quad (A-30)$$

$$\left( \begin{array}{lll} m = EW_F & \text{for} & n = EW_M \text{ or } EW_C \\ m = NS_F & \text{for} & n = NS_M \text{ or } NS_C \end{array} \right)$$

The correction terms are defined as follows:

$Z_n \sim$  same as  $Z_m$  above

$\Delta t_d \sim$  correction due to sequencer delay, plus a 0.15 sec delay due to a 2 Hz bandwidth filter in the digital recording system

$$\Delta t_d = \begin{cases} -0.15 & \text{for EW medium} \\ 0.15 & \text{for EW coarse} \\ 0.25 & \text{for NS medium} \\ 0.45 & \text{for NS coarse} \end{cases} \quad (\text{A-31})$$

The first three terms on the right in Equation (A-28) account (approximately) for the shift in reference time of the ambiguity polynomials.

#### A.4.2.3 Ambiguity Resolution

The time adjusted and calibrated smoothing polynomials provide the proper relative phase difference (time variation). The phase difference magnitudes are reduced to the first ambiguity period when the constant terms  $A'_n$  ( $n = EW_F, EW_M, EW_C, NS_F, NS_M, NS_C$ ) are reduced to their fractional parts in Equations (A-23) and (A-27). Since the time variation of the polynomials is proper, the coefficients  $B_n, C_n$  (and  $D_n$  for fine polynomials) are correct and only  $A'_n$  needs to be altered to accommodate the ambiguity resolution. Furthermore,  $A'_n = b_n (\tau = 0) = b_n^*$  is the smooth, time corrected, and calibrated ambiguous phase difference at approximately the midframe time.

The stepping process, summarized at the beginning of Section A.4.2 and described in detail in References 9 and 10, is now performed to determine the absolute phase differences of the fine baseline polynomials. Throughout the following description,  $[ ]$  denotes fractional part only, and  $\{ \}$  denotes minimum phase difference, i.e.,  $-.500 < \{ \} < .500$ .

The absolute phase difference for a fictitious North-South and East-West 0.5 wavelength baseline is determined from the medium (4.0 wavelength) and coarse (3.5 wavelength) baseline relative phase differences  $b_{4.0}^*$  and  $b_{3.5}^*$  as follows

$$b_{0.5} = \{ [b_{4.0}^* - b_{3.5}^*] \} \quad (\text{A-32})$$

The absolute phase differences for the medium and coarse baselines are obtained as follows

$$\overline{b}'_{3.5} = 7 \overline{b}_{0.5} \quad (\text{A-33})$$

$$\overline{b}_{3.5} = \overline{b}'_{3.5} - \{[\overline{b}'_{3.5} - b_{3.5}^*]\} \quad (\text{A-34})$$

$$\overline{b}'_{4.0} = 8 \overline{b}_{0.5} \quad (\text{A-35})$$

$$\overline{b}_{4.0} = \overline{b}'_{4.0} - \{[\overline{b}'_{4.0} - b_{4.0}^*]\} \quad (\text{A-36})$$

The absolute phase difference for a fictitious 7.5 wavelength baseline is determined from the absolute medium and coarse data  $b_{4.0}$  and  $b_{3.5}$ , as follows

$$\overline{b}_{7.5} = \overline{b}_{3.5} + \overline{b}_{4.0} \quad (\text{A-37})$$

Finally, the absolute phase difference for the fine baseline is determined from the absolute 7.5 wavelength baseline data.

$$\overline{b}'_F = \overline{b}_{7.5} (N_F/7.5) \quad (\text{A-38})$$

$$\overline{b}_F = \overline{b}'_F - \{[\overline{b}'_F - b_F^*]\} \quad (\text{A-39})$$

The above process is performed for both EW and NS baseline data. The resulting EW and NS fine baseline absolute phase difference polynomials are

$$\overline{b}_m(\tau) = \overline{b}_m(\tau = 0) + B_m \tau + C_m \tau^2 + D_m \tau^3 \quad (\text{A-40})$$

$$(m = \text{EW}_F, \text{NS}_F)$$

where

$$\tau = t - t_m^* \quad (m = \text{EW}_F, \text{NS}_F) \quad (\text{A-41})$$

#### A.4.2.4 Antenna Field Correction

The calibration  $Z_n$  given in Equation (A-28) is determined as an average over the usable antenna field. There are distortions in the field patterns, however, and they are corrected by the following calibration polynomials operating on the corrected absolute phase differences  $\bar{b}_{NS_F}$  and  $\bar{b}_{EW_F}$ , obtained from Equation (A-40). These corrections are of the form given below

$$\begin{bmatrix} \bar{b}_{EW_F} \\ \bar{b}_{NS_F} \end{bmatrix}_{\text{corrected}} = \begin{bmatrix} C_1 \\ C_2 \end{bmatrix} + \begin{bmatrix} C_3 & C_5 \\ C_4 & C_6 \end{bmatrix} \begin{bmatrix} \bar{b}_{EW_F} \\ \bar{b}_{NS_F} \end{bmatrix} + \begin{bmatrix} C_7 \\ C_8 \end{bmatrix} \bar{b}_{EW_F} \bar{b}_{NS_F} + \begin{bmatrix} C_9 & C_{11} \\ C_{10} & C_{12} \end{bmatrix} \begin{bmatrix} \bar{b}_{EW_F}^2 \\ \bar{b}_{NS_F}^2 \end{bmatrix} \\ + \begin{bmatrix} C_{13} & C_{15} \\ C_{14} & C_{16} \end{bmatrix} \begin{bmatrix} \bar{b}_{EW_F}^3 \\ \bar{b}_{NS_F}^3 \end{bmatrix} + \begin{bmatrix} C_{17} & C_{19} \\ C_{18} & C_{20} \end{bmatrix} \begin{bmatrix} \sin(2\pi \bar{b}_{EW_F}) \\ \sin(2\pi \bar{b}_{NS_F}) \end{bmatrix} + \begin{bmatrix} C_{21} & C_{23} \\ C_{22} & C_{24} \end{bmatrix} \begin{bmatrix} \cos(2\pi \bar{b}_{EW_F}) \\ \cos(2\pi \bar{b}_{NS_F}) \end{bmatrix} \quad (A-42)$$

where the coefficients  $C_i$  are obtained by field calibration.

#### A.4.2.5 Conversion to Direction Cosines

The direction cosines  $\ell'$  and  $m'$  of the corrected phase differences are determined from the corrected absolute fine baseline phase differences by dividing by the distance between the fine antennas, expressed in wavelengths of the received signal. The fine antennas are positioned to be  $N_F$  (46 or 57) times the nominal 136,000 MHz vacuum wavelength. For transmitted signal frequencies  $\nu_T$ , the baseline length in terms of the transmitted frequency is  $N_F \nu_T / 136,000$ . Therefore, the direction cosine of the received signal from the station centered local tangent east-pointing axes is

$$\ell' = (\bar{b}_{EW_F})_{\text{corrected}} \left( \frac{136,000}{N_F \nu_T} \right) \quad (A-43)$$

and the direction cosine to the local tangent north-pointing axis

$$m' = (\bar{b}_{NS_F})_{\text{corrected}} \left( \frac{136,000}{N_F \nu_T} \right) \quad (A-44)$$



#### A.4.2.5 Procedure

Several aspects of the procedure influence the accuracy and use of direction cosine data in sub-orbit determination processing. First, the sampled data are approximated by a cubic polynomial which is used to determine the direction cosines. The cubic polynomial can introduce time correlated errors into multiple direction cosine pairs obtained from the same station pass. Therefore, the variance of the residuals between the cubic polynomial and the data should be scrutinized, and consideration should be given to limiting the direction cosine data to one pair per station pass. Second, the received signal frequency in Equations (A-43) and (A-44) neglects the downlink Doppler shift and assumes that the transmitted and received signal frequencies are the same (i.e.,  $\nu_R = \nu_T$ ). Finally, the direction cosines  $\ell'$  and  $m'$  correspond to vacuum signal paths. Thus, atmospheric refraction corrections and light time delays must be applied in the processor.

#### A.5 VERY LONG BASELINE INTERFEROMETER (VLBI)

Like Minitrack, the VLBI system measures the phase differences at two or more ground stations when they simultaneously receive the same radio signal. However, in the VLBI system each terminal is controlled by its own independent frequency standard so that there is no necessity to use cable or microwave links to preserve the phase coherence among these stations. This permits the stations to be separated by arbitrarily large distances, typically of the order of thousands of kilometers. Since the angular resolution of any interferometer is directly proportional to the length of the baseline, the VLBI concept permits the position of the radio source (e.g., satellite) to be determined to a much greater degree of accuracy than is possible with a short baseline system like Minitrack.

The principle underlying the VLBI concept is illustrated by the simplified two-dimensional geometry shown in Figure A-5. The figure shows a signal, characterized as a planar wavefront, being simultaneously received at stations A and B, which are separated by distance D. The phase difference  $\Delta\phi$  between the two received signals is related to the separation of the stations D as follows

$$\Delta\phi = (D/\lambda) \cos \theta \quad (\text{A-45})$$

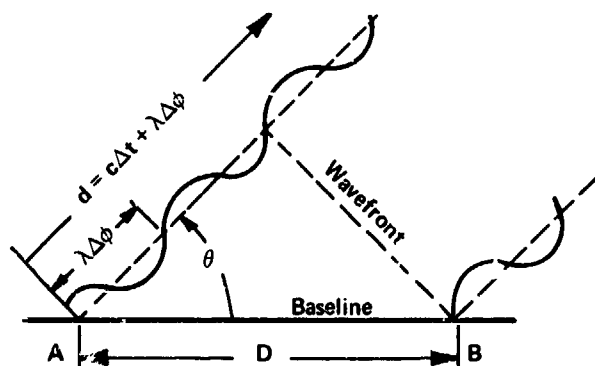


Figure A-5. Simplified Schematic of VLBI

where  $\theta$  is the source direction and  $\lambda$  is the signal wavelength. When the value of  $\theta$  is such that  $\Delta\phi$  is an integral number of half-cycles, i.e.,  $\theta = \cos^{-1} (n\lambda/2D)$  where  $n$  is an integer, the signals received at each terminal are in phase or anti-phase, and a relative extremum of power is available from the interferometer.

As the source transits the interferometer, a power (or intensity) response like that shown in Figure A-6 is produced. The abscissa is time, which is related monotonically to the source direction  $\theta$ . If the time at which a specific fringe is produced can be determined precisely enough, the relationship for  $\Delta\phi$  in Equation (A-45) can be equally precisely specified in terms of source position and baseline parameters. The fringe density is so great, however, that it is very difficult to identify the central fringe (the fringe produced when the source direction is perpendicular to the baseline), and hence very difficult to record accurately the time of passage through any  $n^{\text{th}}$ -order fringe (i.e., the fringe displaced from the central one by  $n$  cycles).

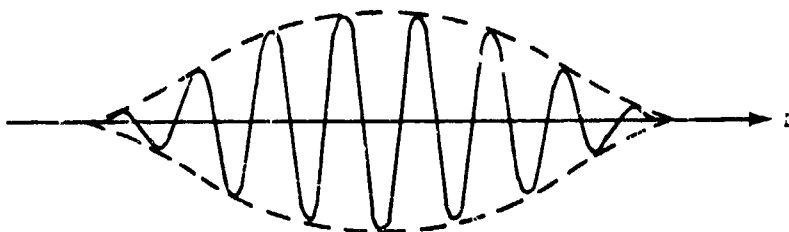


Figure A-6. Interferometer Fringes

The fringe number ambiguity is resolved by recording the received signal onto magnetic tape at as high a bandwidth as possible. These recorded signals are clipped and sampled so that the information is preserved in digital format. Corrections to compensate for the clipping and sampling are applied during preprocessing. Pairs of tapes, one from each station, are crosscorrelated afterwards in a preprocessing program. The correlations are repeated for many trial combinations of relative delay offset and delay-rate offset between the two records. When both digital records are correctly aligned, all of the frequencies within the signal bandwidth will have the same phase, and at this point the superposition of all the harmonic components within the complex correlation function will produce a maximum in its amplitude, as well as in the amplitude of its power spectrum. For each observation, the delay and delay-rate values that produce this maximum are recorded, and the series of such values form the observables that enter as input into the GTDS program.

## A. 6 RADAR ALTIMETER

A satellite is assumed to be in a near earth orbit, and its attitude is assumed to be stabilized so that the axis  $z_1$  of an attached pointing instrument is directed along the local vertical or gravity gradient. This may be accomplished (as for GEOS-C) by gravity gradient stabilization or other attitude stabilization techniques. Such stabilization allows the use of a directional antenna, pointed along the  $z_1$ -axis, for the radar altimeter. The transmitter aboard the satellite transmits X-band signal pulses which form a series of spherical wavefronts directed towards the earth. The antenna beamwidth results in a signal cone with its apex at the transmitter and an axis which coincides approximately with the  $z_1$ -axis of the satellite as shown in Figure A-7. As the wavefront of each pulse intersects the sea surface, it is reflected back towards the satellite. The time difference between the time of transmission and time of reception of the radar pulse is a measure of the height of the satellite above the local surface. If the beamwidth of the transmitted signal is larger than the nominal spacecraft libration in attitude about the local vertical, the first return signal will lie on the transmission path normal to the sea surface and through the satellite. The effective size of the illuminated spot on the surface is determined by the transmitted pulsewidth, the beamwidth, and the type of return pulse detection utilized. As long as the local vertical from the surface to the satellite lies inside the antenna beamwidth cone, the altimeter measurement will represent the shortest distance between the satellite and the sea surface.

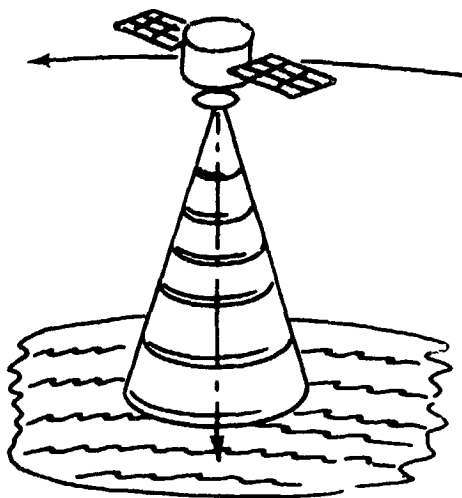


Figure A-7. Radar Altimeter Cone

The satellite timing equipment provides signals for measuring the time interval between the transmitted and received signals, and for time tagging discrete observations. This timing equipment is periodically calibrated from ground stations.

Initial preprocessing of the altimetry data will consist of applying calibration and ambiguity corrections to the two-way time difference between transmitted and received signals, and converting the result to an altitude by multiplying by one-half the speed of light. The time tag is calibrated and corrected to the midinterval time (i.e., the time that the signal is reflected from the sea surface). After these preprocessing computations, each data element is treated as if it were an instantaneous measurement at the midinterval time.

## A.7 SATELLITE-TO-SATELLITE TRACKING

A relay satellite is assumed to be in a near synchronous orbit over a tracking site, and a target satellite is assumed to be in a low elliptical orbit. Figure A-8a presents a schematic of the geometry of the two satellites relative to the tracking site. The tracking station transmits a signal to the relay satellite. The relay satellite then retransmits the signal to the target satellite, which retransmits it back to the relay satellite. Finally, the relay satellite retransmits the signal to the ground station. The signal traverses the path  $S \rightarrow A \rightarrow N \rightarrow A \rightarrow S$ . The return signal, when related to the transmitted signal, can be expressed as the sum of the range segments of the signal path (RS) and the time derivative of the range sum (RSR).

An exaggerated schematic of the signal paths is shown in Figure A-8b. The station transmits a signal at time  $t_0$ . The signal is received by the relay satellite at  $t_1$  and retransmitted to the target satellite at  $t_1 + \Delta\tau_1$  where  $\Delta\tau_1$  is the transponder time delay. The target satellite receives the signal at  $t_2$  and retransmits back to the relay satellite at  $t_2 + \Delta\tau_2$ . The relay satellite receives the retransmitted signal at  $t_3$ , and after a transponder time delay of  $\Delta\tau_3$ , sends it back to the ground station, which receives it at  $t_4$ . The station records the data at UTC tag time  $t_R$ . The signal time delays depicted in Figure A-8b are defined as follows:

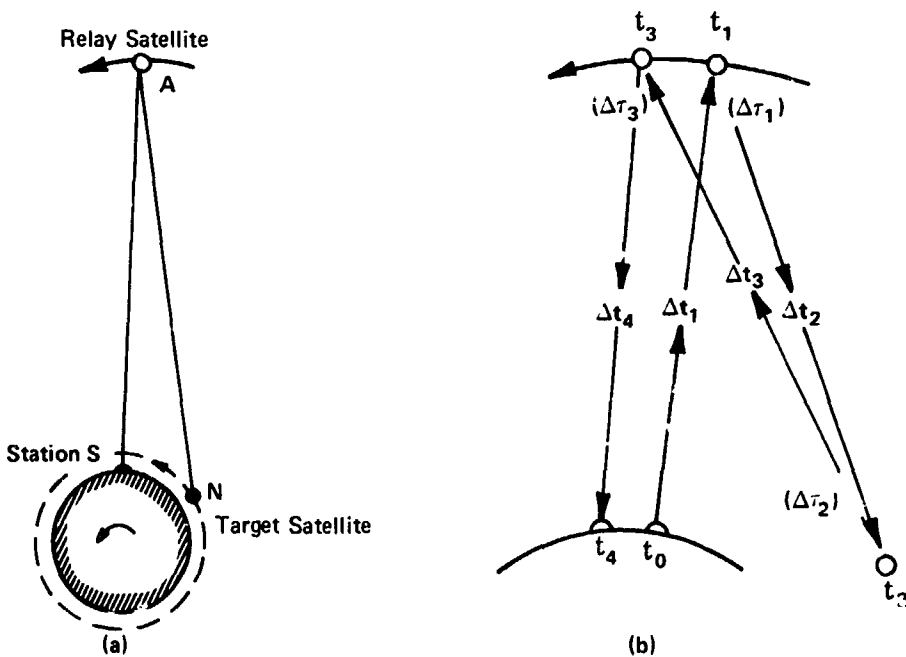


Figure A-8. Range Sum Geometry and Transmission Legs

$\Delta\tau_1 \sim$  time delay due to the transponder on the relay satellite at its first reception

$\Delta\tau_2 \sim$  time delay due to the transponder on the target satellite at its reception

$\Delta\tau_3 \sim$  time delay due to the transponder on the relay satellite at its second reception

$\Delta t_1 \sim$  light time and atmospheric delay during leg 1

$\Delta t_2 \sim$  light time delay during leg 2

$\Delta t_3 \sim$  light time delay during leg 3

$\Delta t_4 \sim$  light time and atmospheric delay during leg 4.

The recorded measurements, described in Section A.1, consist of

- The gimbal angles X and Y defining the direction of the received signal path at time  $t_R$ .
- The four-way range time delay, measured as a count  $C_1$  of the number of cycles of a reference frequency  $\nu_{R1}$  which occurs between the positive-directed zero crossings of the high-frequency ranging tone (frequency  $\nu_h$ ) associated with the transmitted and received signals. The counter is started and the tag time  $t_R$  is signaled simultaneously by a positive zero crossing of the transmitted signal. The counter is stopped at the next zero crossing of the received signal.
- The four-way range-rate measurement can be made in two ways. In the "destruct" method the measurement is  $C_0$ , the number of cycles of a reference frequency  $\nu_{R2}$  required to simultaneously count exactly N cycles of the Doppler-plus-bias signal  $\nu_d + \nu_b$ . The count is begun at time  $t_R$  and ended after the accumulation of N cycles of the  $\nu_d + \nu_b$  signal. In the "non-destruct" method the measurement is N, the number of cycles of the Doppler-plus-bias signal  $\nu_d + \nu_b$  required to simultaneously count  $C_0$ , a fixed number of cycles of the reference frequency, i.e.,  $\Delta t$  for the counting period is constant.

A more detailed description of the Doppler measurement for an existing satellite-to-satellite tracking scheme can be found in Reference 11.

The data sample time  $t_s$  corresponds to the time that the range measurement of the received signal was initiated. Therefore, the end of the measurement occurs at

$$t_0 = t_s + \frac{C_1}{\nu_{R1}} - \Delta t_{RD} \quad (A-46)$$

where  $\Delta t_{RD}$  accounts for the signal propagation delay within the ground station electronics as well as delay in the counter itself, and is determined by on-site calibration. The round trip light time is

$$\Delta t_R = \frac{C_1}{\nu_{R1}} + \frac{\rho_a}{\nu_h} + \frac{\rho_b}{\nu_L} - \Delta\tau - \Delta t_{RD} \quad (A-47)$$

where

$\rho_a, \rho_b \sim$  range ambiguity numbers

$\Delta\tau \sim$  the sum of the transponder time delays

The ambiguity number  $\rho_a$ , the number of cycles of  $\nu_h$ , is determined by range tone methods which superimpose a series of low frequencies on  $\nu_h$ . The ambiguity number  $\rho_b$ , the number of cycles of  $\nu_L$ , is the large ambiguity which results from the light time being greater than  $1/\nu_L$ . Both  $\Delta t_{RD}$  and  $\rho_a/\nu_h$  are accounted for in the logic by the station hardware. The time of the return signal  $t_0$  does not involve the range ambiguity numbers since their effect would be to increase the return time erroneously rather than decrease the transmission time. The range ambiguity can be accounted for in the gross logic of the process, since its omission accounts for large, obvious errors.

## A.8 REFERENCES

1. Grenchik, T. J. and Putney, B. H.: 1969, A Review of Goddard Range and Range-Rate System Measurements and Data Processing Techniques, Goddard Space Flight Center Report X-551-69-137, April 1969.
2. Schmid, P. E.: 1969, The Conversion of Fundamental Tracking Data to Metric Form, Goddard Space Flight Center Report X-551-69-3, January 1969.
3. Watkins, E. R. and Rose, D. H.: 1969, Description of the Goddard Range-Rate Data Processing Program for the CDC-160A, Goddard Space Flight Center Report X-541-69-322, August 1969.
4. Zillig, D. J.: 1969, Data Formats of the Goddard Range and Range-Rate System and the Application Technological Satellite Range and Range-Rate System, Goddard Space Flight Center Report X-571-69-149, April 1969.
5. Scott, J. N.: 1974, STDN User's Guide Baseline Document, Goddard Space Flight Center STDN Report No. 101.1, Revision 2, May 1974.
6. Kallmeyer, F. W.: 1975, Tracking Data Transmission Formats and Reduction Algorithms, Goddard Space Flight Center STDN Report No. 721, Revision 2, May 1975.
7. JPL Design Specification: 1966, MSFN Ground Equipment, Unified S-Band, RF Receiver/Exciter Subsystem, JPL Design Specification No. DNR-1086-DSN-B, July 22, 1966.
8. National Aeronautics and Space Administration Report: 1968, MARK 1A Ranging Subsystem, NASA Report MH-1055, April 1, 1968.
9. Watkins, E. R.: 1969, Preprocessing of Minitrack Data, Goddard Space Flight Center Report TND-5042, May 1969.
10. Control System Research, Inc. Report: 1970, Minitrack Tracking Function Description, March 1970.
11. Ayres, C. L., Stull, H. E., and Teles, J.: 1975, Tracking Data Relay Range and Range Rate Observation Modeling via the Applications Technology Satellite-6 (ATS-6), Goddard Space Flight Center Report X-570-75-53, March 1975.



## APPENDIX B

## TIME ELEMENTS

The Time-Regularized Cowell system of equations achieves analytic stepsize control through the transformation of the independent variable time to a new variable  $s$  defined by

$$\frac{dt}{ds} = r^\alpha \quad (\text{B-1})$$

where  $\alpha$  is called the uniformization constant and  $r$  is the magnitude of the radius vector. The physical time  $t$  is obtained through the integration of Equation (B-1), which involves  $r$ . Any linear error in  $r$  will propagate into a nearly quadratic error in the time. Time elements are introduced to reduce this nearly quadratic error growth to a nearly linear error growth for perturbed motion. An element in two-body motion is defined as a parameter which is either constant or a linear function of the independent variable.

For perturbed motion (assuming small perturbations) an element varies slowly from the two-body solution. Thus, in deriving a time element  $\tau$  for the Time-Regularized Cowell method,  $\tau$  is required to vary linearly with the independent variable  $s$ , i.e.,

$$\frac{d\tau}{ds} = c \quad (\text{B-2})$$

where  $c$  is a constant; it is also required that  $\tau$  be related analytically to the physical time  $t$ . This is done via Kepler's Equation

$$t = t_0 + \frac{1}{n} (E - e \sin E) \quad (\text{B-3})$$

which can be rewritten with the introduction of  $\tau$  as

$$t = t_0 + \tau - \frac{g(\alpha)}{n} + \frac{1}{n} (E - e \sin E) \quad (\text{B-4})$$

where, by definition,

$$\tau = \frac{g(\alpha)}{n} \quad (\text{B-5})$$

and  $g(\alpha)$  is a function relating  $\tau$  to the Kepler element  $\alpha$ .

Differentiating Equation (B-5) with respect to  $s$  and substituting Equations (B-1) and (B-2) yields

$$\frac{dg}{dt} = ncr^{-\alpha} \quad (B-6)$$

## B.1 UNPERTURBED MOTION

The definition of the function  $g$  is obtained for various values of  $\alpha$  by utilizing known integrals of the two-body problem.

### B.1.1 Time Element Corresponding to the Eccentric Anomaly ( $\alpha = 1$ )

In Keplerian motion, the time derivative of the eccentric anomaly  $E$  is given by

$$\frac{dE}{dt} = nar^{-1} \quad (B-7)$$

where the mean motion  $n$  and the semimajor axis  $a$  are constants for two-body motion. Comparing Equations (B-6) and (B-7) for  $\alpha = 1$  yields

$$g = E \quad (B-8a)$$

and

$$c = a \quad (B-8b)$$

Thus,

$$\frac{d\tau}{ds} = \frac{1}{n} \frac{dE}{dt} r^{\alpha} = a \quad (B-9)$$

and, from Equation (B-4)

$$t = t_0 + \tau - \frac{e \sin E}{n} \quad (B-10)$$

which is the desired result for two-body motion.

### B.1.2 Time Element Corresponding to the True Anomaly ( $\alpha = 2$ )

The time derivative of the true anomaly  $f$  is given by

$$\frac{df}{dt} = \sqrt{\mu p} \, r^{-2} \quad (\text{B-11})$$

where the semilatus rectum  $p$  is a constant of the motion for the Kepler problem.

Comparing Equation (B-6) and Equation (B-11) yields

$$g = f \quad (\text{B-12a})$$

and

$$c = \frac{\sqrt{\mu p}}{n} \quad (\text{B-12b})$$

Thus,

$$\frac{d\tau}{ds} = \frac{1}{n} \frac{df}{dt} r^2 = \frac{\sqrt{\mu p}}{n} \quad (\text{B-13})$$

which is the desired differential equation for  $\tau$ . Kepler's equation, Equation (B-4), can then be written as

$$\begin{aligned} t &= t_0 + \tau - \frac{f}{n} + \frac{1}{n} (E - e \sin E) \\ &= t_0 + \tau - \frac{(f - E)}{n} - \frac{e \sin E}{n} \end{aligned} \quad (\text{B-14})$$

## B.2 PERTURBED MOTION

The extension of the time element equation for perturbed motion is presented for  $\alpha = 1$  and  $\alpha = 2$ , using the approach followed in References 1 and 2.

### B.2.1 Time Element Equation Corresponding to the KS Formulation ( $\alpha = 1$ )

Equation (B-10) can be written as

$$\tau = t + \frac{(\bar{\mathbf{r}} \cdot \dot{\bar{\mathbf{r}}})}{2h_k} \quad (\text{B-15})$$

where  $h_k$  is the negative Keplerian energy

$$h_k = \frac{\mu}{r} - \frac{v^2}{2} \quad (\text{B-16})$$

Differentiating Equation (B-15) with respect to the new independent variable  $s$  yields

$$\frac{d\tau}{ds} = \frac{dt}{ds} + \left[ \frac{(\bar{\mathbf{r}} \cdot \ddot{\bar{\mathbf{r}}})}{2h_k} + \frac{(\dot{\bar{\mathbf{r}}} \cdot \dot{\bar{\mathbf{r}}})}{2h_k} - \frac{\bar{\mathbf{r}} \cdot \dot{\bar{\mathbf{r}}}}{2h_k^2} \dot{h}_k \right] \frac{dt}{ds} \quad (\text{B-17})$$

This expression simplifies to

$$\frac{d\tau}{ds} = \frac{\mu}{2h_k} + \frac{r(\bar{\mathbf{r}} \cdot \bar{\mathbf{P}})}{2h_k} + \frac{r(\bar{\mathbf{r}} \cdot \dot{\bar{\mathbf{r}}})(\dot{\bar{\mathbf{r}}} \cdot \bar{\mathbf{P}})}{2h_k^2} \quad (\text{B-18})$$

where  $\bar{\mathbf{P}}$  is the perturbing acceleration, i.e.,

$$\ddot{\bar{\mathbf{r}}} = \frac{-\mu\bar{\mathbf{r}}}{r^3} + \bar{\mathbf{P}} \quad (\text{B-19})$$

The differential equation for the time element in Equation (B-18) clearly has the desired properties in that the element varies linearly with respect to the independent variable  $s$  for unperturbed motion ( $\bar{\mathbf{P}} = 0$ ), and for perturbed motion (providing  $\bar{\mathbf{P}}$  is small) the element varies slowly from the two-body solution. An alternative expression involving the total energy

$$h = h_k - V \quad (\text{B-20})$$

where  $V$  is the perturbing potential, can be derived by beginning with the expression

$$\tau = t + \frac{(\bar{\mathbf{r}} \cdot \dot{\bar{\mathbf{r}}})}{2h} \quad (\text{B-21})$$

Differentiating this equation with respect to the independent variable  $s$  yields

$$\frac{d\tau}{ds} = \frac{1}{2h} [\mu - 2rV - r(\bar{r} \cdot \nabla V) + r(\bar{r} \cdot \bar{P})] - \frac{r(\bar{r} \cdot \dot{\bar{r}})}{2h^2} \dot{h} \quad (B-22)$$

where  $\nabla V$  is the perturbing acceleration due to the perturbing potential function, i.e.,

$$\ddot{\bar{r}} = \frac{-\mu \bar{r}}{r^3} + \bar{P} - \nabla V \quad (B-23)$$

Equation (B-22) can be shown to be the time element equation corresponding to the KS formulation (Equation (5-10a)) by noting that

$$\frac{d}{ds} = 2\omega \frac{d}{dE} \quad (B-24)$$

and

$$\omega = \sqrt{h/2} \quad (B-25)$$

The comparison between Equations (B-18) and the KS equation, Equation (B-22), has been made in Reference 2, and it was found that they give the same amount of accuracy improvement for the tested cases.

## B.2.2 Time Element Equation Corresponding to the DS Formulation ( $\alpha = 2$ )

Equation (B-15) can be written as

$$\tau = t + \frac{(\bar{r} \cdot \dot{\bar{r}})}{2h_k} + \frac{\mu(f - E)}{(2h_k)^{3/2}} \quad (B-26)$$

Differentiating Equation (B-26) with respect to the new independent variable  $s$  yields

$$\begin{aligned} \frac{d\tau}{ds} = \frac{dt}{ds} + \frac{r^2}{2h_k} [(\dot{\bar{r}} \cdot \dot{\bar{r}}) + (\bar{r} \cdot \ddot{\bar{r}})] - \frac{r^2(\bar{r} \cdot \dot{\bar{r}})}{2h_k^2} \dot{h}_k \\ + \frac{\mu r^2}{(2h_k)^{3/2}} (\dot{f} - \dot{E}) - \frac{3\mu r^2(f - E)}{(2h_k)^{5/2}} \dot{h}_k \end{aligned} \quad (B-27)$$

This expression simplifies to

$$\begin{aligned} \frac{d\tau}{ds} = & \frac{\mu}{(2h_k)^{3/2}} \sqrt{\mu p} + \frac{r^2}{2h_k} (\bar{r} \cdot \bar{p}) + \frac{r^2}{2h_k^2} (\bar{r} \cdot \dot{\bar{r}}) (\dot{\bar{r}} \cdot \bar{p}) \\ & + \frac{3\mu r^2}{(2h_k)^{5/2}} (f - E) (\dot{\bar{r}} \cdot \bar{p}) + \frac{\mu r^2}{(2h_k)^{3/2}} \left[ \left( \frac{\partial f}{\partial \dot{\bar{r}}} \right) \cdot \bar{p} - \left( \frac{\partial E}{\partial \dot{\bar{r}}} \right) \cdot \bar{p} \right] \end{aligned} \quad (B-28)$$

Noting that the leading term in this equation is a constant and all other terms are a function of the perturbations, it is clear that this differential equation for  $\tau$  has the desired properties noted previously.

The differential equation for the time element  $\ell$  in the DS formulation (see Equations (5-45), (5-46), and Reference 3) is given by

$$\frac{d\ell}{ds} = \frac{\mu}{(2L)^{3/2}} + v \frac{r}{q} \left( 2 \frac{\partial r}{\partial \beta_4} - \frac{r}{q} \frac{\partial q}{\partial \beta_4} \right) + \frac{r^2}{q} \frac{\partial v}{\partial L} - P_4 \quad (B-29)$$

where  $L$ , the total energy, is one of the elements of the formulation, and  $s$ , the independent variable, is the true anomaly. Transforming the independent variable of Equation (B-28) to the true anomaly using the operator

$$\frac{d}{ds} = (G - \Phi) \frac{d}{df} \quad (B-30)$$

(where  $G$  is the total angular momentum and  $\Phi$  is the perturbing energy) and letting  $Q_1$  represent all terms dependent upon perturbations, yields

$$\frac{d\tau}{df} = \frac{\mu}{(2h_k)^{3/2}} + Q_1 \quad (B-31)$$

If  $Q_2$  represents those terms in Equation (B-29) which are dependent upon perturbations, the following equation results

$$\frac{d\ell}{ds} = \frac{\mu}{(2L)^{3/2}} + Q_2 \quad (B-32)$$

As in the case where  $a = 1$ , the leading term in Equation (B-31) is a function of the Keplerian energy  $h_K$ , whereas the leading term in Equation (B-32) is a function of the total energy  $L$ . This may lead to accuracy improvements for conservative perturbed motion situations, although at present no comparison studies have been performed.

# APPENDIX C

## DEVELOPMENT OF RANGE-RATE FORMULAS

This appendix presents the development of formulas which relate the tracker and spacecraft relative motion to the Doppler shift in an electromagnetic signal transmitted from one to the other. For a further definition of the mathematical symbols used, refer to Appendix A, which describes the GRARR, ATSR, USB and SST Systems.

The general relativistic expression relating the frequencies of an electromagnetic signal propagation from a transmitter to a receiver is

$$\frac{\nu_r}{\nu_t} = \frac{a_t}{a_r} \left[ \frac{1 - F_r \bar{n}_r \cdot \dot{\vec{r}}_r}{1 - F_t \bar{n}_t \cdot \dot{\vec{r}}_t} \right] \quad (C-1)$$

where

$$a = \sqrt{g_{00} + \frac{2}{c} \sum_{i=1}^3 g_{0i} \dot{x}^i + \frac{1}{c^2} \sum_{i,j=1}^3 g_{ij} \dot{x}^i \dot{x}^j} \quad (C-2)$$

$$F = \frac{1}{cg_{00}} \left[ \sqrt{\sum_{i,j=1}^3 (g_{0i}g_{0j} - g_{00}g_{ij}) \frac{dx^i}{dS} \frac{dx^j}{dS}} - \sum_{i=1}^3 g_{0i} \frac{dx^i}{dS} \right] \quad (C-3)$$

and

- $t, r \sim$  subscripts indicating that the designated quantities are evaluated at the transmitter and receiver, respectively
- $\nu_t, \nu_r \sim$  frequencies of the transmitted and received signals
- $\dot{\vec{r}}_t, \dot{\vec{r}}_r \sim$  velocities of the transmitter and receiver, defined as the derivatives of their inertial positions with respect to the coordinate time  $\tilde{t}$
- $g_{ij} \sim$  elements of the metric matrix defining the nature of the space-time frame



$x^i \sim$  components of the space coordinates

$S \sim$  arc length along the propagation path

$\bar{n}_t, \bar{n}_r \sim$  unit vectors along the local propagation path at the transmitter and receiver, respectively

$c \sim$  wave propagation speed

The derivatives  $dx^i/dS$  are simply the direction cosines of the propagation path, and thus are the components of the local unit vector  $\bar{n}$ .

Equation (C-1) is derived under the assumption that the metric elements  $g_{ij}$  vary slowly in time compared with the wave propagation speed  $c$ . This is a good approximation since the variations of the  $g_{ij}$  's are due to planetary motions, which are very slow compared with  $c$ .

In principle, the  $g_{ij}$  should mathematically describe everything that physically affects the propagation of electromagnetic waves in their region of definition, including gravitational influences, the refractive effects of the atmosphere, and any other significant influences. If such a rigorous mathematical description of the space-time frame could be formulated and then solved analytically, propagation paths for specific cases could be computed very accurately as geodesics. However, no such completely general treatment of the problem has yet been produced.

It is generally assumed that the metric coefficients for the case of special relativity are

$$\left. \begin{aligned} g_{00} &= 1 \\ g_{ii} &= -1 \\ g_{ij} &= 0, i \neq j \end{aligned} \right\} i, j = 1, 2, 3 \quad (C-4)$$

Equation (C-2) then becomes

$$a = \sqrt{1 - \frac{\dot{\vec{r}} \cdot \dot{\vec{r}}}{c^2}} \quad (C-5)$$

and Equation (C-3) simplifies to

$$F = \frac{1}{c} \quad (C-6)$$

The propagation path, which is the straight relative position vector from  $\vec{r}_t$  to  $\vec{r}_r$ , is given by

$$\vec{n}_t = \vec{n}_r = \vec{n} = \frac{\vec{r}_r - \vec{r}_t}{|\vec{r}_r - \vec{r}_t|} \quad (C-7)$$

Under the preceding conditions, Equation (C-1) reduces to

$$\frac{\nu_r}{\nu_t} = \sqrt{\frac{1 - \frac{\dot{\vec{r}}_t \cdot \dot{\vec{r}}_t}{c^2}}{1 - \frac{\dot{\vec{r}}_r \cdot \dot{\vec{r}}_r}{c^2}}} \left[ \frac{1 - \frac{\vec{n} \cdot \dot{\vec{r}}_r}{c}}{1 - \frac{\vec{n} \cdot \dot{\vec{r}}_t}{c}} \right] \quad (C-8)$$

which is the formula from special relativity for the one-way Doppler frequency shift.

The metric coefficients in Equation (C-4) describe straight line propagation in a vacuum. The neglect of the ray path bending due to gravitational effects is an acceptable approximation, considering the precision of the radar Doppler measuring equipment. However, the refractive bending of the ray by the atmosphere (troposphere and ionosphere) is not negligible and must be taken into account. The special relativistic formula given by Equation (C-8) is modified to replace the unit vector  $\vec{n}$  along the idealized straight ray path with the unit vectors

$$\begin{aligned} \vec{n}_t &= \vec{n} + \Delta\vec{n}_t \\ \vec{n}_r &= \vec{n} + \Delta\vec{n}_r \end{aligned} \quad (C-9)$$

along the actual curved propagation path. The method by which the refraction difference vectors  $\Delta\vec{n}_t$  and  $\Delta\vec{n}_r$  are estimated is discussed in Chapter 7. Here the terms will simply be introduced into the equations and formally carried through the derivations. As a result of this substitution, Equation (C-8) becomes

$$\frac{\nu_r}{\nu_t} = \sqrt{\frac{1 - \frac{\dot{\bar{r}}_t \cdot \dot{\bar{r}}_t}{c^2}}{1 - \frac{\dot{\bar{r}}_r \cdot \dot{\bar{r}}_r}{c^2}}} \left[ \frac{1 - \frac{\bar{n}_r \cdot \dot{\bar{r}}_r}{c}}{1 - \frac{\bar{n}_t \cdot \dot{\bar{r}}_t}{c}} \right] \quad (C-10)$$

where  $\bar{n}_r$  and  $\bar{n}_t$  are given by Equations (C-9).

The geometry of two-way (or three-way) signal propagation is illustrated in Figure C-1. A continuous wave signal of frequency  $\nu_T$  is emitted by a ground station at position  $\bar{r}_T$  at time  $t_T$ . At a later time  $t_v$ , the spacecraft at position  $\bar{r}_v$  receives this signal along the curved uplink transmission path. Application of Equation (C-10) gives the relationship between the apparent signal frequency at the ground transmitter  $\nu_T$  and at the spacecraft receiver  $\nu_v$ , i.e.,

$$\frac{\nu_v}{\nu_T} = \sqrt{\frac{1 - \frac{\dot{\bar{r}}_T \cdot \dot{\bar{r}}_T}{c^2}}{1 - \frac{\dot{\bar{r}}_v \cdot \dot{\bar{r}}_v}{c^2}}} \left[ \frac{1 - \frac{\dot{\bar{u}}_v \cdot \dot{\bar{r}}_v}{c}}{1 - \frac{\dot{\bar{u}}_T \cdot \dot{\bar{r}}_T}{c}} \right] \quad (C-11)$$

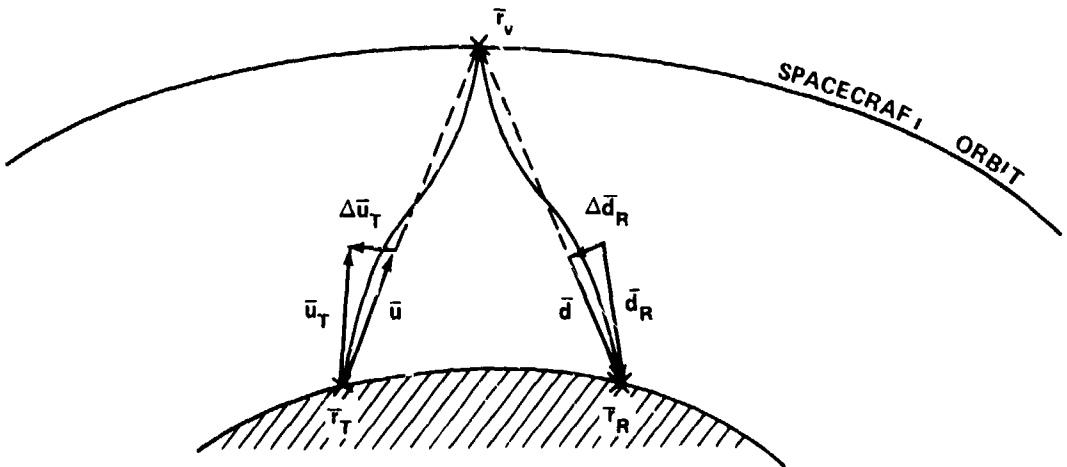


Figure C-1. Signal Propagation Geometry

where

$$\begin{aligned}\bar{u}_T &= \bar{u} + \Delta\bar{u}_T \\ \bar{u}_v &= \bar{u} + \Delta\bar{u}_v \\ \bar{u} &= \frac{\bar{r}_v - \bar{r}_T}{|\bar{r}_v - \bar{r}_T|}\end{aligned}\tag{C-12}$$

and the subscript T refers to quantities evaluated at the ground transmitter.

Although it is not rigorously correct to do so, the spacecraft USB transponder can be modeled as though it coherently turns the received signal around and retransmits it at the received frequency  $\nu_v$ .\* The downlink signal is received by the ground station (either the same station which transmitted the uplink signal or an entirely different station whose oscillator is coherently linked with the transmitter) at position  $\bar{r}_R$  at time  $t_R$ . The one-way frequency shift which occurs on the curved downlink path is

$$\frac{\nu_R}{\nu_v} = \sqrt{\frac{1 - \frac{\dot{\bar{r}}_v \cdot \dot{\bar{r}}_v}{c^2}}{1 - \frac{\dot{\bar{r}}_R \cdot \dot{\bar{r}}_R}{c^2}}} \left[ \frac{1 - \frac{\bar{d}_R \cdot \dot{\bar{r}}_R}{c}}{1 - \frac{\bar{d}_v \cdot \dot{\bar{r}}_v}{c}} \right]\tag{C-13}$$

where

$$\begin{aligned}\bar{d}_v &= \bar{d} + \Delta\bar{d}_v \\ \bar{d}_R &= \bar{d} + \Delta\bar{d}_R \\ \bar{d} &= \frac{\bar{r}_R - \bar{r}_v}{|\bar{r}_R - \bar{r}_v|}\end{aligned}\tag{C-14}$$

The relationship between the transmitted and received ground frequencies for this two- or three-way case is computed by multiplying Equations (C-11) and (C-13) together to obtain

\*The USB uplink frequency capability is 2025 to 2120 MHz, and the downlink frequency capability is 2200 to 2300 MHz.

$$\frac{\nu_R}{\nu_T} = \sqrt{\frac{1 + \frac{\dot{\vec{r}}_T \cdot \dot{\vec{r}}_T}{c^2}}{1 + \frac{\dot{\vec{r}}_R \cdot \dot{\vec{r}}_R}{c^2}}} \left[ \frac{1 - \frac{\vec{u}_v \cdot \dot{\vec{r}}_v}{c}}{1 - \frac{\vec{u}_T \cdot \dot{\vec{r}}_T}{c}} \right] \left[ \frac{1 - \frac{\vec{d}_R \cdot \dot{\vec{r}}_R}{c}}{1 - \frac{\vec{d}_v \cdot \dot{\vec{r}}_v}{c}} \right] \quad (C-15)$$

The frequencies  $\nu_R$  and  $\nu_T$  are defined with respect to the tracking station oscillator. In the language of relativity theory, this "clock" measures the proper time associated with the inertially moving tracking station. The velocities, on the other hand, are all defined in terms of derivatives with respect to coordinate time, the time system associated with the inertial reference frame. This time can be regarded as the same as uniform time for the present development.

If Equations (C-12) and (C-14) are substituted into Equation (C-15), and the factors within the brackets are expanded in terms of no higher order than  $\Delta \vec{u} \cdot (\dot{\vec{r}}/c)$  or  $\Delta \vec{d} \cdot (\dot{\vec{r}}/c)$ , the following form results

$$\frac{\nu_R}{\nu_T} = \sqrt{\frac{1 + \frac{\dot{\vec{r}}_T \cdot \dot{\vec{r}}_T}{c^2}}{1 + \frac{\dot{\vec{r}}_R \cdot \dot{\vec{r}}_R}{c^2}}} \left\{ \left[ \frac{1 - \frac{\vec{u} \cdot \dot{\vec{r}}_v}{c}}{1 - \frac{\vec{u} \cdot \dot{\vec{r}}_T}{c}} \right] \left[ \frac{1 - \frac{\vec{d} \cdot \dot{\vec{r}}_R}{c}}{1 - \frac{\vec{d} \cdot \dot{\vec{r}}_v}{c}} \right] + \frac{\Delta \dot{\rho}}{c} \right\} \quad (C-16)$$

where

$$\Delta \dot{\rho} = \Delta \vec{u}_T \cdot \dot{\vec{r}}_T + \Delta \vec{d}_v \cdot \dot{\vec{r}}_v - \Delta \vec{u}_v \cdot \dot{\vec{r}}_v - \Delta \vec{d}_R \cdot \dot{\vec{r}}_R$$

The first term within the braces (the product of the expressions in brackets) represents the vacuum portion of the Doppler shift. The additional term  $\Delta \dot{\rho}/c$ , involving the propagation path unit vector deflections, represents the refraction effects. Equation (C-16) relates the received frequency to the transmitted frequency via the geometry of the round-trip light path.

The continuously transmitted signal is beat against the received signal, resulting in a signal with a frequency equal to the difference between the two, i.e.,

$$\nu_d = \nu_R - \nu_T = \nu_T \left( \frac{\nu_R}{\nu_T} - 1 \right) \quad (C-17)$$

A fixed frequency bias signal  $\nu_b$  is added to this Doppler signal and the combination is fed to a Doppler-plus-bias cycle counter. Simultaneously, a reference frequency  $\nu_{R_2}$  is fed to a separate time interval counter. At most tracking stations, the bias and reference frequencies are coherently derived from the same source as  $\nu_T$ . The measurement is mechanized in one of two ways, a destruct or a non-destruct count. The destruct count mode (employed in the GRARR and ATSR systems) counts a preassigned fixed number of cycles  $N$  of the Doppler-plus-bias signal and records the measurement as the (variable) number  $C_0$  of cycles of the reference frequency required to accumulate the simultaneous  $N$  cycle count. The nondestruct mode (employed in the USB and ATSR SST systems) continually accumulates the count of the Doppler-plus-bias signal in its counter. The measurement consists of recording this continually increasing number whenever a preassigned fixed number of reference frequency cycles has been accumulated. Differences between the recorded values at different sample times gives the number  $N$  of the Doppler-plus-bias count over the reference time interval. Using either technique, the measurement results in a count of some number  $N$  of Doppler-plus-bias cycles over a period of time

$$\Delta t_{RR} = \frac{C_0}{\nu_{R_2}} \quad (C-18)$$

This measurement count can be modeled mathematically by the equation

$$N = \int_t^{t+\Delta t_{RR}} (\nu_d + \nu_b) dt_R \quad (C-19)$$

If the measurement is made in the destruct mode, the integration time interval  $\Delta t_{RR}$  should be varied until the computed value of  $N$  matches the fixed cycle count number exactly. In the nondestruct mode,  $\Delta t_{RR}$  is fixed and  $N$ , in general, will be some whole number of cycles plus a fractional part. This fractional part should be truncated to simulate more rigorously the actual accumulation of whole cycles.

The integration variable  $t_R$  in Equation (C-19) is the receiving station clock time, or proper time. The significance of this point will become evident during the evaluation of the integral.

Substitution of Equation (C-17) into Equation (C-19) yields

$$\begin{aligned}
N &= \int_t^{t+\Delta t_{RR}} \left[ \nu_T \left( \frac{\nu_R}{\nu_T} \right) + \nu_b - \nu_T \right] dt_R \\
&= (\nu_b - \nu_T) \Delta t_{RR} + \nu_T \int_t^{t+\Delta t_{RR}} \frac{\nu_R}{\nu_T} dt_R
\end{aligned} \tag{C-20}$$

and Equation (C-16) can be substituted for the remaining integrand

$$N = (\nu_b - \nu_T) \Delta t_{RR} + \nu_T \sqrt{\frac{1 + \frac{\dot{\vec{r}}_T \cdot \dot{\vec{r}}_T}{c^2}}{1 + \frac{\dot{\vec{r}}_R \cdot \dot{\vec{r}}_R}{c^2}}} \tag{C-21}$$

$$\times \int_t^{t+\Delta t_{RR}} \left[ \frac{1 - \frac{\vec{u} \cdot \dot{\vec{r}}_v}{c}}{1 - \frac{\vec{u} \cdot \dot{\vec{r}}_T}{c}} \right] \left[ \frac{1 - \frac{\vec{d} \cdot \dot{\vec{r}}_R}{c}}{1 - \frac{\vec{d} \cdot \dot{\vec{r}}_v}{c}} \right] dt_R + \nu_T \Delta t_{RR} \left( \frac{\Delta \dot{\rho}_{avg}}{c} \right) \sqrt{\frac{1 + \frac{\dot{\vec{r}}_T \cdot \dot{\vec{r}}_T}{c^2}}{1 + \frac{\dot{\vec{r}}_R \cdot \dot{\vec{r}}_R}{c^2}}}$$

In writing Equation (C-21), it is assumed that the squares of the inertial speeds  $\dot{\vec{r}}_T \cdot \dot{\vec{r}}_T$  and  $\dot{\vec{r}}_R \cdot \dot{\vec{r}}_R$  are constant, since the motion of the tracking stations is due to the nearly uniform rotation of the earth. The refraction integral is evaluated by the trapezoidal rule, yielding

$$\Delta \dot{\rho}_{avg} = \frac{\Delta \rho_t + \Delta t_{RR} + \Delta \rho_t}{2} \tag{C-22}$$

The remaining integral in Equation (C-21) will now be considered. The geometries of the uplink and downlink ranges are related to the light times by

$$\rho_u = |\vec{r}_v - \vec{r}_T| = c(\tilde{t}_v - \tilde{t}_T) \tag{C-23}$$

and

$$\rho_d = |\vec{r}_R - \vec{r}_v| = c(\tilde{t}_R - \tilde{t}_v) \tag{C-24}$$

The derivatives of these ranges with respect to the coordinate time  $\tilde{t}$  at the receiver are given by

$$\frac{d\rho_u}{d\tilde{t}_R} = \bar{u} \cdot \left( \dot{\tilde{r}}_v \frac{d\tilde{t}_v}{d\tilde{t}_R} - \dot{\tilde{r}}_T \frac{d\tilde{t}_T}{d\tilde{t}_R} \right) = c \left( \frac{d\tilde{t}_v}{d\tilde{t}_R} - \frac{d\tilde{t}_T}{d\tilde{t}_R} \right) \quad (C-25)$$

$$\frac{d\rho_d}{d\tilde{t}_R} = \bar{d} \cdot \left( \dot{\tilde{r}}_R - \dot{\tilde{r}}_v \frac{d\tilde{t}_v}{d\tilde{t}_R} \right) = c \left( 1 - \frac{d\tilde{t}_v}{d\tilde{t}_R} \right) \quad (C-26)$$

Explicit solution for the coordinate time derivatives gives

$$\frac{d\tilde{t}_v}{d\tilde{t}_R} = \frac{1 - \bar{d} \cdot \frac{\dot{\tilde{r}}_R}{c}}{1 - \bar{d} \cdot \frac{\dot{\tilde{r}}_v}{c}} = 1 - \frac{1}{c} \frac{d\rho_d}{d\tilde{t}_R} \quad (C-27)$$

$$\frac{d\tilde{t}_T}{d\tilde{t}_R} = \frac{1 - \bar{u} \cdot \frac{\dot{\tilde{r}}_v}{c}}{1 - \bar{u} \cdot \frac{\dot{\tilde{r}}_T}{c}} \left( \frac{d\tilde{t}_v}{d\tilde{t}_R} \right) = 1 - \frac{1}{c} \left( \frac{d\rho_d}{d\tilde{t}_R} + \frac{d\rho_u}{d\tilde{t}_R} \right)$$

Equations (C-27) show that a coordinate time increment of a given length at the receiving station corresponds to increments of different lengths at the spacecraft and at the transmitter, considering that the arrival of corresponding phases at  $\tilde{t}_T$  and  $\tilde{t}_T + d\tilde{t}_T$  marks the interval.

Substitution of Equations (C-27) into the integrand in Equation (C-21) yields the expression for the integral term

$$\nu_T \sqrt{\frac{1 + \frac{\dot{\tilde{r}}_T \cdot \dot{\tilde{r}}_T}{c^2}}{1 + \frac{\dot{\tilde{r}}_R \cdot \dot{\tilde{r}}_R}{c^2}}} \int_{t_R}^{t_R + \Delta t_{RR}} \left[ 1 - \frac{1}{c} \left( \frac{d\rho_d}{d\tilde{t}_R} + \frac{d\rho_u}{d\tilde{t}_R} \right) \right] dt_R \quad (C-28)$$



At the receiving station, the relationship between coordinate and proper time is

$$dt_R = \sqrt{1 - \frac{\dot{\vec{r}}_R \cdot \dot{\vec{r}}_R}{c^2}} d\tilde{t}_R \quad (C-29)$$

Therefore,

$$\left(1 - \frac{\dot{\vec{r}}_R \cdot \dot{\vec{r}}_R}{c^2}\right) \frac{d\rho}{d\tilde{t}_R} = \frac{d\rho}{dt_R} \quad (C-30)$$

and, since it was assumed that  $\dot{\vec{r}}_R \cdot \dot{\vec{r}}_R = \text{constant}$ , Equation (C-21) becomes

$$N = \nu_b \Delta t_{RR} - \frac{\nu_T}{c} \Delta \rho_c + \frac{\nu_T}{c} \Delta t_{RR} \Delta \dot{\rho}_{avg} \quad (C-31)$$

Terms higher than first order in  $|\dot{\vec{r}}|/c$  have been neglected, and the computed quantity

$$\Delta \rho_c = (\rho_u + \rho_d)_{t_R + \Delta t_{RR}} - (\rho_u + \rho_d)_{t_R} \quad (C-32)$$

is the range difference. Since the quantities  $N$ ,  $\Delta t_{RR}$ ,  $\nu_b$ , and  $\nu_T$  are known, the preprocessor program can compute the "observation"

$$\dot{\rho}_0 = \frac{c}{2\nu_T} \left( \nu_b - \frac{N}{\Delta t_{RR}} \right) \quad (C-33)$$

and Equation (C-31) can be written as

$$\frac{\Delta \rho_c}{2\Delta t_{RR}} = \dot{\rho}_0 + \frac{\Delta \dot{\rho}_{avg}}{2} \quad (C-34)$$

where the division by  $2 \Delta t_{RR}$  causes the range difference to approximate the one-way range rate. Equation (C-34) mathematically describes the modeling of the USB Doppler measurement in GTDS. The quantity on the left side of the equation is the computed measurement and is calculated by means of Equations

(C-32), (C-23), and (C-24). The latter two equations require that two iterative light-time solutions be determined to correspond to the round-trip propagation paths terminating at the receiving station at the start and at the end of the Doppler-plus-bias count interval  $\Delta t_{RR}$ . The first term on the right side of Equation (C-34) represents the actual observation and is calculated in the preprocessor from the basic measurement data according to Equation (C-33). The second term on the right in Equation (C-34) is the refraction correction term. It is computed by Equations (C-22) and (C-16), where the appropriate  $\Delta \bar{u}$  and  $\Delta \bar{d}$  path deflection vectors are computed as described in Section 7.6.3.3.

The GRARR and sidetone ATSR Doppler observations are implemented in GTDS in the form of a very simple model. The Doppler measurements made with the GRARR and ATSR systems differ from those made using the USB system in terms of the hardware details. The GRARR VHF system operates with a nominal uplink carrier frequency of 148.98 MHz and a nominal downlink frequency of 136.89 MHz. The ATSR system, operating in the sidetone Doppler mode, uses C-Band frequencies of approximately 6000 and 4000 MHz on the uplink and downlink legs, respectively.

The simple model for these data types is derived by further restricting the assumptions made in deriving Equation (C-15). As given, that expression for the two-way Doppler-shifted frequency ratio is valid under the assumptions that special relativity holds and that the origin of the inertial coordinate frame is at the center of the earth. If it is assumed instead that the tracking station moves with uniform velocity, i.e.,

$$\dot{\bar{r}}_R = \dot{\bar{r}}_T = \text{constant (inertially)}$$

then the origin of the coordinate system can be considered to be fixed at the tracking station and moving with it. Then

$$\bar{r}_R = \dot{\bar{r}}_T = 0$$

and Equation (C-15) becomes

$$\frac{\nu_R}{\nu_T} = \frac{1 - \frac{\bar{u}_v \cdot \dot{\bar{r}}_v}{c}}{1 - \frac{\bar{d}_v \cdot \dot{\bar{r}}_v}{c}}$$

Substituting Equations (C-12) and (C-14) into this expression, expanding, eliminating higher order terms, and noting that in this case  $\bar{\mathbf{u}} = -\bar{\mathbf{d}}$

$$\frac{\nu_R}{\nu_T} = \frac{1 - \frac{\bar{\mathbf{u}} \cdot \dot{\bar{\mathbf{r}}}_v}{c}}{1 + \frac{\bar{\mathbf{u}} \cdot \dot{\bar{\mathbf{r}}}_v}{c}} + \frac{\Delta \dot{\rho}}{c} \quad (\text{C-35})$$

where

$$\Delta \dot{\rho} = 2 \Delta \bar{\mathbf{u}}_v \cdot \dot{\bar{\mathbf{r}}}_v$$

Since the tracking station is motionless in this coordinate frame, the unit vector  $\bar{\mathbf{u}}$  can be defined in terms of the instantaneous position vector of the vehicle relative to the station

$$\bar{\mathbf{u}} = \frac{\bar{\mathbf{r}}_v(\tilde{t}_v)}{|\bar{\mathbf{r}}_v(\tilde{t}_v)|} \quad (\text{C-36})$$

at the vehicle turnaround time  $\tilde{t}_v$ . The instantaneous relative range at this time is

$$\rho = |\bar{\mathbf{r}}_v(\tilde{t}_v)| \quad (\text{C-37})$$

and the rate of change with respect to coordinate time is

$$\dot{\rho} = \bar{\mathbf{u}} \cdot \dot{\bar{\mathbf{r}}}_v \quad (\text{C-38})$$

If Equation (C-38) is substituted into Equation (C-35) and the result then substituted into Equation (C-20)

$$\begin{aligned} N - \nu_b \Delta t_{RR} &= \nu_T \int_t^{t+\Delta t_{RR}} \left[ \frac{1 - \frac{\dot{\rho}}{c}}{1 + \frac{\dot{\rho}}{c}} - 1 - 2 \frac{\Delta \bar{\mathbf{u}}_v \cdot \dot{\bar{\mathbf{r}}}_v}{c} \right] dt_R \\ &= -2\nu_T \int_t^{t+\Delta t_{RR}} \left[ \frac{\dot{\rho}}{c + \dot{\rho}} + \frac{\Delta \bar{\mathbf{u}}_v \cdot \dot{\bar{\mathbf{r}}}_v}{c} \right] dt_R \end{aligned} \quad (\text{C-39})$$

Applying the Theorem of the Mean gives

$$N + \nu_b \Delta t_{RR} = -2\nu_T \left( \frac{\dot{\rho}}{c + \dot{\rho}} \right)_{avg} \Delta t_{RR} - 2\nu_T \left( \frac{\Delta \bar{u}_v \cdot \dot{\bar{r}}_v}{c} \right)_{avg} \Delta t_{RR} \quad (C-40)$$

The last term on the right is the refraction correction, and it will be assumed that the mean value can be approximated with sufficient accuracy by evaluating  $\Delta \bar{u}_v$  and  $\dot{\bar{r}}_v$  at the vehicle turnaround time  $\tilde{t}_v^*$  corresponding to the counting interval midpoint. With this understanding, the subscript "avg" will be dropped from this term. Writing  $\dot{\rho}_{avg}$  for the value of the range rate which produces the correct average value in Equation (C-40), and solving explicitly for  $\dot{\rho}_{avg}$  gives

$$\dot{\rho}_{avg} = \frac{c \left( \nu_b - \frac{N}{\Delta t_{RR}} - 2\nu_T \frac{\Delta \bar{u}_v \cdot \dot{\bar{r}}_v}{c} \right)}{2\nu_T - \left( \nu_b - \frac{N}{\Delta t_{RR}} - 2\nu_T \frac{\Delta \bar{u}_v \cdot \dot{\bar{r}}_v}{c} \right)} \quad (C-41)$$

Expanding this expression in terms of the small parameter  $\Delta \bar{u}_v \cdot \dot{\bar{r}}_v$  and eliminating higher order terms in this parameter, and terms involving this parameter divided by  $c$ , yields

$$\dot{\rho}_{avg} = \frac{c \left( \nu_b - \frac{N}{\Delta t_{RR}} \right)}{2\nu_T - \left( \nu_b - \frac{N}{\Delta t_{RR}} \right)} - \Delta \bar{u}_v \cdot \dot{\bar{r}}_v \quad (C-42)$$

It is again assumed that the correct average value for  $\dot{\rho}_{avg}$ , the instantaneous relative range rate, is given by Equation (C-38) evaluated at  $\tilde{t}_v^*$ , the vehicle turnaround time corresponding to the counting interval midpoint at the ground station. Equation (C-42) therefore represents the model of the GRARR and sidetone ATSR Doppler measurements in the form of an instantaneous relative range rate. The term on the left is the computed value obtained by evaluating Equation (C-38) for the current estimate of the spacecraft ephemeris. The first term on the right side of Equation (C-42)

$$\dot{\rho}_0 = \frac{c \left( \nu_b - \frac{N}{\Delta t_{RR}} \right)}{2\nu_T - \left( \nu_b - \frac{N}{\Delta t_{RR}} \right)} \quad (C-43)$$

is the algorithm in current use in the preprocessing of the GRARR and ATSR Doppler data (References 1 through 4 in Appendix A) and represents the given observation. The second term on the right side of Equation (C-2),  $\Delta \bar{u}_v \cdot \hat{r}_v$ , is the refraction correction. The vehicle velocity is taken at the time  $t_v^*$  defined above, and  $\Delta \bar{u}_v$  is evaluated as described in Section 7.3.3.3.

A development similar to the one presented in this appendix is carried out in Reference 2 of Chapter 7 for the four-way Doppler measurements used in the ATSR Satellite-to-Satellite (SST) Tracking System (see Section 7.3). The resulting range difference for the Doppler count is

$$N = \nu_b \Delta t_{RR} - \frac{\nu_{R_2}^A}{c} \Delta \rho_L - \frac{\nu_{R_2}^B}{c} \Delta \rho_S \quad (C-44)$$

where

$\nu_{R_2} \sim$  system reference frequency

$\nu_b \sim$  bias frequency

A, B, C  $\sim$  constants which depend on the tracking mode counting method and the frequency option used

$\Delta \rho_L, \Delta \rho_S \sim$  changes in the four-leg and two-leg round trip ranges, respectively, during the count interval  $\Delta t_{RI}$ .

REPRODUCIBILITY OF THE  
ORIGINAL PAGE IS POOR

# APPENDIX D

## OBSERVATION WEIGHTING

Tables D-1 and D-2 define typical dynamic weighting factors and a priori standard deviations for several observation types that are processed in GTDS. The dynamic weighting factors are used in the following manner: If  $\sigma^2$  is the a priori variance for a given observation type and  $\rho_F$  is the dynamic weighting factor, then the data weight for an observation is formed as

$$w = \rho_F / \sigma^2 \quad (D-1)$$

or, for those observations where a dynamic weighting factor is not specified,

$$w = 1 / \sigma^2 \quad (D-2)$$

Table D-1  
Dynamic Weighting Factors

Observation Type	Dynamic Weighting Factor*
Minitrack direction cosine $\ell$	$\sqrt{1 - \ell^2}$
Minitrack direction cosine $m$	$\sqrt{1 - m^2}$
Range	$C_1 \sin (\text{Elevation}) + C_2$
Range Rate	$C_1 \sin (\text{Elevation}) + C_2$
Elevation	$C_1 \sin (\text{Elevation}) + C_2$
Azimuth	$C_3 \cos (\text{Elevation}) + C_4$

\* $C_1$ ,  $C_2$ ,  $C_3$ , and  $C_4$  are user-supplied constants.

Table D-2  
Typical A Priori Data Standard Deviations

Observation Type	A Priori Standard Deviation
Range (VHF)	500 meters
Range Rate (VHF)	30 centimeters/second
X <sub>30</sub> Orientation angle (VHF)	3600 seconds of arc
Y <sub>30</sub> Orientation angle (VHF)	3600 seconds of arc
Minitrack direction cosine $\ell$	0.3 mils
Minitrack direction cosine m	0.3 mils
Range (S-Band)	100 meters
Range Rate (S-Band)	10 centimeters/second
Azimuth (C-Band)	54 seconds of arc
Elevation (C-Band)	54 seconds of arc
Range (USB)	15 meters
Range Rate (USB)	5 centimeters/second
X <sub>30</sub> (USB)	720 seconds of arc
Y <sub>30</sub> (USB)	720 seconds of arc
X <sub>85</sub> (USB)	54 seconds of arc
Y <sub>85</sub> (USB)	54 seconds of arc

## APPENDIX E

### MATRIX IDENTITIES ASSOCIATED WITH SEQUENTIAL ESTIMATION

This appendix presents the derivations of a recursive form of the covariance matrix of error and an alternative form of the optimal linear gain. The results of these derivations are used in Section 8.4.1 to simplify the expressions for the covariance matrix of error and the updated state correction vector.

The following symbols are used in the derivations

$P \sim$  a symmetric, positive definite matrix

$I \sim$  the identity matrix

$w_{m+1} \sim$  the weight of the  $(m+1)^{st}$  measurement; its inverse is equal to the variance of the measurement noise

$F \sim$  the matrix of partial derivatives (see Equation (8-6))

#### E.1 DERIVATION OF THE RECURSIVE FORM OF THE COVARIANCE MATRIX OF ERROR, $P_{\Delta x_{m+1}}$

From Equation (8-80b) the covariance matrix of error is given as

$$P_{\Delta x_{m+1}} = P_{\Delta x_m} + \Delta P \quad (E-1)$$

In order to find an expression for  $\Delta P$ , Equation (E-1) is substituted into

$$P_{\Delta x_{m+1}}^{-1} P_{\Delta x_{m+1}} = I \quad (E-2)$$

yielding

$$P_{\Delta x_{m+1}}^{-1} (P_{\Delta x_m} + \Delta P) = I \quad (E-3)$$

Inverting Equation (8-79), the following expression is obtained

$$P_{\Delta x_{m+1}}^{-1} = (P_{\Delta x_m}^{-1} + F_{m+1}^T w_{m+1} F_{m+1}) \quad (E-4)$$

Substituting Equation (E-4) into Equation (E-3) gives

$$P_{\Delta x_m}^{-1} \Delta P + F_{m+1}^T w_{m+1} F_{m+1} P_{\Delta x_m} + F_{m+1}^T w_{m+1} F_{m+1} \Delta P = 0 \quad (E-5)$$



Premultiplying Equation (E-5) by  $P_{\Delta x_m}$  yields

$$\Delta P + P_{\Delta x_m} F_{m+1}^T w_{m+1} F_{m+1} P_{\Delta x_m} + P_{\Delta x_m} F_{m+1}^T w_{m+1} F_{m+1} \Delta F = 0 \quad (E-6)$$

Solving this expression for  $\Delta P$  yields

$$\Delta P = - (I + P_{\Delta x_m} F_{m+1}^T w_{m+1} F_{m+1})^{-1} P_{\Delta x_m} F_{m+1}^T w_{m+1} F_{m+1} P_{\Delta x_m} \quad (E-7)$$

Premultiplying by  $P_{\Delta x_m}^{-1}$

$$\Delta P = - P_{\Delta x_m} (I + P_{\Delta x_m} F_{m+1}^T w_{m+1} F_{m+1})^{-1} F_{m+1}^T w_{m+1} F_{m+1} P_{\Delta x_m} \quad (E-8)$$

Multiplying  $F_{m+1}^T w_{m+1} F_{m+1}$  into the term in parentheses in Equation (E-8) and factoring forward yields

$$\Delta P = - P_{\Delta x_m} F_{m+1}^T w_{m+1} F_{m+1} (I + P_{\Delta x_m} F_{m+1}^T w_{m+1} F_{m+1})^{-1} P_{\Delta x_m} \quad (E-9)$$

Equation (E-9) is not the best form for  $\Delta P$ . From the definition of the inverse of a matrix, the expression

$$(w_{m+1}^{-1} + F_{m+1} P_{\Delta x_m} F_{m+1}^T)^{-1} (w_{m+1}^{-1} + F_{m+1} P_{\Delta x_m} F_{m+1}^T) = I \quad (E-10)$$

can be obtained.

Postmultiplying Equation (E-10) by  $w_{m+1} F_{m+1}$  and then factoring out  $F_{m+1}$  yields

$$(w_{m+1}^{-1} + F_{m+1} P_{\Delta x_m} F_{m+1}^T)^{-1} F_{m+1} (I + P_{\Delta x_m} F_{m+1}^T w_{m+1} F_{m+1}) = w_{m+1} F_{m+1} \quad (E-11)$$

If Equation (E-11) is then postmultiplied by  $(I + P_{\Delta x_m} F_{m+1}^T w_{m+1} F_{m+1})^{-1}$ ,

$$(w_{m+1}^{-1} + F_{m+1} P_{\Delta x_m} F_{m+1}^T)^{-1} F_{m+1} = w_{m+1} F_{m+1} (I + P_{\Delta x_m} F_{m+1}^T w_{m+1} F_{m+1})^{-1} \quad (E-12)$$

Substituting Equation (E-12) into Equation (E-9) gives

$$\Delta P = - P_{\Delta x_m} F_{m+1}^T (w_{m+1}^{-1} + F_{m+1} P_{\Delta x_m} F_{m+1}^T)^{-1} F_{m+1} P_{\Delta x_m} \quad (E-13)$$

and substituting Equation (E-13) into Equation (E-1) gives

$$P_{\Delta x_{m+1}} = P_{\Delta x_m} - P_{\Delta x_m} F_{m+1}^T (w_{m+1}^{-1} + F_{m+1} P_{\Delta x_m} F_{m+1}^T)^{-1} F_{m+1} P_{\Delta x_m} \quad (E-14)$$

or

$$P_{\Delta x_{m+1}} = (I - K F_{m+1}) P_{\Delta x_m} \quad (E-15)$$

where

$$K \equiv P_{\Delta x_m} F_{m+1}^T (w_{m+1}^{-1} + F_{m+1} P_{\Delta x_m} F_{m+1}^T)^{-1} \quad (E-16)$$

## E.2 DERIVATION OF AN ALTERNATIVE FORM OF THE OPTIMAL LINEAR GAIN

From Equation (8-79), the covariance matrix of error is given as

$$P_{\Delta x_{m+1}} = (P_{\Delta x_m}^{-1} + F_{m+1}^T w_{m+1} F_{m+1})^{-1} \quad (E-17)$$

Postmultiplying this equation by  $F_{m+1}^T w_{m+1}$  and factoring out  $P_{\Delta x_m}^{-1}$  gives

$$P_{\Delta x_{m+1}} F_{m+1}^T w_{m+1} = (I + P_{\Delta x_m} F_{m+1}^T w_{m+1} F_{m+1})^{-1} P_{\Delta x_m} F_{m+1}^T w_{m+1} \quad (E-18)$$

Premultiplying Equation (E-18) by  $F_{m+1}^T w_{m+1} F_{m+1}$  and substituting Equation (E-12) into the result yields

$$\begin{aligned} F_{m+1}^T w_{m+1} F_{m+1} P_{\Delta x_{m+1}} F_{m+1}^T w_{m+1} \\ = F_{m+1}^T (w_{m+1}^{-1} + F_{m+1} P_{\Delta x_m} F_{m+1}^T)^{-1} F_{m+1} P_{\Delta x_m} F_{m+1}^T w_{m+1} \end{aligned} \quad (E-19)$$

Moving the factor  $F_{m+1} P_{\Delta x_m} F_{m+1}^T w_{m+1}$  inside the brackets and factoring out  $w_{m+1}$ ,

$$\begin{aligned} F_{m+1}^T w_{m+1} F_{m+1} P_{\Delta x_m} F_{m+1}^T w_{m+1} \\ = F_{m+1}^T w_{m+1} [w_{m+1}^{-1} (F_{m+1} P_{\Delta x_m} F_{m+1}^T)^{-1} + I]^{-1} \end{aligned} \quad (E-20)$$

Factoring out  $F_{m+1} P_{\Delta x_m} F_{m+1}^T$  from this expression and premultiplying by  $(F_{m+1}^T w_{m+1} F_{m+1})^{-1}$  gives

$$P_{\Delta x_{m+1}} F_{m+1}^T w_{m+1} = P_{\Delta x_m} F_{m+1}^T (w_{m+1}^{-1} + F_{m+1} P_{\Delta x_m} F_{m+1}^T)^{-1} \quad (E-21)$$

Finally, substituting Equation (E-21) into Equation (E-16) yields the following expression for K.

$$K = P_{\Delta x_{m+1}} F_{m+1}^T w_{m+1} \quad (E-22)$$

## GLOSSARY OF MATHEMATICAL SYMBOLS

$A$  - Azimuth angle.

- Reference satellite area for aerodynamic drag in Section 4.5.
- Satellite area exposed to direct solar radiation in Sections 4.6 and 5.4.
- Precession transformation matrix from mean of 1950.0 to mean of date coordinates. See Sections 3.3.1 and 9.1.1.

$\bar{A}$  - External acceleration vector in Section 4.9.

$A, B, C$  - Matrices of time-varying coefficients in variational differential equations in Sections 4.1, 6.4, and 6.5.

- Coefficients used in the SST Doppler count in Section 7.3.3.

$A_m, B_m, C_m, D_m$  - Coefficients of polynomial fitted to Minitrack fine baseline rectified data in Appendix A.

$A_n, B_n, C_n$  - Coefficients of polynomial fitted to Minitrack coarse and medium baseline rectified ambiguity data in Appendix A.

$A_p$  - Solar paddle area in Section 4.5.2.

$A.1$  - Atomic time.

$A'_1, A'_2, A_1, \dots, A_{26}$  - Auxiliary parameters defined in Equations (5-184).

$a$  - Semimajor axis of satellite orbit.

- Semimajor axis of reference ellipsoid in Section 7.4.
- Magnitude of spacecraft thrust acceleration in Section 4.8.

$\dot{\hat{a}}$  - Minitrack fine baseline fractional phase rate in Appendix A.

- $\bar{a}_b$  - Inertial acceleration vector in body-fixed coordinates.  
See Section 4.3.
- $\bar{a}_E(M)$  - Inertial acceleration of the point mass earth due to the moon's oblateness. See Section 4.4.
- $a_F, \bar{a}_F, \bar{a}'_F$  - Minitrack fine baseline fractional phase difference in Appendix A.
- $a_{ij}$  - Polynomial coefficients of polar motion in Section 3.3.2.2 (see Table 3-1).
- Time difference polynomial coefficients in Section 3.5.2.
  - Terms used in the evaluation of the Chebyshev polynomial coefficients ( $b_i$ ) in Section 3.6.
- $a_i, b_{ij}, c_i$  - Shank's coefficients used in the Runge-Kutta integration method in Section 6.6.
- $\bar{a}_j$  - Represents the  $j^{\text{th}}$  row of the matrix of measurement partial derivatives,  $F$ , in Chapter 8.
- $\bar{a}_m$  - Acceleration vector in the nominal dynamical model.  
See Section 8.4.2.
- $a_p$  - Planet radius in Section 4.6.1.
- $\bar{a}_u$  - Vector of unknown or unmodeled accelerations in Section 8.4.2.
- $a_x, a_y, a_z$  - Coefficients of the polynomial characterizing the attitude control system acceleration in Section 4.7.1.
- $a_0, a_1, \dots, a_4$  - Coefficients of the polynomial characterizing the spacecraft thrust acceleration in Section 4.8.
- $a_1, a_2, a_3$  - Parameters in the topside electron density profile in Section 7.6.
- $B$  - Transformation matrix from true equator and equinox of date coordinate system to body-fixed coordinates in Sections 3.3.2.3, 4.3, 9.1, and 9.2.

- $\overline{B}$  - Bias correction vector in Section 4.9.
- B, C, A - See A, B, C above.
- $B_C, B_F, B_M$  - Minitrack coarse, fine, and medium phase rates in Appendix A.
- $B_1$  - Transformation matrix from true of date to pseudo body-fixed coordinates in Section 3.3.2.
- $B_2$  - Simplified transformation matrix from pseudo body-fixed to body-fixed coordinates in Section 3.3.2.
- $B_1, \dots, B_{15}$  - Auxiliary parameters defined in Equation (5-185).
- b - Measurement bias in Sections 7.1 and 8.2.
- $\overline{b}_F$  - Absolute phase difference for the Minitrack fine baseline in Appendix A.
- $b_1$  - Chebyshev coefficients of interpolating polynomial in Section 3.6.
- $b_j, c_j$  - Numerical coefficients in Section 5.6.
- $b_m$  - Polynomial fitted to Minitrack fine baseline rectified data in Appendix A.
- $b_n$  - Polynomial fitted to Minitrack coarse and medium baseline rectified ambiguity data in Appendix A.
- $b_x, b_y, b_z$  - Coefficients of the linear term of the polynomial characterizing the attitude control system acceleration in Section 4.7.1.
- C - Transformation matrix from mean equator and equinox of 1950.0 to true of date coordinate system in Section 3.3.1.3 and Chapters 4 and 9.
- C, A, B - See A, B, C above.
- $C_{A_C}$  - Force coefficient for the force along the cylinder axis in Section 4.5.2 (see Table 4-1).

- $C_D, C_{D\bar{0}}$  - Aerodynamic drag coefficient with and without systematic error corrections in Section 4.5.
- $C_F$  - Nondimensional force coefficient in Section 4.5.2.
- $C_{N_C}$  - Force coefficient for the force normal to the cylinder axis in Section 4.5.2 (see Table 4-1).
- $C_{N_P}$  - Force coefficient for the force normal to the plate in Section 4.5.2 (see Table 4-1).
- $C_R$  - Nondimensional force coefficient for solar radiation pressure in Section 4.6.
- $C_{T_P}$  - Force coefficient for the force tangent to the plate in Section 4.5.2 (see Table 4-1).
- $C_j^i$  - Harmonic coefficients of the earth's nonspherical potential in Section 4.4.
- $C_n^m$  - Gravitational harmonic coefficients.
- $C_{\Delta_s \Delta_u^*}$  - Correlation between errors in  $\bar{s}$  and  $\bar{u}^*$  in Chapter 8.
- $C_{\Delta_x \Delta_z}$  - Correlation between errors in  $\bar{x}$  and  $\bar{z}_0$  in Chapter 8.
- $C_{\Delta_{x_0 n}}$  - Correlation between errors in  $\bar{x}_0$  and  $\bar{n}$  in Chapter 8.
- $C_{\Delta_{x_0} \Delta_z}$  - Correlation between errors in  $\bar{x}_0$  and  $\bar{z}_0$  in Chapter 8.
- $C_{\Delta_{z n}}$  - Correlation between errors in  $\bar{z}$  and  $\bar{n}$  in Chapter 8.
- $C_\psi$  - Dot product in Chapter 9.
- $C_0, C_1$  - Count of the number of cycles of the GRARR and ATSR Doppler reference frequency and the range reference frequency in Chapter 7, and Appendices A and C.
- $c$  - Vacuum speed of light.
- $c_g, c_p$  - The group speed and phase speed of propagation of an electromagnetic signal in Section 7.6.

- $c_i^j$  - Harmonic coefficients of the moon's nonspherical potential in Section 4.4.
- $c_j$  - Coefficients in the expression for  $Y_m(t)$  in Section 3.6.
- $c_x, c_y, c_z$  - Coefficients of the quadratic term of the polynomial characterizing the attitude control system acceleration in Section 4.7.1.
- D - Transformation matrix from true of date to local plane coordinates. See Section 3.3.4.
  - Parameter obtained from Barker's equation for parabolic motion in Section 3.3.8.1.
  - Parameter used to determine if the spacecraft is within the cylindrical shadow of a celestial body in Section 4.6.
  - Linear differentiation operator in Sections 6.1 and 6.4.
- $D, D_{ij}$  - Matrix and its elements in Section 5.5.
- $D_n$  - Quantity used to solve Kepler's equation for elliptical motion in Section 3.3.8.
- $d$  - Spacecraft diameter in Section 4.5.2.
- $\bar{d}$  - Unit vector pointing down along the vacuum downlink path from the spacecraft to the tracking station in Section 7.6.3 and Appendix C.
- $d_e$  - Number of ephemeris days past 0<sup>h</sup> January 1, 1950 ET in Section 3.3.3.
- E - Eccentric anomaly of an orbit.
  - Transformation matrix from body-centered true of date inertial Cartesian coordinates to orbit plane coordinates in Section 3.3.5.
  - Elevation angle measured from the reference plane to the station-to-spacecraft position vector in Section 3.2.4, Chapter 7, Section 9.1, and Appendix A.

- E (cont'd) - Matrix of partial derivatives of the nonlinear measurement equations  $f(x,z)$  with respect to consider variables  $z$  in Section 8.2.
- $E_a$  - Observed elevation angle in Section 7.6.
- $E^s$  - Linear shifting operator in Section 6.1.
- ET - Ephemeris time.
- $e$  - Orbital eccentricity.
- Eccentricity of the planet's figure in Section 3.3.6.
- $\bar{e}$  - Eccentricity vector in Sections 3.2.6 and 3.3.10.
- $e_x, e_y, e_z$  - Herrick eccentricity vector components used in Section 3.3.11.2.
- em - Exponential multiplier in Section 7.6.3.
- F - Hyperbolic anomaly in Section 3.3.8.
- Eccentric longitude in Section 3.3.9. Equals the sum of the eccentric anomaly, argument of perigee, and right ascension of the ascending node.
  - Total force acting on the spacecraft in Chapter 4.
  - Perturbed Hamiltonian in Section 5.5.
  - Matrix of partial derivatives of observations with respect to solve-for variables in Chapter 8 and Appendix E.
- $F'$  - Augmented matrix of partial derivatives in Section 8.2.
- $F_B$  - Aerodynamic acceleration per unit density in Section 4.5.2.
- $F^T W F$  - Normal matrix in Chapter 8.
- $\tilde{F}^T W \tilde{F}$  - Expanded state normal matrix in Chapter 8.
- $F_t, F_r$  - Parameters used in general relativistic expression (defined in Appendix C).



- $F_0$  - Unperturbed Hamiltonian in Section 5.5.
- $F_1, F_2, F_3, F_4$  - Functions used in the evaluation of the density in Section 4.5.4.
- $F_{10.7}$  - Daily average of the 10.7 cm solar flux in Section 4.5.
- $\overline{F}_{10.7}$  - The 81-day running average of  $F_{10.7}$ . See Section 4.5.
- $\mathfrak{J}$  - Augmented observation matrix in Section 8.4.
- $f$  - Planet's flattening coefficient in Sections 3.3.6.1, 4.5.3, 7.2, and 9.1.
- Orbital true anomaly in Sections 3.3.8.1, 4.10, 5.9, 6.1.2, and Appendix B.
- General time-varying function in Chapter 6.
- $f, g$  - Series used to predict spacecraft positions in Chapter 9.
- $\hat{f}, \hat{g}, \hat{w}$  - Equinoctial unit vectors along the equinoctial coordinate directions  $x_{ep}, y_{ep}$ , and  $z_{ep}$ , respectively, in Sections 3.2.5 and 3.3.9.1.
- $f(t_i)$  - Observation model in Section 4.10.
- $f_i$  - Functions used in the Runge-Kutta integration method in Section 6.6.
- $f_0$  - Nonlinear measurement functions in Sections 7.1 and 8.2.
- $f_0 F_2$  - Critical frequency of the F2 layer in Section 7.6.
- $G$  - Universal gravitational constant.
- Total angular momentum in Section 5.5 and Appendix B.
- GHA - Greenwich Hour Angle.
- $g$  - Argument of the pericenter in section 5.5.
- $g, g'$  - Mean anomaly of the moon and sun, respectively, in Section 3.3.3.

- $g(\alpha)$  - Function relating  $\tau$  and  $\alpha$  in the time element formulation in Appendix B.
- $g_i$  - Nonlinear functional form of  $\Delta \hat{s}_i$  in Section 8.2.3.
- $g_{ij}$  - Elements of the metric matrix defining the nature of the space-time frame in Appendix C.
- $g_s$  - Sea-level acceleration due to gravity in section 4.5.4.
- $H$  - Local hour angle of the sun in Section 4.5.4.
- The  $z$  component of the angular momentum in Section 5.5.
  - Matrix used for expressing the Cowell corrector formula in matrix form in Chapter 6.
- $H_I$  - Ionospheric scale height in the expression for refractivity in Section 7.6.
- $H_M, H_m$  - Maximum and minimum scale heights in Section 4.5.6.
- $H, h$  - Transformations of the covariance matrix  $P_{\Delta_s}$  and the estimated state  $\bar{s}$ , respectively, in Chapter 8.
- $H_T$  - Tropospheric scale height in the expression for refractivity in Section 7.6.
- $h$  - Altitude measured as the perpendicular distance from the surface of the ellipsoidal planet model to the point being measured. See Sections 3.2.2, 3.3.6, and Chapter 4.
- Longitude of the ascending node in Section 5.5.
  - Energy of the orbit in Section 5.4 and Appendix B.
  - Integration stepsize in Chapter 6.
- $h, h_r$  - Projection of the vector  $\bar{e}$  on the  $y_{ep}$  axis in Chapter 3 (equinoctial elements).
- $h, \bar{h}, h_x, h_y, h_z$  - Orbital angular momentum vectors and Cartesian components in Section 3.3.3.

- $h_a, h_p$  - Apofocal and perifocal altitude in Section 3.3.8.3.
- $h_K$  - Negative Keplerian energy in Appendix B.
- $h_L$  - Lower altitude limit for the ionosphere in Section 7.6.
- $h_m$  - Altitude corresponding to maximum electron density in Section 7.6.
- $h_s$  - Height of tracking station above reference ellipsoid in Sections 3.3.7, 7.6, and 9.1.
- $h_0, h_1, h_2$  - Parameters in the topside electron density profile in Section 7.6.
- $I$  - Orbital inclination in Section 5.5.
- Linear identity operator in Section 6.1.
  - Abbreviation used in ray angular deflection formula in Section 7.6.3 (Equation (7-157)).
  - Identity matrix in Chapter 8 and Appendix E.
- $I, I_m$  - Inclination of the mean lunar equator to the ecliptic of date in Section 3.3.3.
- $I_{P_n}, II_{P_n}; I_{S_n}, II_{S_n}$  - Summation symbols in Chapter 3.
- $i$  - Orbital inclination.
- Local incidence angle between an electromagnetic ray and a radius vector in Section 7.6.
- $i_p$  - Incidence angle between the spacecraft axis and the paddle surface in Section 4.5.2.
- $i_s$  - Inclination of the moon's equatorial plane to the earth's equatorial plane. (Euler angle used in transformation from selenocentric to selenographic coordinates.) See Section 3.3.3.
- $J_n$  - Zonal harmonic coefficients ( $\bar{C}_n^0 = -C_n^0$ ). See Chapter 4.

$J_2, J_3, J_4, J_5$  - Zonal harmonic coefficients in Chapter 5.

JD - Julian day number.

K - Diagonal matrix of accelerometer scale factor corrections in Section 4.9.

- Kalman filter gain matrix in Chapter 8.

$\mathcal{K}$  - Augmented gain matrix in Section 8.4.

$K_p$  - Geomagnetic planetary index in Section 4.5.4.

k - Solar pressure model parameter in Section 4.6.2.

- Factor used in definition of the average Doppler frequency in Section 7.3.

$\hat{k}$  - Unit vector normal to the orbital plane in Section 9.1.2.

$k, k_r$  - Projection of the vector  $\bar{e}$  on the  $x_{ep}$  axis in Chapter 3 (equinoctial elements).

$k_1$  - Functions used in the Runge-Kutta integration method in Section 6.6.

$k_1, k_2$  - Gain constants used to compute measurement variances in Section 8.1.

$k_1, k_2, k_3$  - Decay constants for the lower, middle, and upper third, respectively, of the topside electron density profile in Section 7.6.

$k_2, k_3, k_4, k_5$  - Auxiliary parameters defined in Section 5.9.

L - Cylinder length in Section 4.5.2.

- Luminosity of the sun in Section 4.6.

- Total energy of the orbit (DS element) in Chapter 5 and Appendix B.

- KS matrix in Section 5.4.

$L$  (cont'd) - Magnitude of the angular momentum vector in Section 4.8.2.

$L, L_b, L_H, L_T$  - Unit vector directed toward the spacecraft from a tracking station in mean of 1950.0, body-fixed, local tangent, or true of date coordinates, respectively. See Section 9.1.

$L_i$  - Components of the angular momentum vector in Section 4.8.2.

$(L^TP)_1, (L^TP)_2, (L^TP)_3$  - Transformed components of perturbing accelerations in Section 5.4.

$\ell$  - Parameter in Robert's temperature profile in Section 4.5.4.

- Mean anomaly in Delaunay elements in Chapter 5 and Appendix B.

- Direction cosine of the angle between the station-spacecraft vector and the local tangent east-pointing axis. This angle is measured by the Minitrack system and is described in Section 7.2.3.

- Number which scales the hyperellipse of constant (normal) probability in terms of the standard deviations. See Section 8.5.2.

- Direction cosine of the corrected phase difference from the east-pointing axis at the station in Appendix A.

$\bar{\ell}, \ell_x, \ell_y, \ell_z$  - Herrick angular momentum vector and its components in Sections 3.2.6, 3.3.10, and 3.3.11.

$M$  - Orbital mean anomaly.

$M(a')$  - Mean molecular mass of atmosphere in Section 4.5.4.

$M, M'$  - Transformation matrices from selenocentric to selenographic coordinates in Sections 3.3.3 and 4.4.

$M, M_{ij}, m_{ij}$  - Notation used in describing the matrix inversion procedure in Section 8.6.

- $M_i$  - Molecular mass of atmospheric constituents in Section 4.5.4.
- $M_{1t}$  - Transformation matrix from body-fixed coordinates, centered at a tracking station, to local tangent coordinates at the station. See Section 3.3.7 and Chapter 9.
- $M_s$  - Sea-level mean molecular mass in Section 4.5.4.
- MJD, MJD<sub>i</sub> - Modified Julian date and tabular modified Julian date.
- MUF(3000)F2 - Highest frequency usable for a 3000-kilometer single-hop propagation via the F2 layer in Section 7.6.
- M-factor - Ratio of MUF(3000)F2 to the critical frequency  $f_oF_2$  in Section 7.6.
- $m$  - Mass of a body in Chapter 4.
- Direction cosine of the angle between the station-spacecraft vector and the local tangent north-pointing axis. This angle is measured by the Minitrack system and is described in Section 7.2.3.
- $\overline{m}$  - Group mean in Section 8.6.
- $m'$  - Direction cosine of the corrected phase difference from the north-pointing axis at the station. See Appendix A.
- $N$  - The distance along the normal vector from the intersection of the normal and the ellipsoid to the  $z_b$  axis. See Figure 3-15 and Section 3.3.6.
- Nutation transformation matrix from mean of date to true of date coordinates in Sections 3.3.1 and 9.1.1.
- $\overline{N}$  - Ascending nodal vector in the equinoctial system. See Figure 3-5 and Section 3.2.
- $N, N_0$  - Number of cycles of the Doppler-plus-bias signal counted over the Doppler counting cycle. See Section 7.3, Appendix A, and Appendix C.

- $N_e, N_m$  - Electron density and maximum electron density in Section 7.6.
- $N_F$  - The Minitrack fine baseline lengths in terms of vacuum wavelengths of the nominal 136.0 MHz frequency signal. See Appendix A.
- $N_I, N_T$  - Ionospheric and tropospheric refractivity in Section 7.6.
- $N_{pq}$  - Brouwer drag parameters in Section 4.10.
- $N_s$  - Magnitude of the normal vector to the surface of the reference ellipsoid at the tracking station in Sections 3.3.7 and 9.1.
- Surface refractivity in Section 7.6.
- $N_0, N_1, N_2$  - Parameters in the topside electron density profile in Section 7.6.
- $n$  - Keplerian mean motion.
- Adjustable parameter exponent of the cosine variation between the Harris-Priester maximum and minimum density profiles in Sections 4.3.5 and 5.3.
  - Uniformization constant in Section 5.1.
  - Variable local index of refraction in Section 7.6.
  - Measurement noise in Section 7.8.
- $\bar{n}$  - Unit vector along the idealized straight signal propagation path in Appendix C.
- Random noise vector in Chapter 8.
- $\hat{n}, \hat{n}'$  - Unit vectors normal to the reference ellipsoid and the geoid, respectively, in Section 7.4.
- $n_s$  - Total number of residuals for a tracking station and data type in Section 8.6.

- $\bar{n}_t, \bar{n}_r$  - Unit vectors along the local signal propagation path at the transmitter and receiver, respectively, in Appendix C.
- $O_c, O_0$  - The computed and actual observations in Sections 7.1, 7.6, and 8.2.
- $P$  - Transformation matrix from orbital rectangular coordinates to true of date coordinates in Sections 3.3.8.1 and 3.3.8.2.
- Orbital period in Section 3.3.8.3.
  - Ionospheric term used in the equation for atmospheric time delay in Section 7.6.3.
  - Symmetric positive definite matrix in Appendix E.
- $\bar{P}$  - Perturbative accelerations additional to the primary body's inverse square gravity in Chapter 5 and Appendix B.
- $\hat{P}$  - Augmented error covariance matrix in Section 8.4.
- $P_A, P_T$  - Adopted and true pole, respectively, of the earth. See Section 3.3.2.2.
- $P_i(\cos \theta)$  - Legendre functions in Section 4.2.
- $P_n^m$  - Legendre functions in Section 4.3.1.
- $P_s$  - The force on a perfectly absorbing surface due to solar radiation pressure at one astronomical unit in Section 4.6.
- $P_T, Y_T$  - Pitch and yaw angles, respectively, defining the thrust direction in Section 4.8.
- $P_{\Delta a}$  - Covariance matrices in Chapter 8.
- $P_{\Delta s}, P'_{\Delta s}$  - Covariance matrix of the estimated state variable errors in Chapter 8.
- $P_{\Delta u}$  - Covariance matrix of the state and model parameter errors in Section 8.2.3.



- $P_{\Delta x}$  - Covariance matrix of estimated solve-for variable errors.
- $P_{\Delta x_0}$  - Covariance matrix of a priori solve-for variable errors in Chapter 8.
- $P_{\Delta z}$  - Covariance matrix of consider variable errors.
- $P_{\Delta z_0}$  - Covariance matrix of a priori consider variable errors in Chapter 8.
- ${}^1P_n, {}^{II}P_n$  - Summation matrices in Section 6.4.
- $P_1, P_2, P_3$  - Components of the perturbing accelerations in Section 5.4.
- $p$  - Semilatus rectum of orbit.
- Dimension of the solve-for vector in Chapter 8.
- $\bar{p}$  - Vector of dynamic parameters in the acceleration model which can be estimated.
- $\bar{p}^*$  - The components of  $\bar{p}$  remaining after excluding satellite position and velocity variables. These components include constant model parameters pertaining to drag, gravitational harmonic coefficients, etc. See Section 4.1.
- $\hat{p}, \hat{q}$  - Unit vectors in the orbit plane in Section 4.10.
- $p, p_r$  - Projection of vector  $\bar{N}$  on the  $Y_{ep}$  axis in Sections 3.2.6, 3.3.9.1, and 3.3.11.1 (equinoctial elements).
- $p_M(\xi)$  - Interpolating polynomial representing a component of acceleration as a function of normalized time in Section 5.6.
- $p_x$  - Normal probability density function in Section 8.5.
- $Q$  - Transformation matrix from spacecraft vehicle-fixed axes to true of date coordinates in Section 3.3.12 and Chapter 4.
- Difference between ephemeris data and the function  $Y_{in}(t)$  in Section 3.6.

- Q (cont'd) - Ionospheric term used in the equation for atmospheric time delay in Section 7.3.3.
- Least squares loss function defined in Sections 8.1 and 8.2.
  - Covariance of the state noise in Section 8.4.
- Q' - Linearized least squares loss function in Sections 8.1 and 8.2.
- q - Pericentric distance in Section 2.3.8.1.
- Scaling factor defining time transformation in Section 5.5 and Appendix B.
  - Dimension of the consider vector in Chapter 8.
- $\bar{q}$  - The total parameter vector of all candidate solve-for variables in Chapter 7.
- q,  $q_r$  - Projection of the vector  $\bar{N}$  on the  $x_{ep}$  axis in Sections 3.2.5, 3.3.9.1, and 3.3.11.1 (equinoctial elements).
- R - Universal gas constant. See Section 4.5.4.
- Covariance matrix of the observation noise in Section 8.4.
- $\bar{R}$  - Position vector in mean equator and equinox of 1950.0 coordinates in Chapter 3.
- Column vector of vehicle position coordinates in Chapter 4.
  - Epoch state elements in Section 7.2.3.
- $\hat{R}$  - Vector from the center of an inertial coordinate system to the satellite in Section 4.2.1.
- $\dot{\bar{R}}$  - Velocity of the spacecraft in Section 4.5.2.
- $\bar{R}'$  - Satellite position vector relative to the shadowing body in Section 4.6.1.

- $\ddot{\bar{\mathbf{R}}}$  - Total acceleration vector expressed in an inertial Cartesian coordinate system in Section 4.1.
- $\ddot{\bar{\mathbf{R}}}_A$  - Sum of nonpotential accelerations expressed in an inertial Cartesian coordinate system in Section 4.9.
- $R_a$  - Polar radius of the earth in Section 4.5.4.
- $\ddot{\bar{\mathbf{R}}}_D$  - Acceleration due to aerodynamic forces expressed in an inertial Cartesian coordinate system in Chapter 4.
- $\bar{\mathbf{R}}_E$  - Inertial acceleration of the earth in an inertial Cartesian coordinate system. See Section 4.4.
- $R_e, R_p$  - Equatorial and polar radii, respectively, of earth or reference body.
- $\bar{\mathbf{R}}_{IO}$  - Acceleration due to the mutual nonspherical gravitational attraction of the earth and moon in an inertial Cartesian coordinate system. See Chapter 4.
- $\bar{\mathbf{R}}_i$  - Geocentric inertial spacecraft position vectors in Chapter 9.
- $\mathbf{R}_{kp}$  - Vector from the  $k^{\text{th}}$  body to the satellite in Chapter 4.
- $\ddot{\bar{\mathbf{R}}}_M$  - Inertial acceleration of the moon in an inertial Cartesian coordinate system in Chapter 4.
- $R_m$  - Equatorial radius of the moon in Section 4.4.
- $\ddot{\bar{\mathbf{R}}}_{NS}$  - Gravitational acceleration due to nonsphericity of the gravitational potential in inertial Cartesian coordinate system. See Chapter 4.
- $\ddot{\bar{\mathbf{R}}}_{PM}$  - Gravitational acceleration due to n-point masses in inertial Cartesian coordinate system in Chapter 4.
- $\bar{\mathbf{R}}_s$  - Position vector of the sun in the inertial mean of 1950.0 coordinate system in Section 4.6.1.
- $\bar{\mathbf{R}}_{s_i}$  - Tracking station position vectors in Chapter 9.

- $\ddot{\mathbf{R}}_{\text{SR}}$  - Acceleration due to solar radiation pressure expressed in an inertial Cartesian coordinate system in Chapter 4.
- $R_{\text{sun}}$  - One astronomical unit in Section 4.6.1.
- $\ddot{\mathbf{R}}_{\text{T}}$  - Acceleration due to thrusting of the spacecraft engines in an inertial Cartesian coordinate system in Chapter 4.
- $\ddot{\mathbf{R}}_{\text{TAC}}$  - Acceleration due to attitude control system corrections in an inertial Cartesian coordinate system in Chapter 4.
- $R_{\text{u}}$  - Right ascension of the fictitious mean sun on the mean equator of date and measured from the mean equinox of date. See Section 3.4.3.
- $R_{\text{vs}}$  - Distance from the spacecraft to the sun in Section 4.6.1.
- $R_{\text{x}}, R_{\text{y}}, R_{\text{z}}$  - Rotational transformations about the x, y, and z axes, respectively, in Section 3.3.
- $\ddot{\mathbf{R}}_{\text{E}}(\text{M})$  - Inertial acceleration of the point mass earth due to an oblate moon in Section 4.4.
- $\ddot{\mathbf{R}}_{\text{M}}(\text{E})$  - Inertial acceleration of the point mass moon due to an oblate earth in Section 4.4.
- $\text{RF}_{\text{c}}$  - Observation correction due to refraction, light time, transponder delay, antenna mount errors, etc., in Chapter 7.
- RMS - Actual root mean square error in Section 8.6.
- RMSP - Predicted root mean square error in Section 8.6.
- RMSB - The smallest RMS over all prior iterations in Section 8.6.
- $r$  - Radial distance from the origin to the satellite or point being measured.
- Magnitude of the satellite position vector in inertial geocentric coordinates in Section 4.5.6 and Appendix B.
  - Geocentric radius in Section 7.4.

- $\bar{\mathbf{r}}$  - Position vector in true of date coordinates in Sections 3.2, 3.3, and 3.4.2.
- Satellite position vector in inertial geocentric coordinates in Section 4.5.6.
- $\bar{\mathbf{r}}, \dot{\bar{\mathbf{r}}}, \ddot{\bar{\mathbf{r}}}$  - Position, velocity, and acceleration vectors in the inertial Cartesian coordinate system in Chapter 5.
- $r_a$  - Magnitude of the apofocal radius vector in Section 3.3.8.
- $\bar{\mathbf{r}}_b, \bar{\mathbf{r}}'_b$  - Position vector expressed in body-fixed and pseudo body-fixed coordinates, respectively.
- $\bar{\mathbf{r}}_E$  - Position vector in Cartesian coordinates referred to the mean equator and equinox of date in Sections 3.2.1 and 3.3.1.
- Position vector of the earth in selenographic coordinates in Section 4.4.
- $\bar{\mathbf{r}}_{EM}$  - Moon's position vector in geocentric coordinates in Section 4.4.
- $\bar{\mathbf{r}}_{lp}$  - Position vector referred to the local plane coordinate system in Section 3.3.4.1.
- $\bar{\mathbf{r}}_{lt}$  - Position vector referred to the local tangent coordinate system in Sections 3.2.4 and 3.3.6.
- $\bar{\mathbf{r}}_M$  - Lunar position vector in true of date coordinates in Section 4.4.
- $\bar{\mathbf{r}}_{ME}$  - Earth's position vector in selenocentric coordinates in Section 4.4.
- $\bar{\mathbf{r}}_{op}$  - Position vector referred to the orbit plane coordinate system. See Sections 3.2.5 and 3.3.4.
- $r_p$  - Magnitude of the perifocal radius vector in Section 3.3.9.1.
- $\bar{\mathbf{r}}_p$  - Position vector referred to the orbital rectangular coordinate system with the  $x_p$  axis directed toward perigees. See Section 3.3.8.

- $\bar{\mathbf{r}}_R$  - Position vector of the tracking station at signal reception in inertial Cartesian coordinates. See Chapter 7.
- $\bar{\mathbf{r}}_r, \bar{\mathbf{r}}_t$  - Position vectors of the generalized receiver and transmitter in inertial Cartesian coordinates in Appendix A.
- $r_s$  - Geocentric radius of a point (tracking station) on the surface of the ellipsoidal planet. See Sections 3.3.6 and 7.6.
- Radius of the earth in Section 4.5.6.
- $\bar{\mathbf{r}}_S$  - Inertial position vector of the ground station in Section 7.3.3.
- $\bar{\mathbf{r}}_s$  - Earth-fixed coordinates of the tracking station.
- $\bar{\mathbf{r}}_T$  - Position vector of the tracking station at signal transmission in inertial Cartesian coordinates in Chapter 7, Appendix A, and Appendix C.
- $\ddot{\mathbf{r}}_T$  - Acceleration due to thrust of the spacecraft engines in Section 4.8.1.
- $\ddot{\mathbf{r}}_{TAC}$  - Acceleration due to attitude control effects in Section 4.7.
- $\bar{\mathbf{r}}_v$  - Vector in vehicle-fixed coordinates in Section 4.7.1.
- Position vector of the spacecraft in inertial Cartesian coordinates in Chapter 7 and Appendix C.
- $\ddot{\mathbf{r}}_E(M)$  - Acceleration of the point mass earth due to the oblate moon in selenographic true of date coordinates in Section 4.4.
- $\ddot{\mathbf{r}}_M(E)$  - Acceleration of the point mass moon due to the oblate earth in geocentric true of date coordinates in Section 4.4.
- $\bar{\mathbf{r}}_0$  - Earth-centered position vector in Section 3.3.5.
- $\mathbf{r}_1$  - Inertial position vector of the relay satellite in satellite-to-satellite tracking. See Section 7.3.3.

- $r_2$  - Inertial position vector of the target satellite in satellite-to-satellite tracking. See Section 7.3.3.
- $S$  - Mean solar flux at one astronomical unit in Section 4.6.
  - Orbital period in regularized time system in Section 6.10.
  - Series involved in atmospheric signal propagation time delay in Section 7.6.3.
  - Epoch sensitivity matrix in Section 8.2.3.
  - Eigenvector transformation from basic coordinate frame to principal axes in Section 8.5.
  - Sum of the squares of the residuals about the mean in each residual group in Section 8.6.
  - Arc length along the signal propagation path in Appendix A.
- $S_c$  - The projection of the spacecraft position vector onto the plane normal to the sun vector in the shadow model of Section 4.6.
- $S_c, S_e, S_p, S_s$  - Coefficients in the aerodynamic force equations in Section 4.5.2.
- $S_e$  - See  $S_c, S_e, S_p, S_s$  above.
- $S_i^j$  - Harmonic coefficients of the earth's nonspherical potential in Section 4.4.
- $S_n^m$  - Gravitational harmonic coefficients in Section 4.3.
- $S_p$  - See  $S_c, S_e, S_p, S_s$  above.
- $S_s$  - See  $S_c, S_e, S_p, S_s$  above.
- $S_u$  - Greenwich Hour Angle of the fictitious mean sun in Section 3.4.3.
- $^1S_n, ^{11}S_n$  - First and second sums, respectively, in the Adams-Cowell formulas in Chapter 6.

- $S_1, S_2, S_3$  - Components of the unit vector to the sun in true of date coordinates in Section 4.5.
- ST - Station time as defined in Section 3.4.8.
- SV - Universal time correction due to seasonal variations in the rotation of the earth in Section 3.4.6.
- $s$  - New independent variable in the time-regularized equation of motion in Chapter 5 and Appendix B.
- $\bar{s}, \bar{s}'$  - The state vector in Chapters 7 and 8.
- $s_i^j$  - Harmonic coefficients of the moon's nonspherical potential in Section 4.4.
- $T$  - Average orbital period defined in terms of the average value of the semimajor axis in Section 5.8.
- $T_{ac1}, T_{ac2}$  - Epoch times at which the attitude control acceleration polynomials are turned on and turned off in Section 4.7.1.
- $T_b$  - Rocket motor's effective burn time in Section 4.8.1.
- $T_c$  - Nighttime minimum global exospheric temperature for zero geomagnetic activity in Section 4.5.4.
- $T_E$  - Time in Julian centuries (36525 Julian days) measured from 1900 January 0<sup>d</sup> 12<sup>h</sup> ET (JD 2415020.0) to specified date. See Section 3.3.1.1.
- $T_e$  - Number of Julian centuries of 36525 Julian ephemeris days past 0<sup>h</sup> January 1, 1950 ET. See Section 3.3.3.
- $T_f, T_0$  - The effective termination and initiation times, respectively, of the spacecraft motor burn in Section 4.8.1.
- $T_i$  - Specified time to which the covariance and correlation matrices are propagated in Chapter 8.
- $T_j$  - Chebyshev polynomials in Sections 3.6 and 5.6.



- $T_U$  - Time in Julian centuries (of 36525 Julian days) from 1950.0 in Section 3.3.1.1.
- $T_U$  - Number of Julian centuries elapsed from 12 hours UT1 January 0, 1900 (JD = 2415020.0) to the UT1 time of date in Sections 3.3.2 and 3.4.3.
- $T_x$  - Inflection point temperature in Section 4.5.4.
- $T(Z)$  - Atmospheric temperature profile in Section 4.5.4.
- $T_0, T_1$  - See  $T_f, T_0$  above.
- $T_1$  - Uncorrected exospheric temperature in Section 4.5.4.
- $T_1, T_2, T_3$  - Numerical integration error bounds in Section 6.9.
- $T_\infty$  - Corrected exospheric temperature in Section 4.5.4.
- $t$  - Coordinate time measured in seconds from epoch. The independent variable of the equations of motion.
- Variable defined in Section 8.2 for testing residuals to determine the confidence interval for the group mean.
- $\tilde{t}$  - Coordinate time in Appendix C.
- $t^*$  - Reference date in Section 3.3.1.3.
- $t_F$  - Time commencing the frame time interval for the GRARE and Minitrack systems in Appendix A.
- $t_{FM}$  - Midframe time for the Minitrack system in Appendix A.
- $t_f$  - Time of the final observation in Section 8.4.
- $t_{in}^*$  - The corrected midframe time of the Minitrack system in Appendix A.
- $t_\eta$  - Reference time associated with the Brouwer drag parameters in Section 4.10.
- $t_x$  - Time tag of the C-Band range data.

- $t_R$  (cont'd) - Time at which the ground station receives the return signal in Chapter 7 and Appendix A.
- Proper time at the receiving station in Appendix C.
- $t_s$  - Sample time of the tracker range and range-rate data in Appendices A and C.
- $t_T$  - Signal transmission time at the ground station in Chapter 7 and Appendix A.
- $t_v$  - Signal turnaround time at the spacecraft in Chapter 7 and Appendix A.
- $t_0$  - Epoch time in Chapter 4 and Section 8.2.3.
- $U$  - Geoidal undulation in Section 7.4.
- $\bar{U}$  - Unit vector directed at the satellite and referred to the geocentric inertial Cartesian coordinate system in Section 3.3.5.
- $U, V$  - Tropospheric delay terms in Section 7.6.3.
- $\bar{U}_B$  - Unit vector directed toward the apex of the diurnal bulge expressed in inertial geocentric coordinates in Section 4.5.6.
- $U_{B_x}, U_{B_y}, U_{B_z}$  - Components of the unit vector  $\bar{U}_B$  in Section 4.5.6.
- $\hat{U}_i$  - Unit vector directed along  $i^{th}$  leg in satellite-to-satellite tracking. See Section 7.3.3.
- $\bar{U}_N$  - Unit vector normal to the orbital plane in the direction of the angular momentum vector. See Section 3.3.4.2.
- $\bar{U}_s$  - Unit vector directed at the sun from a shadowing body in Section 4.6.1.
- $\bar{U}_T$  - Unit vector directed along the thrust axis and referred to the geocentric inertial Cartesian coordinate system. See Section 4.8.1.

- UT - Universal time.
- UTC - Universal time coordinated.
- UT0 - Uncorrected universal time.
- UT1 - UT0 corrected for polar motion.
- UT2 - UT1 corrected for periodic seasonal variations.
- $\bar{U}_{z_{lp}}$  - Unit vector in the local plane  $z_{lp}$ -axis direction and referred to the geocentric inertial Cartesian system. See Section 3.3.4.2.
- $\bar{U}_\alpha, \bar{U}_\delta$  - Partial derivatives of  $\bar{U}_T$  with respect to the right ascension,  $\alpha$ , and declination,  $\delta$ . See Section 4.8.2.
- $\bar{u}$  - Unit vector pointing along the vacuum uplink signal propagation path from the station to the spacecraft. See Section 7.6.3 and Appendix C.
- Expanded state vector containing as components the merged vectors  $\bar{x}$  and  $\bar{z}$ . See Section 8.2.
- Vector of Gaussian noise in Section 8.4.
- $\hat{u}$  - Best estimate of uncertain state and model parameters in Section 8.2.3.
- $\bar{u}^*$  - Uncertain model parameters in  $\hat{u}$  in Section 8.2.3.
- $\bar{u}, \bar{u}'$  - Transformed position and velocity vectors in Section 5.4.
- $\bar{u}_x, \bar{u}_y, \bar{u}_z$  - Unit vectors in the body-centered true of date Cartesian coordinate system in Section 3.3.8.3.
- $u(\zeta)$  - Function used in Section 4.7.1.
- V - Spacecraft's velocity vector magnitude.
- Magnitude of velocity with respect to a medium producing an aerodynamic force in Section 4.5.
- Perturbing potential function in Section 5.4 and Appendix B.

- $\bar{V}$  - Unit vector normal to the geocentric position vector and lying in the orbital plane. See Section 3.3.5.
- $\bar{V}_B$  - Relative wind velocity in the spacecraft body axes coordinate system in Section 4.5.2.
- $\bar{V}_{rel}$  - Velocity of the spacecraft relative to the atmosphere in Section 4.5.
- $v$  - Local vertical at the ground station in Section 7.6.3.
- Magnitude of spacecraft velocity in Appendix B.
- $\bar{v}$  - Velocity vector in Section 8.4.2.
- $v_n$  - Quantity denoting the Cowell velocity integrator for linear systems in Section 6.3.
- $W$  - Weighting matrix in the least squares loss function in Chapter 8.
- $\bar{W}$  - Unit vector directed normal to the orbit plane in the direction of the angular momentum vector. See Section 3.3.5.
- $W'$  - Augmented weighting matrix in Chapter 8.
- $w_{m+1}$  - Weight of the  $(m+1)^{st}$  measurement in Chapter 8 and Appendix E.
- $X, Y, Z$  - Inertial Cartesian components of spacecraft position in the mean of 1950.0 coordinate system in Section 3.2.1.
- $\hat{X}_B$  - Unit vector along the cylinder axis in Section 4.5.2.
- $X_1, Y_1$  - Position coordinates in the equinoctial coordinate system in Sections 3.3.9.1 and 5.7.
- $X_{30}, Y_{30}$  - Gimbal angles for the GRARR, ATSR, and USB systems. See Section 7.2.3.
- $X_{85}, Y_{85}$  - Gimbal angles for the USB system in Section 7.2.3.

- $\mathcal{X}$  - Augmented state matrix in Section 8.4.
- $x$  - Transformed time variable in Section 3.6.
- $\bar{x}$  - Vector of slow osculating orbital elements in Section 5.8.
- $\bar{x}, \hat{x}_i, \bar{x}_i, \bar{x}_0$  - Epoch values of the solve-for or expanded state vector of p-dimension in Chapter 8. The vector  $\hat{x}_i$  is the best estimate of  $\bar{x}$  obtained on the  $i^{\text{th}}$  iteration. The vector  $\bar{x}_{i-1}$  is the reference solution on the  $i^{\text{th}}$  iteration. The vector  $\bar{x}_0$  is the a priori estimate of the reference state.
- $x, y, z$  - Inertial Cartesian components of spacecraft position in the true of date coordinate system.
- $x_b, y_b, z_b$  - Rectangular Cartesian components of spacecraft position in body-fixed (rotating) coordinates of the principal gravitating body.
- $x_b', y_b', z_b'$  - Components of spacecraft position in the pseudo body-fixed coordinate system in Section 3.3.2.
- $x_E, y_E, z_E$  - Inertial components of spacecraft position in the mean of date coordinate system in Section 3.2.1.
- $x_{ep}, y_{ep}, z_{ep}$  - Components of spacecraft position in the equinoctial coordinate system in Section 3.2.5.
- $x^1$  - Components of the space coordinates in Appendix C.
- $x_{lp}, y_{lp}, z_{lp}$  - Components of spacecraft position in geocentric local plane coordinates (up, east, north) in Section 3.2.3.
- $x_{lt}, y_{lt}, z_{lt}$  - Components of spacecraft position in topocentric local tangent coordinates (east, north, up) in Section 3.2.4.
- $x_n$  - Quantity denoting the Cowell position integrator for linear systems.
- $x_{op}, y_{op}, z_{op}$  - Components of spacecraft position in geocentric orbit plane coordinates in Section 3.2.5.

- $x_p, y_p$  - Instantaneous angular coordinates of the polar motion in Section 3.3.2.2 (see Figure 3-11).
- $x_p, y_p, z_p$  - Keplerian Cartesian components of spacecraft position in orbital coordinates, i.e.,  $x_p$  is directed toward perigee and  $z_p$  in the direction of the angular momentum. See Sections 3.2.5 and 5.7.
- $\hat{x}_p, \hat{y}_p, \hat{z}_p$  - Keplerian unit vectors in Sections 3.2.5 and 5.7.
- $x'_s, z'_s$  - Components used in two-dimensional analysis of ellipsoid in Section 3.3.6 to indicate that the y component is omitted.
- $x_s, y_s, z_s$  - Coordinates of a point s on the surface of an ellipsoidal planet expressed in body-centered rotating coordinates. See Section 3.3.6.
- $x_v, y_v, z_v$  - Components of spacecraft position in the vehicle-fixed coordinate system in Sections 3.2.7 and 4.7.1.
- $x_1 \dots x_{19}$  - DODS variables used in the Brouwer-Lyddane theory defined in Section 4.9.1.
- $x_{20} \dots x_{59}$  - DODS drag parameters in Section 4.9.2.
- Y - See X, Y, Z above.
- Dependent variable vector in the second-order linear differential system of variational equations in Sections 4.1 and 6.4.
- $Y_T, P_T$  - Yaw and pitch angles, respectively, defining the thrust direction in Section 4.8.
- $Y(t), \dot{Y}(t)$  - Matrices obtained by integrating the variational equations in Section 4.1.
- Matrices of position partial derivatives and velocity partial derivatives, respectively, in Section 6.4.
- $Y(t_{j+1} | t_j)$  - Predicted measurement residual uncertainty in Section 8.4.

$Y_m(t)$  - Linear combination of functions used in the interpolation of ephemeris data in Section 3.6.

$y$  - See  $x, y, z$  above.

- Fast osculating orbital elements in Section 5.8.

$\bar{y}$  - The  $m$ -dimensional vector of measurement data in Chapter 8.

$y_b$  - See  $x_b, y_b, z_b$  above.

$y'_b$  - See  $x'_b, y'_b, z'_b$  above.

$y_E$  - See  $x_E, y_E, z_E$  above.

$y_{ep}$  - See  $x_{ep}, y_{ep}, z_{ep}$  above.

$y_i$  - JPL ephemeris function value at time  $t_i$  in Section 3.6.

$y_{lp}$  - See  $x_{lp}, y_{lp}, z_{lp}$  above.

$y_{lt}$  - See  $x_{lt}, y_{lt}, z_{lt}$  above.

$y_n$  - Half-thickness of the bottomside layer of the electron density profile in Section 7.6.

$y_p$  - See  $x_p, y_p, z_p$  above.

$y_s$  - See  $x_s, y_s, z_s$  above.

$y_v$  - See  $x_v, y_v, z_v$  above.

$y_{op}$  - See  $x_{op}, y_{op}, z_{op}$  above.

$Z$  - See  $X, Y, Z$  above.

- Altitude in Section 4.5.4.

$Z_m, Z_n$  - Zenith calibration constants in Appendix A.

$z$  - See  $x, y, z$  above.

$z$  (cont'd) - Nondimensional altitude used in the Chapman profile for electron density in Sections 7.6.2 and 7.6.3.

$\bar{z}$  - The  $q$ -dimensional consider vector containing as components all model parameters whose values are known with limited certainty but are not to be estimated. See Chapter 8.

$z_b$  - See  $x_b, y_b, z_b$  above.

$z'_b$  - See  $x'_b, y'_b, z'_b$  above.

$z_E$  - See  $x_E, y_E, z_E$  above.

$z_{ep}$  - See  $x_{ep}, y_{ep}, z_{ep}$  above.

$z_t$  - The  $z_b$  axis intercept of the vector normal to the surface of the ellipsoidal planet model in Section 3.3.6.

$z_{lp}$  - See  $x_{lp}, y_{lp}, z_{lp}$  above.

$z_{lt}$  - See  $x_{lt}, y_{lt}, z_{lt}$  above.

$z_{op}$  - See  $x_{op}, y_{op}, z_{op}$  above.

$z_o$  - See  $x_p, y_p, z_p$  above.

$z_s$  - See  $x_s, y_s, z_s$  above.

$z_v$  - See  $x_v, y_v, z_v$  above.

$\bar{z}_0$  - A priori value of  $\bar{z}$  in Chapter 8.

$u$  - Right ascension of the spacecraft relative to the true of date system.

- Geocentric angle between the ground station and the sub-ionospheric point in Section 7.6.3.

- Uniformization constant in Appendix B.

$\hat{a}$  - Unit vector normal to the orbit plane in Section 4.10.



- $\alpha, \beta$  - Slow and fast elements, respectively, in Section 5.7.
- $\bar{\alpha}, \bar{\rho}$  - Four-vectors in Section 5.4 and Appendix B.
- $\alpha_g$  - True Greenwich sidereal time, the Greenwich Hour Angle of the true equinox of date, or the right ascension of Greenwich.
- $\alpha_{GM}$  - Mean Greenwich sidereal time, measured in the mean equator and equinox of date system.
- $\alpha_i$  - Thermal diffusion coefficient in Section 4.5.4 (see Table 4-2).
- DS elements vector in Section 5.5.
- $\alpha_i, \beta_i; \alpha_i^*, \beta_i^*$  - Coefficients of the Adams-Cowell predictor formulas (ordinate form) in Chapter 6.
- $\alpha_s$  - Right ascension of the sun in Section 4.5.6.
- $\alpha_T$  - Right ascension of the spacecraft's thrust axis in Section 4.8.1.
- $\alpha_t$  - Topocentric right ascension of the spacecraft in Section 9.1.
- $\alpha_v$  - Right ascension of the spacecraft's longitudinal axis in Section 3.3.12.
- $\alpha_0, \dots, \alpha_4$  - Coefficients of polynomial characterizing the thrust axis right ascension in Section 4.8.1.
- $\alpha_1, \alpha_2, \alpha_3$  - Doppler factors for individual transmission legs in satellite-to-satellite tracking in Section 7.3.3.
- $\alpha_1, \dots, \alpha_8$  - DS elements vector in Section 5.5.
- $\phi$  - Flight path angle measured from the geocentric position vector to the velocity vector in Section 3.2.3.
- $\hat{\rho}$  - Unit vector lying in the orbit plane in Section 4.10.

- $\beta_1, \beta_2, \beta_3$  - Doppler factors for individual transmission legs in satellite-to-satellite tracking in Section 7.3.3.
- $\Gamma_n^T$  - Vector containing powers of the thrust burning time in Section 4.8.2.
- $\gamma$  - Normal gravity at a point. See Section 7.4.
- $\hat{\gamma}$  - Unit vector forming right-hand system with  $\hat{a}$  and  $\hat{\beta}$  in Section 4.10.
- $\gamma_e$  - Normal equatorial gravity in Section 7.4.
- $\gamma_i, \gamma'_i, \gamma''_i$  - Coefficients in the Adams-Cowell formulas in Section 6.1.
- $\gamma_2, \gamma_3, \gamma_4, \gamma_5$  - Auxiliary parameters defined on pages 5-44 and 5-45.
- $\gamma'_2, \gamma'_3, \gamma'_4, \gamma'_5$  - Auxiliary parameters defined on pages 5-44 and 5-45.
- $\Delta$  - Auxiliary angle used in determining the transformation from true of date selenocentric to selenographic coordinates in Section 3.3.3.
- $\Delta \vec{d}_R, \Delta \vec{d}_V$  - Correction vectors used in the determination of refraction correction in Section 7.6.3.
- $\Delta E$  - Atmospheric elevation correction in Section 7.6.3.
- $\Delta f_{\text{cesium}}$  - The correction to the frequency  $f_{\text{cesium}} = 9,192,631,770$  cycles of cesium per ephemeris second in Section 3.5.1.
- $\Delta H$  - The correction to the mean right ascension to account for nutation in Section 3.3.2.1.
- $\Delta \ell_{\text{DRAG}}, \Delta M_{\text{DRAG}}$  - First-order correction to the mean anomaly in Sections 3.9 and 4.10, respectively.
- $(\Delta \log_{10} \rho)_G$  - Geomagnetic activity correction to standard density calculation in Section 4.5.4.
- $(\Delta \log_{10} \rho)_{He}$  - Density correction for seasonal latitudinal variation of helium in Section 4.5.4.

- $(\Delta \log_{10} \rho)_{LT}$  - Density correction for seasonal latitude variation of the lower thermosphere in Section 4.5.4.
- $(\Delta \log_{10} \rho)_{SA}$  - Semiannual atmospheric density variation in Section 4.5.4.
- $\Delta r$  - Radius of the error hypersphere in Section 8.5.2.
- $\Delta r, \Delta \dot{r}$  - Range and range-rate antenna mount corrections in Section 7.6.3.
- $\Delta s, \Delta \hat{s}$  - First six components of  $\Delta \hat{x}$  and  $\Delta \bar{x}$  in Chapter 8.
- $\Delta T_{\infty}$  - Correction to exothermic temperature in Section 4.5.4.
- $\Delta T_{1958}$  - The difference ET - UT2 on January 1, 1958, 0<sup>h</sup> 0<sup>m</sup> 0<sup>s</sup> UT2 minus the periodic terms in the ET to A.1 transformation in Section 3.5.1.
- $\Delta t_{A_i}$  - Atmospheric delay in the i<sup>th</sup> leg in satellite-to-satellite tracking in Section 7.3.3.
- $\Delta t_c$  - Counter delay in the phase readout digitizing equipment in Appendix A.
- $\Delta t_d$  - Correction to sequencer delay in Appendix A.
- $\Delta t_p$  - Sequencer delay in Appendix A.
- $\Delta t_R$  - Two-way light time corresponding to range observable in Section A.1.
- $\Delta t_{RD}$  - The reciprocal of the data recording rate in Section A.1.
- $\Delta t_{RR}$  - Doppler count time interval in Chapter 7 and in Appendices A and C.
- $\Delta \bar{u}$  - Perturbations about  $\bar{u}$  in Section 8.2.3.
- $\Delta \hat{u}$  - Best estimate of  $\bar{\Delta u}$  in a weighted least squares sense in Chapter 8.
- $\Delta \bar{u}_T, \Delta \bar{u}_V$  - Correction vectors used in the determination of refraction correction in Section 7.6.3.

- $\overline{\Delta \mathbf{x}}_i$  - Perturbation in the solve-for vector about the  $i^{\text{th}}$  iterated estimate,  $\hat{\mathbf{x}}_i$ . See Section 8.2.
- $\widehat{\Delta \mathbf{x}}_i$  - Best estimate of  $\overline{\Delta \mathbf{x}}$  in a weighted least squares sense in Section 8.2.
- $\widetilde{\Delta \mathbf{x}}_i$  - Deviation of the a priori from the  $i^{\text{th}}$  iterated estimate of  $\overline{\mathbf{x}}$ . See Section 8.2.
- $\overline{\Delta \mathbf{y}}_i$  - Vector of deviation between the actual measurements and the  $i^{\text{th}}$  iterated estimate of the measurements. (Note:  $\overline{\Delta \mathbf{y}} = \overline{\Delta \mathbf{y}}_c$ ). See Sections 8.1 and 8.2.
- $\overline{\Delta \mathbf{z}}$  - Perturbations of the consider vector  $\overline{\mathbf{z}}$  about its a priori value in Section 8.2.
- $\Delta \mathbf{z}_i$  - Components of transformed state vector which constitute the coordinates of a hypersphere in Section 8.5.2.
- $\Delta \lambda$  - Difference between the adopted and true longitude in Section 3.3.2.2.
- $\Delta \rho$  - Atmospheric range correction in Section 7.6.3.
- $\Delta \dot{\rho}$  - Atmospheric range-rate correction in Section 7.6.3.
- $\Delta \rho_c$  - Density correction factor in Section 4.5.5.
  - Computed range difference in Appendix C.
- $\Delta \tau$  - Spacecraft transponder time delay in Chapter 7 and Appendix A.
- $\Delta \phi$  - Difference between the adopted and true latitude in Section 3.3.2.2.
- $\delta$  - Declination angle measured north from the equator.
  - Quantity used in the determination of atmospheric refraction correction to the elevation angle in Section 7.6.4.
  - Dirac delta function in Section 8.4.

- $\delta'_i, \delta''_i$  - Coefficients of the ordinate form of the Adams-Cowell formulas in Section 6.7.
- $\delta_{ij}$  - Polynomial coefficients in density calculation in Section 4.5.4.
  - Kronecker delta function in Sections 4.8.2 and 8.4.
- $\delta_s$  - Declination of the sun.
- $\delta_T$  - Declination of the spacecraft's thrust axis in Section 4.6.1.
- $\delta_t$  - Topocentric declination of the spacecraft in Section 9.1.
- $\delta_v$  - Declination of the spacecraft's longitudinal axis in Section 3.3.12.
- $\delta_0, \dots, \delta_4$  - Coefficients of polynomial characterizing the thrust axis declination in Section 4.8.1.
- $\delta i, \delta \Omega, \delta \omega$  - Perturbations in the orbit inclination, right ascension of the ascending node, and argument of perigee, respectively, in Section 4.10.
- $\delta t$  - Timing bias in observation data in Sections 7.1 and 8.2.
- $\delta \alpha, \delta \beta, \delta \gamma$  - Rotational perturbations around  $\hat{\alpha}$ ,  $\hat{\beta}$ , and  $\hat{\gamma}$ , respectively, in Section 4.10.
- $\delta \epsilon$  - Difference between the true and mean obliquity in Section 3.3.1.2.
- $\delta \psi$  - Nutation in longitude in Section 3.3.1.2.
- $\epsilon$  - Small parameter proportional to the perturbing acceleration in Section 5.8.
  - Improvement ratio criterion specified for least squares iteration convergence in Section 8.6.3.
- $\bar{\epsilon}, \tilde{\epsilon}$  - Mean and true obliquity in Section 3.3.1.2.

- $\bar{\epsilon}(t)$  - First-order Gauss-Markov process representing the unmodeled acceleration  $\bar{a}_u$  in Section 8.4.2.
- $\epsilon_n$  - Local error of the numerical integration in Section 6.9.
- $\mathcal{E}(\ )$  - Denotes the expected value.
- $\zeta_0$  - Precession angle in Section 3.3.1.1.
- $\eta$  - Surface reflectivity coefficient in Section 4.6.
- Auxiliary parameter defined on page 5-44.
- $\theta$  - Flight path angle in Section 4.10.
- Transition matrix between perturbations in solve-for variables and perturbations in consider variables in Section 8.2.3.
- Auxiliary parameter defined on page 5-44.
- $\theta, \theta_M$  - Orbital angle and mean orbital angle, respectively, measured along the lunar equator from the descending node of the earth's orbit to the lunar prime meridian. See Section 3.3.3.
- $\theta_p$  - Precession angle in Section 3.3.1.
- $\iota$  - Euler angle used in the transformation from selenocentric to selenographic coordinates in Section 3.3.3.
- $\lambda$  - Longitude measured east from the prime meridian.
- Equinoctial and Herrick mean longitudes in Sections 3.2.6 and 3.3.9.1.
- $\bar{\lambda}$  - Lag angle between the sun line and the apex of the diurnal bulge in Section 4.5.6.
- $\lambda_A, \lambda_T$  - Adopted and instantaneous (true) longitudes, respectively, in Section 3.3.2.2.
- $\lambda_E$  - Selenographic longitude of the earth in Section 4.4.

- $\lambda_M$  - Geocentric mean longitude of the moon in Section 3.3.3.
- True right ascension of the moon in Section 4.4.
- $\lambda_p$  - Longitude of the magnetic north pole in Section 7.6.
- $\lambda_r$  - Mean longitude for retrograde orbit in Section 3.3.11.1.
- $\lambda_s$  - Longitude of the tracking station in Sections 3.3.7 and 9.1.
- $\mu$  - Gravitational parameter of the reference body, i.e., the product of the universal gravitational parameter and the mass of the body.
- $\nu$  - Eclipse factor in Section 4.6.1.
- Electromagnetic signal frequency in Section 7.6.
- $\nu_b$  - Bias frequency on Doppler signal in Section 7.3.3 and Appendices A and C.
- $\nu_d$  - Doppler signal frequency in Appendices A and C.
- $\nu_h$  - High frequency modulation (ranging) tone in Appendix A.
- $\nu_{in}$  - Counter input frequency in satellite-to-satellite tracking in Section 7.3.3.
- $\bar{\nu}_{in}$  - Average value of  $\nu_{in}$  over the Doppler count interval  $\Delta t_{RR}$  in Section 7.3.3.
- $\nu_L$  - Low frequency modulation (ranging) tone in Appendix A.
- $\nu_R$  - Signal frequency received at the ground station in Appendices A and C.
- System reference frequency for satellite-to-satellite tracking Doppler measurements in Section 7.3.3.
- $\nu_{R1}, \nu_{R2}$  - Reference frequency for the GRARR and ATSR range and range-rate measurements. See Appendices A and C.
- $\nu_T$  - Frequency of signal transmitted at the tracking station in Appendices A and C.

- $\nu_t, \nu_r$  - Frequencies of transmitted and received signals in Appendix C.
- $\nu_v$  - Frequency of signal received at the spacecraft. See Appendices A and C.
- $\xi$  - Normalized time in Section 5.6.
- $\xi_p$  - Precession angle in Section 3.3.1.
- $\rho$  - One-way range from the tracking station to the spacecraft in Chapters 3, 7, and Appendix A.
- Planet's mass density in Section 4.3.
  - Atmospheric density in Section 4.5.
  - Average of the uplink and downlink propagation distances in Section 7.2.
- $\rho, \eta, \theta$  - Oblate spherical coordinates in Section 5.12.
- $\rho_a$  - Atmospheric density in Section 4.5.2.
- $\rho_a, \rho_b$  - Range ambiguity numbers in Appendix A.
- $\dot{\rho}_{avg}$  - Average range rate over the uplink and downlink paths in Chapter 7 and Appendices A and C.
- $\rho_F$  - Dynamic weighting factor in Appendix D.
- $\rho_i$  - Atmospheric constituent densities in Section 4.5.4.
- Slant range from tracking station to spacecraft in Section 9.1.2.
- $\rho_{ij}$  - Correlation coefficient in Section 8.5.
- $\rho_L$  - Four-leg round trip range in satellite-to-satellite tracking in Section 7.3.3 and Appendix C.
- $\overline{\dot{\rho}}_L$  - Average four-leg range rate (in satellite-to-satellite tracking) over the Doppler count interval  $\Delta t_{RR}$ . See Section 7.3.3.



- $\rho_{1t_i}$  - Measurement vector in station-centered topocentric local tangent coordinates in Section 9.2.
- $\rho_M$  - Physical libration in the inclination of the mean lunar equator in Section 3.3.3.
- $\rho_M, \rho_m$  - Maximum and minimum densities in Section 4.5.6.
- $\rho_S$  - Two-leg round trip range in satellite-to-satellite tracking in Section 7.3.3 and Appendix C.
- $\overline{\rho_S}$  - Average two-leg range rate (in satellite-to-satellite tracking) over the Doppler count interval  $\Delta t_{RR}$  in Section 7.3.3.
- $\rho_s$  - Summed atmospheric density in Section 4.5.4.
- $\rho_u, \rho_d$  - One-way range distance corresponding to the uplink and downlink signal path in Section 7.2.3 and Appendix C.
- $\rho_1, \rho_2$  - Ranges from first and second stations to the satellite in VLBI tracking in Section 7.4.
- $\rho_1, \rho_2, \rho_3$  - Systematic error coefficients in the atmospheric density model in Section 4.5.
- $\sigma$  - Sample standard deviation in Section 8.6.4.
- $\sigma_i^2$  - Variance of the measurement noise component  $n_i$  in Chapter 8.
- $\sigma_k$  - The standard deviation of the  $k^{th}$  observation in Chapter 8.
- $\tilde{\sigma}_k$  - A priori standard deviation of the noise on the  $k^{th}$  observation in Section 8.1.
- $\bar{\sigma}_k$  - Standard deviation of the data reduction curve fit obtained during preprocessing of the  $k^{th}$  observation in Section 8.1.
- $\zeta_M$  - Hayn's physical libration in the mean right ascension of the ascending node of the lunar orbit in Section 3.3.3.

- $\sigma_1, \dots, \sigma_6$  - Eigenvalues of  $P_{\Delta x}$  in Section 8.5.
- $\sigma_{\Delta s_i}^2$  - Estimate of the variance of  $\Delta s_i$  in Section 8.2.3.
- $\sigma_{\Delta z_i}^2$  - Estimate of the variance of  $\Delta z_i$  in Section 8.2.3.
- $\tau$  - Auxiliary angle used in the calculation of the uncorrected exospheric temperature in Section 4.5.4.
- Time measured from effective ignition of the thruster in Section 4.8.1.
- The independent variable (time element) for the transformed time-regularized system in Sections 5.4, 6.10, and Appendix B.
- Phase difference time interval in VLBI tracking in Section 7.4.
- $\rho_M$  - Hayn's physical libration in longitude in Section 3.3.3.
- $\Phi$  - Perturbing energy in Section 5.5 and Appendix B.
- State transition matrix in Section 6.5.
- Augmented state transition matrix in Section 8.4.
- $\phi, \phi'$  - Geodetic and geocentric latitudes, respectively, in Chapters 3 and 7.
- Geocentric and geodetic latitudes, respectively, in Chapter 4.
- $\phi(T_i, t_0)$  - State transition matrix relating state perturbations at time  $t_0$  to state perturbations at time  $T_i$ . See Chapter 3.
- $\phi(t, t_0)$  - Transition matrix relating perturbations about  $\bar{u}(t)$  at times  $t$  and  $t_0$  in Chapter 8.
- $\phi_A, \phi_T$  - Latitude corresponding to the adopted and true poles, respectively, in Section 3.3.2.2.
- $\phi_E$  - Selenographic latitude of the earth in Section 4.4.

- $\phi_M$  - Geocentric latitude (declination) of the moon in Section 4.4.
- $\phi_p$  - Geodetic latitude of the magnetic north pole in Section 7.6.
- $\phi_s, \phi'_s$  - Geodetic and geocentric latitude of the tracking station in Sections 3.3.7 and 9.1.
- $\phi_T$  - See  $\phi_A, \phi_T$  above.
- $\phi_v$  - Roll angle of the spacecraft in Section 3.3.12.
- $\psi$  - Gravitational potential in Sections 4.3.1 and 4.4.
  - Angle between the satellite position vector and the apex of the diurnal bulge in Section 4.5.6.
  - Generalized true anomaly in Section 5.5.
  - Geopotential function (sum of the normal geopotential  $\psi_N$  and the disturbing potential  $\psi_D$ ). See Section 7.4.
  - Abbreviation for the covariance matrix of the estimated state in the absence of consider variables in Section 8.3.
- $\psi_D$  - Disturbing potential in Section 7.4.
- $\psi_N$  - Normal geopotential in Section 7.4.
- $\Omega$  - Right ascension of the orbital ascending node.
  - Skew matrix whose elements are components of the earth's rotation vector in Section 4.5.3.
- $\Omega'$  - Euler angle used in transformation from selenocentric to selenographic coordinates in Section 3.3.3.
- $\Omega_M$  - Mean right ascension of the ascending node of the lunar orbit in Section 3.3.3.
- $\omega$  - Argument of perigee of the satellite orbit.
  - Frequency related to the negative of the total energy in Section 5.4 and Appendix B.

$\omega$  (cont'd) - Rotation rate of the earth in Section 7.4.

$\bar{\omega}$  - Angular rotation vector of the earth expressed in mean of 1950.0 coordinates in Section 4.5.2.

- State noise in Chapter 8.

$\omega_M$  - Moon's argument of perigee in Section 3.3.3.

## Subscripts

- ( )<sub>A</sub> - adopted quantity; averaged quantity; or model replacement
- ( )<sub>a</sub> - apofocus; atmospheric; or apparent
- ( )<sub>ac</sub> - attitude control
- ( )<sub>avg</sub> - average
- ( )<sub>B</sub> - spacecraft axis
- ( )<sub>b</sub> - body centered; body fixed; burn; or bias
- ( )<sub>C</sub> - correction; or coarse baseline (Minitrack)
- ( )<sub>c</sub> - computed; cylinder; or minimum exospheric
- ( )<sub>D</sub> - drag; aerodynamic; deviation; or disturbing
- ( )<sub>d</sub> - Doppler; or downlink
- ( )<sub>E</sub> - earth; or mean of date
- ( )<sub>E-W</sub> - east-west
- ( )<sub>e</sub> - equatorial; ephemeris; end plate; or electron density
- ( )<sub>ep</sub> - equinoctial system
- ( )<sub>F</sub> - frame; force; or fine baseline (Minitrack)
- ( )<sub>FM</sub> - midframe
- ( )<sub>f</sub> - final
- ( )<sub>GM</sub> - Greenwich mean
- ( )<sub>g</sub> - geomagnetic; Greenwich; or group
- ( )<sub>I</sub> - ionospheric
- ( )<sub>IO</sub> - mutual nonspherical gravitational attraction of earth and moon

- ( )<sub>in</sub> - counter input
- ( )<sub>j</sub> - reference (central) body
- ( )<sub>k</sub> - Keplerian
- ( )<sub>k</sub> - body k
- ( )<sub>L</sub> - four-way ranging; or low frequency
- ( )<sub>lp</sub> - local plane
- ( )<sub>lt</sub> - local tangent
- ( )<sub>M</sub> - moon; maximum; or medium baseline (Minitrack)
- ( )<sub>M<sub>m</sub></sub> - midpoint
- ( )<sub>m</sub> - minimum; maximum (Chapter 7); or middle point
- ( )<sub>N</sub> - normal
- ( )<sub>NS</sub> - nonspherical
- ( )<sub>N-S</sub> - north-south
- ( )<sub>of</sub> - orbital frame
- ( )<sub>op</sub> - orbit plane
- ( )<sub>PM</sub> - point mass
- ( )<sub>p</sub> - polar; perifocus; precession; solar paddle; geomagnetic; planetary; orbital rectangular coordinates; or phase
- ( )<sub>R</sub> - ground receiver; or reference
- ( )<sub>RR</sub> - Doppler count
- ( )<sub>RT</sub> - round trip
- ( )<sub>r</sub> - generalized receiver (Appendix C)

- ( )<sub>rel</sub> - relative to the atmosphere
- ( )<sub>s</sub> - two-way ranging
- ( )<sub>SA</sub> - semiannual
- ( )<sub>SR</sub> - solar radiation
- ( )<sub>s</sub> - tracking station; solar; sample; selenographic; surface; spherical; or sea level
- ( )<sub>T</sub> - ground transmitter; thrust; tropospheric; or true (instantaneous) pole
- ( )<sub>TAC</sub> - attitude control system
- ( )<sub>t</sub> - time; topside; topocentric; or generalized transmitter (Appendix C)
- ( )<sub>u</sub> - uplink
- ( )<sub>v</sub> - spacecraft; or vehicle fixed
- ( )<sub>x</sub> - inflection point
- ( )<sub>x</sub>, ( )<sub>y</sub>, ( )<sub>z</sub> - corresponding axis
- ( )<sub>0</sub> - mean elements at epoch; earth centered; initial conditions; actual; or a priori (Chapter 7)
- ( )<sub>30</sub> - GRARR and USB 30-foot antennas
- ( )<sub>85</sub> - USB 85-foot antennas
- ( )<sub>∞</sub> - corrected exospheric

## Superscripts

( )<sup>c</sup> - corrected values

( )<sup>d</sup> - day

( )<sup>h</sup> - hour

( )<sup>m</sup> - minute

( )<sup>p</sup> - predicted values

( )<sup>s</sup> - second

( )<sup>T</sup> - transpose

( )<sup>̂</sup> - perturbed initial conditions



## Operational Symbols

$\nabla$  - linear gradient; or backward difference operator

$(\ ) \times (\ )$  - vector cross product

$(\ ) \cdot (\ )$  - vector dot product

$E^s$  - shifting operator (Section 6.1)

$D$  - differential operator (Section 6.1)

$I$  - identity operator

$(\ )'$  - first derivative with respect to time

$(\ )''$  - second derivative with respect to time

$(\ )^\wedge$  - best estimate

$(\ )^\sim$  - vector; or average value

$E(\ )$  - expected value

$\text{cov}(\ )$  - covariance

$\text{var}(\ )$  - variance

$(\ )'_s$  - first derivative with respect to the variable  $s$  (Chapter 5)

$(\ )''_s$  - second derivative with respect to the variable  $s$  (Chapter 5)

## INDEX

This index consists of an alphabetical list of significant topics contained in this document. Cross-referencing is used where appropriate. The notation appearing in parentheses after certain topics refers to the section or chapter which is primarily concerned with that topic. The hyphenated numbers refer to the pages where the specified topic is mentioned. A page number immediately following a section or chapter number indicates the beginning page of that section or chapter. For example, the following entry

Mean of estimate, (8.2.1) 8-8, 8-50

indicates that the "mean of estimate" is discussed in Section 8.2.1, which begins on page 8-8, and that it is also mentioned on page 8-50.

---

Accelerometer data, 4-73

Acceleration,

of earth due to oblateness of earth and moon, 4-20

of moon due to oblateness of earth and moon, 4-20

unknown, 8-42

unmodeled, 8-37

Adams integration formulas, 5-8, 5-9, 6-1, 6-2

Adams-Bashforth formula, 6-1

Adams-Cowell integration formulas, (6.1) 6-9

Adams-Moulton predictor-corrector coefficients, 6-6

Aerodynamic force coefficients, Table 4-1, 4-26

cylindrical spacecraft, 4-25, 4-27, 4-28

cylindrical spacecraft with solar paddles, 4-28, 4-29

spherical spacecraft, 4-25 through 4-27

Aerodynamic forces, (4.5) 4-22 through 4-32

aerodynamic force modeling, (4.5.2) 4-24 through 4-28

associated partial derivatives, (4.5.3) 4-29 through 4-32

Algorithm, batch estimator, (8.2) 8-6

Analytic partial derivatives, (4.10) 4-75 through 4-86

conversion of differential corrections, (4.10.3) 4-83 through 4-86

definition of perturbation variables, (4.10.1) 4-75 through 4-79

state transition matrix elements, (4.10.2) 4-79 through 4-83

Angles only early orbit methods (9.1) 9-1

Antenna mount corrections, (7.7.2) 7-76, 7-77

Applications Technology Satellite Range and Range-Rate (ATSR) System,  
(see Goddard Range and Range-Rate (GRARR) System)

- Atmospheric density models, 4-22, 4-23
  - comparison of, (4.5.8) 4-60
  - Jacchia-Roberts model, (4.5.4) 4-33 through 4-49
  - modified Harris-Priester model, (4.5.6) 4-53 through 4-60
- Atmospheric effects, (7.6) 7-43 through 7-75
  - Chapman profile refraction corrections, (7.6.3) 7-52 through 7-63
    - Doppler corrections, 7-59 through 7-64
    - elevation angle-dependent corrections, 7-56 through 7-59
    - range correction, 7-52 through 7-56
  - ionospheric models, (7.6.2) 7-44 through 7-52
    - electron density profile parameters, 7-49 through 7-52
    - empirical worldwide profile, 7-47 through 7-49
    - modified Chapman profile, 7-46
  - sequential profile refraction corrections (7.6.4) 7-64 through 7-75
    - ionospheric correction, 7-68 through 7-75
    - tropospheric correction, 7-65 through 7-68
  - troposphere model, (7.6.1) 7-43, 7-44
- Attitude control effects, (4.7) 4-64 through 4-65, 2-18
  - partial derivatives, (4.7.2) 4-66
  - perturbation model, (4.7.1) 4-64, 4-65
- Averaging formulation, (5.8) 5-45, 5-5
  - equinoctial VOP formulation, (5.8.3) 5-40
  - Keplerian formulation, (5.8.4) 5-40
- Batch estimator algorithm, (8.2) 8-6
- Besselian solar year, 3-1
- Bouguer's formula, 7-56
- Brouwer drag parameters, 4-78, 4-79
- Brouwer-Lyddane formulation, (5.10) 5-51, 4-75, 5-4, 5-48
- Brouwer theory, (5.9) 5-42, 2-6, 5-1, 5-39, 5-51, 5-58, 5-59, 5-60
- C-Band radar system, A-8, A-10
  - early orbit data, 9-24
  - functional description, A-9
  - preprocessing description, A-10
- Canonical variables, 5-1, 5-2, 5-16
  - force, 5-18
- Cassini's laws, 3-26
- Celestial equator, 3-2
- Celestial sphere, 3-2
- Chapman profile, 7-46
- Chapman profile refraction corrections, (7.6.3) 7-52 through 7-64
  - Doppler corrections, 7-59 through 7-64
  - elevation angle-dependent corrections, 7-56 through 7-59

- Chapman profile refraction corrections (cont'd.)
  - ionospheric model for, 7-46
  - range correction, 7-52 through 7-55
- Chebyshev series, (5.6) 5-26
- Consider variables, 2-13
- Consider variables, a priori, 8-6, 8-3, 8-24
- Consider vector, 8-6, 8-12, 8-15, 8-27
  - uncertainty, 8-51
- Convergence criteria, 8-61
- Correlation, 8-11, 8-19
  - between state and uncertain model parameters, 8-19
  - coefficient, (8.5.4) 8-56
  - of estimate and consider variables, 8-23
  - of errors in a priori solve-for and consider variables, 8-11
  - of errors in solve-for and consider variables, 8-11, 8-12
  - of solve-for and consider variables, timewise propagation, 8-24
- Coordinate systems, (Chapter 3)
  - body-centered equatorial inertial, (3.2.1) 3-3
    - rectangular Cartesian, 3-4
    - spherical polar, 3-4
  - body-centered rotating, (3.2.2) 3-4
    - geodetic, 3-5
    - rectangular Cartesian, 3-5
    - spherical polar, 3-5
  - local plane, (3.2.3) 3-5
    - rectangular Cartesian, 3-6
    - spherical velocity, 3-6
  - orbit plane, (3.2.5) 3-7
    - equinoctial, 3-8
    - Keplerian, 3-7
  - orbital elements, (3.2.6) 3-8
    - equinoctial, 3-9
    - Herrick, 3-9
    - Keplerian, 3-8
  - selenocentric, 3-26
  - selenographic, 3-26
  - topocentric local tangent, (3.2.4) 3-6, 7-5
    - rectangular Cartesian, 3-6
    - spherical position, 3-7
  - vehicle-fixed, (3.2.7) 3-10
    - rectangular Cartesian, 3-10
- Coordinate time, C-6, C-8, C-9, C-10, C-12
- Coordinate time derivatives, C-9

- Coordinate transformations, (3.3) 3-10, 2-18
  - body-centered true of date to orbit plane, (3.3.5) 3-39
  - body-fixed to geographic, (3.3.6) 3-40
    - earth-fixed to geodetic, (3.3.6.3) 3-44
    - geodetic to earth-fixed, (3.3.6.2) 3-43
  - earth-fixed to topocentric local tangent, (3.3.7) 3-47
  - equinoctial to Cartesian, (3.3.9) 3-58
    - Cartesian coordinates to equinoctial elements, (3.3.9.2) 3-60
    - equinoctial elements to Cartesian coordinates, (3.3.9.1) 3-58
  - Herrick to Cartesian, (3.3.10)
    - Cartesian coordinates to Herrick elements, (3.3.10.2) 3-63
    - Herrick elements to Cartesian coordinates, (3.3.10.1) 3-62
  - Keplerian to Cartesian, (3.3.8) 3-49
    - body-centered true of date to Keplerian elements, (3.3.8.3) 3-55
    - Keplerian elements to body-centered true of date, (3.3.8.1) 3-49
  - Keplerian to equinoctial and Herrick, (3.3.11) 3-64
    - Keplerian to equinoctial elements, (3.3.11.1) 3-64
    - Keplerian to Herrick elements, (3.3.12) 3-64
  - mean of 1950.0 to true of date, (3.3.1) 3-11
    - mean of date to true of date, (3.3.1.2) 3-14
    - mean of 1950.0 to mean of date, (3.3.1.1) 3-12
  - spherical to Cartesian, (3.3.4) 3-34
    - Cartesian position and velocity to spherical, (3.3.4.2) 3-36
    - spherical position and velocity to Cartesian, (3.3.4.1) 3-34
  - selenocentric true of date to selenographic, (3.3.3) 3-26
  - true of date to body-fixed, (3.3.2) 3-18
    - pseudo body-fixed to body-fixed, (3.3.2.2) 3-20
    - true of date to pseudo body-fixed, (3.3.2.1) 3-18
  - vehicle-fixed to body-centered true of date, (3.3.12) 3-65
- Covariance,
  - of estimate, (8.2.1) 8-8, 8-23
  - of state noise, 8-31, 8-32, 8-42
- Covariance matrix,
  - of error, 8-3, 8-4, 8-12, 8-29, 8-30
    - augmented, 8-44, 8-50
    - derivation of, (E.1) E-1
    - uncertainty (error), 8-5
  - interpretation, (8.5) 8-50
  - of state, 8-18
    - timewise propagation of, 8-17, 8-24
  - transformations, (8.2.3) 8-15
- Cowell method, (5.2) 5-8, 4-2, 5-1, 5-3, 5-5, 5-26, 6-1, 6-2, 6-11, 6-20, 6-25
  - time-regularized, (5.3) 5-9, 5-3, 5-5, 5-9, 6-1
- Critical frequency, 7-49

- Data Management Program, (2.1.8) 2-4
- Data Simulation Program, (2.1.6) 2-3
- Delaunay elements, (5.5) 5-16, 5-42, 5-43, 5-59
- Delaunay-Similar formulation, (5.5) 5-16, 2-9, 5-3, 5-4
- Density corrections, 4-36, 4-37
  - geomagnetic activity, 4-36, 4-45
  - seasonal latitudinal, 4-36, 4-37, 4-45, 4-54
  - seasonal latitudinal, helium, 4-37, 4-45
  - semiannual variation, 4-36, 4-45, 4-54
- Differential correction process, 7-1, 7-2
- Differential Correction Program, (2.1.1) 2-2
  - a priori input, 8-19
  - computational procedure, (8.2.4) 8-19
  - data management, 8-19
  - estimation computation, 8-22
  - inner processing loop, 8-21
  - outer iteration loop, 8-21
  - termination of outer iteration loop, 8-22, 8-60
- Differential equations,
  - class I, 5-2, 5-9, 5-26, 6-1, 6-2
  - class II, 5-2, 5-8, 5-9, 6-1, 6-2
- Direction cosines, Minitrack, 7-11
- Dispersion, 8-12 (see also measurement uncertainty)
- Diurnal bulge, 4-54, 4-56, 4-57
- Divergence, filter, 8-36
- DODS variables, 2-14, 4-75 through 4-86, 6-12
- Doppler corrections due to atmospheric refraction, 7-59 through 7-64
- Doppler cycle count, 7-15, A-3, A-7, A-11, A-12, A-13, A-32
  - destruct, 7-27, 7-28, A-32, C-7
  - nondestruct, 7-28, A-12, A-32, C-7
- Doppler measurements, 2-12, 7-20
- Doppler observation, (7.3.4) 7-27 through 7-34
  - formulation of, 7-28 through 7-30
  - partial derivatives of, 7-30 through 7-34
- Doppler shift, relativistic, C-3, C-4, C-5, C-6, C-11, C-14
- Double r-iteration method, early orbit, (9.1.3) 9-14, 2-14, 9-1, 9-2
- Dynamic model compensation,
  - advantages of, 8-37
  - procedure, 8-41
- Dynamic stability, 5-5
- Dynamic weighting factor, D-1, D-2
- Dynamics, spacecraft, (2.3) 2-17, 2-18

- Early orbit, angles only methods, (9.1) 9-1
- Early Orbit Determination Program, (2.1.5) 2-3
- Early orbit methods, (Chapter 9)
  - Double r-Iteration method, (9.1.3) 9-14, 2-3, 9-1, 9-2
  - Gauss method, (9.1.2) 9-6, 2-3, 9-1, 9-14, 9-17
  - Range and Angles method, (9.2) 9-24, 2-3, 9-1
- Earth-moon system, (4.4) 4-18
- Editing of observation residuals, (8.5.2) 8-60
- Electron density profile, 7-49 through 7-52
- Electron density profile parameters, 7-49 through 7-52
- Element sets,
  - Brouwer mean, 5-45
  - Delaunay-Similar, (5.5) 5-16, 5-4
  - equinoctial, (5.7.2) 5-33, 5-4, 5-31, 5-38
  - Keplerian, 5-4, 5-31, 5-38, 5-45
  - Kustaanheimo-Stiefel, 5-4
  - rectangular, 5-4, 5-31, 5-34
- Encke method, 5-58
- Ephemeris Comparison Program, (2.1.3) 2-2
- Ephemeris Generation Program, (2.1.2) 2-2
- Ephemeris data, 3-74 through 3-80
  - polynomial representation of, (3.6) 3-74
- Equations of motion, 6-2, 6-8, 8-37
- Error analysis,
  - application, (8.3) 8-22
  - problems, 8-24
- Error Analysis Program, (2.1.7) 2-3
- Error control, (6.9) 6-21
- Estimate,
  - a priori, 8-3
  - bias, 8-8
  - classical equation for best, 8-3
  - covariance of error, 8-10, 8-29
  - mean, 8-10
  - minimum variance, 8-30
  - state correction, 8-29
- Estimation, (Chapter 8)
- Estimation model, (7.8) 7-77 through 7-79
- Estimation, sequential, (8.4) 8-27, (Appendix E) E-1
  - process, 8-1
- Estimator,
  - advantage of recursive, 8-33
  - algorithm, 9-1
  - gain matrix, 8-11

## Estimator, (cont'd.)

- Kalman minimum variance, 8-27
- sequential adaptive, 8-42
- sequential weighted least squares, 8-27
- weighted least squares, 8-1, 8-22
- weighted least squares variation,
  - with respect to consider parameters, 8-25
  - with respect to dynamic parameters, 8-25

## Expected value of deviation, 8-8

- of linearized observation residuals, 8-9

## Fast elements, 5-17, 5-31, 5-38, 5-40

## Figure of the earth, (3.3.6.1) 3-40

## Filter

- Extended Kalman, (8.4) 8-27, 2-3, 2-13
  - derivation of, (8.4.1) 8-28
  - nonupdated reference trajectory, 8-33
  - prediction formulas of, 8-31
  - update equations of, 8-30
  - updated reference trajectory, 8-33, 8-34
- Jazwinski, (8.4.3) 8-42, 2-3
  - derivation of, 8-44
  - prediction equations, 8-47
  - update equations, 8-47

## Filter Program, (2.1.4) 2-2, 2-3

- a priori input, 8-48
- computational procedure, (8.4.4) 8-47
- data management, 8-48
- data set loop, 8-50
- processing loop, 8-48

## Filtering,

- dynamic model compensation, (8.4.2) 8-37
- statistical adaptive, (8.4.3) 8-42

## Flight sectioning, 2-18

## Gain matrix, 8-11, 8-30, 8-35, 8-45

## Gauss method, early orbit, (9.1.2) 9-6, 2-14, 9-1, 9-14, 9-17

## Gaussian planetary equation, 5-31

## Gaussian VOP formulation, (5.7) 5-30, 5-38

## General perturbation method, 2-6, 5-1, 5-3, 5-4

## Geoid, 7-34 through 7-38

## Geoidal undulation, 7-36, 7-37, 7-40

## Gibbs method, 9-6, 9-11



- Global iteration, 8-34
- Goddard Range and Range-Rate (GRARR) and ATSR systems, A-1 through A-8, C-11, C-13, C-14
  - data smoothing, A-8
  - early orbit data, 9-24
  - functional description, A-1, A-2, A-3
  - gimbal angles, A-6
  - preprocessing description, A-4, A-5, A-6
  - processing computations and interfaces, A-5
  - range computation, A-6, A-7
  - range-rate computation, A-7, A-8
- Greenwich Hour Angle, 3-67
- GTDS overview, (Chapter 2)
- GTDS programs, (2.1) 2-1 through 2-4
  - Data Management, (2.1.8) 2-4
  - Data Simulation, (2.1.6) 2-3, 2-16, 2-17
  - Differential Correction, (2.1.1) 2-2, 2-16, 2-17
  - Early Orbit Determination, (2.1.5) 2-3
  - Ephemeris Comparison, (2.1.3) 2-2
  - Ephemeris Generation, (2.1.2) 2-2, 2-6, 2-16
  - Error Analysis, (2.1.7) 2-3, 2-4, 2-17
  - Filter, (2.1.4) 2-2, 2-3
- GTDS system capabilities, (2.2) 2-4 through 2-17
  - early orbit determination, (2.2.4) 2-14, 2-15
  - estimation techniques, (2.2.3) 2-13, 2-14
  - observation modeling, (2.2.2) 2-9 through 2-13
    - data preprocessing, 2-10
    - observation models, 2-12
    - observation types, 2-10
  - optional modes of operation, (2.2.5) 2-16, 2-17
  - trajectory generation, (2.2.1) 2-6 through 2-8
- Hamilton-Jacobi differential equations, 5-1, 5-60
- Hamiltonian, 5-17, 5-18
- Harris-Priester atmospheric density model, (4.5.6) 4-53 through 4-59, 4-23
  - partial derivatives, (4.5.7) 4-57 through 4-59
- Index of refraction, 7-44
- Indirect oblation perturbation model, (4.4) 4-18 through 4-22
- Intermediate Orbit formulation, (5.11) 5-58, 2-8, 5-3, 5-4, 5-5
- Interpolation, 6-21
- Introduction, 1-1, 1-2
- Ionosphere models, (7.6.2) 7-44 through 7-52

- JPL ephemeris, 3-14, 3-17
- Jacchia-Roberts atmospheric density model, (4.5.4) 4-33 through 4-49, 4-23
  - partial derivatives, (4.5.5) 4-50 through 4-53
- KS matrix, 5-13
- Kalman gain, 8-30, (see also gain matrix)
- Kalman filter, (see Extended Kalman Filter)
- Kepler's equation, 5-51
- Kustaanheimo-Stiefel formulation, (5.4) 5-10, 2-9, 5-3, 5-4
- Laplacian, 4-9
- Least squares, weighted, 8-1, 8-6, 8-7
- Legendre functions, 4-11
- Libration of the moon, 4-18
- Light time correction, (7.7.1) 7-76
- Light time modeling, (7.3.2) 7-21
- Linear gain, optimal, E-3
- Linearity, 8-3, 8-6, 8-34
- Loss function, 8-2, 8-3, 8-6, 8-7
- Lunisolar precession and nutation, 3-12, 4-18
- Magnetic dip, 7-51
- Matrix identities (sequential estimation), (Appendix E) E-1
- Matrix inversion, (8.6.1) 8-57
- Matrix of functional sensitivities, 8-26
- Matrix of partial derivatives, 8-2
- Mean of estimate, (8.2.1) 8-8, 8-50
- Measurement model, 8-43
- Measurement noise, 8-9, 8-12, 8-42, 8-43 (see also observation noise)
  - covariance, 8-9
  - expected value, 8-9
- Measurement process, statistical assumption of, 8-3, 8-4
- Measurement residuals, 8-7, 8-9
- Measurement uncertainty, 8-12, 8-30
- Meridian,
  - local, 3-2
  - prime, 3-2
- Minimization, nonlinear, 8-2
- Minitrack system, A-14 through A-27
  - ambiguity data, A-20
  - ambiguity resolution, A-24
  - antenna field corrections, A-26
  - data linearization and smoothing, A-19

- Minitrack system, (cont'd.)
  - fine baseline data, A-21, A-22
  - functional description, A-14
  - preprocessing description, A-17
  - processor considerations, A-27
  - time adjustment and zenith calibration, A-22, A-23, A-24
- Model parameters, uncertain, 8-18
- Multistep integration methods, 6-1
  
- Near real-time operation, 2-19
- Newton-Raphson iteration, 5-41
- Newtonian interpolation, 6-5
- Nonspherical gravitational effects, (4.3) 4-9 through 4-18, 2-17
  - associated partial derivatives, (4.3.2) 4-14 through 4-18
  - perturbation model, (4.3.1) 4-9 through 4-14
- Normal matrix, 8-3, 8-14, 8-59
- Numerical integration methods, (Chapter 6)
  - corrector-only, 6-9 through 6-14
  - multistep methods, 6-1 through 6-16
  - predict-pseudo-correct, 6-7 through 6-9
  - predictor-corrector, 6-2 through 6-6
  - Runge-Kutta, 6-16 through 6-18
  - starting procedures, 6-19 through 6-22
- Numerical stability, 5-2, 5-3, 6-2, 6-7, 6-9
- Nutation, 3-12, 3-14, 3-15
  
- Obliquity of the ecliptic, 3-12, 3-14, 3-15
- Observation equation, nonlinear, 8-14
- Observation model, GTDS, 7-2
- Observation models, (Chapter 7)
  - additional corrections, (7.7) 7-76, 7-77
  - atmospheric effects, (7.6) 7-43 through 7-75
  - estimation model, (7.8) 7-77 through 7-79
  - general description of, (7.1) 7-1 through 7-4
  - ground-based tracker models, (7.2) 7-4 through 7-17
  - radar altimeter model, (7.4) 7-34 through 7-41
  - satellite-to-satellite tracking model, (7.3) 7-18 through 7-41
  - Very Long Baseline Interferometer, (7.5) 7-41, 7-42
- Observation noise, 8-1, 8-4, 8-41, (see also measurement noise)
- Observation partial derivatives, (8.2.2) 8-12
  - with respect to consider variables, 8-15
  - with respect to solve-for variables, 8-14
- Observation vector, linearized, 8-2

- Observational model parameters, 7-2
- Optimal linear gain, derivation of, (E.2) E-3
- Orbit estimation problem, 8-1, 8-27
- Orbit generation methods, (Chapter 5)
  - averaged equinoctial, (5.8.3) 5-40
  - averaged Keplerian, (5.8.4) 5-40
  - Brouwer, (5.9) 5-42 through 5-50
  - Brouwer-Lyddane, (5.10) 5-51 through 5-57
  - Chebyshev-Picard, (5.6) 5-26 through 5-29
  - Cowell, (5.2) 5-8
  - Cowell, time regularized, (5.3) 5-9
  - Delaunay-Similar, (5.5) 5-16 through 5-26
  - Intermediate Orbit, (5.11) 5-58
  - Kustaanheimo-Stiefel, (5.4) 5-10 through 5-15
  - Vinti, (5.12) 5-59, 5-60
  - VOP - equinoctial, (5.7.2) 5-33
  - VOP - Keplerian, (5.7.1) 5-31, 5-32
  - VOP - rectangular, (5.7.3) 5-34 through 5-36
- Orbit generators, characteristics of, (Table 5-1) 5-6, (Table 5-2) 5-7
- Orbital equations of motion, (Chapter 5)
- Origin of coordinates, 3-2
- Overview of GTDS, (Chapter 2)

## Partial derivatives,

- of acceleration due to nonspherical gravitational effects, (4.3.2) 4-14 through 4-32
- of acceleration due to attitude-control effect, (4.7.2) 4-66
- of acceleration due to nonspherical gravitational effects, (4.3.2) 4-14 through 4-18
- of acceleration due to point mass effects, (4.2.2) 4-8
- of acceleration due to solar radiation pressure, (4.6.2) 4-63
- analytic, (4.10) 4-75 through 4-86
- of atmospheric density,
  - Harris-Priester model, (4.5.7) 4-53 through 4-59
  - Jacchia-Roberts model, (4.5.5) 4-50 through 4-53
- of Cartesian state with respect to DODS variables, 4-80 through 4-83
- of Doppler measurement, 7-30 through 7-34
- of expected range, 7-15
- of geodetic coordinates with respect to body-fixed coordinates, 3-47
- of gimbal angles, 7-7 through 7-10
- of indirect oblateness effects, 4-20, 4-21
- Keplerian to Cartesian, (3.3.8.2) 3-53
- of Keplerian with respect to Cartesian, 3-58

Partial derivatives, (cont'd.)

- mapping of, (6.5) 6-15
- of Minitrack direction cosines, 7-11
- of nonspherical potential with respect to  $r$ ,  $\phi$ , and  $\lambda$ , 4-10
- of observation measurements, 7-4
- of observation measurements in local tangent coordinates, 7-6
- of radar altimeter observations, 7-40, 7-41
- of range observation, 7-25 through 7-27
- of range rate (average), 7-18
- of range rate (instantaneous method), 7-17
- of range rate (iterative method), 7-16
- of USB expected range, 7-14
- of VLBI measurements, 7-42

Perturbation methods,

- general, 5-1
- special, 5-1

Perturbation models, (Chapter 4)

- aerodynamic and atmospheric models, (4.5) 4-22 through 4-60
- indirect oblation perturbation model, (4.4) 4-18 through 4-22
- model parameters, 4-3
- N-point masses model, 4-5
- nonspherical gravitational effects, (4.3) 4-9 through 4-18
- point mass effects, (4.2) 4-4 through 4-8
- total perturbation model, (4.1) 4-2 through 4-4

Perturbing accelerations, (Chapter 4)

- aerodynamic force effects, (4.5) 4-22
- analytic partial derivatives, (4.10) 4-75
- atmospheric effects, (4.5) 4-22
- attitude control effects, (4.7) 4-64
- earth-moon indirect oblation effects, (4.4) 4-18
- nonspherical gravitational effects, (4.3) 4-9
- point mass effects, (4.2) 4-4
- replacement acceleration, (4.9) 4-73
- solar radiation pressure, (4.6) 4-60
- thrust effects, (4.8) 4-66

Picard iteration method, (5.6) 5-26

Poincaré variables, 5-4, 5-59

Point mass effects, (4.2) 4-4 through 4-8

- associated partial derivatives, (4.2.2) 4-8
- N-point masses perturbation model, (4.2.1) 4-5 through 4-8

Poisson's equation, 4-9

Polar motion, 3-18, 3-20, 3-21, 3-22, 3-23, 3-24

Polar motion coefficients, (Table 3-1) 3-25

- Postflight processing, 2-19
- Precession, 3-12
- Predictor-corrector integration methods, 6-1, 6-2, 6-7
- Predictor-pseudo-corrector methods, (6.2) 6-7
- Preprocessing, (Appendix A) A-1, 7-1, A-4, A-5, A-6, A-8, A-10, A-17, A-18, A-19, A-27, A-29, A-30
- Preprocessor/processor interfaces, A-1, A-5, A-17, A-18
- Prime Meridian, 3-2
  - Greenwich, 3-2
  - lunar, 3-2
- Principal directions, 3-3
- Probabilities,
  - hyperellipse, (8.5.2) 8-51, (Table 8-1) 8-53
  - hyperrectangle, (8.5.3) 8-54, (Table 8-2) 8-55
- Probability density function, 8-51
- Proper time, C-6, C-7, C-10
  
- Radar altimeter model, (7.4) 7-34 through 7-41
  - measurement equation, (7.4.2) 7-38 through 7-40
  - partial derivatives, (7.4.3) 7-40, 7-41
  - surface model, (7.4.1) 7-34 through 7-38
- Radar altimeter system, A-29, A-30
- Range (GRARR, ATSR, USB, and C-Band), 7-11 through 7-15
  - instantaneous method, 7-14
  - iterative method, 7-12 through 7-14
- Range ambiguity, A-3, A-6, A-11, A-33
- Range and Angles method, early orbit, (9.2) 9-24, 2-14
- Range difference, C-10
- Range observation, (7.3.3) 7-21 through 7-27
- Range rate (GRARR, ATSR, USB), 7-15 through 7-18
  - average range rate, 7-17, 7-18
  - instantaneous range difference method, 7-17
  - iterative range difference method, 7-16
- Range-rate formulas, (Appendix C) C-1
- Range sum calculation, 7-24, 7-25
- Range sum measurement, 7-19
- Real-time operation, near, 2-19
- Reference ellipsoid, 7-35 through 7-38
- Reference planes, 3-2
- Reference trajectory, 8-32, 8-33
- Reference trajectory, a priori, 8-23
- Refraction (see atmospheric effects)
- Refraction difference vectors, C-3

- Refraction effects, C-3, C-6, C-8, C-11, C-13, C-14
- Regression equation, nonlinear, 8-1, 8-7
- Regularization, (6.10) 6-22, 5-4, 5-10
- Relativistic Doppler frequency shift, C-3, C-4, C-5, C-6, C-11, C-14
- Relativistic signal propagation, (Appendix C) C-1
- Replacement acceleration, (4.9) 4-73 through 4-75, 2-18
  - acceleration model, (4.9.1) 4-73
  - partial derivatives, (4.9.2) 4-74, 4-75
- Residual error, predicted measurement, 8-32
- Residual uncertainty, predicted measurement, 8-32
- Runge-Kutta integration method, (6.6) 6-16, 6-1
  - starter for multi-step integration methods, 6-20
- Satellite-to-satellite tracking (SST) model, (7.3) 7-18 through 7-34
- Satellite-to-satellite tracking (SST) system, A-30 through A-33, C-14
- Schur identity, 8-57
- Sensor systems (see trajectory sensor systems)
- Solar/Lunar/Planetary File, 3-17
- Solar radiation pressure, (4.6) 4-60 through 4-63, 2-18
  - partial derivatives, (4.6.2) 4-63
  - perturbation model, (4.6.1) 4-60 through 4-63
- Solve-for variables, 2-13
  - a priori values, 8-6, 8-7, 8-24
  - best estimate of, 8-8
- Solve-for vector, 8-6, 8-12, 8-13, 8-27, 8-32
- Spacecraft dynamics, (2.3) 2-17, 2-18
- Space-time matrix, C-1 through C-3
- Special perturbations method, 2-6, 5-1, 5-2, 5-3, 5-4
- Stability,
  - dynamic, 5-5, 5-10
  - numerical, 5-2, 5-3
- Standard deviations, a priori, D-1, D-2
- Starting procedures, (6.7) 6-19, 6-20
- State correction vector, E-1
- State noise, 8-31, 8-32, 8-40, 8-42
- State transition matrix, 2-18, 4-1, 6-15, 6-16, 8-35
  - augmented, 8-44
  - elements, 4-72 through 4-81
- State vector,
  - augmented, 8-38, 8-43, 8-50
  - expanded, 8-15
- Statistical adaptive filtering, (8.4.3) 8-42
- Statistics, weighted least squares and filter, (8.6.4) 8-61
  - confidence interval for group mean, 8-63

Statistics, weighted least squares and filter, (cont'd.)

- group mean, 8-62
- observation residual groups, 8-63
- root mean square error, 8-62
- sample standard deviation, 8-63
- sum of squares about mean, 8-62

Stepsize regulation, 2-8, 5-5, 5-10, 6-1, 6-2, 6-21, 6-22

Störmer-Cowell integration formulas, 5-8, 5-9, 6-1, 6-6

System capabilities, (see GFDS system capabilities)

Thrust effects, (4.8) 4-66 through 4-72, 2-18

- acceleration model, (4.8.1) 4-67 through 4-69
- partial derivatives, (4.8.2) 4-69 through 4-72

Time,

- coordinate, C-6, C-8, C-9, C-10, C-12
- proper, C-6, C-7, C-10

Time correlation coefficients, 8-38

Time dependency of solve-for and consider variables, 3-12

Time difference coefficients, (Table 3-2) 3-74

Time element, 5-10, 5-11

Time regularization, (6.10) 6-22, 2-9, 2-18

Time regularized Cowell method, (5.3) 5-9, 2-9, 5-3, 5-5, 6-1, 6-20

Time systems, (3.4) 3-66

- atomic time, A.1, (3.4.3) 3-67
- ephemeris time, ET, (3.4.1) 3-67
- station time, ST, (3.4.8) 3-71
- transformation between, (3.5) 3-71
- uncorrected universal time, UT0, (3.4.4) 3-69
- universal time, UT, (3.4.3) 3-67
- universal time, UT1, (3.4.5) 3-69
- universal time, UT2, (3.4.6) 3-70
- universal time coordinated, UTC, (3.4.7) 3-70

Time tag, A-2, A-4, A-9, A-11, A-17, A-20, A-21, A-30, A-31, A-32

Timewise propagation of estimate, covariance matrix, 8-17

Tracker models, ground based, (7.2) 7-4 through 7-17

Tracking modes, 7-19

- coherent mode, 7-19
- crystal mode, 7-19
- phase-locked mode, 7-19

Tracking process, (7.2.1) 7-4

Tracking stations,

- ATSR, A-2
- C-Band, A-9



Tracking stations, (cont'd.)

GRARR, A-2, A-8

Minitrack, A-14

USB, A-10

Tracking system data types, 7-1, 7-2

Trajectory sensor systems, (Appendix A) A-1

ATSR, A-1 through A-8

C-Band radar, A-9, A-10

GRARR, A-1 through A-8

Minitrack, A-14 through A-27

radar altimeter, A-29, A-30

satellite-to-satellite, A-30 through A-33

USB, A-10 through A-13

VLBI, A-27 through A-29

Transformations,

from Brouwer mean elements to osculating Keplerian elements, (5.9.2)

5-46, (5.10.2) 5-52

from C-Band, GRARR, and USB data vectors to local tangent coordinates,  
9-24

from Cartesian position and velocity to DS elements, (5.5.2) 5-20

from Cartesian position and velocity to KS elements, (5.4.2) 5-13

from DS elements to Cartesian position and velocity, (5.5.3) 5-25

from KS parametric variables to Cartesian position and velocity, (5.4.3)  
5-15

from osculating orbital elements to averaged elements, (5.8.5) 5-40

from osculating orbital elements to Brouwer mean elements, (5.9.1) 5-45,  
(5.10.1) 5-52

from topocentric gimbil angles to inertial coordinates, (9.1.1) 9-2

Transformations between time systems, (3.5) 3-71, 3-72

by standard formula, (3.5.1) 3-71

by time polynomials, (3.5.2) 3-72

Transponder delay correction, (7.7.3) 7-77

Troposphere model, (7.6.1) 7-43, 7-44

Unified S-Band (USB) System, A-10 through A-13, C-10, C-11

early orbit data, 9-24

functional description, A-10, A-11, A-12

preprocessing description, A-13

Uniformization, 5-2, 5-3, 5-5, 5-9, 5-16

Variance, D-1

Variance estimation, 8-26

Variance for each observation, 8-5, 8-30

Variation of estimator with respect to consider parameters, 8-25  
 Variation of parameters formulations, 2-8, 4-7, 5-2, 5-4, 5-11, 5-16, 5-17, 5-20, 5-31, 5-38, 5-58, 6-1, 6-9  
 Variation of state with respect to consider dynamic parameters, 8-25  
 Variation of transformed state with respect to consider variables, 8-26  
 Variational equations, (Chapter 4) 4-1, 4-3, 4-4, 6-2, 6-11, 6-12, 6-14, 6-20, 8-14, 8-24  
     regularized, 6-24  
 Vehicle-fixed to body-centered true of date transformations, (3.3.12) 3-65  
 Vernal equinox, 3-3  
 Very Long Baseline Interferometer (VLBI) model, (7.5) 7-41, 7-42  
 Very Long Baseline Interferometer (VLBI) System, A-27 through A-29  
 Vinti theory, (5.12) 5-59  
 Von Zeipel method, 5-2, 5-42  
  
 Weighting factors, dynamic, D-1, D-2  
 Weighting matrix, 8-2, 8-4, 8-14, 8-63  
 Weighting, observation, D-1